

Copyright is owned by the Author of the thesis. Permission is given for a copy to be downloaded by an individual for the purpose of research and private study only. The thesis may not be reproduced elsewhere without the permission of the Author.

Understanding the largest-scale explosive volcanism at Mt. Taranaki, New Zealand

A thesis presented in partial fulfilment of the requirements for the
degree of

Doctor of Philosophy

in

Earth Science

Rafael Torres-Orozco

Massey University, Palmerston North

New Zealand

2017





“In solitude we find ourselves, defeat our ego, discover our worst, our best, love, real life and real friends” Photo: Sharks Tooth from the summit of Mt. Taranaki, Jul/2016.

Dedicated to my mother - the strongest person I've ever met,
and to my beloved adopted sisters and brothers

Abstract

Over the last 5000 years B.P., at least 53 explosive eruption episodes occurred at Mt. Taranaki, (western North Island, New Zealand) from either the summit-crater (2500 m), or a satellite vent on Fanthams Peak (1966 m). These eruptions are represented in well-preserved pyroclastic successions on the upper volcano flanks. At least 16 episodes produced deposits with lithostratigraphic characteristics comparable to those of the last sub-Plinian eruption at AD 1655, suggesting an average recurrence of one Plinian/sub-Plinian eruption episode every 300 years. Several large-scale mafic-intermediate (~48-60 wt.% SiO₂) eruption episodes sourced from the two vents were studied in detail to determine the “maximum” intensity, magnitude and eruptive styles from this volcano. These episodes comprised climactic phases with sustained and steady, 14-29 km-high eruption columns, often starting and ending with unsteady pulsating, oscillating and collapsing plumes. The columns erupted 0.1-0.5 km³ DRE at mass and volume discharge rates of 10⁷-10⁸ kg/s and 10³-10⁴ m³/s, respectively, indicating magnitudes of 4.1-5.1. The unsteady initial, pre- and post-climactic eruptive phases were dominated by dome-collapse, column-collapse and lateral-blast pyroclastic density currents (PDCs), with run-out distances of 3-19 km and volumes of up to 0.02 km³ DRE. The steadiest phases were associated with eruption of rheologically homogeneous magmas producing homogenous pumice textures. Unsteady phases produced density and porosity pumice gradients by magma stalling in upper conduit levels. Three eruption onset scenarios were developed from this work: a) initial closed-conduit decompression by vent unroofing and dome-collapse, b) transient open and clogged conduits produced by repeated plugging-and-bursting of chilled or gas-depleted magma, and c) rapid conduit opening with more mafic eruptives. In all scenarios, the climactic phases are comparable, with pyroclastic fallouts

covering 1500-2500 km². The most violent phases of these events, however, are lateral-blast PDCs that could reach a broad arc between 14-19 km from source. This reappraisal of the hazardscape at Mt. Taranaki integrates many new details that enable a more realistic hazard management and provides a range of findings that can be applied to other similar andesitic volcanoes prior to reawakening.

Acknowledgements

The first time I heard about New Zealand was in 2009 during an outstanding poster presentation about Mt. Ruapehu at the Jorullo conference in Mexico, by PhD student Natalia Pardo. The next thing I discovered was an incredibly beautiful, almost perfect cone-shaped stratovolcano, confusingly named both Taranaki and Egmont. This I wished to climb if I ever had the chance to go for any reason to the other side of the world. A few years later I emailed Shane Cronin inquiring about PhD opportunities and he replied by asking if I would be interested in working on explosive volcanism at Mt. Taranaki - I felt that I had just won the lottery. Doing fieldwork in this volcano has been challenging, slow, and at times frustrating due to the multiple obstacles posed by topography and vegetation and the very intricate stratigraphy. Disentangling a little part of such complexity whilst walking on its slopes has been extremely rewarding, and I would never choose differently, even if I could.

For this once-in-a-life opportunity, and for his aid in my receiving a Massey University Doctoral scholarship, I am very thankful to my chief supervisor Dr. Shane J. Cronin. I was also greatly benefited from his extraordinary understanding of the “big and small picture” of volcanic processes, from his ability in quickly recognising the core relevance of data and in choosing the exact sentence and the right paper among limitless possibilities, from his enthusiasm and cheering during these years, and from his skills in writing, organizing, discussing and developing ideas.

I am also greatly thankful to my co-supervisor Dr. Natalia Pardo. Her advice was essential in coming to New Zealand. Her expertise and cheerful disposition in reviewing, discussing and providing work-related and personal support were vital in pursuing this

work. Natalia is a field and research geologist and volcanologist worth to be followed and emulated, but additionally her patience and friendship have been second to none.

Many thanks to my co-supervisor Dr. Alan S. Palmer for his great disposition, reviews and encouraging, especially valuable during fieldwork. And I also wish to thank my other co-supervisors Dr. Robert B. Stewart and Assoc. Prof. Ian E.M. Smith (The University of Auckland) for their support, advice, reviews, explanations and discussion at different moments during completion of this work. I also thank Drs. Vince Neall, Karoly Nemeth, Georg F. Zellmer, Gert Lube, John Procter, and Eric Breard for their collegial support, Dr. Kate Arentsen for her reviews and her assistance with logistics and procedures, and Dr. Anja Moebis, Bob Toes and Ian F. Furkert for their help during labwork. Drs. Darren Gravley, Ian Fuller, and Roberto Sulpizio are acknowledged for their deep and fruitful reviews of the final thesis.

My infinite thanks go to my friend and colleague Magret Damaschke. This work simply would not have been properly finished without her deep discussions and endless energy, care, support and encouraging, especially during the worst times. Working alongside such a determined, honest and clever person enriched every chapter of this thesis, and her work brought light into solving Mt. Taranaki's stratigraphic puzzle which otherwise would have remained unclear.

Very especial thanks to my friend, colleague volcanologist, and mountain-climbing partner in Mexico Juan Ramón de la Fuente. His selfless care, humbleness, disposition and honesty despite distance are admirable. I benefited from his ongoing support and his taking charge of personal issues and financial and legal procedures back home, including the bureaucratic and tedious processing of my CONACyT Doctoral scholarship.

Additional thanks go to my first mentor in Volcanology, Dr. Jose Luis Arce, who has never stopped providing advice, discussion, reviews, appreciation and concern. Many

thanks to my friend Dr. Gabor Kereszturi who provided outstanding personal and academic advice, cheering and support, interesting discussions (and rum-based drinks at any opportunity!). His enthusiasm and determination during fieldwork were greatly appreciated. I am also very thankful to my colleague and half-Mexican friend Szabolcs Kósik, who demonstrated an exceptional personality and interest, and did not vacillate in supporting me, my work and my future outcomes, at times by fuelling up with Palinka.

Endless thanks to friends and people I met at Palmerston North who provided their support in many different ways and at different moments during these years, including words of encouraging and comprehension, discussion, field-assistance, tramps and good memories: Angela Denes, István Hajdu, Eduardo A. Sandoval, Gaby Gómez, Kwan Maitrarat, Marcela Humphrey, Friederike von Schlippe, Soledad Navarrete, Javier Agustín Flores, Diana Cabrera, Manuela Tost, Omar Cristobal, Zsuzsa Szmolinka, Jimena Rodríguez and “Negrito” Adimar.

Last but not least, to my grandma and uncles, and to my non-blood family who have kept their unconditional support, encouraging and inspiration at any time during these years of PhD regardless of distance: David Alvarez, Juan Angel Torres-Rechy, Pasquinel de la Fraga, Heriberto Oliva, Francisca Vidal, Edgar Ocampo, Laura Scheffler, Mariela Díaz, and Emma Cesta.

This work was supported by a Massey University Doctoral scholarship, a CONACyT (Mexico) Doctoral scholarship, and the George Mason Trust of Taranaki.

Table of Contents

Abstract	i
Acknowledgements	iii
Table of Contents	vii
List of Tables	xi
List of Figures	xi
Chapter 1 Introduction	17
1.1 Introduction	18
1.2 Research outline and objectives	24
1.3 Literature review	25
1.3.1 Explosive volcanism	25
1.3.2 Eruption dynamics	31
1.3.3 Previous research at Mt. Taranaki	34
1.4 Background geology	41
1.4.1 Regional framework	41
1.4.2 The Taranaki Basin	45
1.4.3 Mt. Taranaki / Egmont	48
1.4.3.1 <i>Volcanic history of Mt. Taranaki</i>	50
1.4.3.2 <i>Petrology and geochemistry</i>	54
1.5 References	57
Chapter 2 Methodology	77
2.1 Outline	78
2.2 Field methodology	79
2.2.1 Mapping criteria	81
2.3 Radiocarbon dating	82
2.4 Granulometry and componentry	83
2.5 Geochemical analysis	84
2.6 Density and porosity (gas pycnometry)	84

2.7	Eruptive parameters	86
2.8	References	88

Chapter 3 New Holocene eruption episodes from proximal deposit sequences93

3.1	Abstract	95
3.2	Introduction	96
3.3	Geological setting and previous work	98
3.4	Methodology	102
3.4.1	Field methodology.....	102
3.4.2	Mapping criteria.....	109
3.4.3	Radiocarbon dating.....	111
3.5	The late-Holocene eruption records of Mt. Taranaki	111
3.5.1	The Mt. Taranaki Lithosome.....	114
3.5.1.1	<i>Bed-sets Tw-I to Tw-VII</i>	114
3.5.1.2	<i>Bed-sets Tw-VIII and Tw-IX</i>	118
3.5.1.3	<i>Bed-sets Tw-X and Tw-XI</i>	118
3.5.1.4	<i>The Kokowai bed-set</i>	118
3.5.1.5	<i>Bed-sets KkF-I and KkF-II</i>	119
3.5.1.6	<i>The Kapuni-A bed-set</i>	120
3.5.1.7	<i>The Kapuni-B bed-set</i>	120
3.5.1.8	<i>The Korito bed-set</i>	121
3.5.1.9	<i>The Lower Inglewood bed-set</i>	122
3.5.1.10	<i>The Upper Inglewood bed-set</i>	123
3.5.1.11	<i>The Maketawa I bed-set</i>	125
3.5.1.12	<i>The Maketawa II bed-set</i>	125
3.5.1.13	<i>The Maero Formation</i>	127
3.5.2	The Fanthams Peak Lithosome.....	128
3.5.2.1	<i>The Manganui Formation</i>	128
3.6	Interpretation of deposits and associated volcanic hazard	132
3.6.1	Pyroclastic fall deposits.....	132
3.6.2	Pyroclastic density currents (PDCs).....	134

3.7	Revised eruption history	136
3.7.1	Comparison with previous work.....	136
3.7.2	Late-Holocene eruptions of Mt. Taranaki.....	137
3.8	Conclusions	143
3.9	Next chapters	145
3.10	References	145

Chapter 4 Diverse dynamics of mafic-intermediate Plinian eruptions..... 151

4.1	Abstract	153
4.2	Introduction	154
4.3	Geological setting	156
4.4	Methods	159
4.5	Late-Holocene large explosive eruptions at Mt. Taranaki	165
4.5.1	The 4700 - 4600 cal BP Kokowai eruptive episode	165
4.5.2	The 3300 cal BP Upper Inglewood eruptive episode	168
4.5.3	The ~2600 cal BP Manganui-D eruptive episode.....	174
4.5.4	The ~1200 cal BP Kaupokonui eruptive episode	177
4.5.5	The AD 1655 Burrell eruptive episode.....	179
4.6	Whole-rock chemistry	180
4.7	Eruptive metrics	183
4.7.1	Dispersal	183
4.7.2	Eruptive volumes	187
4.7.3	Column heights, wind speed and classification	188
4.7.4	Eruption rates, magnitudes and durations.....	191
4.8	Discussion	192
4.8.1	Constraints on the eruptive volume estimates	192
4.8.2	Mt. Taranaki summit-vent: eruptive successions and processes	193
4.8.3	Fanthams Peak vent: parasitic cone/flank vent eruptions.....	195
4.8.4	Implications for Plinian and sub-Plinian eruptions.....	198
4.9	Conclusions	200
4.10	References	202

Chapter 5	Volcanic hazard scenarios for Plinian eruptions: insights into PDC diversity	209
5.1	Abstract.....	211
5.2	Introduction.....	212
5.3	Geological background.....	215
5.4	Methods and terms	218
5.5	Summary lithostratigraphy of proximal Plinian and sub-Plinian eruption deposits at Mt. Taranaki	224
5.6	Discussion	231
5.6.1	Interpretation of eruptive processes	231
5.6.1.1	<i>Plinian, sub-Plinian, and small-scale eruption columns</i>	<i>234</i>
5.6.1.2	<i>Concentrated – flow type – PDCs</i>	<i>235</i>
5.6.1.3	<i>Dilute – surge type - PDCs</i>	<i>236</i>
5.6.1.4	<i>Transitional – flow-and-surge type – PDCs</i>	<i>236</i>
5.6.2	Constraints of depositional environment to hazard distribution.....	238
5.6.3	Volcanic hazard scenarios	242
5.6.3.1	<i>Scenario I: dome collapse and conduit decompression</i>	<i>245</i>
5.6.3.2	<i>Scenario II: transient conduit clogging by magma plug-and-burst</i>	<i>248</i>
5.6.3.3	<i>Scenario III (Fanthams Peak): rapid conduit clearing at satellite vents</i>	<i>250</i>
5.6.4	Event-tree scenario sequence.....	251
5.7	Conclusions.....	252
5.8	References.....	254
Chapter 6	Conclusions	261
6.1	Avenues for future research.....	268
Appendices	273

List of Tables

Table 3.1.....	112
Radiocarbon dating of material from proximal sections of Mt. Taranaki.	
Table 4.1.....	164
Eruptive volumes obtained by different methods using bulk-isopach data of fall deposits, and area and bulk-average thickness of pyroclastic density current deposits.	
Table 4.2.....	169
Bulk and solid densities, bulk porosities, dense-rock-equivalent volumes, and eruptive parameters calculated from fall and pyroclastic density current deposits produced by different eruptions at Mt. Taranaki.	
Table 5.1.....	213
Summary of key lithostratigraphic characteristics and componentry of deposits produced by late-Holocene eruptions at Mt. Taranaki.	
Table 5.2.....	215
Late-Holocene Plinian / sub-Plinian eruptions at Mt. Taranaki.	
Table 5.3.....	219
Lithofacies classification scheme to describe proximal pyroclastic deposits at Mt. Taranaki.	
Table 5.4.....	221
Summary descriptions of the lithofacies associations identified from pyroclastic deposits at Mt. Taranaki.	
Table 5.5.....	232
Summary interpretations of the lithofacies associations identified from pyroclastic deposits at Mt. Taranaki.	

List of Figures

Figure 1.1.....	42
a Tectonic setting of the North Island of New Zealand (modified from King and Thrasher 1996; Henrys et al. 2003; Price et al. 2005; Platz et al. 2007). b Zoomed area of the Taranaki Volcanic Lineament (Neall 1979), which comprises four Pleistocene-Holocene, southwards-younging andesitic volcanoes or their eroded volcanic edifice-remnants: Paritutu, Kaitake, Pouakai and Mt. Taranaki (along with the parasitic cone of Fanthams Peak). Coordinate system: NZGD 2000 New Zealand Transverse Mercator.	
Figure 3.1.....	99
a Tectonic setting of the North Island (NI) of New Zealand (modified from King and Thrasher 1996; Henrys et al. 2003; Price et al. 2005; Platz et al. 2007). <i>CEFZ</i> Cape Egmont Fault Zone, <i>R</i> Mount Ruapehu, <i>SI</i> South Island, <i>TVL</i> Taranaki Volcanic Lineament (yellow line), <i>TVZ</i> Taupo Volcanic Zone. b Zoomed area of the Taranaki Volcanic Lineament (Neall 1979); which comprises four Pleistocene-Holocene, southwards-younging andesitic volcanoes or their eroded volcanic edifice-remnants: Paritutu, Kaitake, Pouakai and Mt. Taranaki (along with the parasitic cone of Fanthams Peak). <i>AS</i> Ahukawakawa swamp, <i>DOC</i> Department of Conservation visitor centre, <i>SH</i> principal state highways and other roads connecting	

residential areas. **c** Zoomed area of the proximal eastern flanks of Mt. Taranaki and the studied key sections. Coordinate system: NZGD 2000 New Zealand Transverse Mercator.

Figure 3.2..... 103
Stratigraphic correlation of the late-Holocene pyroclastic sequence studied in proximal sections on the eastern flanks of Mt. Taranaki.

Figure 3.3..... 105
Composite stratigraphic log of the late-Holocene proximal pyroclastic sequence of Mt. Taranaki. Members of the Manganui Formation (i.e. Manganui-A to G) are abbreviated: *MA*...*MG*. *CR* Curtis Ridge Lapilli bed-set (Turner et al. 2008b). Main juvenile pyroclasts are indicated (dense-vesicular). Solid lines indicate sharp contacts; bold solid lines indicate sharp-erosive (often angular) contacts; dashed lines indicate transitional contacts. Grain-size simplified from White and Houghton (2006): *FA* Fine-ash, *CA* Coarse-ash, *FL* Fine-lapilli, *CL* Coarse-lapilli, *B* Blocks/Bombs. Sorting: poor (psr), moderate (ms), well (ws) and very well sorting (vs) from Cas et al. (2008). Clast (cs) and matrix-support (ms) framework, and angular (a), sub-angular (sa), sub-rounded (sr), rounded (rd) and well-rounded (wr) clast-shape are indicated. *DF* Debris-Flow, *C-PDC* Column-collapse Pyroclastic Density Current, *BAF* Block-and-Ash Flow, *PDC* Undefined Pyroclastic Density Current. **a** Comparison of a segment from the previous ring-plain and distal tephrostratigraphy with the equivalent proximal lithostratigraphy of this work and a few earlier studies. See text and Table 1 for ¹⁴C age references.

Figure 3.4..... 115
Photographs showing the deposit features of representative late-Holocene bed-sets/Members exposed at different eastern-flank sections of Mt. Taranaki. Bed-sets/Members are Tw-I to Tw-XI, *Kw* Kokowai, *KA* and *KB* Kapuni-A and B, *Ko* Korito, *Lig* Lower Inglewood, *Uig* Upper Inglewood, *MA* to *MF* Manganui-A to F, *MkI* and *MkII* Maketawa I and II, *CR* Curtis Ridge, *Kp* Kaupokonui, *GI* to *GIII* Grey PDC-I to -III, *Tp* Te Popo, *Bu* Burrell. **a** Deposits of the ~5 ka bed-sets and stratigraphic relationships with younger 4.7-3.3 cal ka B.P. deposits. **b** Complete *Kw* bed-set. Radiocarbon (¹⁴C) dating of charcoal from layers 3 and 5-6 is indicated. **c** Northern stratigraphic relationships between different 4.7-3.3 cal ka B.P. and younger ~2.6-0.7 cal ka B.P. bed-sets. ¹⁴C dated layers from bed-sets *Ko* and *Uig* are indicated. **d** Zoom of the *Ko*. **e** Impact sags produced by pumice bombs of different 4.7-3.3 cal ka B.P. bed-sets. **f** Fall deposits of the *Kw* layer 4. Bombs and blocks are signalled. **g** Fall deposits of bed-sets *KA* and *KB* separated by weathered ash. **h** Block-and-ash flow and fall deposits of the *Kw* constitute the base of the exposed section. Lava flows (MD 2b) from Fanthams Peak erode fall deposits of the MD. **i** Stratigraphic relationships and ¹⁴C dated deposits of 3.4-0.3 cal ka B.P. bed-sets. Block-and-ash flow deposits underlying layer 2 of the *Lig* bed-set make the base of the exposed section. Notice Block-and-ash flow deposits of the *Uig* (layer 1). **j-l** Deposit features of the *Uig* in southeastern-northeastern locations. Notice lithofacies transitions of layer 6 and ¹⁴C dating of charcoal from bracketing bed-sets. **m** Deposits of the <3.0-2.2 cal ka B.P. *MA* to *MD* Members and other bracketing and/or younger deposits. **n** Zoom of the *MC*-*MD* Members and bracketing debris-flow deposits. **o** Zoom of the *MA*-*MC* Members. Notice the cauliflower bomb of the *MB* Member deforming deposits of the *MA*. Notice grey-lithic ash deposits of bed-sets *MkP*-I and *MkP*-II (not labelled), which pass laterally into ¹⁴C dated 2.6 cal ka B.P. lithic breccias. **p-t** Deposit features and facies transitions of the *Mk* II. **s** Notice the commonly overlying deposits of the *MF* and their distinctive scarlet-red lithics. **t** Notice deposits of the *GI* bed-set. **u-w** Deposit features of the *Tp*. Notice ash deposits of layer 1 (*Tp*1), which correlate with western 0.7 cal ka B.P. lithic breccias. *x* cross-, *p* parallel- or *fp/fx* faint parallel/cross-stratified and *m* massive deposits. Spade is 70.5 cm-long, large scraper is 32.5 cm-long, small scraper is 20 cm-long. See text and Table 1 for ¹⁴C age references.

Figure 3.5..... 133
a Total accumulated thickness of fall and pyroclastic density current (PDC) deposits per bed-set (Bdst) in centimetres, and total thickness per pyroclastic deposit-type in metres (see inset). Numbers accompanying bars (e.g. 71-29) indicate volume percentages of fall-PDC deposits. The line-diagram indicates number of

layers of Fall and PDC deposits (units) per bed-set. *Unconf* Unconformity, *pl/wa* Intervening paleosol and/or weathered ash deposits in centimetres-thick. Refer to text and figure 3 for bed-set abbreviations. **b** Calibrated ^{14}C ages from this work and previous works. The size of each circle is proportional with the corresponding dating error (see Table 1 for complete data and references).

Figure 4.1..... 157

a Tectonic setting of the North Island (NI) of New Zealand (modified from King and Thrasher 1996; Henrys et al. 2003; Sherburn and White 2006; Stagpoole and Nicol 2008). *CEFZ* Cape Egmont Fault Zone, *R* Mount Ruapehu, *SI* South Island, *TVL* Taranaki Volcanic Lineament (yellow line), *TVZ* Taupo Volcanic Zone. **b** Zoomed area of the Taranaki Peninsula and the TVL. The latter comprises four <1.75 Ma and NNW-SSE migrating andesitic volcanoes or their eroded volcanic edifice-remnants (Neall 1979): Paritutu, Kaitake, Pouakai and Mt. Taranaki (and the satellite cone of Fanthams Peak). *IGF* Inglewood Fault, *MF* Manaia Fault, *NFF* Norfolk Fault. **c** Zoomed area of the proximal eastern flanks of Mt. Taranaki and type sections of this study. Coordinate system: NZGD 2000 New Zealand Transverse Mercator.

Figure 4.2..... 162

a Diagram of median diameter ($\text{Md}\phi$) vs. Inman sorting coefficient ($\sigma 1\phi$), modified from Walker (1971), and corresponding to grain-size of samples from different <5000 to 300 cal BP fall (Fallouts) and pyroclastic density current (PDCs) deposits of Mt. Taranaki. **b** Bulk-deposit isopach data plotted on square root (Area) vs. log (Thickness) of each fall deposit studied.

Figure 4.3..... 166

Lithostratigraphic characteristics, modified from Torres-Orozco et al. (2017), componentry, granulometry, and pumice density and porosity data, of the 4700-4600 cal BP Kokowai bed-set (layers Kw1 to Kw8). Grain-size modified from White and Houghton (2006). Notice the slight bimodality in some fall deposit histograms (e.g., basal and middle deposit levels of layer Kw7) produced at 4ϕ mode by ash deposits from associated pyroclastic density currents. Connected and bulk porosities (p), and bulk densities (d) were calculated from texturally different pumice clasts, hand-picked from different vertical fall deposit levels (30 clasts per texture per level).

Figure 4.4..... 171

Lithostratigraphic characteristics, modified from Torres-Orozco et al. (2017), componentry, granulometry, and pumice density and porosity data, of the 3300 cal BP Upper Inglewood (layers Uig1 to Uig7). Notice the slight bimodality in some fall deposit histograms (e.g., basal level of layer Uig7) produced at $\sim 3\phi$ mode by ash deposits from associated pyroclastic density currents. Connected and bulk porosities (p), and bulk densities (d) calculated from texturally different pumice clasts (30 clasts per texture per layer). See Fig. 4.3 for complete symbology and details.

Figure 4.5..... 175

Lithostratigraphic characteristics, modified from Torres-Orozco et al. (2017), componentry, granulometry, and density and porosity data of vesicular juvenile clasts, of deposits of the 2600 cal BP Manganui-D bed-set (layers MD1 to MD3). Deposits of lower and upper debris flows (L-DF and U-DF) are also represented. Connected and bulk porosities (p), and bulk densities (d) were calculated from similar vesicular juvenile clasts, hand-picked from different vertical levels within each pyroclastic layer (30 clasts per level per layer). See Fig. 4.3 for complete symbology and definitions.

Figure 4.6..... 178

Lithostratigraphic characteristics, modified from Torres-Orozco et al. (2017), componentry, granulometry, and pumice density and porosity data, of the 1200 cal BP Kaupokonui bed-set (Kp), and the AD 1655 Burrell fall deposit (Bu). Connected and bulk porosities (p), and bulk densities (d) were calculated from texturally different pumice clasts, hand-picked from different vertical fall deposit levels (30 clasts per texture per level). See Fig. 4.3 for complete symbology and definitions.

- Figure 4.7**.....182
 Whole-rock analyses of volcanic rocks from Mt. Taranaki, normalized to anhydrous basis, plotted on the total alkalis vs. silica diagram modified from Le bas et al. (1986), and on binary diagrams of some major elements. Dotted line discriminates between alkaline (above the line) and sub-alkaline (below the line) series (Irvine and Baragar 1971). Data taken from previous work (*) correspond to Franks (1984), May (2003), Turner (2008), Turner et al. (2011b) and Platz et al. (2007, 2012).
- Figure 4.8**.....184
 Isopach maps of fall deposits corresponding to bed-sets: **a** Manganui-D, layers MD1 to MD3, sourced at the satellite vent of Fanthams Peak, **b** Burrell, modified from Platz et al. (2007), **c** Upper Inglewood, layer Uig7, **d** Kaupokonui, modified and corrected from Whitehead (1976), **e** Kokowai, layer Kw4, and **f** Kokowai, layer Kw7. Grey numbers represent thickness data measured in centimeters. Some contours are labeled with black numbers inside white squares (in centimeters). Black contours were interpolated from field data (Appendix 4.1) using methods described in the text. Red contours were partially or fully extrapolated using parameters described in the methodology. Coordinate system: NZGD 2000 New Zealand Transverse Mercator.
- Figure 4.9**.....185
 Isopleth maps of the diameters of pumice clasts, vesicular juvenile clasts (scoriaceous) of the Manganui-D bed-set, and dense andesitic clasts in centimeters, corresponding to fall deposits of bed-sets: **a** Burrell, modified from Platz et al. (2007), **b-c** Kaupokonui, **d-f** Manganui-D, layers MD1 to MD3, sourced at the satellite vent of Fanthams Peak, **g-h** Upper Inglewood, layer Uig7, **i-j** Kokowai, layer Kw4, and **k-l** Kokowai, layer Kw7. Grey numbers indicate average diameters measured in the field. Black contours were interpolated from field data (Appendix 4.1) using methods described in the text. Red contours were partially extrapolated using parameters described in the methodology. Coordinate system: NZGD 2000 New Zealand Transverse Mercator.
- Figure 4.10**... ..187
 Maps of area of distribution of pyroclastic density current deposits from bed-sets Upper Inglewood (layers Uig1 to Uig6) and Kokowai (layers Kw1 to Kw3, Kw6 and Kw8). Coordinate system: NZGD 2000 New Zealand Transverse Mercator.
- Figure 4.11**... ..190
 Eruptive parameters and classification of the studied deposits. **a** Normal distribution of total column heights (HT) in kilometers, calculated by using different methods (Table 4.1, Appendix 4.9). Numbers indicate minimum, maximum and average HT corresponding to individual fall deposits. **b-c** Isopleth data plotted in the diagram of Carey and Sparks (1986) to determine HT and wind speeds, based on diameters of dense andesitic clasts and pumice clasts (or vesicular juvenile clasts of the Manganui-D bed-set), ranging from 0.8 to 2 cm and 1.6 to 4 cm, respectively, and on the corresponding clast's bulk-densities (kg/m^3). **d** Diagram of Pyle (1989) of classification of the eruptions based on parameters (bc, bt) calculated from isopach and average isopleth (pumice and dense andesitic clast) data, and on the dispersal index of Walker (1973, Appendix 4.9). **e** Diagram of Bonadonna and Costa (2013) of classification of eruptions based on HT, and on parameters (λ_{th} , λ_{ML}) calculated from isopach and isopleth data (Appendix 4.9). **f** Diagram modified from Sparks (1986) and Carey and Bursik (2000) to determine volume and mass eruption rates (Q and MER, respectively), considering the average HT calculated from each individual fall deposit. The curve of HT calculated by using the model of Sparks (1986) is indicated. Neutral buoyancy column heights (HB) were estimated by using the average HT of each fall deposit and "bc" of Pyle (1989, Appendix 4.9). Fields corresponding to Plinian and sub-Plinian eruptions were modified from Bonadonna and Costa (2013). **g** Plot of average HT vs. Minimum dense-rock-equivalent (DRE) eruptive volumes. The latter were calculated from average total volumes, and bulk and solid densities (Table 4.2). **h** Plot of average HT vs. Magnitude ($M = \text{Log}_{10}(\text{mT}) - 7$) calculated using the method of Pyle (2000). Total mass in kilograms ($\text{mT} = (\text{solid-density}) (\text{DRE volume})$) calculated using the method of Wilson (1976). **i** Plot of average HT vs.

minimum duration of the eruption, in hours ($T=mT/MER$, Table 4.2), estimated using the method of Wilson (1976).

- Figure 5.1**.....216
A Tectonic setting of the North Island (NI) of New Zealand (modified from King and Thrasher 1996; Henrys et al. 2003; Sherburn and White 2006). *CEFZ* Cape Egmont Fault Zone, *R* Mount Ruapehu, *SI* South Island, *TVL* Taranaki Volcanic Lineament (yellow line), *TVZ* Taupo Volcanic Zone. **B** Zoomed area of the TVL. The latter comprises four <1.75 Ma and NNW-SSE migrating andesitic volcanoes (Neall 1979) or their eroded volcanic edifice-remnants: Kaitake, Pouakai and Mt. Taranaki (and the satellite cone of Fanthams Peak – topped by Syme Hut). **C** Zoomed transect of the proximal eastern flanks of Mt. Taranaki and the type sections of this study (points A to Y, Appendix 5.1). Digital profile modified from Google Images (2017). **D** 10 cm-thick isopachs of fall deposits produced during <5 ka Plinian (white ellipses) and sub-Plinian (grey ellipses) eruptive episodes at Mt. Taranaki (modified from Torres-Orozco et al. 2017b, Table 5.2). Red circles indicate the position of the summit crater and the Fanthams Peak vent. Coordinate system of all insets: NZGD 2000 New Zealand Transverse Mercator.
- Figure 5.2**.....225
 Proximal lithofacies transitions of the 4700-4600 cal BP Kokowai (Kw1-Kw8). *KA* Kapuni-A, *KB* Kapuni-B, *Ko* Korito. Sections indicated on top of each profile (A-Y, Fig. 5.1). Yellow lines on photographs indicate lower and uppermost bed-set contacts. Lithofacies codes (Table 5.3) indicated to the right of each profile and inside white boxes on pictures. *FA* fine-ash, *CA* coarse-ash, *FL* fine-lapilli, *CL* coarse-lapilli, *B* block/bombs. Scale on pictures represented by a black bar or a scraper (32.5 cm-long).
- Figure 5.3**.....226
 Proximal lithofacies transitions of the 3800 to 3500 cal BP Kapuni-A (*KA*: KA1-KA2), Kapuni-B (*KB*: KB1-KB4) and Korito (*Ko*: Ko1-Ko8). *Kw* Kokowai, *Uig* Upper Inglewood. Sections indicated on top of each profile (A-Y, Fig. 5.1). Yellow lines on photographs indicate lower and uppermost bed-set contacts. See Fig. 5.2 for more details. The scale on pictures is represented by a black bar or a scraper (32.5 cm-long).
- Figure 5.4**.....227
 Proximal lithofacies transitions of the 3300 cal BP Upper Inglewood (*Uig1-Uig7*). Sections indicated on top of each profile (A-Y, Fig. 5.1). Yellow lines on photographs indicate lower and uppermost bed-set contacts. See Fig. 5.2 for more details. The scale on pictures is represented by a black bar, a long (32.5 cm-long) or a small scraper (20 cm-long), or a 10 cm-long scale.
- Figure 5.5**.....228
 Proximal lithofacies transitions of 3000-2600 cal BP members Manganui-A (*MA*: MA1-MA3), Manganui-B (*MB*), Manganui-C (*MC*), Manganui-D (*MD*: MD1-MD3) and Manganui-E (*ME*) of the Manganui Formation (Torres-Orozco et al. 2017a; b). *Uig* Upper Inglewood, *DF* debris flow. Sections are indicated on top of each profile (A-X, Fig. 5.1). Yellow lines on photographs indicate lower and uppermost bed-set contacts. See Fig. 5.2 for more details. The scale on pictures is represented by a black bar, and a long (32.5 cm-long) or a small scraper (20 cm-long).
- Figure 5.6**.....237
A Example of landscape elements that integrate the present-day micro-topography of the upper eastern flanks of Mt. Taranaki. The gradient of deposit confinement is indicated (modified from Schwarzkopf et al. 2005). **B** Profile of the general lateral transitions, relative to landscape, of deposits corresponding to each lithofacies association. Dotted white line indicates section not represented (not rep.) in the profile. Proximal (P-lateral) and proximal-medial (M-lateral) lateral lithofacies transitions relative to a reference incision-channel (i) are sketched. Digital image modified from Google Images (2017).

Figure 5.7.....	239
Hazard maps indicating the possible distribution of different types of eruptive activity, throughout distinct eruptive phases, during a future Plinian eruption at Mt. Taranaki. Insets A to D correspond to opening, pre- or post-climactic eruptive phases. A dome-collapse block-and-ash flows, B blast type PDCs and lithic-rich surges, C column-collapse PDCs, D fallout, ballistics, and lava flow distributions. Insets E to G correspond to climactic eruptive phases. E blast type PDCs, F fallout, ballistics and lava flow distributions, G column-collapse PDCs. Inset H represents possible distributions of channel-confined lahars and small-scale landslides during any eruptive phase. Coordinate system of all insets: NZGD 2000 New Zealand Transverse Mercator.	
Figure 5.8.....	243
Volcanic hazard scenarios for Plinian eruptions at Mt Taranaki's summit-crater and Fanthams Peak vent. A-F Scenario I: initial eruptive phases of close-conduits and conduit-decompression by vent unroofing and dome collapse. G-K Scenario II: transient open and clogged conduits by repeated plugging-and-bursting of gas-depleted or chilled magma. L-O Scenario III: rapid progression into steady phases by open-conduits. The possible upper conduit dynamics for each scenario were sketched based on data and interpretations of Torres-Orozco et al. (2017a; b).	
Figure 5.9.....	247
Event-tree sequence of the volcanic scenarios expected at Mt. Taranaki during a possible Plinian eruptive episode (magnitudes 4 to 5), produced at either the summit crater, or a satellite vent. For any vent, the eruptive sequence progresses from an opening and pre-climactic phase (1), throughout a climactic phase (2), to a post-climactic phase (3). Vent and/or conduit conditions (A to H) may direct into different processes and events (i.e., Scenarios I to III). Dotted lines indicate subsequent, alternative directions. Run-out distances simplified from Fig. 5.7.	

Chapter 1 Introduction

This chapter introduces the justification of this research within the overall hazardscape of New Zealand and for andesitic volcanoes worldwide. Guiding questions and the objectives of the work are outlined. Furthermore, a literature review briefly summarizes contributions concerning the study of explosive volcanism at andesitic volcanoes and summarises research carried out at Mt. Taranaki, as well as explaining its geologic and tectonic setting.

1.1 Introduction

New Zealand's hazardscape is well recognized worldwide for its recurrent explosive volcanic activity. The Taupo Volcanic Zone (TVZ) has been frequently the centre of attention, having erupted some of the largest and environmentally most disruptive Quaternary rhyolitic ignimbrites ever recorded in Earth's history (Wilson et al. 1995; Wilson 1997; Manville et al. 2009). The smaller andesitic volcanoes, however, can be equally hazardous, with many historical examples of destructive, and deadly eruptions including: AD 79 Mt. Vesuvius (Carey and Sigurdsson 1987), 1902 Mt. Pelée (Bourdier et al. 1989), 1980 Mt. St. Helens (Tilling et al. 1990), 2008 Chaiten (Carn et al. 2009), and the 2010 Eyjafjallajökull eruptions (Gudmundsson and Pedersen 2010; Langmann et al. 2012). These show that sub-Plinian and Plinian events in the order of 0.1-1 km³ are able to produce huge human, environmental and quantitative harm.

Little is known about the largest-scale explosive eruptions in subduction-related andesitic stratovolcanoes in New Zealand (NZ) and human consequences that they may hold. By contrast, knowledge of the 100-1000 times less explosive "typical" or most-likely eruptions has been better examined over the last decade (Platz et al. 2012; Turner et al. 2009, 2011b), and after the latest 2012 activity at Mt. Tongariro (e.g. Lube et al. 2014). Recently, Pardo et al. (2012a, 2012b) calculated minimum volumes of 0.6 km³ for the five <27 ka largest possible eruptions at Mt. Ruapehu in south TVZ. These Plinian events were characterized by columns of up to 37 km high that dispersed ash and pumice to north, east, and southeast flanks of the volcano, as far as 30 km from its summit. Mt. Taranaki, located in the centre of western NZ's Taranaki region, is the second largest major andesitic stratovolcano that can produce Plinian and sub-Plinian events as seen as

lapilli units found extensively in ring-plain deposits downwind of the volcano (Alloway et al. 1995).

According to the 2006 NZ census (Statistics NZ 2013) 104,126 people, 2.6% of NZ's total population, live in the Taranaki region (as defined by the Taranaki Regional Council 2013). About 8,892 people inhabit the eastern Stratford District, 26,484 residents live in the South Taranaki District, and 68,901 people live in the northern New Plymouth District. The economy in the region increased 46.9% between 2007 and 2010 contributing 4.2% (\$NZ8.0 billion) of the total national Gross Domestic Product (GDP), which denotes the largest increase for any region in NZ during that interval (Statistics NZ 2013). Excluding the regions of Auckland, Canterbury, and Wellington, the GDP of Taranaki is comparable to that of Bay of Plenty and Otago regions. Such escalation mainly rests upon the expansion of the energy industry. The Taranaki region is home of almost all of the nation's oil, natural gas and petrochemical production, making 1.3% of the national GDP, and comprising 90% of this branch's national employment (New Zealand's Oil and Gas Industry 2013). Of the total 18 natural gas fields in the region, 13 are located onshore in the proximities of Mt. Taranaki. This region also hosts 1,900 dairy farms (two-thirds of the regional area) concentrated along the ring-plain of the volcano which produce about 20% of NZ's milk for domestic and foreign markets (Fonterra 2013). Fonterra operates three major plants in the region: a manufacturing plant at Kapuni, a cheese factory at Eltham, and the largest milk-processing plant in the South Hemisphere near Hawera. Agriculture is another prime regional industry. Whilst 40% of the land is covered by indigenous and/or exotic forest, including the Egmont National Park, over 60% is in grassland or crops. Around 6,600 people work in the industry of agriculture alone, and 4,000 full-time-position employees work in the food processing and manufacturing

industry in general (Taranaki Regional Council 2013). Forestry, fishing, mining, electricity, water, and waste services are other socio-economically relevant activities in the region.

In the eventuality of a Plinian eruption at Mt. Taranaki not only all the economic activities representing 4.2% of NZ's GDP would be truncated, but thousands of people within the region would find their lives and livelihoods at severe risk. Considering the common northeast and southeast wind regional directions recorded in the distributions of the Holocene explosive events (Neall 1972; Alloway et al. 1995; Turner et al. 2009), people settled over the lee-side of the volcano would face the most hazardous scenarios. Ash transported by plumes through the atmosphere can generate long-lasting air and water pollution yielding serious respiratory illnesses, stomach intoxications, eye diseases, and water poisoning. There are 286 separate river catchments flowing throughout the Taranaki region (Taranaki Regional Council 2013), and most of them could potentially be polluted by acid pyroclasts. Lives could be threatened by pyroclastic material deposited over the roofs of houses, buildings and infrastructure (e.g. roads, bridges, pylons, sewers, water reservoirs) disabling them and possibly causing them to collapse. The worst possible pyroclastic-scenario would be the occurrence of Plinian columns coupled with deadly pyroclastic density currents (PDCs) traveling through valleys, burning settlements outside of the National Park boundaries, in a manner identical to the deadly eruptions of AD 79 Mt. Vesuvius (in today's Italy), and 1902 Mt. Pelée, in the island of Martinique.

Even if an eruption did not directly endanger people, the environmental and industrial consequences could be devastating. Large extensions of forest, rivers, lakes, grassland and crops can be easily lost, once covered under centimetres to decimetres of ash and

pumice as observed after the 1980 eruption of Mt. St. Helens, US, and the 2008 eruption of Chaiten, Chile. Livestock of any type may die as a consequence of water poisoning, loss of crops and grassland, lack of food and/or food intoxications, and respiratory failures. After ash cools down, it becomes very sticky and as resistant as concrete, breaking down any sort of machinery, and hence forcing any industrial activity to stop. The national energy and dairy production lying on Taranaki region's facilities would be on risk of collapse. Additionally, it is noteworthy that NZ holds an important income from tourism. In 2012, international tourism expended \$NZ9.6 billion and contributed to 15.4% of the total exports of goods and services. Domestic tourism expended \$NZ13.8 billion, and both branches together represented 3.3% of the national GDP. The industries supporting tourism generated 5.2% of the GDP and employed 119,800 full-time people (Statistics NZ 2013). National tourism would be threatened from an eruption of Mt. Taranaki in a similar way as the Icelandic Eyjafjallajökull volcano disturbed Europe in April-May 2010 (Langmann et al. 2012). Tephra dispersed from Iceland damaged the turbines of aircrafts flying above European territory as far as 2100 km from the volcano in, for example, the city of Paris; paralyzing the domestic and international European air traffic and tourism industry. Many other productive and manufacturing Icelandic industries were distorted. Fortunately, fast response strategies based on volcanological assistance were deployed, preventing aerial accidents.

The loss of primary, secondary, and tertiary activities would simply make most of the Taranaki region inhabitable. Moreover, there would be likely significant beyond-regional impacts, considering that fall deposits of at least 43 different events produced at Mt. Taranaki were identified in sediments from paleolakes in the city of Auckland (Shane 2005), about 270 km to the north of the volcano. This fact suggests that the largest

explosive eruption at Mt. Taranaki could be of Plinian-scale, and thus would be capable to inject at least 0.1-1.0 km³ in volume of material into the atmosphere, which would be distributed across distances of 100's of kilometres. In this case, New Zealand would face national hazard scenarios and a socio-economic crisis (e.g., by the impacts of ash on the national air traffic and crop lands).

Thereafter, the acknowledgement of the properties, scale and dynamics behind the largest explosive volcanism is fundamental to define the extreme bounds of a potential eruption, and the upper limits of hazard possible from major andesitic volcanoes. However, previous work carried out at Mt. Taranaki has focused on mapping general tephrostratigraphic units (e.g., Neall 1972; Alloway et al. 1995), lava flows and domes (e.g., Stewart et al. 1996; Platz et al. 2012), debris avalanche deposits produced by catastrophic edifice collapses (e.g., Procter et al. 2009; Zernack et al. 2009, 2011), or deposits from singular explosive events (e.g., Platz et al. 2007). While these data have been fundamental to understand the broad geological and magmatic history of this volcano (e.g., Neall 2003; Neall and Alloway 2004; Price et al. 2005; Zernack et al. 2012a), and to delineate probabilistic models to forecast eruptive or edifice-collapse recurrence (e.g., Turner et al. 2008a, b; 2009; 2011a, b; Zernack et al. 2012b), the specific boundaries and characteristics of separate eruptive episodes, comprising multiple eruptive phases of different style, length, volume, dynamics, intensity, magnitude, and controlled by distinct triggering mechanisms and conduit processes, have remained obscured. Consequently, numerical modelling of hazards and hazard assessment (e.g., Procter et al. 2010) have been applied in detail only to particular phenomena (e.g., lahars, debris avalanches, and block-and-ash flows), occurring on restricted locations at Mt. Taranaki (e.g., Procter et al. 2009; Platz et al. 2012).

In this work, the late-Holocene eruptive history of Mt. Taranaki was refined and expanded, based on new and detailed mapping and lithostratigraphic analysis of proximal pyroclastic deposits, and on new geochronological constraints (see Chapter 3). The complex pyroclastic succession necessitated development of a hierarchical basis for description of deposits and of the parental eruptions and processes that generated them. These data were employed to build a strong geological framework by filling out gaps between distal lake and swamp sediment records and medial tephra existing within soils on the ring-plain. Furthermore, the best preserved, thickest and coarsest deposits, corresponding to five <5 ka eruptive episodes, were used to explore the transitions in style and mechanisms of explosive eruptions in mafic-intermediate volcanic systems, quantify the uppermost eruptive limits (in terms of intensity and magnitude) at this volcano, and to understand differences between hazards at separate vents (i.e., the summit crater and the satellite vent on Fanthams Peak) on a single stratovolcano (see Chapter 4). In addition, by analysing the lithofacies associations resulting from the lateral and longitudinal variations in deposition, eruption styles and magnitudes were qualitatively approximated when field deposit-data were insufficient to empirically estimate eruptive parameters (see Chapter 5). The latter approach had its major impact on the diversity of PDC processes identified in this work, and for the first time at this volcano. By these means, this work captures a broad spectrum of eruptive styles, transitions, and spatial distribution of impacts during Plinian eruptive episodes, that have been distilled into volcanic hazard scenarios (see Chapter 5), aiming to be used during, and to improve hazard assessment and emergency management at this and other similar andesitic stratovolcanoes.

1.2 Research outline and objectives

The present research intends to understand the dynamics of the largest explosive volcanism possible in the andesitic stratovolcano Mt. Taranaki. These results will be put toward development of comprehensive volcanic hazard scenarios. For this purpose, the eruptive dynamics, intensity, magnitude, conduit processes of bubble nucleation and the triggering conditions of the most explosive eruptions in Mt. Taranaki's geological records will be examined and quantified.

The eruptive dynamics are given by the interpretation of pyroclastic deposits, and can provide solutions to questions such as: What kind of volcanic phenomena should we anticipate and what magnitude will it represent? Would it comprise a single volcanic column, and under what conditions could it include massive pyroclastic density currents (PDC)? What are the maximum column heights, eruptive volumes, fall and PDC distributions, volume-and-mass discharge rates that we can expect? What would be the size and nature of the ejected pyroclasts?

To understand how such large-scale eruptions may develop, it is necessary to comprehend the process of the explosivity, and hence formulate questions like, for example: What was the chemical composition of magma? How did magma degas before a large explosive eruption? Did it reach overpressure before, or could it openly degas? What magmatic properties constrained and triggered degassing? How did degassing processes affect fragmentation and the textures of pyroclasts? How did magma vesiculation and fragmentation occur? How vesiculation changed along with the conduit during eruption? What was the role of decompression in triggering fragmentation? Was vesiculation homogeneous or heterogeneous, fast or delayed?

Milestones towards answering these questions include:

- 1) To define the explosive eruptive history of Mt. Taranaki: comprising number and characteristics of the events and/or episodes represented by the preserved pyroclastic records.
- 2) To define the longitudinal and lateral run-out distributions and lithofacies transitions related to deposits produced by the largest and most explosive events recognised.
- 3) To quantify the eruptive parameters during large explosive eruptions: such as column height, area of dispersal, eruption volume, volume-and-mass discharge rates, magnitude and duration.
- 4) To determine the chemical composition of magmas associated with large explosive eruptions.
- 5) To quantify the variability of magma vesiculation involved in the origin of large explosive volcanism.
- 6) To determine pre-climactic, climactic and post-climactic eruptive dynamics and styles to get insights into pre-eruptive conditions triggering large eruptions.
- 7) To document the maximum potential hazard scenarios posed by large explosive volcanism at andesitic volcanoes in New Zealand like Mt. Taranaki.

1.3 Literature review

1.3.1 Explosive volcanism

Explosive eruptions produce fragmental material (pyroclasts) carried upwards inside convective columns or laterally transported through pyroclastic density currents, and later on accumulated in the land surface forming deposits of diverse character. Eruptions can

be triggered by magmatic processes where gases dissolved in magma play a key role in volatile saturation and thus in the inception, sustainability, depth and speed of vesiculation, and afterwards in the fragmentation process. Explosive eruptions can also be triggered by phreatomagmatic activity as a result of the interaction between magma and external water.

Vesiculation is the formation of a separate, exsolved gas phase, and starts with nucleation of the smallest possible stable bubble up to its maximum expansion (Sparks 1978; Gardner et al. 1996; Freundt and Rosi 1998; Gilbert and Sparks 1998; Cashman et al. 2000). The rapid acceleration of bubble growth and expansion along with enough overpressure to disrupt the confining conduit, or coupled with rapid decompression of the volcano, can trigger fragmentation which controls the explosivity of an eruption itself.

Fragmentation is the process of transformation of magma from a liquid with dispersed expanding gas bubbles and solids (crystals and inclusions) into a gas with dispersed liquid drops (trapped-quenched bubbles) and solid particles (Sugioka and Bursik 1995; Gardner et al. 1996; Cashman et al. 2000). During this process, the potential energy of bubble expansion is released and transformed into kinetic energy of the fragments, and then into thermal energy of the convective plume. The fragmentation has been studied to explain different types of explosive eruptions and transitions (Alidibirov 1994; Sugioka and Bursik 1995; Gardner et al. 1996; Zimanowski et al. 1997; Freundt and Rosi 1998; Gilbert and Sparks 1998; Spieler et al. 2004b; Platz et al. 2007) in relationship to diverse conditions and triggering mechanisms such as, rapid decompression and rapid vesiculation (Alidibirov and Dingwell 1996, 2000; Gardner 2007), degassing and permeability (Klug and Cashman 1996; Platz et al. 2007; Mueller et al. 2008), conduit flow dynamics (Mader 1998; Papale 1999; Palladino et al. 2008), magma viscosity and

composition (Koyaguchi and Mitani 2005; Koyaguchi et al. 2008; Namiki and Manga 2008), magma rheology (Zhang 1999; Wright and Weinberg 2009), etc; using field, theoretical, and experimental data (Wohletz et al. 1989; Dellino et al. 2001; Spieler et al. 2004a).

Although fragmentation only occurs after vesiculation, and the latter does not necessarily yield explosive eruptions (e.g. it may be followed by extensive degassing and effusive activity), the complete process leading to fragmentation needs to be understood. This is primarily because pre-eruptive volatile-crystal-related magmatic processes take place during storage, prior to volatile saturation and exsolution, and limit maximum bubble growth (Sugioka and Bursik 1995; Cashman et al. 2000; Spieler et al. 2004b).

Studies on magma storage, magma chambers and processes involve different petrological and chemical approaches, and have discussed topics such as open magma systems (Couch et al. 2001; Cashman and McConnell 2005), convective mechanisms and chemical zoning (Hervig and Dunbar 1992; Couch et al. 2001), mineral crystallization and disequilibrium (Couch et al. 2001; Takeuchi and Nakamura 2001; Nakagawa et al. 2002; Sosa-Ceballos et al. 2012), mixing and mingling processes (McBirney 1977; Venezky and Rutherford 1997; Nakagawa et al. 2002; Sosa-Ceballos et al. 2012), assimilation of wall-rock and mush chambers (Nakagawa et al. 2002; Huber et al. 2011), and multiple level magma storage (Cashman and McConnell 2005). Pre-eruptive conditions at the interior of the magma storage, including pressure, temperature, and volatile saturation have been also evaluated (Gardner et al. 1995; Venezky and Rutherford 1997; Takeuchi and Nakamura 2001; Arce et al. 2006; Sosa-Ceballos et al. 2012).

After magma ascends from storage, volatiles acquire a crucial role in fragmenting magma and in triggering explosive eruptions by developing a saturation surface from which vesiculation might initiate. Therefore, volatiles constitute one of the major focuses in physical volcanology. Determining the source of volatiles (Schmidt and Poli 1998) and the pre-eruptive volatile contents driving explosive eruptions, especially water content, is carried out using diverse techniques such as the analysis of glass and melt inclusions, FTIR, and experimental petrology (Stolper 1982; Sisson and Layne 1993; Ihinger et al. 1994; Johnson et al. 1994; Symonds et al. 1994; Devine et al. 1995; Gardner et al. 1995; Lowenstern 1995; Wallace et al. 1995; Wallace and Anderson 1998, 2000; Wallace 2001; Newman and Lowenstern 2002; Burgisser and Gardner 2005; Nichols and Wysoczansk 2007). Volatile data can be correlated, for example, with pre-eruptive pressure and temperature conditions (Rutherford and Devine 1996), effects on density and viscosity (Lange 1994), effects on heat transfer and crystallization (Tait et al. 1989; Huber et al. 2010), oversaturation limits, generation of gas overpressure, and triggering mechanisms of explosive eruptions (Blake 1984; Bursik 1993; Massol and Jaupart 1999), and with instability of explosive events (Jaupart and Allegre 1991). The solubility of volatiles in magma is a key factor in understanding saturation, exsolution, and degassing (McMillan 1994; Holloway and Blank 1994; King and Holloway 2002).

The viscosity of magmas at a given temperature and pressure is also fundamental, as it may constrain the viability of volatiles to exsolve, to participate in vesiculation, and to degas. Viscosity was studied especially through experimental methods to understand how magma viscosity varies with different temperatures, pressures and compositions (Anilkumar et al. 1993; Hess and Dingwell 1996; Stein and Spera 2002; Giordano and Dingwell 2003; Costa and Macedonio 2005), and the effects of such changes in volatile

saturation and exsolution, vesiculation, ascent rates and decompression processes. Viscosity has important implications for the rheology of magma and often relates to the rheological properties and microstructure of different silicate melts, although studies have mainly focused on dacite and rhyolite compositions (Dingwell and Webb 1989; Stein and Spera 1992; Mueller et al. 2009; Whittington et al. 2009).

Depending on the character of degassing during explosive eruptions (Sparks and Brazier 1982; Cashman and Mangan 1994; Mader et al. 1994, 1996; Dixon 1997; Mangan and Sisson 2000; Blower et al. 2001), it may affect vesiculation (Cashman and Mangan 1994), microlite crystallization before the eruption and crystallization during ascent (Hammer et al. 1999; Cashman and Blundy 2000), and consequently the explosivity of an eruption. Several experiments have been performed to understand how degassing relates to nucleation, decompression, permeability and porosity (Jaupart 1998; Gardner et al. 1995; 1999; Mangan and Sisson 2000; Burgisser and Gardner 2005; Marziano et al. 2007; Takeuchi et al. 2009; Kennedy et al. 2010).

Another branch of studies examines the effect of solid particles on magma properties, including examining fractional crystallization, crystal zoning and disequilibrium, crystal size distributions and kinetics and dynamics (Cashman and Ferry 1988; Higgins 2000), as well as microlite crystallization during ascent, fast-ascent eruptions and decompression, and groundmass crystallization (Geschwind and Rutherford 1995; Nakada and Motomura 1999; Blundy and Cashman 2001). Different proportions of solid, vesicle and dissolved gas phases modify the inception of fragmentation and the nature of the explosive volcanism (Cashman and Blundy 2000; Blundy and Cashman 2001).

Vesiculation driving fragmentation in explosive volcanism, including homogeneous and heterogeneous bubble nucleation, gas diffusion and bubble expansion, has been extensively discussed. Publications comprise a wide range of theoretical and field observations, and analog experiments concerning conditions involved in the process including: pressure, temperature, volatile supply, degassing, decompression, chemical magma composition, viscosity and crystallinity (Sparks 1978; Houghton and Wilson 1989; Walker 1989; Proussevitch et al. 1993; Hurwitz and Navon 1994; Klug and Cashman 1994; Sparks et al. 1994; Lyakhovsky et al. 1996; Mangan and Cashman 1996; Navon and Lyakhovsky 1998; Mourtada-Bonnefoi and Laporte 1999; Zhang 1999; Cashman et al. 2000; Gardner and Denis 2004; Gardner 2007; Polacci et al. 2009a, 2009b; Giachetti et al. 2010).

The bubble size distribution and the bubble number density constitute important parameters in quantifying vesiculation, degassing, and fragmentation; and in correlating such mechanisms with pyroclastic textures (Toramaru 1989, 1990; Cashman and Mangan 1994; Kaminski and Jaupart 1997; Larsen and Gardner 2000; Blower et al. 2002; Klug et al. 2002; Rust and Manga 2002; Okumura et al. 2006; Toramaru 2006; Proussevitch et al. 2007; Cluzel et al. 2008; Polacci et al. 2008; Hamada et al. 2010; Shea et al. 2010; Proussevitch et al. 2011; Rust and Cashman 2011). The permeability and porosity are also important factors to determine how feasible is magma to nucleate bubbles and/or degas (Saar and Manga 1999; Rust and Cashman 2004; Costa 2006; Wright et al. 2006).

Large improvements in quantifying bubbles have been reached since Houghton and Wilson (1989) and Walker (1989) worked on counting vesicles, analyzing textures and on integrating a vesicularity index of pyroclasts. Modern 3D particle size distributions and X-ray computed microtomography have increased the quality of data (Sahagian and

Proussevitch 1998; Ketchman and Carlson 2001; Song et al. 2001; Mess et al. 2003; Ketcham 2005; Gualda and Rivers 2006; Polacci et al. 2006; Gualda et al. 2010; Zandomenighi et al. 2010; Baker et al. 2011; Giachetti et al. 2011).

Magma ascent rates have been calculated through diverse petrological observations and experiments, by measuring diffusion in crystals and crystal textures, decompression, by using different compositions, volatile contents and viscosities, and varying ascent conditions in general (Rutherford and Hill 1993; Papale and Dobran 1993; Eichelberger 1995; Papale et al. 1998; Polacci et al. 2001; Martel and Schmidt 2003). Ascent and decompression are usually studied in parallel, especially on the basis of decompression-induced crystallization (Nelson and Montana 1992; Mangan and Sisson 2000; Hammer and Rutherford 2002; Blundy and Cashman 2005). Decompression is one of the most important mechanisms to trigger rapid ascent and fragmentation.

The structure of conduits, vents and plumbing systems, as well as the erosion processes of conduits, also have an important influence in changes in eruptive style and magma discharge rates (Scandone and Malone 1985; Varekamp 1993; Macedonio et al. 1994; Houghton et al. 2004; Scandone et al. 2007), shearing, overpressure and extrusion rates (Hale and Mühlhaus 2007), degassing, permeability, pressure and decompression (Mangan et al. 2004; Degruyter et al. 2010), and crystallization processes (Jerram and Martin 2008) during fragmentation, and all along the explosive eruption.

1.3.2 Eruption dynamics

Numerous contributions to understand explosive volcanism have been discussed since Walker (1971, 1973) proposed the first classification of volcanic eruptions based on grain-size characteristics and distribution of pyroclastic deposits. Contemporaneously, Walker

and Croasdale (1971) and Lirer et al. (1973) described some of the first Plinian-type fall deposits, whilst Wilson (1972) and McBirney (1973) with their works on pyroclastic trajectories and factors controlling the intensity of explosive eruptions, respectively, made some of the first attempts at quantification. Later, Wilson (1976) and Wilson et al. (1978; 1980) studied the Plinian eruption columns, their heights, and the influence of magma properties and conduit geometry into their behaviour and Sparks and Wilson (1976) proposed a model for column collapse and ignimbrite formation.

After the eruption of Mt. St. Helens in 1980, an outbreak of new publications characterized by broadly detailed and robust quantitative data followed. Complete treatises on pyroclastic rocks, their deposits and their interpretation, and eruption dynamics as well, became available (Fisher and Schmincke 1984; Whitham and Sparks 1986; Cas and Wright 1987; White and Houghton 2006; Parfitt and Wilson 2008; Manville et al. 2009). Further, new classifications, field approaches, descriptions of deposits and interpretations of rock textures, and an advanced understanding of the processes of the explosive eruption dynamics followed with successive eruption studies. Quantitative studies have focussed on: plume dynamics, vertical and lateral eruptions, column vs. pyroclastic density current development, ballistic trajectories and impacts, ash dispersal, eruption velocities and temperatures, among others. Diverse works to calculate the dimensions and the physical dynamics of the eruptive column (Sparks 1986; Thomas and Sparks 1992; Koyaguchi and Tokuno 1993; Sparks et al. 1997), fall and dispersal of deposits from the column (Carey and Sparks 1986; Bursik et al. 1992; Orsi et al. 1992; Bursik 1998; Watt et al. 2009; Biass and Bonadonna 2010), the thickness, grain-size and volume of the pyroclastic fall deposits (Pyle 1989; Fierstein and Nathenson 1992; Bonadonna et al. 1998; Bonadonna and Houghton 2005; Sulpizio 2005; Biass and

Bonadonna 2010; Kratzmann et al. 2010), the intensity and size of volcanic eruptions (Carey and Sigurdsson 1989; Carey et al. 1995; Pyle 2000), and the sizes, densities and textures of the resulting pyroclasts (Wilson 1999; Polacci et al. 2003; Shea et al. 2010), constitute the basis of eruption dynamics.

The modern classification of volcanic eruptions also lies on these collective models, tailored with field and stratigraphic studies of the individual study site. Hydromagmatic volcanism (phreatomagmatic and phreatic eruptions; Sheridan and Wohletz 1983; Wohletz 1983, 1986; Wohletz and Sheridan 1983; White 1991; Zimanowski et al. 1991) is distinguished from magmatic explosive activity (Plinian, sub-Plinian and vulcanian eruptions; Hoblitt et al. 1996; Stix et al. 1997; Cioni et al. 2000; Morrissey and Mastin 2000; Sulpizio et al. 2005; Pérez et al. 2009) on the basis of the agents triggering fragmentation, although in many situations both might alternate. The particular lithostratigraphic and sedimentological characteristics of the deposits, along with the textural analysis of pyroclasts (Waite et al. 1981; Brazier et al. 1983; Williams 1983; Sigurdsson et al. 1984; Fagents and Wilson 1993; Coltelli et al. 1998, Gardner et al. 1998; Arce et al. 2003, 2005; Sable et al. 2006; Pardo et al. 2012a), is a further mainstream approach to distinguish a range of differing eruption types.

Many works exemplify the definition of eruption dynamics in diverse volcanoes. Some use geophysical approaches (Woods 1995; Polacci 2005), experimental techniques (Scheu et al. 2006), yet most remain focusing on geological methods (Cioni et al. 2000, 2003; Wright et al. 2007; Arana-Salinas et al. 2010; Saucedo et al. 2010; Pardo et al. 2012b). One of the important features addressed for eruption scenario development are transitions between differing levels of explosivity during eruptions (Rosi et al. 2001;

Gurioli et al. 2005; Adams et al. 2006; Susuki and Koyaguchi 2012), and from explosive to effusive activity and vice versa (Woods and Koyaguchi 1994; Platz et al. 2007, 2012).

1.3.3 Previous research at Mt. Taranaki

Diverse topics have been aimed at studying Mt. Taranaki over the last 50 years. Publications on tectonics, structural geology and geophysics, regional seismicity, regional geology, tephrochronology, tephrostratigraphy, and geochemistry are the most abundant; while volcanic stratigraphy, physical volcanology, statistical forecasting and hazard assessment remained untreated until last decade.

Tephrochronology and tephrostratigraphy have been substantially discussed since Grant-Taylor (1964) and Druce (1966) resumed the observations made in previous works by Skeet (1901), Oliver (1931), Grange and Taylor (1933), and Taylor (1954). According to Oliver (1931), A.W. Burrell in 1883 made the first ever documented observations of pumice fragments hanging in the forks of living matai and rimu trees. Burrell estimated an age of ca. AD 1430 for such deposits based on tree ring counting. It was later supported when in 1929 a Maori oven “umu” was found close to the Stratford Mountain House beneath the Burrell Lapilli during a soil survey (Oliver 1931).

Druce (1966) provided field descriptions and correlations of ash and lapilli beds (P1-P5) of sections around and across Mt. Taranaki; and defined the age (based on tree ring dating) and distribution of Newall (AD 1604), Burrell (AD 1655) and Taurangi (AD 1755) Formations. He recognized the lateral-directed nature of the Newall eruptives. Topping (1971) defined three lobes of distribution for the Burrell Lapilli (SE, ESE and NE) based on sedimentology, and suggested that the two Puniho Lapilli units were deposited by “nuees ardentes” towards the west. However, Neall (1972, 1976) was the

first to provide extensive tephrostratigraphical and tephrochronological records centred on the western ring-plain of Mt. Taranaki. He defined and redefined the sequence and distribution of 13 tephra formations from AD 1755 to ca. >16,100 BP: Tahurangi, Burrell, Newall, Inglewood, Korito, Oakura-Okato “Egmont Shower”, Saunders Ash, Carrington, Koru, Pukeiti, Weld, and New Plymouth Ashes and Buried Soils.

Whitehead (1976) subsequently studied and named the Kaupokonui (P4 of Druce 1966) and Manganui Tephra. She produced isopach maps for both and defined the SE distribution of Kaupokonui, and the three lobe distribution (SE, E, and N) of Manganui Tephra. The latter was explained as a result of three different pulses from Fanthams Peak; and Whitehead estimated an age of ca. 3200 BP based on the stratigraphic position of the deposits above (a 1990 BP unnamed tephra) and below (a 4030 BP lahar deposit). Franks (1984) separated the Inglewood Tephra in two different pumice units (P2a and P2b), and also studied the distribution and the chemical and mineralogical characteristics of Korito and a sequence of older tephra in the SE sector of Mt. Taranaki, from E5-E4 (5000-7000 BP Oakura Tephra of Neall 1972), E3, E2-E1 (Okato Tephra and Ahuahu Lapilli; Neall 1972), to Mahoe Tephra. Later on, Petrie (1988) carried out a basic study of Manganui Tephra in three proximal sections, where he identified 10 to 11 Manganui beds divided by two soils in at least three different eruptive periods.

McGlone et al. (1988) studied the effects on vegetation of climatic changes and recent volcanic events at Mt. Taranaki by performing pollen analysis in two cores from the Ahukawakawa Swamp and the Potaema Bog. Along the cores, they identified an Inglewood tephra-like pumice lapilli, Manganui, Maketawa-like, and Kaupokonui Tephra, Newall and Burrell Ash and Lapilli, and Tahurangi Ash. Carbon dating on peat below and within the Inglewood-like pumice was 3510-3630 BP, 3110 BP inside the

Maketawa-like tephra, and 1350 BP on peat below Kaupokonui. Following McGlone's approach, Lees and Neall (1993) focused on the impacts on vegetation of the last 1500 yrs of volcanic activity. They found a time-break between Burrell Ash and Burrell Lapilli of >70 yrs. Furthermore, in contrast to Druce (1966), who estimated 100 yrs between the eruption of the Burrell and the Tahurangi events; Lees and Neall suggested that the Tahurangi Ash is closer to AD 1860, according to soil forming rates.

Alloway et al. (1995) recorded the ca. 3-28 ka north-eastern to eastern Mt. Taranaki ring-plain tephrostratigraphy. They defined and redefined 16 andesite tephra formations: Manganui, Inglewood, Korito (P1 of Druce 1966), Mangatoki (E5 of Franks 1984), Tariki (a-f, E4 of Franks 1984), Waipuku (basal Oakura Tephra of Neall 1972; and E3 of Franks), Kaponga (E2 to upper-E1 of Franks 1984), Konini (basal-E1 of Franks 1984), Mahoe, Kaihourai (Ahuahu Lapilli of Neall 1972), Paetahi, Poto (Saunders Ash and Carrington Tephra of Neall 1972), Tuikonga, Koru, Pukeiti, and Waitepuku. Based on different interspersed andic soil units, they divided the tephra succession in three periods: a ca. 2.9-10.5 ka period from Manganui to Mahoe Tephra, a ca. 12-24 ka interval from Kaihourai to Poto Tephra, and the oldest studied period of 24-28 ka from Tuikonga to Waitepuku Tephra. Each formation comprised a variable number of individual beds, for a total of 76 eruptive events with volumes of $>10^7$ m³, mainly distributed to NNE and SSE from present day summit. Alloway et al. (1995) suggested a periodicity of one eruption of this magnitude every 300-330 years.

Aiming to establish an andesite tephrochronological framework in New Zealand, Shane (2005) drilled cores and studied sediments from paleolakes in the Auckland city (e.g. the Pukaki lagoon). They found 14 tephras of 8-28 ka, and 43 tephras of 10-70 ka

respectively; able to be related to Mt. Taranaki (ca. 270 km to the south) based on glass shard compositions.

Turner et al. (2008a) continued coring in areas adjacent to Mt. Taranaki, looking to statistically forecast the volcanic recurrence. In Lake Umutekai, 25 km NNE of the summit, they identified 123 events for the last 9.5 ka. By integrating ^{14}C dates from cores and deposits in proximal sections into a statistical model, they calculated a 37-48% chance of an eruption from Mt. Taranaki in the next 50 years. However, Turner et al. (2009) added new data from cores of Lake Rotokare (30 km SE of the summit) which they correlated with Lake Umutekai using titanomagnetites as chemical fingerprints. They identified at least 138 separate ash fall-producing eruptions between 96 and 10150 yr BP; and forecasted a probability of 0.52 for an eruption every 50 yrs, and a present annual eruption probability of 1.6%. As part of the same work, Turner et al. (2008b) used titanomagnetite (tmg) textures to differentiate and quantify slow (exsolved tmg of dome-building and block-and-ash flow deposits) and fast ascent eruptions (non-exsolved tmg of open-system, sub-Plinian events) among 103 individual tephra from Lake Umutekai spanning 10-1.5 ka. They found a periodicity of ca. 1500 yr for fast events, which they explained to reflect the periodicity of magma replenishment, the recurrence of tectonic events, or the time for magma to gain enough pressure to rise and erupt.

Following a statistical approach like Turner et al. (2008a, 2008b, 2009), Zernack et al. (2012b) estimated a maximum of <16.2 ka before the next edifice collapse in Mt. Taranaki. They calculated the current annual collapse probability of ca. 0.00018 (0.018 %), and the most likely collapse to be <2km³ (e.g. similar to that of St. Helens, 1980), with debris avalanche deposits in Mt. Taranaki's geological records ranging from volumes of 1 to a maximum of 7.9 km³. They concluded that edifice growth and collapse in Mt.

Taranaki was governed by magma supply rates, since the volcano rests over an invariant basement and edifice structure, and appears to exhibit to a stable-slow magma evolution over 130 ka.

Before Zernack et al. (2012b), extensive stratigraphic and sedimentological studies on Mt. Taranaki's debris flow and debris avalanche ring-plain deposits preceded (Neall 1979; Palmer et al. 1991; Procter et al. 2009; Zernack et al. 2009; and Zernack et al. 2011). In Zernack et al. (2011) medial-distal >25 ka volcanoclastic deposits of SW Taranaki were studied. They identified at least 14 widespread debris avalanches deposited during the last <200 ka, suggesting one major collapse every 14 ka, with an increase in frequency for the last 40 ka. Rhyolitic tephra from Taupo (ca. 4000 BP Stent Ash, ca. 22590 BP Kawakawa Tephra/Aokautere Ash, ca. 45-55000 BP Rotoehu Tephra, and ca. 350-400 ka Rangitawa Tephra; some previously identified by Neall 1972, and Alloway et al. 1995) were employed as stratigraphic markers. After observing Mangati debris avalanche deposits underlying Motunui Formation, and lying on top of cemented iron-stained sands and over the Ngarino Marine Bench, Zernack et al. (2011) proposed that Mt. Taranaki might be ca. 200 ka, in contrast to the ca. >130 ka suggested by Alloway et al. (2005).

Zernack et al. (2011) also provided a chronostratigraphic framework with a summary of the entire volcanic-volcanoclastic succession of Mt. Taranaki. Turner et al. (2011b) integrated records from proximal and distal explosive and effusive activity for the last 10 ka. The latter authors identified two periods of different activity: a 5-6 ka period of east-directed effusive, block-and-ash flow (BAF) generating eruptions; and an 8-9 ka period of explosive, sub-Plinian events; separated by a 7 ka episode of a south-directed Opuia edifice collapse (Neall 1979). They concluded that Mt. Taranaki has switched from extended periods of explosive volcanism to periods of dome-forming events, suggesting

that much of the current edifice was constructed between 5-6 ka. This is supported by the fact that Warwicks Castle lavas are of an age similar to east and west BAF deposits (Neall 1979; Stewart et al. 1996), while younger lavas of the upper summit match the ages of ca. 1 ka BAF deposits.

A few works on physical volcanology are centred on the last 2000 yr BP. Turner (2008) studied a period of vulcanian events in between Kaupokonui and Maketawa tephra, where he identified a sequence of pyroclastic density currents (PDC) consisting of two east-directed block-and-ash flow (BAF) deposits, an unnamed pumice fall, a wet surge, a column-collapse PDC deposit that he named Curtis Ridge Lithic Lapilli, and a top lateral-erupted basaltic unit. Most of the sequence was interpreted to have erupted directly from the summit of Mt. Taranaki, while the top basaltic unit was related to the formation of a cinder cone over the NE flank of the Rangitoto flat.

Platz et al. (2007, 2012) focused on the AD 1040 Maero Formation (Cronin et al. 2003). They redefined the AD 1655 Burrell eruption, and identified the AD 1785-1820 Sisters eruption. The Burrell sequence included a dome extrusion, followed by a NW-directed BAF, a sub-Plinian eruption depositing pumice from SE to NE (Burrell Lapilli; Neall 1972), and three pumice PDC deposits over the summit flanks of Mt. Taranaki triggered by column instability (a grey column-collapse PDC, a brown unstable PDC, and a last grey PDC). The authors calculated volumes of fall, BAF and PDC deposits; densities, isopachs, isopleths, and determined the height of the sub-Plinian column (14 km). They explained the transition from an effusive to an explosive activity through a model of vertical conduit stratification after exploring clast textures, porosity, vesicularity, glass and whole-rock geochemistry, and crystal content (viscosity). The Sisters eruption followed the AD 1755 Tahurangi event, and the sequence included the extrusion of the

Sisters crater dome (present-day summit), the Sisters lapilli, and an ensuing rock-avalanche from partial collapse of the Sisters dome. After performing mineral chemistry, whole-rock geochemistry, calculating temperatures of emplacement with a magnetometer and porosity with a He-pycnometer, and measuring hornblende reaction rims; they concluded that the Sisters dome collapsed after cooling once it reached metastability, perhaps decades to centuries subsequent to emplacement.

Cronin et al. (2003), Turner (2008), Platz et al. (2007, 2012), Turner et al. (2008b), and Zernack et al. (2009, 2011), published the first works on modern volcanic stratigraphy and physical volcanology of Mt. Taranaki, intending to understand not only the stratigraphic and the chronological sequence of events, but the nature and quantification of the volcanic phenomena.

In geochemistry and petrology, Gow (1968), in its pioneering work, classified the andesites of Mt. Taranaki in five types based on different proportions of augite, hornblende and olivine crystals; and suggested a rough petrogenetical model. Further on, Price et al. (1992) defined the main chemical characteristics of Mt. Taranaki rocks (subduction-related, hornblende-bearing, high-k rocks) based on trace element geochemistry and isotopic compositions of young lavas, and proposed a more sophisticated model for magma genesis. Stewart et al. (1996), Price et al. (1999, 2005), and Zernack et al. (2012a) looked deep into the genesis and evolution of the high-k arc magmas of Mt. Taranaki. May (2003) and Turner et al. (2011a) studied the variability of eruptions relative to changes on magma composition; and Gruender et al. (2010) focused on xenoliths found in Mt. Taranaki's rocks. Further details of these works are addressed in the section of Petrology and Geochemistry.

General contributions in tectonics, seismicity, structural geology and geophysics will be discussed below. Further specific geophysical work on the Taranaki edifice is so far limited and includes an analysis of the nature of the edifice (lava vs. pyroclastic content; Locke and Cassidy 1997), as well as views into the crustal structure beneath it (Sherburn and White 2005, 2006; Sherburn et al. 2006).

1.4 Background geology

1.4.1 Regional framework

New Zealand lies on the plate boundary between the Pacific and the Australian Plates, to the south of the circum-Pacific belt (The Ring of Fire). In the North Island, the oceanic Pacific Plate is subducted beneath the continental crust of the Australian Plate along the Hikurangi Trough (Henrys et al. 2003, Fig. 1.1). In the South Island, the Chatham Rise and the Campbell Plateau comprise a continental block within the Pacific Plate that collides against the Challenger Plateau in the Australian Plate, accommodating plate motion in a strike-slip fault system, mainly along the parallel shear-margins of the Alpine Fault (de Mets et al. 1994). South of the transform boundary, the Australian Plate becomes subducted beneath the Pacific Plate along the Puysegur Trench.

The Hikurangi Trough is located to the east of the NE-SW Axial Ranges (Raukumara-Tararua Ranges), on the eastern side of the North Island (Fig. 1.1); and constitutes the southernmost part of the Tonga-Kermadec Trench. Plate convergence rates along the trench decrease from north to south (98 mm/yr in the Tonga Trench to 42-50 mm/yr in the Hikurangi Trough; de Mets et al. 1994; Wallace et al. 2004) in response to subduction resistance that the Hikurangi Plateau upholds, east of the lower North Island. From this

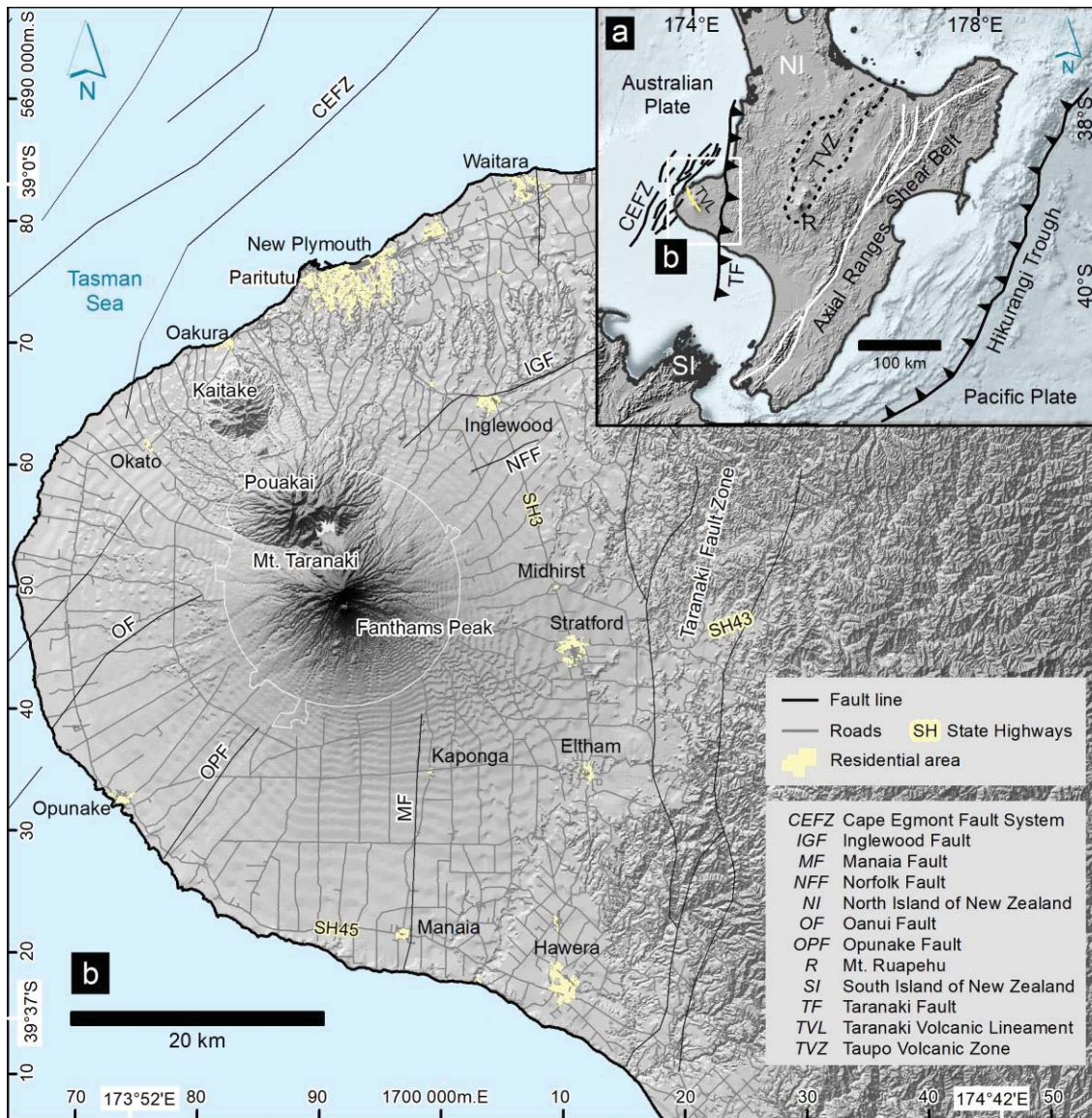


Fig. 1.1 **a** Tectonic setting of the North Island of New Zealand (modified from King and Thrasher 1996; Henrys et al. 2003; Price et al. 2005; Platz et al. 2007). **b** Zoomed area of the Taranaki Volcanic Lineament (Neall 1979), which comprises four Pleistocene-Holocene, southwards-younging andesitic volcanoes or their eroded volcanic edifice-remnants: Paritutu, Kaitake, Pouakai and Mt. Taranaki (along with the parasitic cone of Fanthams Peak). Coordinate system: NZGD 2000 New Zealand Transverse Mercator.

resistance, fore-arc clockwise rotation of microplates and back-arc extension of the central North Island are produced, and influence the parallel to sub-parallel angle of the Hikurangi Trough to the Axial Ranges (Wallace et al. 2004, Fig. 1.1).

The Taupo Volcanic Zone (TVZ, Fig. 1.1) rises where rapid (8-10 mm/yr) pull-apart tensional stress weakens the crust (12-15 km thick), following the rifting of the active Tonga-Kermadec intra-oceanic arc (de Mets et al. 1994; Villamor and Berryman 2001; Henrys et al. 2003). It is one of the most productive Quaternary magmatic systems on Earth owing to its high heat flows (ca.700 mW/m²), and the principal centre of volcanic activity in New Zealand (Stern 1987; Wilson et al. 1995). The TVZ has andesites in its NE and SW extremes, including White Island and the Tongariro Volcanic Centre (TgVC) respectively. The central portion however is dominated by rhyolites such as the Taupo caldera (Wilson et al. 1995). The TgVC is located at the southern low-spreading edge of the TVZ and consists of the N-S aligned stratovolcanoes Mt. Tongariro (and the satellite cone of Mt. Ngauruhoe) and Mt. Ruapehu (Hobden et al. 2002, Fig. 1.1).

About 130 km to the west of Mt. Ruapehu, in the Taranaki Peninsula (Fig. 1.1), the Taranaki Volcanic Lineament (TVL) is located. This Quaternary NNW-SSE lineament comprises four southwards younging hornblende-rich andesite volcanoes (Fig. 1.1): the 1.75 Ma Sugar Loaf Islands-Paritutu, the 0.57 Ma Kaitake, the 0.25 Ma Pouakai, and the <0.13 Ma Mt. Taranaki (and its parasitic cone Fanthams Peak; Neall 1979; Alloway et al. 2005). The Sugar Loaf Islands-Paritutu are remnants of plugs and dikes of an earlier volcano (Grant-Taylor 1964). The younger three stratovolcanoes denote different stages of erosion, but share common histories as all have experienced multiple edifice collapses inside explosive-effusive periods of activity, recorded in ring plain volcanoclastic deposits along the Peninsula (Neall 1979, 1986). For instance, the coastal city of New Plymouth is mostly built over debris avalanche deposits from Pouakai (Maitahi Formation; Neall 1979). Contemporaneous hornblende and pyroxene andesite domes (German Hill, The

Dome, Skinner Hill, and North and South Beehive), and an andesite cone (Pukeiti), also form part of the TVL.

The TVZ and the TVL are both related to subduction of the Pacific Plate beneath the continental crust of the North Island; however, they portray differences in petrology, geochemistry and tectonics. Contrasting mineralogy and potassium contents in their rocks (2-pyroxenes, low-K in the TVZ; and hornblende, high-K in the TVL; Price et al. 2005), associated to differences in crustal compositions, define the principal chemical distinctions. Changes in the thermal and structural regimes and in the position of the subducted slab may influence the mantle input (Price et al. 2005). The Pacific Plate sinks into the mantle to a depth of ca. 100 km below the ca. 40 km thick crust of Mt. Ruapehu, at about 280 km west of the Hikurangi Trough (Henrys et al. 2003). The slab descends to a depth of 250 km beneath the ca. 25 km crust of the Taranaki Peninsula, 400 km west of the trough (Henrys et al. 2003; Boddington et al. 2004, Fig. 1.1).

To explain how magma originates in the TVL, Price et al. (1992, 1999, 2005) hypothesise that melting of the mantle wedge is triggered by slab-derived fluids. However, the slab is only traceable up to ca. 35 km SE of Mt. Taranaki, indicating that the TVL does not directly overlie the subducted Plate (Stern et al. 2006). Boddington et al. (2004), by contrast, interprets that isolated ca. 600 km depth earthquakes beneath Mt. Taranaki are produced by a horizontal lying, detached sliver of the plate. In counter model, Stern et al. (2006) suggest that an area to the west of the TVZ, and to the north of a line between Mt. Ruapehu and Mt. Taranaki, has lost the lower portion of the lithospheric mantle by convective instability, so that the asthenosphere is able to rise and melt the hydrous mantle.

1.4.2 The Taranaki Basin

The Taranaki Volcanic Lineament lies within the Eastern Mobile Belt of the Taranaki Basin. The basin is composed of sediments on average 6 km and up to 9 km-thick, rich in oil and gas reserves (King and Thrasher 1996). It is delimited to the east by the Miocene N-S reverse Taranaki Fault (Fig. 1.1), which offsets basement rocks by ca. 6 km and has vertically moved 12-15 km for the last 80 Ma (King and Thrasher 1996; Nicol et al. 2004). A Stable Platform defines the western limit of the basin and is separated from the Eastern Mobile Belt by the Cape Egmont Fault Zone (CEFZ, Fig. 1.1) – the mid-Cretaceous and still active western limit of deformation of the Pacific-Australian convergent boundary in the North Island (Nodder 1993; King and Thrasher 1996).

The CEFZ is characterized by subduction-related NW-SE extension, and consequent NE trending faults. The Cape Egmont fault, the largest individual normal fault inside the CEFZ, is a 1-5 m high, 53 km long scarp on the seafloor, moving on average to a slip rate of ca. 0.8 mm/yr for the last 225 ka (Nodder 1993). The onshore Oaonui fault (Fig. 1.1) has experienced 5 m of vertical displacement in the last 6.5 ka. The Inglewood fault, close to the homonymous town (Fig. 1.1), comprises a 3 m scarp with individual offsets of >1 m for the last 13 ka (Hull and Delow 1993; Hull 1994). A NE-SW lineation of hypocentres beneath Mt. Taranaki appears to link the southern Oaonui fault with the northern Inglewood and Norfolk faults, suggesting the presence of a fault, or a fault zone, beneath the volcano (Cavill et al. 1997; Sherburn and White 2005).

Based on data from the 1974 Opunake earthquake, Sherburn and White (2006) propose that the last 3.3-3.5 Ma Inglewood fault movement could be related to intrusion of magma along N-S dikes, responsible for the ca. 3.0 Ma formation of Fanthams Peak and some N-

S aligned flank domes on Mt. Taranaki. According to the authors, such intrusions would produce E-W compressive stress able to replace the NE-SW dip-slip motion in western Taranaki Peninsula by oblique reverse, right lateral strike-slip motion. When eruptions occur, the stress is released and normal faulting re-activates.

Tectonics from the eastern boundary of the Taranaki Basin are related to extension of the TVZ by means of an E-W swarm of earthquakes producing strike-slip and dip-slip faulting along the Taranaki-Ruapehu Line (Stern 1987; Sherburn and White 2005).

The Taranaki Basin opened after the early to mid-Cretaceous uplift, at the end of the subduction along the Pacific margin of Gondwana (King and Thrasher 1996). The basin was developed over mid-Palaeozoic to mid-Cretaceous calc-alkaline subduction-related plutonic rocks which are part of a major basement terrane, the Median Tectonic Zone (MTZ; Mortimer et al. 1997). Late-Palaeozoic to early-Cretaceous sequences of lithic, feldspathic meta-greywackes with some volcanic and intrusive rocks from the East Provinces lie to the east of the MTZ (Mortimer et al. 1997).

The geological history of the Taranaki Basin (TB) is similar to the neighbouring King Country (KC) and Whanganui Basins. Eocene to mid-Miocene sediments were the first deposits accumulated inside the TB and the KC basins once the modern collisional margin between the Pacific and Australian Plates was established (King and Thrasher 1996). Marine sedimentation dominated during New Zealand's maximum subsidence at the early-Oligocene, when the TB and the KC basins remained jointed (Kamp et al. 2004). Clastic rock deposits and shallow water sedimentation (e.g. early to mid-Miocene Mokau Group; Kamp et al. 2004) followed the mid-Oligocene uplift (reverse motion of the Taranaki Fault and uplift of the Patea-Tongaporutu High) in association with the

beginning of the NE-SW Alpine Fault (Mills 1990). This uplift divided the TB and the KC basins (Mills 1990; Kamp et al. 2004).

Both basins merged again after the mid-Miocene subsidence of the Patea-Tongaporutu High, driving the formation of clastic and organic sediments (Kamp et al. 2004). These sediments overwhelmed subsidence, generating SE-NW progradation during the mid-Miocene to early-Pliocene (e.g. Whangamomona Group; Kamp et al. 2004). *Phialopecten* shell fossils inside the Matemateaonga Formation delimit the Miocene-Pliocene boundary (Vonk and Kamp 2004).

An early-Pliocene regional subsidence, the Tangahoe Pull-down, marks the initiation of the Whanganui Basin as a separate depocentre subdivided into west and east portions (the Rangitikei Supergroup; Kamp et al. 2004). Terraces of intercalated clastic deposits and marine to estuarine organic sediments in the basin show continuous transgressions and subsidence that exceeded sedimentation along the mid-Pliocene (Naish and Kamp 1995; 1997; Kamp et al. 2004). The late-Pliocene Hautawa shellbed member of the Upper Okiwa Group (Tikapu Group in eastern Whanganui Basin; Naish and Kamp 1995) constitutes a stratigraphic marker since it contains fossils of the first cool water bivalve *Zygochlamys delicatula* (Naish and Kamp 1997). Rhyolitic tephtras of 2.8, 2.17, 1.79 and 1.75 Ma (Naish et al. 1996; McIntyre 2002; Pillans et al. 2005) intercalated within late-Pliocene Formations of the eastern Whanganui basin (contemporary to the western Nukumaru Group; Naish and Kamp 1995) bracket the Plio-Pleistocene boundary. The 1.75 Ma Sugar Loaf-Paritutu andesites from west Taranaki (Neall 1979; Neall et al. 1986) coincide into this period and represent the first evidence of Quaternary volcanism within the Taranaki Volcanic Lineament (TVL).

East and west Whanganui sub-basins coalesced into a south directed depocentre at the Pleistocene, following uplift of the central North Island (Kamp et al. 2004). Abundant terrestrial, non-marine sediments which preserve pollen; and marginal marine rocks containing rare Moa bones were deposited (Maxwell Group; Naish and Kamp 1995). The 1.72 Ma Ototoka tephra overlies these sequences (Alloway et al. 2004; Pillans et al. 2005).

A 1.58 Ma tephra rests under several regional early to mid-Quaternary non-marine, shallow water, and marine deposits (Pillans et al. 2005). These sequences resulted from intercalated uplift and transgression periods that sculpted wave-cut coastal platforms, topped by mid to late-Quaternary alluvial and marine deposits (e.g. Pouakai Group; Fleming 1953) contemporaneous to the initiation of the volcanism at the TVL.

1.4.3 Mt. Taranaki / Egmont

Mt. Taranaki, also known as Mt. Egmont, is the second highest mountain in the North Island (after Mt. Ruapehu), the largest andesite volcano in New Zealand, and the youngest and most southerly volcano of the Taranaki Volcanic Lineament (Fig. 1.1). It is a nearly perfect cone-shaped stratovolcano rising up to 2518 meters above the sea level (masl) on its summit, and whose symmetry is only interrupted on its south flank by the parasitic cone of Fanthams Peak (1962 masl, Fig. 1.1). Mt. Taranaki comprises a volcanic edifice topped by a dome inside a crater, and a volumetrically much larger flat surface termed the volcanic ring-plain (Neall et al. 1986).

The volcanic edifice encloses a basal area of 25 km² (Neall et al. 1986) and a volume of ca. 12 km³ (Zernack et al. 2011), and is made up of lava flows extruded over the last ca. 8 ka (Stewart et al. 1996). Bluffs of lava crop out between 1000 masl and the summit, and

are especially clear above the bush line (ca. 1300 masl). Some of the youngest blocky lava flows to the north and south sides of the cone can be tracked up to the west-breached crater rim, where remnants of the northwest-collapsed, ca. AD 1800 Sisters dome (Platz et al. 2012) make up the summit of Mt. Taranaki. Radial drainage developed over the mountain owing to its geomorphological configuration into lava bluffs and gorges. Except for the north-northeast, where the Ahukawakawa swamp serves as a transitional depocentre in between Mt. Taranaki and Pouakai, most rivers flow directly from the upper parts of the volcano to the lowland, barely incising into the ring-plain.

The ring-plain is a 1000 km² area (Neall et al. 1986) and a ca. 150 km³ volume (Zernack et al. 2011) of extensive coalesced fans, composed of volcanic and volcanoclastic sequences that were deposited during the last >130 ka (Alloway et al. 2005) beyond the current coastline, extending from the inside of the Egmont National Park. Its near-circular outline symmetry is broken to the north-northeast by the remnants of the Pouakai and Kaitake volcanoes, to the north by the dissected Eltham laharic surface (strongly influenced by the Inglewood fault; Alloway et al. 1995), and to the east by hills of eroded Tertiary marine sediments. Further north of the Eltham surface, uplifted marine terraces shape cliffs that run close parallel to the present-day coastline between the city of New Plymouth and Urenui, but are interfered by coastal flatland of the volcanic ring-plain between Waitara and Bell Block towns. In the south and west coasts of the ring-plain, from Manaia to Oaonui, the interplay between marine erosion and tectonic uplift has formed coastal cliffs of up to 30 m high. A hummocky geomorphology dominates the land surface of this area. It is the product of debris avalanches deposited during the last <200 ka after repeated collapses of Mt. Taranaki's edifice (Neall 1979; Zernack et al. 2009, 2011).

1.4.3.1 Volcanic history of Mt. Taranaki

According to Alloway et al. (2005), volcanism in Mt. Taranaki began >130 ka since the earliest known debris avalanche deposits of the Motunui Formation closely underlie the ca. 127 ka NT2/Rapanui wave-cut surface. This age has remained the most accepted for the last decade. Nonetheless, in sections along north coastal cliffs, near Bell Block town, Zernack et al. (2011) observed debris avalanche deposits of the Mangati Formation underlying the Motunui Formation beneath peat and interbedded layers of andesite tephra; and lying directly on top of sands of the ca. 210 ka NT3/Ngarino marine bench. Mangati Fm. clasts appears to have more Taranaki-like chemical affinities, although the database of Pouakai eruptives is currently very small. If it is Taranaki sourced, it would suggest that the volcano might have initiated closer to ca. 200 ka.

Cycles of cone growth and edifice collapse describe the volcanic history of Mt. Taranaki (Neall et al. 1986; Palmer and Neall 1991; Neall and Alloway 2004; Alloway et al. 2005; Zernack et al. 2009, 2011). Cone-growth is defined as the accumulation of lava flows and domes that build up the volcanic edifice, as well as pyroclastic deposits of fall and flow origin that mantle the pre-existing topography and fill in channels and depressions. The ca. 8 ka lavas of the Warwicks Castle Group (Stewart et al. 1996) constitute the core of the youngest and present-day volcanic cone (Neall 1979). Pyroclastic deposits of the last 6 ka crop out in either proximal sections around the volcano, or in mid to distal lowland areas (Neall 1972; Alloway et al. 1995; Turner et al. 2011b). Deposits older than 7 ka appear only along the ring-plain (Alloway et al. 1995). Edifice collapses have been recorded in Mt. Taranaki after mapping several ring-plain debris avalanche deposits spanning the last ca. 200 ka (Neall 1979; Palmer and Neall 1991; Zernack et al. 2011). A

diversity of lahar (debris to hyperconcentrated flows) and alluvial deposits are also preserved.

The volcanic history of Mt. Taranaki can be summarized in four periods:

- 1) ca. 200 ka to ca. 14 ka: during this period, 13 edifice collapses spread debris avalanche deposits (DAD) to NE, SE and SW flanks of the current volcano, thus defining distinct episodes of edifice regrowth (Zernack et al. 2011). Intercalated with the DADs are sediments recording 12 edifice growth periods, including many explosive eruptions that deposited pyroclasts mapped within about 20 tephra formations (e.g. from Okato and Kaihoura Tephra to Waitepuku Tephra; Neall 1972; Alloway et al. 1995, 2005). These edifice growth periods also saw the deposition of debris and hyperconcentrated flow deposits (e.g. Punehu and Warea deposits; Neall 1979; Zernack et al. 2011); and marine, shallow water and fluvial deposits during the first 130 ka (Alloway et al. 2005; Zernack et al. 2011).

- 2) ca. 14 ka to 7 ka. sub-Plinian eruptions around ca. 13 -8 ka created thick fall deposits (e.g. Konini and Kaponga Tephra; Alloway et al. 1995). These events were contemporaneous with the first dated block-and-ash flow deposits (BAF) directed to east and west sides of the present cone which were accompanied by lahars flowing down the volcano (the ca. 13-7 ka Kahui BAFs and debris flow deposits; Neall 1979). The Kahui deposits possibly represented a dome-forming/dome-collapse cycle. At around 8 ka, Warwicks Castle lavas started building the core of the present-day cone; however, south-eastern lavas of this group collapsed at ca. 7.5 ka to form the Opuia debris avalanche which represents the last known edifice collapse of Mt. Taranaki (Neall 1979; Zernack et al. 2011).

3) <7 ka to ca. AD 1000. After the Opuia collapse, the volcano went into a stage of effusive activity during which much of the current cone was built; such as that displayed by Colima, Merapi, and Mt. St. Helens volcanoes. The 7-3.3 ka Peters lavas (Neall 2003) built the edifice up again by flowing through valleys carved on Warwicks Castle deposits. Fanthams Peak is believed to have formed early during this period (Stewart et al. 1996). Different sub-Plinian eruptions produced some of the thickest fall deposits in Taranaki's history distributed in eight tephra formations (e.g. ca. 5.4 ka Tariki, ca. 3.6 ka Inglewood, and ca. 2.9-3.3 ka Manganui Tephra; Whitehead 1976; Alloway et al. 1995) whose outcrops can be found in either proximal areas of the volcanic edifice or in the ring-plain. The Manganui Tephra is a very distinct mafic sequence of at least three separate eruptions distributed SE, E, and NE of the volcano. It lies on top of the Ngatoro lahar deposits and over the Inglewood Tephra, and is interbedded with the two units of the Te Popo debris flows (Whitehead 1976; Alloway et al. 1995). Turner et al. (2011b) observed that most <5ka tephtras rest upon BAF deposits to east and west sides of the present volcano (e.g. ca. 5 ka Piakau Formation; Neall et al. 2012). Similarly, two east-directed BAFs were deposited over the Maketawa Tephra at about 2 ka, and below the Curtis Ridge Lithic Lapilli (Turner 2003). These events suggest that transitions between effusive dome-forming activity and explosive sub-Plinian eruptions are a common cyclical characteristic of volcanism in Mt. Taranaki (Platz et al. 2007; Turner et al. 2011b). The Staircase and Skeet lavas extruded at around 1.6-1.3 ka (Stewart et al. 1996; Neall 2003) and partially filled in the amphitheatre left by the Opuia edifice collapse. The eruption that

deposited the ca. 1.3 ka Kaupokonui Tephra (McGlone et al. 1988) might be related to this effusive activity. Lava domes also extruded on the lower flanks of the volcano during this period (e.g. The Dome, Skinner Hill, Beehives domes; Neall et al. 1986; Platz et al. 2012).

- 4) < AD 1000 to present. The 0.8-0.4 ka Summit lavas (Stewart et al. 1996) flowed over the Skeet and Staircase lavas to configure most of the upper part of the present-day cone and the remnants of the crater. Between AD 1150-1600 at least five BAF and surge units, mainly directed towards the west, developed sequences of ash and thin lapilli layers around the proximal areas (e.g. Newall, Waiweranui and Puniho events; Druce 1966; Neall 1972; Alloway and Neall 1994); indicating an active period of dome-forming effusive and minor explosive activity. The ca. AD 1655 Burrell eruption ensued (Druce 1966; Neall 1972) and released 1.7×10^6 m³ of BAF and surge deposits, and a sub-Plinian 14 km column that deposited the 3.2×10^8 m³ Burrell Lapilli and three column-collapse pumice density currents of 1.3×10^6 m³ in total over the summit slopes (Platz et al. 2007). It was followed by the AD 1755 Tahurangi event (Druce 1966; Neall 1972), including two BAF and surge producing eruptions. The extrusion of the ca. AD 1800 Sisters dome (Platz et al. 2012) inside the crater of Mt. Taranaki represents the last known eruption of the volcano (Platz et al. 2012). It also showed that dome extrusion in Mt. Taranaki may or may not yield transitions into sub-Plinian explosive activity. The Burrell eruption comprised post-BAF explosive episodes, the Tahurangi event did not, and neither did the Sisters dome extrusion (Platz et al. 2007, 2012).

In total, Alloway et al. (1995) observed at least 76 individual eruptions of about $>10^7$ m³ each, within the last <28 ka tephra records. Most of these tephras were dispersed by plumes to NNE and SSE from the present-day summit, and show a periodicity of one eruption of this magnitude every 300-330 yr. (Alloway et al. 1995). However, Turner et al. (2008b, 2009) identified a minimum of 138 separate ash fall-producing eruptions between 96 and 10150 BP after correlating cores from lakes Umutekai and Rotokare (30 km SE of the summit). Using these data, they forecasted a probability of 0.52 for an eruption every 50 yr., a present annual eruption probability of 1.6%, and a periodicity of ca. 1500 yr. for fast-ascent sub-Plinian events. The latter was interpreted to reflect the periodicity of magma replenishment, the recurrence of tectonic events, or the periodicity of magma to gain enough pressure to rise and erupt (Turner et al. 2008b, 2009).

For the next edifice collapse to occur, Zernack et al. (2012b) determined a maximum interval of <16.2 ka, a current annual collapse probability of 0.018 %, and the most likely collapse to be <2 km³, similar to the AD 1980 Mt. St. Helens debris avalanche (2.5 km³; Glicken 1996); while 7.9 km³ is the maximum volume estimated for a debris avalanche deposit in Mt. Taranaki's geological record (DAD volumes of 1 to >7.5 km³; Zernack et al. 2012b).

1.4.3.2 Petrology and geochemistry

Rocks from Mt. Taranaki are generally porphyritic and contain different proportions of phenocrysts and microphenocrysts of plagioclase (plg), clinopyroxene (cpx), Fe-Ti oxides (oxs; titanomagnetite and ilmenite), hornblende (hb), and few olivine crystals (ol); set in a groundmass of glass, plg, oxs, cpx, rare ol, orthopyroxene (opx) and hb. Biotite phenocrysts exist in some pumice rocks (e.g. Burrell Lapilli; Platz et al. 2007).

Glomerocrysts of $\text{cpx}\pm\text{oxs}\pm\text{plg}\pm\text{ol}$ with rare opx and hb are common, as well as accessories of apatite and zircon (Gow 1968; Neall et al. 1986; Stewart et al. 1996; Price et al. 1999). A diverse range of lithospheric xenoliths are also common in many lavas and fragments from the volcano. These inclusions were classified by Gruender et al. (2010) as: supracrustal sedimentary rocks, mafic hornfels, garnet gneiss, granite, granodiorite, and banded amphibolitic gneiss from either the Median Tectonic Zone or the Taranaki Basin; and in co-magmatic gabbros and ultramafic rocks.

Chemically, Mt. Taranaki's rocks are calc-alkaline, low-Mg# (<53), high-k (1.25-3.25 K_2O wt. %) basalts, basaltic-andesites and andesites (49-62 SiO_2 wt. %; Price et al. 1992; 1999, 2005; Zernack et al. 2012a). Whole-rock concentrations of major elements (FeO, MgO, TiO_2 , and CaO) compatible with the most abundant mineral phases tend to diminish with both decreasing age and silica increments (Price et al. 1992, 1999). In counterpart, sodium and potassium increase, whilst alumina shows scattered values. Therefore, the youngest rocks tend to be the most evolved on average (e.g. Summit lavas; Price et al. 1992, 1999; Zernack et al. 2012a).

Trace element compositions relative to mid-ocean ridge basalts show subduction signatures such as: enrichment of Large Ion Lithophile Elements (LILE), depletion of High Field Strength Elements (HFSE), enrichment of Light Rare Earths (LREE) relative to High Rare Earth Elements (HREE) and Y, along with negative anomalies of Nb, depletion in Nb/K, Nb/Th and enrichment in Pb/Ce (Price et al. 1992, 1999, 2005; Zernack et al. 2012a). Isotopic compositions of lead, strontium and neodymium comprise a limited range; and overlap, for example, a restricted area of the more radiogenic isotopic field of the Taupo Volcanic Zone (Price et al. 1992, 1999, 2005), suggesting a lack of significant crustal assimilation. Oxygen isotopes indicate similar conclusions. Only the

strontium isotopes change as the age decreases; making the young Summit lavas to be more radiogenic than any of the old groups, although no correlation with silica and/or trace elements ensues (Price et al. 1992, 1999, 2005; Zernack et al. 2012a).

According to Price et al. (1992, 1999, 2005) magmas parental to Mt. Taranaki are under-saturated, hydrous, high-Mg, LILE-rich and HFSE-depleted basalts; generated after slab-derived fluids enriched the depleted mantle and triggered its partial melting in low-degrees. These primitive basalts fractionate in the lower crust, yielding melts of basaltic-andesite composition and ultramafic cumulates. Later progressive interaction between basaltic-andesites and amphibolitic melts generated in the lower underplated crust, produce K-rich magmas. However, Stewart et al. (1996) proposed that early fractionation of magnesium-ol and chromite, and subsequent fractionation of ol±cpx±titanomagnetite turns the underplating primitive basalts into high-alumina compositions. Crystallisation of amphibole in the lower crustal wall rocks drives the high-Al basalts into basaltic-andesites (BA). These melts leave the amphibole stability field once they reach higher levels in the crust, producing decompressive melting of their amphibole crystals and incongruent melting of amphibole in the lower-mid crustal confining walls which constitute the major source of K-enrichment in Mt. Taranaki (Stewart et al. 1996). The BA melts may ascend, fractionate at lower pressures, and erupt as dry, plg±ol±cpx bearing magmas. Hydrous melts may re-enter the amphibole stability field, fractionate amphibole crystals and evolve into dacite compositions; whereas dry melts, unable to fractionate amphibole, only evolve into andesites. More recently, Zernack et al. (2012a) suggested that magmas in Mt. Taranaki have progressively become richer in K₂O and LILE, reflecting a gradual evolution to high-K andesite. Early, <100 ka primitive basalts and basaltic-andesites were able to rise and erupt without modifications. Subsequently,

as underplating of the lower crust developed, a hot zone evolved (Turner et al. 2011a), and underplated mafic material was partially re-melted. The interaction of these re-melts with mantle-derived fractionating magmas generated high-K, LILE-rich compositions.

Low-pressure crystal fractionation and crustal storage into a complex dikes-and-sills system, along with crystal accumulation and mixing/mingling processes, may diversify the range of andesite rock textures (Price et al. 1999, 2005; Turner et al. 2011a). Shear processes at the interior of the volcanic conduit relate to differences in magma viscosity and may also produce a range on pumice density and vesicularity (number density, size, and shape of vesicles) and an evident colour banding (Platz et al. 2007).

1.5 References

- Adams NK, Houghton BF, Hildreth W (2006) Abrupt transitions during sustained explosive eruptions: examples from the 1912 eruption of Novarupta, Alaska. *Bull Volcanol* 69:189-206
- Alidibirov M (1994) A model for viscous magma fragmentation during volcanic blasts. *Bull Volcanol* 56: 459-465
- Alidibirov M, Dingwell DB (1996) Magma fragmentation by rapid decompression. *Nature* 380: 146-149
- Alidibirov M, Dingwell DB (2000) Three fragmentation mechanisms for highly viscous magma under rapid decompression. *J. Volcanol. Geotherm. Res.* 100: 413-421
- Alloway B, McComb P, Neall V, Vucetich C, Gibb J, Sherburn S, and Stirling M (2005) Stratigraphy, age, and correlation of voluminous debris-avalanche events from an ancestral Egmont Volcano: implications for coastal plain construction and regional hazard assessment. *Journal of the Royal Society of New Zealand* 35, 229-267
- Alloway B, Neall VE and Vucetich CG (1995) Late Quaternary (post 28,000 year B.P.) tephrostratigraphy of northeast and central Taranaki, New Zealand. *Journal of the Royal Society of New Zealand* 25, 385-458
- Alloway BV and Neall VE (1994) Late Quaternary Volcaniclastic Stratigraphy of Central & North-east Taranaki. In: Briggs R and Moon V (eds) 1994 Annual Conference. Field Trip Guides, Geological Society of New Zealand Miscellaneous Publication 80B: 97-126
- Alloway BV, Pillans BJ, Naish TR and Westgate JA (2004) Age and correlation of Ototoka tephra. Appendix 1 in: Beu AG, Marine Mollusca of oxygen isotope stages of the last 2 million years in New Zealand. *J.Roy.Soc.of N.Z.* 34: 261-265

- Anilkumar AV, Sparks RSJ, Sturtevant B (1993). Geological implications and applications of high velocity two-phase flow experiments. *J. Volcanol. Geotherm. Res.* 56: 145-160
- Arana-Salinas L, Siebe C, Macías JL (2010) Dynamics of the ca. 4965 yr 14C BP “Ochre Pumice” Plinian eruption of Popocatepetl volcano, México. *J. Volcanol. Geotherm. Res.* 192: 212-231
- Arce JL, Cervantes KE, Macías JL, Mora JC (2005) The 12.1 ka middle Toluca pumice: a dacitic Plinian-subplinian eruption of Nevado de Toluca in Central México: *J. Volcanol. Geotherm. Res.* 147: 125-143
- Arce JL, Macías JL, Gardner JE, Layer PW (2006) A 2.5 ka history of dacitic magmatism at Nevado de Toluca, Mexico: petrological, ⁴⁰Ar-³⁹Ar dating, and experimental constraints on petrogenesis. *J. Petrol.* 47 (3): 457- 479
- Arce JL, Macías JL, Vázquez SL (2003) The 10.5 Ka Plinian eruption of Nevado de Toluca, México: stratigraphy and hazard implications: *Geol. Soc. Am. Bull.* 115 (2): 230-248
- Baker DR, Polacci M, LaRue A (2011) A study on the reproducibility of counting vesicles in volcanic rocks. *Geosphere* 7: 79-86
- Bias S, Bonadonna C (2010) A quantitative uncertainty assessment of eruptive parameters derived from tephra deposits: the example of two large eruptions of Cotopaxi volcano, Ecuador. *Bull Volcanol* 73: 73-90
- Blake S (1984) Volatile oversaturation during the evolution of silicic magma chambers as an eruption trigger. *J. Geophys. Res.* 89: 8237-8244
- Blower JD, Keating JP, Mader HM, Phillips JC (2001) Inferring volcanic degassing processes from vesicle size distributions. *Geophys. Res. Lett.* 28 (2): 347–350
- Blower JD, Keating JP, Mader HM, Phillips JC (2002) The evolution of bubble size distributions in volcanic eruptions. *J. Volcanol. Geotherm. Res.* 120: 1-23
- Blundy J, Cashman KV (2001) Ascent-driven crystallization of dacite magmas at Mount St Helens 1980-1986. *Contrib. Mineral. Petrol.* 120: 631-650
- Blundy J, Cashman KV (2005) Rapid decompression-driven crystallization recorded by melt inclusions from Mount St. Helens volcano. *Geology* 33 (10): 193-196
- Boddington T, Parkin CJ and Gubbins D (2004) Isolated deep earthquakes beneath the North Island of New Zealand. *Geophysical Journal International* 158, 972-982
- Bonadonna C, Ernst GGJ, Sparks RSJ (1998) Thickness variations and volume estimates of tephra fall deposits: the importance of particle Reynolds number. *J. Volcanol. Geotherm. Res.* 81: 173-187
- Bonadonna C, Houghton BF (2005) Total grain-size distribution and volume of tephra-fall deposits. *Bull Volcanol* 67: 441-456
- Bourdier JL, Boudon G and Gourgaud A (1989) Stratigraphy of the 1902 and 1929 nuee-ardente deposits, Mt Pelee, Martinique. *J. Volcanol. Geotherm. Res.* 38 (1–2): 77-96.

- Brazier S, Sparks RSJ, Carey SN, Sigurdsson H, and Westgate JA (1983) Bimodal grain-size distribution and secondary thickening in air-fall ash layers. *Nature* 301 (5896): 115-119
- Burgisser A, Gardner JE (2005) Experimental constraints on degassing and permeability in volcanic conduit flow. *Bull Volcanol* 67: 42-56
- Bursik MI (1993) Subplinian eruption mechanisms inferred from volatile and clast dispersal data. *J. Volcanol. Geotherm. Res.* 57: 47-60
- Bursik MI (1998) Tephra dispersal. In: Gilbert, J.S., Sparks, R.S.J. (Eds.). *The physics of explosive volcanic eruptions*, Geol. Soc. Lon. Spec. Publ. 145: 115-144
- Bursik MI, Sparks RSJ, Gilbert JS, and Carey SN (1992) Sedimentation of tephra by volcanic plumes I, Theory and its comparison with a study of the Fogo A Plinian deposit, Sao Miguel (Azores). *Bull Volcanol* 54: 329-344
- Carey S and Sigurdsson H (1987) Temporal variations in column height and magma discharge rate during the A.D. 79 eruption of Vesuvius. *Geological Society of America Bulletin* 99: 303-314
- Carey S, Gardner J, Sigurdsson H (1995) The intensity and magnitude of Holocene Plinian eruptions from Mount St. Helens volcano. *J. Volcanol. Geotherm. Res.* 66: 185-202
- Carey S, Sigurdsson H (1989) The intensity of Plinian eruptions. *Bull Volcanol* 51: 28-40
- Carey S, Sparks RSJ (1986) Quantitative models of the fall and dispersal of tephra from volcanic eruption columns. *Bull Volcanol* 48: 109-125
- Carn SA, Pallister JS, Lara L, Ewert JW, Watt S, Prata AJ, Thomas RJ, Villarosa (2009) The unexpected awakening of Chaitén Volcano, Chile. *EOS Transactions, AGU* 90 (24): 205-206
- Cas RAF, Wright JV (1987) *Volcanic successions*. Allen and Unwin. 528p.
- Cashman KV, Blundy J (2000) Degassing and crystallization of ascending andesite and dacite. *Phil. Trans. Roy. Soc.* 358: 1487-1513
- Cashman KV, Ferry JM (1988) Crystal size distribution (CSD) in rocks and the kinetics and dynamics of crystallization. *Contrib. Mineral. Petrol.* 99: 401-415
- Cashman KV, Mangan MT (1994) Physical aspects of magmatic degassing II. Constraints on vesiculation processes from textural studies of eruptive products. In: Carroll MR, Holloway JR (eds) *Volatiles in magmas*. *Rev Mineral* 30: 447-478
- Cashman KV, McConnell SM (2005) Multiple levels of magma storage during the 1980 summer eruptions of Mount St. Helens, WA. *Bull Volcanol* 68: 57-75
- Cashman KV, Sturtevant B, Papale P, Navon O (2000). Magmatic fragmentation. In: Sigurdsson H, Houghton BF, McNutt SR, Rymer H, Stix J (eds) *Encyclopedia of volcanoes*. Academic Press, San Diego, CA: 421-430
- Cavill AW, Cassidy J and Brennan BJ (1997) Results from the new seismic monitoring network at Egmont Volcano, New Zealand: tectonic and hazard implications. *NZ. J. Geol. Geophys.* 40:69-78

- Cioni R, Marianelli P, Stantacrocce R, Sbrana A (2000) Plinian and subplinian eruptions. In: Sigurdsson H, Houghton BF, McNutt SR, Rymer H, Stix J (eds) *Encyclopedia of Volcanoes*. Academic Press, San Diego: 477-494
- Cioni R, Sulpizio R, Garruccio N (2003) Variability of the eruption dynamics during a Subplinian event: Greenish Pumice eruption of Somma-Vesuvius (Italy). *J. Volcanol. Geotherm. Res.* 124: 89-114
- Cluzel N, Laporte D, Provost A, Kannevischer I (2008) Kinetics of heterogeneous bubble nucleation in rhyolitic melts: implications for the number density of bubbles in volcanic conduits and for pumice textures. *Contrib. Mineral. Petrol.* 156: 745-763
- Coltelli M, Del Carlo P, Vezzoli L (1998) Discovery of a Plinian basaltic eruption of Roman age at Etna volcano, Italy. *Geol* 26(12):1095-1098
- Costa A (2006) Permeability-porosity relationship: A re-examination of the Kozeny-Carman equation based on a fractal pore-space geometry assumption: *Geophys. Res. Lett.*, 33: L02318
- Costa A, Macedonio G (2005) Viscous heating effects in fluids with temperature dependent viscosity: triggering of secondary flows. *J. Fluid Mech.* 540: 21-38
- Couch S, Sparks RSJ, Carroll MR (2001) Mineral disequilibrium in lavas explained by convective self-mixing in open magma chambers. *Nature* 411: 1037-1039
- Cronin SJ, Stewart RB, Neall VE, Platz T and Gaylord D (2003). The AD1040 to present Maero eruptive period of Egmont Volcano, Taranaki, New Zealand. Abstract. Geological Society of New Zealand Miscellaneous Publication 116A, 43
- Degruyter W, Bachmann O, Burgisser A (2010) Controls on magma permeability in the volcanic conduit during the climactic phase of the Kos Plateau Tuff eruption (Aegean Arc). *Bull Volcanol* 72 (1): 63-74
- Dellino P, Isaia R, La Volpe L, Orsi G (2001) Statistical analysis of textural data from complex pyroclastic sequences: implications for fragmentation processes of the Agnano-Monte Spina Tephra (4.1 ka), Phlegraean Fields, southern Italy. *Bull Volcanol* 63: 443-461
- Devine JD, Gardner JE, Brack HP, Layne GD, and Rutherford MJ (1995). Comparison of microanalytical methods for estimating H₂O contents of silicic volcanic glasses. *Am. Mineral.* 80: 319-328
- Dingwell DB, Webb SL (1989) Structural relaxation in silicate melts and non-Newtonian melt rheology in geological processes. *Phys. Chem. Miner.* 16: 508-516
- Dixon J E (1997) Degassing of alkalic basalts. *Am. Mineral.* 82: 368-378
- Druce AP (1966) Tree-ring dating of recent volcanic ash and lapilli, Mt Egmont. *New Zealand Journal of Botany* 4, 3-41
- Eichelberger JC (1995) Silicic volcanism: ascent of viscous magmas from crustal reservoirs. *Annu. Rev. Earth Planet. Sci.* 23:41-63
- Fagents SA, Wilson L (1993) Explosive eruptions-VII. The ranges of pyroclasts ejected in transient volcanic explosions. *Geophys. J. Int.* 113 (2): 359-370

- Fierstein J, Nathenson M (1992) Another look at the calculation of fallout tephra volumes. *Bull Volcanol* 54: 156-167.
- Fisher R, Schmincke HU (1984) *Pyroclastic Rocks*, Springer-Verlag, Berlin. 472 p.
- Fleming CA (1953) The geology of Wanganui subdivision. Waverly and Wanganui sheet districts (N137 and N138). *NZ Geol. Surv. Bull.* 52. 372 p.
- Fonterra (2013) About us. <http://www.fonterra.com/nz/en> Accessed 1 January 2013
- Franks AM (1984) Soils of Eltham County and the tephrochronology of central Taranaki. Unpublished PhD thesis. Massey University, Palmerston North, New Zealand.
- Freundt A, Rosi M (1998) From magma to tephra: modelling physical processes of explosive volcanic eruptions. Elsevier, 334p.
- Gardner CA, Cashman KV, Neal CA (1998) Tephra-fall deposits from the 1992 eruption of Crater Peak, Alaska: implications of clast textures for eruptive processes. *Bull Volcanol* 59: 537-555
- Gardner JE (2007) Heterogeneous bubble nucleation in highly viscous silicate melts during instantaneous decompression from high pressure. *Chem. Geol.* 236: 1-12
- Gardner JE, Denis MH (2004) Heterogeneous bubble nucleation on Fe-Ti oxide crystals in high-silica rhyolitic melts. *Geochim. Cosmochim. Acta* 68: 3587-3597
- Gardner JE, Hilton M, Carrol MR (1999) Experimental constraints on degassing of magma: Isothermal bubble growth during continuous decompression from high pressure. *Earth Planet. Sci. Lett.* 168: 201-218
- Gardner JE, Rutherford M, Carey S, Sigurdsson H (1995) Experimental constraints on preeruptive water contents and changing magma storage prior to explosive eruptions of Mount St. Helens volcano. *Bull Volcanol* 57: 1-17
- Gardner JE, Thomas RME, Jaupart C, Tait S (1996) Fragmentation of magma during Plinian volcanic eruptions. *Bull Volcanol* 58 (2-3): 144-162
- Geschwind CH and Rutherford MJ (1995) Crystallisation of microlites during magma ascent: the fluid mechanics of 1980-1986 at Mount St Helens. *Bull. Volcanol.* 57: 356-370
- Giachetti T, Burgisser A, Arbaret L, Druitt TH, Kelfoun K (2011) Quantitative textural analysis of Vulcanian pyroclasts (Montserrat) using multi-scale X-ray computed microtomography: comparison with results from 2D image analysis. *Bull Volcanol* 73: 1295-1309
- Giachetti T, Druitt TH, Burgisser A, Arbaret L, Galven C (2010) Bubble nucleation and growth during the 1997 Vulcanian explosions of Soufrière Hills Volcano, Montserrat. *J. Volcanol. Geotherm. Res.* 193 (3-4): 215-231
- Gilbert and R.S.J. Sparks eds. (1998) *The physics of explosive volcanic eruptions*. Geol. Soc.Lon. Spec. Publ 145, 186p.
- Giordano D, Dingwell DB (2003) Viscosity of hydrous Etna basalt: implications for Plinianstyle basaltic eruptions. *Bull Volcanol* 65: 8-14

- Glicken H (1996) Rock-slide debris avalanche of May 18, 1980, Mount St. Helens Volcano, Washington. US Geological Survey Open-File Report 96-677, 90 p.
- Gow AJ (1968) Petrographic and petrochemical studies of Mt. Egmont andesites. *New Zealand Journal of Geology and Geophysics* 11, 166-190.
- Grange LI and Taylor NH (1933) Report on soil surveys for 1932-33. Department of Scientific and Industrial Research, Annual Report 1932-1933
- Grant-Taylor TL (1964) Volcanic history of western Taranaki. *New Zealand Journal of Geology and Geophysics* 7, 78-86.
- Gruender K, Stewart RB, and Foley S (2010) Xenoliths from the sub-volcanic lithosphere of Mt. Taranaki, New Zealand. *Journal of Volcanology and Geothermal Research* 190, 192-202.
- Gualda GAR, Baker DR, Polacci M (2010) Introduction: Advances in 3D imaging and analysis of geomaterials. *Geosphere* 6: 468-469
- Gualda GAR, Rivers M (2006) Quantitative 3D petrography using X-ray tomography: Application to Bishop Tuff pumice clasts. *J. Volcanol. Geotherm. Res.* 154 (1-2): 48- 62
- Gudmundsson M and Pedersen R (2010) Eruptions of Eyjafjallajökull Volcano, Iceland. *Eos* 91 (21): 190-191
- Gurioli L, Houghton BF, Cashman KV, Cioni R (2005) Complex changes in eruption dynamics during the 79 AD eruption of Vesuvius. *Bull Volcanol* 67: 144-159
- Hale A, Mühlhaus HB (2007) Modelling shear bands in a volcanic conduit: Implications for over-pressures and extrusion-rates. *Earth and Planet. Sci. Lett.* 263: 74-87
- Hamada M, Laporte D, Cluzel N, Koga KT, Kawamoto T (2010) Simulating bubble number density of rhyolitic pumices from Plinian eruptions: constraints from fast decompression experiments. *Bull Volcanol* 72: 735-746
- Hammer JE and Rutherford (2002) An experimental study of the kinetics of decompression-induced crystallization in silicic melt: *J. Geophys. Res.* 107, 0.1029/2001JB00281
- Hammer JE, Cashman KV, Hoblitt RP, Newman S (1999) Degassing and microlite crystallization during pre-climactic events of the 1991 eruption of Mt. Pinatubo, Philippines. *Bull Volcanol* 60: 355-380
- Henrys S, Reyners M and Bibby H (2003) Exploring the plate boundary structure of North Island, New Zealand. *EOS, Trans Am. Geophys. Union* 84: 289-294
- Hervig RL, Dunbar NW (1992) Cause of chemical zoning in the Bishop (California) and Bandelier (New Mexico) magma chambers. *Earth Planet. Sci. Lett.* 111: 97-108
- Hess KU, Dingwell DB (1996) Viscosities of hydrous leucogranitic melts: A non-Arrhenian model. *Am. Mineral.* 81: 1297-1300
- Higgins MD (2000) Measurement of crystal size distributions. *Am. Mineral.* 85: 1105-1116

- Hobden BJ, Houghton BF and Nairn IA (2002) Growth of a young, frequently active composite cone: Ngauruhoe volcano, New Zealand. *Bulletin of Volcanology* 64, 392-409.
- Hoblitt RP, Wolfe EW, Scott WE, Couchman MR, Pallister JS, Javier D (1996) The preclimactic eruptions of Mount Pinatubo, June 1991. In: Newhall CG, Punongbayan RS (eds.), *Fire and Mud: Eruptions and Lahars of Mount Pinatubo, Philippines*. University of Washington Press, Hong Kong: 457-511
- Holloway JR, Blank JG (1994) Application of experimental results to C-O-H species in natural melts. In: Carroll MR, Holloway JR (eds) *Volatiles in magmas*. *Rev Mineral* 30: 188-230
- Houghton BF, Wilson CJN (1989) vesicularity index for pyroclastic deposits. *Bull Volcanol* 51: 451-462
- Houghton BF, Wilson CJN, Del Carlo P, Coltelli M, Sable JE, Carey R (2004) The influence of conduit processes on changes in style of basaltic Plinian eruptions: Tarawera 1886 and Etna 122 BC. *J. Volcano. Geotherm. Res.* 137: 1-14
- Huber C, Bachman O, Dufek J (2011). Thermo-mechanical reactivation of locked crystal mushes: Melting-induced internal fracturing and assimilation processes in magmas. *Earth Planet. Sci. Lett.* 304: 443-454
- Huber C, Bachmann O, Manfa M (2010) Two competing effects of volatiles on heat transfer in crystal-rich magmas: thermal insulation vs defrosting. *J. Petrol.* 51: 847-867
- Hull AG (1994) Past earthquake timing and magnitude along the Inglewood fault, Taranaki, New Zealand. *Bulletin of the New Zealand National Society for Earthquake Engineering* 27, 155-162.
- Hull, A.G. and Dellow, G. 1993. Earthquake hazards in the Taranaki region. Institute of Geological and Nuclear Sciences Client Report 1993/03.
- Hurwitz S, Navon O (1994) Bubble nucleation in rhyolitic melts: experiments at high pressure, temperature and water content. *Earth Planet. Sci. Lett.* 122: 267-280
- Ihinger PD, Hervig RL, and McMillan PF (1994) Analytical Methods for Volatiles in Glasses. In: Carroll MR, Holloway JR (eds) *Volatiles in magmas*. *Rev Mineral* 30: 67-121
- Jaupart C (1998) Gas loss from magmas through conduit walls during eruption, *Geol. Soc. Lon. Spec. Publ* 145: 73-90
- Jaupart C, Allegre CJ (1991) Gas content, eruption rate and instabilities of eruption regime in silicic volcanoes. *Earth Planet. Sci. Lett.* 102: 413-429
- Jerram DA, Martin VM (2008) Understanding crystal populations and their significance through the magma plumbing system. In: *Dynamics of crustal Magma Transfer, Storage and Differentiation* (Annen and Zellmer Eds). *Geological Society Special Publication* 304: 144-148
- Johnson MC, Anderson AT, Rutherford MJ (1994) Pre-eruptive volatile contents of magmas. In: Carroll MR, Holloway JR (eds) *Volatiles in magmas*. *Rev Mineral* 30: 281-330
- Kaminski E, Jaupart C (1997) Expansion and quenching of vesicular magma fragments in Plinian eruptions. *J. Geophys. Res.* 102: 12,187-12,203

- Kamp PJJ, Vonk AJ, Bland KJ, Hansen RJ, Hendy AJW, McIntyre AP, Ngatai M, Cartwright SJ, Hayton S and Nelson CS (2004) Neogene stratigraphic architecture and tectonic evolution of Wanganui, King Country, and eastern Taranaki basins, New Zealand. *NZ. J. Geol. Geophys.* 47: 625-644
- Kennedy B, Jellinek AM, Russel JK, Nichols ARL, Vigouroux N (2010) Time-and temperature-dependent conduit wall porosity: a key control on degassing and explosivity at Taurewa volcano, New Zealand. *Earth. Planet. Sci. Lett* 299: 126-137
- Ketcham RA (2005) Three-dimensional textural measurements using high-resolution X-ray computed tomography. *J. Struct. Geol.* 27: 1217-1228
- Ketcham RA, and WD Carlson (2001) Acquisition, optimization and interpretation of X-ray computed tomographic imagery: applications to the geosciences. *Computers & Geosciences* 27: 381-400
- King PL, Holloway JR (2002). CO₂ solubility and speciation in intermediate (andesitic) melts: the role of H₂O and composition. *Geochim. Cosmochim. Acta* 66 (9); 1627-1640
- King PR and Thrasher GP (1996) Cretaceous-Cenozoic geology and petroleum systems of the Taranaki Basin, New Zealand. Institute of Geological and Nuclear Sciences Monograph 13.
- Klug C, Cashman KV (1994) Vesiculation of May 18, 1980. Mount St. Helens magma. *Geology* 22: 468-472
- Klug C, Cashman KV (1996) Permeability development in vesiculating magmas: implications for fragmentation. *Bull Volcanol* 58: 87-100
- Klug C, Cashman KV, Bacon CR (2002). Structure and physical characteristics of pumice from the climactic eruption of Mt Mazama (Crater Lake), Oregon. *Bull Volcanol* 64: 486-501
- Koyaguchi T, Mitani NK (2005) A theoretical model for fragmentation of viscous bubbly magmas in shock tubes. *J. Geophys. Res.* 110, B10202: doi:10.1029/2004JB003513
- Koyaguchi T, Schew B, Mitani N, Melnik O (2008) A fragmentation criterion for highly viscous bubbly magmas estimated from shock tube experiments. *J. Volcanol. Geotherm. Res.* 178: 58-71
- Koyaguchi T, Tokuno M (1993) Origin of the giant eruption cloud of Pinatubo, June 15, 1991. *J. Volcanol. Geotherm. Res.* 55: 85-96
- Kratzmann DJ, Carey SN, Fero J, Scasso RA, Naranjo JA (2010) Simulations of tephra dispersal from the 1991 explosive eruptions of Hudson volcano, Chile. *J. Volcanol. Geotherm. Res.* 190: 337-352
- Lange RA (1994) The effect of H₂O, CO₂ and F on the density and viscosity of silica melts In: Carroll MR, Holloway JR (eds) *Volatiles in magmas.* *Rev Mineral* 30: 331-370
- Langmann B, Folch A, Hensch M and Matthias V (2012) Volcanic ash over Europe during the eruption of Eyjafjallajökull on Iceland, April-May 2010. *Atmospheric Environment* 48: 1-8
- Larsen JR, Gardner JE (2000) Experimental constraints on bubble interactions in rhyolite melts: implications for vesicle size distributions. *Earth Planet. Sci. Lett.* 180: 201-214
- Lees CM and Neall VE (1993) Vegetation response to volcanic eruptions on Egmont Volcano, New Zealand, during the last 1500 years. *Journal of the Royal Society of New Zealand* 23, 91-127.

- Lirer L, Pescatore T, Booth B, Walker GPL (1973) Two Plinian pumice fall deposits from Somma-Vesuvius, Italy. *Geol. Soc. Am. Bull.* 84: 759-772
- Locke CA and Cassidy J (1997) Egmont volcano, New Zealand: three-dimensional structure and its implications for evolution. *J. Volc. Geoth. Res.* 76: 149-161
- Lowenstern JB (1995) Applications of silicate melt inclusions to the study of magmatic volatiles. In: JFH Thompson (ed). *Magma, Fluids and Ore Deposits*. Mineralogical Association of Canada Short Course 23: 71-99
- Lube G, Breard EC, Cronin SJ, Procter JN et al. (2014) Dynamics of surges generated by hydrothermal blasts during the 6 August 2012 Te Maari eruption, Mt. Tongariro, New Zealand. *J Volcanol Geoth Res* 286:348-366
- Lyakhovskiy V, Hurwitz S, Navon O (1996). Bubble growth in rhyolitic melts: experimental and numerical investigation. *Bull Volcanol* 58: 19-32
- Macedonio G, Dobran F, Neri A (1994) Erosion processes in volcanic conduits and application to the AD 79 eruption of Vesuvius. *Earth Planet. Sci. Lett.* 121 (1-2): 137-152
- Mader HM (1998) Conduit flow and fragmentation. In: J.S. Gilbert and R.S.J. Sparks (Eds), *The physics of explosive volcanic eruptions*. *Geol. Soc. Lon. Spec. Publ* 145: 51-71
- Mader HM, Phillips JC, Sparks RSJ, Sturtevant B (1996) Dynamics of explosive degassing of magma: Observations of fragmenting two-phase flows. *J. Geophys. Res.* 101B:5547-5560
- Mader HM, Zgang Y, Phillips JC, Sparks RSJ, Sturtevant B, Stolper E (1994) Experimental simulations of explosive degassing of magma. *Nature* 372: 85-88
- Mangan M, Mastin L, Sisson T (2004) Gas evolution in eruptive conduits: combining insights from high temperature and pressure decompression experiments with steady-state flow modelling. *J. Volcanol. Geotherm. Res.* 129 (1-3): 23-36
- Mangan MT, Cashman KV (1996) The structure of basaltic scoria and reticulite and inferences for vesiculation, foam formation, and fragmentation in lava fountains. *J. Volcanol. Geotherm. Res.* 73: 1-18
- Mangan MT, Sisson T (2000) Delayed, disequilibrium degassing in rhyolite magma: decompression experiments and implications for explosive volcanism. *Earth Planet. Sci. Lett.* 183: 441-455
- Manville V, Németh K, Kano K (2009). From source to sink: a review of three decades of progress in the understanding of volcanoclastic processes, deposits, and hazards. *Sedimentary Geology* 220: 136-161
- Martel C, Schmidt BC (2003) Decompression experiments as an insight into ascent rates of silicic magmas. *Contrib. Mineral. Petrol.* 144: 397-415
- Marziano GI, Schmidt BC, Dolfi D (2007) Equilibrium and disequilibrium degassing of phonolitic melt (Vesuvius AD 79 “white pumice”) simulated by decompression experiments. *J. Volcanol. Geotherm. Res.* 161:151-164

- Massol H, Jaupart C (1999) The generation of gas overpressure in volcanic eruptions. *Earth Planet. Sci. Lett.* 166: 57-70
- May DJ (2003) The correlation of recent tephra with lava flows on Egmont volcano, Taranaki, New Zealand using evidence of mineral chemistry. Unpublished Masters thesis. The University of Auckland, Auckland, New Zealand.
- McBirney AR (1973) Factors governing the intensity of explosive andesitic eruptions: *Bull Volcanol* 37: 443-453
- McBirney AR (1977) Mixing and unmixing of magmas. *J. Volcanol. Geotherm. Res.* 7: 357-371
- McGlone MS, Neall VE and Clarkson BD (1988) The effect of recent volcanic events and climatic changes on the vegetation of Mt Egmont (Mt Taranaki), New Zealand. *New Zealand Journal of Botany* 26, 123-144.
- McIntyre AP (2002) Geology of Mangapanian (Late Pliocene) strata, Wanganui Basin: lithostratigraphy, paleontology and sequence stratigraphy. PhD thesis, University of Waikato, Hamilton.
- McMillan PF (1994) water solubility and speciation models. In: Carroll MR, Holloway JR (eds) Volatiles in magmas. *Rev Mineral* 30: 131-156
- Mess F, Swennen R, Van Geet M, Jacobs P (2003) Applications of X-ray computed tomography in the geosciences. *Geol. Soc. Lon. Spec. Publ.*, 215p
- Mets C de, Gordon RG, Argus DF and Stein S (1994) Effect of recent revisions to the geomagnetic reversal time scale on estimates on current plate motions. *Geophys. Res. Letters* 21:2191-2194
- Mills C (1990) Gravity expression of the Patea-Tongaporutu High and subsequent model for the Taranaki Basin margin. In: 1989 New Zealand Oil Exploration Conference: proceedings. Wellington, Petroleum and Geothermal Unit, Ministry of Commerce. 191-200
- Morrissey MM, Mastin LG (2000) Vulcanian eruptions. In: Sigurdsson H, Houghton BF, McNutt SR, Rymer H, Stix J (eds) *Encyclopedia of volcanoes*. Academic Press, San Diego, CA: 463-475
- Mortimer N, Tulloch AJ and Ireland TR (1997) Basement geology of Taranaki and Wanganui Basins, New Zealand. *New Zealand Journal of Geology and Geophysics* 40, 223-236.
- Mourtada-Bonnefoi and Laporte (1999) Experimental study of homogeneous bubble nucleation in rhyolitic magmas. *Geophys. Res. Lett.* 26: 3505-3508
- Mueller S, Llewellyn EW, Mader HM (2009) The rheology of suspensions of solid particles. *Proc. R. Soc. A.* 466 (2116): 1201-1228, doi: 10.1098/rspa.2009.0445
- Mueller S, Scheu B, Spieler O, Dingwell DB (2008). Permeability control on magma fragmentation. *Geology* 36 (5): 399-402
- Naish TR and Kamp PJJ (1995) Pliocene-Pleistocene marine cyclothems, Wanganui Basin, New Zealand: a lithostratigraphic framework. *NZ. J. Geol. Geophys.* 38: 223-243

- Naish TR and Kamp PJJ (1997) Sequence stratigraphy of sixth-order (41 k.y.) Pliocene-Pleistocene cyclothems, Wanganui Basin, New Zealand: a case for the regressive systems tract. *Geol. Soc. Of Am. Bull.* 109: 978-999
- Naish TR, Kamp PJJ, Alloway BV, Pillians B, Wilson GS and Westgate JA (1996) Integrated tephrochronology and magnetostratigraphy for cyclothem marine strata, Wanganui Basin: Implications for the Pliocene-Pleistocene boundary in New Zealand. *Quaternary International* 34-36: 29-48
- Nakada S, Motomura Y (1999) Petrology of the 1991-1995 eruption at Unzen: effusion pulsation and groundmass crystallization. *J. Volcanol. Geotherm. Res.* 89: 174-196
- Nakagawa M, Wada K, Wood PC (2002) Mixed magmas, mush chambers and eruption triggers: Evidence from zoned clinopyroxene phenocrysts in andesitic scoria from the 1995 eruptions of Ruapehu Volcano, New Zealand. *J. Petrol.* 43 (12): 2279-2303
- Namiki A, Manga M (2008) Transition between fragmentation and permeable outgassing of low viscosity magmas. *J. Volcanol. Geotherm. Res.* 169: 48-60
- Navon O and Lyakhovsky V (1998) Vesiculation processes in Silicic Magmas. In: Gilbert, J. and Sparks R.S.J. (eds.) *The Physics of Explosive Volcanism* *Geol. Soc. Lond., Spec. Publ.* 145: 29-52
- Neall VE (1972) Tephrochronology and tephrostratigraphy of western Taranaki (N108-109), New Zealand. *New Zealand Journal of Geology and Geophysics* 15, 507-557.
- Neall VE (1976) *Volcanology of Egmont National Park*. Department of Soil Science, Massey University, Palmerston North.
- Neall VE (1979) Sheets P19, P20, and P21. New Plymouth, Egmont and Manaia. 1st ed. Geological map of New Zealand 1:50,000. 3 maps and notes. New Zealand Department of Scientific and Industrial Research. Wellington.
- Neall VE (2003) *The volcanic history of Taranaki*. Institute of Natural Resources, Massey University, Soil & Earth Sciences Occasional Publication 2.
- Neall VE and Alloway BE (2004) *Quaternary Geological Map of Taranaki*. Institute of Natural Resources, Massey University, Soil and Earth Sciences Occasional Publication 4.
- Neall VE, Hogg AG and Zernack AV (2012) Revision of Volcaniclastic Stratigraphy in Eastern Egmont National Park, Taranaki (abstract). 2012 *Geol. Soc. NZ. Conference*.
- Neall VE, Stewart RB and Smith IEM (1986) History and petrology of the Taranaki volcanoes. In: Smith IEM (ed.) *Late Cenozoic volcanism*. *Royal Society of New Zealand Bulletin* 23, 251-263.
- Nelson ST, Montana A (1992) Sieve-textured plagioclase in volcanic rocks produced by rapid decompression. *Am. Mineral.* 77: 1242-1249
- New Zealand's Oil and Gas Industry (2013) *Why NZ*. <http://www.energystream.co.nz/> Accessed 1 January 2013
- Newman S, Lowerstern JB (2002) VolatileCalc: A silicate melt-H₂O-CO₂ solution model written in Visual Basic for Excel. *Comp Geosci* 28: 597-604

- Nichols ARL, and Wysoczansk RJ (2007) Using micro-FTIR spectroscopy to measure volatile contents in small and unexposed inclusions hosted in olivine crystals. *Chem. Geol.* 242: 371-384
- Nicol A, Stagpoole V and Maslen G (2004) Structure and petroleum potential of the Taranaki fault play. Abstract. 2004 New Zealand Petroleum Conference Proceedings. Ministry of Economic Development, Wellington, New Zealand.
- Nodder SD (1993) Neotectonics of the offshore Cape Egmont Fault Zone, Taranaki Basin, New Zealand. *New Zealand Journal of Geology and Geophysics* 36, 167-184.
- Okumura S, Nakamura M, Tsuchiyama A (2006) Shear-induced bubble coalescence in rhyolitic melts with low vesicularity. *Geophys. Res. Lett.* 33 (20): 1-5
- Oliver WRB (1931) An ancient Maori oven on Mount Egmont. *Journal of the Polynesian Society* 40, 73-80.
- Orsi G, Gallo G, Heiken G, Wohletz K, Yu E, Bonani G (1992) A comprehensive study of pumice formation and dispersal: the Cretaceous Tephra of Ischia (Italy). *J. Volcanol. Geotherm. Res.* 53: 329-354
- Palladino DM, Simei S, Kyriakopoulos K (2008) On magma fragmentation by conduit shear stress: Evidence from the Kos Plateau Tuff, Aegean Volcanic Arc. *J. Volcanol. Geotherm. Res.* 178: 807-817
- Palmer BA and Neall VE (1991) Contrasting lithofacies architecture in ring plain deposits related to edifice construction and destruction, the Quaternary Stratford and Opunake Formations, Egmont Volcano, New Zealand. *Sedimentary Geology* 74, 71-88.
- Palmer BA, Alloway BV and Neall VE (1991) Volcanic-debrisavalanche deposits in New Zealand: lithofacies organisation in unconfined, wet-avalanche flows. In: Fisher, R. V. and Smith, G. A. (eds) *Sedimentation in Volcanic Settings*. SEPM Special Publications 45, 89-98.
- Papale P (1999). Strain-induced magma fragmentation in explosive eruptions: *Nature* 397: 425-428
- Papale P, Dobran F (1993) Modelling of the ascent of magma during the plinian eruption of Vesuvius in A.D. 79. *J. Volcanol. Geotherm. Res.* 58: 101-132
- Papale P, Neri A, Macedonio G (1998) The role of magma composition and water content in explosive eruptions, 1. Conduit ascent dynamics. *J. Volcanol. Geotherm. Res.* 87: 75-93
- Pardo N, Cronin SJ, Palmer A, Németh K (2012a) Reconstructing the largest explosive eruptions of Mt. Ruapehu, New Zealand: lithostratigraphic tools to understand subplinian-Plinian eruptions at andesitic volcanoes. *Bull Volcanol* 74: 617-640.
- Pardo N, Cronin SJ, Palmer A, Procter J, Smith I (2012b). Andesitic Plinian eruptions at Mt. Ruapehu: quantifying the uppermost limits of eruptive parameters. *Bull Volcanol* 74: 1161-1185.
- Parfitt EA, Wilson L (2008) *Fundamentals of Physical Volcanology*. Oxford, Blackwell, 256p.
- Pérez W, Freundt A, Kutterolf S, Schmincke HU (2009) The Masaya Triple Layer: A 2100 year old basaltic multi-episodic Plinian eruption from the Masaya Caldera Complex (Nicaragua). *J. Volcanol. Geotherm. Res.* 179: 191-205

- Petrie RA (1988) Unpublished Honours Dissertation in Soil Sciences. Massey University, Palmerston North.
- Pillans B, Alloway BV, Naish TR, Westgate J, Abbott S and Palmer A (2005) Silicic tephra in Pleistocene shallow-marine sediments of Wanganui Basin, New Zealand. *J. Roy. Soc. NZ.* 35: 43-90
- Platz T, Cronin SJ, Cashman KV, Stewart RB, Smith IEM (2007) Transitions from effusive to explosive phases in andesite eruptions-A case-study from the AD 1655 eruption of Mt. Taranaki, New Zealand. *J. Volcanol. Geotherm. Res.* 161: 15-34
- Platz T, Cronin SJ, Procter JN, Neall VE and Foley SF (2012) Non-explosive dome-forming eruptions at Mt. Taranaki, New Zealand. *Geomorphology* 136: 15-30
- Polacci M, (2005) Constraining the dynamics of volcanic eruptions by characterization of with Vp and Vp/Vs. *Geophys. J. Int.*, 165: 565–583 imaging. *Earth Sci. Rev.* 29: 9-26
- Polacci M, Baker DR, Bai L, Mancini L (2008) Large vesicles record pathways of degassing at basaltic volcanoes. *Bull Volcanol* 70: 1023-1029
- Polacci M, Baker DR, Mancini L, Favretto S, Hill RJ (2009a) Vesiculation in magmas from Stromboli and implications for normal Strombolian activity and paroxysmal explosions in basaltic systems. *J. Geophys. Res.* 114: B01206, doi:10.1029/2008JB005672
- Polacci M, Baker DR, Mancini L, Tromba G, Zanini F (2006) Three-dimensional investigation of volcanic textures by X-ray microtomography and implications for conduit processes. *Geophys. Res. Lett.* 33(13): L13312
- Polacci M, Burton MR, La Spina A, Muré F, Favretto S, Zanini F (2009b) The role of syneruptive vesiculation on explosive basaltic activity at Mt. Etna, Italy. *J. Volcanol. Geotherm. Res.* 179: 265-269
- Polacci M, Papale P, Rosi M (2001) Textural heterogeneities in pumices from the climactic eruption of Mount Pinatubo, 15 June 1991, and implications for magma ascent dynamics. *Bull Volcanol* 63: 83-97
- Polacci M, Pioli L, Rosi M (2003) The Plinian phase of the Campanian Ignimbrite eruption (Phlegrean Fields, Italy): evidences from density measurements and textural characterization of pumice. *Bull Volcanol* 65: 418-432
- Price RC, Gamble JA, Smith IEM, Stewart RB, Eggins S, Wright IC (2005). An integrated model for the temporal evolution of andesites and rhyolites and crustal development in New Zealand's North Island. *J. Volcanol. Geotherm. Res.* 140 (1-3): 1-24
- Price RC, McCulloch MT, Smith IEM and Stewart RB (1992) Pb-Nd-Sr isotopic compositions and trace element characteristics of young volcanic rocks from Egmont Volcano and comparisons with basalts and andesites from the Taupo Volcanic Zone, New Zealand. *Geochimica et Cosmochimica Acta* 56, 941-953.
- Price RC, Stewart RB, Woodhead JD and Smith IEM (1999) Petrogenesis of high-K arc magmas: evidence from Egmont Volcano, North Island, New Zealand. *Journal of Petrology* 40, 167-197.

- Procter JN, Cronin SJ, Zernack AV (2009) Landscape and sedimentary response to catastrophic debris avalanches, western Taranaki, New Zealand. *Sed. Geol.* 220: 271-287
- Procter JN, Cronin SJ, Platz T, et al. (2010) Mapping block-and-ash flow hazards based on Titan 2D simulations: a case study from Mt. Taranaki, NZ. *Natural Hazards* 53: 483-501
- Proussevitch AA, Mulukutla GK, Sahagian DL (2011) A new method of measuring bubble size distributions from vesicle fragments preserved on surface of volcanic ash particles. *Geosphere* 7: 62-69
- Proussevitch AA, Sahagian DL, Anderson AT (1993) Dynamics of diffusive bubble growth in magmas: isothermal case. *J. Geophys. Res.* 98 (B12): 22283-22307
- Proussevitch AA, Sahagian DL, Tsentalovich EP (2007) Statistical analysis of bubble and crystal size distributions: Formulations and procedures. *J. Volcanol. Geotherm. Res.* 164: 95-111
- Pyle DM (1989) The thickness, volume and grain size of tephra fall deposits. *Bull Volcanol* 51: 1-15
- Pyle DM (2000) Sizes of volcanic eruptions. In: Sigurdsson H, Houghton BF, McNutt SR, Rymer H, Stix J (eds) *Encyclopedia of volcanoes*. Academic Press, San Diego, CA: 263-269
- Rosi M, Palladio-Melosantos ML, Di Muro A, Leoni R, Bacolcol T (2001) Fall vs flow activity during the 1991 climatic eruption of Pinatubo Volcano (Philippines) *Bull Volcanol* 62: 549-566
- Rust AC, Cashman KV (2004). Permeability of vesicular silicic magma: Inertial and hysteresis effects, *Earth Planet. Sci. Lett.* 228: 93-107
- Rust AC, Cashman KV (2011) Permeability controls on expansion and size distributions of pyroclasts. *J. Geophys. Res.* 116, B11202, 17p. doi:10.1029/2011JB008494
- Rust AC, Manga M (2002) Bubble shapes and orientation in low Re simple shear flow. *J Colloid Interface Sci* 249: 476
- Rutherford MJ and Hill PM (1993) Magma ascent rates from amphibole breakdown: An experimental study applied to the 1980-1986 Mount St. Helens eruptions. *J. Geophys. Res.* 98: 19667-19685
- Rutherford MJ, Devine JD (1996) Preeruption pressure-temperature conditions and volatiles in the 1991 dacitic magma of Mount Pinatubo. In: Newhall CG, Punongbayan RS (eds) *Fire and Mud: Eruptions and lahars of Mount Pinatubo, Philippines*. University of Washington Press, Seattle and London, 1126p.
- Saar MO, Manga M (1999). Permeability-porosity relationship in vesicular basalts. *Geophys. Res. Lett.* 26: 111-114
- Sable JE, Houghton BF, Wilson CJN, Carey RJ (2006) Complex proximal sedimentation from Plinian plumes: the example of Tarawera 1886. *Bull Volcanol* 69: 89-103
- Sahagian DL, and Proussevitch AA (1998) 3D Particle size distributions from 2D observations: stereology for natural applications, *J. Volcanol. Geotherm. Res.* 84: 173-196

- Saucedo R, Macías JL, Gavilanes JC, Arce JL, Komorowski JC, Gardner JE, Valdez-Moreno G (2010) Eyewitness, stratigraphy, chemistry, and eruptive dynamics of the 1913 Plinian eruption of Volcán de Colima, México. *J. Volcanol. Geotherm. Res.* 191: 149-166
- Scandone R, Cashman KV, Malone SD (2007) Magma supply, magma ascent and the style of volcanic eruptions. *Earth Planet. Sci. Lett.* 253: 513-529
- Scandone R, Malone SD (1985) Magma supply, magma discharge and readjustment of the feeding system of Mount St. Helens during 1980. *J. Volcanol. Geotherm. Res.* 23: 239-262
- Scheu B, Spieler O, Dingwell DB (2006) Dynamics of explosive volcanism at Unzen volcano: an experimental contribution. *Bull Volcanol* 69: 175-187
- Schmidt MW, Poli S (1998) Experimentally based water budgets for dehydrating slabs and consequences for arc magma generation. *Earth Planet. Sci. Lett.* 163: 361-379
- Shane P (2005) Towards a comprehensive distal andesitic tephrostratigraphic framework for New Zealand based on eruptions from Egmont volcano. *Journal of Quaternary Science* 20, 45-57.
- Shea T, Houghton BF, Gurioli L, Cashman KV, Hammer JE, Hobden BJ (2010) Textural studies of vesicles in volcanic rocks: An integrated methodology. *J. Volcanol. Geotherm. Res.* 190: 271-289
- Sherburn S and White RS (2005) Crustal seismicity in Taranaki, New Zealand using accurate hypocentres from a dense network. *Geophysical Journal International* 162, 494-506.
- Sherburn S and White RS (2006) Tectonics of the Taranaki region, New Zealand: earthquake focal mechanisms and stress axes. *N.Z.J.Geol and Geoph.* 49:269-279
- Sherburn S, White RS and Chadwick M (2006) Three-dimensional tomographic imaging of the Taranaki volcanoes, New Zealand. *Geophysical Journal International* 166, 957-969.
- Sheridan MF, Wohletz KH (1983). Hydrovolcanism: basic considerations and review. In: *Explosive Volcanism* (MF Sheridan and F Barberi Eds). *J Volcanol. Geotherm. Res.* 17: 1-29
- Sigurdsson H, Carey S, Espíndola JM (1984) The 1982 eruption of El Chichón volcano, Mexico; stratigraphy of pyroclastic deposits. *J. Volcanol. Geotherm. Res.* 23: 11-37
- Sisson TW, Layne GD (1993) H₂O in basalt and basaltic andesite glass inclusions from four subduction-related volcanoes, *Earth Planet. Sci. Lett.* 117: 619-635
- Skeet HM (1901) Mt. Egmont and the Pouakai Range. *NZ Dep. Lands Surv. Ann. Rep. 1900-1901*: 136-7.
- Song SR, Jones KW, Lindquist WB, Dowd BA, and Sahagian DL (2001) Synchrotron X-ray computed microtomography: studies on vesiculated basaltic rocks, *Bull Volcanol* 63 (4): 252-263
- Sosa-Ceballos G, Gardner JE, Siebe C, Macías JL (2012) A caldera-forming eruption ~14,100 14C yr BP at Popocatepétl volcano, México: Insights from eruption dynamics and magma mixing. *J. Volcanol. Geotherm. Res.* 213-214: 27-40
- Sparks RSJ (1978) The dynamics of bubble formation and growth in magmas: a review and analysis. *J. Volcanol. Geotherm. Res.* 3: 1-37

- Sparks RSJ (1986) The dimension and dynamics of volcanic eruption columns. *Bull Volcanol* 48: 13-15
- Sparks RSJ and Wilson L (1976) A model for the formation of ignimbrite by gravitational column collapse. *J Geol. Soc. Lond.* 132: 441-451
- Sparks RSJ, Barclay J, Jaupart C, Mader HM, Phillips JC (1994) Physical aspects of magma degassing I. Experimental and theoretical constraints on vesiculation. In: Carroll MR, Holloway JR (eds) *Volatiles in magmas*. *Rev Mineral* 30: 413-445
- Sparks RSJ, Brazier S (1982) New evidence for degassing processes during explosive eruptions. *Nature* 295: 218-220
- Sparks RSJ, Bursik M, Carey SN, Gilbert JS, Glaze LS, Sigurdsson H, Woods AW (1997) *Volcanic plumes*. Wiley, Chichester, 574 p.
- Spieler O, Dingwell DB, Alidibirov M (2004a) Magma fragmentation speed: an experimental determination. *J. Volcanol. Geotherm. Res.* 129: 109-123
- Spieler O, Kennedy B, Kueppers U, Dingwell DB, Scheu B, Taddeucci J (2004b) The fragmentation threshold of pyroclastic rocks. *Earth Planet. Sci. Lett.* 226: 139-148
- Statistics New Zealand (2013) 2013 Census: Taranaki Region. <http://www.stats.govt.nz/> Accessed 1 January 2017
- Stein D J, Spera FJ (1992) Rheology and microstructure of magmatic emulsions: theory and experiments. *J. Volcanol. Geotherm. Res.* 49: 157-174
- Stein DJ, Spera FJ (2002) Shear viscosity of rhyolite-vapor emulsions at magmatic temperatures by concentric cylinder rheometry. *J. Volcanol. Geotherm. Res.* 113: 243-58
- Stern TA (1987) Asymmetric back-arc spreading, heat flux and structure beneath the central volcanic region of New Zealand. *Earth and Planetary Science Letters* 85, 265-276.
- Stern TA, Stratford WR and Salmon ML (2006) Subduction evolution and mantle dynamics at a continental margin, Central North Island, New Zealand. *Reviews of Geophysics* 44, 1-36.
- Stewart RB, Price RC, Smith IEM (1996) Evolution of high-K arc magma, Egmont volcano, Taranaki, New Zealand: evidence from mineral chemistry. *J. Volcanol. Geotherm. Res.* 74: 275-295
- Stix J, Torres RC, Narváez LM, Cortés GP, Raigosa JA, Gómez D, Castonguay R (1997) A model of vulcanian eruptions at Galeras volcano, Colombia. *J. Volcanol. Geotherm. Res.* 77: 285-303
- Stolper EM (1982) Water in silicate glasses: An infrared spectroscopic study. *Contrib. Mineral. Petrol.* 81: 1-17
- Sugioka I, Bursik M (1995) Explosive fragmentation of erupting magma. *Nature* 373: 689-692
- Sulpizio R (2005) Three empirical methods for the calculation of distal volume of tephra-fall deposits. *J. Volcanol. Geotherm. Res.* 145 (3-4): 315-33

- Sulpizio R, Mele D, Dellino P, La Volpe L (2005) A complex, subplinian-type eruption from low-viscosity, phonolitic to tephri-phonolitic magma: the AD 472 (Pollena) eruption of Somma-Vesuvius, Italy. *Bull Volcanol* 76: 743-767
- Susuki YJ, Koyaguchi T (2012) 3-D numerical simulations of eruption column collapse: effects of vent size on pressure-balance jet/plumes. *J. Volcanol. Geotherm. Res.* 221-222: 1-13
- Symonds RB, Rose WI, Bluth GJS, Gerlach TM (1994) Volcanic-gas studies: methods, results, and applications. In: Carroll MR, Holloway JR (eds) *Volatiles in magmas*. *Rev Mineral* 30: 10-66
- Tait S, Jaupart C, and Vergnolle S (1989) Pressure, gas content and eruption periodicity of a shallow crystallizing magma chamber. *Earth Planet. Sci. Lett.* 92: 107-123
- Takeuchi S, Nakamura M (2001) Role of precursory less-viscous, mixed magma in the eruption of phenocryst-rich magma: evidence from the Hokkaido-Komagatake 1929 eruption. *Bull Volcanol* 63: 365-376
- Takeuchi S, Tomiya A, Shinohara H (2009) Degassing conditions for permeable silicic magmas: Implications from decompression experiments with constant rates. *Earth Planet. Sci. Lett.* 283 (1-4): 101-110
- Taranaki Regional Council (2013) Regional priorities and economy. <https://www.trc.govt.nz/council/> Accessed 1 January 2013
- Taylor NH (1954) Soils of the North Island of New Zealand (with map of ash showers) NZ Soil Bureau Bull 5
- Thomas RME, Sparks RSJ (1992) Cooling of tephra during fallout from eruption columns. *Bull Volcanol* 54: 542-553
- Tilling RI, Topinka L and Swanson DA (1990) The Eruptions of Mount St. Helens: Past, Present, and Future. USGS Information Publication.
- Topping WW (1971) Burrell Lapilli eruptives, Mount Egmont, New Zealand. *New Zealand Journal of Geology and Geophysics* 15, 476-490.
- Toramaru A (1989) Vesiculation process and bubble size distributions in ascending magmas with constant velocities. *J. Geophys. Res.* 94: 17523-17542
- Toramaru A (1990) Measurement of bubble-size distributions in vesiculated rocks with implications for quantitative estimation of eruption processes. *J. Volcanol. Geotherm. Res.* 43: 71-90
- Toramaru A (2006) BND (bubble number density) decompression rate meter for explosive volcanic eruptions. *J. Volcanol. Geotherm. Res.* 154: 303-316
- Turner MB (2008) Eruption cycles and magmatic processes at a reawakening volcano, Taranaki, New Zealand. PhD thesis, Massey University, Palmerston North.
- Turner MB, Bebbington MS, Cronin SJ and Stewart RB (2009) Merging eruption datasets: building an integrated Holocene eruptive record for Mt. Taranaki, New Zealand. *Bull. Volcanol.* 71: 903-918

- Turner MB, Cronin SJ, Bebbington MS, Smith IEM and Stewart RB (2011a) Relating magma composition to eruption variability at andesitic volcanoes: A case study from Mount Taranaki, New Zealand. *GSA Bulletin* 123 (9/10): 2005-2015
- Turner MB, Cronin SJ, Bebbington MS, Smith IEM and Stewart RB (2011b) Integrating records of explosive and effusive activity from proximal and distal sequences: Mt. Taranaki, New Zealand. *Quaternary International* 246: 364-373
- Turner MB, Cronin SJ, Smith IEM, Stewart RB and Neall VE (2008a) Eruption episodes and magma recharge events in andesitic systems, Mt Taranaki, New Zealand. *Journal of Volcanology and Geothermal Research* 177, 1063-1076.
- Turner MB, Cronin SJ, Stewart RB, Bebbington M and Smith IEM (2008b) Using titanomagnetite textures to elucidate volcanic eruption histories. *Geology* 36, 31[^]34.
- Varekamp JC (1993) Some remarks on volcanic vent evolution during Plinian eruptions. *J. Volcanol. Geotherm. Res.* 54: 309-318
- Venezky DY, Rutherford MJ (1997) Preeruption conditions and timing of dacite-andesite magma mixing in the 2.2 ka eruption at Mt. Ranier. *J. Geophys. Res.* 102: 20069-20086
- Villamor P and Berryman k (2001) A late Quaternary extension rate in the Taupo Volcanic Zone, New Zealand, derived from fault slip data. *NZ J. Geol. Geophys.* 44: 243-270
- Vonk AJ and Kamp PJJ (2004) Late Miocene-Early Pliocene Matamateonga Formation in eastern Taranaki Peninsula: a new 1:50,000 geological map and stratigraphic framework. In: 2004 New Zealand Petroleum Conference proceedings. Wellington Crown Minerals, Ministry of Economic Development.
- Waitt RB, Hansen VL, Sarna-Wojcicki AM, Wood SH (1981) Proximal air-fall deposits of eruptions between May 24 and August 7, 1980-stratigraphy and field sedimentology. *US Geol Surv Prof Pap* 1250: 617-628
- Walker GPL (1971) Grain-size characteristics of pyroclastic deposits. *J. Geol.* 79: 696-714
- Walker GPL (1973) Explosive Volcanic Eruptions -A new Classification Scheme. *Geologische Rundschau* 62: 431-446
- Walker GPL (1989) Spongy pahoehoe in Hawaii: a study of vesicle-distribution patterns in basalt and their significance. *Bull Volcanol* 51: 199-209
- Walker GPL, Croasdale R (1971) Two Plinian-type eruptions in The Azores. *J Geol Soc Lond* 127:17-55
- Wallace LM, Beavan J, McCaffrey R and Darby D (2004) Subduction zone coupling and tectonic block rotations in the North Island, New Zealand. *Journal of Geophysical Research-Solid Earth* 109, B12406.
- Wallace P (2001) Volcanic SO₂ emissions and the abundance and distribution of exsolved gas in magmas. *J. Volcanol. Geotherm. Res.* 108: 85-106
- Wallace P, Anderson AT (2000) Volatiles in Magmas. In: Sigurdsson H, Houghton BF, McNutt SR, Rymer H, Stix J (eds) *Encyclopedia of volcanoes*. Academic Press, San Diego, CA: 149-170

- Wallace PJ, Anderson AT (1998) Effects of eruption and lava drain back on the H₂O contents of basaltic magmas at Kilauea volcano. *Bull Volcanol* 59: 327-344
- Wallace PJ, Anderson AT, and Davis AM (1995) Quantification of pre-eruptive exsolved gas contents in silicic magmas: *Nature* 377: 612-616
- Watt SFL, Pyle DM, Tamsin AM, Martin RS, Matthews NE (2009) Fallout and distribution of volcanic ash over Argentina following the May 2008 explosive eruption of Chaitén, Chile. *J. Geophys. Res.* 114: B04207, doi:10.1029/2008JB006219
- White JDL (1991) Maar-diatreme phreatomagmatism at Hopi Buttes, Navajo Nation (Arizona), USA. *Bull Volcanol* 53: 239-258
- White JDL, Houghton BF (2006) Primary volcanoclastic rocks. *Geology* 34: 677-680
- Whitehead SJ (1976) Granulometric studies on selected tephra eruptions, North Island, New Zealand. Unpublished Honours Dissertation, Massey University, Palmerston North.
- Whitham AG, Sparks RSJ (1986) Pumice. *Bull Volcanol* 48: 209-223
- Whittington AG, Hellwig M, Behrens H, Joachim B, Stechern A, Vetere F (2009) The viscosity of hydrous dacitic liquids: implications for the rheology of evolving silicic magmas. *Bull Volcanol* 71: 185-199
- Williams SN (1983) Plinian airfall deposits of basaltic composition. *Geology* 11: 211-214
- Wilson CJN (1997) Emplacement of Taupo ignimbrite. *Nature scientific correspondence* 385: 306-307
- Wilson CJN, Houghton BF, McWilliams MO, Lanphere MA, Weaver SD, Briggs RM (1995) Volcanic and structural evolution of Taupo Volcanic Zone, New Zealand: a review. *J. Volcanol. Geotherm. Res.* 68: 1-28
- Wilson L (1972) Explosive volcanic eruptions-II: the atmospheric trajectories of pyroclasts. *Geophys J Royal Astronom Soc* 30: 381-392
- Wilson L (1976) Explosive volcanic eruptions III. Plinian eruption columns. *Geophys J Royal Astronom Soc* 45: 543-56
- Wilson L (1999) Explosive volcanic eruptions-X. The influence of pyroclast size distributions and released magma gas contents on the eruption velocities of pyroclasts and gas in Hawaiian and Plinian eruptions. *Geophys. J. Int.* 136: 609-619
- Wilson L, Sparks RSJ, Huang TC, Watkins ND (1978) The control of volcanic column heights by eruption energetics and dynamics, *J. Geophys. Res.* 83 (B4): 1829-1836
- Wilson L, Sparks RSJ, Walker GPL (1980) Explosive volcanic eruptions - IV. The control of magma properties and conduit geometry on eruption column behaviour. *Geophys J Royal Astronom Soc* 63: 117-148
- Wohletz KH (1983) Mechanisms of hydrovolcanic pyroclast formation: size, scanning electron microscopy, and experimental studies. In: *Explosive Volcanism* (MF Sheridan and F Barberi, Eds). *J. Volcanol. Geotherm. Res.* 17: 31-63.

- Wohletz KH (1986) Explosive magma-water interactions: thermodynamics, explosion mechanisms, and field studies. *Bull Volcanol* 48: 245-264
- Wohletz KH, Sheridan MF (1983) Hydrovolcanic explosions; II. Evolution of basaltic tuff rings and tuff cones: *Am. J. Sci.* 283: 385-413
- Wohletz KH, Sheridan MF, Brown WK (1989) Particle-size distributions and the sequential fragmentation/transport theory applied to volcanic ash. *J. Geophys. Res.* 94 (B11): 15703-15721
- Woods AW (1995) The dynamics of explosive volcanic eruptions. *Reviews of Geophysics* 33: 495-530
- Woods AW and Koyaguchi T (1994) Transitions between explosive and effusive eruptions of silicic magma. *Nature* 370: 641-644
- Wright HMN, Cashman KV, Rosi M, Cioni R (2007) Breadcrust bombs as indicators of Vulcanian eruption dynamics at Guagua Pichincha volcano, Ecuador. *Bull Volcanol* 69: 281-300
- Wright HMN, Roberts JJ, Cashman KV (2006) Permeability of anisotropic tube pumice: Model calculations and measurements. *Geophys. Res. Lett.* 33: L17316, doi:10.1029/2006GL027224
- Wright HMN, Weinberg RF (2009) Strain localization in vesicular magma: Implications for rheology and fragmentation. *Geology* 37: 1023-1026
- Zandomenighi D, Voltolini M, Macini L, Brun F, Dreossi D, Polacci M (2010) Quantitative analysis of X-ray microtomography images of geomaterials: Application to volcanic rocks. *Geosphere* 6 (6): 793-804
- Zernack AV, Cronin SJ, Bebbington MS, Price RC, Smith IEM, Stewart RB and Procter JN (2012b) Forecasting catastrophic stratovolcano collapse: A model based on Mount Taranaki, New Zealand. *Geology* 40 (11): 983-986
- Zernack AV, Cronin SJ, Neall VE and Procter JN (2011) A medial to distal volcanoclastic record of an andesite stratovolcano: Detailed stratigraphy of the ring-plain succession of south-west Taranaki, New Zealand. *International Journal of Earth Sciences* 100, 1936-1966.
- Zernack AV, Price RC, Smith IEM, Cronin SJ and Stewart RB (2012a) Temporal Evolution of a High-K Andesitic Magmatic System: Taranaki Volcano, New Zealand. *J. Petrol.* 53 (2): 325-363
- Zernack AV, Procter JN and Cronin SJ (2009) Sedimentary signatures of cyclic growth and destruction of stratovolcanoes: A case study from Taranaki, NZ. *Sedimentary Geology* 220, 288-305.
- Zhang YX (1999) A criterion for the fragmentation of bubbly magma based on brittle failure theory. *Nature* 402: 648-650
- Zimanowski B, Büttner R, Lorenz V, Häfele HG (1997) Fragmentation of basaltic melt in the course of explosive volcanism. *J. Geophys. Res.* 102: 803-814
- Zimanowski B, Fröhlich G, Lorenz V (1991) Quantitative experiments on phreatomagmatic explosions. *J. Volcanol. Geotherm. Res.* 48: 341-358

Chapter 2 Methodology

In this chapter, all methods that were employed to accomplish the research objectives outlined in Chapter 1 are described.

2.1 Outline

The research objectives described in Chapter 1 required the completion of the following activities:

1) Field mapping and development of a precise (mm-scale) event lithostratigraphy in accordance to the international stratigraphic code (Salvador 1994) covering the last 5000 yrs of pyroclastic deposition at Mt. Taranaki. This was used to define individual eruption units (pyroclastic falls and density currents) integrating complex eruption events and episodes (see Chapter 3).

2) Systematic sampling of bulk deposits and primary components (pumice and lithic clasts), and sampling of organic material for radiocarbon dating (see Chapters 3-5).

3) Detailed mapping and high-resolution sampling of deposits produced by five of the largest Holocene explosive eruption episodes representing diverse eruption styles (i.e. Kokowai, Upper Inglewood, Manganui-D, Kaupokonui and Burrell; see Chapters 3-5).

4) Calculation of eruptive parameters to quantify the dynamics, magnitudes and intensities of the largest eruption episodes (see Chapter 4).

4) Analyses of granulometry, componentry, whole-rock chemistry (by x-ray fluorescence), density and porosity (by envelope and gas pycnometry) to investigate about the physical and chemical properties behind the triggers and diversity of large eruption episodes (see Chapter 4).

2.2 Field methodology

A total of 112 exposures, located at ~1 and up to 42 km from the summit crater, were studied on the eastern flanks of Mt. Taranaki. Some proximal sections located at <10 km from the crater were examined by Turner et al. (2008b, 2011). Most ring-plain sections studied in previous works (Neall 1972; Whitehead 1976; Franks 1984; Alloway et al. 1995; May 2003), located on farmland at 10-24 km from the crater, and few distal exposures (e.g. northeastern coastal cliff exposures at Onaero; Alloway et al. 1995) were reinterpreted and in the majority of the cases had to be re-excavated in nearby sites. Lake and peat sediment records, recovered at 22-34.5 km from the crater and interpreted by Damaschke et al. (2017), were employed to constrain the distal distribution of fall deposits. Other ring-plain deposits and distal lake-core profiles (Neall 1972; Alloway et al. 1995, Turner et al. 2008a, 2009) were used to aid overall correlation. Some distinctive fall deposits are useful marker horizons in the proximal stratigraphic profiles, defined earlier as the Maketawa and Kaupokonui Tephra Formations (Whitehead 1976; Franks 1984); however, the proximal stratigraphy is much more intricate, such that close hand-over-hand mapping was needed to reconstruct complex pyroclastic lithofacies architecture.

On the central eastern proximal flanks of Mt. Taranaki, 3-8 m-thick pyroclastic deposits generally cap flat-topped ridges and interfluves between >100 m-deep, steep-sided valleys. The pumice-dominated deposits generally overlie 12-20 m-thick stacks of coarse lithic-rich breccias and volcaniclastic sands and gravels. On the southern, southeastern and northern volcano flanks, the uppermost pyroclastic deposits expand to 12-15 m-thickness and cap thinner massive-ash deposits, along with ubiquitous volcaniclastic gravelly sands. These uppermost pyroclastic deposits preserve an eruptive record of up to

~10 ka B.P. (Turner et al. 2011); however, at the majority of sites, <5 ka B.P. deposits are best preserved. By contrast, the western proximal flanks are covered by thick post-AD 1000 lithic breccias interpreted as BAFs and associated downslope lahar deposits (Platz et al. 2012), that overlie a thick paleosol formed within a sequence of deeply weathered medial ash (Neall 1972).

At every exposure, data of maximum pyroclastic deposit thickness and the three maximum axes of the largest five pumice and lithic clasts of the corresponding fall deposits were measured (Appendix 4.1). Thickness measurements from ring-plain deposits had the largest uncertainties caused by the effect of localized upper-deposit reworking and by deposit-modification produced by agriculture. For this reason, in ring-plain locations, the thickest – unaltered – pyroclastic deposits were considered to represent minimum deposit thicknesses.

The most detailed observations were recorded in field sedimentary logs from 25 proximal exposures (~900-1350 m-high) at 1-4 km from the crater, inside the Egmont National Park; including data of: bed thickness, geometry, contacts, sedimentary structures, sorting (using first-order field terminology of Cas et al. 2008), framework, grain-size (using terminology of White and Houghton 2006), grading and syn-depositional deformational structures, clast texture (e.g. colour, shape, crystallinity and vesicularity), and lithology/componentry (vesicular and dense-lithic juveniles and altered or accidental lithics); following schemes applied in similar types of deposits (e.g. Macias et al. 1997; Arce et al. 2003, 2005; Cioni et al. 2000, 2008; Cronin et al. 2013; Kim et al. 2014).

Descriptions were combined into a composite stratigraphic column (see Chapter 3, Fig 3.3) which approximates a theoretical maximum thickness for the whole pyroclastic,

epiclastic (i.e. sediments produced from syn- and post-eruptive remobilization [erosion, re-sedimentation and/or reworking] of pyroclastic deposits; Cas et al. 2008) and soil deposits studied, combining field thicknesses of the most representative exposures.

2.2.1 Mapping criteria

The mapping criteria in this work follows the rules of the International Stratigraphic Guide (Salvador 1994). Deposits mappable at 1:25000 scale with clear recognizable lithology, lithofacies variations and basal-and-capping boundaries were formally classified into *Formations*, subdivided in *Members*. Where the criteria for defining Formations was not achieved, deposits were only referred as individual *bed-sets* (informal equivalent to Members) constituted by single or multiple *layers* (or beds). The term “Tephra Formation” is here only referred for citation of deposits previously named and described in that way. We prefer not to use a genetic terminology for the lithostratigraphic nomenclature, considering potential lithofacies variations with distance and following the recommendations of Salvador (1994).

The upper and lower contacts of a bed-set are given by the embedding fine ash-dominated paleosols, thick medial ash deposits (mostly centimetres to tens of cm-thick deposits of moderately weathered, massive fine-medium ash), and the base and top, respectively, of deep-erosion surfaces (including paleochannels). All these features suggest quiescence periods in the eruptive deposition.

Fine-grained, mud- and sand-dominated hyperconcentrated flow deposits (mostly 10's of cm thick) may represent time breaks in the volcanic activity when they show signs of weathering and paleosol development. By contrast, debris- and hyperconcentrated-flow deposits containing abundant juvenile clasts from the underlying pyroclastic deposit

indicate only short intervals, or may represent deposits of syn-eruptive events. In addition, one 3rd order unconformity (Lucchi 2013) was identified, demarking a significant repose period represented by a surface of erosion extended in a ~10-15 km arc-sector around the eastern volcano flanks (see Chapter 3).

Following the terminology of Fisher & Schmincke (1984), each of the lithostratigraphic bed-sets analysed could be products of a definable *eruption* bounded by paleosols that suggest a significant period without eruptive activity. Thereafter, each of the layers within a bed-set, separated by sharp, gradational and/or locally mildly-erosive boundaries that suggest no evident pause in deposition (e.g. contacts given by sharp differences in grain-size, clast framework and/or bed structure), represents an *eruption unit* deposited from an individual fallout, pyroclastic density current (PDC) or a lava flow. An eruption consisting of a single eruption unit will be referred as an *eruption event*; whereas an eruption consisting of multiple eruption units will be referred as an *eruption episode*. In this latter case, each of the composing eruption units could be interpreted as the accumulation of an eruption phase.

2.3 Radiocarbon dating

Samples of charcoal from inside deposits of selected bed-sets were hand-picked and packed in aluminium foil during transportation, to carry out radiocarbon (¹⁴C) dating. In addition, sites of earlier ¹⁴C dates (e.g., Turner et al. 2008b, 2011) were reviewed where sampling sites were clearly known. Six new dates were obtained using the Accelerator Mass Spectrometer technique at the Radiocarbon Dating Laboratory of Waikato University, New Zealand (see Chapter 3, Table 3.1). Results were determined following Stuiver and Polach (1977), based on the Libby half-life of 5568 yrs with correction for

isotopic fractionation. All ages were calibrated using OxCal 4.2 (Bronk-Ramsey 2009). The southern hemisphere atmospheric curve was employed (Hogg et al. 2013). The ^{14}C dates from previous works were also calibrated in the same manner for consistency.

2.4 Granulometry and componentry

Samples of ~0.5-5 kg from each layer, and in some cases from different stratigraphic levels (base, middle and top) of every individual layer, were collected from deposits of most bed-sets at proximal type exposures, cleaned in distilled water and oven-dried for minimum 48 hours at ~45°C. In order to determine vertical granulometric variations, selected samples were dry-sieved at 0.5 pre-harvest intervals (ϕ) between -5ϕ and 4.5ϕ . The granulometric statistical parameters ($Md\phi$ and $\sigma 1$) of Inman (1952) and the sorting categories of Folk and Ward (1957) were determined for each sample by using a self-built excel spreadsheet (Appendix 2.1). In addition, fall and PDC deposits were discriminated by using the diagram of Walker (1971).

For componentry analyses, two different ϕ fractions were employed: the main coarse mode (-1ϕ to -3.5ϕ) and a secondary finer mode (commonly 0.5ϕ) from all samples processed for granulometry. In each sample, ~300-500 particles were counted and qualitatively classified into vesicular juvenile, dense (lithic) juvenile and other lithic (altered and accidental) clasts and free crystals (mostly in fine $<0\phi$ fractions). Three counts per each fraction were completed, giving errors of ~0.6-0.2 vol.%.

The vesicular juvenile clasts of each studied bed-set were qualitatively classified according to their colour, vesicularity (Houghton and Wilson 1989) and crystallinity (Cas et al. 2008) into: (1) finely (i.e. ~0.5-3 mm vesicles) to coarsely (i.e. ~3-6 mm vesicles) vesicular yellow-white, pink, grey or brown pumice; (2) dense, ~microvesicular (i.e.

often deformed vesicles only visible in the microscope) grey, dark-grey or brown pumice; (3) very-dense (i.e. firm, heavy clasts of thick-walled vesicles), finely vesicular and ~microvesicular dark-grey and dark-brown pumice (only present in deposits of the Manganui Formation; see Chapter 4); and (4) crystalline (i.e. very crystal rich, ~60 vol.% crystals) yellow-white or grey-violet pumice.

2.5 Geochemical analysis

Samples of bulk and hand-picked vesicular and dense juvenile clasts were selected from different layers and stratigraphic levels of some of the studied bed-sets to determine whole-rock major element concentrations (Appendix 4.4). Dried samples were crushed with a tungsten carbide ring mill to produce powders. The whole-sample powders were fused into disks following the Norrish fusion method (Harvey et al. 1973) with a dilution factor of 2:6 (ignited sample at 12:22 lithium tetraborate:lithium metaborate flux). The disks were analysed in triplicate using a PANalytical Axios 1 kW wavelength dispersive X-ray fluorescence (XRF) spectrometer at the University of Auckland, New Zealand. For calibration, 28 international standards analysed in triplicate were used. U.S. Geological Survey glass standard BCR-2G was analysed to provide an independent assessment of accuracy and precision. The results for BCR-2G were consistent with the reference values within <1% for elements used in this study, and replicate analyses indicated an analytical precision (2s) of <1% (mostly ~0.7%).

2.6 Density and porosity (gas pycnometry)

A total of 1542 cylinders of 10-20 mm-diameter were drilled from vesicular juvenile lapilli clasts (i.e. -4ϕ to -3ϕ) from selected bed-sets, and from dense lithics for reference (32 cylinders). Bulk densities (bulk-d) were calculated from envelope volumes (cm^3)

obtained with a Micrometrics GeoPyc 1360 envelope density analyser ($\pm 1.1\%$ reproducibility). Skeletal density (sk-d, which considers only the volume of connected pores across the sample) and solid density (solid-d, which excludes all the porosity) were acquired with a Quantachrome's gas pycnometer using pure nitrogen (N_2) as the flowing gas ($\pm 0.2\%$ reproducibility of gas flow). Five measurements per sample were performed. All the cylinders were manually crushed in a porcelain mortar (down to ~ 2 to 3ϕ) in order to perform analyses of solid-d. Total porosity (bulk-p) with average standard error $\sigma = 0.1-0.5\%$ was calculated from:

$$(2.6.1) \text{ Bulk\%} = (1 - (\text{bulk-d} / \text{solid-d})) * 100$$

following Houghton and Wilson (1989). Connected porosity (conn-p, pores accessible to N_2 gas though and interconnected pore network) and isolated porosity (iso-p, pores inaccessible to N_2 gas) were calculated from:

$$(2.6.2) \text{ Conn\%} = ((\text{envelope volume} - \text{skeletal volume}) / \text{envelope volume}) * 100$$

$$(2.6.3) \text{ Iso\%} = \text{Bulk\%} - \text{Conn\%}$$

following Klug and Cashman (1996). All density analyses were completed at Massey University, New Zealand. Corresponding data are given in Appendix 4.2.

The heterogeneity of the deposits of the different bed-sets necessitated different analytical approaches. The most complete analyses include the range of vesicular clast textures contained in every layer of a single bed-set (e.g. Upper Inglewood bed-set; see Chapters 3-4). In some cases, due to field sampling limitations (e.g. inaccessibility to complete exposures), this scale of analysis was performed in different levels (base, middle and top) of only deposits interpreted as the climactic explosive phase of an eruption (e.g. Kokowai

bed-set; see Chapters 3-4). In the cases where clast textures are relatively homogeneous (e.g. Manganui-D and Kaupokonui bed-sets; see Chapters 3-4), the analyses were performed only in different levels per layer.

2.7 Eruptive parameters

Isopach and isopleth contours were digitally drawn in ArcMap 10.1 using a natural neighbour interpolation for reference, and later on tested against contours generated from a single-segment regression combined with an ordinary kriging interpolation in a similar way than the model of Yang and Bursik (2016). For consistency, distal isopachs of <5 cm-thick were partially or fully extrapolated using a constant minimum isopach area^{1/2} ($A^{1/2}$) of $d_{0.1\text{ cm}} = 60$ and 80 km for interpolated isopach $A^{1/2}$ of $d_{5\text{ cm}} = \sim 20$ and $35\text{-}40$ km, respectively (cf. Klawonn et al. 2014). Fully extrapolated distal isopachs were assumed to have elliptical and ~circular shape factors of <1 to 1 and aspect ratios of >1 to 1, with eccentricities ($0 < \text{ellipse} < \sim 1.05$) equal to the mean eccentricity of the proximal and medial isopachs (e.g. Cioni et al. 2000; Sulpizio 2005). In the same manner, isopleths of <0.8 cm-diameter were partially extrapolated using a constant minimum isopleth $A^{1/2}$ of $d_{0.1\text{ cm}} = 15\text{-}20$ and $40\text{-}50$ km for interpolated isopleth $A^{1/2}$ of $d_{1.6\text{ cm}} = <10$ and $\sim 15\text{-}25$ km, correspondingly. Constant minimum $A^{1/2}$ values were averaged from exponential regressions (cf. Pyle 1989) of all the isopachs or isopleths interpolated (cf. Klawonn et al. 2014).

Minimum fall deposit volumes were calculated by using a suite of methods (Cole and Stephenson 1972; Fierstein and Nathenson 1992; Pyle 1989, 1995; Bonadonna et al. 1998; Legros 2000; Sulpizio 2005; Bonadonna and Costa 2012, 2013; see Chapter 4, Table 4.1) applied with data from both interpolated-extrapolated isopachs and

interpolated isopachs alone, for comparison. Minimum pyroclastic density current volumes were calculated by constraining a minimum area and average deposit thickness (e.g. Arce et al. 2005; Platz et al. 2007). Dense rock equivalent volumes (DRE vol., see Chapter 4, Table 4.2) were estimated for each layer by calculating weighted averages of bulk-d and solid-d based on vol.% of pumice and lithics, using:

$$(2.7.1) \text{ DRE vol.} = ((\text{wt. average bulk-d}) (\text{average volume})) / \text{wt. average solid-d}$$

Total eruption column heights (HT) were calculated following the methods of Carey and Sparks (1986), Sparks (1986), Pyle (1989), Sulpizio (2005) and Bonadonna and Costa (2012, 2013). The results were compared to estimate neutral buoyancy column heights (HB). Minimum, maximum and average HTs (see Chapter 4, Fig 4.11; Appendix 4.9) were determined from a normal distribution fitted to the results produced by the different methods. Mass-and-volume eruption rates (MER and Q, respectively) were calculated by the equations of Sparks (1986) and Wilson and Walker (1987):

$$(2.7.2) \text{ HT} = 1.67 ((\text{Q}) (0.259)) \text{ and}$$

$$(2.7.3) \text{ HT} = 0.236 (\text{MER}^{1/4})$$

and by graphic interpolation using Carey and Bursik (2000). Following Wilson (1976), the total erupted mass (mT) and minimum eruption duration (T) were determined by:

$$(2.7.4) \text{ mT} = \text{solid-d (DRE vol.) and}$$

$$(2.7.5) \text{ T} = \text{mT} / \text{MER}$$

The eruptive magnitude was estimated following Pyle (2000) by:

$$(2.7.6) \text{ M} = \text{Log}_{10} (\text{mT}) - 7$$

The eruption columns were classified according to Pyle (1989, 1995) by calculating the half distance of both the maximum clasts extrapolated from the isopleth data (bc) and the maximum thickness extrapolated from the isopachs (bt), and by estimating the dispersal area (D) inside the 0.01 Thickness-maximum isopach (0.01Tmax) of Walker (1973). The classification of Bonadonna and Costa (2013) based on Weibull-function parameters derived for both thinning rates of deposits (λ_{th}) and decreasing rates of grain-size (λ_{ML}) was also employed (see Chapter 4, Fig 4.11; Appendix 4.9).

2.8 References

- Alloway B, Neall VE, Vucetich CG (1995) Late Quaternary (post 28,000 years B.P.) tephrostratigraphy of northeast and central Taranaki, New Zealand. *J Royal Soc NZ* 25:385-458
- Arce JL, Cervantes KE, Macías JL, Mora JC (2005) The 12.1 ka Middle Toluca Pumice: A dacitic Plinian–subplinian eruption of Nevado de Toluca in Central Mexico. *J Volcanol Geotherm Res* 147:125-143
- Arce JL, Macias JL, Vazquez-Selem L (2003) The 10.5 ka Plinian eruption of Nevado de Toluca volcano, Mexico: Stratigraphy and hazard implications. *Geol Soc Am Bull* 115:230-248
- Bonadonna C, Costa A (2012) Estimating the volume of tephra deposits: a new simple strategy. *Geology* G32769-1
- Bonadonna C, Costa A (2013) Plume height, volume, and classification of explosive volcanic eruptions based on the Weibull function. *Bull Volcanol* 75(8):1-19
- Bonadonna C, Ernst GGJ, Sparks RSJ (1998) Thickness variations and volume estimates of tephra fall deposits: the importance of particle Reynolds number. *J Volcanol Geotherm Res* 81:173-187
- Bronk-Ramsey C (2009) Bayesian analysis of Radiocarbon dates. *Radiocarbon* 51(1):337–360
- Carey S, Bursik M (2000) Volcanic plumes. In: Sigurdsson H, Houghton BF, McNutt SR, Rymer H, Stix J (eds) *Encyclopedia of volcanoes*. Academic Press, San Diego, CA: 527-544
- Carey S, Sparks RSJ (1986) Quantitative models of the fall and dispersal of tephra from volcanic eruption columns. *Bull Volcanol* 48:109-125
- Cas R, Porritt L, Pittari A, Hayman P (2008) A new approach to kimberlite facies terminology using a revised general approach to the nomenclature of all volcanic rocks and deposits: Descriptive to genetic. *J Volcanol Geotherm Res* 174:226-240
- Cioni R, Bertagnini A, Santacroce R, Andronico D (2008) Explosive activity and eruption scenarios at Somma-Vesuvius (Italy): Towards a new classification scheme. *J Volcanol Geotherm Res* 178:331-346

- Cioni R, Marianelli P, Stantacroe R, Sbrana A (2000) Plinian and subplinian eruptions. In: Sigurdsson H, Houghton BF, McNutt SR, Rymer H, Stix J (eds) *Encyclopedia of Volcanoes*. Academic Press, San Diego, pp:477-494
- Cole JW, Stephenson TM (1972) Calculation of the volume of a tephra deposit. In: Cole JW (Ed) *Distribution of high alumina basalts in the Taupo Volcanic Zone*. Geology Department, Victoria University of Wellington, vol.1, 13-15
- Cronin SJ, Lube G, Dayudi DS et al (2013) Insights into the October-November 2010 Gunung Merapi eruption (Central Java, Indonesia) from the stratigraphy, volume and characteristics of its pyroclastic deposits. *J Volcanol Geoth Res* 261:244-259
- Damaschke M, Cronin S, Holt K, Bebbington M, Hogg A (2017) A 30,000-year high-precision eruption history for the andesitic Mt Taranaki, North Island, New Zealand. *Quaternary Res*, 1–23. DOI:10.1017/qua.2016.11
- Fierstein J, Nathenson M (1992) Another look at the calculation of fallout tephra volumes. *Bull Volcanol* 54:156-167
- Fisher R, Schmincke HU (1984) *Pyroclastic Rocks*, Springer-Verlag, Berlin. 472 pp
- Folk RL, Ward WC (1957) Brazos River bar: a study in the significance of grain size parameters. *J Sedimentary Res* 27(1)
- Franks AM (1984) *Soils of Eltham County and the tephrochronology of central Taranaki*. Dissertation, Massey University, Palmerston North, New Zealand
- Harvey PK, Taylor DM, Hendry RD, Bancroft F (1973) An accurate fusion method for the analysis of rocks and chemically related materials by X-ray fluorescence spectrometry. *X-ray Spectrom* 2:33-34
- Hogg AG, Hua Q, Blackwell PG et al (2013) SHCAL13 Southern hemisphere calibration, 0-50,000 years cal BP. *Radiocarbon* 55(4):1889-1903.
- Houghton BF, Wilson CJN (1989) Vesicularity index for pyroclastic deposits. *Bull Volcanol* 51:451-462
- Inman DL (1952) Measures for describing the size distribution of sediments. *J Sedimentary Res* 22(3)
- Kim GB, Cronin SJ, Yoon WS, Sohn YK (2014) Post 19 ka B.P. eruptive history of Ulleung Island, Korea, inferred from an intra-caldera pyroclastic sequence. *Bull Volcanol* 76:802. doi 10.1007/s00445-014-0802-1
- Klawonn M, Houghton BF, Swanson DA et al (2014) From field data to volumes: constraining uncertainties in pyroclastic eruption parameters. *Bull Volcanol* 76(7):1-16
- Klug C, Cashman KV (1996) Permeability development in vesiculating magmas: implications for fragmentation. *Bull Volcanol* 58:87-100
- Legros F (2000) Minimum volumen of a tephra fallout deposit estimated from a single isopach. *J Volcanol Geotherm Res* 96:25-32
- Lucchi F (2013) Stratigraphic methodology for the geological mapping of volcanic areas: insights from the Aeolian archipelago (southern Italy). *Geological Society, London, Memoirs* 37:35-53

- Macias JL, Sheridan MF, Espindola JM (1997) Reappraisal of the 1982 eruptions of El Chichón Volcano, Chiapas, Mexico: new data from proximal deposits. *Bull Volcanol* 58:459-471
- May DJ (2003) The correlation of recent tephra with lava flows on Egmont volcano, Taranaki, New Zealand using evidence of mineral chemistry. Dissertation, University of Auckland, Auckland, New Zealand
- Neall VE (1972) Tephrochronology and tephrostratigraphy of western Taranaki (N108-109), New Zealand. *NZ J Geol Geoph* 15:507-557
- Platz T, Cronin SJ, Cashman KV et al (2007) Transitions from effusive to explosive phases in andesite eruptions-A case-study from the AD 1655 eruption of Mt. Taranaki, New Zealand. *J Volcanol Geoth Res* 161:15-34
- Platz T, Cronin SJ, Procter JN et al (2012) Non-explosive dome-forming eruptions at Mt. Taranaki, New Zealand. *Geomorphology* 136:15-30
- Pyle DM (1989) The thickness, volume and grainsize of tephra fall deposits. *Bull Volcanol* 51:1-15
- Pyle DM (1995) Assessment of the minimum volume of tephra fall deposits. *J Volcanol Geotherm Res* 69(3):379-382
- Pyle DM (2000) Sizes of volcanic eruptions. In: Sigurdsson H, Houghton BF, McNutt SR, Rymer H, Stix J (eds) *Encyclopedia of volcanoes*. Academic Press, San Diego, CA: 263-269
- Salvador A (1994) *International stratigraphic guide. A guide to stratigraphic classification, terminology and procedure*, 2nd ed. Subcommittee of Stratigraphic Classification of IUGS International Commission on Stratigraphy and Geological Society of America. Boulder, Colorado, 214 pp
- Sparks RSJ (1986) The dimension and dynamics of volcanic eruption columns. *Bull Volcanol* 48:13-15
- Stuiver M, Polach HA (1977) Discussion: Reporting of ¹⁴C data. *Radiocarbon* 19:355-63
- Sulpizio R (2005) Three empirical methods for the calculation of distal volume of tephra-fall deposits. *J Volcanol Geotherm Res* 145(3-4):315-33
- Turner MB, Bebbington MS, Cronin SJ, Stewart RB (2009) Merging eruption datasets: building an integrated Holocene eruptive record for Mt. Taranaki, New Zealand. *Bull. Volcanol.* 71:903-918
- Turner MB, Cronin SJ, Bebbington MS et al (2011) Integrating records of explosive and effusive activity from proximal and distal sequences: Mt. Taranaki, New Zealand. *Quaternary Intl* 246:364-373
- Turner MB, Cronin SJ, Bebbington MS, Platz T (2008a) Developing probabilistic eruption forecasts for dormant volcanoes: a case study from Mt Taranaki, New Zealand. *Bull Volcanol* 70:507-515
- Turner MB, Cronin SJ, Smith IEM et al (2008b) Eruption episodes and magma recharge events in andesitic systems, Mt Taranaki, New Zealand. *J Volcanol Geoth Res* 177:1063-1076
- Walker GPL (1971) Grain-size characteristics of pyroclastic deposits. *J. Geol.* 79: 696-714
- Walker GPL (1973) Explosive Volcanic Eruptions -A new Classification Scheme. *Geologische Rundschau* 62: 431-446

White JDL, Houghton BF (2006) Primary volcaniclastic rocks. *Geology* 34:677-680

Whitehead SJ (1976) Granulometric studies on selected tephra eruptions, North Island, New Zealand. Dissertation, Massey University, Palmerston North, New Zealand

Wilson L (1976) Explosive volcanic eruptions III. Plinian eruption columns. *Geophys J Res Astron Soc* 45:543-56

Wilson L, Walker GPL (1987) Explosive volcanic eruptions VI. Ejecta dispersal in plinian eruptions: the control of eruption conditions and atmospheric properties. *Geophys J Res Astron Soc* 89:657-679

Yang Q, Bursik M (2016) A new interpolation method to model thickness, isopachs, extent, and volume of tephra fall deposits. *Bull Volcanol* 78(10):68

Chapter 3 New Holocene eruption episodes from proximal deposit sequences

This chapter contains the backbone lithostratigraphy and correlation of Holocene proximal pyroclastic deposits at Mt. Taranaki. The interpretation of deposits provides the definition of individual eruption units (pyroclastic falls and density currents) produced by different eruption events and episodes.

Chapter 3 comprises the full version of a published journal paper. Its format has been modified to match the overall thesis.

Title New insights into Holocene eruption episodes from proximal deposit sequences at Mt. Taranaki (Egmont), New Zealand.

Authors Rafael Torres-Orozco, Shane J. Cronin, Natalia Pardo, Alan S. Palmer.

Status published in *Bulletin of Volcanology* (2017) 79:3, doi: 10.1007/s00445-016-1085-5

Principal author Rafael Torres-Orozco

Carried out

- field descriptions, mapping and sampling,
- laboratory preparation of samples,
- manuscript and figures preparation, writing and submission.

Co-authors Shane J. Cronin, Natalia Pardo and Alan S. Palmer

Aided the study by

- discussing results,
- reviewing and commenting the manuscript.

3.1 Abstract

Upper stratovolcano flanks contain the most nuanced depositional record of long eruption episodes, but steep, irregular terrain makes these sequences difficult to correlate and interpret. This necessitates development of a detailed and systematic approach to describing localised depositional facies and relating these to eruptive processes. In this work, the late-Holocene eruption history of Mt. Taranaki/Egmont, New Zealand, was reassessed based on study of proximal deposits spanning the ^{14}C -dated age range of ~5.0-0.3 cal ka B.P. Mt. Taranaki is a textbook-example stratovolcano, with geological evidence pointing to sudden switches in scale, type and frequency of eruptions over its ~130 kyr history. The proximal stratigraphy presented here almost doubles the number of eruptions recognised from previous soil-stratigraphy studies. A total of 53 lithostratigraphic bed-sets record eruptions of the summit crater and parasitic vents like Fanthams Peak (the latter between ~3.0-1.5 cal ka B.P.). At least 12 of the eruptions represented by these bed-sets comprise deposits comparable to or thicker than those of the latest sub-Plinian eruption of AD 1655. The largest eruption episode represented is the 4.6-4.7 cal. ka B.P. Kokowai. Contrasting eruption styles were identified, from stable basaltic-andesite eruption columns at Fanthams Peak, to andesitic lava-dome extrusion, blasts and partial collapse of unstable eruption columns at Mt. Taranaki's summit. The cm-scale proximal deposit descriptions were used to identify several previously unknown, smaller eruption events. These details are indispensable for building a comprehensive probabilistic event record and in the development of realistic eruptive scenarios for complex eruption episodes prior to reawakening of a volcano.

3.2 Introduction

Andesitic stratovolcanoes have generated some of the most disruptive and deadliest Plinian and sub-Plinian historical eruptions (e.g. Bourdier et al. 1997; Coltelli et al. 1998; Cioni et al. 2000; Carn et al. 2009; Saucedo et al. 2010; Surono et al. 2012; Cronin et al. 2013). Ongoing population growth on the fertile ring-plains and debris fans surrounding active volcanoes constantly exacerbates vulnerability to volcanic activity (e.g. Alberico et al. 2011; Cronin et al. 2013). Within increasing populations at risk, there is a need to develop the most comprehensive eruptive frameworks possible prior to re-awakening of andesitic volcanoes, in order to develop high-precision hazard assessments and scenarios that encompass diverse paths of progression that an eruption sequence might follow.

In many past studies, eruption histories have been inferred from investigations of medial and distal deposits in locations where undisturbed deposits in low-relief depositional environments allow accurate sedimentological determinations (e.g. Pardo et al. 2012a, b) and regional tephrostratigraphic reconstructions (e.g. Neall 1972; Alloway et al. 1995; Andreastuti et al. 2000). There are, however, limitations of medial-distal volcanic records, particularly in humid tropical or temperate environments where rapid weathering and soil formation, along with vegetation, obscures and modifies primary deposits, hindering detailed volcanological interpretation (e.g. Alloway et al. 1995; Espindola et al. 2010; Saucedo et al. 2010; Avellan et al. 2014). Moreover, the medial pyroclastic/volcaniclastic data sets could be biased towards events that produce widely dispersed fallouts, i.e., mainly large-volume and highly explosive events. Also, medial deposits usually provide little detail of the progression of any eruption (i.e., opening, pre-, syn- and post-climactic phases), and they certainly do not represent all eruptions (e.g., lavas don't reach the medial environment). For this reason, it is often difficult to develop detailed eruption scenarios,

of a clear understanding of the physical processes involved (cf. Houghton et al. 2004; Platz et al. 2007; Cioni et al. 2008).

Proximal pyroclastic sequences, while challenging to access, may contain a more complete and less-modified record of eruptive episodes than do more-distal sites. Their main limitation is that they normally preserve only the youngest part of the geological record due to remobilization and burying of older deposits by e.g., repeated cone collapse and lava flow deposition, in addition to other erosive processes (e.g. fluvial, mass-movement and eolian). Despite this, many interfluvial and ridge areas contain well-preserved deposit sequences that may represent most, or even all, of the phases of an ancient eruption (e.g. Macias et al. 1997; Houghton et al. 2004; Arce et al. 2003, 2005; Platz et al. 2007, 2012; Cronin et al. 2013; Avellan et al. 2014; Kim et al. 2014) and consequently may provide the foundation for understanding the potential pre-eruptive, opening, syn- and post-eruptive phases of a future eruption episode (e.g. Cioni et al. 2008).

The andesitic stratovolcano Mt. Taranaki (in the western part of the North Island of New Zealand) has produced several large, explosive eruptions and frequent mildly-explosive activity since 5 ka, as seen primarily from ring-plain records and studies of isolated deposits from single events in proximal sites (Alloway et al. 1995; Platz et al. 2007; Turner et al. 2008a, b). Past studies of ring-plain deposits included lapilli fall beds contained within soils, together with interbedded debris-flow and debris-avalanche deposits (e.g. Zernack et al. 2009, 2011). These were used to set up a Tephra Formation-based stratigraphic framework (Neall 1972; Alloway et al. 1995), and an understanding of major periods of cone growth and cone collapse. Apart from good information about fall-deposit distribution, the available stratigraphic data lack the detail needed for precise

volcanological assessment, and many of the lateral correlations are tentative because they are based primarily on stratigraphic proximity and similar lapilli features (colour, grainsize, shape etc.). A parallel set of studies has focussed on the radiocarbon dating of volcanic deposits (mainly fall deposits) in swamp and lake sediments. This provided the event data for forecasting eruption frequencies and magmatic evolution paths, suggesting a probability of 0.52 for an eruption over the next 50 years from Mt. Taranaki (Turner et al. 2008a, 2009, 2011a).

In this work, we aim to refine and expand knowledge of the late-Holocene eruption history of Mt. Taranaki/Egmont, New Zealand, based on detailed analysis of proximal pyroclastic sequences, particularly concentrating on bed, contact and sedimentological features (cf. Arce et al. 2003, 2005; Cronin et al. 2013; Kim et al. 2014). We use these data to fill the gaps between the distal lake- and swamp-core deposits and the sparse tephra within medial soils, and to build a strong geological framework for understanding the opening and closing phases of typical explosive andesitic eruptions. The complex suite of deposits necessitated development of a hierarchical framework for description of the deposits and of the parental eruptions and processes that generated them. This approach can be broadly applied to any pyroclastic sequence, but is especially valuable in proximal deposit sequences where a wide variety of deposits may represent emplacement periods from seconds to a few years.

3.3 Geological setting and previous work

The North Island of New Zealand lies along the convergent boundary between the Australian and Pacific Plates, with the latter being subducted along the Hikurangi Trough

(HT; Henrys et al. 2003; Fig 3.1). This subduction system is associated with the NNE-SSE aligned Taupo Volcanic Zone (TVZ; Wilson et al. 1995), located ~280 km to the

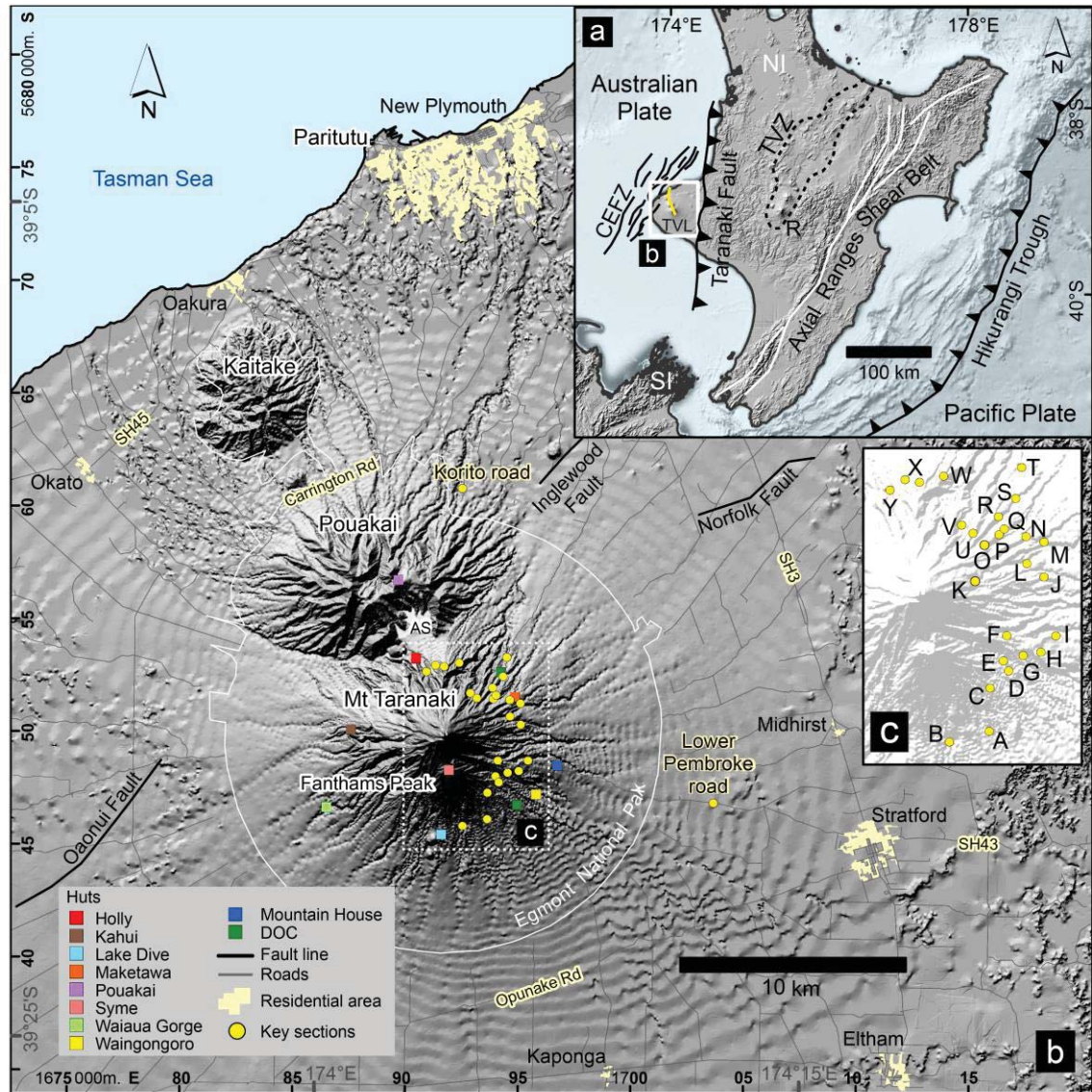


Fig 3.1 **a** Tectonic setting of the North Island (NI) of New Zealand (modified from King and Thrasher 1996; Henrys et al. 2003; Price et al. 2005; Platz et al. 2007). *CEFZ* Cape Egmont Fault Zone, *R* Mount Ruapehu, *SI* South Island, *TVL* Taranaki Volcanic Lineament (yellow line), *TVZ* Taupo Volcanic Zone. **b** Zoomed area of the Taranaki Volcanic Lineament (Neall 1979); which comprises four Pleistocene-Holocene, southwards-younging andesitic volcanoes or their eroded volcanic edifice-remnants: Paritutu, Kaitake, Pouakai and Mt. Taranaki (along with the parasitic cone of Fanthams Peak). *AS* Ahukawakawa swamp, *DOC* Department of Conservation visitor centre, *SH* principal state highways and other roads connecting residential areas. **c** Zoomed area of the proximal eastern flanks of Mt. Taranaki and the studied key sections. Coordinate system: NZGD 2000 New Zealand Transverse Mercator.

west of the HT and dominated by rhyolitic volcanoes in the central portion (Fig 3.1); but also with the andesitic volcanism produced at the northern and southern extremities of the TVZ (e.g. Mt. Ruapehu), and with the most westerly andesitic volcanism in the North Island (e.g. Mt. Taranaki; Price et al. 2005; Fig 3.1).

About 400 km to the west of the HT, 130 km from the TVZ, lies the Quaternary and NNW-SSE trending Taranaki Volcanic Lineament (TVL; Neall 1979; Fig 3.1) over the eastern side of the mid-Cretaceous to present-day extensional and NE-SW trending Cape Egmont Fault Zone (King and Thrasher, 1996). The TVL is made up of four high-K hornblende-rich andesitic volcanoes, <1750 ka B.P. and younging to the south (i.e. Paritutu, Kaitake, Pouakai and Mt. Taranaki; Price et al. 2005; Fig 3.1), that contrast in mineralogy with two-pyroxene andesitic products being produced concurrently in the southern TVZ. Volcanic products of the TVL cover the entire ~1500 km² Taranaki Peninsula and cap mid-Palaeozoic to mid-Cretaceous plutonic rocks of the Median Tectonic Zone (Mortimer et al. 1997) and a 6-9 km thick early to mid-Cretaceous sequence of oil- and gas-rich sediments of the Taranaki Basin (King and Thrasher 1996).

Mt. Taranaki/Egmont is the youngest volcano in the extreme south of the TVL with a known eruption record spanning ~130 ka B.P. to AD 1800 (Alloway et al. 2005; Zernack et al. 2011; Platz et al. 2012; Fig 3.1). It comprises a 2518 m-high upper cone with a basal area of 25 km² and ~12 km³ in volume, surrounded by a 1000 km² ring plain of volcanoclastic debris, which is up to 150 km³ in volume (Neall et al. 1986; Zernack et al. 2011). The edifice above ~1400 m is considerably younger than the ring plain, with past cones having been repeatedly destroyed by at least 12 massive debris avalanches since ~130 ka. The latest, and one of the smallest, collapses was at ~7.5 ka B.P. (i.e. Opuia Formation; Neall 1979; Zernack et al. 2011). On the volcano, lava flows of the ~8 ka B.P.

Warwicks Castle Group (Neall 1979; Stewart et al. 1996) constitute the core of the present-day volcanic edifice. The western side of the crater rim likely collapsed in a series of eruptions over the last 800 years (Procter et al. 2010), and remnants of the AD 1800 Sisters dome make up the present summit inside the crater (Platz et al. 2012). The symmetry of the volcano is broken in the southeast by the 1962 m-high, basaltic and basalt-andesitic parasitic cone of Fanthams Peak (Stewart et al. 1996; Fig 3.1). Due to the splitting of the Opuā Debris avalanche deposit, Fanthams Peak is postulated to have existed before 7 ka B.P. (Neall 1979), but only eruptions since ~3.3 ka B.P., continuing until ~1.8 ka B.P. from this vent have been confirmed (Whitehead 1976; Turner et al. 2008b).

The volcanic history of Mt. Taranaki is characterised by cycles of cone growth to a critical height/size, followed by a catastrophic edifice collapse (Neall et al. 1986; Zernack et al. 2009, 2011). Cone growth includes effusive, lava and dome-forming volcanism, intercalated with periods of highly explosive, Plinian to sub-Plinian eruptions on average 300-500 year intervals; and smaller, Strombolian or Vulcanian-style eruptions on intervals of ~50-80 years (Alloway et al. 1995; Platz et al. 2007; Turner et al. 2011a). Many of the pyroclastic fall deposits over the last ~30 ka B.P. were mapped northeast and southeast of the volcano within 20 “Tephra Formations” (Neall 1972; Alloway et al. 1995, 2005). Some of the largest known explosive eruptions in Mt. Taranaki’s history are recorded by fall deposits dated to within the last 5 ka B.P. and distributed generally east of the volcano, including: the ~5-4.5 ka B.P. Tariki, ~4.1 ka B.P. Korito, ~3.6 ka B.P. Inglewood, and ~3.3-2.9 ka B.P. Manganui tephra (Whitehead 1976; Alloway et al. 1995). Some of the youngest fall deposits, e.g. the ~1.5-1.3 ka B.P. Kaupokonui Tephra (Neall and Jansen 1984), were deposited concurrently with ~1.6-1.3 ka B.P. lava flows

(Stewart et al. 1996; Neall 2003). In addition to such explosive vents, lava domes also erupted on the northern and southern volcano flanks during the last ~7 ka (Neall et al. 1986; Platz et al. 2012).

The most recent volcanism includes the 0.8-0.4 ka B.P. summit lavas (Downey et al. 1994) that shape most of the present-day upper cone and, at least, six dome-growth and collapse phases recorded by block-and-ash flows (BAFs) and related surge units. These PDC deposits are exposed in proximal areas, mostly on the western flanks (Platz et al. 2012), associated with the Newall, Waiweranui and Puniho ash deposits (Druce 1966; Neall 1972).

The most recent sub-Plinian eruption produced the AD 1655 Burrell Lapilli (Druce 1966; Neall 1972; Topping 1971), $3 \times 10^6 \text{ m}^3$ of pyroclastic density current deposits and $3.2 \times 10^8 \text{ m}^3$ of fall deposits from a ~14 km-high eruption column (Platz et al. 2007). It was followed by AD 1800-1755 effusive and small explosive events producing the Taururangi Ash (Druce 1966; Neall 1972), then finally the Sisters dome (Platz et al. 2012).

3.4 Methodology

3.4.1 Field methodology

Twenty-five proximal exposures (~900-1350 m-high) were studied around Mt. Taranaki, inside the Egmont National Park and within ~1-4 km of the summit (Figs 3.1-3.2). Some of these sections were examined by Turner et al. (2008b, 2011a). On the central eastern flanks of Mt. Taranaki, 3-8 m-thick pyroclastic deposits generally cap flat-topped ridges and interfluvies between >100 m-deep, steep-sided valleys. The pumice-dominated deposits generally overlie 12-20 m-thick stacks of coarse lithic-rich breccias and volcani

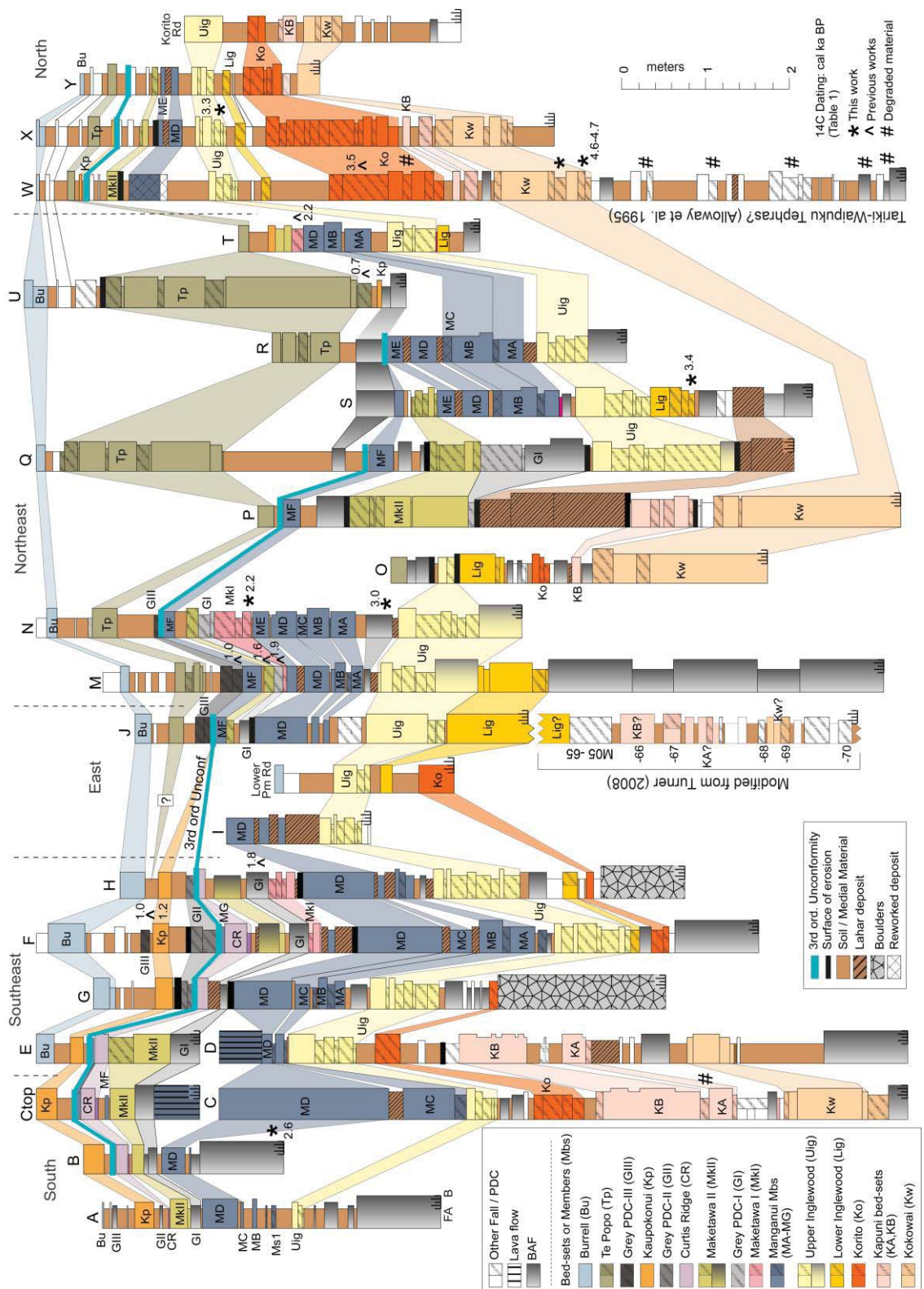
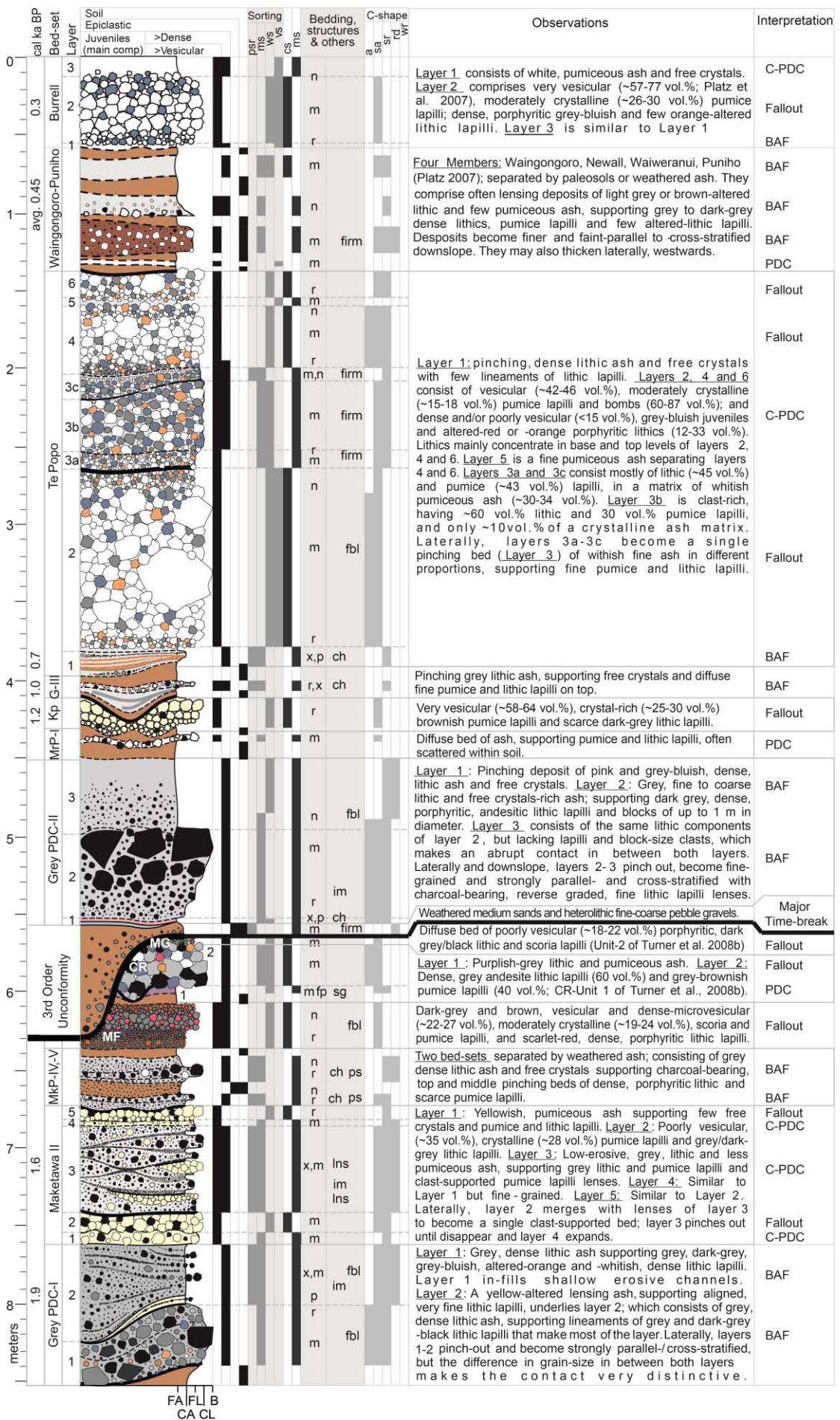


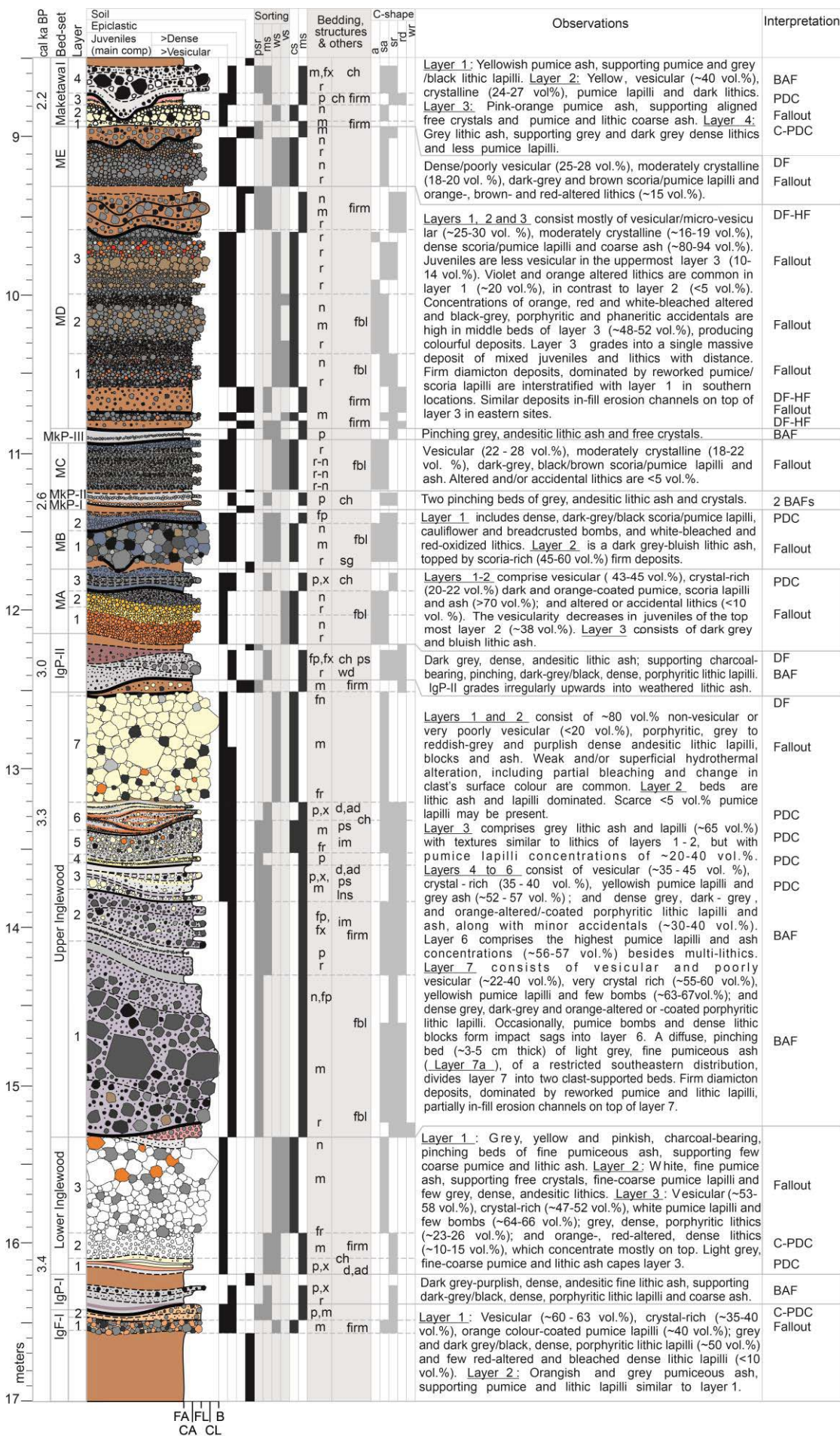
Fig 3.2 Stratigraphic correlation of the late-Holocene pyroclastic sequence studied in proximal sections on the eastern flanks of Mt. Taranaki.

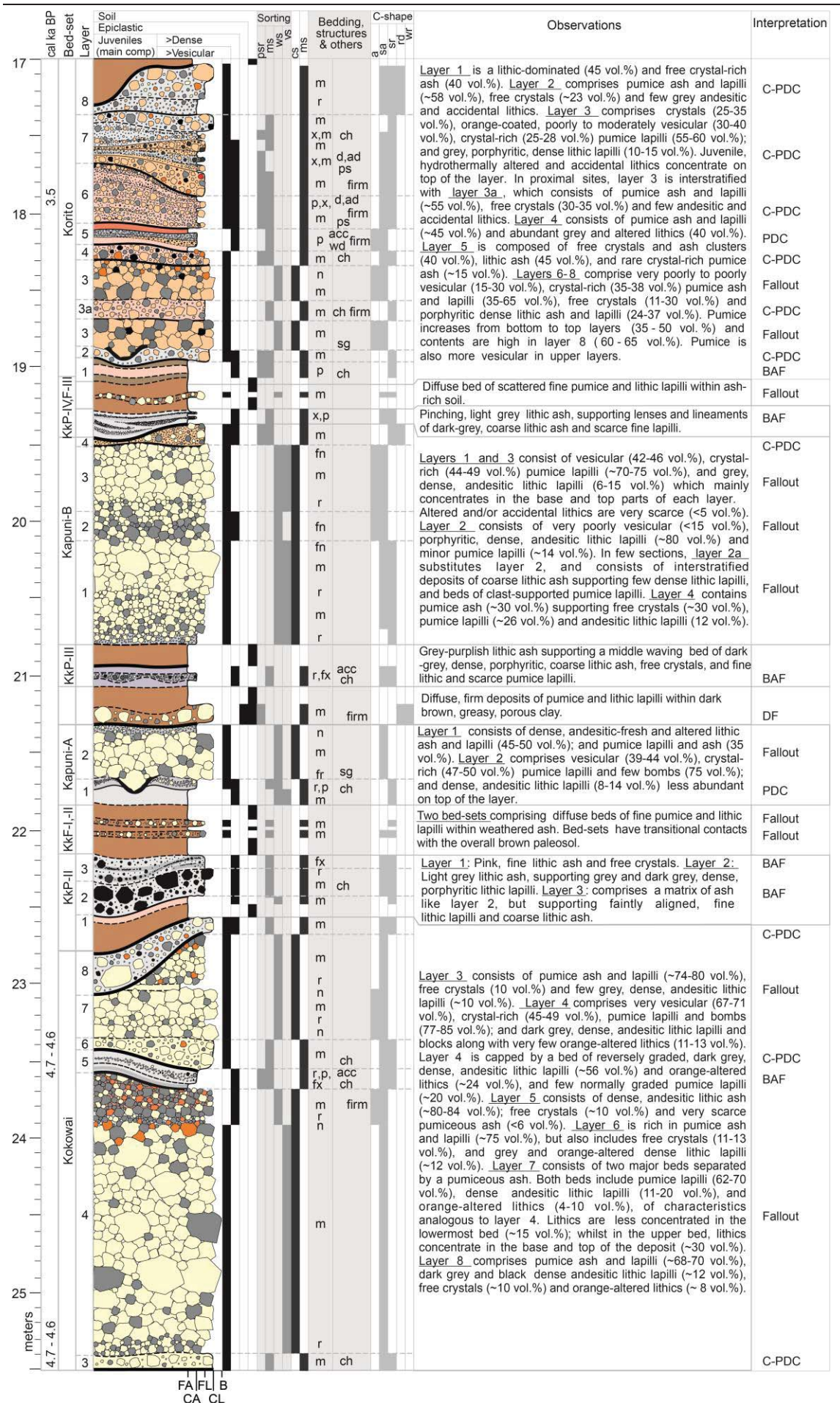
clastic sands and gravels. On the southern, southeastern and northern volcano flanks, the uppermost pyroclastic deposits expand to 12-15 m-thickness and cap thinner massive-ash deposits, along with ubiquitous volcanoclastic gravelly sands. These uppermost pyroclastic deposits preserve an eruptive record of up to ~10 ka B.P. (Turner et al. 2011a); however, at the majority of sites, <5 ka B.P. deposits are best preserved. By contrast, the western flanks are covered by thick post-AD 1000 lithic breccias interpreted as BAFs and associated downslope lahar deposits (Platz et al. 2012), that overlie a thick paleosol formed within a sequence of deeply weathered medial ash (Neall 1972).

Some distinctive fall deposits are useful marker horizons in the studied stratigraphic profiles, defined earlier as the Maketawa and Kaupokonui Tephra Formations (Whitehead 1976; Franks 1984; Fig 3.2). Medial ring-plain deposits and distal lake-core profiles (Neall 1972; Alloway et al. 1995, Turner et al. 2008a, 2009) were used to aid overall correlation; however, the proximal stratigraphy is much more intricate, such that close hand-over-hand mapping was needed to reconstruct complex pyroclastic lithofacies architecture.

At each flank exposure, field sedimentary logs were recorded, including data of: bed thickness, geometry, contacts, sedimentary structures, sorting (using first-order field sorting classes of Cas et al. 2008), framework, grain-size (using terminology of White and Houghton 2006), grading and syn-depositional deformational structures, clast texture (e.g. colour, shape, crystallinity and vesicularity), and lithology/componentry (vesicular and dense-lithic juveniles and altered or accidental lithics); following schemes applied in similar types of deposits (e.g. Macias et al. 1997; Arce et al. 2003, 2005; Cioni et al. 2000, 2008; Cronin et al. 2013; Kim et al. 2014). Detailed descriptions were combined into a composite stratigraphic column (Fig 3.3) which approximates a theoretical maximum







FA | FL | B
CA | CL

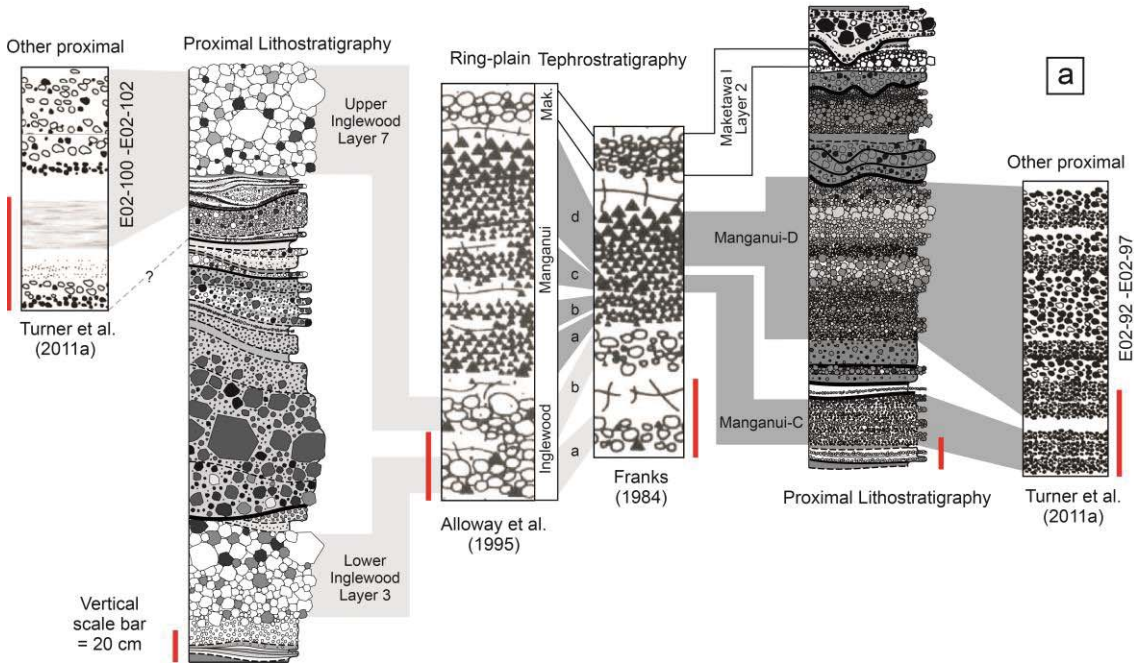
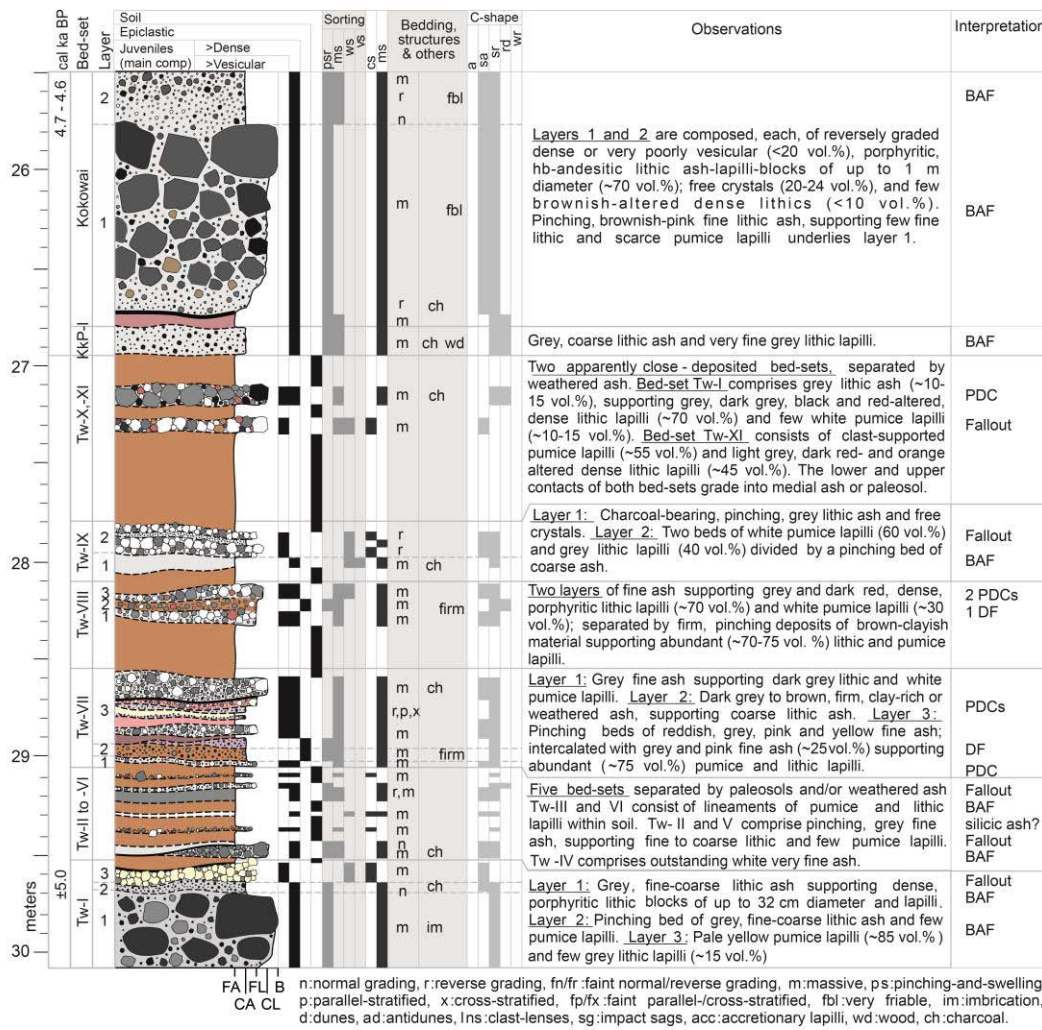


Fig 3.3 Composite stratigraphic log of the late-Holocene proximal pyroclastic sequence of Mt. Taranaki. Members of the Manganui Formation (i.e. Manganui-A to G) are abbreviated: *MA*...*MG*. *CR* Curtis Ridge Lapilli bed-set (Turner et al. 2008b). Main juvenile pyroclasts are indicated (dense-vesicular). Solid lines indicate sharp contacts; bold solid lines indicate sharp-erosive (often angular) contacts; dashed lines indicate transitional contacts. Grain-size simplified from White and Houghton (2006): *FA* Fine-ash, *CA* Coarse-ash, *FL* Fine-lapilli, *CL* Coarse-lapilli, *B* Blocks/Bombs. Sorting: poor (psr), moderate (ms), well (ws) and very well sorting (vs) from Cas et al. (2008). Clast (cs) and matrix-support (ms) framework, and angular (a), sub-angular (sa), sub-rounded (sr), rounded (rd) and well-rounded (wr) clast-shape are indicated. *DF* Debris-Flow, *C-PDC* Column-collapse Pyroclastic Density Current, *BAF* Block-and-Ash Flow, *PDC* Undefined Pyroclastic Density Current. a Comparison of a segment from the previous ring-plain and distal tephrostratigraphy with the equivalent proximal lithostratigraphy of this work and a few earlier studies. See text and Table 1 for ^{14}C age references.

thickness for the whole pyroclastic, epiclastic (i.e. sediments produced from syn- and post-eruptive remobilization [erosion, resedimentation and/or reworking] of pyroclastic deposits; Cas et al. 2008) and soil deposits studied, combining field thicknesses of the most representative exposures.

3.4.2 Mapping criteria

Deposits mappable at 1:25000 scale with clear recognizable lithology, lithofacies variations and basal-and-capping boundaries were formally classified into *Formations*, subdivided in *Members*, according to the rules of the International Stratigraphic Guide (Salvador, 1994). Member is the formal name for a *bed-set* within a defined Formation. However, in most cases, the criteria for defining Formations was not achieved, and deposits were only referred as individual bed-sets constituted by single or multiple *layers*.

The term “Tephra Formation” is here only referred for citation of deposits previously named and described in that way. We prefer not to use a genetic terminology for the

lithostratigraphic nomenclature, considering potential lithofacies variations with distance and following the recommendations of Salvador (1994).

The upper and lower contacts of a bed-set are given by the embedding fine ash-dominated paleosols, thick medial ash deposits (mostly centimetres to tens of cm-thick deposits of moderately weathered, massive fine-medium ash), and the base and top, respectively, of deep-erosion surfaces (including paleochannels). All these features suggest quiescence periods in the eruptive deposition.

Fine-grained, mud- and sand-dominated hyperconcentrated flow deposits (mostly 10's of cm thick) may represent time breaks in the volcanic activity when they show signs of weathering and paleosol development. By contrast, debris- and hyperconcentrated-flow deposits containing abundant juvenile clasts from the underlying pyroclastic deposit indicate only short intervals, or may represent deposits of syn-eruptive events. In addition, one 3rd order unconformity was identified (Fig 3.2), demarking a significant repose period, which can be traced in a ~10-15 km arc around the eastern volcano flanks.

Following the terminology of Fisher & Schmincke (1984), each of the lithostratigraphic bed-sets analysed could be products of a definable *eruption* bounded by paleosols that suggest a significant period without eruptive activity. Thereafter, each of the layers within a bed-set, separated by sharp, gradational and/or locally mildly-erosive boundaries that suggest no evident pause in deposition (e.g. contacts given by sharp differences in grain-size, clast framework and/or bed structure), represents an *eruption unit* deposited from an individual fallout, pyroclastic density current (PDC) or a lava flow. An eruption consisting of a single eruption unit will be referred as an *eruption event*; whereas an eruption consisting of multiple eruption units will be referred as an *eruption episode*. In

this latter case, each of the composing eruption units could be interpreted as the accumulation of an eruption phase.

3.4.3 Radiocarbon dating

Samples of charcoal from distinct bed-sets were collected for radiocarbon (^{14}C) dating, and sites of earlier ^{14}C dates (e.g., Turner et al. 2008b, 2011a) were reviewed where sampling sites were clearly known. Six new dates were obtained using the Accelerator Mass Spectrometer technique at the Radiocarbon Dating Laboratory of Waikato University, New Zealand (Table 3.1). Results were determined following Stuiver and Polach (1977), based on the Libby half-life of 5568 yrs with correction for isotopic fractionation. All ages were calibrated using OxCal 4.2 (Bronk-Ramsey 2009). The southern hemisphere atmospheric curve was employed (Hogg et al. 2013). The ^{14}C dates from previous works were also calibrated in the same manner for consistency.

3.5 The late-Holocene eruption records of Mt. Taranaki

In the proximal exposures on Mt. Taranaki 53 bed-sets were identified (Fig 3.3), each one capped by 10-20 cm-thick ash-rich paleosols or weathered ash deposits. Among these 53 bed-sets, 36 underlie a 3rd order unconformity which is traceable over the eastern flank of the volcano. Based on the nearest stratigraphically underlying 7.5 cal ka B.P. debris-avalanche deposits (Neall 1979; Zernack et al. 2011), these 36 bed-sets could be considered part of the Opuā Formation defined by Neall and Alloway (2004). Nevertheless, it was not possible to corroborate this stratigraphic position, because the base of the stratigraphic sequence studied here remains unknown, and there are not enough outcrops to construct mappable units. In contrast, the uppermost ~3 to >1.2 cal ka

Table 3.1 Radiocarbon dating of material from proximal sections of Mt. Taranaki

Lab code	Location	Section	Material		BP	1s	cal BP	1s	Bed-set / Member
<u>This work</u>									
Wk-39445	Maketawa Hut	N	charcoal	*	2223	25	2210	60	Maketawa I
Wk-19168	York track	A	log	*	2277	39	2240	55	Maketawa I
Wk-19169	Kaupokonui stm	B	punga log	*	2515	38	2560	100	MkP-I
Wk-39446	Maketawa Hut	N	charcoal	*	2946	25	3040	55	IgP-II
Wk-39436	Holly Hut 1	X	charcoal	*	3115	25	3280	50	Upper Inglewood
Wk-39437	Camphouse	S	charcoal	*	3180	29	3350	55	Lower Inglewood
Wk-39439	Kokowai	W	charcoal	*	4140	25	4630	90	Kokowai
Wk-39440	Kokowai	W	charcoal	*	4213	25	4710	70	Kokowai
<u>Calibrated from previous works</u>									
Wk-11586	Maero stream	-	flakes	a	878	39	745	40	Te Popo
Wk-16391	Little Maketawa	M	charcoal	c	1130	34	995	40	Grey PDC-III
Wk-16390	Little Maketawa	M	charcoal	c	1739	35	1615	50	Maketawa II
Wk-16392	Little Maketawa	M	charcoal	c	1989	45	1900	60	Grey PDC-I
NZ-3886C	Stratford Plateau	H	charcoal	b	1934	70	1830	90	Grey PDC-I
Wk-16397	North Egmont Rd	T	charcoal	c	2217	36	2200	70	Maketawa I
Wk-16393	Holly Hut 1	X	charcoal	c	3102	37	3270	60	Upper Inglewood
Wk-16395	Okahu stream	-	charcoal	c	3362	37	3545	55	Korito
Wk-16396	Okahu stream	-	charcoal	c	4429	45	4980	100	Undefined PDC

a. Cronin et al. 2003. b. Neall and Alloway 1986. Original age of 1990 ± 70 a BP was recalculated for the Libby half-life of 5568 years. c. Turner 2008.

* Uncalibrated radiocarbon ages in this work (and Lab codes Wk-) were determined by the Radiocarbon Dating Laboratory of the University of Waikato, New Zealand, using the Accelerator Mass Spectrometer technique. Results correspond to a conventional age or Percent Modern Carbon (pMC) following Stuiver and Polach 1977. This is based on the Libby half-life of 5568 years with correction for isotopic fractionation applied.

All ages were calibrated using OxCal 4.2 of the Oxford Radiocarbon Accelerator Unit (Bronk-Ramsey 2009). The Southern hemisphere atmospheric curve (SHCal13) of Hogg et al. 2013 was employed.

B.P. bed-sets are interdigitated with the well-recognized and mappable Manganui Formation (Whitehead 1976; Alloway et al. 1995), which includes seven bed-sets sourced at Fanthams Peak, as we demonstrate below. Another ten pyroclastic bed-sets (~1.2 cal ka B.P. to AD 1655) overlying the 3rd order unconformity are Mt. Taranaki-sourced and, given their better exposure, could be grouped and mapped as part of the Maero Formation (cf. Neall 1979; Neall et al. 1986; Cronin et al. 2003; Platz 2007).

A significant feature within the reconstructed stratigraphic sequence is a 3rd-order unconformity (i.e. a surface of erosion that is extended over a specific sector of the volcano; Lucchi et al. 2013), which consists of an irregular disconformity lying, with a sharp-erosive contact, on top of <1.6 cal. ka B.P. deposits of the Manganui-G Member (q.v. Manganui Formation) and the Curtis Ridge bed-set (cf. Turner et al. 2008b) in southeastern sections (e.g. sections F-G; Figs 3.1-3.2), and most commonly on top of deposits of the Manganui-F Member in the northeast (of the Manganui Formation). In few northeastern locations (e.g. sections Q and R; Figs 3.1-3.2), the unconformity cuts as a ~30°-angular contact down into >2.2 cal ka B.P. deposits of the Manganui-E Member (q.v. Manganui Formation).

Deposits associated with the unconformity consist of up to 70 cm-thick, massive, poorly-sorted, fine to medium sands supporting heterolithic fine to coarse pebbles (Fig 3.3), capping and in-filling erosion surfaces (e.g. paleochannels). These deposits generally exhibit a flat top, grading into ~10 cm-thick paleosols, or a sharp contact with capping lithic breccias and fine lithic ash deposits (i.e. the Grey PDC-II Member, Fig 3.3). Applying ¹⁴C dating of bed-sets below and above indicates that the unconformity occupied an interval between ~1.6 to 1.2 cal ka B.P. (calibrated from Neall and Jansen 1984 and Turner 2008).

In general, deposits of the different bed-sets of Mt. Taranaki comprise white-yellow pumice, grey porphyritic juvenile lithics, altered lithics and accidental clasts; containing crystals of plagioclase, hornblende, Fe-Ti oxides, ortho and clinopyroxene and minor biotite consistent with basaltic-andesitic and andesitic compositions reported elsewhere (53.5-60 wt.% SiO₂; e.g. Neall et al. 1986; Price et al. 1992; Stewart et al. 1996; Turner et al. 2011b; Platz et al. 2007; 2012). In contrast, the basaltic and few basaltic-andesitic

deposits of the Manganui Formation (48-53 wt.% SiO₂, Price et al. 1992; Stewart et al. 1996; May 2003; Turner et al. 2011b) comprise mostly grey and dark grey porphyritic juvenile lithics, few dark grey scoria and dark brown pumice; bearing ortho and clinopyroxene, hornblende, Fe-Ti oxides and olivine crystals.

Below, we describe the the thickest and most readily followed deposits of the stratigraphic sequence in depositional order (Figs 3.2-3.3), separately grouping bed-sets identified from the Mt. Taranaki summit vent, vs. those from Fanthams Peak.

3.5.1 The Mt. Taranaki Lithosome

The oldest deposits studied in this work include 11 bed-sets recognized on the northern flanks of Mt. Taranaki. Bed-sets Tw-I, Tw-VII, and Tw-IX to -XI contain the thickest deposits of the suite (Fig 3.3) and are likely associated to fall deposits within the Tariki and Waipuku Tephra Formations mapped by Alloway et al. (1995) on the ring-plain. They are poorly exposed in only two adjacent sections: W and X (Figs 3.1-3.2) and charcoal fragments were too small or degraded to perform ¹⁴C dating, thus their estimated age is ~5 ka, based on the ¹⁴C age of the closest overlying bed-set (i.e. ~4.7-4.6 cal ka B.P. Kokowai, Table 3.1), and on their approximate correlation with western ~5 cal ka B.P. lithic breccias (Turner 2008; Figs 3.2-3.3).

3.5.1.1 *Bed-sets Tw-I to Tw-VII*

The oldest Tw-I bed-set comprises three layers (Figs 3.3-3.4). The basal contact of the lowermost layer (layer 1) is exposed within an inaccessible ~100 m vertical valley wall. The accessible part of this layer is a massive, poorly-sorted lithic breccia, tens of metres-thick and dominated by dense, porphyritic andesitic blocks and lapilli, at times imbricated

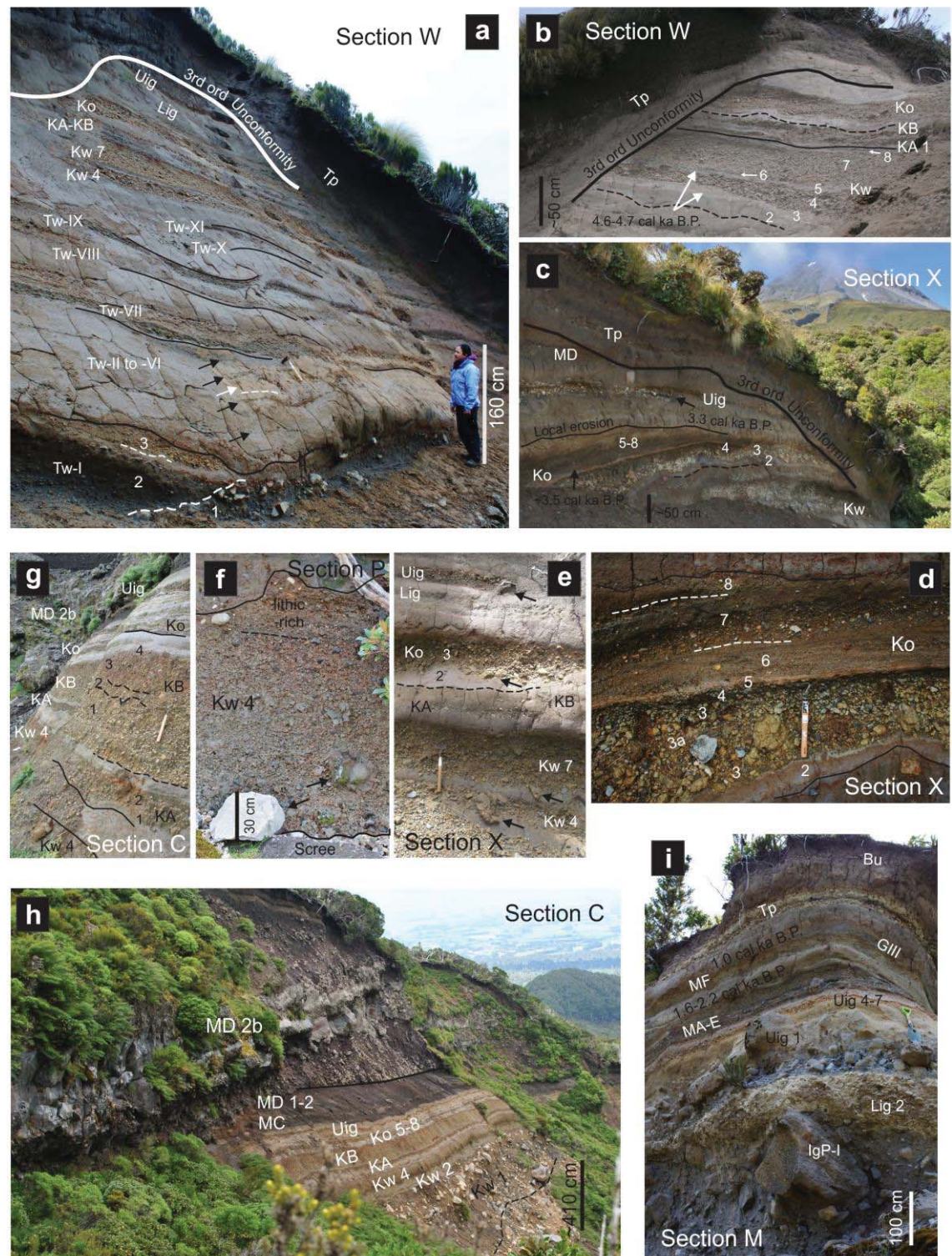
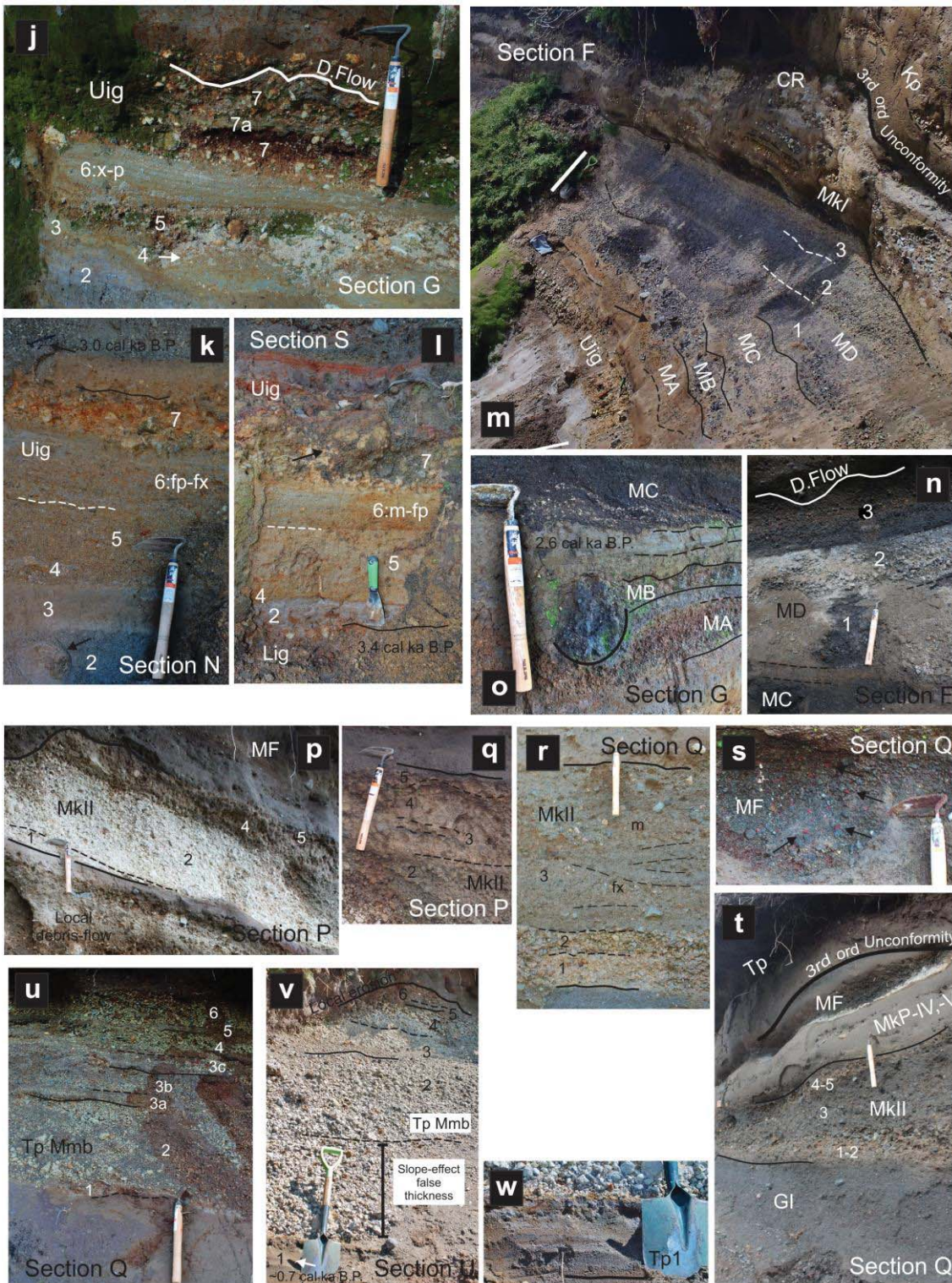


Fig 3.4 Photographs showing the deposit features of representative late-Holocene bed-sets/Members exposed at different eastern-flank sections of Mt. Taranaki. Bed-sets/Members are Tw-I to Tw-XI, Kw Kokowai, KA and KB Kapuni-A and B, Ko Korito, Lig Lower Inglewood, Uig Upper Inglewood, MA to MF Manganui-A to F, Mkl and MklI Maketawa I and II, CR Curtis Ridge, Kp Kaupokonui, GI to GIII Grey PDC-I to -III, Tp Te Popo, Bu Burrell. **a** Deposits of the ~5 ka bed-sets and stratigraphic relationships with



younger 4.7-3.3 cal ka B.P. deposits. **b** Complete Kw bed-set. Radiocarbon (^{14}C) dating of charcoal from layers 3 and 5-6 is indicated. **c** Northern stratigraphic relationships between different 4.7-3.3 cal ka B.P. and younger ~2.6-0.7 cal ka B.P. bed-sets. ^{14}C dated layers from bed-sets Ko and Uig are indicated. **d** Zoom of the Ko. **e** Impact sags produced by pumice bombs of different 4.7-3.3 cal ka B.P. bed-sets. **f** Fall deposits of the Kw layer 4. Bombs and blocks are signalled. **g** Fall deposits of bed-sets KA and KB separated by

weathered ash. **h** Block-and-ash flow and fall deposits of the Kw constitute the base of the exposed section. Lava flows (MD 2b) from Fanthams Peak erode fall deposits of the MD. **i** Stratigraphic relationships and ^{14}C dated deposits of 3.4-0.3 cal ka B.P. bed-sets. Block-and-ash flow deposits underlying layer 2 of the Lig bed-set make the base of the exposed section. Notice Block-and-ash flow deposits of the Uig (layer 1). **j-l** Deposit features of the Uig in southeastern-northeastern locations. Notice lithofacies transitions of layer 6 and ^{14}C dating of charcoal from bracketing bed-sets. **m** Deposits of the <3.0-2.2 cal ka B.P. MA to MD Members and other bracketing and/or younger deposits. **n** Zoom of the MC-MD Members and bracketing debris-flow deposits. **o** Zoom of the MA-MC Members. Notice the cauliflower bomb of the MB Member deforming deposits of the MA. Notice grey-lithic ash deposits of bed-sets MkP-I and MkP-II (not labelled), which pass laterally into ^{14}C dated 2.6 cal ka B.P. lithic breccias. **p-t** Deposit features and facies transitions of the Mk II. **s** Notice the commonly overlying deposits of the MF and their distinctive scarlet-red lithics. **t** Notice deposits of the GI bed-set. **u-w** Deposit features of the Tp. Notice ash deposits of layer 1 (Tp1), which correlate with western 0.7 cal ka B.P. lithic breccias. *x* cross-, *p* parallel- or *fp/fx* faint parallel/cross-stratified and *m* massive deposits. Spade is 70.5 cm-long, large scraper is 32.5 cm-long, small scraper is 20 cm-long. See text and Table 1 for ^{14}C age references.

within an ash matrix. This deposit is capped by layer 2, which comprises normal-graded, poorly-sorted lithic ash of similar composition to the underlying deposit. The uppermost layer 3 is a distinctive mantling bed of massive, well-sorted, clast-supported pumice lapilli (Figs 3.3-3.4).

Each of the Tw-II to Tw-VII bed-sets comprises deposits with transitional or diffuse contacts within encapsulating lower and upper paleosols (Fig 3.3). Tw-II and -V comprise massive, moderately to poorly-sorted pinching beds of ash supporting lithic lapilli. Tw-IV comprises diffuse, massive and well-sorted very fine white ash. Tw-III and VI consist of diffuse and often lensing, massive, moderately-sorted beds of pumice and lithic ash or lapilli. Bed-set Tw-VII consists of two very similar layers (layers 1 and 3) comprising several parallel, cross-stratified and massive, moderately-sorted pinching beds of ash supporting pumice and lithic lapilli; divided by layer 2, which is a massive firm brown ash supporting abundant coarse ash and few lithic lapilli.

3.5.1.2 *Bed-sets Tw-VIII and Tw-IX*

Bed-sets Tw-VIII and -IX lie over ~30 cm-thick paleosols and weathered ash developed on top of bed-set Tw-VII; and are separated by transitional contacts with ~15 cm-thick weathered ash deposits. At its maximum thickness, bed-set Tw-VIII comprises two layers of massive, moderately-sorted pumice and lithic lapilli within an ash matrix, divided by a layer of firm, massive and poorly-sorted pinching clay-rich ash (Fig 3.3). These three layers merge rapidly into a single bedded deposit, which is the most common appearance. Bed-set Tw-IX consists of two layers (Fig 3.3). Layer 1 is a charcoal-rich, massive, well-sorted pinching lithic ash; and layer 2 consists of two reverse-graded, well-sorted and clast-supported mantling beds of distinctive white pumice lapilli, divided by a pinching bed of pumice ash.

3.5.1.3 *Bed-sets Tw-X and Tw-XI*

Bed-sets Tw-X and Tw-XI overlie ~50 cm-thick paleosols and weathered ash developed on top of Tw-IX (Fig 3.3), and are separated by <10 cm-thick weathered ash deposits with sharp contacts between. Tw-X comprises massive, moderately to well-sorted, clast-supported, mantling pumice and lithic lapilli deposits. Tw-XI consists of a massive, moderately-sorted, pinching-swelling bed of lithic-rich lapilli with an interstitial lithic ash matrix, bearing rare charcoal twigs.

3.5.1.4 *The Kokowai bed-set*

The Kokowai bed-set (Kw) contains the thickest and coarsest pyroclastic deposits studied in this work. A sharp contact with up to 30 cm-thick paleosols developed on top of weathered ash deposits separate the Kw from older bed-sets (Fig 3.3). The Kw comprises

eight layers (Fig 3.3) exposed in sections along the eastern flank of the volcano, which are best seen at the Kokowai section (section W, Figs 3.1-3.2).

The most distinctive deposits of the Kw correspond to layers 1, 4 and 7 (Figs 3.3-3.4). Layer 1 consists of up to 10 m-thick, reverse-graded, poorly to moderately-sorted lithic breccias on the volcano southeast flanks, containing porphyritic andesitic blocks of up to 1 m-diameter through to coarse lapilli. Layers 4 and 7 contain almost exclusively massive or stratified, well and very well-sorted, clast-supported, crystal-rich pumice lapilli beds. Layer 4 reaches up to 1.7 m-thick at northeast exposures (Fig 3.4), where it is capped by a bed of dense lithic lapilli. The remaining layers comprise poorly to moderately-sorted, matrix-supported pinching beds of ash, rich in either pumice lapilli or andesitic lithic ash and lapilli.

^{14}C dating of charcoal fragments within layers 3 and 6 at section W indicates an age of 4.7-4.6 cal ka B.P. for the Kw (Table 3.1), which approximately correlates with deposits described by Turner (2008) at Waipuku Stream and Wilkies Pools sections (i.e. deposits M05-69 and M06-54, respectively; sections J and ~D, Figs 3.1-3.2). These ages suggest that the Kw lies stratigraphically above ~5 ka B.P. ring-plain deposits of the Tariki Tephra Formation mapped within soils east and south of Mt. Taranaki by Alloway et al. (1995).

3.5.1.5 *Bed-sets KkF-I and KkF-II*

Two bed-sets (i.e. KkF-I and KkF-II) are separated in between by an intervening ~5-8 cm-thick paleosol with diffuse contacts (Fig 3.3). In southeastern locations, they lie over ~15 cm-thick paleosols developed on top of weathered ash from older deposits (e.g. sections C and D, Figs 3.2-3.3). Each bed-set consists of a single massive, moderately-sorted and very thin bed of fine pumice and lithic lapilli; which might stratigraphically

correlate with the Mangatoki Tephra (~4.4 ka B.P.) mapped by Alloway et al. (1995) in ring-plain locations.

3.5.1.6 The Kapuni-A bed-set

The Kapuni-A bed-set (KA) lies with a gradational contact over ~10-40 cm-thick weathered ash deposits on top of bed-sets KkF-I, -II, or KkP-II at southeast sections (Figs 3.2-3.3). The KA includes two layers (Fig 3.3), with the best exposure near Hooker Shelter (section C, Figs 3.1-3.2). Layer 2 is the thickest (Figs 3.3-3.4) and comprises a massive, well-sorted and clast-supported bed of mostly crystal-rich pumice lapilli; which correlates with >3.8 ka B.P. pumice beds (i.e. between M05-67-M05-68) described by Turner (2008) at Waipuku stream (section J, Figs 3.1-3.2).

3.5.1.7 The Kapuni-B bed-set

The Kapuni-B bed-set (KB) lies with either sharp or gradational contact above a well-developed ~15 cm-thick paleosol, or at Wilkies Pools section, directly over ~20 cm-thick, lithic ash deposits (i.e. bed-set KkP-III; Fig 3.3) and onto the KA bed-set (section D, Figs 3.1-3.2). The KB bed-set consists of at least four layers (Fig 3.3) exposed on the volcano's southeastern, northeastern and northern flanks, best observed at section C (Figs 3.1-3.2). Layers 1 and 3 are the most distinctive as near-identical reverse-graded to massive, well to very well-sorted, clast-supported beds (Fig 3.4), comprising mostly crystal-rich pumice lapilli, but also lithic lapilli. The latter mainly concentrate at the base and top levels of each layer. Layer 2 separates the pumice layers 1-and-3, and consists of a reverse to normal-graded, well-sorted and clast-supported bed, dominated by dense, porphyritic hornblende-rich andesitic lithic lapilli (Fig 3.3). In northeastern sections, layer 2 is

replaced by multiple reverse-graded and clast-supported beds of pumice ash and lapilli, interstratified with massive beds of ash supporting pumice and andesitic lithic lapilli.

Based on its stratigraphic position, the KB correlates with one or more <3.8 ka B.P. unnamed pumice beds described by Turner (2008) on the eastern flanks at section J (i.e. M05-66 and M05-67; Figs 3.1-3.2).

3.5.1.8 *The Korito bed-set*

The Korito bed-set (Ko) lies with a transitional contact over ~10-30 cm-thick paleosols developed on weathered ash (Fig 3.3) on top of different deposits depending on the location (Fig 3.2). The Ko deposits are unique in Taranaki's studied <5 ka sequence due to their varied lithologies and very distinctive yellow- to red-orange coloured pumice. This bed-set is a useful marker horizon in proximal exposures.

The Ko comprises nine layers (1-8, and 3a; Fig 3.3), best observed at Kokowai and Holly Hut 1 sections (sections W and X, Figs 3.1-3.2). Layer 3 contains two massive, well-sorted and clast-supported pumice-dominated lapilli beds, which are separated by matrix-supported deposits (layer 3a) in northern exposures (Figs 3.3-3.4). Hydrothermally altered and accidental dense lithics are common at the normal-graded top part of layer 3 (Fig 3.3). In southern sites, only a single lapilli bed is seen.

Layer 5 is an unusual orange to pink-coloured, parallel-stratified, pinching and fine-grained deposit, useful to correlate the Ko (Figs 3.3-3.4). This layer is firm, appears cemented and is composed of particle clusters (in some cases accretionary lapilli) of highly angular, dense lithic and loose-crystal ash and rare crystal-rich pumice ash, bearing common wood fragments. Layers 6-8 are the most widely distributed and thickest

deposits of the overall bed-set. They comprise intercalated cross-, parallel-stratified and massive, poorly to moderately-sorted, pinching-swelling beds of ash and lapilli (Figs 3.3-3.4), made up of very poorly to poorly vesicular, crystal-rich pumice, and porphyritic lithics. Charcoal twigs are common in layers 7-8.

Some of these layers are traceable ~8 km northwards, across the neighbouring Pouakai volcano and down to Korito road (Figs 3.1-3.2). With distance, layers 5-7 merge, become finer-grained, and together with lensing or scattered pumice lapilli of layers 3 and 8 correlate with the Korito Tephra mapped by Neall (1972). On the ring-plain, Alloway et al. (1995) assigned maximum and minimum ^{14}C ages of 4.1 and 3.5 ka B.P. for the Korito Tephra from coastal cliff exposures, ~42 km northeast of Mt. Taranaki; and suggested that the silicic ~3.9 ka B.P. Stent Tephra (sourced from the TVZ; Alloway et al. 1994) should overlie the Korito Tephra. By contrast, Turner (2008) obtained an ^{14}C age of 3.5 cal ka B.P. (Table 3.1) for charcoal within a cross-stratified and lithic-rich “surge” deposit at Okahu Stream, northwest of Mt. Taranaki, which correlates with layer 6. Ages of underlying Kokowai and overlying Upper Inglewood bed-sets (Table 3.1; Figs 3.2-3.3) support the Turner (2008) age estimate of 3.5 cal ka B.P. for the Ko.

3.5.1.9 *The Lower Inglewood bed-set*

The Lower Inglewood bed-set (Lig) consists of three layers (Fig 3.3) restricted to the east and north flanks of Mt. Taranaki, which are best seen at Waipuku stream, Little Maketawa and Camphouse sections (J, M and S, Figs 3.1-3.2). In northern flank locations (e.g. section W, Fig 3.2), sharp contacts with ~90 and 15 cm-thick deposits of weathered ash and paleosols separate the Lig from the Korito bed-set below and from the Upper Inglewood bed-set above, respectively (Figs 3.2-3.4). On the northeast flanks of Mt.

Taranaki (e.g. section S, Fig 3.2), transitional contacts with similar weathered ash separate the Lig from bed-sets IgFC-I and IgPC-I below (Fig 3.3).

Layers 2-3 comprise the most distinctive deposits. Layer 2 is a firm, massive, moderately to well-sorted pinching deposit of ash supporting white pumice and rare lithic lapilli. Layer 3 consists of mostly massive, well to very well-sorted and clast-supported deposits, dominated by crystal-rich pumice lapilli with andesitic and altered lithics in upper deposit levels (Fig 3.3).

At eastern flank locations (e.g. section J and Lower Pembroke road, Figs 3.1-3.2), layer 3 correlates with the Inglewood-a bed of the Inglewood Tephra mapped by Alloway et al. (1995). An age of 3.6 ka B.P. was proposed by Alloway et al. (1995) for the Inglewood Tephra based on ^{14}C dating of peat and wood from encapsulating ring-plain and distal deposits. In this work, ^{14}C dating of charcoal within layer 1 at section S provides an age of 3.4 cal ka B.P. for the Lig (Table 3.1), which is consistent with under and overlying bracketing bed-sets of 3.5 and 3.3 cal. ka B.P., respectively (Table 3.1).

3.5.1.10 The Upper Inglewood bed-set

The Upper Inglewood bed-set (Uig) lies with sharp and erosive contacts directly upon deposits of the Lig in most northeastern areas (Fig 3.3); whereas in southern and northern locations, transitional and sharp contacts separate the Uig from 10-20 cm-thick paleosols developed on top of bed-sets Lig, IgP-I, IgF-I or Ko (Fig 3.2). The Uig is one of the most complex deposits seen during this study, with seven layers (Fig 3.3) recording one of the largest explosive eruptions in Mt. Taranaki's history. Most layers are exposed across the entire eastern flank and, with its distinctive field appearance, form an ideal proximal stratigraphic marker (Fig 3.2).

Layer 1 is a reverse-graded to massive and poorly sorted lithic breccia, containing dense grey and few hydrothermally altered porphyritic lithic blocks and coarse lapilli (Figs 3.3-3.4). This layer laterally passes into massive, parallel- or cross-stratified pinching thin beds of ash and lapilli. Layers 2 and 3 are reverse-graded, parallel- and cross-stratified and poorly to moderately-sorted lithic-dominated ash beds; that cap interfluves in a similar way to the lateral parts of layer 1; however, layer 3 additionally contains pumice lapilli in some areas. Layers 4-6 comprise overall poorly- to moderately-sorted and pinching-swelling, matrix-supported beds of multiple lithics and crystal-rich pumice (Figs 3.3-3.4). They graduate vertically from basal, parallel-stratified, very thin beds of ash and lapilli (layer 4), into clast-rich massive beds of lapilli (layer 5); and finally into upper parallel- and cross-stratified thin beds of ash showing occasional dune structures (layer 6). The uppermost layer 7 comprises a massive, well-sorted and clast-supported bed (Figs 3.3-3.4) of crystal-rich pumice lapilli and dense, porphyritic lithic lapilli (Fig 3.3).

From Holly Hut 1 section (section X, Fig 3.1) layer 7 was traced northwards, down to Maude, Kent and Korito roads, where it correlates with the Inglewood Tephra mapped by Neall (1972). To the east flanks of Mt. Taranaki (e.g. sections F-I, Figs 3.1-3.2), layer 7 correlates with the Inglewood-b bed of the Inglewood Tephra defined by Alloway et al. (1995). In the present study, ^{14}C dating of ~30 cm-long charcoal logs within layer 6 at section X (Fig 3.4) indicates an age of 3.3 cal ka B.P. for the Uig (Table 3.1); which is near identical to the ^{14}C date obtained by Turner (2008) in a correlative deposit. ^{14}C dating of charcoal within immediate over- and under-lying deposits at Maketawa Hut and Camphouse sections (N and S, Figs 3.1-3.2) confirms maximum and minimum ages of 3.4 and 3.0 cal ka B.P., respectively (Table 3.1).

3.5.1.11 The Maketawa I bed-set

The Maketawa I bed-set (MkI) lies with sharp and parallel contact on top of ~10-15 cm-thick deposits of massive, poorly-sorted and firm conglomerates (Fig 3.3), which in southeastern locations consist of fine to coarse pebble gravels within a clay-rich matrix. In other locations, the MkI rests with sharp contact upon ~5-10 cm-thick paleosols developed on top of other Members of the Manganui Formation.

The MkI includes four layers (Fig 3.3) mainly exposed along southeastern and eastern flanks (Fig 3.2). It is best seen at Curtis Ridge (Fig 3.4) and Maketawa Hut sections (F and N, Figs 3.1-3.2). Deposits of layers 2 and 3 are the most frequently exposed. Layer 2 comprises a normal-graded, well-sorted and clast-supported bed of yellow and crystalline pumice lapilli and dark-grey lithic lapilli. Layer 3 comprises a characteristic set of pink and orange coloured, parallel-stratified, moderately-sorted and occasionally pinching firm beds of pumice ash supporting aligned pumice and lithic lapilli and rare 1-5 cm-long charcoal twigs. Layers 2-3 are frequently deformed by blocks produced during deposition of the overriding lithic breccia of layer 4.

Layer 2 correlates with the Maketawa Tephra Formation mapped by Franks (1984) and dated at 2.9 ka B.P. by McGlone et al. (1988). Here, ^{14}C dating of charcoal within layers 3-4 at sections N and York track (Figs 3.1-3.2) indicates an age of 2.2 cal. ka B.P. for the MkI (Table 3.1), which is consistent with the ^{14}C age of 2.2 cal. ka B.P. obtained by Turner (2008) for correlated deposits at section T (Fig 3.1).

3.5.1.12 The Maketawa II bed-set

In most locations, the Maketawa II bed-set (MkII) lies with sharp contact over massive lithic breccias passing laterally into cross-stratified coarse lithic ash deposits (i.e. Grey

PDC-I bed-set, Figs 3.2-3.3). The latter are rarely separated with sharp contacts from a ~5-6 cm-thick paleosol developed on top of the MkI (Fig 3.3). In a few sections, transitional contacts with weathered ash separate the MkII from the Grey PDC-I bed-set.

The MkII comprises five layers (Figs 3.3-3.4) best seen at northeast locations (e.g. sections P-Q, Figs 3.1-3.2). Although the MkII is traceable all along the eastern flanks of the volcano, its correlation is complex in proximal locations. Layers 1 and 4 consist of massive, moderately-sorted, pinching beds of yellow pumice lapilli and dark-grey andesitic lithic lapilli supported by a matrix of pumice ash. Layers 2 and 5 comprise massive or reverse-graded, well-sorted and clast-supported beds of poorly vesicular and crystalline yellow pumice and andesitic lithic lapilli. Layer 3 comprises cross-stratified and massive, poorly to moderately-sorted pinching beds of grey lithic ash supporting imbricated lithic and pumice lapilli, interstratified with massive, clast-supported lenses of yellow pumice lapilli (Figs 3.3-3.4).

In rare exposures (e.g. section P, Figs 3.1-3.2), layer 3 thins to ~2-5 cm and becomes a distinctive grey, lithic-rich bed that contrasts with the bracketing yellow-white pumice deposits (Fig 3.4). In addition, layer 2 and the pumice-rich lenses of layer 3 merge and expand to form a single, stratified, clast-supported and up to 75-80 cm-thick pumice-rich bed (Fig 3.4). Layer 4 thickens to ~25 cm. Frequent, sharp-erosive angular contacts between layer 4 and several overriding lithic breccias occur where layer 5 has been completely eroded. These rapid transitions occur along sections spaced at ~50 m apart near the North Summit Track (e.g. sections P-Q and S, Figs 3.1-3.2).

In several locations (e.g. section M; Figs 3.1-3.2), the MkII is bracketed between deposits ¹⁴C dated at 1.9 and 1.6 cal ka B.P. by Turner (2008; Table 3.1). This is consistent with

the age of 1.8 cal ka B.P. of the underlying GI bed-set (e.g. section H; Figs 3.1-3.2) calibrated from Neall and Alloway (1986).

3.5.1.13 The Maero Formation

The Maero Formation lies above the 3rd-order unconformity, and comprises deposits of the last ~850 yrs of volcanic activity of Mt. Taranaki (Druce 1966; Neall 1972; 1979; Neall et al. 1986; Cronin et al. 2003; Platz et al. 2012), represented by a minimum of 19 Members (Platz 2007). The most prominent deposits from oldest to youngest correspond to Members Te Popo Breccia and Te Popo Ash, Waingongoro Ash, Newall Ash, Waiweranui Ash, Puniho Ash and Burrell Lapilli. The most recent deposits of the Maero Formation correspond to three different post AD 1755 Members (Platz 2007).

Based on the identification and correlation of the basal 3rd order unconformity, the Maero Formation was here redefined to comprise a total of 23 Members, which includes older >1.0 ka deposits of Members Grey PDC-II, MrP-I, Kaupokonui and Grey PDC-III (Fig 3.3). The Kaupokonui Member correlates with the ~1.2 cal ka B.P. Kaupokonui Tephra mapped by Franks (1984) and calibrated from Neall and Jansen (1984). ¹⁴C dating of charcoal within deposits of the Grey PDC-III indicates an age of 1.0 cal ka B.P. (calibrated from Turner 2008).

The Te Popo Member (Tp) contains some of the thickest deposits of the Maero Formation, representing the Te Popo Episode recorded by Platz (2007). These deposits lie with sharp contacts on top of 10-15 cm-thick paleosols developed over Members Grey PDC-III or Kaupokonui (Fig 3.3), or above of up to 100 cm-thick weathered ash deposits (section Q, Fig 3.2). Paleosols and massive coarse-fine ash deposits of the Newall, Waiweranui, Puniho and Burrell Lapilli Members overlie the Tp in few sections (Figs 3.2-3.3).

The Tp comprises six layers exposed mainly on the northeastern volcano flanks (Figs 3.3-3.4) and best preserved at the Veronica Slip and North Summit Track sections (U and Q, Figs 3.1-3.2). Layers 2, 4 and 6 consist of mostly massive, well and very well-sorted, clast-supported beds; composed of crystalline pumice lapilli and grey, bluish and altered-red dense or poorly vesicular porphyritic lithic lapilli (Fig 3.3). These layers are interbedded with massive or parallel-stratified, poorly to well-sorted, matrix-supported deposits of layers 1 and 3 (Figs 3.3-3.4). Layer 3 consists of three beds of lithic and pumice lapilli, at times reverse- or normal-graded (i.e. 3a to 3c; Figs 3.3-3.4). Beds 3a and 3c are firm and the matrix includes a large fraction of white pumice ash, similar to the massive ash of layer 5. Bed 3b is clast rich, but contains interstitial ash matrix.

Deposits of layer 1 (Figs 3.3-3.4) correlate with westward-distributed 0.7 cal. ka B.P. BAF deposits (^{14}C age calibrated from Cronin et al. 2003) of the Te Popo Breccia (Platz 2007), consistent with the ages of underlying 1.2-1.0 cal ka B.P. deposits at northeastern locations. The Te Popo Member encompasses both the Te Popo Breccia and likely the Te Popo Ash Members of Platz (2007).

3.5.2 The Fanthams Peak Lithosome

3.5.2.1 *The Manganui Formation*

At least four Members of the Manganui Formation, sourced at Fanthams Peak, were earlier mapped as the “Manganui Tephra Formation” along the eastern area of Mt. Taranaki, up to ~20-25 km from the summit crater (Whitehead 1976; Alloway et al. 1995). In this work, the Manganui Formation encompasses a series of seven Members (Manganui-A [MA] to Manganui-G [MG], Fig 3.3) with a characteristically basaltic composition (avg. 50.6 wt.% SiO_2 ; Price et al. 1992; Stewart et al. 1996; May 2003;

Turner et al. 2011b) which contrasts with the typical avg. 57 wt.% SiO₂ for bed-sets above and below (Neall et al. 1986; Price et al. 1992; Stewart et al. 1996; Turner et al. 2011b; Platz et al. 2007; 2012) and sourced from the summit vent of Mt. Taranaki. The basal contact of the Manganui Formation is a sharp surface between a ~10 cm-thick paleosol developed on top of the 3.0 cal ka B.P. Ig-P-II bed-set and the lowermost Manganui-A Member (Fig 3.3, Table 3.1). The top of the Formation corresponds to a sharp, conformable contact between the uppermost <1.6 cal ka B.P. Manganui-G Member and the Taranaki-sourced Curtis Ridge bed-set (cf. Turner et al. 2008b), both underlying the 3rd order unconformity (Figs 3.2-3.3).

Members Manganui-A to D correlate with Manganui tephra beds a-d of Alloway et al. (1995). The Manganui-G Member was previously included by Turner et al. (2008b) as part of the “Curtis Ridge Lapilli” (CR Unit-1, Fig 3.3), but at that time, Members Manganui-E and F had not been identified. In southern flanks, Members Manganui-B, C and D are interdigitated with at least three bed-sets sourced at Mt. Taranaki and consisting of pinching beds of light-grey andesitic lithic ash (i.e. MkP-I, -II and -III, Fig 3.3) that pass laterally into lithic breccias. Similarly, Members Manganui-E, F and G are intercalated with deposits of other six Mt. Taranaki-sourced bed-sets (e.g. Maketawa I, Maketawa II and Curtis Ridge; Fig 3.3).

Alloway et al. (1995) dated Members Manganui-A to D between 3.3-2.9 ka B.P. Here, ¹⁴C dating of charcoal within deposits of bed-sets IgP-II and Maketawa I (e.g. section N, Figs 3.1-3.2) bracket Members Manganui-A to E between 3.0-2.2 cal ka B.P. (Table 3.1). ¹⁴C dating of a log within lithic breccias of bed-sets MkP-I and -II (section B, Figs 3.1-3.2) indicates that Members Manganui-A and B are >2.6 cal ka B.P. in age (Table 3.1). ¹⁴C dating of charcoal within deposits of the encapsulating bed-sets Maketawa II and

Grey PDC-III (section M, Figs 3.1-3.2) indicate that Members Manganui-F and G are <1.6 to >1.0 cal ka B.P. (calibrated from Turner 2008).

The Manganui-A Member (MA) comprises at least three layers (Fig 3.3) resting with a sharp lower contact above ~6 cm-thick paleosols and up to 10 cm-thick weathered ash, best seen at Curtis Ridge and Veronica track sections (F and R, Fig 3.1). Layers 1-2 are reverse to normally-graded, very well-sorted, clast-supported and often firm deposits of crystal-rich, dark-brown pumice and dark-grey scoria lapilli and ash. Layer 3 consists of distinctive parallel- and cross-stratified, moderately-sorted and pinching-swelling beds of dark bluish-grey lithic ash (Fig 3.3). The MA contains the most vesicular pyroclasts of the Manganui Formation.

The Manganui-B Member (MB) lies above ~5-6 cm-thick edafized and firm deposits of fine sand capping the MA (Fig 3.3). The MB comprises a very distinctive reverse-graded and occasionally massive, moderately to well-sorted, clast-supported and rarely matrix-supported bed of heterogeneous lithic lapilli, rich in cauliflower and bread-crust bombs. The Manganui-C Member (MC) is separated from the underlying MB by bed-sets MkP-I and -II (Fig 3.3), ~5 cm-thick edafized ash deposits and occasional firm deposits of coarse sand. The MC is made up of very friable, reverse to normal-graded, well to very well-sorted and clast-supported thin beds of moderately crystalline dark-grey lithic lapilli, dark-brown pumice and black scoria lapilli and ash.

The Manganui-D Member (MD) contains the thickest deposits of the Manganui Formation (Fig 3.3). The MD rests with sharp contact on top of edafized firm deposits of coarse sand, rich in dark juvenile clasts from the underlying Manganui Members. These same types of sand deposits are also interstratified with basal beds of the MD (Fig 3.3).

The MD comprises at least three pyroclastic layers, exposed in most sections (Fig 3.2), and a lava flow (layer 2b, Fig 3.4). Layers 1 and 2 comprise reverse to normal-graded, well and very well-sorted and clast-supported beds, made up of dense dark lithic lapilli and moderately crystalline pumice and scoria lapilli and ash. Violet-red and orange altered lithics are common in layer 1 but rare in layer 2. Layer 3 is a very distinctive deposit of four reverse to normal-graded, well-sorted and clast-supported lapilli beds (Fig 3.3) made up of juvenile clasts similar to layers 1-2, but with higher altered and accidental lithic concentrations in middle beds (i.e. orange, red and white-bleached altered angular lithics; and black-grey dioritic accidentals).

With distance, layer 3 passes into a single stratified deposit of evenly mixed juveniles and altered and accidental lithics. In eastern and southeastern locations, layer 3 is partially or fully replaced by firm sand deposits rich in juvenile clasts from the MD (Figs 3.3-3.4); whereas in few southeastern sections (e.g. sections C and D; Figs 3.1-3.2), layers 1-3 are capped and partially or fully eroded by lava flows sourced at Fanthams Peak (Fig 3.4).

The Manganui-E Member (ME) is found in only few locations (e.g. sections N and R, Figs 3.1-3.3), lies above ~2-6 cm-thick paleosols developed on top of lapilli-rich breccias and is often partially eroded or fully replaced by overriding breccias rich in ME-lapilli. The ME consists of reverse to normally-graded, well and very well-sorted and clast-supported beds of poorly vesicular, dark-grey lithic lapilli, scoria lapilli and brown pumice lapilli. Orange-reddish scoriaceous fragments give ME a distinctive appearance compared to earlier Manganui Members.

The Manganui-F Member (MF) comprises a rarely preserved deposit exposed in northeastern locations (e.g. section Q, Figs 3.2-3.4). The MF rests with a gradational

contact upon weathered massive fine ash deposits, and consists of reverse to normally-graded, well-sorted and clast-supported beds of moderately crystalline, dark-brown and grey lithics, pumice and scoria lapilli, and the Member's most distinctive poorly vesicular, scarlet-red lithic lapilli (Figs 3.3-3.4).

3.6 Interpretation of deposits and associated volcanic hazard

The lithofacies associations of the different bed-sets that comprise the late-Holocene Members deposited on Mt. Taranaki (Fig 3.3) allow them to be classified within three categories: (a) fall deposits from a sustained, convective eruption column (cf. Cioni et al. 2000, 2008; Arce et al. 2003, 2005; Pardo et al. 2012a, b); (b) PDC deposits, including column-collapse and dome-collapse sourced currents (cf. Brown and Branney 2004; Lube et al. 2011; Cronin et al. 2013; Kim et al. 2014); and (c) lahar deposits from syn- and post-eruptive debris flows and hyperconcentrated flows.

3.6.1 Pyroclastic fall deposits

The diagnostic features of fall deposits in the proximal areas are mantling of paleotopography, even thickness, good-sorting (according to first-order visual classes of Cas et al. 2008), and clast-supported framework. Beds range from massive to graded (both reverse and normal) and/or have "shower-bedded" stratification, reflecting vertical grainsize or compositional changes. The deposits are generally friable and dominated by pumice clasts, which are normally lapilli-grade with local blocks and bombs (the latter being mainly ballistically emplaced).

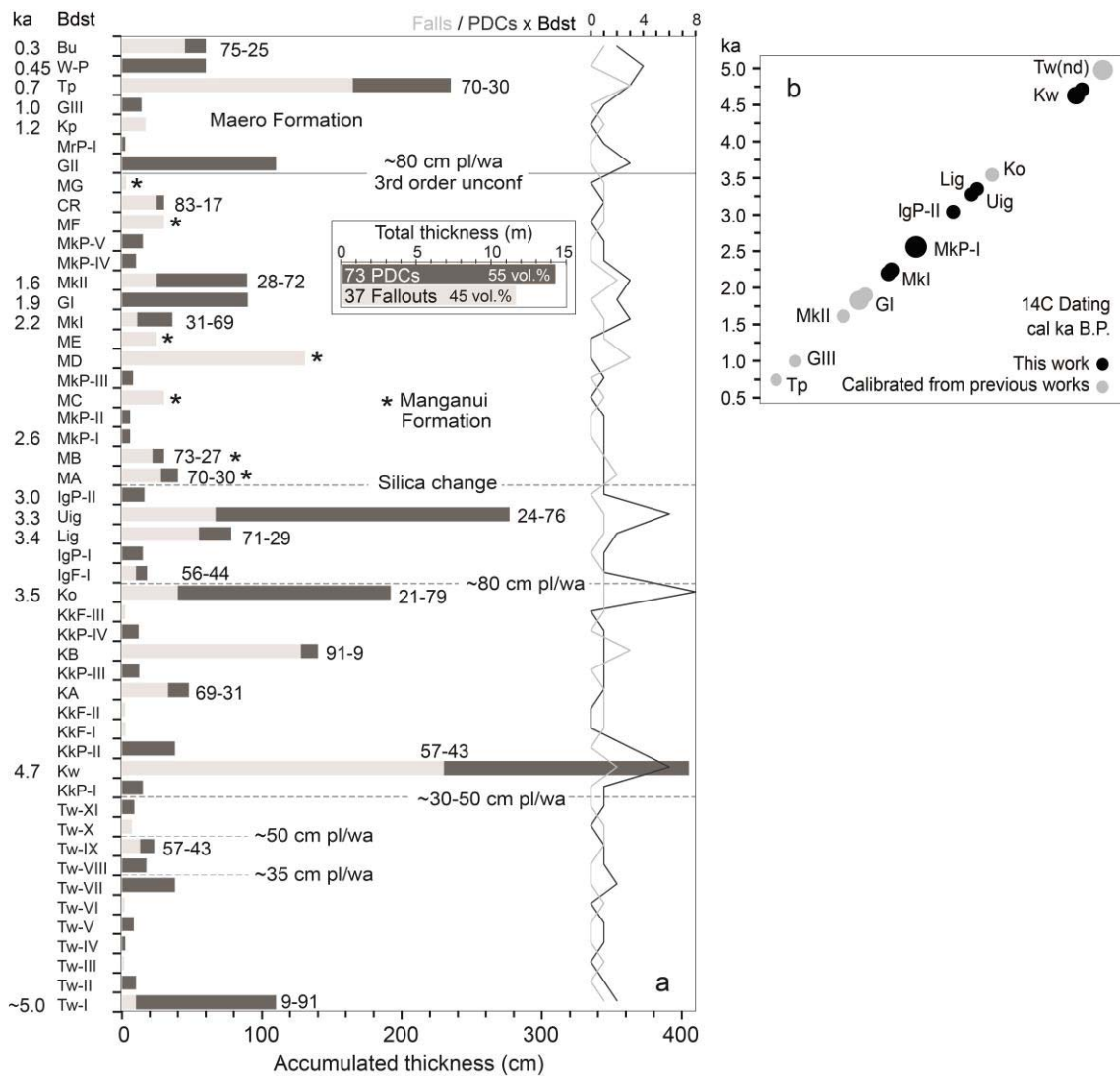


Fig 3.5 a Total accumulated thickness of fall and pyroclastic density current (PDC) deposits per bed-set (Bdst) in centimetres, and total thickness per pyroclastic deposit-type in metres (see inset). Numbers accompanying bars (e.g. 71-29) indicate volume percentages of fall-PDC deposits. The line-diagram indicates number of layers of Fall and PDC deposits (units) per bed-set. *Unconf* Unconformity, *pl/wa* Intervening paleosol and/or weathered ash deposits in centimetres-thick. Refer to text and figure 3 for bed-set abbreviations. **b** Calibrated ^{14}C ages from this work and previous works. The size of each circle is proportional with the corresponding dating error (see Table 1 for complete data and references).

Single fallout units are up to 2 m-thick, such as from the Kokowai and Te Popo eruptions (Fig 3.5). Fallout-generated deposits are associated with 28 of the 53 eruptions, and 45% of the total thickness of the studied pyroclastic succession. Around 57% of the fall

deposits are widespread, significantly coarse-grained and thick enough to be representative of the maximum eruption column heights produced at Mt. Taranaki over the Holocene (cf. ~14 km-height column of the AD 1655 Burrell eruption, Platz et al. 2007).

Pyroclastic debris dispersed by clouds or plumes is an expected hazard from large eruptions at andesitic volcanoes. Ash has impacts in the air (including air-transport routes), on land (agriculture), and in water environments, and may severely damage infrastructure due to its abrasive, corrosive, acidic and conductive properties (Cronin et al. 1998, 2003; Wilson et al. 2011). Ash from Mt. Taranaki plumes was distributed dominantly across the northeastern and east-southeastern flanks (Fig 3.2) due to New Zealand's North Island's prevailing winds, covering currently populated areas of ~1,600 km² (Neall 1972; Topping 1971; Whitehead 1976; Alloway et al. 1995). Distal fall deposits from Mt. Taranaki have also been identified in maar-crater sediments in Auckland, 280 km away from the volcano (Shane 2005).

3.6.2 Pyroclastic density currents (PDCs)

PDC units in Mt. Taranaki include both pumice and lithic-rich proximal deposits, with a common pinching and pinching-and-swelling geometry, that drape ridges and thicken in paleovalleys. The diagnostic features of PDC deposits are their generally poor sorting and matrix support; they vary from massive to parallel- and cross-stratified and contain a mixture of ash, lapilli and blocks, with common charcoal fragments.

The stratigraphic succession suggests that PDCs were the most frequent proximal volcano-sedimentary process during Holocene Mt. Taranaki eruptions, generating deposits during 38 of the 53 eruption events/episodes studied, and producing 55 vol.% of

the total composite pyroclastic deposit thickness (Fig 3.5). PDC units can be up to 2 m-thick on ridges, and much thicker in valleys. In this proximal area, the PDC deposits may constitute up to ~80 vol.% of the record of an eruption episode (e.g. Upper Inglewood and Korito eruptions; Fig 3.5), and could be deposited both by one-off flows, or from a sequence of events (e.g. Grey PDC-I and -II eruptions, Fig 3.3). PDC units almost universally accompanied eruptions that produced thick fall deposits during complex eruption episodes (e.g. Kokowai eruption, Fig 3.3).

Pumice-dominated PDC deposits, commonly associated with pumice-rich fall deposits, are interpreted as resulting from column collapse under open-conduit conditions. In contrast, lithic-dominated PDC deposits are interpreted as resulting from lava-dome collapse, under initially closed-conduit conditions. The massive to stratified lithofacies is attributed to concentrated to dilute PDCs, respectively. Both types of PDCs have been observed in recent historical eruptions of similar composition, type and scale (e.g. Saucedo et al. 2010; Lube et al. 2011; Cronin et al. 2013).

The run-out of PDCs is commonly influenced by their volumes. Previous studies indicated that low-volume PDCs at Mt. Taranaki commonly reached 10-15 km from the crater (Procter et al. 2010; Platz et al. 2007, 2012). However, longer run outs could be expected during extended eruption episodes, because deep valleys become in-filled and smoothed by earlier deposits (e.g. Lube et al. 2011; Cronin et al. 2013).

Field evidence for the distribution of PDC deposits of Mt. Taranaki from multiple past studies suggests that any of the volcanic flanks could be impacted, with arguably the northwestern sector being at present most susceptible due to the collapsed northwestern crater margin (Procter et al. 2010; Platz et al. 2007, 2012). During future eruptions, PDCs

would pose a very high threat to all the forested areas of the Egmont National Park and the adjacent inhabited farmland (Figs 3.1-3.2). Given the high abundance of PDC units within the deposits studied, it must be assumed by hazard managers that almost every eruption of Mt. Taranaki will produce at least one PDC of some type.

3.7 Revised eruption history

3.7.1 Comparison with previous work

The example of figure 3.3a demonstrates that the volcanic processes during the <5 ka eruption events and episodes at this volcano are far more complex than those interpreted from previous ring-plain and distal deposits. Previous studies of ring-plain deposits at Mt. Taranaki estimated 27 tephra beds within 12 Tephra Formations (cf. Neall 1972; Franks 1984; Alloway et al. 1995). However, according to the International Stratigraphic Code (Salvador 1994), genetic terms should be avoided when naming lithostratigraphic units. In addition, the significance of each lithostratigraphic unit defined in previous works, in terms of eruption activity and source, remains unclear. Each of the defined “Tephra Formations” could either be: (a) deposits produced by only one fallout/PDC during a single eruption event (e.g. The Kaupokonui Member), (b) deposits produced by one or more fall/PDCs within a multiple-eruption episode (e.g. The Maketawa I bed-set), or (c) deposits produced during several different eruption events or episodes (e.g. The Manganui Formation). In this respect, some of the “Formations” defined might provide information about layers (e.g. a flow), but do not contain details about distinct eruption events/episodes. Furthermore, using “Tephra Formations” to define volcanic units excludes any potential syn-eruptive lithofacies variation with distance, from a proximal

pyroclastic deposit to a distal volcanoclastic and/or epiclastic deposit (e.g. syn-eruptive lahars).

In the present study, we therefore propose abandonment of the previously defined “Tephra Formations”, as has been done in schemes earlier applied by Cronin et al. (2003) and Platz (2007) to redefine the uppermost Maero Formation following the international rules for the definition of lithostratigraphic units. There is only one more Formation that is mappable, distinctive in the field and with clear basal-and-top contacts, which is the Manganui Formation. For the rest of the stratigraphy, we redefined units bounded by erosive surfaces or paleosols, suggesting time-breaks in eruptive activity, as bed-sets.

We estimated a total of 37 pyroclastic fall deposits and 73 individual PDC units formed during 53 different eruptions (events or episodes), in the period between 5 and 0.3 cal ka B.P. (Fig 3.5). Previous studies recognized only 10 fall deposits as being related to PDCs (Turner et al. 2008b; Platz et al. 2007, 2012). This poor representation of PDC deposits in ring-plain areas was also noted in high-resolution distal swamp- and lake-core sediment pyroclastic fallout records surrounding Mt. Taranaki (Turner et al. 2008b, 2009, 2011a).

Despite the improved resolution obtained in the present research, the new proximal record still doesn't represent all eruptions with deposits known from distal swamp- and lake-core sediment records over the same time-period (e.g. up to 62 in Green et al. 2016).

3.7.2 Late-Holocene eruptions of Mt. Taranaki

For simplicity, we have organized the 53 late-Holocene eruptions, sourced from the summit of Mt. Taranaki and Fanthams Peak, according to peaks in pyroclastic and epiclastic (in this case only for sediments clearly produced from post-eruptive pyroclast-

remobilization during inferred periods of volcanic quiescence; Fisher and Schmincke 1984) bed-set deposition and soil formation, interpreted from maximum deposit thickness through time (Fig 3.5). Similarly, the peaks in pyroclastic deposition associated with the largest eruption episodes during the last 5 ka, were compared to the maximum thickness produced by the $3.2 \times 10^8 \text{ m}^3$ fall deposits generated by a ~14 km-high column during the eruption of the sub-Plinian Burrell episode (Bu, Platz et al. 2007; Fig 3.5).

At least 11 different eruption events/episodes, separated by periods of quiescence of different length, occurred between ~5 and 4.7 cal ka B.P. (Fig 3.5), producing five pyroclastic fall deposits and ten PDC units localised down the north and northeast volcano flanks (Fig 3.2). The largest eruption during this period (Tw-I bed-set, Fig 3.3) began with BAFs in-filling the Kokowai Stream valley, which was followed by a short-lived eruption column that produced pumice-rich deposits. Subsequent events produced sequences of hot column-collapse PDCs from brief, short-lived eruption columns, similar or smaller than the Tw-I eruption based on the thinner deposits generated (Fig 3.5).

Following a period of quiescence, the largest late-Holocene eruption episode of Mt. Taranaki produced the thickest deposits of the 4.7-4.6 cal ka B.P. Kokowai bed-set (Figs 3.3 and 3.5). The Kokowai eruption started with BAFs in-filling the southeastern valleys of the Kaupokonui Stream. Two eruption columns accompanied by column-collapse PDCs produced thick and widespread fall deposits blanketing the north and east Taranaki Peninsula.

Subsequently, ten eruptions produced eight fallouts and 16 PDCs between 4.7-3.5 cal ka B.P., many of which produced only ~5-15 cm-thick deposits (Fig 3.5). The Kapuni-B episode produced a particularly thick, southeast-dispersed fallout succession, without any

large PDC deposits (Fig 3.5). The Korito bed-set was deposited from the last large eruption episode during this time-period; but, in contrast to the others, it was dominated by production of a succession of column-collapse PDCs (Fig 3.5) with minor fall units (Fig 3.3).

The next major eruptions occurred after a period during which up to 80 cm-thick weathered fine ash accumulated at many sites, either due to very small eruptions or by wind-remobilised ash. Five eruption episodes produced three fallouts and 10 PDCs between 3.4-3.3 cal. ka B.P. (Fig 3.5). The earliest, Lower Inglewood eruption produced pumice-rich PDC and fall deposits similar in thickness to the sub-Plinian Burrell eruption (Platz et al. 2007; Figs 3.3-3.5). Following a brief interval of quiescence, the Upper Inglewood eruption produced the thickest PDC succession in the late-Holocene history of Mt. Taranaki, having northeast-dispersed pumice fallout (Figs 3.3-3.5).

A brief quiescence, during which ~20 cm-thick of weathered massive fine-ash accumulated, preceded a sudden shift to paired eruption of basaltic (avg. 50.6 wt.% SiO₂) and andesitic (avg. 57 wt.% SiO₂) variants (Price et al. 1992; Stewart et al. 1996; May 2003; Turner et al. 2011b) from two centres, the parasitic Fanthams Peak (1952 m-elevation) and the summit crater (2518 m), respectively. From these two centres, 17 eruptions occurred between ~3-1.5 cal ka B.P., producing 14 fall and 17 PDC units (Fig 3.5). Seven of these eruptions were sourced at Fanthams Peak and produced eight fallouts and two PDC units that deposited seven bed-sets (i.e. The Manganui Formation) encompassing ten layers formed by distinctive basaltic, dark-grey and black lithics, dark-grey scoria (i.e. ~dense clasts of thick-walled vesicles) and brown pumice (i.e. ~fragile clasts of thin-walled vesicles). The other ten eruptions deposited 19 layers of andesitic

pumice and lithic compositions, corresponding with four fallouts and 15 PDC units (Fig 3.5).

The contrast between fall-dominated eruptions of basaltic composition and prevalent PDCs from the andesitic eruptions of this period (Fig 3.3) is noteworthy, and potentially reflects differing conduit conditions, magma supply rates and volatile contents; this needs to be further investigated. Preliminarily, the key feature of the summit crater appears to be choked conduits, with crystalline mush within the conduit and/or capping lava domes (cf. Platz et al. 2007, 2012 and data presented above). This means that eruption events/episodes are more complex, involving a range of BAFs, vulcanian blasts with unstable columns producing further column-collapse PDCs and eventually sustained columns, only when the conduit has been cleared. By contrast, the Fanthams Peak eruptions appear to be characterised by more open-vent conditions, producing fall deposits from stable eruption columns. Occasional lava flows interspersed within the eruption sequence (e.g. Manganui-D bed-set; Figs 3.2 and 3.4) and the basaltic and less crystalline composition of the Fanthams eruptive products suggest lower viscosity magmas and rapid transit through the upper conduit system. Some of the most mafic eruptions of the period were also located from subsidiary vents just below and north of the Fanthams Peak area, in the Rangitoto flat (noted by Turner et al. 2008a, b).

Despite the basaltic compositions (Price et al. 1992; Stewart et al. 1996; May 2003; Turner et al. 2011b), the largest eruption of the Fanthams Peak area produced the east and northeast-dispersed Manganui-D fall succession (Figs 3.2-3.3), which is similar in thickness to the fall deposits of the Kapuni-B bed-set, and thicker than the $3.2 \times 10^8 \text{ m}^3$ fall deposits produced by the ~14 km-high column of the sub-Plinian Burrell eruption (Platz et al. 2007; Fig 3.5). Many of other Mt. Taranaki's summit eruptions, contemporaneous

with the activity of Fanthams Peak, generated thick BAFs and column-collapse PDCs but comparatively thin pumice fall deposits (e.g. Maketawa I and II bed-sets; Figs 3.3 and 3.5).

Most deposits of the Manganui Formation appear similar to the deposits produced during the eruptions of monogenetic basaltic volcanoes (e.g. Rowland et al. 2009) but, in contrast, the former span ~1500 yrs and so are much longer than the eruption of a single monogenetic volcano. In addition, the relatively thin (~1-6 cm) paleosols and weathered massive fine-ash deposits that separate some of the Manganui Members (e.g. MA-MB, MB-MC, and MD-ME; Fig 3.3) represent longer intervals of quiescence than were observed during, e.g., the 10-15 yrs. eruption episodes of Paricutin and Jorullo (Rowland et al. 2009), even if we assume that other intervening pyroclastic and volcanoclastic deposits were produced by syn-eruptive units, e.g., lahars and BAFs.

First-order estimates considering segments of 120 and 250 cm-thick pyroclastic, epiclastic and paleosol deposits bracketing 3.0-2.6 and 2.6-2.2 cal ka B.P., respectively, and comprising Members MA-ME (Fig 3.3), suggest the accumulation of 1 cm of soil or weathered massive ash in 16 to 27 yrs. In this hypothetical rapid soil-forming environment of Mt. Taranaki, and considering ^{14}C dating errors of max.100 yrs. (Table 3.1), Members MA-ME were likely deposited during a single yet very long ~190-320 yrs episode at ~2.6 ka, separated by quiescence intervals of ~400 yrs from deposition of the under and overlying bed-sets (i.e. from ~3-2.6 ka and ~2.6-2.2 ka, respectively, Fig 3.3). By contrast, Members MF-MG rest on top of Taranaki-sourced deposits of <1.6 cal ka B.P., suggesting that at least 600-1000 yrs. separate the youngest from the oldest Manganui Members.

By this means, the Manganui Formation was produced from relatively frequent and multi-episodic eruptions. Fanthams Peak must be considered a potential future eruptive vent together with the summit crater of Mt. Taranaki, able to produce large-volume basaltic eruption episodes (cf. Coltelli et al. 1998) as have other multi-vent basaltic to andesitic volcanoes (e.g. Tongariro Volcanic Complex, Nairn et al. 1998).

The stratigraphic sequence indicates that Fantham's vent became quiescent at ~1.6-1.4 ka, but the Summit vent remained active, producing at least nine <1.5 ka eruptions that generated five fall deposits and at least 14 PDC units (Fig 3.5). Some of the eruptions produced thick fall deposits that correspond to the 1.2 cal ka B.P. Kaupokonui Member (calibrated from Neall and Jansen 1984) and the ~AD 1655 Burrell Lapilli (Druce 1966; Topping 1971; Platz et al. 2007). Also, many eruptions of this period produced thin fine ash layers on the proximal eastern volcanic flanks, but emplaced valley-filling BAF layers on the northwestern flanks (Druce 1966; Neall 1972; Platz 2007; Platz et al. 2012).

The thickest deposit, suggesting the largest eruption of the last ~1000 years at Mt. Taranaki, corresponds to the ~0.7 cal ka B.P. Te Popo Member, involving three fallouts and three PDC units that formed deposit sequences distributed to the northeast and west (Fig 3.3). The episode started with the emplacement of hot BAFs within the western valleys of the volcano (Platz et al. 2012), with correlative ash blankets on the northeastern side (Fig 3.2). The following three eruption columns covered the east of Mt. Taranaki under ash and pumice fall, with one collapsing to produce a PDC. The eruption column(s) generated fall deposits intermediate in thickness between those of the Burrell and the Kokowai bed-sets (Figs 3.3-3.5).

Within this context, it remains clear that proximal data are essential for increasing the precision of eruptive frequency records. Where these are missing, tephrochronological and hazard-related studies should specify and document the limitations of their interpretations based on incomplete datasets. Statistical models accounting for missing proximal data need to be established in order to assess eruption frequencies and repose-time periods.

Interpretations based only on intermediate-to-distal records could also oversimplify the eruption dynamics, particularly when short run-out depositional events are not represented in medial or distal sites. Hence, we suggest conservative documentation when reporting, for example, sustained eruption columns based on intermediate-to-distal tephra records could be miss-inferred when the proximal PDC deposits are not included.

3.8 Conclusions

A detailed new stratigraphy of proximal volcanic deposits on Mt. Taranaki provides stratigraphical and volcanological data for analysis of 53 eruption events and episodes in the period from ~5 ka to 0.3 ka. The proximal deposits record nine fewer eruptions than does the highest-resolution compilation of medial fall deposits in swamp and lake sequences (Green et al. 2016), but the proximal record gives greater detail about eruption processes (e.g. Fig 3.3a). This additional information is particularly important for developing an understanding of the volcanic hazards, including the style and sequence of events, as well as realistic eruption scenarios for hazard management planning.

From these new proximal details, it is clear that pyroclastic density currents (block and ash flows and column-collapse PDCs) are the most common hazards at Mt. Taranaki, in spite of the fact that they have been poorly recognised from past studies. Furthermore, it

is clear that many eruptions are complex, with multiple phases, including dome growth and collapse, and the repeated production of eruption columns which often collapse (e.g. Fig 3.3a). The new data also shows the great diversity of eruptive styles of largest eruption episodes. We infer tentatively that diversity might be controlled by magma composition and conduit conditions (e.g. Kokowai vs. Upper Inglewood vs. Manganui-D eruptions; Fig 3.3). In the period between ~3-1.5 cal. ka B.P. two vents were erupting and displayed a contrast in composition and eruptive style. Fanthams peak produced basaltic magmas with steady eruptive columns and dominantly fallouts, while the andesitic summit vent produced many domes, short-lived dense vulcanian eruption columns and dominantly PDCs. The hazard profiles of these two, potentially simultaneous eruption sources must be carefully considered in future hazard studies.

In addition, we have revised fall deposit correlations drawn between northeast-distributed and east to southeast-distributed fallout lobes of apparently similar relative stratigraphic position surrounding Mt. Taranaki. At this and other similar volcanoes around the world, medial soil stratigraphies without precise chronology do not provide ideal conditions to relate similar-appearing fall deposits at different sectors around a volcano. By showing more precisely breaks between eruption events/episodes and the strong-sector based variations in stratigraphy, proximal studies can provide a more realistic number of eruptions and a more reliable expectation for eruptions. It remains to be seen whether the large pre-5 ka B.P. tephra in the Taranaki record, which are also depicted with a bilobate form (e.g., Alloway et al. 1995), represent single or multiple eruption events or episodes.

This work shows the importance of recording, where possible, detailed lithostratigraphic data for the nearest-vent sites possible on stratovolcanoes. This approach provides unique insights into the eruptive record. Not only are some eruptions newly recorded, but also

the depth of understanding about the diversity and style of eruption processes can be evaluated, along with the range of eruption sequences that may help develop realistic scenarios for emergency managers.

3.9 Next chapters

In the present chapter, the late-Holocene eruptive history of Mt. Taranki has been reinterpreted, providing a new and highly-detailed stratigraphic basis at this volcano, which resulted from at least 53 different eruptive episodes recognised. In chapter 4, the five best preserved and coarsest deposits from such pyroclastic succession were reassessed in order to estimate eruptive parameters, understand eruptive dynamics, and quantify the magnitude and intensity of the maximum-likely eruptions at Mt. Taranaki. In chapter 5, lithofacies associations were assembled from deposits produced by eruptions studied in chapter 4, and from other eight eruptions recognized in chapter 3. Out of these associations, further deep interpretations on eruptive style and fallout and pyroclastic density current dynamics were established, and three volcanic hazard scenarios were proposed in case of future re-awakening at this volcano.

3.10 References

- Alberico I, Petrosino P and Lirer L (2011) Volcanic hazard and risk assessment in a multi-source volcanic area: the example of Napoli city (Southern Italy). *Nat Hazards Earth Syst Sci* 11:1057-1070
- Alloway B, Lowe DJ, Chan RPK et al (1994) Stratigraphy and chronology of the Stent tephra, a c. 4000 year old distal silicic tephra from Taupo Volcanic Centre, New Zealand. *NZ J Geol Geoph* 37:37-47
- Alloway B, McComb P, Neall V et al (2005) Stratigraphy, age, and correlation of voluminous debris-avalanche events from an ancestral Egmont Volcano: implications for coastal plain construction and regional hazard assessment. *J Royal Soc NZ* 35:229-267
- Alloway B, Neall VE, Vucetich CG (1995) Late Quaternary (post 28,000 year B.P.) tephrostratigraphy of northeast and central Taranaki, New Zealand. *J Royal Soc NZ* 25:385-458

- Andreastuti SD, Alloway BV, Smith IEM (2000) A detailed tephrostratigraphic framework at Merapi Volcano, Central Java, Indonesia: implications for eruption predictions and hazard assessment. *J Volcanol Geoth Res* 100:51-67
- Arce JL, Cervantes KE, Macias JL, Mora JC (2005) The 12.1 ka Middle Toluca Pumice: A dacitic Plinian–subplinian eruption of Nevado de Toluca in Central Mexico. *J Volcanol Geoth Res* 147:125-143
- Arce JL, Macias JL, Vazquez-Selem L (2003) The 10.5 ka Plinian eruption of Nevado de Toluca volcano, Mexico: Stratigraphy and hazard implications. *Geol Soc Am Bull* 115:230-248
- Avellan DR, Macias JL, Sosa-Ceballos G, Velasquez G (2014) Stratigraphy, chemistry, and eruptive dynamics of the 12.4 ka plinian eruption of Apoyeque volcano, Managua, Nicaragua. *Bull Volcanol* 76:792
- Bourdier JL, Pratomo I, Thouret JC et al (1997) Observations, stratigraphy and eruptive processes of the 1990 eruption of Kelut volcano, Indonesia. *J Volcanol Geoth Res* 79:181–203
- Bronk-Ramsey C (2009) Bayesian analysis of Radiocarbon dates. *Radiocarbon* 51(1):337–360
- Brown RJ, Branney MJ (2004) Event-stratigraphy of a caldera-forming ignimbrite eruption on Tenerife: the 273 ka Poris Formation. *Bull Volcanol* 66:392-416
- Carn SA, Pallister JS, Lara L et al (2009) The unexpected awakening of Chaitén Volcano, Chile. *EOS Transactions, AGU* 90(24):205-206
- Cas R, Porritt L, Pittari A, Hayman P (2008) A new approach to kimberlite facies terminology using a revised general approach to the nomenclature of all volcanic rocks and deposits: Descriptive to genetic. *J Volcanol Geotherm Res* 174:226-240
- Cioni R, Bertagnini A, Santacroce R, Andronico D (2008) Explosive activity and eruption scenarios at Somma-Vesuvius (Italy): Towards a new classification scheme. *J Volcanol Geotherm Res* 178:331-346
- Cioni R, Marianelli P, Santacroce R, Sbrana A (2000) Plinian and subplinian eruptions. In: Sigurdsson H, Houghton BF, McNutt SR, Rymer H, Stix J (eds) *Encyclopedia of Volcanoes*. Academic Press, San Diego, pp:477-494
- Coltelli M, Del Carlo P, Vezzoli L (1998) Discovery of a Plinian basaltic eruption of Roman age at Etna volcano, Italy. *Geol* 26(12):1095-1098
- Cronin SJ, Hedley MJ, Neall VE, Smith G (1998) Agronomic impact of tephra fallout from 1995 and 1996 Ruapehu volcano eruptions, New Zealand. *Environ Geol* 34:21-30
- Cronin SJ, Lube G, Dayudi DS et al (2013) Insights into the October–November 2010 Gunung Merapi eruption (Central Java, Indonesia) from the stratigraphy, volume and characteristics of its pyroclastic deposits. *J Volcanol Geoth Res* 261:244-259
- Cronin SJ, Stewart RB, Neall VE et al (2003) The AD1040 to present Maero eruptive period of Egmont Volcano, Taranaki, New Zealand. *Geol Soc NZ Misc Publ* 116A: 43
- Downey WS, Kellett RJ, Smith IEM et al (1994) New palaeomagnetic evidence for the recent eruptive activity of Mt. Taranaki, New Zealand. *J Volcanol Geoth Res* 60:15-27

- Druce AP (1966) Tree-ring dating of recent volcanic ash and lapilli, Mt Egmont. *NZ J Botany* 4:3-41
- Espindola JM, Zamora-Camacho A, Godinez ML et al (2010) The 1793 eruption of San Martín Tuxtla volcano, Veracruz, Mexico. *J Volcanol Geoth Res* 197:188-208
- Fisher R, Schmincke HU (1984) *Pyroclastic Rocks*, Springer-Verlag, Berlin. 472 pp
- Franks AM (1984) *Soils of Eltham County and the tephrochronology of central Taranaki*. Dissertation, Massey University, Palmerston North, New Zealand
- Green RM, Bebbington MS, Jones G et al (2016) Estimation of tephra volumes from sparse and incompletely observed deposit thicknesses. *Bull Volcanol* 78:25
- Henry S, Reyners M, Bibby H (2003) Exploring the plate boundary structure of North Island, New Zealand. *EOS, Trans Am. Geophys Union* 84:289-294
- Hogg AG, Hua Q, Blackwell PG et al (2013) SHCAL13 Southern hemisphere calibration, 0-50,000 years cal BP. *Radiocarbon* 55(4):1889-1903.
- Houghton BF, Wilson CJN, Del Carlo P et al (2004) The influence of conduit processes on changes in style of basaltic Plinian eruptions: Tarawera 1886 and Etna 122 BC. *J Volcanol Geoth Res* 137:1-14
- Kim GB, Cronin SJ, Yoon WS, Sohn YK (2014) Post 19 ka B.P. eruptive history of Ulleung Island, Korea, inferred from an intra-caldera pyroclastic sequence. *Bull Volcanol* 76:802. doi 10.1007/s00445-014-0802-1
- King PR, Thrasher GP (1996) *Cretaceous-Cenozoic geology and petroleum systems of the Taranaki Basin, New Zealand*. Institute of Geological and Nuclear Sciences Monograph 13
- Lube G, Cronin SJ, Thouret JC, Suroño (2011) Kinematic characteristics of pyroclastic density currents at Merapi and controls on their avulsion from natural and engineered channels. *GSA Bull* 123(5/6):1127-1140
- Lucchi F (2013) *Stratigraphic methodology for the geological mapping of volcanic areas: insights from the Aeolian archipelago (southern Italy)*. Geological Society, London, Memoirs 37:35-53
- Macias JL, Sheridan MF, Espindola JM (1997) Reappraisal of the 1982 eruptions of El Chichón Volcano, Chiapas, Mexico: new data from proximal deposits. *Bull Volcanol* 58:459-471
- May DJ (2003) *The correlation of recent tephra with lava flows on Egmont volcano, Taranaki, New Zealand using evidence of mineral chemistry*. Dissertation, University of Auckland, Auckland, New Zealand
- McGlone MS, Neall VE, Clarkson BD (1988) The effect of recent volcanic events and climate changes on the vegetation of Mt Taranaki (Egmont), New Zealand. *N Z J Bot* 26:123-144
- Mortimer N, Tulloch AJ, Ireland TR (1997) *Basement geology of Taranaki and Wanganui Basins, New Zealand*. *NZ J Geol Geoph* 40:223-236
- Nairn IA, Kobayashi T, Nakagawa M (1998) The ~10 ka multiple vent pyroclastic eruption sequence at Tongariro Volcanic Centre, Taupo Volcanic Zone, New Zealand: Part 1. Eruptive processes during regional extension. *J Volcanol Geoth Res* 86:19-44

- Neall VE (1972) Tephrochronology and tephrostratigraphy of western Taranaki (N108-109), New Zealand. *NZ J Geol Geoph* 15:507-557
- Neall VE (1979) Sheets P19, P20, and P21. New Plymouth, Egmont and Manaia. 1st ed. Geological map of New Zealand 1:50,000. 3 maps and notes. NZ Dept of Scientific and Industrial Res, Wellington
- Neall VE (2003) The volcanic history of Taranaki. Institute of Natural Resources, Massey University, Soil & Earth Sciences Occasional Publication 2
- Neall VE, Alloway BV (1986) Quaternary volcanoclastics and volcanic hazards of Taranaki. *NZ Geol Surv Rec* 12:101-137.
- Neall VE, Alloway BV (2004) Quaternary geological map of Taranaki. Institute of Natural Resources-Massey University, Soil and Earth Sciences Occasional Publication No.4
- Neall VE, Jansen HS (1984) Anomalous radiocarbon dates from Mt. Egmont. *Geol Soc of NZ, Miscellaneous Publication* 31A.
- Neall VE, Stewart RB, Smith IEM (1986) History and petrology of the Taranaki volcanoes. In: Smith IEM (ed) Late Cenozoic volcanism. *Royal Society of New Zealand Bulletin* 23:251-263
- Pardo N, Cronin SJ, Palmer A, Németh K (2012a) Reconstructing the largest explosive eruptions of Mt. Ruapehu, New Zealand: lithostratigraphic tools to understand subplinian-Plinian eruptions at andesitic volcanoes. *Bull Volcanol* 74:617-640
- Pardo N, Cronin SJ, Palmer A et al (2012b). Andesitic Plinian eruptions at Mt. Ruapehu: quantifying the uppermost limits of eruptive parameters. *Bull Volcanol* 74:1161-1185
- Platz T (2007) Aspects of dome-forming eruptions from Andesitic Volcanoes exemplified through the Maero Eruptive Period (1000 yrs B.P. to Present) activity at Mt. Taranaki, New Zealand. Dissertation, Massey University, Palmerston North, New Zealand
- Platz T, Cronin SJ, Cashman KV et al (2007) Transitions from effusive to explosive phases in andesite eruptions-A case-study from the AD 1655 eruption of Mt. Taranaki, New Zealand. *J Volcanol Geoth Res* 161:15-34
- Platz T, Cronin SJ, Procter JN et al (2012) Non-explosive dome-forming eruptions at Mt. Taranaki, New Zealand. *Geomorphology* 136:15-30
- Price RC, Gamble JA, Smith IEM et al (2005). An integrated model for the temporal evolution of andesites and rhyolites and crustal development in New Zealand's North Island. *J Volcanol Geoth Res* 140(1-3):1-24
- Price RC, McCulloch MT, Smith IEM, Stewart RB (1992) Pb-Nd-Sr isotopic compositions and trace element characteristics of young volcanic rocks from Egmont Volcano and comparisons with basalts and andesites from the Taupo Volcanic Zone, New Zealand. *Geochimica et Cosmochimica Acta* 56:941-953
- Procter JN, Cronin SJ, Platz T et al (2010) Mapping block-and-ash flow hazards based on Titan 2D simulations: a case study from Mt. Taranaki, NZ. *Nat Hazards* 53:483-501

- Rowland SK, Jurado-Chichay Z, Ernst G, Walker GPL (2009) Pyroclastic deposits and lava flows from the 1759-1774 eruption of El Jorullo, Mexico: aspects of 'violent Strombolian' activity and comparison with Parícutin. In: Thordarson T et al (eds) *Studies in Volcanology: The Legacy of George Walker*. Geol Soc, Special Publications of IAVCEI, 2:105-128
- Salvador A (1994) *International stratigraphic guide. A guide to stratigraphic classification, terminology and procedure*, 2nd ed. Subcommission of Stratigraphic Classification of IUGS International Commission on Stratigraphy and Geological Society of America. Boulder, Colorado, 214 pp
- Saucedo R, Macías JL, Gavilanes JC, Arce JL et al (2010) Eyewitness, stratigraphy, chemistry, and eruptive dynamics of the 1913 Plinian eruption of Volcán de Colima, México. *J Volcanol Geoth Res* 191:149-166
- Shane P (2005) Towards a comprehensive distal andesitic tephrostratigraphic framework for New Zealand based on eruptions from Egmont volcano. *J Quaternary Sc* 20:45-57
- Stewart RB, Price RC, Smith IEM (1996) Evolution of high-K arc magma, Egmont volcano, Taranaki, New Zealand: evidence from mineral chemistry. *J Volcanol Geoth Res* 74:275-295
- Stuiver M, Polach HA (1977) Discussion: Reporting of ¹⁴C data. *Radiocarbon* 19:355-63
- Surono, Jousset P, Pallister J et al (2012) The 2010 explosive eruption of Java's Merapi volcano – A '100-year' event. *J Volcanol Geoth Res* 241-242:121-135
- Topping WW (1971) Burrell Lapilli eruptives, Mount Egmont, New Zealand. *NZ J Geol Geoph* 15:476-490
- Turner MB (2008) *Eruption cycles and magmatic processes at a reawakening volcano, Taranaki, New Zealand*. Dissertation, Massey University, Palmerston North, New Zealand
- Turner MB, Bebbington MS, Cronin SJ, Stewart RB (2009) Merging eruption datasets: building an integrated Holocene eruptive record for Mt. Taranaki, New Zealand. *Bull. Volcanol.* 71:903-918
- Turner MB, Cronin SJ, Bebbington MS, Platz T (2008a) Developing probabilistic eruption forecasts for dormant volcanoes: a case study from Mt Taranaki, New Zealand. *Bull Volcanol* 70:507-515
- Turner MB, Cronin SJ, Bebbington MS et al (2011a) Integrating records of explosive and effusive activity from proximal and distal sequences: Mt. Taranaki, New Zealand. *Quaternary Intl* 246:364-373
- Turner MB, Cronin SJ, Bebbington MS et al (2011b) Relating magma composition to eruption variability at andesitic volcanoes: A case study from Mount Taranaki, New Zealand. *GSA Bulletin* 123 (9/10):2005-2015
- Turner MB, Cronin SJ, Smith IEM et al (2008b) Eruption episodes and magma recharge events in andesitic systems, Mt Taranaki, New Zealand. *J Volcanol Geoth Res* 177:1063-1076
- White JDL, Houghton BF (2006) Primary volcaniclastic rocks. *Geology* 34:677-680
- Whitehead SJ (1976) *Granulometric studies on selected tephra eruptions, North Island, New Zealand*. Dissertation, Massey University, Palmerston North, New Zealand

- Wilson CJN, Houghton BF, McWilliams MO et al (1995) Volcanic and structural evolution of Taupo Volcanic Zone, New Zealand: a review. *J Volcanol Geoth Res* 68:1-28
- Wilson TM, Stewart C, Sword-Daniels V et al (2011) Volcanic ash impacts on critical infrastructure. *J Phys Chem Earth*, doi:10.1016/j.pce.2011.06.006
- Zernack AV, Cronin SJ, Neall VE, Procter JN (2011) A medial to distal volcanoclastic record of an andesite stratovolcano: Detailed stratigraphy of the ring-plain succession of south-west Taranaki, New Zealand. *Intl J Earth Scs* 100:1936-1966
- Zernack AV, Procter JN, Cronin SJ (2009) Sedimentary signatures of cyclic growth and destruction of stratovolcanoes: A case study from Taranaki, NZ. *Sed Geol* 220:288-305

Chapter 4 Diverse dynamics of mafic-intermediate Plinian eruptions

This chapter provides the quantification of the main eruptive parameters of the largest-scale and most diverse eruptions at Mt. Taranaki (i.e. dispersal, eruptive volume, column height, mass-and-volume eruption rates, magnitude and duration). It also discusses these in relation to the chemical composition of magmas and pyroclastic density and porosity determinations. New implications for Plinian/sub-Plinian eruptions at andesitic volcanoes worldwide are proposed.

Chapter 4 comprises the full version of a published journal paper. Its format has been modified to match the overall thesis.

Title Diverse dynamics of Holocene mafic-intermediate Plinian eruptions at Mt. Taranaki (Egmont), New Zealand

Authors Rafael Torres-Orozco, Shane J. Cronin, Magret Damaschke, Natalia Pardo

Status in press at Bulletin of Volcanology (2017), doi: 10.1007/s00445-017-1162-4

Principal author Rafael Torres-Orozco

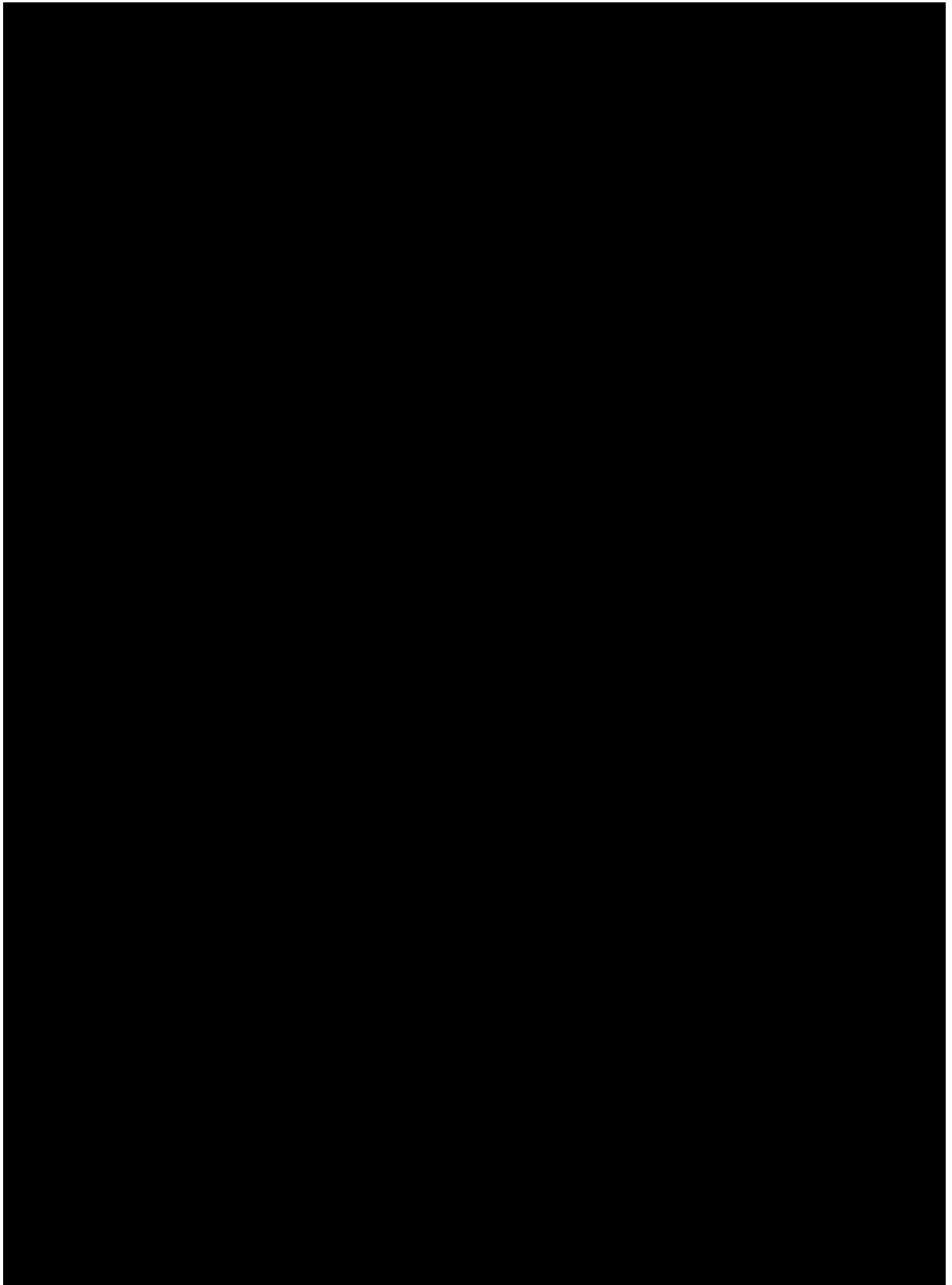
Carried out

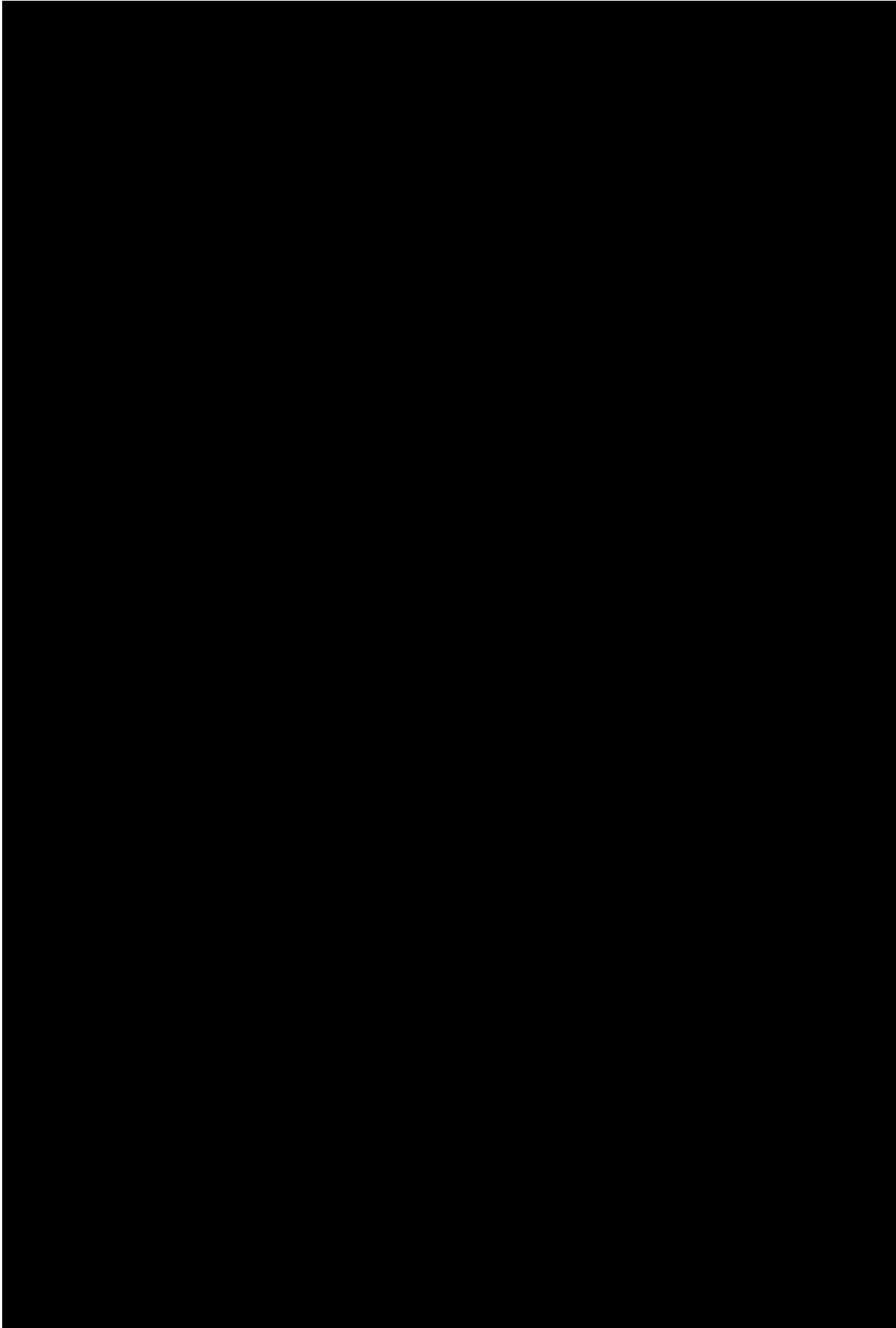
- field descriptions, mapping and sampling,
- laboratory preparation of samples for all the analyses,
- analyses of granulometry, componentry and pycnometry,
- all calculations of eruptive parameters,
- manuscript and figures preparation, writing and submission.

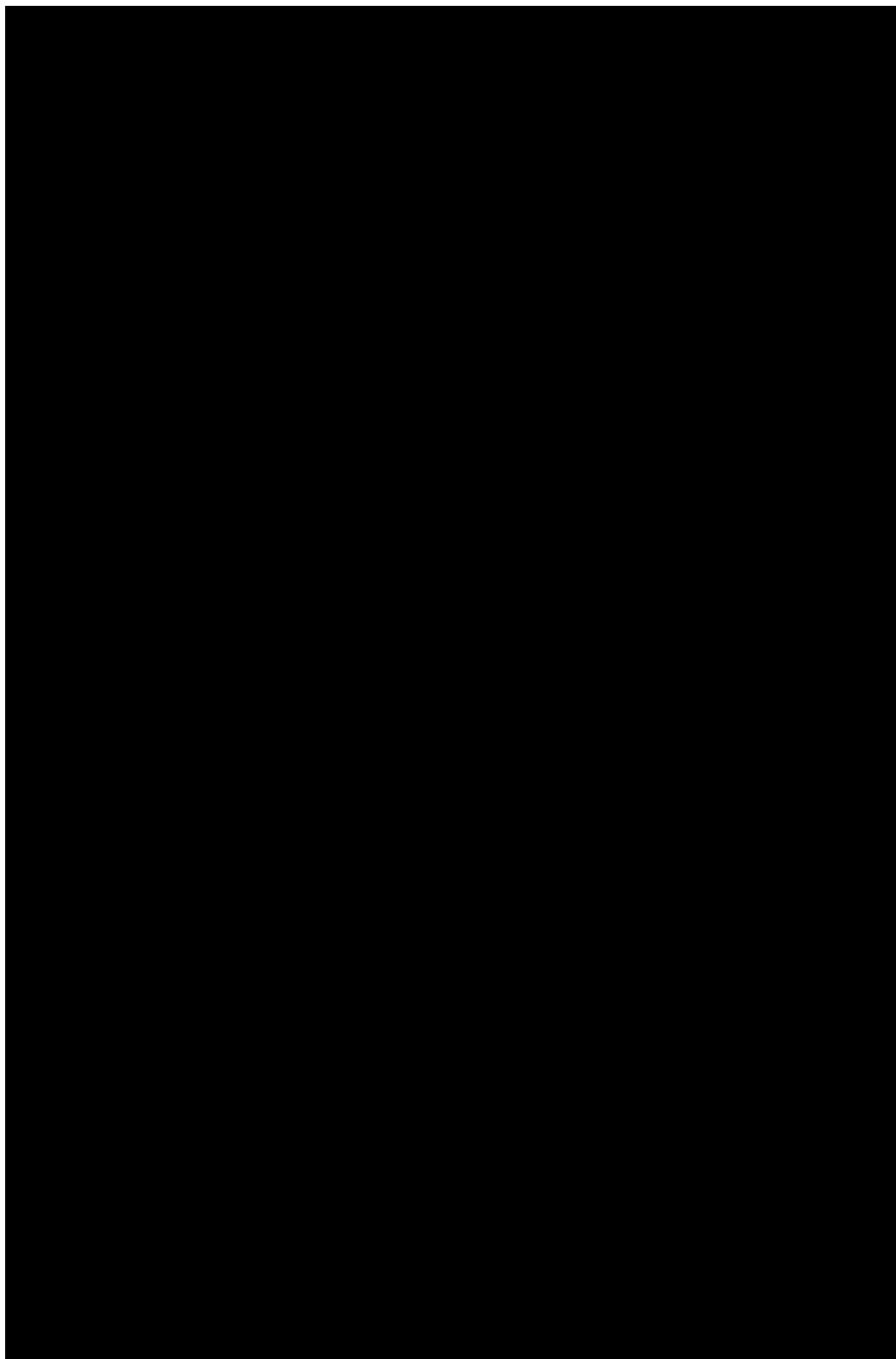
Co-authors Shane J. Cronin, Magret Damaschke and Natalia Pardo

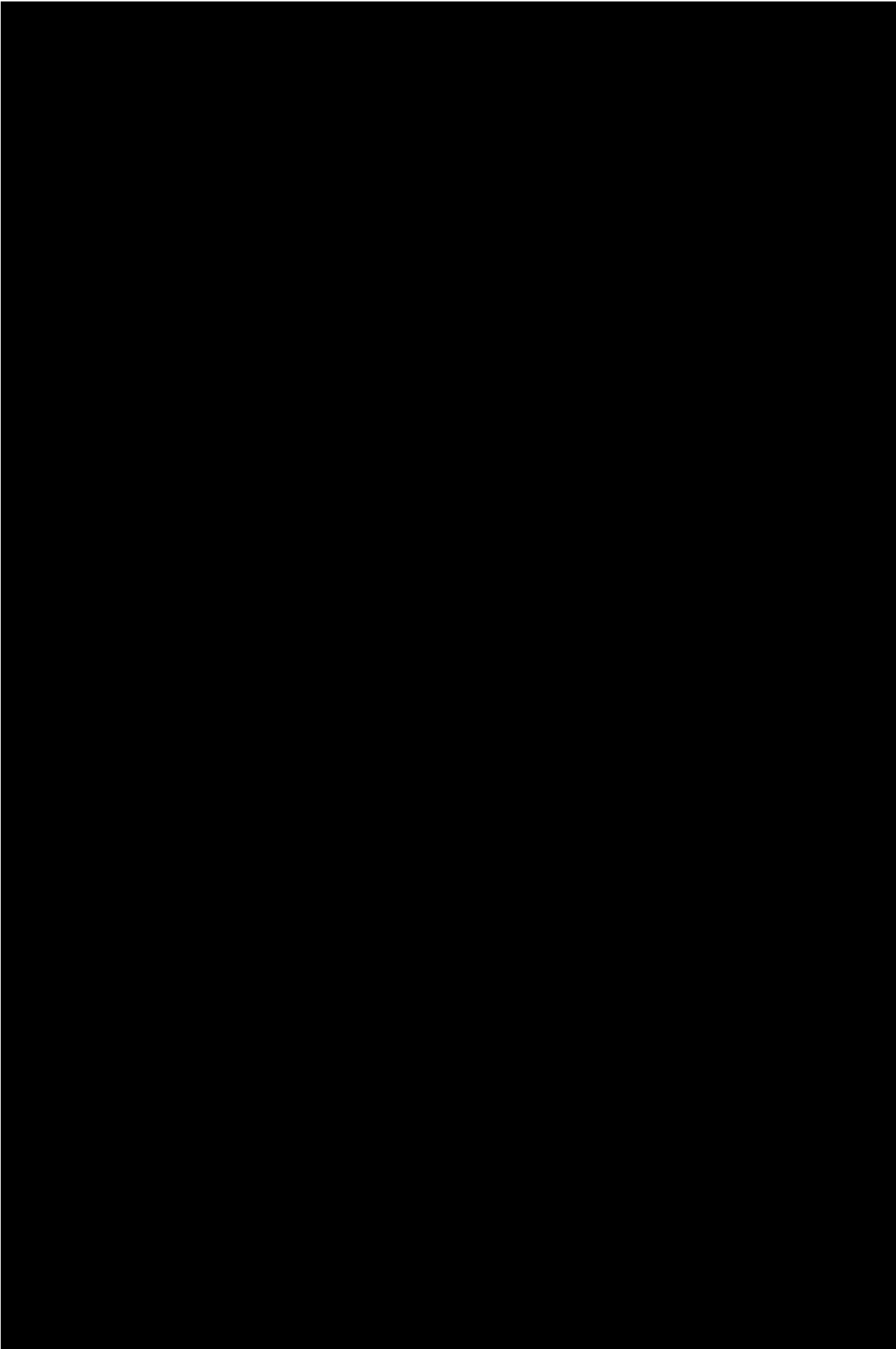
Aided the study by

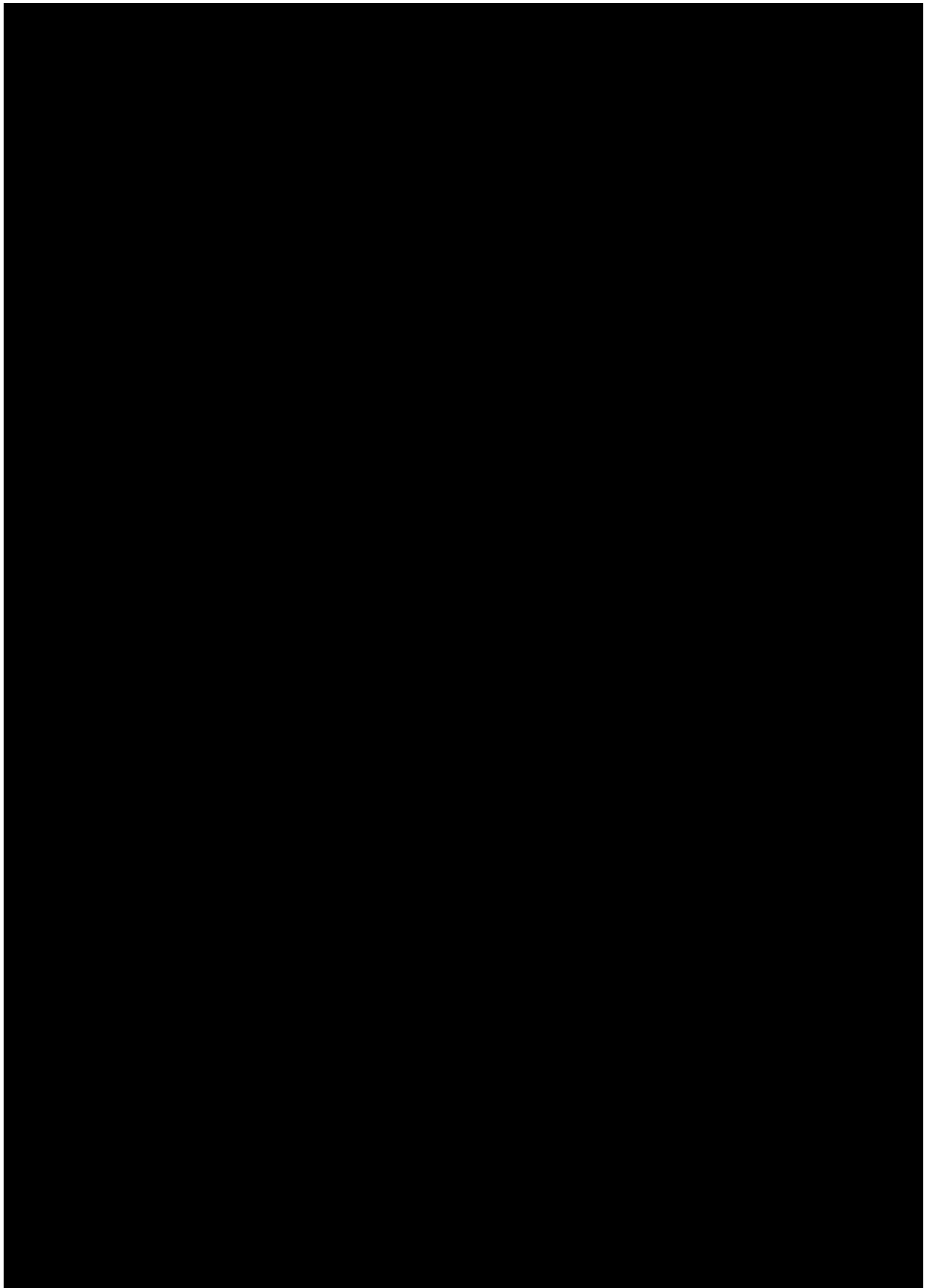
- discussing results,
- reviewing and commenting the manuscript.

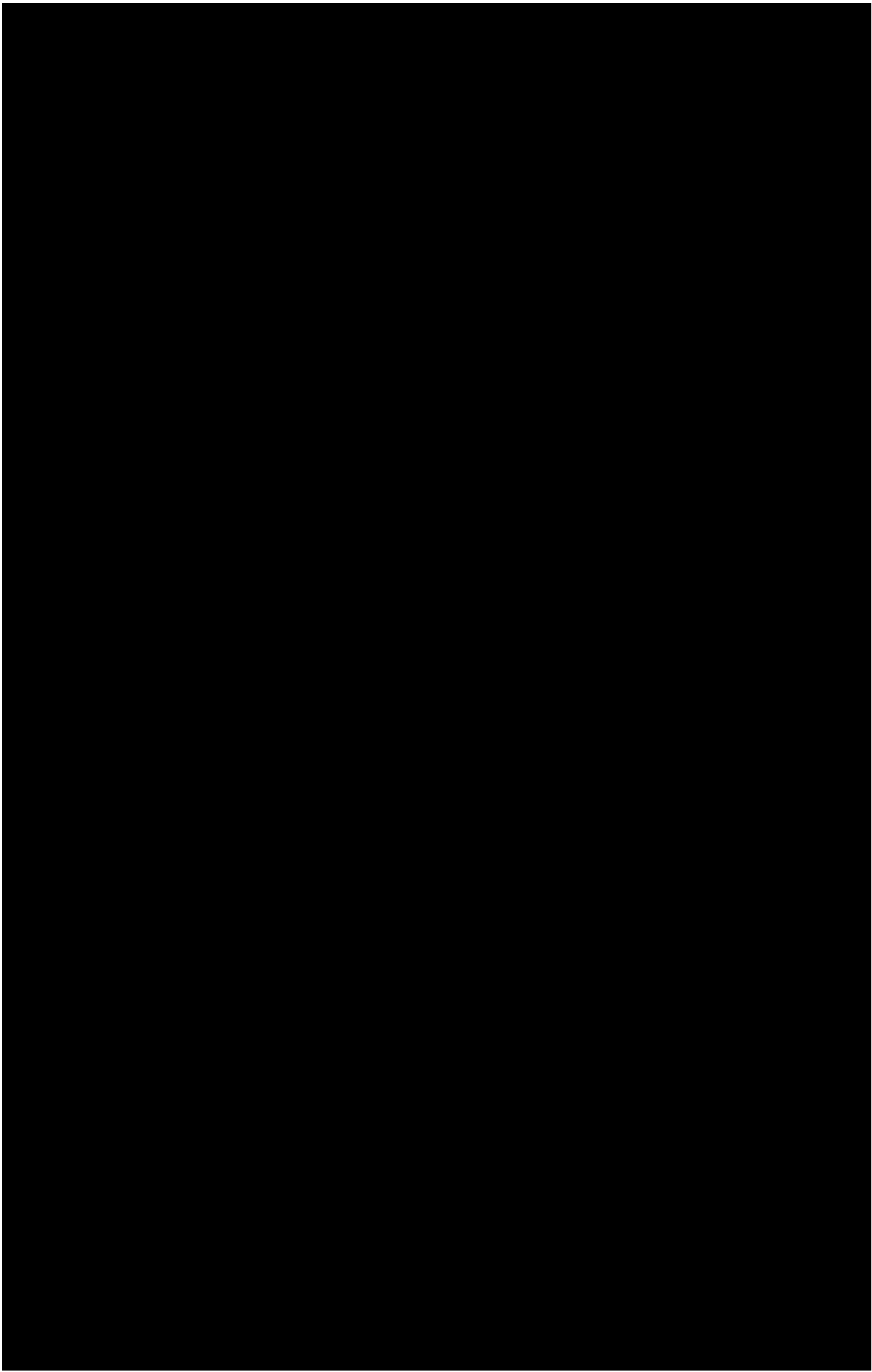


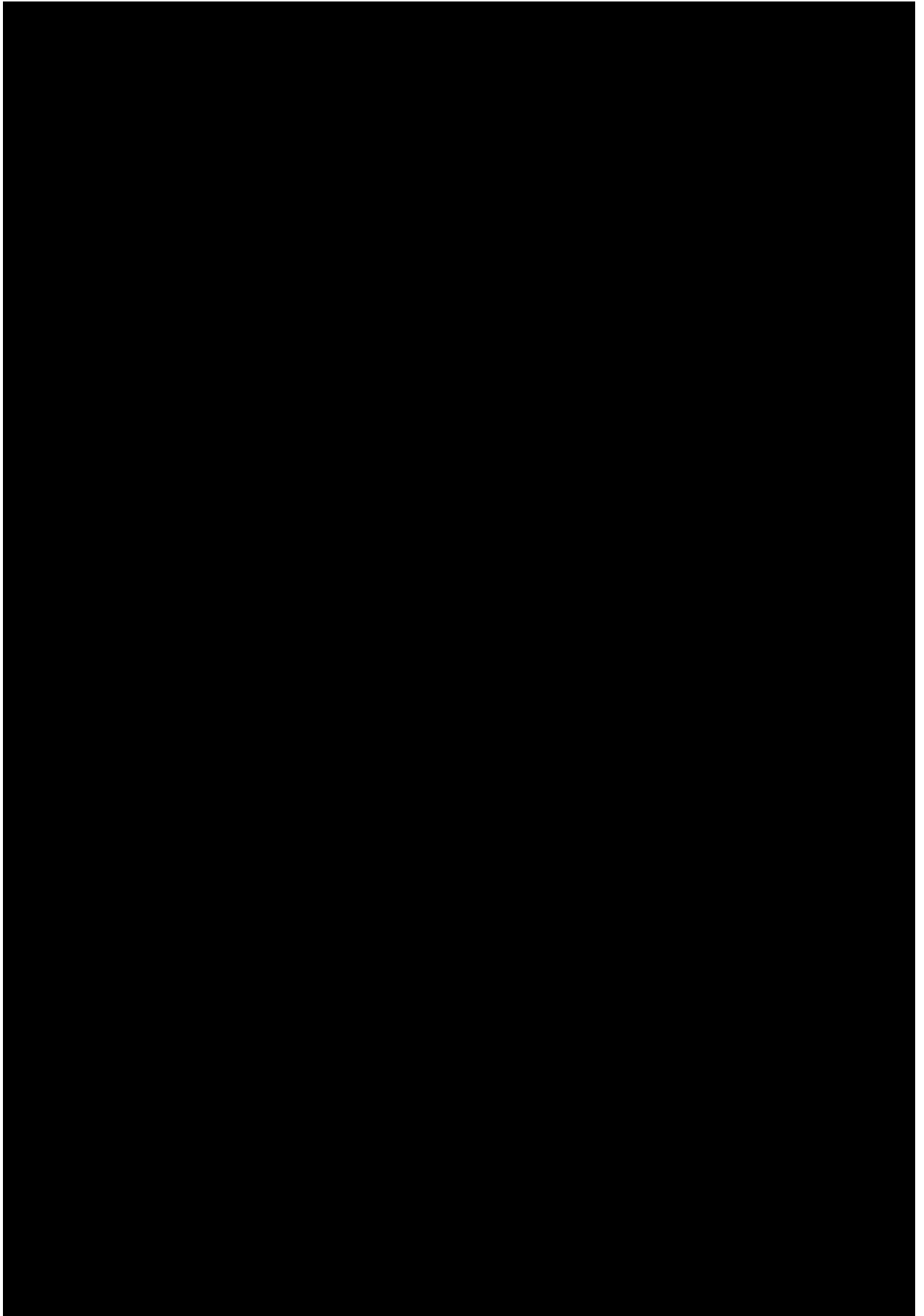


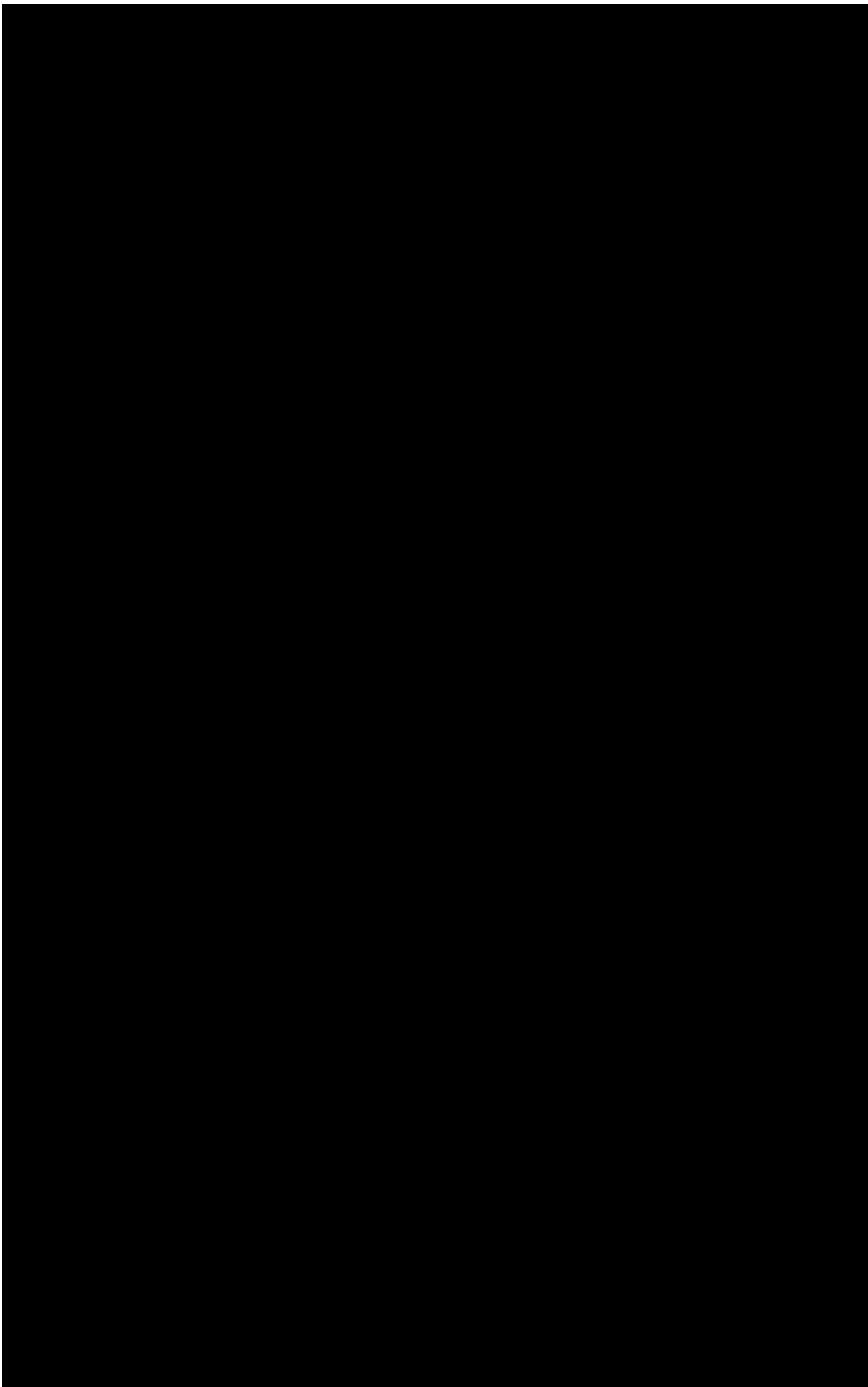


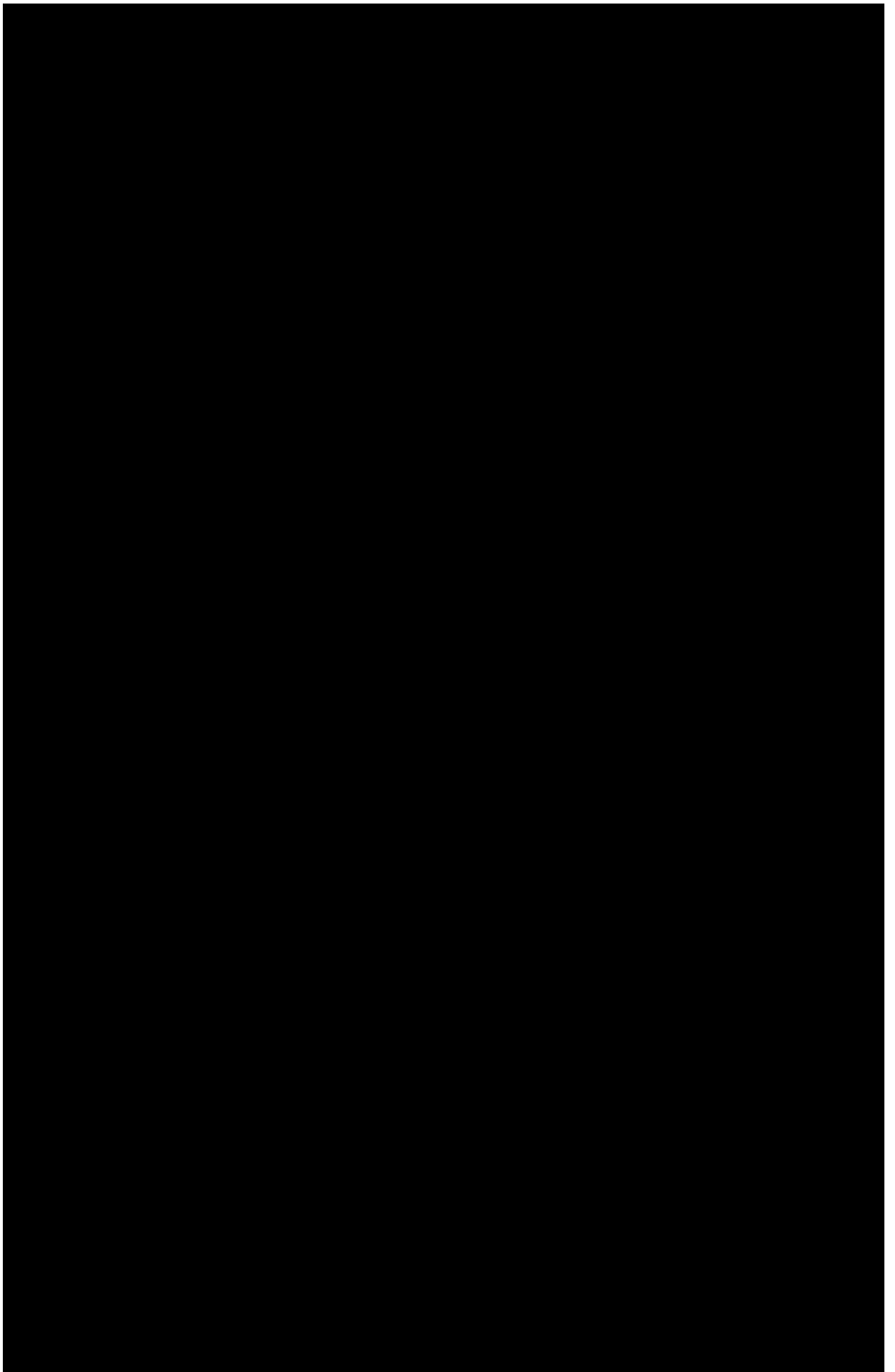


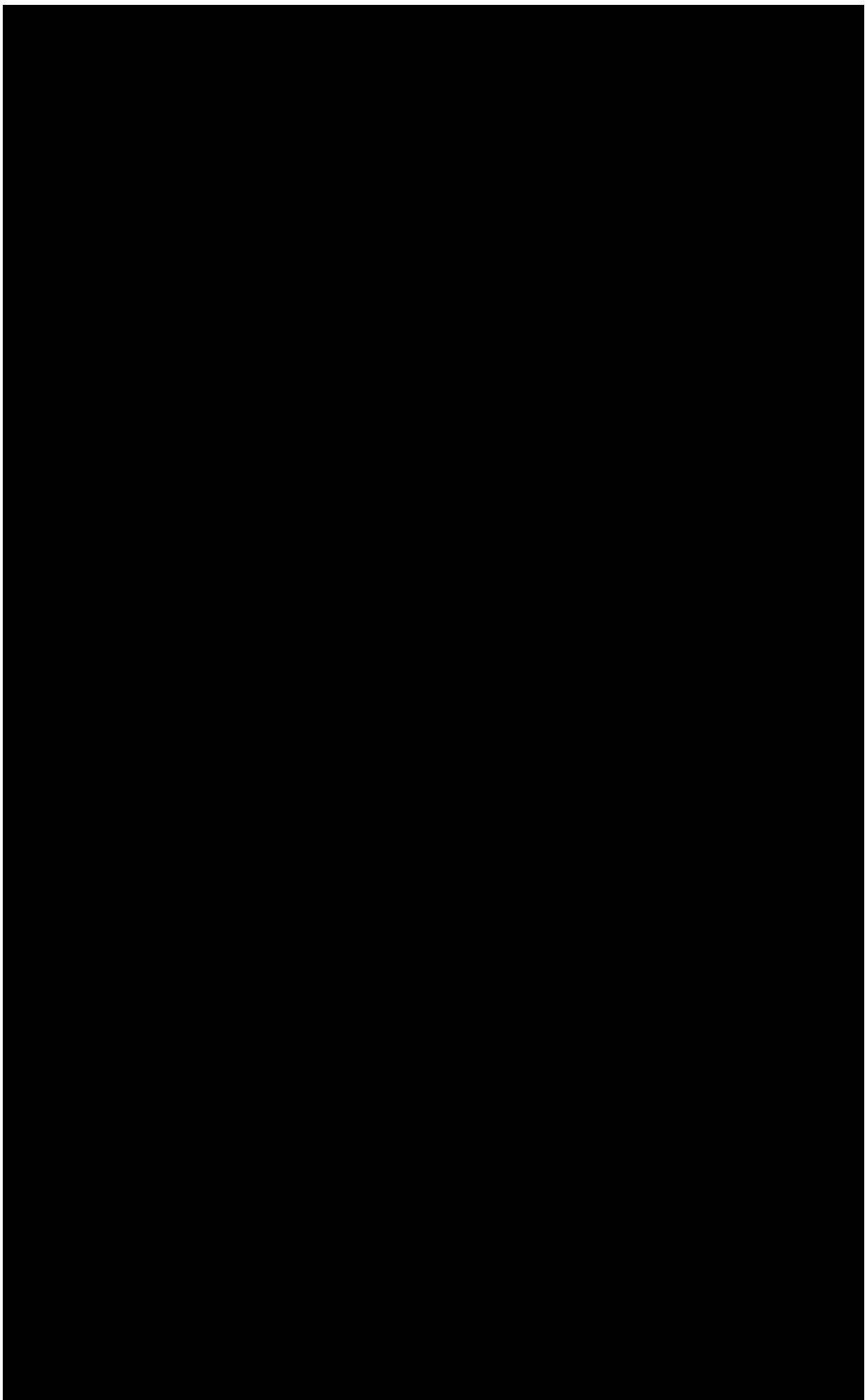


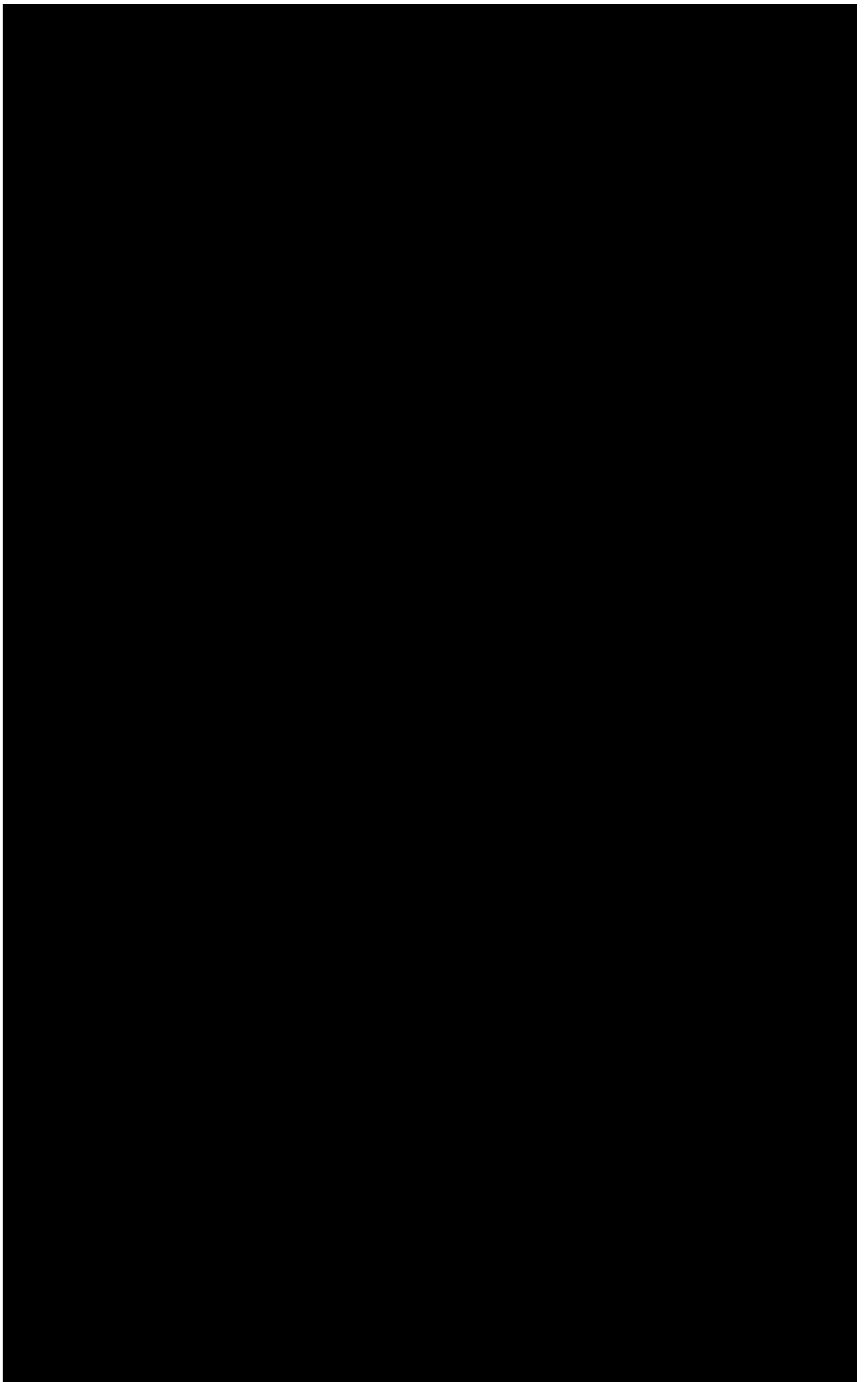


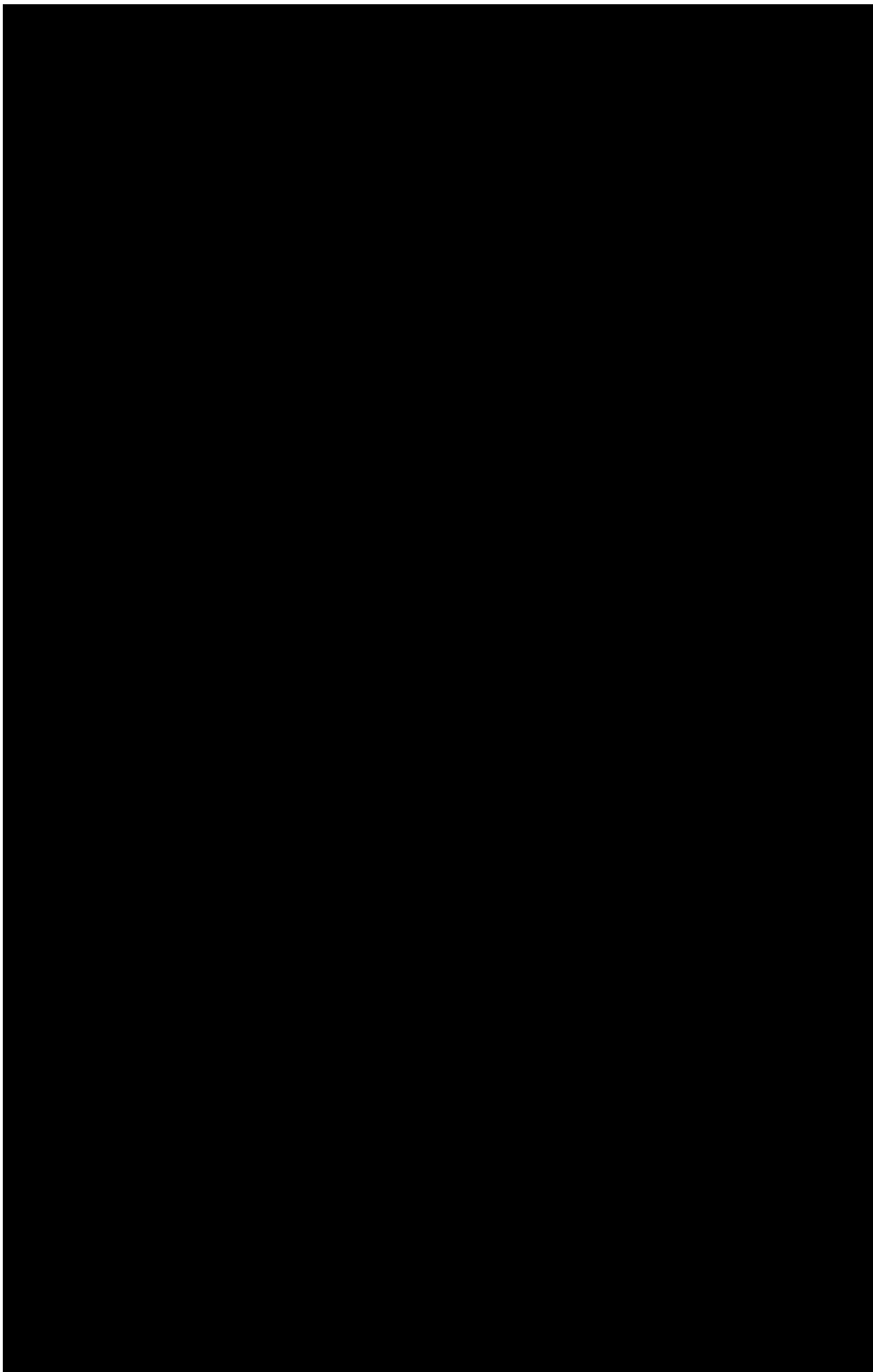


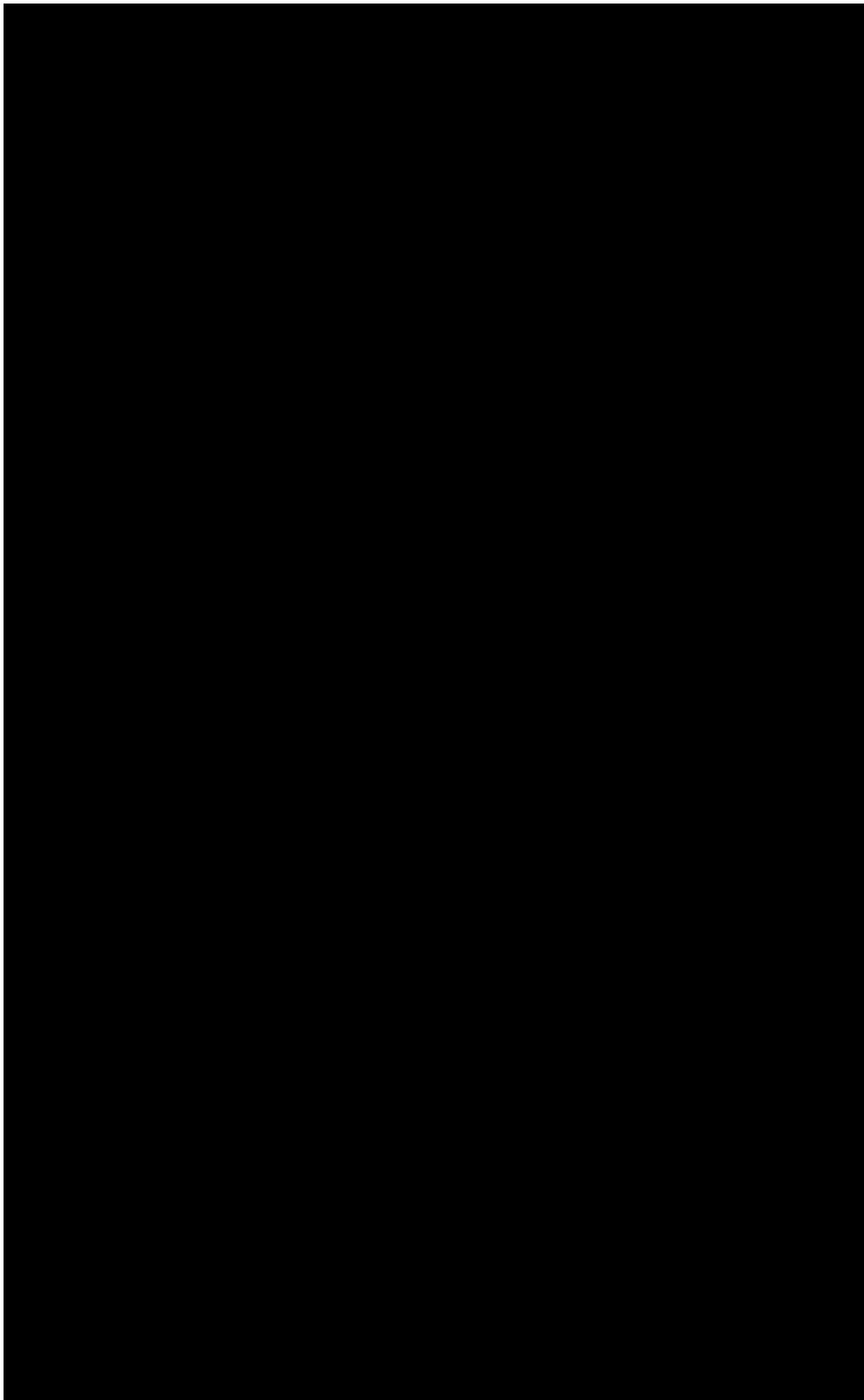


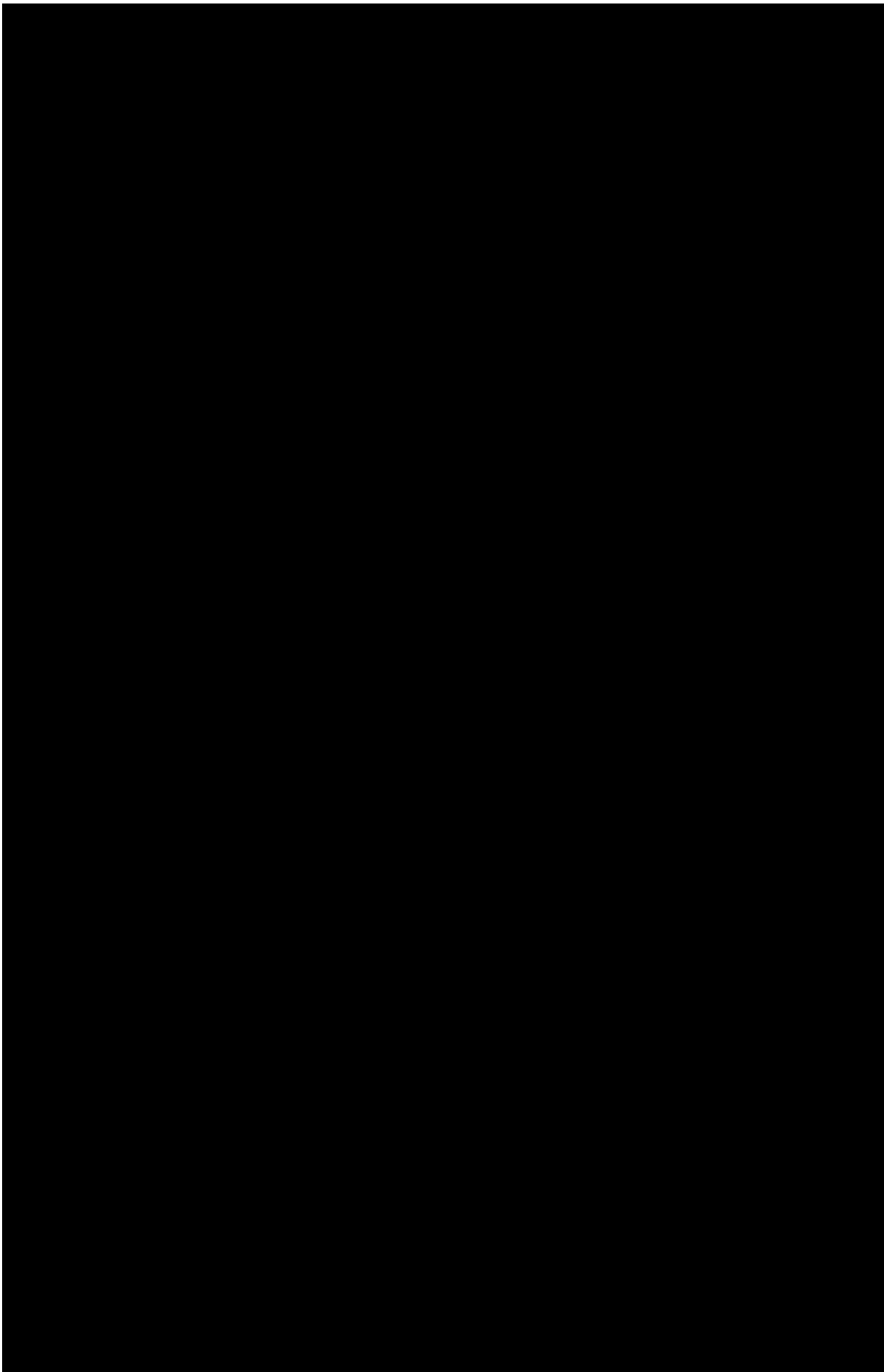


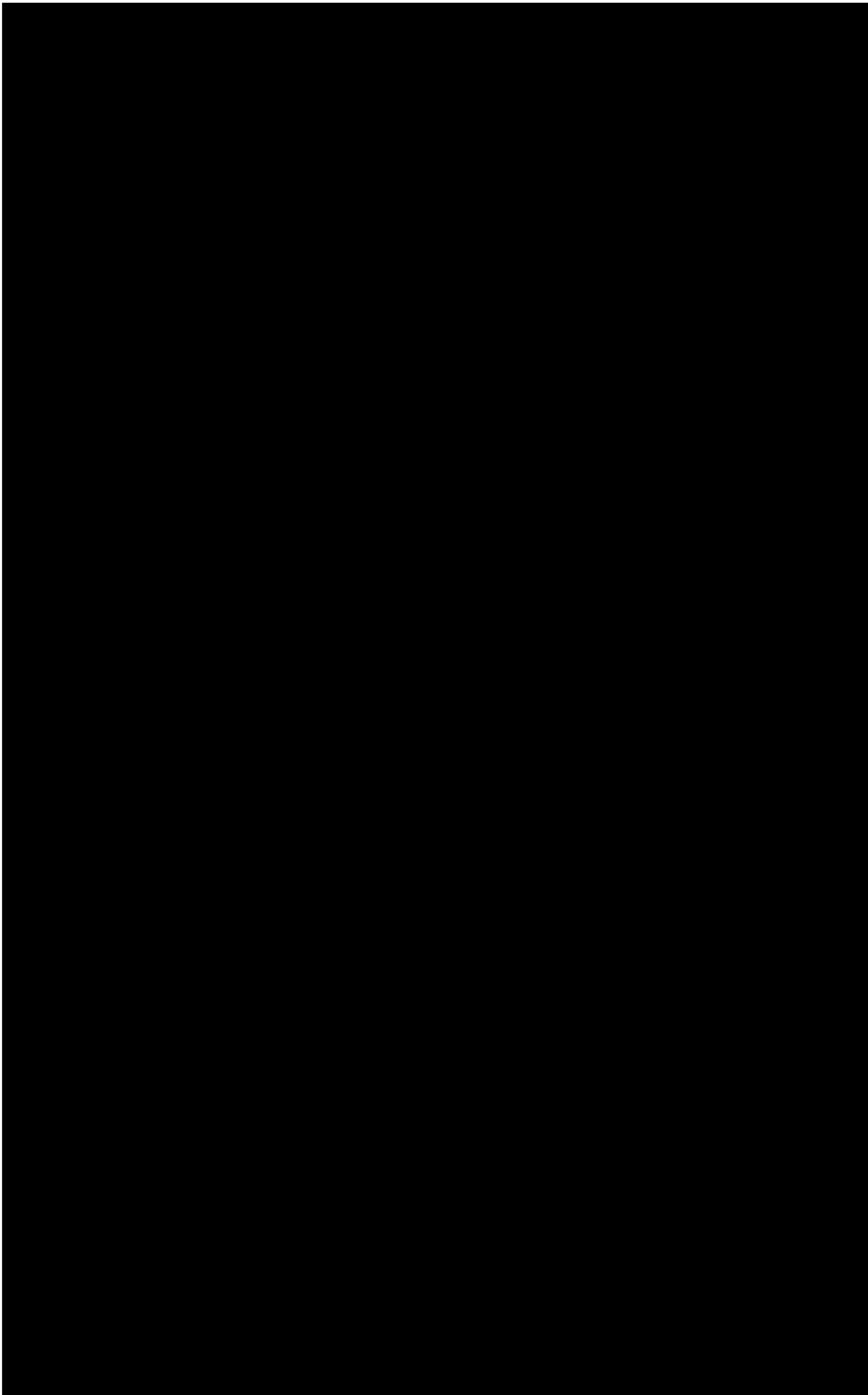


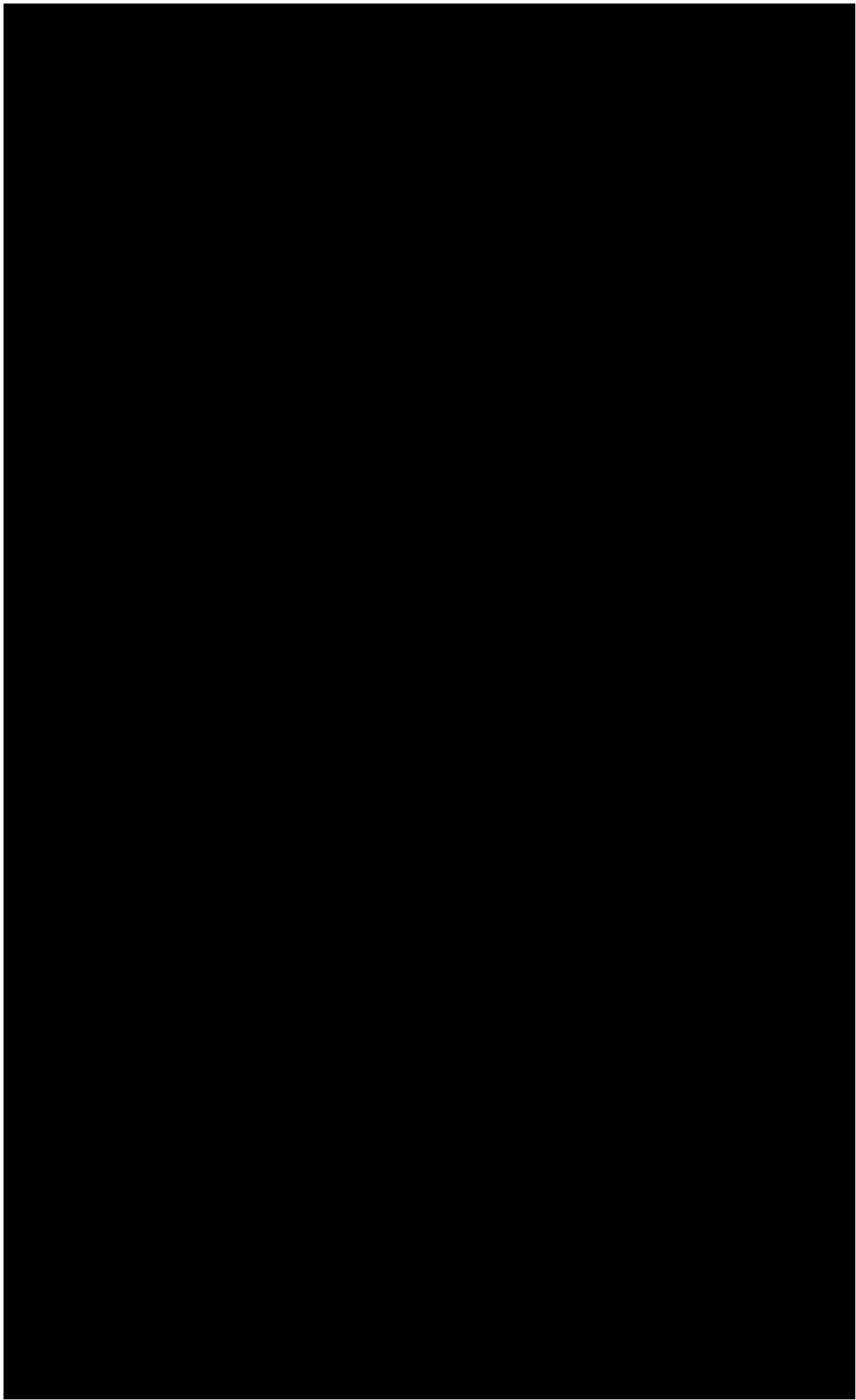


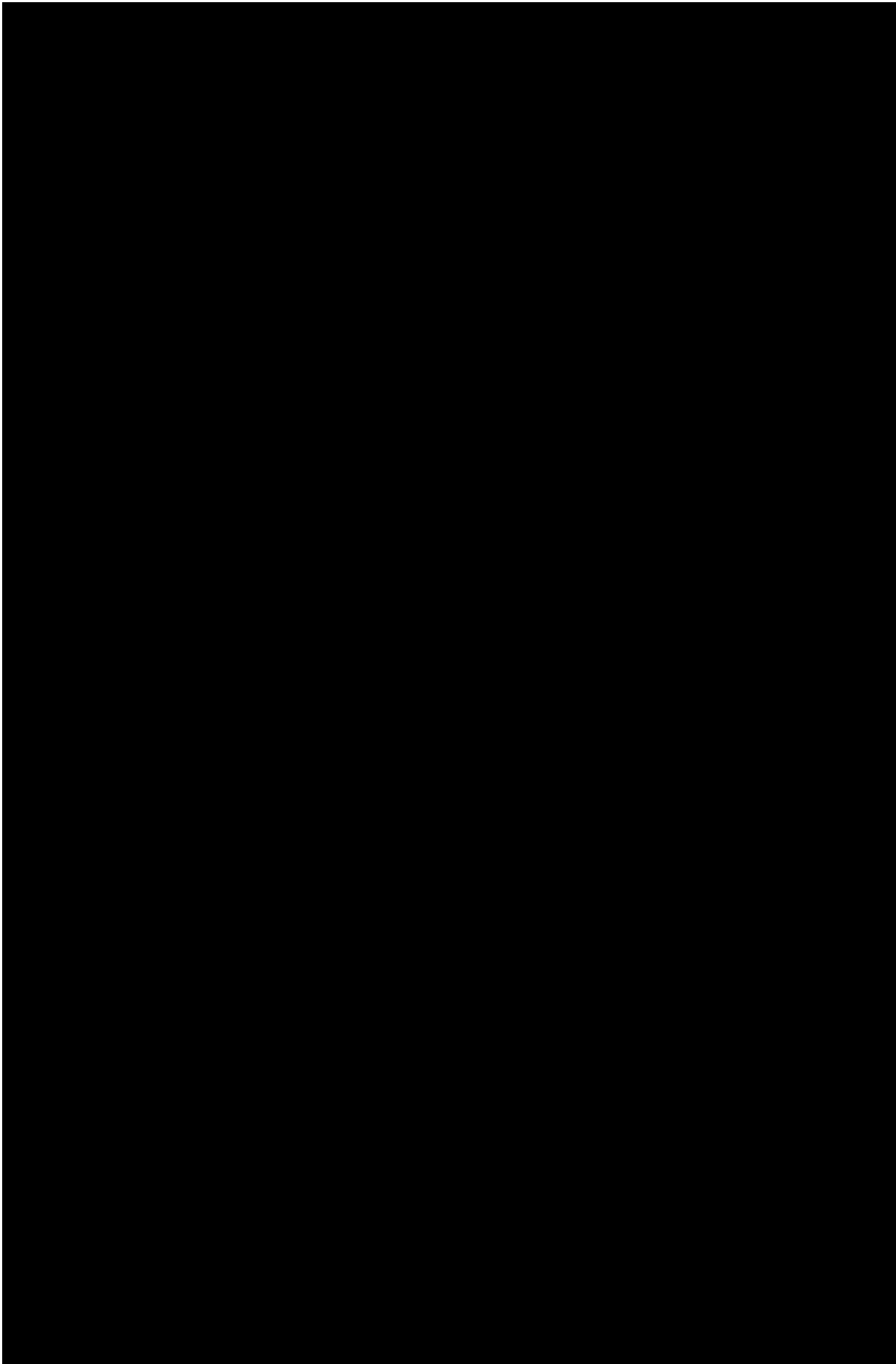


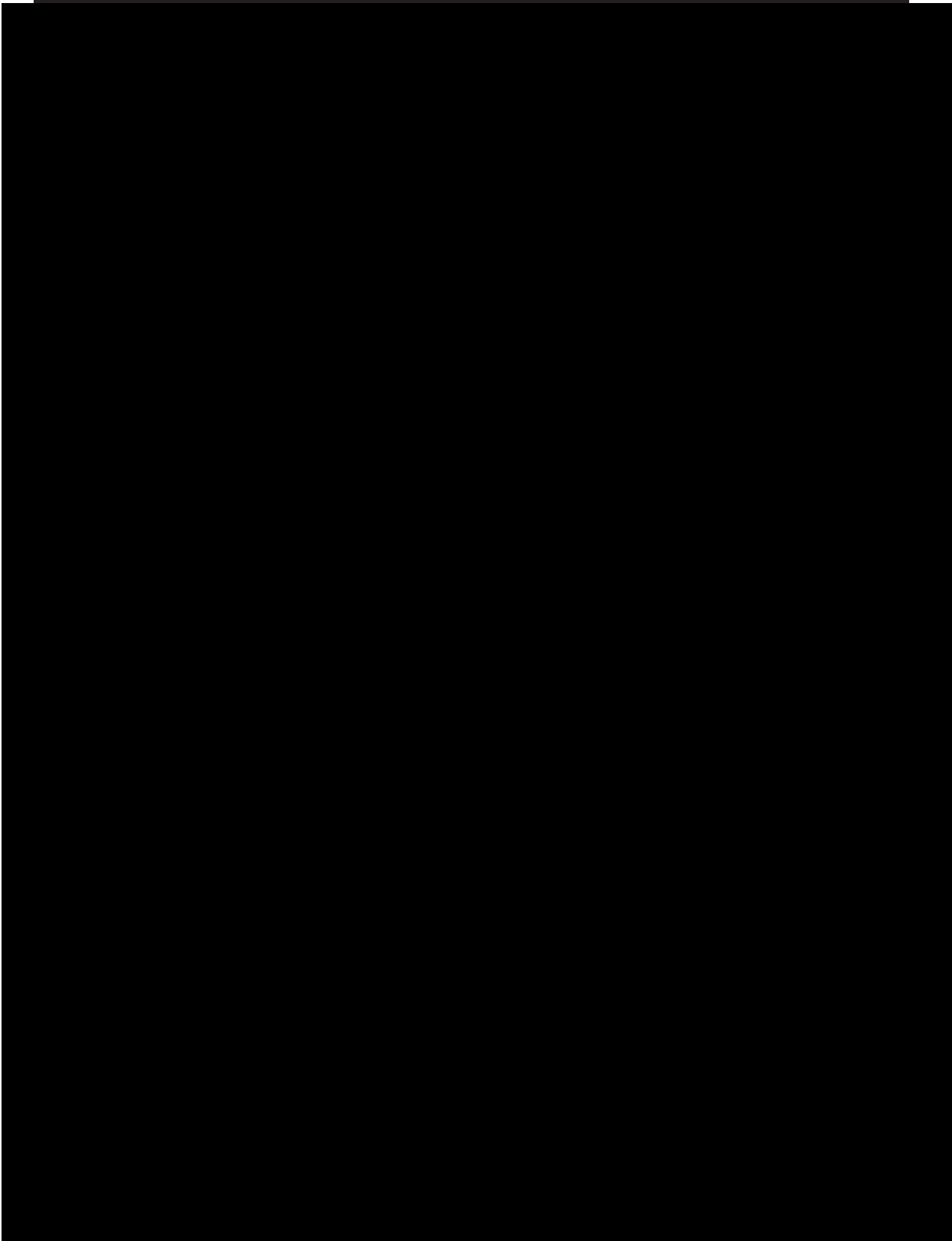


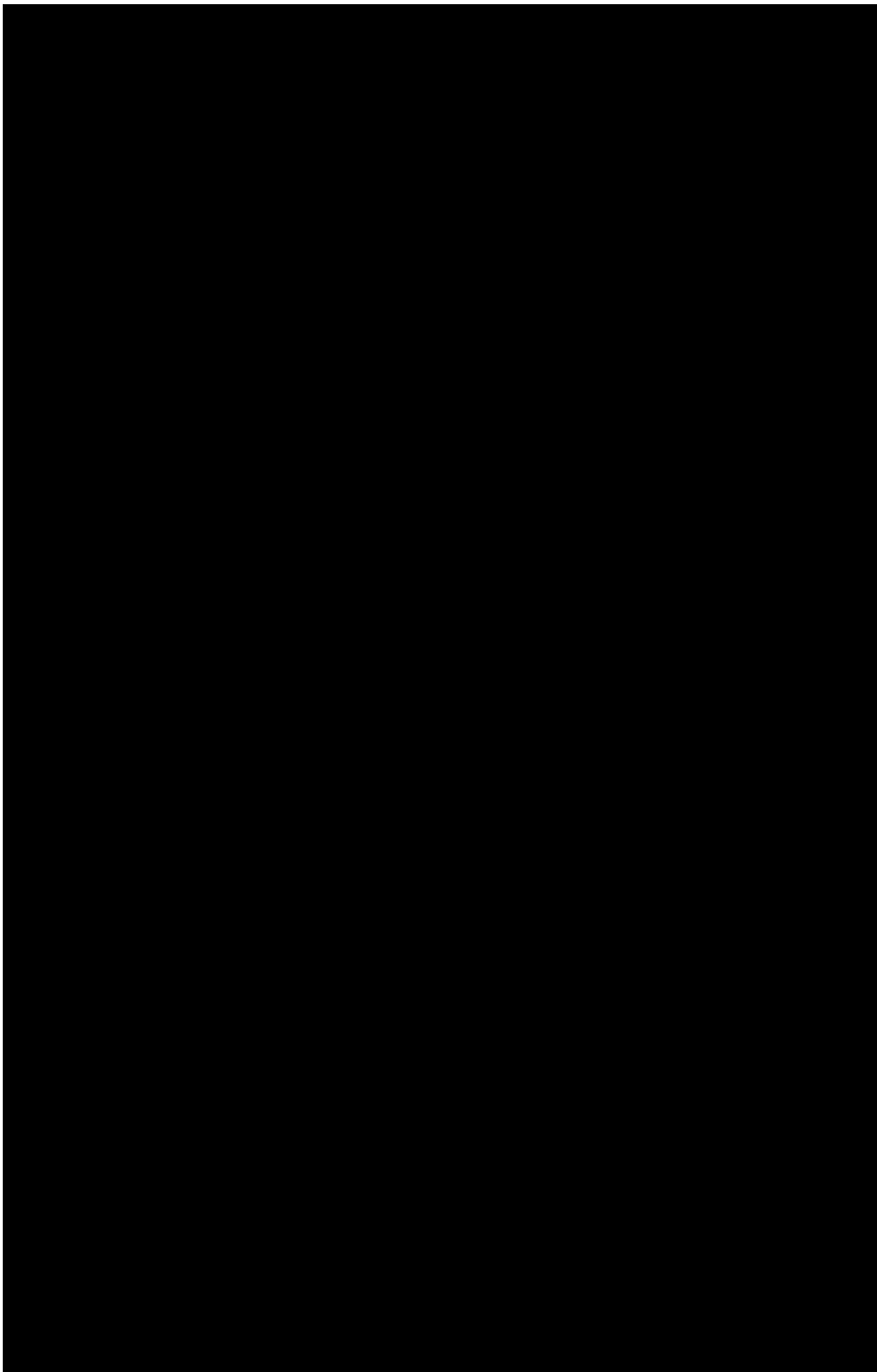


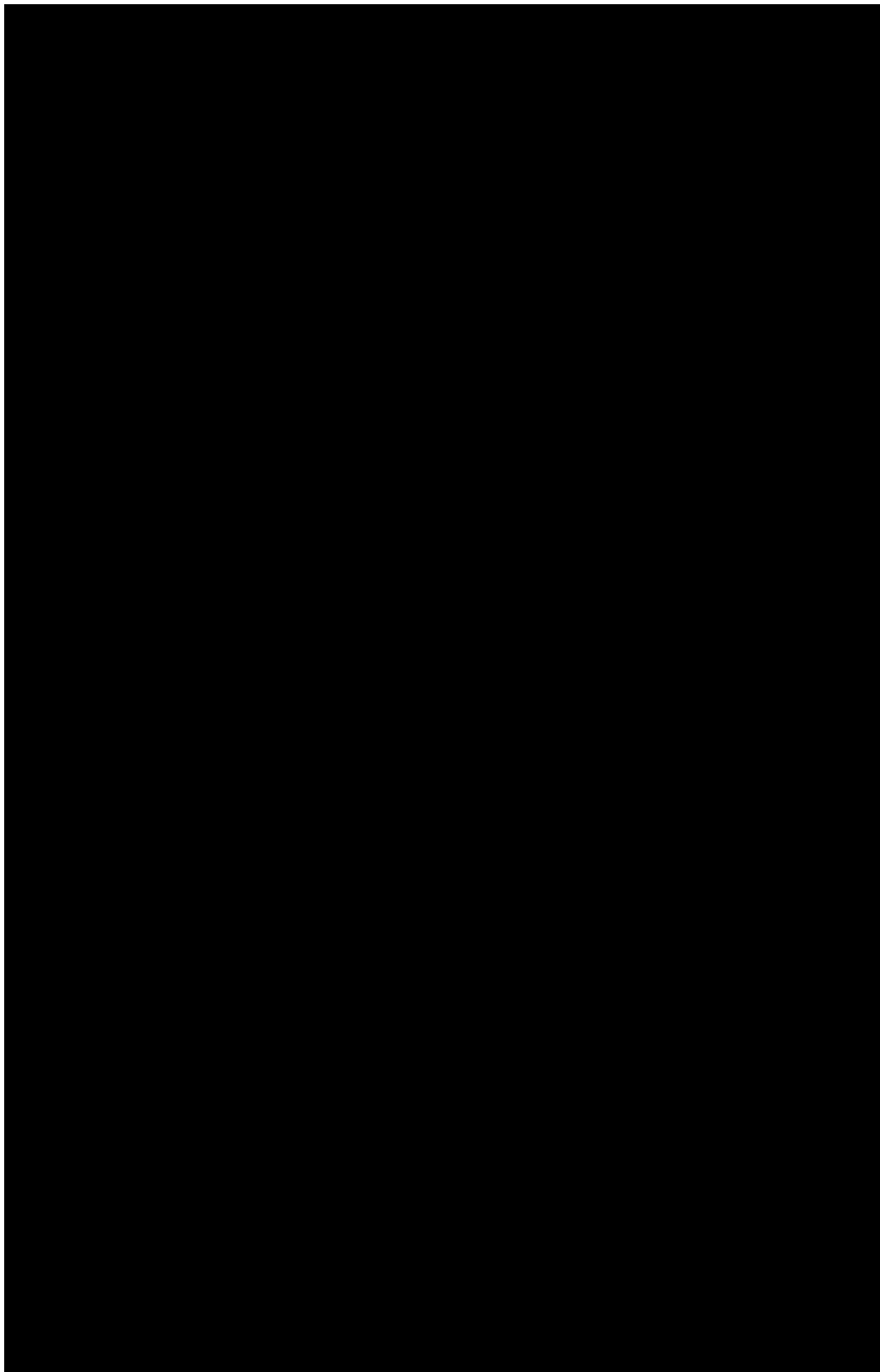


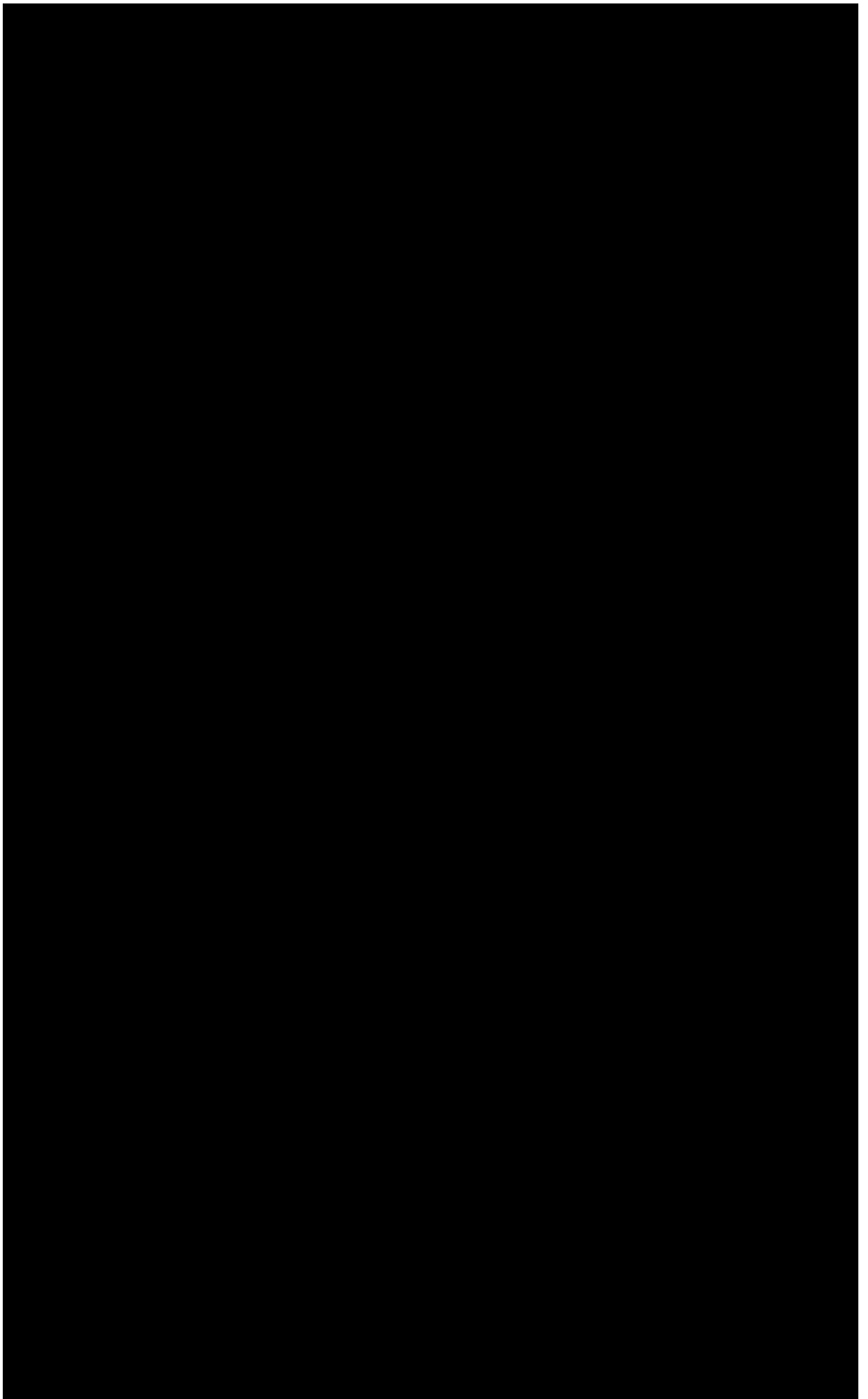


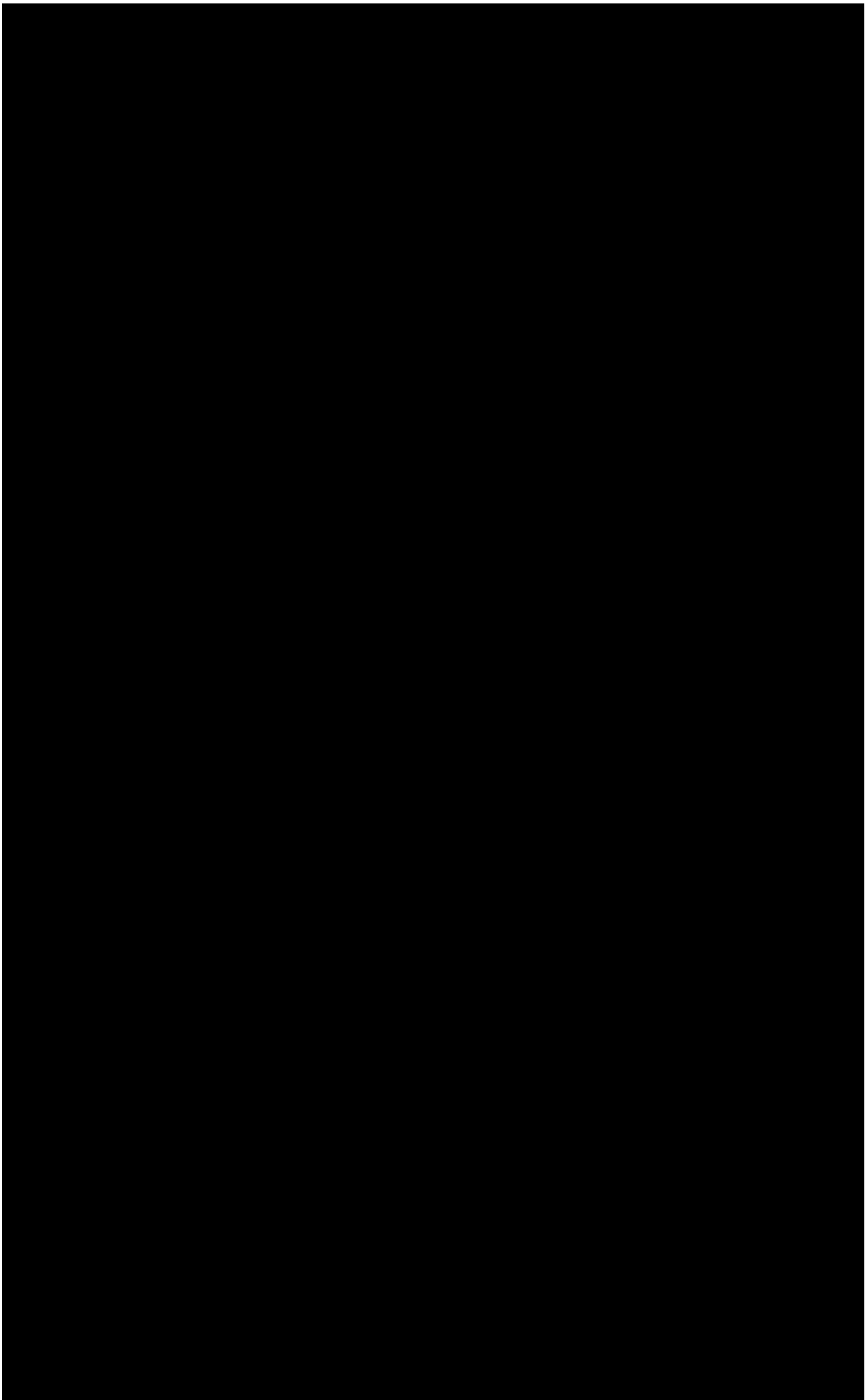


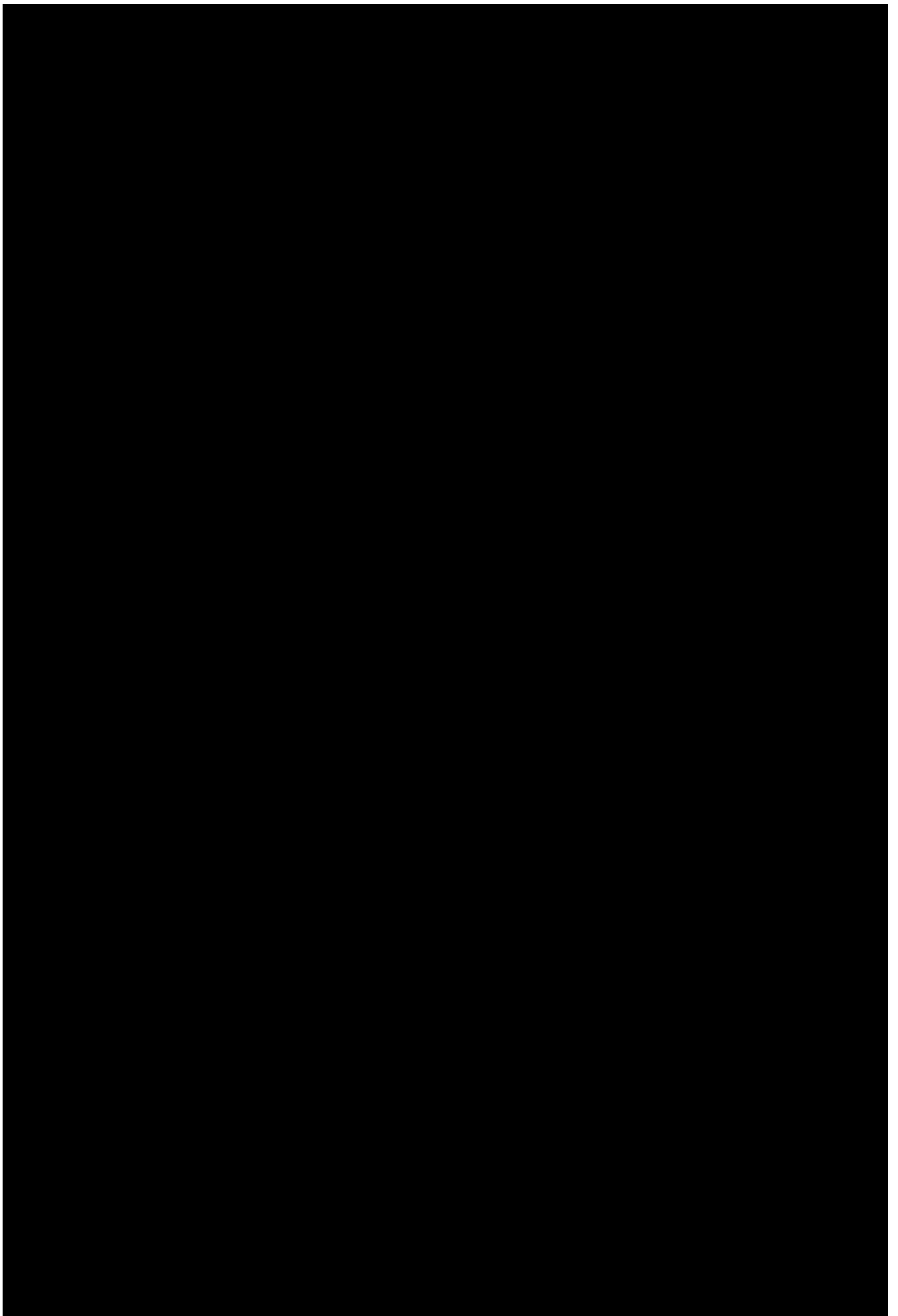












Chapter 5 Volcanic hazard scenarios for Plinian eruptions: insights into PDC diversity

This chapter contains the unification of the geological data produced in this work, into complete volcanic hazard scenarios for Plinian eruptions. These are based on insightful analyses of lithofacies associations assembled from the deposits of eight large-scale late-Holocene eruptive episodes at Mt. Taranaki, and on the interpretation of eruptive processes. The eruptive scenarios demonstrate onset style variations, dynamics and magnitudes expected in case of renewed explosive activity at Mt. Taranaki. In addition, they provide evidence of the variety of pyroclastic density currents (PDCs) erupted at this volcano, and thus, demonstrate the major role that PDCs must have during the hazardscape assessment. These scenarios can be tailored to other similar andesitic stratovolcanoes by completing basic lithostratigraphic studies.

Chapter 5 comprises the full version of a submitted journal paper. Its format has been modified to match the overall thesis.

Title Volcanic hazard scenarios for multi-phase andesitic Plinian eruptions from lithostratigraphy: insights into PDC diversity at Mt. Taranaki, New Zealand

Authors Rafael Torres-Orozco, Shane J. Cronin, Natalia Pardo, Alan S. Palmer

Status in review at the Geological Society of America Bulletin (2017)

Principal author Rafael Torres-Orozco

Carried out

- field descriptions, mapping and sampling,
- laboratory preparation of samples
- analyses of componentry
- manuscript and figures preparation, writing and submission.

Co-authors Shane J. Cronin, Natalia Pardo, Alan S. Palmer

Aided the study by

- discussing results,
- reviewing and commenting the manuscript.

5.1 Abstract

Over the last 5000 years at Mt. Taranaki, a Plinian eruption occurred at least every 300 years, the latest at AD 1655. Based on detailed lithofacies analysis at this volcano, three Plinian eruption scenarios are possible at either the andesitic summit-crater (2500 m-high), or the basaltic Fanthams Peak satellite-vent (1960 m), during future magmatic unrest. These scenarios comprise comparable climactic phases of steady to oscillating eruption columns. Yet contrasting pre- and post-climactic phases, represented by diverse deposits of concentrated to dilute pyroclastic density currents, highlight the major role that PDCs must have during the hazardscape evaluation. The most common scenario (I) begins with closed conduits, rapidly decompressed via unroofing by dome collapse, triggering block-and-ash flows and laterally-directed blast type PDCs. Scenario II involves transient unsteady conditions between open and clogged conduits, by repeated plugging-and-release of chilled magma, producing a range of PDC styles. Scenario III is mainly restricted to satellite vents, and reflects a sudden and rapid progression into open-conduits and quasi-steady Plinian phases. In every case, pyroclastic falls would cover under 10 cm-thick deposits the most populated areas of Taranaki at 20-30 km from the crater, while blast PDCs could threaten farmlands and urban locations at 15-18 km. These scenarios are consistent with recent eruptions at similar andesitic volcanoes, and can be tailored to different sites around the world by localised lithostratigraphic studies. They can also be used to plan emergency management if specific magma compositions, eruption sites, or eruptive styles are confirmed at the outset of episodes.

5.2 Introduction

Plinian and sub-Plinian eruptions from andesitic volcanoes consist of multi-phase eruptive episodes with shifting styles, producing complex pyroclastic successions over intervals of hours to months (e.g., Arce et al. 2003; 2005; Cioni et al. 2000; 2003; 2008; Saucedo et al. 2010; Kim et al. 2014; Torres-Orozco et al. 2017a). Fully understanding the patterns of phases and consequent hazards of these eruptions is challenging despite having comparable peak intensities and magnitudes. A single Plinian eruption can comprise pre-, syn- and post-climactic eruptive phases of variable length, during which eruption columns of different height, duration and stability can occur while affected by variable wind directions. Similarly, pyroclastic density currents (PDCs) triggered by different mechanisms, having diverse mobility, volume, composition and footprint, within the range from concentrated – flow type – to dilute – surge type – PDCs can be produced (e.g., Druitt 1998; Coltelli et al. 1998; Branney and Kokelaar 2002; Brown and Branney 2004; Belousov et al. 2007; Cioni et al. 2000; 2008; Saucedo et al. 2010; Sulpizio et al. 2014; Capra et al. 2014; 2016). Such complex eruptions result from variations in, e.g., mass eruption rate, conduit and vent geometry, gas content, or chemical and rheological magma variability (cf. Cashman et al. 2000; Cioni et al. 2000; Houghton et al. 2004; Shea et al. 2011; 2012). In addition, the steep volcano topography engenders sudden transitions in deposition environment that must be accounted for when interpreting hazards (e.g., Brown and Branney 2004; Belousov et al. 2007; Cronin et al. 2013; Lube et al. 2011; 2014; Kim et al. 2014). Over long periods of inactivity at typical stratovolcanoes, communities grow around them, benefiting from the fertile soils, abundant water and aggregate resources (e.g., Boudon and Lajoie 1989; Bourdier et al. 1997; Macias et al. 1997; Coltelli et al. 1998; Cioni et al. 2000; Carazzo et al. 2012;

Table 5.1 Summary of key lithostratigraphic characteristics and componentry of deposits produced by late-Holocene eruptions at Mt. Taranaki

Layer	Main Lithofacies	Componentry (vol.%)			
		P	DJ	L	C
<u>~2600 cal BP Manganui-D Member</u>					
MD2b	Coherent, poorly vesicular or non-vesicular, porphyritic, andesite blocks				
MD3	Clast-supported, four reversely-graded beds of scoria and hetero-lithic lapilli	66	14	10	10
MD2	Clast-supported, reverse to normally-graded, scoria, basaltic and lithic lapilli	76	14	2	8
MD1	Clast-supported, reverse to normally-graded, scoria, basaltic and lithic lapilli	76	10	8	6
<u>>2600 cal BP Manganui-C Member *</u>					
MC	Clast-supported, thinly and reversely-bedded, scoria, basaltic and lithic lapilli	78	10	2	10
<u><3000 cal BP Manganui-A Member *</u>					
MA3	Matrix-supported, parallel and cross-stratified, pinching-swelling, lithic lapilli-and-ash	13	67	8	12
MA1-2	Clast-supported, two reversely-graded layers of scoria lapilli-and-ash	76	12	8	4
<u>3300 cal BP Upper Inglewood bed-set</u>					
Uig7a	Matrix-supported, massive, pinching, pumice ash				
Uig7	Clast-supported, massive, pumice and andesitic lapilli	67	13	8	12
Uig6	Matrix-supported, parallel and cross-stratified, pinching-swelling, pumice and lithic ash	57	19	7	17
Uig5	Firm, matrix-supported, massive, pinching-swelling, pumice and lithic lapilli-and-ash	53	32	8	7
Uig4	Matrix-supported, parallel-stratified, pinching, pumice and lithic ash	52	35	6	7
Uig3	Matrix-supported, parallel and cross-stratified, pinching-swelling, andesitic lapilli-and-ash	20	61	3	16
Uig2	Firm, matrix-supported, reverse to parallel and cross-stratified, andesitic lapilli-and-ash	5	66	8	21
Uig1	Friable, matrix-supported, reverse to massive, andesitic blocks or blocks-and-ash	2	72	8	18
<u>3500 cal BP Korito bed-set *</u>					
Ko8	Matrix-supported, reverse and massive, pinching, pumice lapilli-and-ash	65	19	5	11
Ko7	Matrix-supported, cross or massive, pinching-swelling, pumice and lithic lapilli-and-ash	46	23	13	18
Ko6	Matrix-supported, parallel or cross, pinching-swelling, pumice and lithic lapilli-and-ash	35	21	14	30
Ko5	Firm, matrix-supported, parallel-bedded or massive, pinching, lithic ash	15	26	19	40
Ko4	Matrix-supported, massive, pinching, pumice and hetero-lithic lapilli-and-ash	45	26	14	15
Ko3a	Matrix-supported, massive, pinching, pumice lapilli-and-ash	55	11	3	31
Ko3	Clast-supported, massive to normally-graded, pumice and topmost lithic lapilli	59	17	10	14
Ko2	Matrix-supported, massive, pinching, pumice and lithic lapilli-and-ash	58	14	5	23
Ko1	Matrix-supported, parallel-bedded, pinching, andesitic ash	12	35	8	45
<u>~3800 cal BP Kapuni-B bed-set *</u>					
KB4	Matrix-supported, massive, pinching, pumice and andesitic lapilli-and-ash	56	12	2	30
KB3	Clast-supported, reverse to massive to normally-graded, pumice lapilli	73	7	3	17
KB2	Clast-supported, reverse to normally-graded, andesitic and lithic lapilli	14	80	1	5
KB1	Clast-supported, reverse to massive, pumice lapilli	72	8	4	16
<u>~3800 cal BP Kapuni-A bed-set *</u>					
KA2	Clast-supported, massive to normally-graded, pumice lapilli	75	9	2	14
KA1	Matrix-supported, parallel and cross-stratified, pinching, andesitic lapilli-and-ash	35	42	8	15
<u>4700-4600 cal BP Kokowai bed-set</u>					
Kw8	Matrix-supported, massive, pinching, pumice and hetero-lithic lapilli-and-ash	70	12	8	10
Kw7	Clast-supported, reverse, massive to normally-graded, pumice lapilli	67	16	7	11
Kw6	Matrix-supported, massive, pinching, pumice lapilli-and-ash	75	10	2	13
Kw5	Matrix-supported, reverse, parallel or faintly cross-stratified, pinching, lithic ash	6	80	4	10
Kw4	Clast-supported, reverse to massive, pumice and topmost andesitic lapilli	82	9	2	7
Kw3	Matrix-supported, massive, pinching, pumice lapilli-and-ash	80	6	4	10
Kw2	Friable, matrix-supported, reversely-graded, andesitic lapilli-and-ash	1	70	5	24
Kw1	Friable, matrix-supported, reverse to massive, andesitic blocks-and-ash	1	70	9	20

All the lithostratigraphic data modified from Torres-Orozco et al. (2017a). P: pumice (or scoria), DL: dense juvenile andesitic or basaltic clasts, L: combined accessory and accidental lithics, C: free crystals.

*Componentry estimated in this work, otherwise modified from Torres-Orozco et al. (2017a; b).

Surono et al. 2012; Cronin et al. 2013). Consequently, aside from defining intensity and magnitude, developing comprehensive hazard scenarios that account for different phases, styles, durations, and hazard types and areas of distribution, throughout complex eruptive episodes, will be important to achieve an effective volcanic hazard management.

Mt. Taranaki/Egmont is a stratovolcano located in the centre of a populous (>100,000 inhabitants) and productive (4.2% Gross Domestic Product) region of New Zealand (Statistics NZ 2013), home to the nation's energy and a large portion of the dairy industry (Taranaki Regional Council 2017). This andesitic cone has experienced at least 16 Plinian and sub-Plinian eruptive episodes during the last 5000 years (Torres-Orozco et al. 2017a), forming successions of intercalated fall and PDC deposits in proximal sites that represent climactic phases, and a variety of pre- and post-climactic eruptive styles (Torres-Orozco et al. 2017a; b). Comparable Plinian eruptions have been produced throughout the >170 ka geological history of Mt. Taranaki (Alloway et al. 1995; Zernack et al. 2011; Turner et al. 2011; Damaschke et al. 2017), however, only the <5 ka eruption deposits remain well preserved.

In this work, multiphase volcanic hazard scenarios applicable to a broad range of andesitic stratovolcanoes were developed from the proximal lithostratigraphic records of eight of the largest <5 ka eruptions at Mt. Taranaki, corresponding to the Kokowai, Kapuni-A, Kapuni-B, Korito, Upper Inglewood, Manganui-A, Manganui-C, and Manganui-D eruptive episodes. The defining lithostratigraphic characteristics and geochronology of deposits produced by these eruptions were studied by Torres-Orozco et al. (2017a, Table 5.1). The chemical composition, distribution, intensity and magnitude of the best preserved sub-Plinian and Plinian eruption deposits were estimated by Torres-Orozco et al. (2017b, Table 5.2). Here we focus on analysing the lithofacies associations resulting

Table 5.2 Late-Holocene Plinian / sub-Plinian eruptions at Mt. Taranaki

Age (cal BP)	Eruptive Episode	Column Height (km)	Min. Volume (km ³)	MDR (kg/s)	Magnitude*	Eruption Type	SiO ₂ [†] (wt.%)
300	Burrell	14-17	0.10	1.3 x 10 ⁷	4.1	sub-Plinian	56.5
1200	Kaupokonui	14-16	0.13	1.2 x 10 ⁷	4.3	sub-Plinian	54.0
2600	Manganui-D	25-27	0.50	1.1 x 10 ⁸	4.9	Plinian	49.8
3300	Upper Inglewood	22-24	0.30	7.6 x 10 ⁷	4.7	Plinian	58.5
4700-4600	Kokowai 7	21-22	0.10	5.8 x 10 ⁷	4.2	sub-Plinian	54.0
4700-4600	Kokowai 4	27-29	1.10	1.8 x 10 ⁸	5.1	Plinian	55.2

All data were sourced from Torres-Orozco et al. (2017a, b). Min: minimum, MDR: mass-discharge-rate.

*Calculated by the original authors following the method of Pyle (2000).

[†]Corresponds to the average SiO₂ wt.% estimated from the source data.

from the lateral and longitudinal variations in deposition. These provide qualitative approximations to the eruptive style and magnitude, when field deposit-data are insufficient to empirically estimate eruptive parameters (e.g., Nemeth and White 2003; Brown and Branney 2004; Cioni et al. 2008; Lucchi 2013; Kim et al. 2014). Based upon our new evidence, we also report an up-to-date examination on the variety of PDC processes at Mt. Taranaki, before only suggested (e.g., Procter et al. 2010; Turner et al. 2008a; 2011; Platz et al. 2012). By these means, our lithofacies analysis captures a broad spectrum of eruptive styles, transitions, and spatial distribution of impacts during Plinian eruptive episodes, that support hazard scenarios, assessment, and emergency management.

5.3 Geological background

New Zealand's North Island lies over the south-Pacific convergent boundary between the Australian and Pacific Plates, with the latter being subducted along the Hikurangi Trough (Henrys et al. 2003; Fig. 5.1). The ~170 ka to AD 1800 Mt. Taranaki constitutes New Zealand's westernmost (~400 km west of the Trough) and largest andesitic stratovolcano associated with this subduction system (Price et al. 2005; Zernack et al. 2011).

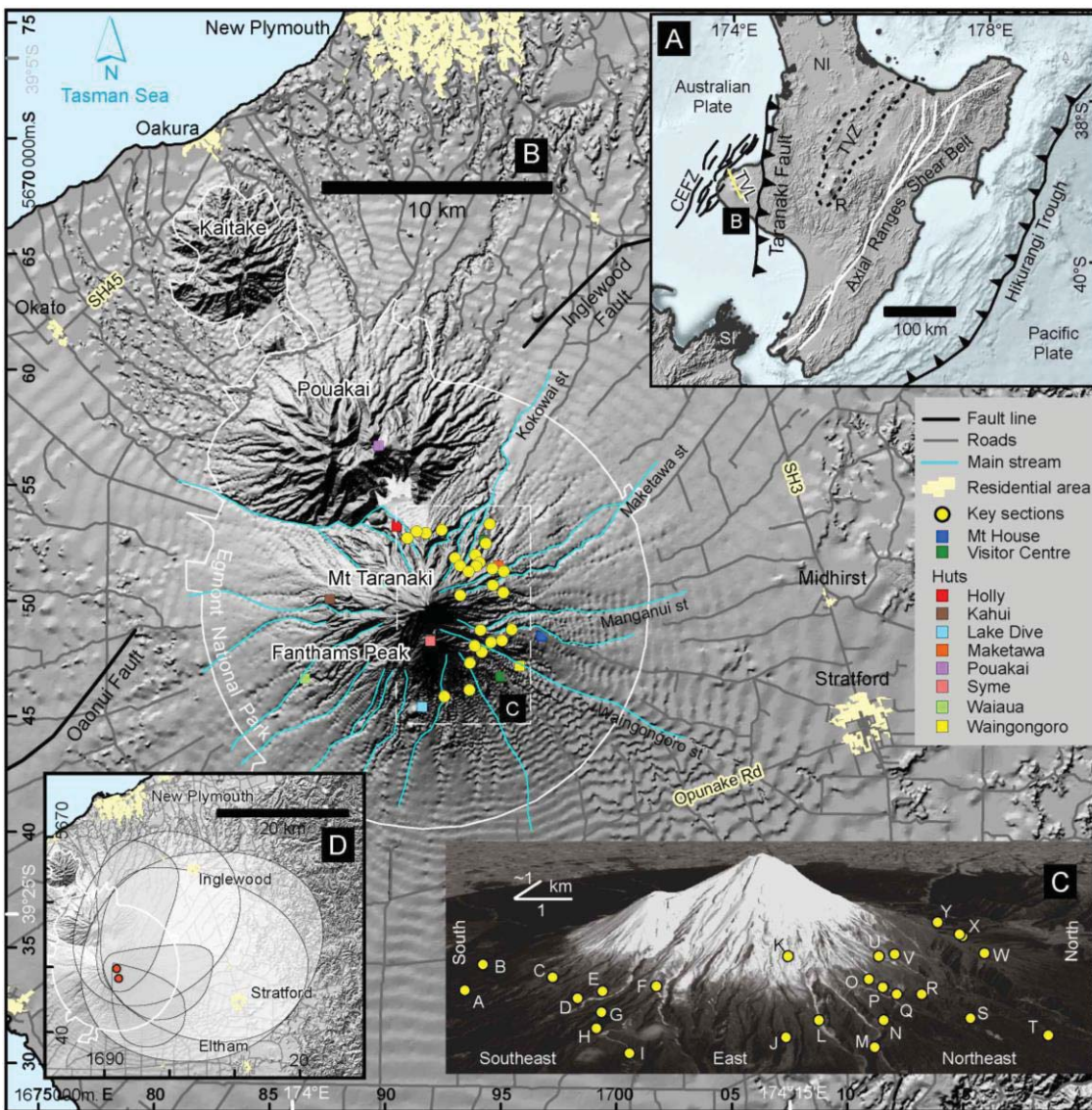


Fig. 5.1 A Tectonic setting of the North Island (NI) of New Zealand (modified from King and Thrasher 1996; Henrys et al. 2003; Sherburn and White 2006). CEFZ Cape Egmont Fault Zone, R Mount Ruapehu, SI South Island, TVL Taranaki Volcanic Lineament (yellow line), TVZ Taupo Volcanic Zone. B Zoomed area of the TVL. The latter comprises four <1.75 Ma and NNW-SSE migrating andesitic volcanoes (Neall 1979) or their eroded volcanic edifice-remnants: Kaitake, Pouakai and Mt. Taranaki (and the satellite cone of Fanthams Peak – topped by Syme Hut). C Zoomed transect of the proximal eastern flanks of Mt. Taranaki and the type sections of this study (points A to Y, Appendix 5.1). Digital profile modified from Google Images (2017). D 10 cm-thick isopachs of fall deposits produced during <5 ka Plinian (white ellipses) and sub-Plinian (grey ellipses) eruptive episodes at Mt. Taranaki (modified from Torres-Orozco et al. 2017b, Table 5.2). Red circles indicate the position of the summit crater and the Fanthams Peak vent. Coordinate system of all insets: NZGD 2000 New Zealand Transverse Mercator.

Mt. Taranaki is also the youngest and southernmost volcano of a NNW-SSE trending chain of four <1.75 Ma volcanoes that form the Taranaki Volcanic Lineament (Neall et al. 1986; Alloway et al. 1995; Fig. 5.1), which is located at the eastern side of the mid-Cretaceous to recent extensional Cape Egmont Fault Zone (King and Thrasher 1996; Fig. 5.1).

The present-day 2518-m high Mt. Taranaki's edifice above 1400 m is a maximum of 10 ka in age (Neall 1979; Downey et al. 1994) and constitutes 12 km³ in volume (Zernack et al. 2011). Lava flows aged between 2 and 0.4 ka shape the uppermost cone of Mt. Taranaki (Downey et al. 1994), and remnants of the youngest AD 1800 Sisters dome make up the present summit (Platz et al. 2012). The conical edifice symmetry is broken in the southeast by the 1966-m high Fanthams Peak basaltic satellite cone (Fig. 5.1), with known eruptions between 3000 to 1200 cal BP (Turner et al. 2008b; Torres-Orozco et al. 2017a; b).

The long-term volcanic history of Mt. Taranaki consists of cycles of cone growth to a critical volume/height during explosive and effusive volcanism, followed by catastrophic edifice collapse to generate massive debris avalanches – the latest at ~7.5 ka (Neall 1979; Neall et al. 1986; Procter et al. 2010; Zernack et al. 2009; 2011). Over the last 30 ka, >20 Tephra Formations were mapped in ring plain soils (Neall 1972; Alloway et al. 1995) and within lake and peat sediments (Turner et al. 2008b; 2009; 2011; Damaschke et al. 2017). Recent studies show that at least 16 sub-Plinian and Plinian eruptions, of a total of 53 explosive bursts generated from the summit-crater of Mt. Taranaki and the Fanthams Peak satellite-vent, were produced over the last 5000 years (Torres-Orozco et al. 2017a; b). These Plinian eruptions (Table 5.2) formed 14-29 km-high steady, oscillating or partially collapsing plumes, and ejected minimum volumes of 10⁸ to 10⁹ m³ at mass

discharge rates of 10^7 to 10^8 kg/s and magnitudes of 4.1 to 5.1 during climactic phases (Torres-Orozco et al. 2017b). Associated dome- and/or column-collapse occurred during the pre- and post-climactic phases, generating block-and-ash flows and pumice flows. Yet blast type PDCs, produced during abrupt climactic bursts, had the largest run-out distances of up to 18 km, and minimum volumes of 10^7 m³ (Torres-Orozco et al. 2017b). Whole-rock analysis of deposits formed during these episodes (Torres-Orozco et al. 2017b) revealed that the summit crater has produced mainly andesite (54-60 wt.% SiO₂), while basaltic and basaltic-andesitic magmas have erupted at Fanthams Peak (47-54 wt.% SiO₂; Table 5.2).

5.4 Methods and terms

Deposits of the Kokowai, Kapuni-A, Kapuni-B, Korito, and Upper Inglewood bed-sets, and the Manganui-A, Manganui-C, and Manganui-D members of the Manganui Formation, as defined by Torres-Orozco et al. (2017a, Table 5.1), were mainly studied at 25 eastern-flank exposures, ~1-18 km from the summit of Mt. Taranaki (Fig. 5.1). Following the mapping criteria of the latter authors, in agreement with Salvador (1994), each individual *bed-set* (or member) is constituted by single or multiple *layers* (pyroclastic or epi-volcaniclastic), has uppermost and lowermost contacts defined by paleosols, weathering horizons or deep-erosion surfaces, and represents the accumulation of sediments during an *eruptive episode* (cf. Torres-Orozco et al. 2017a). Accordingly, each *pyroclastic layer* is separated by sharp or gradational boundaries marked by differences in grain-size, clast framework or bed structure, and represents an individual fallout or PDC *unit* (cf. Fisher and Schmincke 1984).

Table 5.3 Lithofacies classification scheme to describe proximal pyroclastic deposits at Mt. Taranaki

Volcanic facies	B	BA	LA	L	A
<u>Clast-supported</u>					
<i>Pumice / Scoria-rich</i>					
1			LA1	L1	A1
2			LA2	L2	
3			LA3	L3	A3
4			LA4	L4	
5				L5	
6				L6	
<i>Dense clast-rich</i>					
7			LA7	L7	
8			LA8	L8	
9				L9	
10			LA10	L10	
11					
12				L12	
<u>Matrix-supported</u>					
<i>Pumice-rich</i>					
13			LA13		
14			LA14		
15			LA15		A15
16					A16
17			LA17		
18			LA18		A18
19			LA19		A19
<i>Pumice-and-dense clasts</i>					
20			LA20	L20	
21			LA21		
22			LA22		
23			LA23		A23
24			LA24	L24	A24
25			LA25		A25
26			LA26		A26
27					A27
28			LA28		A28
29			LA29		A29
<i>Dense clast-rich</i>					
30	B30	BA30	LA30		A30
31	B31	BA31	LA31		A31
32		BA32	LA32		
33		BA33			A33
34			LA34		A34
35			LA35		A35
36			LA36		A36
37			LA37		A37
38			LA38		A38

Pyroclastic blocks (B, >75 % blocks), Blocks-and-Ash (BA, mixture of ash, lapilli and blocks or bombs), Lapilli-and-Ash (LA, mixture of ash and lapilli), Lapilli (L, >75% lapilli), Ash (A, >75% ash).

Pumice / Scoria- or Dense clast-rich: >60 vol.%.

Terms and diagram modified from Fisher and Schmincke (1984), Chough and Sohn (1990), Nemeth and White (2003) and Lucchi (2013)

Field descriptions were recorded as lithostratigraphic profiles. A total of 70 lithofacies (Table 5.3) were identified following terminology schemes applied by Fisher and Schmincke (1984), Chough and Sohn (1990), Nemeth and White (2003) and Lucchi (2013). The profiles contain data of vertical bed thickness, contacts, clast framework, bed geometry and stratification, grading, grain-size (White and Houghton 2006), and other sedimentary structures (e.g., syn-depositional deformational structures), as well as textural data, such as clast rounding and colour. Pre-eruptive landscape and paleotopographic settings were reconstructed from the interpretation of lithofacies associations (e.g., Brown and Branney 2004; Cronin et al. 2013; Lube et al. 2011; 2014). Chief characteristics were lateral lithofacies transitions, deposit shape (e.g., draping of topography, lenticular shape, pinch-and-swell structures), contacts, and restrictions in dispersal (e.g., channel confinement, unconfinement, topography deflection or surmounting). The stream order of Strahler was employed to distinguish between 1st order rills-and-gullies and 2nd order incision-channels (cf. Gutierrez-Elorza 2008). Based upon lithostratigraphic characteristics analogous to deposits of the most extensively mapped Plinian and sub-Plinian eruptions (e.g., Table 5.2), eruptive styles, intensities and magnitudes were qualitatively extrapolated to pyroclastic successions lacking sufficient field data.

Componentry analysis followed counts of 350 particles from the coarse mode (-1ϕ to -3.5ϕ) and from a finer secondary mode (commonly 0.5ϕ) by using a binocular stereoscope, and were added to data reported in Torres-Orozco et al. (2017a; b; Table 5.1). Volume percentages were determined for pumice, dense juvenile clasts (i.e., light-grey, dark-grey and black, porphyritic or aphanitic, plagioclase and hornblende dominated, andesitic clasts), accessory (i.e., red-oxidized, white-bleached, and other fully

Table 5.4 Summary descriptions of the lithofacies associations identified from pyroclastic deposits at Mt. Taranaki

Lith. Asc.	Characteristics
Asc1	<p><i>Lithology:</i> Clast-supported, poorly to moderately-well sorted deposits, dominated by angular to subangular pumice lapilli (60–82 vol.%).</p> <p><i>Boundaries:</i> Lowermost sharp-parallel, rarely gradational. Uppermost gradational, often sharp-irregular.</p> <p><i>Description:</i> Mostly firm, 35–170 cm-thick, massive lapilli deposits, commonly having thin (<10 cm-thick) basal and top lapilli horizons that comprise faint reversely-graded and normally and reversely-graded lithofacies, respectively, and are often andesitic clast-rich. Deposits thin laterally and longitudinally in km-distance, but preserve massive lapilli lithofacies. Deposits mantle the paleo-topography and rarely form lenticular geometries thinning over paleo-ridges, interpreted from associated under or overlying channel-fill deposits. Ballistically emplaced pumice bombs and andesitic blocks commonly produce impact sags into underlying deposits. Very common impact-fractured pumice lapilli clasts.</p> <p><i>Lithofacies:</i> Dispersal axis: L1. Occasional lowermost: L2 or L8 and L5, and topmost: L3, L6 and L8. Lateral and longitudinal variations: L1.</p> <p><i>Occurrence:</i> Layers Kw4, KB3, Ko3, Ulg7. <i>Other associations lithologically or stratigraphically related:</i> Asc5, Asc6, Asc7.</p>
Asc2	<p><i>Lithology:</i> Clast-supported, poorly to moderately sorted deposits, lapilli-grade dominated, angular to subangular pumice (67–75 vol.%), or angular to subrounded dense scoria (76–77 vol.%) of the Manganui Formation.</p> <p><i>Boundaries:</i> Lowermost sharp-parallel, commonly gradational. Uppermost gradational, often sharp-irregular.</p> <p><i>Description:</i> Moderately friable, 25–85 cm-thick, massive or reversely-graded lapilli deposits, grading from basal reversely-graded lapilli or lapilli-and-ash horizons, and upwards into normally-graded lapilli, lapilli-and-ash or ash deposits. Deposits thin laterally and longitudinally in km-distance and become dominated by core massive lapilli deposits encapsulated within reverse and normally-graded lapilli-and-ash or ash beds. Deposits mantle the paleo-topography and often form lenticular geometries thinning over paleo-ridges. Common impact-fractured pumice clasts and impact sags produced by pumice bombs and andesitic blocks.</p> <p><i>Lithofacies:</i> Dispersal axis: L1, L7, L2, LA2. Occasional lowermost: L2, LA2. Occasional lowermost: L2, LA2, A3, A1. Lateral and longitudinal variations: L1, L2, LA2.</p> <p><i>Occurrence:</i> Layers Kw7, KA2, KB1, MD1, MD2. <i>Other associations lithologically or stratigraphically related:</i> Asc7.</p>
Asc3	<p><i>Lithology:</i> Clast-supported, poorly to moderately sorted deposits, lapilli-grade dominated, angular to subrounded dense scoria (75–78 vol.%) of the Manganui Formation, and associated hetero-lithic horizons (45 vol.%).</p> <p><i>Boundaries:</i> Lowermost gradational-subparallel, rarely sharp. Uppermost gradational, often sharp-irregular.</p> <p><i>Description:</i> Very friable, 30–50 cm-thick, strongly bedded deposits, comprising multiple reverse, normally-graded and massive lapilli beds, grading from basal reversely-graded lapilli-and-ash or ash horizons, and normally-graded lapilli, lapilli-and-ash or ash deposits. Andesitic and heterolithic-rich horizons are common. Deposits thin laterally and longitudinally in km-distance and fine into lapilli-and-ash dominated beds, but preserve strongly stratified lithofacies. More than ±10 km-distance, deposits shift towards unsorted massive and reversely-graded ash lithofacies. Deposits mantle the paleo-topography and very frequently form lenticular geometries produced either by channel margin deposition or by irregular uppermost erosion.</p> <p><i>Lithofacies:</i> Dispersal axis: L4, L10 and LA4, dominated by beds of L1, L2, L3, L7 or L8, and LA2 lithofacies. Occasional lowermost: A2, LA2 and LA3, and topmost: L3, L9, LA3 and A1. Lateral and longitudinal variations: LA4 and LA10, dominated by beds of LA2, LA3, L7, L8 and L1 lithofacies. Distal variations: A2 and A1.</p> <p><i>Occurrence:</i> Layers MA1–2, MC, MD3. <i>Other associations lithologically or stratigraphically related:</i> Asc6.</p>
Asc4	<p><i>Lithology:</i> Clast-supported, poorly to moderately sorted deposits, dominated by angular, juvenile andesitic clast lapilli (~81 vol.%).</p> <p><i>Boundaries:</i> Lowermost gradational-subparallel. Uppermost gradational-irregular.</p> <p><i>Description:</i> Very friable, 10–25 cm-thick, reversely to massive and topmost normally-graded lapilli deposits. These deposits mantle the paleo-topography and are interstratified within pumice-rich lithofacies associations.</p> <p><i>Lithofacies:</i> Dispersal axis: L8, L9, L7.</p> <p><i>Occurrence:</i> Layer KB2. <i>Other associations lithologically or stratigraphically related:</i> Asc1, Asc2, Asc7.</p>

(continue)	Lith. Asc.	Characteristics
Asc5		<p><i>Lithology:</i> Very-poorly to poorly sorted, matrix-supported, subangular to rounded lapilli, and fine to coarse-grained ash of ~evenly proportional pumice (35-57 vol.%) and andesitic clasts (26-50 vol.%). Common individual pumice, andesitic and lithic lapilli clasts aligned in the ash.</p> <p><i>Boundaries:</i> Lowermost sharp-subparallel to low-angular, often undulating. Uppermost gradational-subparallel, often sharp.</p> <p><i>Description:</i> Very firm, lenticular or pinching-and-swelling in m-distance, 9-45 cm-thick channel-fill massive lapilli-and-ash, grading vertically from lowermost stratified lapilli-and-ash, and into uppermost, moderately firm, 4-25 cm-thick, parallel thinly bedded and faintly stratified ash. These deposits change laterally and longitudinally into 6-11 cm-thick lapilli-and-ash beds of unsorted massive, faintly stratified, cross-stratified or diversely stratified, i.e., scour-fill or parallel-thinly bedded lithofacies. Deposits often pinch out upslope. May contain charcoal branches and twigs and ash pellets.</p> <p><i>Lithofacies:</i> Channel-fill (~dispersal axis): LA20-22. Lowermost: LA23, and topmost: A24, LA/A25-28. Lateral and longitudinal variations: LA/A23-29.</p> <p><i>Occurrence:</i> Layers KA1, Ko4-Ko7, Ulig4-Ulig5. <i>Other associations lithologically or stratigraphically related:</i> Asc1.</p>
Asc6		<p><i>Lithology:</i> Very-poorly to poorly sorted, andesitic or lithic-dominated (43-84 vol.%), subangular to subrounded fine to coarse-grained ash. Common andesitic and lithic lapilli clasts matrix-supported in the ash.</p> <p><i>Boundaries:</i> Lowermost sharp-subparallel to highly-angular and undulating, rarely gradational-irregular. Uppermost gradational-subparallel.</p> <p><i>Description:</i> Moderately to very firm, 5-16 cm-thick, pinching and swelling in m-distance, unsorted massive ash deposits, shifting into deposits of faintly stratified lithofacies and commonly developing cross-stratification and scour-fill bedding laterally and longitudinally. May contain charcoal twigs and ash pellets.</p> <p><i>Lithofacies:</i> ~Dispersal axis: A33-37. Lateral and longitudinal variations: A36 and LA34</p> <p><i>Occurrence:</i> Layers Kw5, Ko1, MA3. <i>Other associations lithologically or stratigraphically related:</i> Asc3, Asc8, Asc9.</p>
Asc7		<p><i>Lithology:</i> Very-poorly sorted deposits, dominated by subangular to subrounded pumice lapilli (55-80 vol.%) matrix-supported in a fine-grained ash.</p> <p><i>Boundaries:</i> Lowermost sharp-subparallel to low-angular, occasionally undulating, rarely highly-angular. Uppermost gradational-subparallel, often undulating and rarely sharp low-angular.</p> <p><i>Description:</i> Moderately firm, 8-30 cm-thick, lenticular in m-distance, channel-fill massive or reversely-graded lapilli-and-ash deposits, grading vertically from and into secondary lowermost and uppermost ash deposits of massive and faintly stratified lithofacies or thinly bedded lithofacies, respectively, and passing laterally into m-distance pinching, 3.5-14 cm-thick lapilli-and-ash or ash deposits of unsorted massive and faintly stratified lithofacies or subparallel reversely and very thinly bedded lithofacies. May contain charcoal twigs</p> <p><i>Lithofacies:</i> Channel-fill (~dispersal axis): LA13-14. Lowermost: A15 and 19, and topmost: A16. Lateral and longitudinal variations: LA or A15, 16, 17 and 19, A24 and 28, and LA25.</p> <p><i>Occurrence:</i> Layers Kw3, Kw6, Kw8, KB2a, KB4, Ko2, Ko3a, Ko8. <i>Other associations lithologically or stratigraphically related:</i> Asc1, Asc2, Asc4.</p>
Asc8		<p><i>Lithology:</i> Extremely-poorly to very-poorly sorted deposits, dominated by subangular to rounded andesitic and lithic lapilli (64-79 vol.%) matrix-supported in a fine- to coarse-grained ash.</p> <p><i>Boundaries:</i> Lowermost sharp-subparallel to low-angular, often gradational-subparallel and undulating. Uppermost gradational-subparallel, rarely sharp.</p> <p><i>Description:</i> Very firm to weakly firm, 25-50 cm-thick, lenticular or pinching-and-swelling in m-distance, channel-fill massive or reversely-graded lapilli-and-ash or ash deposits, grading vertically from secondary lowermost lapilli-and-ash dominated deposits of strongly stratified lithofacies, and passing laterally into pinching-and-swelling, 4-13 cm-thick, ash-dominated deposits of unsorted massive and faintly stratified lithofacies or scour-fill, parallel and dune bedded lithofacies. Occasional imbrication in channel-fill lithofacies. May contain charcoal twigs and rare ash pellets.</p> <p><i>Lithofacies:</i> Channel-fill (~dispersal axis): LA20-21, LA or A30-31. Secondary lowermost: LA23 and 25-26, A35 and LA or A37. Lateral and longitudinal variations: LA or A23, A24 and 28, LA or A33, 34, 35, 37 and 38.</p> <p><i>Occurrence:</i> Layers Kw2, Ulig2, Ulig3. <i>Other associations lithologically or stratigraphically related:</i> Asc6, Asc9.</p>

(continue)

Lith. Asc.	Characteristics
Asc9	<p><i>Lithology:</i> Very-poorly sorted blocks or blocks and lapilli-grade, subangular to rounded, andesitic clasts (~80 vol.%), matrix-supported in coarse-grained andesitic ash. Fines-depleted basal block horizons commonly observed.</p> <p><i>Boundaries:</i> Lowermost sharp-subparallel to low-angular, rarely highly-angular. Uppermost sharp-subparallel, rarely gradational-irregular.</p> <p><i>Description:</i> Mostly weakly to moderately firm, ~85-500 cm-thick, pinching in m to km-distance, channel-fill massive, reversely or normally-graded pyroclastic blocks and block-and-ash beds, often grading from fines-depleted basal block horizons, followed by massive lapilli-and-ash or ash deposits; and passing downstream into finer and thinner, ~20-80 cm-thick, channel-fill lapilli-and-ash or ash deposits or into ~unconfined massive ash deposits. Deposits can also be very firm in cases in which they normally show imbrication. May contain carbonized logs and charcoal branches and twigs.</p> <p><i>Lithofacies:</i> Channel-fill (~dispersal axis): B30-31, BA31-32. Secondary lowermost: LA30 and A31. Downstream longitudinal variations: BA33, LA30-32, A31.</p> <p><i>Occurrence:</i> Layers Kw1, Ulg1. <i>Other associations lithologically or stratigraphically related:</i> Asc6, Asc8.</p>

Lith. Asc. = Lithofacies Association.

Sorting categories of Folk and Ward (1957).

Sorting (σ_1) and componentry data modified and/or completed from Torres-Orozco et al. (2017a; b).

altered, nearly unclassifiable clasts) and accidental lithics (dioritic or gabbroic clasts), and loose crystals (i.e., plagioclase, hornblende, pyroxene, oxides, and rare olivine and biotite).

5.5 Summary lithostratigraphy of proximal Plinian and sub-Plinian eruption deposits at Mt. Taranaki

Nine lithofacies associations (i.e., Asc1 to Asc9) were assembled by integrating lateral and longitudinal lithofacies variations (Table 5.4). Associations Asc1 to Asc4 comprise poorly to moderately-well sorted, massive to ‘shower-bedded’ stratified, clast-supported deposits, formed by prevailing angular to subangular clasts. In contrast, associations Asc5 to Asc9 comprise extremely-poorly to poorly sorted, matrix-supported deposits with a wide range of stratification and clast characteristics, having pinch-and-swell or channel-fill structures, and often carrying charcoal twigs, logs, or wood fragments.

In specific, lithofacies association Asc1 (Table 5.4) comprises dominating, laterally and longitudinally, L1 lithofacies, basal L2, L8 or L5 lithofacies, and occasional topmost L3 lithofacies (Table 5.3). Examples of Asc1 correspond to the 40-180 cm-thick, mostly massive, and pumice-rich lapilli layers Kw4 (Fig. 5.2), KB3 and Ko3 (Fig. 5.3), and Uig7 (Fig. 5.4). Layers Ko3 and Uig7 are often interdigitated with deposits of association Asc7 (e.g., Ko3a and Uig7a, Figs. 5.3 and 5.4). Lithofacies association Asc2 (Table 5.4) is comparable to Asc1 by comprising L1, L7, L2 and LA2 lithofacies, and topmost L/LA/A3 and A1 lithofacies (Table 5.3). However, layers of Asc2 are 10-80 cm-thick, and have well developed stratification (e.g., reverse and normal grading). Examples of Asc2 are pumice-dominated lapilli layers Kw7 (Fig. 5.2), KA2 and KB1 (Fig. 5.3), and scoria-dominated layers MD1 and MD2 (Fig. 5.5). All deposits of Asc1 and Asc2 thin laterally

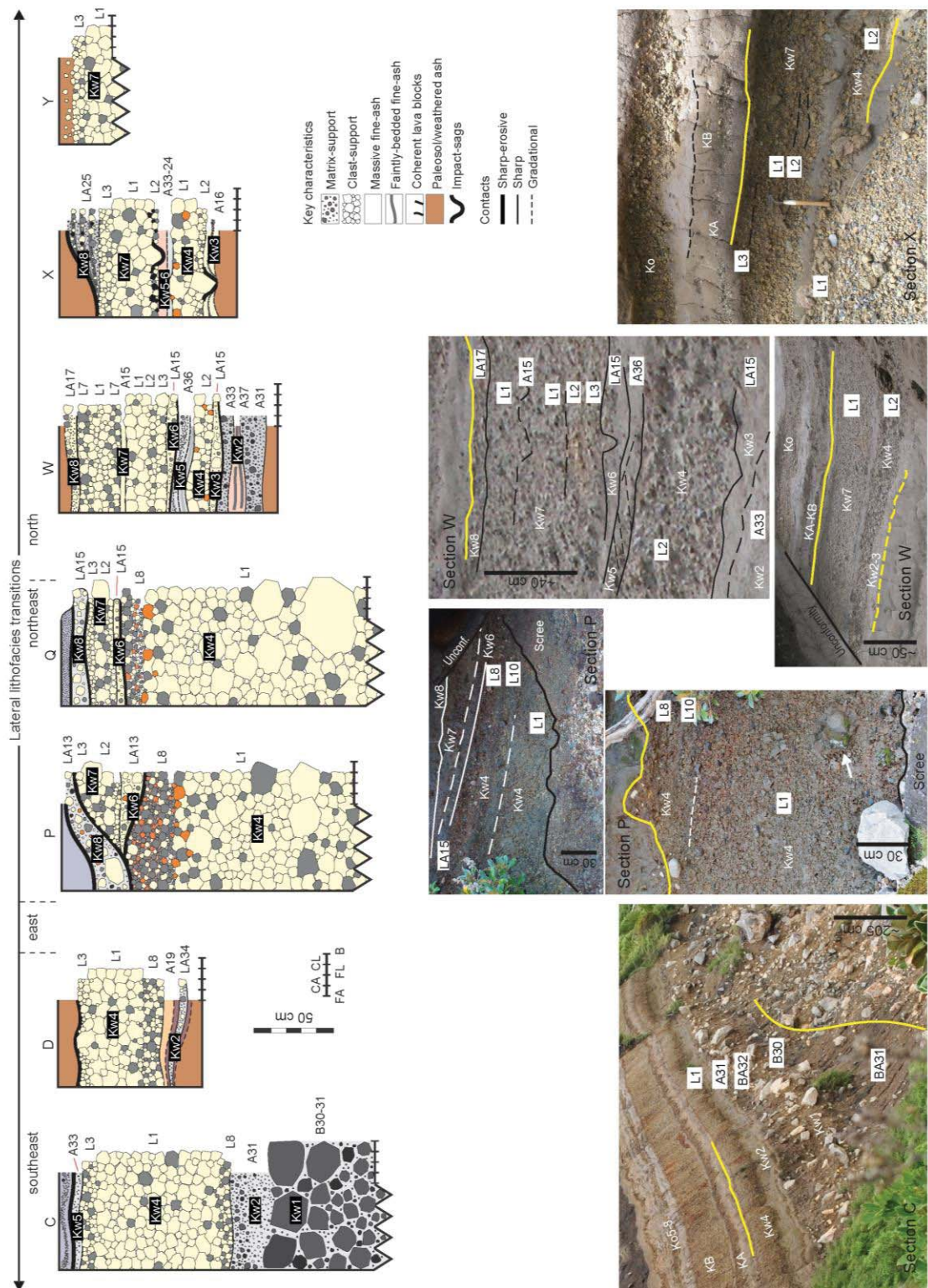


Fig. 5.2 Proximal lithofacies transitions of the 4700-4600 cal BP Kokowai (Kw1-Kw8). *KA* Kapuni-A, *KB* Kapuni-B, *Ko* Korito. Sections indicated on top of each profile (A-Y, Fig. 5.1). Yellow lines on photographs indicate lower and uppermost bed-set contacts. Lithofacies codes (Table 5.3) indicated to the right of each profile and inside white boxes on pictures. *FA* fine-ash, *CA* coarse-ash, *FL* fine-lapilli, *CL* coarse-lapilli, *B* block/bombs. Scale on pictures represented by a black bar or a scraper (32.5 cm-long).

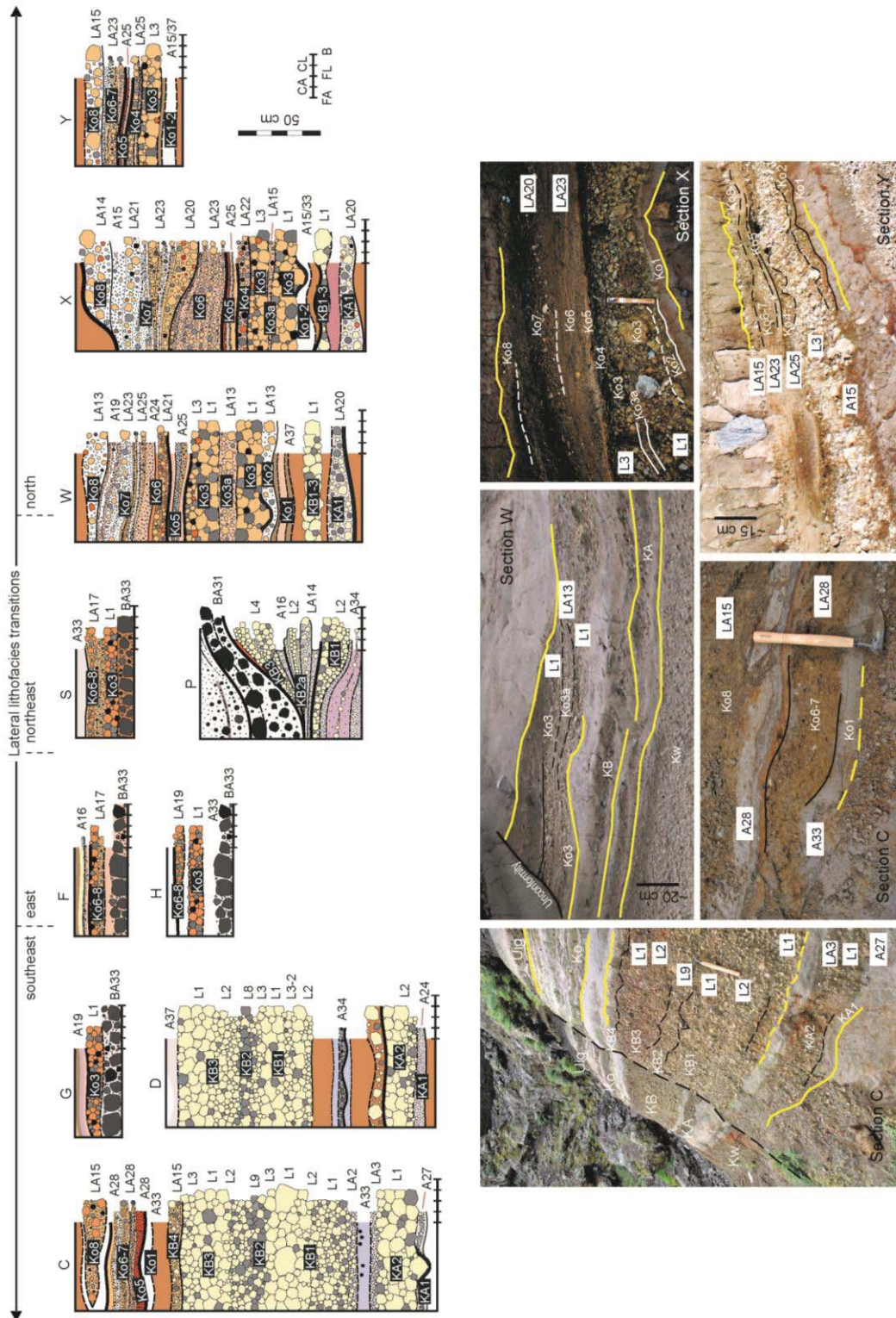


Fig. 5.3 Proximal lithofacies transitions of the 3800 to 3500 cal BP Kapuni-A (KA: KA1-KA2), Kapuni-B (KB: KB1-KB4) and Korito (Ko: Ko1-Ko8). *Kw* Kokowai, *Uig* Upper Inglewood. Sections indicated on top of each profile (A-Y, Fig. 5.1). Yellow lines on photographs indicate lower and uppermost bed-set contacts. See Fig. 5.2 for more details. The scale on pictures is represented by a black bar or a scraper (32.5 cm-long).

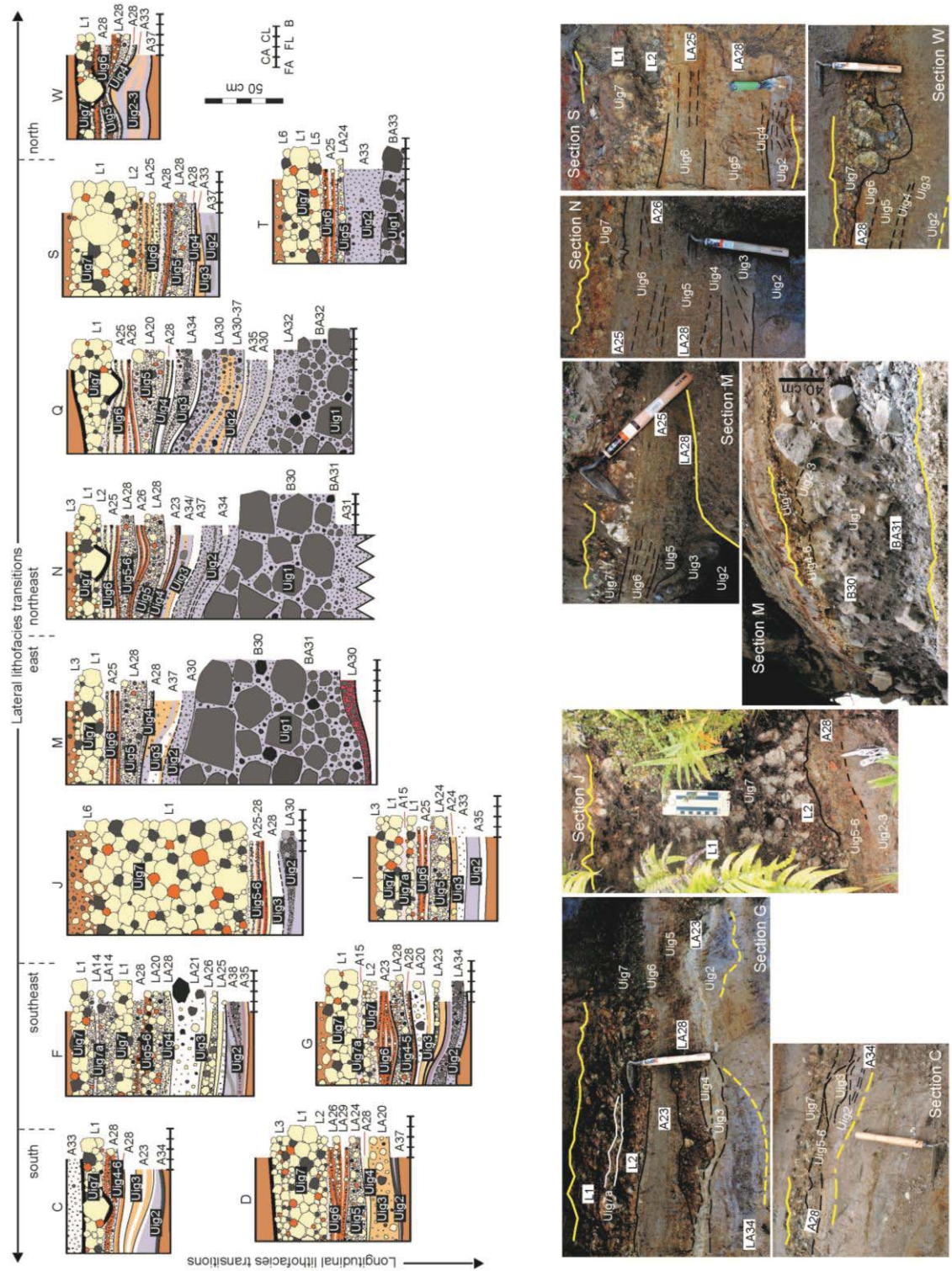


Fig. 5.4 Proximal lithofacies transitions of the 3300 cal BP Upper Inglewood (Uig1-Uig7). Sections indicated on top of each profile (A-Y, Fig. 5.1). Yellow lines on photographs indicate lower and uppermost bed-set contacts. See Fig. 5.2 for more details. The scale on pictures is represented by a black bar, a long (32.5 cm-long) or a small scraper (20 cm-long), or a 10 cm-long scale.

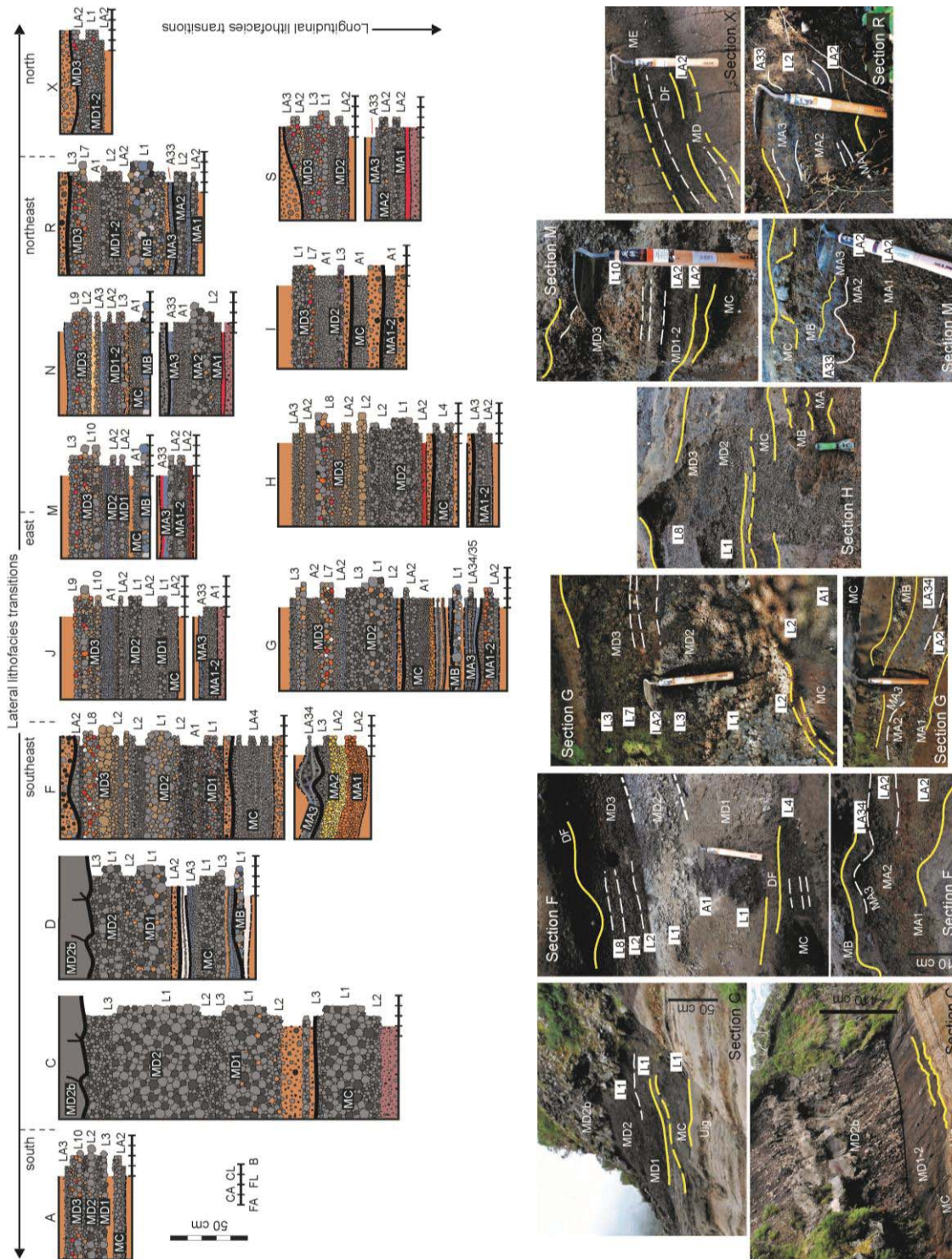


Fig. 5.5 Proximal lithofacies transitions of 3000-2600 cal BP members Manganui-A (MA: MA1-MA3), Manganui-B (MB), Manganui-C (MC), Manganui-D (MD: MD1-MD3) and Manganui-E (ME) of the Manganui Formation (Torres-Orozco et al. 2017a; b). *Uig* Upper Inglewood, *DF* debris flow. Sections are indicated on top of each profile (A-X, Fig. 5.1). Yellow lines on photographs indicate lower and uppermost bed-set contacts. See Fig. 5.2 for more details. The scale on pictures is represented by a black bar, and a long (32.5 cm-long) or a small scraper (20 cm-long).

and longitudinally, yet preserve the dominating lapilli grain-size. The only exceptions are layers MD1 and MD2, which also pass into deposits of alternating lapilli, ash, and lapilli-and-ash sub-layers (Fig. 5.5), similar to deposits of association Asc3. Lithofacies association Asc3 (Table 5.4) includes distinctive ‘shower-bedded’ L/LA4 and L/LA10 lithofacies, comprising multiple reversely to normally-graded sub-layers of L/LA1-3 and L7-8 lithofacies, and distal A1-2 lithofacies (Table 5.3). Examples of Asc3 are the scoria, or dense juvenile clast, and lithic-dominated lapilli and lapilli-and-ash layers MA1, MA2, MC, and MD3, of up to 30-50 cm-thick each (Fig. 5.5). These layers thin and become mostly fine-grained, laterally and longitudinally, and beyond 10 km pass into massive or reversely-graded ash. Lithofacies association Asc4 (Table 5.4) comprises deposits of L7-9 lithofacies (Table 5.3). The only example in this work corresponds to layer KB2 (Fig. 5.3), which consists of a 10-15 cm-thick, stratified deposit of lapilli-grade, dense andesitic clasts. Laterally, deposits of Asc4 pass into massive or ‘shower-bedded’ ash-and-lapilli, interdigitated with deposits of Asc7 (e.g., layer KB2a, Fig. 5.3).

Lithofacies association Asc5 (Table 5.4) comprises deposits with lowermost LA23, middle LA20-22, and topmost A24 and LA/A25-28 lithofacies, passing laterally and longitudinally into LA/A23-29 lithofacies (Table 5.3). Examples of Asc5 are the 8-45 cm-thick, dominantly massive, pumice-and-lithic, lapilli-and-ash layers KA1, Ko4, Ko5, Ko6, and Ko7 (Fig. 5.3), and Uig4-Uig6 (Fig. 5.4). These layers grade either gently (e.g., topmost levels of layers Ko6 and Ko7, Fig. 5.3), or sharply (e.g., layer Uig6, Fig. 5.4), into ash-dominated, uppermost deposits, which are characterized by a wide range of stratification (e.g., reverse grading, subparallel-stratification, scour-bedding, pinch-and-swell, and dune structures). Laterally and longitudinally, layers of Asc5 become faintly-stratified, or massive ash deposits, which can be found up to 14-18 km from the crater of

Mt. Taranaki (cf. Torres-Orozco et al. 2017b). Lithofacies association Asc6 (Table 5.4) includes main A33-37 lithofacies, and A36 and LA34 lateral and longitudinal lithofacies variations (Table 5.3). Examples of Asc6 are the 2-20 cm-thick, dominantly massive, or faintly-stratified, dense andesitic clast-rich, or lithic-rich, ash or ash-and-lapilli layers Kw5 (Fig. 5.2), Ko1 (Fig. 5.3) and MA3 (Fig. 5.5). Layer MA3 stands out by comprising a wide range of cross-stratification, similar to deposits of Asc5, but restricted to the most proximal areas (Fig. 5.5).

Lithofacies association Asc7 (Table 5.4) comprehends dominating LA13-14 lithofacies, complemented by lowermost A15 and 19, and uppermost A16 lithofacies, and passing laterally and longitudinally into LA/A15-17 and 19, or LA/A24-25 and 28 lithofacies (Table 5.3). Examples of Asc7 are the 5-20 cm-thick, channel-fill, massive, or reversely-graded, and topmost thinly-bedded, pumice-dominated, lapilli-and-ash layers Kw3, Kw6 and Kw8 (Fig. 5.2), KB2a, KB4, Ko2, Ko3a and Ko8 (Fig. 5.3), and Uig7a (Fig. 5.4), which become, laterally and longitudinally, massive, faintly-stratified, or parallel-stratified, ash deposits. Lithofacies association Asc8 (Table 5.4) has intermediate characteristics between deposits of Asc5 and Asc7. Asc8 includes main LA20-21, or LA/A30-31 lithofacies, complemented by lowermost LA23, 25-26, A35, or LA/A37 lithofacies, passing laterally and longitudinally into LA/A23-24, 28, or LA/A33-38 lithofacies (Table 5.3). Examples correspond to the 10-40 cm-thick, channel-fill, massive, or reversely-graded, dense andesitic clast-dominated, or lithic-dominated, ash, or lapilli-and-ash layers Kw2 (Fig. 5.2), Uig2 and Uig3 (Fig. 5.4). Laterally, these layers thin and have massive, faintly-stratified, and parallel- or cross-stratified variations (e.g. Uig2-Uig3, Fig. 5.4). Layer Uig3 stands out by alternating between pumice-and-lithic and lithic-rich lithofacies. Lithofacies association Asc9 (Table 5.4) comprises main B/BA30-

32, and lowermost LA/A30-31 lithofacies, passing downstream into BA33 or LA/A30-32 lithofacies (Table 5.3). Examples of Asc9 are the up to 3 m-thick, channel-fill, massive, or reversely-graded, block, or block-and-ash, dense andesitic clast-rich layers Kw1 (Fig. 5.2) and Uig1 (Fig. 5.4). Deposits of these layers are restricted to channel walls and ridges, located up to 6-7 km from the crater of Mt. Taranaki, and correlate, laterally, with deposits of Asc6 and Asc8 (e.g., Uig1-Uig2, Fig. 5.4).

5.6 Discussion

5.6.1 Interpretation of eruptive processes

Layers that exemplify this work's lithofacies associations Asc1 to Asc4 were interpreted by Torres-Orozco et al. (2017a; b) to have been produced by fall deposition, and layers Kw1 to Kw3, Kw6, Kw8, and Uig1 to Uig6 (i.e., Kokowai and Upper Inglewood eruptive episodes, respectively), exemplifying this work's Asc5 to Asc9, to have been generated by different types of PDCs. Our results, provided by the interpretation of the lithofacies associations (e.g., Nemeth and White 2003; Brown and Branney 2004; Lucchi 2013; Table 5.5), indicate that fall deposits produced by the Kapuni-A, Kapuni-B, Korito, Manganui-A, and Manganui-C eruptive episodes were generated by Plinian and sub-Plinian eruption columns, matching the lithostratigraphic characteristics, transitions, and distribution of the most extendedly studied fallouts (e.g., Table 5.2, Fig. 5.1 D). Furthermore, this work's evidence reveals that the erupted PDCs at Mt. Taranaki encompass a wide range of time and space dependant depositional processes, matching different styles and distributions within the spectrum from concentrated – flow type – to dilute – surge type – PDCs (e.g., Druitt 1998; Branney and Kokelaar 2002; Kim et al. 2014; Sulpizio et al. 2014). Other epiclastic and volcanoclastic deposits produced by, e.g.,

Table 5.5 Summary interpretations of the lithofacies associations identified from pyroclastic deposits at Mt. Taranaki

Lith. Asc.	Interpretation
Asc1	<ul style="list-style-type: none"> - Pumice fall deposits: by $\sigma 1 = 0.6-1.4$, composition, clast angularity, mantle bedding and extent. - Plinian eruption columns* by massive texture, coarse and impact-fractured pumice clasts. - Fast column waxing, and crosswind plume effects or brief column waning* by basal faint reverse grading, and topmost faint normal grading. - Minor conduit erosion, or eruption of either chilled or gas-depleted magma† by dense juvenile clasts- or lithic-rich horizons. - Column unsteadiness and minor collapse§ from interstratification with deposits of Asc7.
Asc2	<ul style="list-style-type: none"> - Pumice fall deposits: by $\sigma 1 = 1.0-1.9$, composition, clast angularity, mantle bedding and extent. - Gradual waxing conditions into steady columns* by strong reverse grading and middle massive beds. - Progressive column waning§ by marked uppermost normal grading. - Plinian or sub-Plinian columns smaller or sustained for shorter intervals* than columns of Asc1: by lateral and longitudinal thinning-and-finning lithofacies. - Column unsteadiness and partial collapse§ by interstratification with deposits of Asc7.
Asc3	<ul style="list-style-type: none"> - Pumice fall deposits: by $\sigma 1 = 1.0-1.3$, composition, clast angularity, mantle bedding and extent. - Sub-Plinian columns oscillating in height due to fluctuations in intensity§; by characteristic strong, multiple grain-size grading. - Eruption of gas-depleted or chilled magma, intense conduit erosion† or possible phreatomagmatism# by well-developed dense juvenile clasts- and lithic-rich horizons.
Asc4	<ul style="list-style-type: none"> - Pumice fall deposits: by $\sigma 1 = -1.0$, composition, clast angularity and mantle bedding. - Brief, unsteady Strombolian or Vulcanian columns* by marked reverse to normal and thinly-bedded grain-size stratification, and by limited deposit preservation. - Collapsing columns: by lateral interstratification with deposits of Asc7. - Eruption of gas-depleted or chilled magma†, possible phreatomagmatism#, or likely effusive activity**, or likely effusive activity** by dense andesitic clast- or lithic-dominated lithology
Asc5	<ul style="list-style-type: none"> - PDC deposits: by $\sigma 1 = 1.5-2.5$, clast angularity and pinching-and-swelling structures. - Current unsteadiness and non-uniformity†† by lateral thickness variations, faint stratification and low-angle truncations. - Waxing and/or waning flow conditions§§ by reverse and/or normal grading - Rapid suspension-sedimentation and mild traction of highly to moderately-concentrated 'flow type' PDCs§§ by grain-size, channel-fill massive and faintly stratified lithofacies, and progression from lowermost faintly stratified lithofacies. - Full tractional deposition from dilute, turbulent and unconfined 'surge type' (hot) PDCs§§ by grain-size, progression into uppermost or transition into lateral/longitudinal parallel and cross-stratification, obstacle scours, often undulating contacts and occasional charcoal branches and twigs. - Deposition from energetic, highly mobile, laterally-directed 'blast type' PDCs## by elliptical lateral and longitudinal large run-out extensions (e.g. 10-18 km), pinching-and-swelling shape and minimum topographic deflection interpreted from deposition-landscape relationships.
Asc6	<ul style="list-style-type: none"> - PDC deposits: by $\sigma 1 = 3.2$, clast angularity and pinching-and-swelling structures. - Rapid suspension-sedimentation and moderate traction of unsteady, non-uniform PDCs†† §§ by massive and faintly stratified lithofacies. - Full tractional deposition from fully dilute, turbulent and unconfined 'surge type' PDCs§§ by lateral and longitudinal transitions into stratified lithofacies. - 'Ash-cloud' PDCs by dome-collapse and rapid generation and segregation of fine particles***, or by hydrothermal or phreatomagmatic activity# by lithic lithology and fine, angular ash. - Magmatic, "hot" PDCs: by occasional charcoal content.
Asc7	<ul style="list-style-type: none"> - PDC deposits: by $\sigma 1 = 3.1-3.2$, clast angularity and lenticular architecture. - Waxing flow conditions§§§ by reverse grading. - Sedimentation from gravity-driven, unsteady, non-uniform and confined dense underflows†† §§§ by dominating channel-fill massive lithofacies and small deposit volumes (e.g. 10^3-10^4 km³). - Tractional deposition from dilute, turbulent, 'ash-cloud' PDCs, or from laterally waning 'surge type' PDCs§§§ by progression into uppermost thin-bedding, in addition to lateral transitions into pinching-and-finning, subparallel-bedded lithofacies. - PDC produced by partial collapse of unsteady eruption columns§§§ by pumice lithology, channel-confinement, short run-out distances (e.g. 2-5 km), and interstratification with deposits of Asc1-Asc4.

(continue)	Lith. Asc.	Interpretation
Asc8	<ul style="list-style-type: none"> - PDC deposits: by $\sigma_1 = 2.1-4.1$, clast angularity and pinching-and-swelling structures. - Waxing flow conditions^{†† §§} by marked reverse grading. - Tractional deposition of low-concentrated basal PDCs^{§§} by strongly stratified lowermost horizons. - Rapid suspension-sedimentation of moderately-concentrated, unsteady, non-uniform, relatively confined PDCs^{§§} by grain-size, and dominating channel-fill and unsorted massive textures. - Tractional deposition from dilute, turbulent and unconfined 'surge type' PDCs^{§§} by lateral thinning-and-finning into massive and faintly stratified lithofacies, and later development of scour, parallel and dune bedding with undulating contacts. - 'Ash-cloud' PDCs by explosive dome-collapse and rapid generation and segregation of fine particles^{***} by lithic lithology, charcoal content and interstratification with deposits of Asc9. - Deposition from energetic, mobile, laterally-directed 'blast type' PDCs[#] by elliptical distribution and lateral/longitudinal run-out distances (e.g. 5-8 km). 	
Asc9	<ul style="list-style-type: none"> - PDC deposits: by $\sigma_1 = 3.5-3.9$, clast angularity and strong lenticular channel architecture. - Sedimentation from dense, gravity-driven, non-turbulent, confined PDCs, or en-mass deposition of highly-concentrated granular underflows at the basal level of density-stratified PDCs^{†† §§} ^{***} by fines-depleted, dominant channel-fill massive or reversely and normally-graded lithofacies. - Dispersive pressure due to grain-to-grain collisions^{†† §§} by reverse and reverse to normal grading. - Suspension-sedimentation from moderately-dilute PDCs and/or current waning^{***} by deposits thinning-and-finning downstream into confined and weakly-confined massive lithofacies. - Sedimentation from dense basal avalanches produced by explosive dome-collapse^{***} by dense andesitic clast or lithic lithology, short downstream run-out distances (e.g. 6-7 km), and carried carbonized logs and branches. 	

Lith. Asc. = Lithofacies Association.

Sorting (σ_1), volumes, and pyroclastic density current (PDC) run-out distances modified from Torres-Orozco et al. (2017b).

*cf. Cioni et al. (2000; 2003; 2008).

†cf. Cashman et al. (2000); Cioni et al. (2000); Torres-Orozco et al. (2017a).

§cf. Arce et al. (2003); Brown and Branney (2004); Cioni et al. (2000; 2003; 2008); Bonadonna et al. (2016).

#e.g., Nemeth and White (2003); Lube et al. (2014).

**cf. Cioni et al. (2000; 2008); Houghton et al. (2004); Shea et al. (2012).

††cf. Branney and Kokelaar (2002); Brown and Branney (2004).

§§cf. Druitt (1998); Brown and Branney (2004); Belousov et al. (2007); Kim et al. (2014).

##cf. Boudon and Lajole (1989); Belousov et al. (2007); Cronin et al. (2013); Lube et al. (2014).

***cf. Schwarzkopf et al. (2005); Lube et al. (2011); Cronin et al. (2013).

lahars, were not studied in detail and are only referred as debris or hyperconcentrated flows.

5.6.1.1 Plinian, sub-Plinian, and small-scale eruption columns

The characteristics of Asc1 (Table 5.4), especially massive deposits lacking bedding structures, suggest deposition from fast waxing, sustained and steady Plinian eruption columns (e.g., Arce et al. 2003; Cioni et al. 2000; 2003; 2008; Bonadonna et al. 2016; Table 5.5). Despite deposits of Asc1 and Asc2 being similar (Table 5.4), the defining stratified lithofacies of Asc2 indicate longer and more gradual waxing and waning phases (Table 5.5), and could also represent crosswind plume effects (cf. Cioni et al. 2000; 2003; Bonadonna et al. 2016). In counterpart, the sub-layered – ‘shower-bedded’ – structure of deposits of Asc3, suggests deposition from unsteady sub-Plinian eruption columns, waxing and waning in intensity and height (e.g., Cioni et al. 2000; 2003; 2008; Bonadonna et al. 2016; Table 5.5). Deposits of Asc1 and Asc2 are often interdigitated or topped by PDC deposits of Asc7, suggesting column unsteadiness, and marginal or total column collapse (e.g., Arce et al. 2003; Cioni et al. 2000; 2003; 2008; Bonadonna et al. 2016). Deposits of Asc2 and Asc3 have comparable, laterally and longitudinally, thin and fine-grained lithofacies, which suggest that, in both cases, deposition occurred over similar areas and from columns either smaller (e.g. Kw7 and KA2, Fig. 5.2 and 5.3), or sustained for shorter periods (e.g., KB1 and MD1-MD2, Fig. 5.3 and 5.5), than the Plinian columns of Asc1. Compared to deposits of Asc1-Asc3, deposits of Asc4 are the thinnest and least preserved (Table 5.4), suggesting deposition from short-lived and small Strombolian or Vulcanian eruption columns (cf. Houghton et al. 2004; Cioni et al. 2000; 2008). Lateral correlation of deposits of Asc4 and Asc7 suggests that the unsteady Asc4 columns collapsed. Deposits of Asc3 and Asc4 often comprise sub-layers rich in dense

andesitic clasts or accidental lithics, which are occasionally topped by lava flow deposits (e.g., MD2a, Fig. 5.5). The latter features reflect that column unsteadiness could have different origins that need to be further investigated, for e.g., gas depletion, magma chilling, groundwater interaction, and/or intense vent or conduit erosion (cf. Nemeth and White 2003; Houghton et al. 2004; Bonadonna et al. 2016).

5.6.1.2 *Concentrated – flow type – PDCs*

The characteristics of Asc7 (Table 5.4), mainly pumice-dominated lithology, massive channel-fill deposit structures, and interdigitation with fall deposits of Asc1-Asc4, suggest sedimentation from gravity-driven, confined, dense underflows, at the basal level of density-stratified PDCs produced by collapsing eruption columns (cf. Druitt 1998; Branney and Kokelaar 2002; Brown and Branney 2004; Kim et al. 2014; Sulpizio et al. 2014; Table 5.5). Deposits of Asc7 and Asc9 have comparable lithofacies (Table 5.4), suggesting similar processes of sedimentation. However, Asc9 comprises a dense andesitic clast-dominated lithology, block-and-ash grain-size, and charcoal content, that indicate deposition from dense avalanches, at the basal level of ‘block-and-ash flows’, produced by the explosive collapse of a dome (cf. Schwarzkopf et al. 2005; Lube et al. 2011; Cronin et al. 2013; Table 5.5). The common reverse grading in deposits of Asc9 (e.g., Uig1, Fig. 5.4) suggests dispersive pressure due to grain-to-grain collisions (cf. Branney and Kokelaar 2002; Kim et al. 2014). With distance, the longitudinal lithofacies in both associations comprise, gradually, dominating massive and thinning, fine-grained deposits, that indicate PDC waning, and possible shifts into suspension-sedimentation from moderately-dilute PDCs (cf. Druitt 1998; Schwarzkopf et al. 2005; Lube et al. 2011). Deposits of Asc7 and Asc9 are also topped by, and correlate laterally with, deposits of

Asc6 and Asc8, suggesting shifts into tractional deposition from dilute ‘surge type’ PDCs (cf. Druitt 1998; Brown and Branney 2004; Kim et al. 2014).

5.6.1.3 *Dilute – surge type - PDCs*

Deposits of Asc6 are chiefly defined by fine-grained, faintly-stratified lithofacies, that laterally become subparallel or cross-stratified (pinch-and-swell, Table 5.4). These characteristics suggest rapid suspension-sedimentation and moderate traction, and lateral shifts into complete traction, consistent with deposition from dilute and turbulent ‘surge type’ PDCs (cf. Druitt 1998; Brown and Branney 2004; Kim et al. 2014; Sulpizio et al. 2014; Table 5.5). In addition, dense andesitic clast-dominated lithologies, along with lateral correlations with deposits of Asc9, suggest deposition from ‘ash-cloud surges’, produced by rapid generation and segregation of fine particles following dome-collapse (e.g., Lube et al. 2011; Table 5.5). In the absence of lateral relationships with Asc9, alongside the frequent presence of lithic-rich lithologies (e.g., MA3, Fig. 5.5), deposition could have occurred from explosive hydrothermal or phreatomagmatic ‘surge type’ PDCs (e.g., Nemeth and White 2003; Lube et al. 2014; Table 5.5).

5.6.1.4 *Transitional – flow-and-surge type – PDCs*

The characteristics of Asc5 and Asc8 (Table 5.4), mainly massive and faint-stratification, and uppermost subparallel- and cross-stratification, suggest rapid suspension-sedimentation and weak traction of highly to moderately-concentrated ‘flow type’ PDCs, and topmost full traction from dilute and turbulent ‘surge type’ PDCs (cf. Druitt 1998; Brown and Branney 2004; Kim et al. 2014; Sulpizio et al. 2014; Table 5.5). Laterally, the wide range of stratified lithofacies (e.g., pinch-and-swell structures, low-angle truncations, dune-bedding, and undulating contacts; Ko5-Ko7 and Uig4-Uig6, Fig. 5.3

and 5.4), indicates complete tractional sedimentation from highly unsteady ‘surge type’ PDCs. These vertical and lateral transitions, in addition to the elliptical shape of the PDC depositional areas (cf. Torres-Orozco et al. 2017b), suggest deposition from highly-energetic, laterally-directed, ‘blast type’ PDCs (e.g., Boudon and Lajoie 1989; Belousov et al. 2007; Cronin et al. 2013; Lube et al. 2014; Table 5.5). The occasional reverse to normal grading of deposits of Asc5 and Asc8 could indicate deposition from waxing to vertically diluting PDCs (cf. Brown and Branney 2004; Kim et al. 2014). The defining dense andesitic clast-dominated lithologies of Asc8 (e.g., Kw2 and Uig2, Fig.5.2 and 5.4)

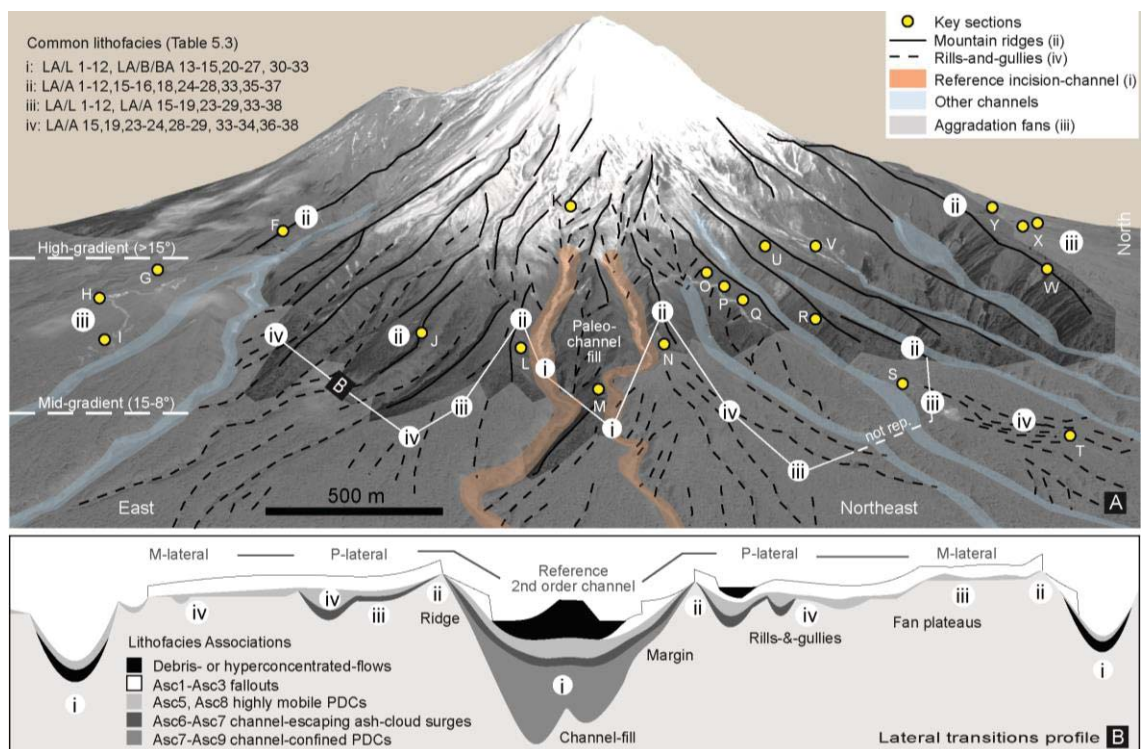


Fig. 5.6 A Example of landscape elements that integrate the present-day micro-topography of the upper eastern flanks of Mt. Taranaki. The gradient of deposit confinement is indicated (modified from Schwarzkopf et al. 2005). **B** Profile of the general lateral transitions, relative to landscape, of deposits corresponding to each lithofacies association. Dotted white line indicates section not represented (not rep.) in the profile. Proximal (P-lateral) and proximal-medial (M-lateral) lateral lithofacies transitions relative to a reference incision-channel (i) are sketched. Digital image modified from Google Images (2017).

and correlation with deposits of Asc9, suggest additional relationship with explosive dome-collapse (cf. ash-cloud surges; Table 5.5). Transitions between dense andesitic clast-dominated and pumice-dominated lithologies (e.g., Uig3, Fig. 5.4), suggest on-going conduit decompression (e.g., Boudon and Lajoie 1989; Belousov et al. 2007; Kim et al. 2014).

5.6.2 Constraints of depositional environment to hazard distribution

The lenticular and channel-fill, coarse-grained lithofacies of Asc7 and Asc9 (Table 5.4) demonstrate that flow type PDCs (Table 5.5) could invariably move downstream through 2nd order incision-channels (cf. Blair and McPherson 1994) with high-confinement gradients (>15-8°, cf. Schwarzkopf et al. 2005; Fig. 5.6). Pinching structures perpendicular to the inferred flow direction (e.g., Kw6, Kw8, Uig1, Fig. 5.2 and 5.4) suggest deposition on channel-margins near to ridge slopes (cf. Schwarzkopf et al. 2005; Lube et al. 2011; 2014). Channel-confined flow type PDC deposits of Asc7 and Asc9 were found commonly at distances varying from 6 to 8 km from the crater of Mt. Taranaki (Fig. 5.7 A and C), however, pumice-rich flows, triggered by column collapse (i.e., Asc7), can reach run-out distances of 15 km during the most explosive eruptive phases (e.g., Saucedo et al. 2010; Capra et al. 2014), and thus, at Mt. Taranaki, constitute potential hazards beyond the boundary of the Egmont National Park (Fig. 5.7 G). Additionally, the lateral association of flow type PDC deposits with fine-grained and stratified surge type PDC deposits (e.g., Kw8, Kw5, Fig. 5.2) suggests deposition over ridge crests and interfluves (e.g., Lube et al. 2011; 2014). These surge deposits were identified across 1.5 km distance from nearly every incision-channel, and downstream, forming the substrate below present-day farmlands at distances varying from 4 to 14 km from the summit crater

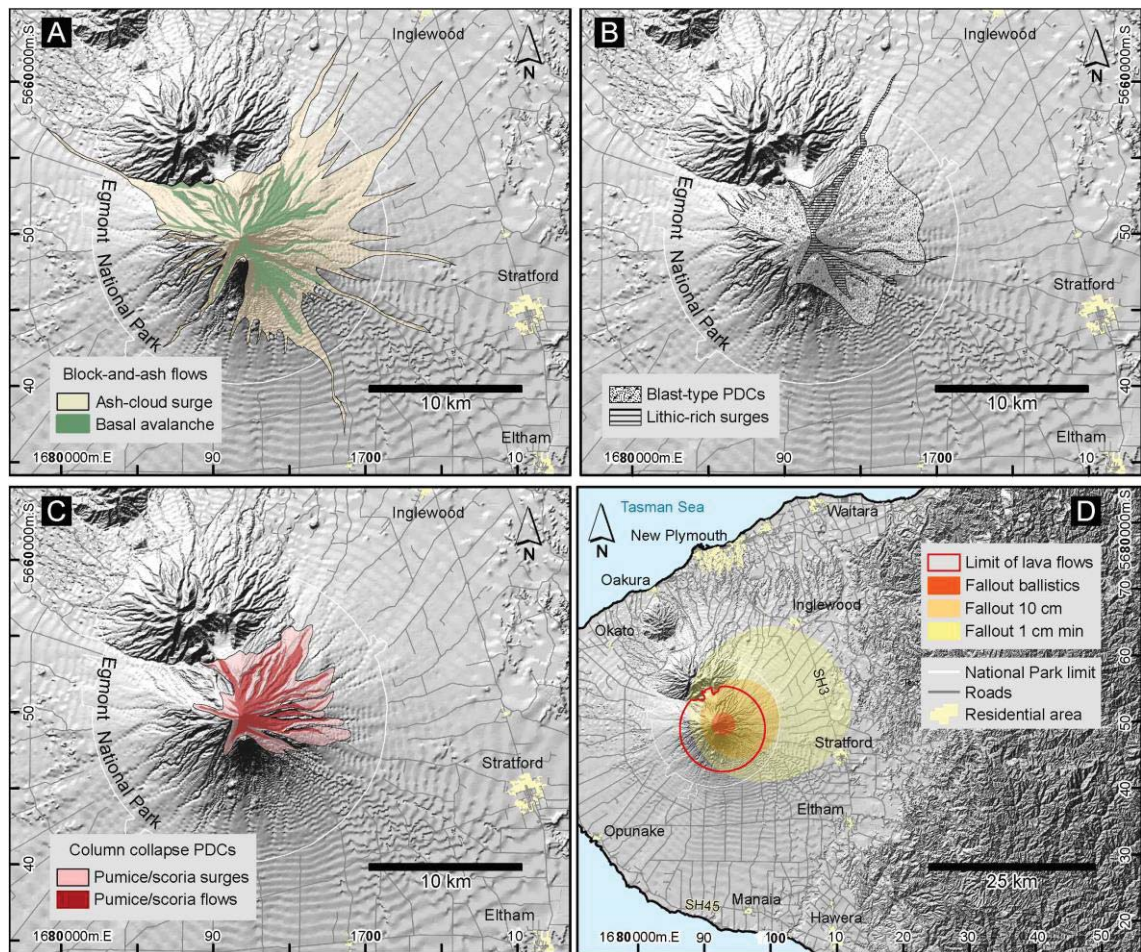
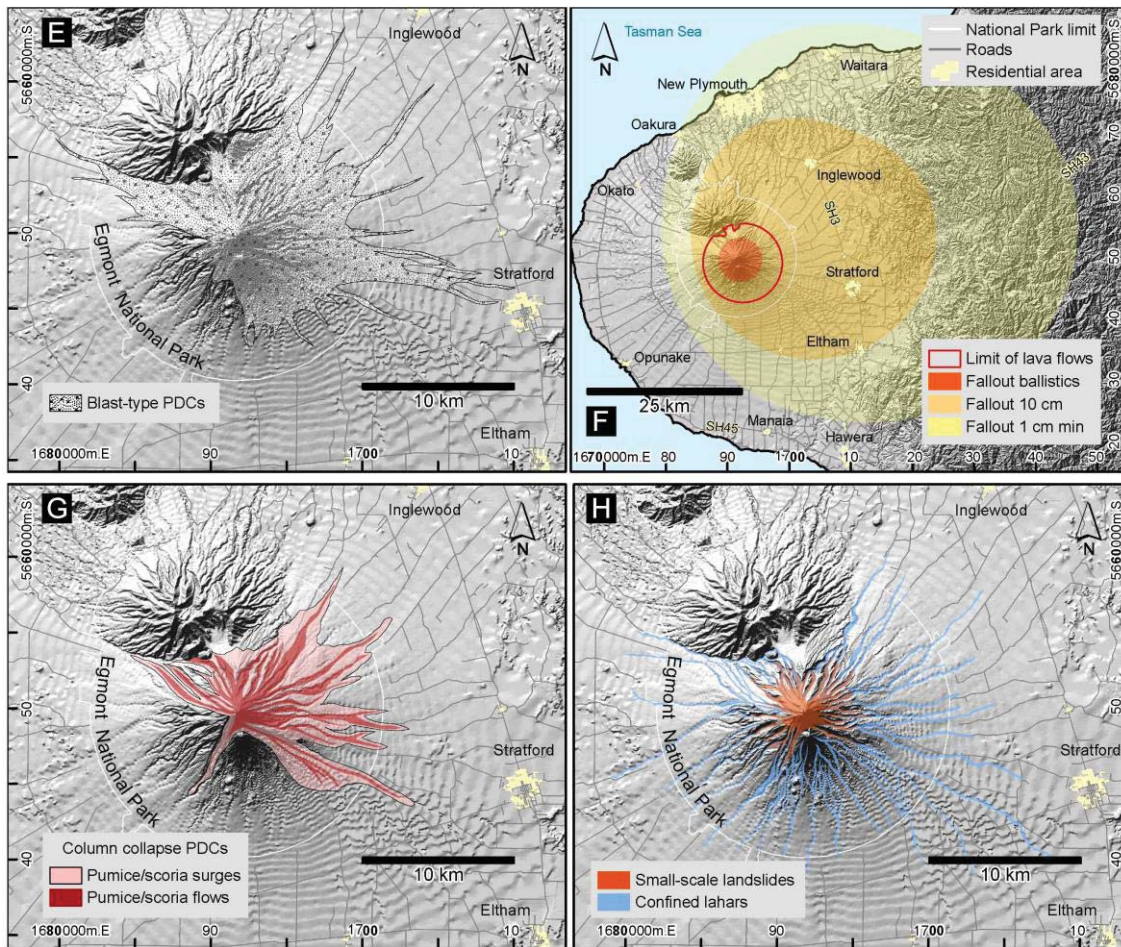


Fig. 5.7 Hazard maps indicating the possible distribution of different types of eruptive activity, throughout distinct eruptive phases, during a future Plinian eruption at Mt. Taranaki. Insets A to D correspond to opening, pre- or post-climactic eruptive phases. A dome-collapse block-and-ash flows, B blast type PDCs and lithic-rich surges, C column-collapse PDCs, D fallout, ballistics, and lava flow distributions. Insets E to G correspond to climactic eruptive phases. E blast type PDCs, F fallout, ballistics and lava flow distributions, G column-collapse PDCs. Inset H represents possible distributions of channel-confined lahars and small-scale landslides during any eruptive phase. Coordinate system of all insets: NZGD 2000 New Zealand Transverse Mercator.

(Fig. 5.7 A, C and G). Yet, deposits of ash-cloud surge (i.e., Asc6), associated with basal avalanches produced by dome-collapse block-and-ash flows (i.e., Asc9), have been predicted to be able to reach distances of 15 km west-northwest (e.g., Procter et al. 2010; Platz et al. 2012; Fig. 5.7 A). Also, lithic-rich deposits of other surge type PDCs (i.e., Asc

Fig. 5.7 (continue)



6), lacking any association with deposits produced by flow type PDCs, were recognised over channels and interfluves (Fig. 5.6), at distances varying from 5 to 14 km downslope, mainly at northeastern and eastern flanks from the summit crater (Fig. 5.7 B). These surge distributions and run-outs demonstrate the capacity of dilute PDCs to surmount topographic obstacles and cover large extensions (e.g., Kim et al. 2014; Lube et al. 2011; 2014), and provide evidence of their potential impacts over Mt. Taranaki's surrounding inhabited areas (Fig. 5.7 A, B, E and G).

The multiple transitions from massive and faintly-stratified, throughout diversely subparallel, pinch-and-swell, and cross-stratified, to waving, massive, and parallel-stratified lithofacies of deposits produced by blast type PDCs of Asc5 and Asc8 (e.g., Uig4 to Uig6, transect of sections C-F-J-M-N, Fig. 5.4), indicate deposition inside incision-channels, over ridge crests, and across interfluves (e.g., Brown and Branney 2004; Belousov et al. 2007; Cronin et al. 2013; Kim et al. 2014; Lube et al. 2011; 2014; Fig. 5.6) dissected by 1st order rills-and-gullies (cf. Blair and McPherson 1994; Menendez et al. 2008), and further over flat low-land areas. Blast type PDC deposits were recognised covering extensions varying from 10 to 12 km across northern, eastern and southern areas of Mt. Taranaki, and downslope, up to 18 km east from the crater (Fig. 5.7 B and E). Such characteristics of deposition and distribution demonstrate that blast type PDCs can travel mostly unconfined and surmount elevated topographic barriers due to their high mobility and energy (e.g., Boudon and Lajoie 1989; Belousov et al. 2007; Cronin et al. 2013; Lube et al. 2011; 2014; Fig. 5.6), and therefore prove that blast type PDCs could cover the broadest PDC extensions during a future eruptive episode at Mt. Taranaki, including urban areas such as at Stratford (Fig. 5.7 E).

Additionally, in contrast to equivalent deposits in southeastern and western channels (cf. Procter et al. 2010; Platz et al. 2012), no charcoal has been found inside northeastern and eastern channel-fill PDC deposits, suggesting that the northeastern to eastern flanks of Mt. Taranaki must have been denuded of vegetation by active PDC and/or fall deposition throughout much of the last 5000 years. Similarly, in proximal sections, fall deposits of associations Asc1 to Asc4 often constitute lenticular drapes produced by capping erosive PDC, debris-flow, or colluvial deposits (e.g., section P, Fig. 5.2 and 5.3), supporting the existence of a very active channel setting (e.g., Saucedo et al. 2010; Cronin et al. 2013;

Capra et al. 2016). In such landscape, thick successions of overlapping PDC deposits (e.g., Ko5-Ko8 at sections W to X, and Uig4-Uig6 at sections N to Q, Fig. 5.3 and 5.4) could have in-filled channels and smoothed the topography (e.g., Procter et al. 2010; Cronin et al. 2013; Capra et al. 2016), easing the passage for further PDCs to develop the long run-out distances recognised beyond the present-day limits of the Egmont National Park (Fig. 5.7 A, E and G).

Conversely, it is well documented that Plinian fallouts produced at most stratovolcanoes can deposit pyroclasts over the largest extensions, irrespective of topography and depending on the prevailing wind directions (e.g., Arce et al. 2003; 2005; Cioni et al. 2000; 2003; 2008; Saucedo et al. 2010; Capra et al. 2014; Bonadonna et al. 2016). Consequently, fallout hazards (e.g., 10 cm-thick fall deposits, Capra et al. 2014) generated during a potential Plinian eruption at Mt. Taranaki could affect the most populated areas located at distances of minimum 20 to 30 km from the summit crater (Fig. 5.7 F), as indicated by the existing isopach maps (e.g., Platz et al. 2007; Torres-Orozco et al. 2017b; Fig. 5.1 D).

5.6.3 Volcanic hazard scenarios

We discuss the expected hazard scenarios during a future Plinian eruptive episode at Mt. Taranaki, taking into account the lithofacies analysis and the interpretations on eruptive processes and hazard distributions. These scenarios are consistent with <5 ka Plinian and sub-Plinian eruptive episodes produced at the summit crater of Mt. Taranaki and at the satellite vent of Fanthams Peak (Table 5.2), characterised by climactic eruptive phases of magnitude 4 to 5, during which eruption columns varying in height from 14 to 29 km, and PDCs having minimum volumes of 10^6 to 10^7 m³ are formed (Torres-Orozco et al.

Fig. 5.8

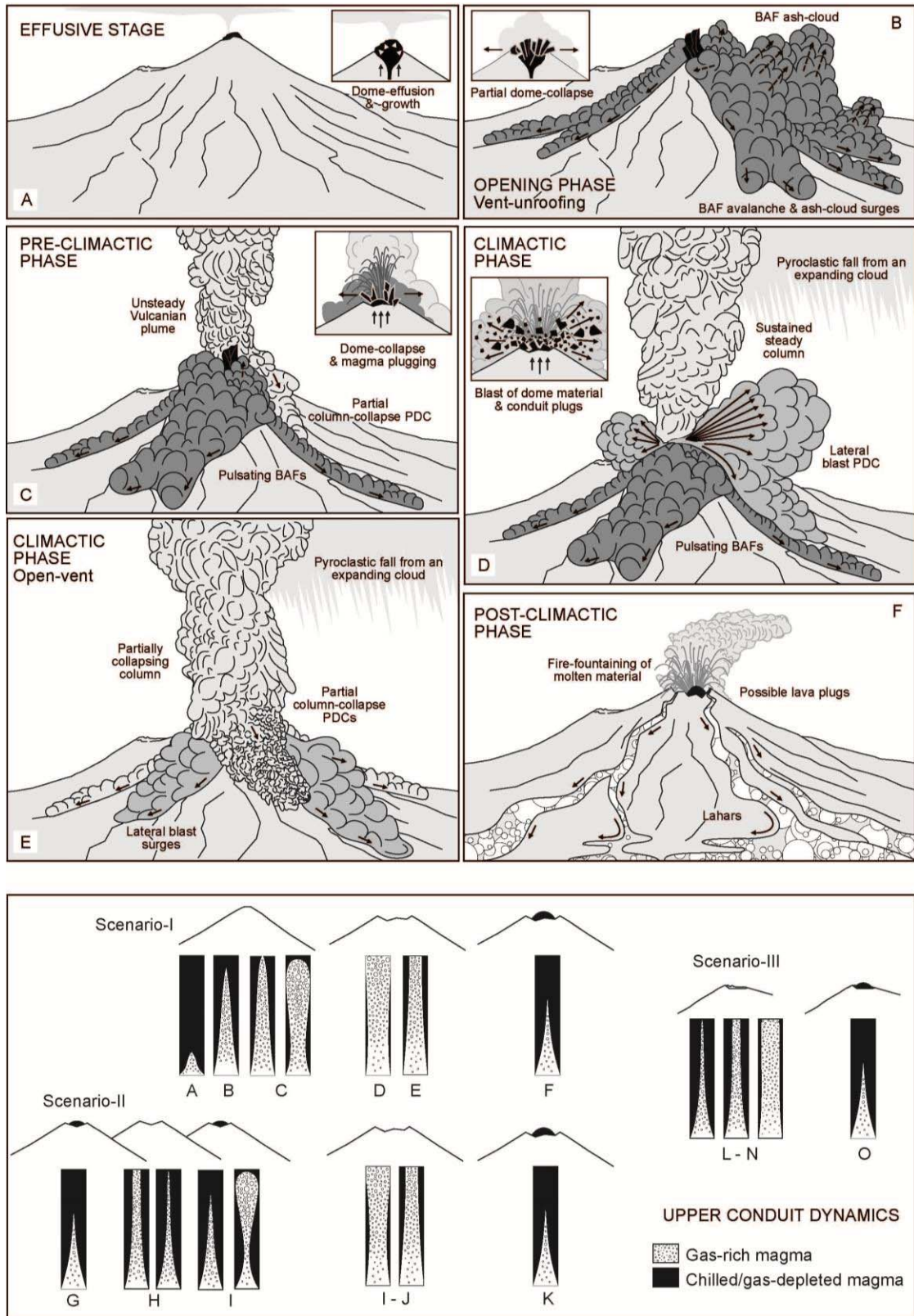


Fig. 5.8 (continue)

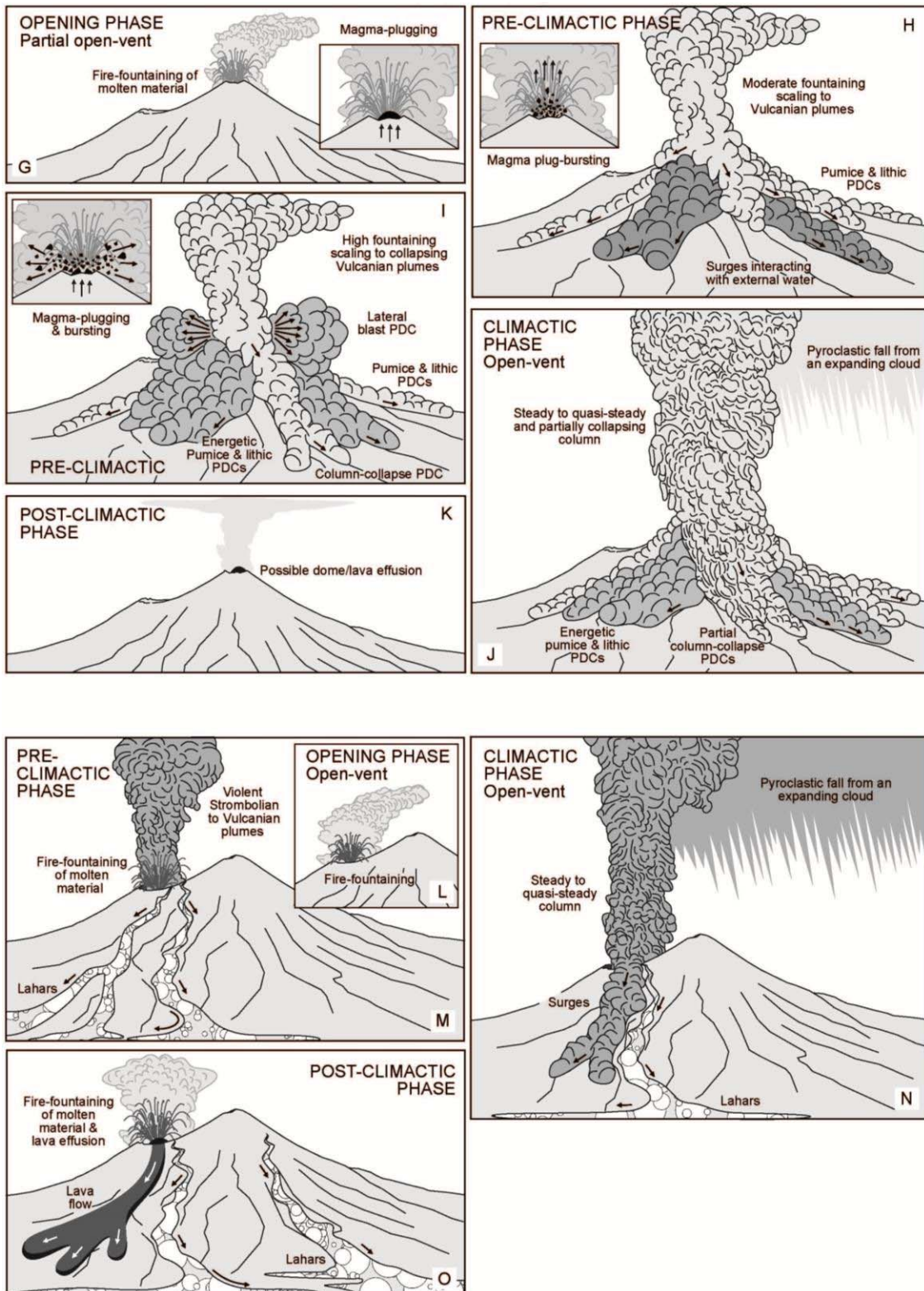


Fig. 5.8 Volcanic hazard scenarios for Plinian eruptions at Mt Taranaki's summit-crater and Fanthams Peak vent. **A-F** Scenario I: initial eruptive phases of close-conduits and conduit-decompression by vent unroofing and dome collapse. **G-K** Scenario II: transient open and clogged conduits by repeated plugging-and-bursting of gas-depleted or chilled magma. **L-O** Scenario III: rapid progression into steady phases by open-conduits. The possible upper conduit dynamics for each scenario were sketched based on data and interpretations of Torres-Orozco et al. (2017a; b).

2017b). Earlier interpretations on block-and-ash flow (Procter et al. 2010; Platz et al. 2012), lahar and landslide distributions (Zernack et al. 2009; 2011) were also considered.

5.6.3.1 Scenario I: dome collapse and conduit decompression

Scenario I is the most typical to be expected from the summit vent of Mt. Taranaki (cf. Turner et al. 2009; 2011; Torres-Orozco et al. 2017a; b). It begins with effusion of a 10^7 to 10^8 m³ dome (cf. Platz et al. 2007; 2012) capping the vent and conduit (Fig. 5.8 A). Days, weeks, or even years later, the vent is unroofed by pulsating or single dome-collapse, prompting conduit decompression and more rapid magma ascent. Multiple block-and-ash flows descend the flanks and form basal avalanches confined to deep-channels (Fig. 5.8 B), reaching up 6 to 8 km (Fig. 5.7 A). Associated ash-cloud surges spread laterally, onto interfluves, and downstream from the basal avalanches (Fig. 5.8 B), threatening most areas inside the Egmont National Park (Fig. 5.7 A). In cases of very rapid conduit decompression, more violent ash-cloud PDCs can develop, spreading across a broader fan and reaching farmlands located at 15 km from the summit crater (Fig. 5.7 A). Once the vent is unroofed, short-lived Vulcanian plumes erupt dense pyroclasts (e.g., Torres-Orozco et al. 2017b) that fall over areas close to the crater, and produce minimum 1 cm-thick ash deposits in urban areas such as at Stratford and Inglewood (Fig. 5.7 D). These unsteady plumes usually collapse and generate PDCs (Fig. 5.8 C) with varying run-

out distances (Fig. 5.7 C). This phase may lead directly into conduit opening (Fig. 5.9 D) and onset of climactic steady sub-Plinian or Plinian columns (Fig. 5.8 E).

In some cases, stalling of magma in the conduit due to lower magma flux or higher viscosity magma may briefly plug it (Fig. 5.8 C), trapping gases that are released by further Vulcanian explosions that produce collapsing columns. Ultimately, once gas-rich magma is erupted at high rates, the conduit pressure increases and more violent climactic explosions occur (Fig. 5.9 C) These produce sub-vertical and laterally-directed blast type PDCs (Fig. 5.8 D) that spread widely over obstacles and may reach distances of 18 km from the crater, affecting mainly the eastern rural areas and urban locations, such as Stratford and Inglewood, if directed to the east and northeast (Fig. 5.7 E). Blast type PDC deposits observed near Pouakai hut, on top of the homonymous volcano (Fig. 5.1), indicate that during the climactic phase of a Scenario I eruption even the upper ridges of Pouakai, delimiting the northern lower flanks of Mt. Taranaki, could be threatened by a blast type PDC.

Increasingly violent blasts clear the conduit before onset of a steady phase. Once the latter phase is reached, sustained and steady or quasi-steady Plinian and sub-Plinian eruption columns develop (Fig. 5.8 D-E). These can disperse at least 10 cm-thick pyroclastic fall deposits in the direction of prevailing stratospheric winds (e.g., Torres-Orozco et al. 2017b), 20 to 30 km away from the crater, over the urban areas of Eltham, Stratford and Inglewood (Fig. 5.7 F), but could also drape most of the Taranaki Peninsula, including the most populated urban fringe, from New Plymouth to Waitara (Fig. 5.7 F), under minimum 1 cm-thick ash deposits. Slowing magma supply rates and degassing ultimately reduce the ejection velocity, leading to eruption waning and partial or total column-collapse, and triggering PDCs (Fig. 5.8 E). Channel filling and smoothing from earlier

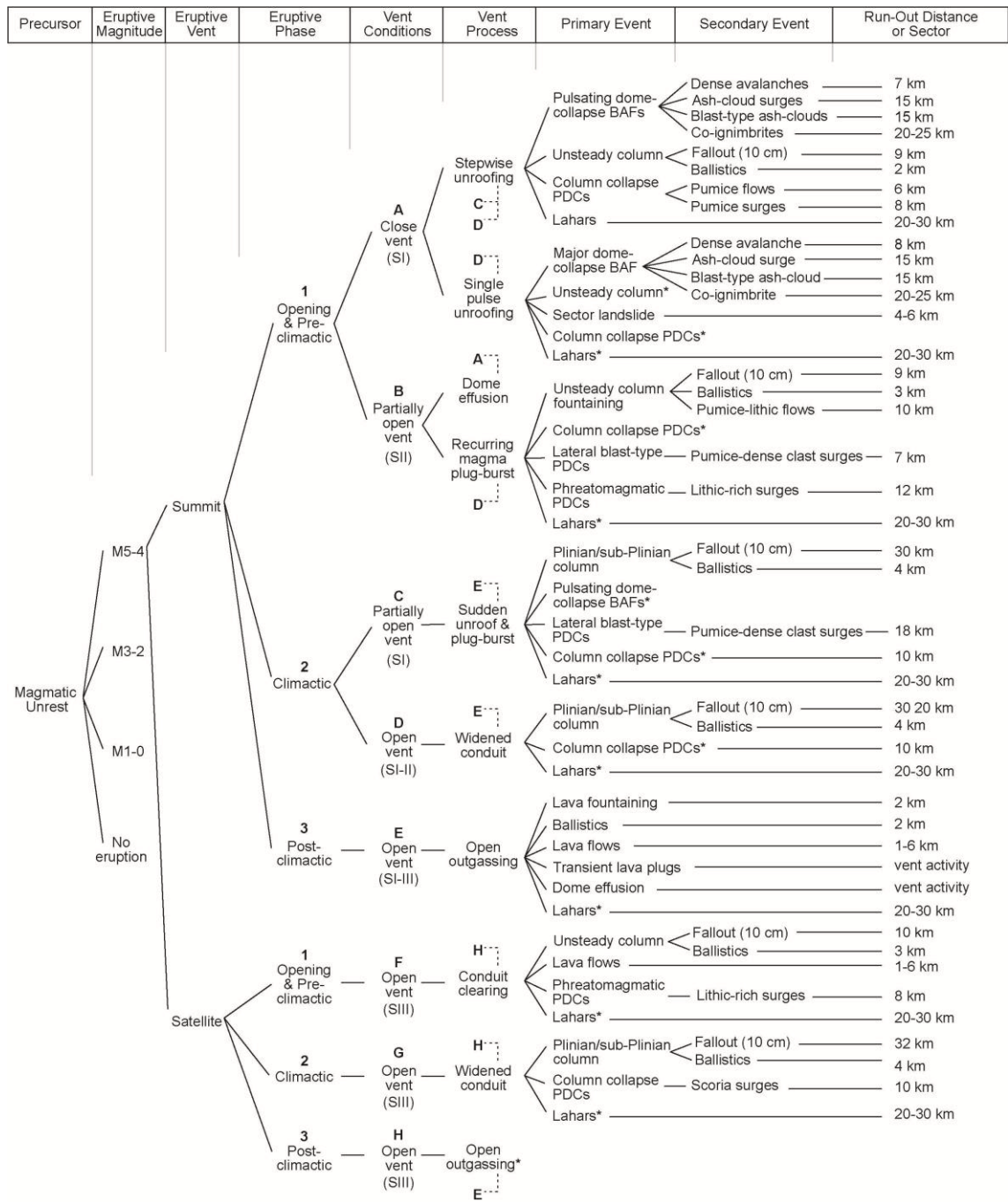


Fig. 5.9 Event-tree sequence of the volcanic scenarios expected at Mt. Taranaki during a possible Plinian eruptive episode (magnitudes 4 to 5), produced at either the summit crater, or a satellite vent. For any vent, the eruptive sequence progresses from an opening and pre-climactic phase (1), throughout a climactic phase (2), to a post-climactic phase (3). Vent and/or conduit conditions (A to H) may direct into different processes and events (i.e., Scenarios I to III). Dotted lines indicate subsequent, alternative directions. Run-out distances simplified from Fig. 5.7.

activity allow PDCs to run-out up to 15 km from the crater, covering farmlands and triggering fires in different areas (Fig. 5.7 G).

The post-climactic phase (Fig. 5.9 E) can extend for hours to weeks, and produce many short lived columns and ballistically ejected pyroclasts, deposited inside the limits of the National Park (Fig. 5.7 D and F). Eruptions generally cease with declining rates of magma rise. In some cases, fire fountaining may produce proximal spatter (Fig. 5.8 F). During and following eruptions, rain and snow melt and, along with exposed areas with burnt and damaged vegetation, combine to source small-scale landslides and widespread lahars (Fig. 5.8 F). The latter can reach minimum run-out distances of 15 to 20 km throughout channels (Fig. 5.7 H), but their deposits have been recognised forming coastal cliffs at 30 to 35 km from the summit crater (cf. Zernack et al. 2009; 2011), and can potentially flood complete farmlands and urban areas around the volcano peak. This eruption scenario is similar to witnessed sub-Plinian and Plinian episodes at Colima (Saucedo et al. 2010; Capra et al. 2014), Merapi (Surono et al. 2012; Cronin et al. 2013), Soufriere Hills (Druitt et al. 2002) and Pelée (Carazzo et al. 2012).

5.6.3.2 *Scenario II: transient conduit clogging by magma plug-and-burst*

This scenario is characterised by short-lived and repeated plugging of, and explosive bursting through conduits, as viscous magma chills and outgasses (Fig. 5.9 B). These relatively sustained, rapid explosions prevent the formation of large-volume lava domes over the vent (Fig. 5.8 G), thus suppressing the generation of dome-collapse block-and-ash flows, in contrast with Scenario I. The first phase of the Scenario II eruptions begins with small phreatomagmatic explosions and dense fountains from the summit crater,

before the conduit is plugged by gas-depleted magma (Fig. 5.8 G). As magma and gas pressure increases and explosions begin from conduit margins, establishing pyroclastic fountaining and small collapsing plumes, and eventually disintegrating the lava plug, ice, rain and/or groundwater infiltration accelerates the frequency of explosions and speeds up the plug fragmentation (Fig. 5.8 H). These explosions generate lithic-rich surges and pumice-and-lithic column-collapse PDCs (Fig. 5.8 H) that can travel distances varying from 4 to 12 km down the volcano flanks, and would threaten the areas of the Egmont National Park and of the neighbouring farmlands (Fig. 5.7 B-C). As slugs of gas-rich magma rise into the conduit, blast type PDCs (Fig. 5.8 I) having run-out distances of up to 7 km may occur (Fig. 5.7 B). This also leads to higher pyroclastic fountaining, and the establishment of larger yet highly unsteady and collapsing Vulcanian columns (Fig. 5.8 I), which disperse fall deposits over rural and urban areas close to the volcano (Fig. 5.7 D).

Once these finally clear the conduit, climactic, open-conduit conditions (Fig. 5.9 D) produce steady or oscillating Plinian and sub-Plinian eruption columns (Fig. 5.8 J). These columns disperse pyroclastic fall deposits downwind, over similar extensions than those of Scenario I (Fig. 5.7 F). However, the Scenario II convective columns are commonly interrupted by slugs of chilled or gas-depleted magma that destabilise the conduit and cause pauses in discharge and column-collapse (Fig. 5.8 J). The largest column-collapse PDCs can reach distances of 15 km downslope, comparable to the analogous PDCs of Scenario I (Fig. 5.7 G), affecting inhabited farmlands and triggering fires.

The eruption ceases (Fig. 5.9 E) as the magma discharge rate and gas content drops, with final effusion of a dome inside the crater (Fig. 5.8 K). Small-scale landslides and lahars can be produced in a similar way, and cover comparable channel and flat land extensions

(Fig. 5.7 H) than during a Scenario I eruption. Eruptions of Scenario II are similar to, but larger than the Vulcanian 2014-2015 activity at Colima volcano (Capra et al. 2016), and comparable to the initial explosive phases of Soufriere Hills (Druitt et al. 2002), but lacking dome-collapse block-and-ash flows. They are also similar to sub-Plinian phases of different eruptions at Cabulco (Petit-Breuilh 1999; Castruccio et al. 2016) and Somma-Vesuvius (Cioni et al. 2003).

5.6.3.3 Scenario III (Fanthams Peak): rapid conduit clearing at satellite vents

Scenario III involves rapid vent-opening, with brief conduit-clearing eruptive phases at satellite vents such as Fanthams Peak (Fig. 5.9 F-H). The initial eruptive phase is characterised by low-viscosity magma that quickly ascends and reaches the surface (Fig. 5.8 L), prompting initial fire-fountains and small-scale, explosive, or violent Strombolian bursts (Fig. 5.8 M). Pyroclastic falls can be deposited over rural and urban areas located near to the eruptive vent (e.g., Fig. 5.7 D), similarly to Scenarios I and II.

During the climactic eruptive phase (Fig. 5.9 G), the waxing and unsteady pre-climactic columns scale into high, steady or oscillating Plinian and sub-Plinian eruption columns (Fig. 5.8 N). These plumes disperse pyroclastic falls downwind, into areas located mainly 20 to 30 km from the vent, but, as described for Scenarios I and II, minimum 1 cm-thick ash deposits can drape most of the Taranaki Peninsula and affect the most populated areas (Fig. 5.7 F). Unsteadiness driven by chilling magma, degassing along conduit walls, and/or magma-water interactions, may lead to column-collapse and the formation of surges (Fig. 5.8 N) which can reach run-out distances of 15 km over the volcano flanks and farmlands (Fig. 5.7 G).

Eruptions of this type cease after gradual outgassing and decrease in magma flux (Fig. 5.9 H). The eruptive column dissipates and transforms into fire-fountaining (Fig. 5.8 O). The post-climactic phase may also include effusion of lava flows (Fig. 5.8 O), having run-out distances of 1 to 6 km from the vent, and threatening the area of the National Park (Fig. 5.7 F). If erupted onto ice/snow, and during heavy rainfalls, spatter and ballistically ejected pyroclasts produced alongside this scenario can trigger syn- and post-eruptive lahars (Fig. 5.8 M-O). Alike Scenarios I and II, lahars produced during a Scenario III eruption can reach minimum distances of 15 to 20 km from the vent throughout channels distributed radially around Mt. Taranaki (Fig. 5.7 H), depending on the vent position, and flood farmlands. Scenario III eruptions are similar to mafic Plinian eruptions produced at, e.g., Etna and Tarawera volcanoes (e.g., Coltelli et al. 1998; Houghton et al. 2004).

5.6.4 Event-tree scenario sequence

The above described scenarios can be distilled into a progression of possible eruptive events (e.g., Newhall and Hoblitt 2002; Martí et al. 2008; Marzocchi et al. 2010; Fig. 5.9) occurring, depending on different vent conditions and processes, during eruptive phases of scaling intensity and magnitude: from opening and pre-climactic phases, mainly characterised by the generation of a range of PDC styles, throughout the most explosive climactic phases, during which the thickest fall and broadest PDC deposits are produced, to post-climactic phases, comprising eruptive activity restricted mostly to near vent areas. Accordingly, this event-tree sequence can be envisaged for eruptions produced at either the summit crater of Mt. Taranaki, or at a satellite vent such as Fanthams Peak (Fig. 5.9). This would be of major use for hazard managers facing potential magmatic unrest at this volcano because of the directions provided to different eruptive phases, associated eruptive styles, and run-out distances of hazard impacts. In addition, this event-tree

sequence also provides insights into the scaling explosivity throughout eruptive phases, common to most andesitic eruptions, and delineates the volcanological basis that can support advance research on numerical modelling of the spatial distribution of hazards at Mt. Taranaki (e.g., Procter et al. 2010). In this work, estimating the probability for each event inside the progression is out of scope. Nevertheless, event probabilities must be further investigated due to their proven value and application on hazard assessment (e.g., Newhall and Hoblitt 2002; Martí et al. 2008; Marzocchi et al. 2010).

5.7 Conclusions

For the last 5000 years, Mt. Taranaki has produced minimum one Plinian/sub-Plinian eruption every 300 years (Torres-Orozco et al. 2017a). This frequency is roughly higher than the historical records (Global Volcanism Program 2013) of recently active andesitic volcanoes such as Colima (1/600 yrs), Merapi (1/750 yrs) and Pelée (1/500 yrs). With the last sub-Plinian eruption produced ± 360 years ago (Druce 1966; Platz et al. 2007), the future volcanic threat at Mt. Taranaki should not be overlooked. In order to achieve a better understanding of the potential hazards produced by Plinian eruptions at volcanoes such as Mt. Taranaki, it is important to analyse the spatial and temporal lithofacies transitions and associations of the proximal pyroclastic successions. This work provides evidence of the application of lithofacies associations to the determination of eruptive styles and magnitudes, when field deposit-data is insufficient to empirically estimate eruptive parameters. Our results expand the range of PDC styles and distributions identified at Mt. Taranaki, and consequently highlight the major role that PDCs must have during the evaluation of the hazardscape at this volcano. This work also remarks the importance of assessing the main landscape elements of the present-day volcano micro-topography, common to most stratovolcanoes (e.g., Lube et al. 2011; Carazzo et al. 2012;

Cronin et al. 2013; Sulpizio et al. 2014; Capra et al. 2014; 2016), so as to envisage possible pathways of distribution of PDCs and other comparable hazards during a future eruptive episode. This requires development of carefully constructed deposition models to compare units formed by different processes and scales within channels, ridges, interfluves, and more distant fans.

From our interpretations of eruptive processes and hazard distributions, three volcanic hazard scenarios (Scenario I to III) can be expected in case of future Plinian eruptive episodes at either Mt. Taranaki's summit crater, or at the satellite vent on top of Fanthams Peak. During a Scenario I eruption, the pre-climactic phase can be sudden by explosive or passive collapse of a dome, rapidly progressing into violent large-volume blast type PDCs. However, when repeatedly blocked conduits occur during Scenario II eruptions, gas and magma pressure combine to also generate explosive blasts and other types of PDCs of smaller volume. These are arguably the greatest hazards to life, associated with the entire eruption sequence, due to their unpredictability and sudden onsets. The longest PDC run-out distances are also associated with large-scale explosive dome collapses, as well as events occurring at the end of eruptive episodes after channels are filled and smoothed. In the Taranaki case, PDC run-out distances of at least 18 km are expected during climactic explosions. Column and fountain fed PDCs generally reach only up to 15 km. Additionally, climactic pyroclastic falls will directly impact rural and urban locations hosting over 100,000 inhabitants in the Taranaki area (Statistics NZ 2013). In both early and late phases of eruption, sudden blast type events are also likely to generate violent PDCs extending >8 km from Park boundaries. If the onset of eruptions at the summit crater is slow, it should be assumed that a Scenario II event is most likely at this volcano – and hazard planning should account for PDC scenarios that may affect areas

well outside the current deep channels. In the case of satellite vent eruptions (Scenario III), Taranaki experiences suggest that these are more mafic and lower viscosity magmas, hence large PDCs are less likely. Climactic scale hazards are still equivalent to other scenarios, but the explosiveness more predictable than in the case of a summit eruption.

The major proximal deposition record shows that Mt. Taranaki may erupt a great range of styles during relatively short intervals. Such complexity should be considered a hallmark for large-scale andesitic eruptions everywhere. The scenario types here can be applied easily to other similar stratovolcanoes and would be especially valuable when tailored to fit proximal depositional successions described in a similar structured way. The proximal evidence provides the most nuanced view of the range and possible duration of entire eruptive episodes, and not just their largest (and arguably most stable) climactic phase.

5.8 References

- Alloway B, Neall VE, Vucetich CG (1995) Late Quaternary (post 28,000 year B.P.) tephrostratigraphy of northeast and central Taranaki, New Zealand. *J Royal Soc NZ* 25:385-458
- Arce JL, Macías JL, Vázquez SL (2003) The 10.5 Ka Plinian eruption of Nevado de Toluca, México: stratigraphy and hazard implications: *Geol. Soc. Am. Bull.* 115 (2): 230-248
- Arce JL, Cervantes KE, Macías JL, Mora JC (2005) The 12.1 ka Middle Toluca Pumice: A dacitic Plinian–subplinian eruption of Nevado de Toluca in Central Mexico. *J Volcanol Geotherm Res* 147:125-143
- Belousov A, Voight B, Belousova M (2007) Directed blast and blast-generated pyroclastic density currents: a comparison of the Bezymianny 1956, Mount St Helens 1980, and Soufriere Hills, Montserrat 1997 eruptions and deposits. *Bull. Volcanol.* 69: 701-740
- Blair TC, McPherson JG (1994) Alluvial fans and their natural distinction from rivers based on morphology, hydraulic processes, sedimentary processes, and facies assemblages. *Journal of sedimentary research*, 64(3):450-489
- Bonadonna C, Cioni R, Costa A et al (2016) MeMoVolc report on classification and dynamics of volcanic explosive eruptions. *Bull Volcanol* 78:84

- Boudon D, Lajoie J (1989) The 1902 Peleean deposits in the Fort Cemetery of St. Pierre, Martinique: a model for the accumulation of turbulent nuees ardentes. *J Volcanol Geoth Res* 38:113-129
- Bourdier JL, Pratomo I, Thouret JC et al (1997) Observations, stratigraphy and eruptive processes of the 1990 eruption of Kelut volcano, Indonesia. *J Volcanol Geoth Res* 79:181–203
- Branney MJ, Kokelaar P (2002) *Pyroclastic Density Currents and the Sedimentation of Ignimbrites*. Geological Society, London, Memoirs 27, 143 p
- Brown RJ, Branney MJ (2004) Event-stratigraphy of a caldera-forming ignimbrite eruption on Tenerife: the 273 ka Poris Formation. *Bull Volcanol* 66:392-416
- Capra L, Gavilanes-Ruiz JC, Bonasia R, Saucedo-Giron R, Sulpizio R (2014) Re-assessing volcanic hazard zonation of Volcán de Colima, Mexico. *Natural Hazards*, doi: 10.1007/s11069-014-1480-1
- Capra L, Macias JL, Cortes A, Davila N et al. (2016) Preliminary report on the July 10–11, 2015 eruption at Volcán de Colima: Pyroclastic density currents with exceptional runouts and volume. *J Volcanol Geoth Res* 310:39-49
- Carazzo G, Tait S, Kaminski E, Gardner JE (2012) The recent Plinian explosive activity of Mt. Pelée volcano (Lesser Antilles): The P1 AD 1300 eruption. *Bull Volcanol* 74:2187-2203
- Cashman KV, Sturtevant B, Papale P, Navon O (2000) Magmatic fragmentation. In: Sigurdsson H, Houghton BF, McNutt SR, Rymer H, Stix J (eds) *Encyclopedia of volcanoes*. Academic Press, San Diego, CA: 421-430
- Castruccio A, Clavero J, Segura A, Samaniego P, Roche O, Le Pennec JL, Droguett B (2016) Eruptive parameters and dynamics of the April 2015 sub-Plinian eruptions of Calbuco volcano (southern Chile). *Bull Volcanol* 78(9):62
- Chough SK, Sohn YK (1990) Depositional mechanics and sequences of base surges, Songaksan tuff ring, Cheju Island, Korea. *Sedimentology* 37 (6):1115-1135
- Cioni R, Marianelli P, Stantacroe R, Sbrana A (2000) Plinian and subplinian eruptions. In: Sigurdsson H, Houghton BF, McNutt SR, Rymer H, Stix J (eds) *Encyclopedia of Volcanoes*. Academic Press, San Diego, pp:477-494
- Cioni R, Sulpizio R, Garruccio N (2003) Variability of the eruption dynamics during a Subplinian event: Greenish Pumice eruption of Somma-Vesuvius (Italy). *J Volcanol Geotherm Res* 124:89-114
- Cioni R, Bertagnini A, Santacroe R, Andronico D (2008) Explosive activity and eruption scenarios at Somma-Vesuvius (Italy): Towards a new classification scheme. *J Volcanol Geotherm Res* 178:331-346
- Coltelli M, Del Carlo P, Vezzoli L (1998) Discovery of a Plinian basaltic eruption of Roman age at Etna volcano, Italy. *Geol* 26(12):1095-1098
- Cronin SJ, Lube G, Dayudi DS et al (2013) Insights into the October-November 2010 Gunung Merapi eruption (Central Java, Indonesia) from the stratigraphy, volume and characteristics of its pyroclastic deposits. *J Volcanol Geoth Res* 261:244-259

- Damaschke M, Cronin S, Holt K, Bebbington M, Hogg A (2017) A 30,000-year high-precision eruption history for the andesitic Mt Taranaki, North Island, New Zealand. *Quaternary Res*, 1–23. DOI:10.1017/qua.2016.11
- Downey WS, Kellett RJ, Smith IEM, Price RC, Stewart RB (1994) New palaeomagnetic evidence for the recent eruptive activity of Mt. Taranaki, New Zealand. *J Volcanol Geoth Res* 60:15-27
- Druce AP (1966) Tree-ring dating of recent volcanic ash and lapilli, Mt Egmont. *NZ J Botany* 4:3-41
- Druitt TH (1998) Pyroclastic density currents. In: Gilbert JS, Sparks RSJ (eds) *The Physics of Explosive Volcanic Eruptions*. Geological Society, London, Special Publication 145, 145-182
- Druitt TH, Calder ES, Cole PD, Hoblitt RP et al (2002) Small-volume, highly mobile pyroclastic flows formed by rapid sedimentation from pyroclastic surges at Soufriere Hills Volcano, Montserrat: an important volcanic hazard. In: Druitt TH and Kokelaar BP (eds) *The Eruption of Soufriere Hills Volcano, Montserrat, from 1995 to 1999*. Geological Society, London, Memoirs 21, 263-279
- Fisher R, Schmincke HU (1984) *Pyroclastic Rocks*, Springer-Verlag, Berlin, 472 p
- Folk RL, Ward WC (1957) Brazos River bar: a study in the significance of grain size parameters. *J Sedimentary Res* 27(1)
- Global Volcanism Program (2013) *Volcanoes of the World*, v. 4.5.3. Venzke E (ed) Smithsonian Institution. <http://dx.doi.org/10.5479/si.GVP.VOTW4-201> Downloaded 9 February 2017
- Google Images (2017) Taranaki Regional - Stratford - South Taranaki Councils. Astrium, CNES, Spot Image, DigitalGlobe, Landsat, Copernicus. Software Google Earth v.7.1.8.3036 <http://www.google.com/maps/@-39.28321,174.09825,14z/data=!3m1!1e3> Downloaded 26 February 2017
- Gutiérrez-Elorza M (2008) *Geomorfología*. Madrid, Pearson Educación, 920 p
- Henry S, Reyners M, Bibby H (2003) Exploring the plate boundary structure of North Island, New Zealand. *EOS, Trans Am. Geophys Union* 84:289-294
- Houghton BF, Wilson CJN, Del Carlo P et al (2004) The influence of conduit processes on changes in style of basaltic Plinian eruptions: Tarawera 1886 and Etna 122 BC. *J Volcanol Geoth Res* 137:1-14
- Kim GB, Cronin SJ, Yoon WS, Sohn YK (2014) Post 19 ka B.P. eruptive history of Ulleung Island, Korea, inferred from an intra-caldera pyroclastic sequence. *Bull Volcanol* 76:802. doi 10.1007/s00445-014-0802-1
- King PR, Thrasher GP (1996) *Cretaceous-Cenozoic geology and petroleum systems of the Taranaki Basin, New Zealand*. Institute of Geological and Nuclear Sciences Monograph 13
- Lube G, Cronin SJ, Thouret JC, Surono (2011) Kinematic characteristics of pyroclastic density currents at Merapi and controls on their avulsion from natural and engineered channels. *GSA Bull* 123(5/6):1127-1140. doi: 10.1130/B30244.1

- Lube G, Breard EC, Cronin SJ, Procter JN et al. (2014) Dynamics of surges generated by hydrothermal blasts during the 6 August 2012 Te Maari eruption, Mt. Tongariro, New Zealand. *J Volcanol Geoth Res* 286:348-366
- Lucchi F (2013) Stratigraphic methodology for the geological mapping of volcanic areas: insights from the Aeolian archipelago (southern Italy). *Geological Society, London, Memoirs* 37:35-53
- Macias JL, Sheridan MF, Espindola JM (1997) Reappraisal of the 1982 eruptions of El Chichón Volcano, Chiapas, Mexico: new data from proximal deposits. *Bull Volcanol* 58:459-471
- Martí J, Aspinall WP, Sobradelo R, Felpeto A et al (2008) A long-term volcanic hazard event tree for Teide-Pico Viejo stratovolcanoes (Tenerife, Canary Islands). *Journal of Volcanology and Geothermal Research*, v. 178, p. 543-552.
- Marzocchi W, Sandri L, Selva J (2010) BET_VH: a probabilistic tool for long-term volcanic hazard assessment. *Bulletin of Volcanology*, v. 72, p. 705-716.
- McGlone MS, Topping WW (1977) Aranuiian (postglacial) pollen diagrams from Tongariro region, North Island, New Zealand. *New Zealand Journal of Botany* 15(4):749-760
- Menéndez I, Silva PG, Martín-Betancor M, Pérez-Torrado FJ, Guillou H, Scaillet S (2008) Fluvial dissection, isostatic uplift, and geomorphological evolution of volcanic islands (Gran Canaria, Canary Islands, Spain). *Geomorphology* 102(1):189-203
- Neall VE (1972) Tephrochronology and tephrostratigraphy of western Taranaki (N108-109), New Zealand. *NZ J Geol Geoph* 15:507-557
- Neall VE (1979) Sheets P19, P20, and P21. New Plymouth, Egmont and Manaia. 1st ed. Geological map of New Zealand 1:50,000. 3 maps and notes. NZ Dept of Scientific and Industrial Res, Wellington
- Neall VE, Stewart RB, Smith IEM (1986) History and petrology of the Taranaki volcanoes. In: Smith IEM (ed) Late Cenozoic volcanism. *Royal Society of New Zealand Bulletin* 23:251-263
- Nemeth K, White JDL (2003) Reconstructing eruption processes of a Miocene monogenetic volcanic field from vent remnants: Waipiata Volcanic Field, South Island, New Zealand. *J Volcanol Geoth Res* 124(1-2):1-21
- Newhall, CG, Hoblitt RP (2002) Constructing event trees for volcanic crises. *Bulletin of Volcanology*, v. 64, p. 3-20.
- Petit-Breuilh M (1999) Cronología eruptiva histórica de los volcanes Osorno y Calbuco, Andes del Sur (41°-41°30'S). *Boletín No. 53, Servicio Nacional de Geología y Minería, Chile*, 46 p
- Platz T, Cronin SJ, Cashman KV et al (2007) Transitions from effusive to explosive phases in andesite eruptions-A case-study from the AD 1655 eruption of Mt. Taranaki, New Zealand. *J Volcanol Geoth Res* 161:15-34
- Platz T, Cronin SJ, Procter JN et al (2012) Non-explosive dome-forming eruptions at Mt. Taranaki, New Zealand. *Geomorphology* 136:15-30

- Price RC, Gamble JA, Smith IEM, Stewart RB, Eggins S, Wright IC (2005). An integrated model for the temporal evolution of andesites and rhyolites and crustal development in New Zealand's North Island. *J. Volcanol. Geotherm. Res.* 140 (1-3): 1-24
- Procter JN, Cronin SJ, Platz T et al (2010) Mapping block-and-ash flow hazards based on Titan 2D simulations: a case study from Mt. Taranaki, NZ. *Nat Hazards* 53:483–501
- Pyle DM (2000) Sizes of volcanic eruptions. In: Sigurdsson H, Houghton BF, McNutt SR, Rymer H, Stix J (eds) *Encyclopedia of volcanoes*. Academic Press, San Diego, CA: 263-269
- Salvador A (1994) *International stratigraphic guide. A guide to stratigraphic classification, terminology and procedure*, 2nd ed. Subcommittee of Stratigraphic Classification of IUGS International Commission on Stratigraphy and Geological Society of America. Boulder, Colorado, 214 p
- Saucedo R, Macías JL, Gavilanes JC, Arce JL et al (2010) Eyewitness, stratigraphy, chemistry, and eruptive dynamics of the 1913 Plinian eruption of Volcán de Colima, México. *J Volcanol Geoth Res* 191:149-166
- Schwarzkopf LM, Schmincke HU, Cronin SJ (2005) A conceptual model for block-and-ash flow basal avalanche transport and deposition, based on deposit architecture of 1998 and 1994 Merapi flows. *J Volcanol Geoth Res* 139:117-134
- Shea T, Gurioli L, Houghton BF et al (2011) Column collapse and generation of pyroclastic density currents during the AD 79 eruption of Vesuvius: the role of pyroclast density. *Geology* 39(7):695-698
- Shea T, Gurioli L, Houghton BF (2012) Transitions between fall phases and pyroclastic density currents during the AD 79 eruption at Vesuvius: building a transient conduit model from the textural and volatile record. *Bull Volcanol* 74(10):2363-2381
- Sherburn S, White RS (2006) Tectonics of the Taranaki region, New Zealand: earthquake focal mechanisms and stress axes. *NZ J Geol and Geoph* 49:269-279
- Statistics New Zealand (2013) 2013 Census: Taranaki Region. <http://www.stats.govt.nz/> Accessed 1 January 2017
- Sulpizio R, Dellino P, Doronzo DM, Sarocchi D (2014) Pyroclastic density currents: state of the art and perspectives. *Journal of Volcanology and Geothermal Research*, v. 283, p. 36-65
- Surono, Jousset P, Pallister J et al (2012) The 2010 explosive eruption of Java's Merapi volcano – A '100-year' event. *J Volcanol Geoth Res* 241-242:121-135. doi: 10.1016/j.jvolgeores.2012.06.018
- Taranaki Regional Council (2017) Regional priorities and economy. <https://www.trc.govt.nz/council/> Accessed 1 January 2017
- Torres-Orozco R, Cronin SJ, Pardo N, Palmer AS (2017a) New insights into Holocene eruption episodes from proximal deposit sequences at Mt. Taranaki (Egmont), New Zealand. *Bull Volcanol* 79(3):1-25, doi 10.1007/s00445-016-1085-5
- Torres-Orozco R, Cronin SJ, Damaschke M, Pardo N (2017b) Diverse dynamics of Holocene mafic-intermediate Plinian eruptions at Mt. Taranaki (Egmont), New Zealand. *Bull Volcanol (BUVO-D-17-00023)*, in review by editor.

-
- Turner MB, Cronin SJ, Bebbington MS, Platz T (2008a) Developing probabilistic eruption forecasts for dormant volcanoes: a case study from Mt Taranaki, New Zealand. *Bull Volcanol* 70:507-515
- Turner MB, Cronin SJ, Smith IEM et al (2008b) Eruption episodes and magma recharge events in andesitic systems, Mt Taranaki, New Zealand. *J Volcanol Geoth Res* 177:1063-1076
- Turner MB, Bebbington MS, Cronin SJ, Stewart RB (2009) Merging eruption datasets: building an integrated Holocene eruptive record for Mt. Taranaki, New Zealand. *Bull. Volcanol.* 71:903-918
- Turner MB, Cronin SJ, Bebbington MS et al (2011) Integrating records of explosive and effusive activity from proximal and distal sequences: Mt. Taranaki, New Zealand. *Quaternary Intl* 246:364-373
- White JDL, Houghton BF (2006) Primary volcanoclastic rocks. *Geology* 34:677-680
- Zernack AV, Procter JN and Cronin SJ (2009) Sedimentary signatures of cyclic growth and destruction of stratovolcanoes: A case study from Taranaki, NZ. *Sedimentary Geology* 220, 288-305
- Zernack AV, Cronin SJ, Neall VE, Procter JN (2011) A medial to distal volcanoclastic record of an andesite stratovolcano: Detailed stratigraphy of the ring-plain succession of south-west Taranaki, New Zealand. *International Journal of Earth Sciences*, v. 100, p. 1936-1966

Chapter 6 Conclusions

Over the last 5000 years of explosive volcanism at Mt. Taranaki, andesitic (53-60 wt.% SiO₂) eruptives have occurred at its summit-crater (2500 m), and basaltic and basaltic-andesitic (48-52 wt.% SiO₂) episodes from its satellite-vent, Fanthams Peak (1966 m). This period has seen at least 53 eruption episodes as evidenced from pyroclastic deposit successions recorded in this study. Each of the 53 bed-sets comprises single or multiple layers with lithostratigraphic properties suggesting deposition from intercalated fall, pyroclastic density current (PDC) or lava flow eruptive units. Fall units were produced during 28 of the 53 eruption episodes, whilst PDC units formed within 38 of them. Twenty-six of the bed-sets are included in two Formations mapable at 1:25000 scale with distinctive lithology, chemical composition and lithofacies variations: the 3.0 to 1.2 cal ka B.P. Manganui Formation, and the <1000 years B.P. Maero Formation.

Fall deposits are dominated by up to 82 vol.% pumice clasts, whereas PDC deposits consist of diverse proportions of pumice and lithic clasts, with some of them comprising up to 99 vol.% dense lava "lithics". The mineralogy of these units consist of varying volumetric proportions of plagioclase, hornblende, Fe-Ti oxides, orthopyroxene, clinopyroxene and minor biotite. Eruptives from the Fanthams Peak vent contrast to the Summit Vent eruptives, by being dominated by ortho and clinopyroxene, hornblende, Fe-Ti oxides and olivine crystals.

The lithostratigraphic characteristics, including lateral and longitudinal lithofacies transitions, componentry, clast shape, grain-size and textures, framework, bedding structures, deposit architecture and upper and lower contacts, indicate that at least 16

eruption episodes were of Plinian or sub-Plinian character and scale. This suggests roughly one large-scale explosive eruption every 300 years, although they are not evenly distributed in time. In stratigraphic order, the largest eruptions produced bed-sets (or Members) ± 5 ka Tw-I, 4.7-4.6 cal ka B.P. Kokowai, ± 3.8 cal ka B.P. Kapuni-A and Kapuni-B, 3.5 cal ka B.P. Korito, 3.4 cal ka B.P. Lower Inglewood, 3.3 cal ka B.P. Upper Inglewood, < 3.0 cal ka B.P. Manganui-A, > 2.6 cal ka B.P. Manganui-C, ~ 2.6 cal ka B.P. Manganui-D, 2.2 cal ka B.P. Maketawa-I, 1.6 cal ka B.P. Maketawa-II, < 1.6 cal ka B.P. Manganui-F, ~ 1.2 cal ka B.P. Kaupokonui, 0.7 cal ka B.P. Te Popo, and AD 1655 Burrell.

PDCs were produced during the sub-Plinian to Plinian eruption sequences by (1) collapse of domes from the summit-crater (generating typical dense lava-rich valley confined basal avalanche deposits); (2) column-collapse during unsteady eruptive phases (forming pumice-rich deposits); (3) boiling-over small fountains (forming mixed pumice/lithic deposits; or (4) laterally directed or vertical blasts from domes or conduit-plugs (forming fan shaped dispersals of pumice-and-lithic deposits). The most widespread of these were types (1) and (4), reaching up to 19 km from source, although it was generally noted that PDC's erupting late in an eruption sequence may travel farther due to pre-smoothing of the topography.

The findings of this study demonstrate the complex nature of the eruption episodes at Mt. Taranaki, even over the short interval of ~ 5 kyr. While past attention has often been paid to the thick pyroclastic fall successions formed during climactic eruptive phases, it was here shown that the main eruptive diversity was due to the variable onset and waning phases of eruption episodes. In these pre- and post-climactic phases, PDCs of different sorts, were the most common depositional processes in the late-Holocene history of this volcano.

Eight Members comprise the Fanthams Peak-sourced Manganui Formation (Manganui-A to Manganui-G and Kaupokonui), each representing a separate eruption episode of relatively mafic composition for this volcano. The Manganui-D Member was produced by the largest basaltic eruption episode recorded in Mt. Taranaki's late-Holocene history. The Manganui Formation is interdigitated with other 2.6-1.2 cal ka B.P. deposits sourced from intermediate composition eruptions at Taranaki's summit vent. These include sequences of PDCs and falls from Vulcanian, Peleean and Plinian eruptions. The two vents were concurrently active for an at least ~1400 years period. This shows that they are both capable of producing large eruption episodes although they have contrasting mafic to intermediate compositions. This implicates a more complex hazardscape at Mt. Taranaki than considered before.

The Taranaki's summit-sourced and youngest Maero Formation comprises 18 Members, including the newly defined Te Popo eruption episode of Plinian style, as well as the youngest sub-Plinian AD1655 Burrell eruption episode from the volcano. The two large eruptions were separated and followed by 350 years of small-scale Vulcanian and Peleean eruptions and intervals of quiescence. According to both the last 5 kyr records, and longer sequences seen on the ring-plain, reawakening at Mt. Taranaki has the potential to produce complex sub-Plinian to Plinian scale eruptions, consistent with the typical behavior registered after long periods of quiescence at similar andesitic volcanoes (e.g. Colima, Copahue, Merapi, Pelée, Mt. St. Helens, Soufriere Hills).

In order to determine the possible intensities, magnitudes, durations and plume and PDC dispersals during future large eruption episodes at Mt. Taranaki, bed-sets produced by the Kokowai, Upper Inglewood, Manganui-D, Kaupokonui and Burrell eruption episodes were mapped and examined in detail. These episodes were erupted from the two different

vents, and encapsulate examples of diverse eruption styles and contrasting compositions representative of the range of large-scale explosive volcanism at Mt. Taranaki. Results from these studies show that the summit-crater of Mt. Taranaki typically produced basaltic trachy-andesitic and trachy-andesitic Plinian and sub-Plinian eruption episodes, during which 14-29 km-high eruption columns ejected 0.1-1.1 km³ (0.05-0.5 km³ DRE) at mass discharge rates of 10⁷-10⁸ kg/s and volume discharge rates of 10³-10⁴ m³/s, indicating magnitudes of 4.1-5.3 and climactic-phase eruption durations of 1-3 hours. In comparison, the Fanthams Peak vent has generated basaltic, trachy-basaltic and basaltic trachy-andesitic Plinian and sub-Plinian eruptions, comprising 14-27 km-high eruption columns that discharged 0.1-0.4 km³ (0.07-0.3 km³ DRE) at mass and volume rates of 10⁷-10⁸ kg/s and 10³-10⁴ m³/s, respectively, involving magnitudes of 4.3-5.0 and climactic-phase eruption durations of 2-4 hours. PDCs were produced almost exclusively from the summit-crater, preceding or accompanying the eruption columns. These PDCs consisted of dome-collapse BAFs of 0.01-0.02 km³ DRE, run-out distances of 3-8 km and magnitudes of 3.4-3.7, column-collapse pumice-and-ash currents of 10⁻⁴-10⁻³ km³ DRE, run-out distances of up to 6 km and magnitudes of 2.5-3, and lateral-blast PDCs of up to 0.01 km³ DRE, run-out distances of 14-19 km and magnitudes of 3.5-3.7.

This study has shown that the Kokowai was the largest eruption episode of the last 5 kyr of Mt. Taranaki, producing a 28 km-high Plinian eruption column which dispersed a 0.5 km³ DRE fallout, followed by a 21 km-high sub-Plinian column that dispersed another 0.05 km³ DRE fallout. The second largest eruption episode, the Upper Inglewood, produced an avg. 22 km-high Plinian column that dispersed a 0.2 km³ DRE fallout. This eruption, was however noteworthy, because it was preceded by one of the largest dome-collapse and lateral-blast PDC successions, forming a total of 0.03 km³ DRE of PDC

deposits dispersed up to 19 km from the summit-crater. The largest basaltic Plinian eruption produced at the Fanthams Peak vent – the Manganui-D – comprised an avg. 25 km-high column that distributed a 0.3 km³ DRE fallout.

The eruption columns were mostly established during climactic eruptive phases, and were sustained and steady to quasi-steady, steady and short-lived, pulsating, height-oscillating, or unsteady and collapsing. PDCs were produced during unsteady to highly unsteady Vulcanian-style eruptive phases, characterized by clearing of conduits, during initial waxing phases and also from the collapse of margins of climactic convective columns under open-conduit conditions. PDCs also occurred during unsteady column phases, and associated with post-climactic waning and collapsing columns. The density and porosity analyses of pumice clasts at different phases during eruption episodes, showed that the steadiest eruptive phases were associated with texturally and chemically homogeneous pumice (with bulk porosities of up to 60-70 vol.%), interpreted to represent eruption of large volumes of rheologically homogeneous magmas at high intensities. By contrast, the unsteady eruptive phases were related to diverse pumice density, porosity and textures (e.g. with bulk porosities ranging from 20 to 60 vol.%), interpreted as the result of contrasts in volatile and crystal contents and viscosity, possibly developed by magma repeatedly stalling, expanding and contracting within shallow conduits.

By these means, it was demonstrated that Plinian and sub-Plinian eruption episodes of nearly-identical magnitudes and intensities may comprise a vast range of contrasting eruption dynamics and shifts in eruption style, also shown for these examples in divergent major element magma compositions. Consequently, to adequately model volcanic hazards from such volcanoes, it is necessary to assess the complete geological record to distinguish among different eruption episodes. Just concentrating on the estimated

intensities and magnitudes alone, does not reflect the huge potential range in style, dynamics, durations and hazards of eruptions; for example, the Upper Inglewood in contrast with the identically “sized” Manganui-D.

In conclusion, three volcanic hazard scenarios for Plinian eruptions are proposed for the case of renewed explosive activity at Mt. Taranaki. These scenarios comprise unsteady initial and pre-climactic eruptive phases of different conduit conditions, intensities, duration, style and dynamics, but steady and quasi-steady climactic phases of eruption columns with comparable intensities and magnitudes.

Scenario I comprises: initial close-conduit conditions and conduit-decompression by vent-unroofing with collapse or blasting of a dome/plug at the summit-crater, leading rapidly to a climactic sub-Plinian to Plinian eruption phase.

Scenario II involves: initial transient open and clogged conduit conditions produced by plugging-and-bursting of chilled or gas-depleted magma that may last for some time before gradual transition to a climactic sub-Plinian to Plinian phase.

Scenario III involves: a rapid vent opening followed by progression from waxing explosive bursts leading rapidly into steady sub-Plinian to Plinian phases by open-conduit conditions.

During scenarios I and II, initial eruptive events produce repeated BAFs or fountain collapse pumice-and-ash currents, intercalated with unsteady and short-lived Vulcanian plumes. Further pre-climactic activity can involve repeated collapse of domes and consequent BAFs, recurrent column collapse PDCs, scaling up to violent blasts and lateral blast-PDCs. By contrast, Scenario III, involves fire-fountaining and Strombolian or

Vulcanian plumes that occur in pre- and post-climactic stages. All three scenarios, lead into steady to quasi-steady Plinian and sub-Plinian climactic eruption columns. The steadiest conditions will commonly produce the highest sustained columns, whereas quasi-steady and late or transient unsteady conditions favor height-oscillating and collapsing columns. The post-climactic eruptive phases are likewise similar in all scenarios, consisting of column waning and dissipation accompanied often by column collapse, fire-fountaining, possible lava dome and/or flow effusion, and lahars triggered by rains.

In every scenario, the pyroclastic fallouts produced by eruption columns constitute the widest dispersed hazard associated with land, air and water pollution, deterioration of human health, and damage of urban (e.g. dwellings), transport and industrial infrastructure. Fall deposits erupted from Mt. Taranaki could affect areas of at least 1500-2500 km² (inside 1-2 cm isopachs), covering the whole eastern Taranaki Peninsula. This includes complete farmlands, the largest city of New Plymouth, and towns of Hawera, Eltham, Stratford, Inglewood and up to Waitara, with most of their population (>100,000 inhabitants) working on the energy and dairy industry. This would also affect one of the most transited highways in New Zealand (i.e. SH3) and disrupt the air traffic. Most dangerous to life, however, are PDCs although they mainly affect areas of 5-30 km². In many cases these may extend beyond the ~9.5 km distant Egmont National Park boundaries, reaching up to 19 km from source. PDCs burn and destroy the vegetation and anything in their paths, can trigger and spread fires into farmlands, pollute most headwaters, and ultimately provide the main source of material for deadly lahars even long after the end of the explosive activity. The most hazardous of the PDCs at Mt. Taranaki relate to violent lateral-blast currents which are highly energetic and mobile,

and thereby spread across topographic barriers. Blast PDC deposits were identified at the western proximities of Stratford, 19 km from the crater, covering areas of 60-70 km² and have also been found by previous studies with a similar distribution pattern to the west. A future blast would burn and obliterate farmlands, villages and urban localities outside the National Park, at least over the eastern sectors.

In this work, an integrative approach was employed to define the large-scale explosive volcanism at the andesitic Mt. Taranaki, and its potential hazards during future reawakening. A set of geological data comprising fine-detail lithostratigraphy, quantitative determinations of eruptive parameters from field data, and componentry, chemical and density-porosity analyses was evaluated, and the results were unified into complete volcanic hazard scenarios for Plinian eruptions. This approach demonstrates the value and need of applying geological methods alongside other resources (e.g. geophysical modeling and monitoring) in order to attain realistic hazard models. Therefore, this work is also important for hazard managers looking for assessing the complexity of large-scale eruption episodes not only at this volcano, but at other similar andesitic cones.

6.1 Avenues for future research

In this thesis work, better understanding magma fragmentation processes during Plinian and sub-Plinian, mafic to intermediate explosive eruptions by complementing the density-porosity determinations with SEM and high-resolution X-ray tomography data remained incomplete, however, work is still in progress and it will provide better constraints on timescales of degassing and bubble nucleation (i.e. bubble and crystal number densities).

Nevertheless, further scientific questions about explosive volcanism and volcanic hazards emerged alongside this work and could be addressed in future studies.

Some of these questions are: What were the reasons for co-existing basaltic and andesitic volcanism of similar scale, style and explosivity to be produced? What processes affected the chemical composition of magma while it crystallized inside the magma chamber? What triggered magma degassing and vesiculation? What was the depth of the magma chamber, temperature and magma volatile content prior to Plinian/sub-Plinian eruptions, and how these conditions changed to produce basaltic or andesitic explosive eruptions? What were the ascent rates and ascent steps: was the magma column fully buoyant or did it stagnate? How many changes in temperature and pressure occurred and how did they affect the magma composition?

These research problems could be solved by employing mineral chemistry and petrology methods such as analyses of specific crystal phases (e.g. two-pyroxenes, hornblende or plagioclase) by Electron-Microprobe and chemical-mapping using CT-scanning, geothermometry and geobarometry, measurement of crystal disequilibrium by rim-growth (e.g. in olivine), aided with the use of glass inclusions to better constrain degassing processes from volatiles. In addition, petrological experiments of pressure-temperature could be performed to understand crystallization and changes in magma composition during ascent and at different depths, and this could be associated to different eruption styles, different scales of explosivity, compositions, and hazard potential.

Many questions also remain in studies of PDC dynamics, along with lateral and longitudinal dispersal. This information is often due to poorly preserved, or poorly recognised PDC deposits. Better simulation and geophysical models can, however, be

achieved by applying the geological data, such as that produced in this work, especially by using the best preserved example of the Upper Inglewood blast PDC. It also remains to better understand how paleotopography and present-day topography could limit PDC distributions, and under which conditions PDCs remain confined, compared, for example, to a highly mobile blast PDC. Quantitative PDC particle concentrations, temperatures and velocities are also missing for every type of PDC studied in this work, i.e. dome-collapse BAFs, ash-cloud surges, column-collapse pumice-and-ash flows, fountain-produced currents, and the very energetic and mobile lateral-blast PDCs.

Considering that dome-collapse from the summit-crater is the most typical eruptive style at Mt. Taranaki, it will be important to define what are the conditions under which this may progress into a large-scale eruption, a small-scale event, or ultimately into triggering a single “hot or cold” BAF without any subsequent relevant activity. These questions could require further field work, thermal analyses of charcoal, analyses of magnetism in deposits, detailed sedimentology and componentry studies of PDC deposits, mineral chemistry, PDC experiments by using the examples of Mt. Taranaki.

Considering the long history of edifice-collapse at Mt. Taranaki, it would be interesting to unveil and understand whether there is a relationship between edifice destruction and large-scale explosive volcanism. What would be the worst-case hazard scenarios in case of having both occurring together, what would be the timescales, distributions and consequences.

And finally, from the results of this work, it is clear that Mt. Taranaki can erupt multiple and even synchronous large-scale explosive eruptions at the summit-crater and at satellite vents like Fanthams Peak. It would be crucial to understand what are the causes for

magma to erupt from any of these vents, what is the potential for a new vent to open and what could be the locations. To this regard, it remains to further study what are the tectonic mechanisms involved and what is the stress regime in the area responsible for faulting and dike propagation.

Appendices

Appendices are contained inside a CD stored in a pocket at the rear of the thesis:

A. Supplementary material

Appendix 1.1 Digital copy of the Thesis.

Appendix 2.1 Excel spreadsheet for calculation of sorting parameters from sieved-data of different bed-sets from Mt. Taranaki.

Appendix 4.1 Deposit thickness and average pumice and lithic diameters measured at different sections located on the eastern flanks of Mt. Taranaki.

Appendix 4.2 Density and volume analyses and porosity determinations of pyroclasts from different bed-sets produced by large eruptions at Mt. Taranaki.

Appendix 4.3 Summary of key lithostratigraphic characteristics of deposits produced by large eruptions at Mt. Taranaki.

Appendix 4.4 Whole-rock chemical analyses of juvenile pyroclasts from different bed-sets deposited by eruptions from Mt. Taranaki.

Appendix 4.5 MgO vs. SiO₂ diagrams of bulk-deposit (black symbols), pumice or “vesicular juvenile clasts of the Manganui-D Member” (P and VJ, respectively, both represented with white symbols), and dense lithic clasts (Lith, represented with grey symbols) from different layers or from different stratigraphic levels within a layer (base, middle “mid” and top), of bed-sets deposited by distinct eruptions from Mt. Taranaki. Data modified from previous works (*) correspond to Franks 1984, May 2003, Platz et al. 2007 and Turner et al. 2011b. *BAF* block-and-ash flow deposits, *PDC* pyroclastic density current deposits.

Appendix 4.6 Isopach data of individual or combined fall deposit layers and resulting geometrical values.

Appendix 4.7 Isopleth data of individual fall deposit layers and resulting geometrical values.

Appendix 4.8 Bulk-fall deposit isopach and isopleth data of each bed-set studied. Isopach data were plotted on Log (Thickness) in metres vs. distance expressed as Isopach Area^{1/2}, comprising: **a** individual segments, **a1** proximal single segments (0a) of selected isopachs; **b** two to three individual segments (proximal 0 or 0b, and others: 1 or 1a, 1b and 2). Isopleth data were plotted on Major Pumice (or vesicular juvenile clasts of the Manganui-D bed-set) or Lithic clast diameters (in centimetres) vs. distance expressed as Isopleth Area^{1/2}, comprising: **c** only individual segments, and **c1** proximal (0) segments only constrained for the Upper Inglewood layer Uig7 to prevent the use of inconsistent data. Data modified from previous works (*) correspond to Whitehead 1976 and Platz et al. 2007.

Appendix 4.9 a Column height (HT) in kilometres, calculated by applying different methods using isopleth and isopach data. **b** Eruption classification parameters calculated from isopleth and isopach data.

Appendix 5.1 Geographic location of the studied sections.

B. Statements of contribution

This thesis contains two published chapters (chapters 3 and 4), and one chapter under editorial review (chapter 5) at international peer-reviewed scientific journals. This appendix contains the corresponding “Statement of contribution to doctoral thesis containing publications” forms (DRC16) of Massey University.

A. Supplementary material

Appendix 2.1. Excel spreadsheet for calculation of sorting parameters from sieved-data of different bed-sets from Mt. Taranaki.

The spreadsheet is not entitled to be read on text/image files. For complete display and best resolution go to electronic spreadsheet.

Burrell fall deposit

		Burrell Fall								
		Bu Top			Bu Middle			Bu Base		
phi	mm	Initial wt.g		600.39	Initial wt.g		1251.49	Initial wt.g		1447.79
		wt.g	wt.%		wt.g	wt.%		wt.g	wt.%	
-5.5	45									
-5	32	21.08	3.539288113	3.54	226.2	18.13517197	18.14	59.81	4.135580094	4.14
-4.5	23	179.29	30.10241773	33.64	365.96	29.34017478	47.48	100.95	6.980217531	11.12
-4	16	127.52	21.41034251	55.05	311.54	24.97715065	72.45	179.5	12.41158045	23.53
-3.5	11	120.28	20.19476158	75.25	196.6	15.76204602	88.21	210.65	14.56545639	38.09
-3	8	55.75	9.360308932	84.61	72.53	5.814960314	94.03	211.05	14.59311451	52.69
-2.5	6	24.07	4.041302888	88.65	37.62	3.016114808	97.05	158.58	10.96506088	63.65
-2	4	18.59	3.121222297	91.77	17.49	1.402228814	98.45	128.46	8.882404597	72.53
-1.5	3	9.06	1.521155138	93.29	5.09	0.408081456	98.86	92.68	6.408385941	78.94
-1	2	5	0.83948959	94.13	4.77	0.38242604	99.24	69.4	4.798683474	83.74
-0.5	1.4	2.95	0.495298858	94.63	1.7	0.136294396	99.37	42.03	2.906176749	86.65
0	1.0	2.41	0.404633983	95.03	0.81	0.064940271	99.44	44.37	3.06797674	89.71
0.5	0.7	2.5	0.419744795	95.45	0.86	0.06894893	99.51	46.19	3.193821176	92.91
1	0.5	3.2	0.537273338	95.99	0.84	0.067345466	99.58	25.56	1.76735374	94.68
1.5	0.35	4.2	0.705171256	96.69	0.78	0.062535076	99.64	19.41	1.342110176	96.02
2	0.25	3.9	0.65480188	97.35	0.75	0.060129881	99.70	16.43	1.136057197	97.15
2.5	0.18	3.6	0.604432505	97.95	0.69	0.05531949	99.75	12.84	0.887825588	98.04
3	0.13	3.1	0.520483546	98.47	0.69	0.05531949	99.81	13.27	0.917558065	98.96
3.5	0.09	2.7	0.453324379	98.93	0.7	0.056121222	99.87	3.86	0.266900839	99.23
4	0.06	2.9	0.486903962	99.41	0.78	0.062535076	99.93	6.43	0.444604247	99.67
>4		3.5	0.587642713	100.00	0.9	0.072155857	100.00	4.76	0.329131604	100.00
Tot		595.6	100		1247.3	100		1446.23	100	

MD phi50	-4.1	-4.47	-3.1
phi84	-3.04	-3.66	-0.97
phi16	-4.8	-5.1	-4.3
SD phi	0.88	0.72	1.665

Kaupokonui fall deposit

		Kaupokonui					
		Kp Base			Kp Middle-Top		
phi	mm	Initial wt.g	245.45		Initial wt.g	2101.5	
		wt.g	wt.%	c wt.%	wt.g	wt.%	c wt.%
-5.5	45						
-5	32	9.86	4.093834337	4.09	215.31	10.25056297	10.25
-4.5	23	14.32	5.9456093	10.04	405.68	19.31377263	29.56
-4	16	17.45	7.245173344	17.28	397.52	18.92528815	48.49
-3.5	11	21.3	8.843678638	26.13	321.3	15.29657648	63.79
-3	8	21.5	8.926717874	35.06	213.56	10.16724828	73.95
-2.5	6	24.78	10.28856135	45.34	103.2	4.913186096	78.87
-2	4	23.2	9.632551381	54.98	98.42	4.685617981	83.55
-1.5	3	20.5	8.511521694	63.49	74.13	3.529210129	87.08
-1	2	16.33	6.780153623	70.27	61.3	2.918394455	90.00
-0.5	1.4	13.68	5.679883745	75.95	40.29	1.91814213	91.92
0	1.0	9.84	4.085530413	80.03	42.13	2.005741572	93.92
0.5	0.7	9.07	3.765829354	83.80	40.1	1.909096536	95.83
1	0.5	7.65	3.176250778	86.98	31.26	1.488238347	97.32
1.5	0.35	6.18	2.565912394	89.54	15.46	0.736025747	98.06
2	0.25	5.21	2.163172099	91.70	14.78	0.70365204	98.76
2.5	0.18	4.56	1.893294582	93.60	5.8	0.276128676	99.04
3	0.13	4.12	1.710608262	95.31	5.16	0.245659305	99.28
3.5	0.09	4.35	1.806103384	97.11	5.78	0.275176508	99.56
4	0.06	3.25	1.349387586	98.46	4.98	0.237089794	99.79
>4		3.7	1.536225867	100.00	4.31	0.205192171	100.00
Tot		240.85	100		2100.47	100	

MD phi50	-2.25	-3.92
phi84	0.5	-1.92
phi16	-4.1	-4.87
SD phi	2.3	1.475

Manganui-D fall deposits

phi	mm	M11			M12			M13			M14			M15		
		Initial wt.g 463.8			Initial wt.g 569.5			Initial wt.g 519.45			Initial wt.g 558.6			Initial wt.g 525.96		
		wt.g	wt.%	c wt.%	wt.g	wt.%	c wt.%	wt.g	wt.%	c wt.%	wt.g	wt.%	c wt.%	wt.g	wt.%	c wt.%
-5.5	45															
-5	32	0	0	0.00	0	0	0.00	0	0	0.00	0	0	0.00	0	0	0.00
-4.5	23	0	0	0.00	0	0	0.00	17.51	3.3758121	3.38	0	0	0.00	0	0	0.00
-4	16	6.11	1.3191985	1.32	46.93	8.2595611	8.26	25.76	4.9663576	8.34	0	0	0.00	0	0	0.00
-3.5	11	32.03	6.9155367	8.23	115.56	20.338267	28.60	31.77	6.1250458	14.47	9.13	1.6385499	1.64	33.52	6.383546	6.38
-3	8	42.36	9.1458675	17.38	87.26	15.357539	43.96	31.26	6.0267212	20.49	17.03	3.0563532	4.69	82.41	15.694153	22.08
-2.5	6	38.91	8.4009845	25.78	84.26	14.829546	58.78	28.23	5.4425572	25.94	32.96	5.9152907	10.61	102.63	19.544849	41.62
-2	4	52.91	11.423698	37.21	68.64	12.080466	70.87	43.93	8.4694133	34.41	50.17	9.0039483	19.61	90.85	17.301466	58.92
-1.5	3	49.87	10.767337	47.97	52.27	9.1993875	80.06	52.43	10.108157	44.51	57.8	10.373295	29.99	67.06	12.770901	71.69
-1	2	53.78	11.611538	59.58	38.96	6.8568613	86.92	65.72	12.670381	57.18	70.44	12.64178	42.63	59.79	11.386403	83.08
-0.5	1.4	59.41	12.827101	72.41	30.04	5.2869639	92.21	86.94	16.761457	73.95	90.69	16.276023	58.91	42.18	8.0327557	91.11
0	1.0	50.24	10.847223	83.26	18.37	3.230734	95.44	66.11	12.745571	86.69	81.1	14.554917	73.46	20.18	3.8430775	94.96
0.5	0.7	31.01	6.6953105	89.95	11.67	2.0538904	97.50	39.64	7.6423297	94.33	62.71	11.254487	84.71	10.86	2.0681775	97.03
1	0.5	21.89	4.7262285	94.68	5.13	0.902867	98.40	18.94	3.6515067	97.99	38.55	6.9185212	91.63	5.89	1.3216911	98.15
1.5	0.35	8.26	1.783401	96.46	1.97	0.346715	98.75	4.72	0.9099848	98.90	17.77	3.1891601	94.82	2.91	0.5541802	98.70
2	0.25	3.85	0.8312462	97.29	1.21	0.2129569	98.96	1.67	0.321965	99.22	9.53	1.7103374	96.53	1.92	0.3656446	99.07
2.5	0.18	2.51	0.5419294	97.84	0.9	0.1583977	99.12	0.9	0.173514	99.39	6.32	1.1342426	97.67	1.48	0.2818511	99.35
3	0.13	2.2	0.4749978	98.31	1.2	0.211197	99.33	0.76	0.146523	99.54	4.44	0.7968413	98.46	1.15	0.2190059	99.57
3.5	0.09	2.27	0.4901114	98.80	1.07	0.1883173	99.52	0.79	0.1523068	99.69	3.6	0.6460876	99.11	0.71	0.1352123	99.70
4	0.06	2.08	0.4490889	99.25	1.02	0.1795174	99.70	0.57	0.1098922	99.80	2.58	0.4630294	99.57	0.82	0.1561607	99.86
~4		3.47	0.7492011	100.00	1.73	0.3044756	100.00	1.04	0.2005051	100.00	2.38	0.4271357	100.00	0.74	0.1409255	100.00
Tot		463.16	100		568.19	100		518.69	100		557.2	100		525.1	100	

MD phi50	-1.4	-2.8	-1.28	-0.75	-2.25
phi84	-0.07	-1.39	-0.2	0.37	-1.05
phi16	-3.1	-3.8	-3.4	-2.2	-3.2
SD phi	1.515	1.205	1.6	1.285	1.075

Manganui-D																
M16			M17			M18			M19			M20			M21-22	
Initial wt.g 409.7			Initial wt.g 507.08			Initial wt.g 441			Initial wt.g 626.3			Initial wt.g 1620.8			Initial wt.g 623.94	
wt.g	wt.%	c wt.%	wt.g	wt.%	c wt.%	wt.g	wt.%	c wt.%	wt.g	wt.%	c wt.%	wt.g	wt.%	c wt.%	wt.g	wt.%
0	0	0.00	0	0	0.00	0	0	0.00	0	0	0.00	0	0	0.00	0	0
0	0	0.00	0	0	0.00	0	0	0.00	0	0	0.00	0	0	0.00	34.46	5.5297025
53.75	13.143095	13.14	0	0	0.00	22.83	5.1859255	5.19	0	0	0.00	0	0	0.00	170.66	27.385346
91.04	22.261346	35.40	15.35	3.0291071	3.03	34.58	7.8549849	13.04	103.5	16.546763	16.55	193.5	11.940022	11.94	148.83	23.882345
84.53	20.669503	56.07	26.3	5.1899359	8.22	56.5	12.8342	25.88	109.3	17.474021	34.02	241.4	14.895718	26.84	90.37	14.501428
66.06	16.153169	72.23	29.99	5.9181056	14.14	72.45	16.457306	42.33	84.7	13.541167	47.56	269.1	16.604961	43.44	43.37	6.959466
46.27	11.314065	83.54	61.57	12.149975	26.29	65.82	14.951275	57.28	102	16.306954	63.87	223.1	13.766506	57.21	34.25	5.4960044
29.22	7.1449531	90.69	89.42	17.645782	43.93	54.26	12.325375	69.61	67.1	10.727418	74.60	200.4	12.36579	69.57	25.91	4.1577072
16.83	4.1153169	94.80	97.52	19.244203	63.18	39.09	8.8794494	78.49	45.8	7.3221423	81.92	141.8	8.7498457	78.32	21.23	3.4067204
10.72	2.6212833	97.42	94.07	18.563394	81.74	33.07	7.5119824	86.00	39.9	6.3788969	88.30	109.9	6.781439	85.10	14.79	2.3733111
4.46	1.0905712	98.51	54.43	10.740997	92.48	20.74	4.7111737	90.71	23.8	3.804956	92.10	59.1	3.6467975	88.75	8.34	1.3382971
2.21	0.5403951	99.05	25.74	5.0794277	97.56	14.23	3.2324012	93.94	13	2.0783373	94.18	38	2.3448106	91.10	5.41	0.868128
1.46	0.3570031	99.41	9.13	1.8016774	99.36	8.84	2.0080413	95.95	8.6	1.3749001	95.56	26.5	1.6351968	92.73	3.59	0.5760775
0.65	0.1589397	99.57	1.74	0.3433646	99.71	5.28	1.1993731	97.15	6.2	0.991207	96.55	21.7	1.3390102	94.07	2.83	0.4541224
0.46	0.1124804	99.68	0.6	0.1184016	99.82	4.06	0.9222452	98.07	6.8	1.0871303	97.63	29.7	1.8326546	95.90	5.11	0.8199878
0.38	0.0929186	99.78	0.35	0.0690676	99.89	2.98	0.6769189	98.75	6.2	0.991207	98.63	30	1.8511662	97.75	6.55	1.0510607
0.29	0.0709116	99.85	0.18	0.0355205	99.93	2.05	0.4656657	99.22	3.6	0.5755396	99.20	17.4	1.0736764	98.83	3.47	0.5568215
0.24	0.0586854	99.90	0.16	0.0315738	99.96	1.46	0.3316448	99.55	2.3	0.3677058	99.57	8.7	0.5368382	99.36	1.59	0.255143
0.19	0.0464593	99.95	0.09	0.0177602	99.98	0.95	0.2157963	99.76	1.6	0.2557954	99.82	5.3	0.3270394	99.69	1.03	0.1652813
0.2	0.0489045	100.00	0.11	0.021707	100.00	1.04	0.2362401	100.00	1.1	0.1758593	100.00	5	0.3085277	100.00	1.39	0.2230495
408.96	100		506.75	100		440.23	100		625.5	100		1620.6	100		623.18	100
-3.15			-1.33			-2.25			-2.4			-2.25			-3.65	
-2.1			-0.5			-0.9			-0.98			-0.71			-2.31	
-3.9			-2.4			-3.38			-3.5			-3.35			-4.3	
0.9			0.95			1.24			1.26			1.32			0.995	

M23-24			
c wt.%	Initial wt.g 828.26		c wt.%
	wt.g	wt.%	
0.00	0	0	0.00
5.53	0	0	0.00
32.92	65.82	7.9560015	7.96
56.80	220.58	26.662637	34.62
71.30	184.54	22.306298	56.92
78.26	116.51	14.083162	71.01
83.75	81.58	9.8609936	80.87
87.91	59.73	7.2198719	88.09
91.32	37.46	4.5279826	92.62
93.69	23.23	2.8079294	95.42
95.03	14.51	1.7538982	97.18
95.90	9.62	1.1628188	98.34
96.47	5.38	0.6503082	98.99
96.93	2.38	0.2876828	99.28
97.75	1.65	0.199444	99.48
98.80	1.27	0.1535114	99.63
99.36	1.19	0.1438414	99.78
99.61	0.76	0.0918651	99.87
99.78	0.49	0.0592288	99.93
100.00	0.6	0.0725251	100.00
	827.3	100	

-3.19

-1.9

-3.92

1.01

Upper Inglewood fall and PDC deposits

phi	mm	Uig 7 (ES)			Uig 7 (Mak Hut)			Uig 6 top (B1-Mak Hut)			Uig 6 bs (B2-Mak Hut)	
		Initial wt.g	1917.3	c wt.%	Initial wt.g	1435.5	c wt.%	Initial wt.g	1198.72	c wt.%	Initial wt.g	1609.69
-5.5	45	0.00		0.00								
-5	32	997.01	52.06	52.06	0.00	0.00	0.00	0.00	0.00	0.00	0.00	0.00
-4.5	23	532.97	27.83	79.88	231.51	16.13	16.13	0.00	0.00	0.00	78.70	4.91
-4	16	99.70	5.21	85.09	260.60	18.16	34.29	0.00	0.00	0.00	17.23	1.07
-3.5	11	55.29	2.89	87.98	230.96	16.09	50.39	1.26	0.11	0.11	4.62	0.29
-3	8	25.75	1.34	89.32	133.85	9.33	59.72	3.21	0.27	0.37	22.71	1.42
-2.5	6	31.75	1.66	90.98	97.76	6.81	66.53	9.26	0.78	1.15	53.07	3.31
-2	4	26.53	1.39	92.36	66.64	4.64	71.17	18.53	1.55	2.70	67.62	4.22
-1.5	3	21.78	1.14	93.50	49.28	3.43	74.61	20.08	1.68	4.38	78.03	4.87
-1	2	15.89	0.83	94.33	40.52	2.82	77.43	31.09	2.60	6.98	87.66	5.47
-0.5	1.4	14.53	0.76	95.09	36.75	2.56	79.99	51.33	4.30	11.28	118.83	7.41
0	1.0	13.36	0.70	95.79	33.51	2.34	82.33	41.74	3.49	14.77	116.27	7.25
0.5	0.7	15.54	0.81	96.60	33.60	2.34	84.67	48.22	4.04	18.81	113.16	7.06
1	0.5	14.66	0.77	97.36	31.93	2.23	86.89	84.89	7.11	25.92	149.40	9.32
1.5	0.35	12.92	0.67	98.04	35.31	2.46	89.35	119.43	10.00	35.91	153.97	9.61
2	0.25	10.76	0.56	98.60	34.19	2.38	91.74	189.39	15.85	51.77	160.78	10.03
2.5	0.18	8.57	0.45	99.05	34.80	2.43	94.16	228.40	19.12	70.89	149.12	9.30
3	0.13	6.69	0.35	99.40	30.53	2.13	96.29	108.42	9.08	79.96	98.82	6.17
3.5	0.09	4.68	0.24	99.64	21.99	1.53	97.82	96.87	8.11	88.07	62.93	3.93
4	0.06	3.93	0.21	99.85	16.77	1.17	98.99	64.44	5.39	93.46	33.11	2.07
>4		2.94	0.15	100.00	14.50	1.01	100.00	78.07	6.54	100.00	36.82	2.30
Tot		1915.25	100		1435	100		1194.63	100.00		1602.85	100.00

MD phi50	-5	-3.5	1.95	0.68
phi84	-4.2	0.5	3.25	2.41
phi16	-5.4	-4.5	0.18	-1.92
SD phi	0.6	2.5	1.535	2.165

Upper Inglewood

c wt.%	Uig 5a (C1, Mak Hut)			Uig 5b (C2, Mak Hut)			Uig 4 (D-Mak Hut)			Uig 3 (E, Mak Hut)		
	Initial wt.g	1592.1		Initial wt.g	1552.47		Initial wt.g	1577.1		Initial wt.g	518.1	
	wt.g	wt.%	c wt.%	wt.g	wt.%	c wt.%	wt.g	wt.%	c wt.%	wt.g	wt.%	c wt.%
0.00	61.51	3.87	3.87	0.00	0.00	0.00	0.00	0.00	0.00	65.83	12.72	12.72
4.91	26.73	1.68	5.55	118.60	7.64	7.64	0.00	0.00	0.00	50.23	9.70	22.42
5.98	25.76	1.62	7.16	25.07	1.62	9.26	13.53	0.86	0.86	36.50	7.05	29.47
6.27	34.12	2.14	9.31	65.19	4.20	13.46	10.91	0.69	1.55	18.37	3.55	33.02
7.69	41.90	2.63	11.94	77.55	5.00	18.46	66.32	4.21	5.76	3.12	0.60	33.62
11.00	81.27	5.11	17.05	100.54	6.48	24.94	72.65	4.61	10.37	6.14	1.19	34.81
15.22	79.81	5.02	22.07	106.06	6.84	31.77	96.97	6.15	16.53	3.67	0.71	35.52
20.09	86.82	5.46	27.52	107.02	6.90	38.67	103.96	6.60	23.13	3.78	0.73	36.25
25.56	123.54	7.76	35.29	99.40	6.41	45.08	112.45	7.14	30.26	5.80	1.12	37.37
32.97	122.49	7.70	42.99	111.88	7.21	52.29	127.17	8.07	38.33	9.84	1.90	39.27
40.22	115.35	7.25	50.24	104.80	6.75	59.04	126.94	8.06	46.39	11.47	2.22	41.48
47.28	142.48	8.95	59.19	104.92	6.76	65.80	134.95	8.57	54.96	16.01	3.09	44.58
56.61	148.92	9.36	68.55	120.75	7.78	73.58	159.88	10.15	65.11	20.09	3.88	48.46
66.21	139.41	8.76	77.31	109.96	7.09	80.67	153.90	9.77	74.87	24.35	4.70	53.16
76.24	118.06	7.42	84.73	108.66	7.00	87.67	142.02	9.01	83.89	28.57	5.52	58.68
85.55	98.40	6.18	90.92	83.14	5.36	93.03	121.11	7.69	91.57	36.50	7.05	65.73
91.71	62.88	3.95	94.87	54.32	3.50	96.53	65.58	4.16	95.74	47.34	9.14	74.88
95.64	40.83	2.57	97.44	30.44	1.96	98.49	35.98	2.28	98.02	58.22	11.25	86.12
97.70	24.63	1.55	98.98	14.72	0.95	99.44	17.23	1.09	99.11	40.29	7.78	93.91
100.00	16.16	1.02	100.00	8.67	0.56	100.00	13.95	0.89	100.00	31.55	6.09	100.00
	1591.07	100		1551.69	100.00		1575.5	100.00		517.67	100	

0	-0.66	-0.24	1.25
1.96	1.76	2	3.4
-2.6	-3.25	-2.02	-4.8
2.28	2.505	2.01	4.1

Uig 2 (F-Mak Hut)			Uig 1 (H-Lil Mak)		
Initial wt.g	1542.64		Initial wt.g	5428.2	
wt.g	wt.%	c wt.%	wt.g	wt.%	c wt.%
0	0.00	0.00	795.12	14.67	14.67
57.09	3.70	3.70	513.66	9.47	24.14
23.78	1.54	5.25	342.9	6.32	30.46
20.12	1.31	6.55	150.33	2.77	33.24
33.45	2.17	8.72	76.5	1.41	34.65
37.84	2.46	11.18	62.61	1.15	35.80
42	2.73	13.90	107.04	1.97	37.78
54.67	3.55	17.45	120.42	2.22	40.00
79.71	5.17	22.62	271.35	5.00	45.00
111.5	7.23	29.86	261.31	4.82	49.82
159.04	10.32	40.18	336.36	6.20	56.03
163.41	10.60	50.78	300.15	5.54	61.56
170.43	11.06	61.84	347.22	6.40	67.97
142.91	9.27	71.11	480.96	8.87	76.84
119.26	7.74	78.85	424.8	7.84	84.67
100	6.49	85.34	261.63	4.83	89.50
69.98	4.54	89.88	120.5	2.22	91.72
53.1	3.45	93.32	172.65	3.18	94.91
45.46	2.95	96.27	154.17	2.84	97.75
57.47	3.73	100.00	121.98	2.25	100.00
1541.22	100.00		5421.66	100.00	

0.48	-0.45
2.4	1.95
-1.7	-4.94
2.05	3.445

Kokowai fall and PDC deposits

		Kokowai 7											
		Kw5			Kw6			Kw7 Top			Kw7 Middle		
phi	mm	Initial wt.g	2308.12		Initial wt.g	2131.14		Initial wt.g	1278.27		Initial wt.g	1643	
		wt.g	wt.%	c wt.%	wt.g	wt.%	c wt.%	wt.g	wt.%	c wt.%	wt.g	wt.%	
-5.5	45												
-5	32	0	0	0.00	17.36	0.965307859	0.97	0	0	0.00	24.3	1.482647533	
-4.5	23	31.92	1.385218263	1.39	63.1	3.508693887	4.47	27.82	2.176481173	2.18	152.47	9.302850588	
-4	16	50.42	2.188054662	3.57	125.11	6.956778007	11.43	62.71	4.906079596	7.08	219.84	13.4133841	
-3.5	11	93.46	4.055842696	7.63	184.15	10.23971441	21.67	144.57	11.31034806	18.39	229.14	13.9808171	
-3	8	151.3	6.565899849	14.20	162.09	9.013061683	30.68	155.83	12.19126748	30.58	221.94	13.54151413	
-2.5	6	231.8	10.0593231	24.25	154.11	8.569331458	39.25	135.17	10.57494465	41.16	176.08	10.74339825	
-2	4	154.97	6.725165232	30.98	91.77	5.102897592	44.36	140.58	10.99819279	52.16	136.74	8.343095622	
-1.5	3	99.27	4.307976722	35.29	122.2	6.794966609	51.15	114.34	8.945321974	61.10	107.83	6.579172158	
-1	2	78.25	3.395780986	38.68	65.38	3.635473952	54.79	91.21	7.135760165	68.24	72.35	4.414384732	
-0.5	1.4	73.37	3.184005763	41.87	47.14	2.621233437	57.41	88.23	6.902621635	75.14	54.55	3.328330161	
0	1.0	45.23	1.962826505	43.83	30.99	1.72320798	59.13	80.98	6.335422192	81.48	43.91	2.67913799	
0.5	0.7	38.39	1.66599402	45.50	66.78	3.71332136	62.84	64.93	5.079759977	86.56	24.97	1.523527115	
1	0.5	50.24	2.180243281	47.68	87.06	4.840996669	67.68	68.4	5.351233365	91.91	31.58	1.926831649	
1.5	0.35	75.24	3.265157334	50.94	83.31	4.632476826	72.32	55.67	4.355309378	96.26	13.81	0.842607507	
2	0.25	103.94	4.510638667	55.45	84.9	4.72088924	77.04	21.03	1.645269557	97.91	10.97	0.66932689	
2.5	0.18	122.71	5.325192138	60.78	95.91	5.333103498	82.37	6.07	0.474882844	98.38	9.03	0.550959145	
3	0.13	216.31	9.387110353	70.16	111.72	6.212223155	88.58	4.15	0.324672785	98.71	8.51	0.519231708	
3.5	0.09	290.08	12.58847474	82.75	91.55	5.090664428	93.67	3.77	0.29494371	99.00	12.37	0.754746913	
4	0.06	300.53	13.04196882	95.79	86.36	4.802072965	98.48	4.48	0.350490139	99.35	35.52	2.167227998	
>4		96.9	4.20512687	100.00	27.4	1.523584984	100.00	8.27	0.646998537	100.00	53.05	3.236808708	
Tot		2304.33	100		1798.39	100		1278.21	100		1638.96	100	

MD phi50	1.38	-1.6	-2.1	-3.09
phi84	3.58	2.65	0.25	-0.65
phi16	-2.9	-3.75	-3.6	-4.3
SD phi	3.24	3.2	1.925	1.825

c wt. %	Kw7 Base			Kw8			Kw1			Kw2		
	Initial wt.g	1851.7		Initial wt.g	2271.1		Initial wt.g	6875.9		Initial wt.g	1720.53	
	wt.g	wt. %	c wt. %	wt.g	wt. %	c wt. %	wt.g	wt. %	c wt. %	wt.g	wt. %	c wt. %
1.48	20.84	1.123450135	1.12	0	0	0.00	1011.60	14.73	14.73	109.1	6.35	6.35
10.79	174	9.380053908	10.50	15.13	0.667622725	0.67	781.92	11.39	26.12	77.84	4.53	10.89
24.20	141.32	7.618328841	18.12	89.22	3.936900165	4.60	494.63	7.20	33.32	63.22	3.68	14.57
38.18	243.94	13.15040431	31.27	219.44	9.682956426	14.29	278.14	4.05	37.37	39.6	2.31	16.87
51.72	260.61	14.0490566	45.32	186.11	8.212244898	22.50	202.20	2.94	40.31	36.92	2.15	19.02
62.46	283.42	15.2787062	60.60	163.26	7.203971318	29.70	137.59	2.00	42.31	29.43	1.71	20.74
70.81	181.62	9.79083558	70.39	158.97	7.014671815	36.72	86.01	1.25	43.57	30.7	1.79	22.53
77.39	132.72	7.154716981	77.55	127.6	5.630446773	42.35	66.89	0.97	44.54	38.7	2.25	24.78
81.80	92.88	5.007008086	82.55	90.2	3.980143409	46.33	71.47	1.04	45.58	41.35	2.41	27.19
85.13	68.33	3.683557951	86.24	97.16	4.287258687	50.62	126.58	1.84	47.42	61.11	3.56	30.75
87.81	43.25	2.331536388	88.57	70.15	3.095421953	53.71	214.46	3.12	50.55	61.63	3.59	34.33
89.33	35.45	1.911051213	90.48	93.99	4.147380033	57.86	244.75	3.56	54.11	96.48	5.62	39.95
91.26	36.11	1.946630728	92.43	166.32	7.338996139	65.20	312.00	4.54	58.65	98.74	5.75	45.70
92.10	21.67	1.16819407	93.59	151.73	6.695201324	71.89	442.15	6.44	65.09	121.8	7.09	52.80
92.77	15.9	0.857142857	94.45	121.11	5.344070601	77.24	502.39	7.32	72.41	114.32	6.66	59.45
93.32	14.03	0.756334232	95.21	109.98	4.85295091	82.09	523.47	7.62	80.03	124.26	7.24	66.69
93.84	10.6	0.571428571	95.78	101.5	4.478764479	86.57	393.96	5.74	85.77	147.39	8.58	75.27
94.60	11.98	0.645822102	96.42	120.08	5.29862107	91.87	365.50	5.32	91.09	164.02	9.55	84.82
96.76	16.98	0.915363881	97.34	95	4.191947049	96.06	340.37	4.96	96.04	131.73	7.67	92.50
100.00	49.35	2.660377358	100.00	89.3	3.940430226	100.00	271.68	3.96	100.00	128.86	7.50	100.00
	1855	100		2266.25	100		6867.75	100.00		1717.2	100.00	

-2.85		-0.6		-0.1		1.4
-0.82		2.7		2.85		3.45
-4.1		-3.4		-4.93		-3.7
1.64		3.05		3.89		3.575

Kokomi 4											
Kw3			Kw4 Top			Kw4 Middle			Kw4 Base		
Initial wt.g	1314.2		Initial wt.g	3346.1		Initial wt.g	4538.68		Initial wt.g	2073.8	
wt.g	wt. %	c wt. %	wt.g	wt. %	c wt. %	wt.g	wt. %	c wt. %	wt.g	wt. %	c wt. %
38.26	2.92	2.92	0	0	0.00	91.75	2.02261805	2.02	124.81	6.033520093	6.03
57.65	4.39	7.31	88.92	2.675855013	2.68	467.28	10.30113311	12.32	246.62	11.92201527	17.96
54.3	4.14	11.45	129.42	3.894614887	6.57	652.3	14.37987743	26.70	248.35	12.0056463	29.96
60.08	4.58	16.03	483.46	14.54868269	21.12	792.8	17.47718355	44.18	332.35	16.06634407	46.03
82.34	6.28	22.31	604.3	18.18510104	39.30	673.2	14.84061549	59.02	347.66	16.80645458	62.83
88.31	6.73	29.04	641.8	19.3135824	58.62	459.67	10.13337154	69.15	263.31	12.72883724	75.56
90.66	6.91	35.95	418.97	12.60799567	71.23	334.91	7.383051894	76.54	165.46	7.998607761	83.56
60.26	4.59	40.54	234.27	7.049848783	78.28	218.18	4.809752656	81.35	88.77	4.291287386	87.85
41.15	3.14	43.68	173.87	5.232241465	83.51	137.86	3.039107623	84.39	52.03	2.515215531	90.37
49.22	3.75	47.43	133.37	4.013481591	87.52	104.47	2.303028967	86.69	41.79	2.020197137	92.39
54.03	4.12	51.55	95.23	2.86574081	90.39	62.26	1.372514439	88.06	35.56	1.71902872	94.11
67.16	5.12	56.67	78.39	2.358977445	92.75	37.43	0.825139985	88.89	28.66	1.385471404	95.49
70.69	5.39	62.06	70.24	2.113720829	94.86	68.24	1.504342842	90.39	23.84	1.152464699	96.65
88.46	6.74	68.80	55.24	1.662328283	96.52	71.25	1.570697941	91.96	15.32	0.740593925	97.39
99.99	7.62	76.42	33.94	1.021350867	97.54	64.67	1.425642608	93.39	9.9	0.478582236	97.86
66.21	5.05	81.47	22.71	0.683408315	98.23	65.34	1.44041268	94.83	7.67	0.370780379	98.24
69.72	5.31	86.79	16.31	0.490814162	98.72	62.34	1.37427803	96.20	7.23	0.349510057	98.58
61.47	4.69	91.47	12.08	0.363521464	99.08	82.47	1.818041533	98.02	7.12	0.344192477	98.93
61.17	4.66	96.13	15.53	0.467341749	99.55	41.75	0.920373881	98.94	11.08	0.535625372	99.46
50.71	3.87	100.00	15	0.451392546	100.00	48.03	1.058815749	100.00	11.08	0.535625372	100.00
1311.84	100.00		3323.05	100		4536.2	100		2068.61	100	

-0.19		-2.7		-3.3		-3.4
2.75		-0.92		-1.1		-1.97
-3.5		-3.65		-4.39		-4.6
3.125		1.365		1.645		1.315

Appendix 4.1 Deposit thickness and average pumice and lithic clasts diameters measured at different sections located on the eastern flanks of Mt. Taranaki

Kaupokonui bed-set

Id	Section's author	Section	Th cm	UTM coordinates		P cm	L cm
				x	y		
1	Torres-Orozco et al	H	15	1695054	5648216	3.60	2.50
2	Torres-Orozco et al	F	15	1694126	5648670	4.50	3.40
3	Torres-Orozco et al	DFrd2	20	1695390	5646375	3.40	2.30
4	Torres-Orozco et al	MThouse	14	1696428	5648665	1.90	1.60
5	Torres-Orozco et al	DFvc2	33	1694558	5645376	2.90	1.60
6	Torres-Orozco et al	LowKaupo	30	1695676	5644152	2.50	1.70
7	Torres-Orozco et al	Radnord1	6	1702687	5648059	0.20	0.20
8	Torres-Orozco et al	Radnord2	4	1703502	5648455	0.20	0.20
9	Torres-Orozco et al	Pembroke2	10	1704691	5646546	0.20	0.20
10	Torres-Orozco et al	Pembroke4	9	1698999	5647954	0.70	0.50
11	Torres-Orozco et al	Pembroke3	12	1701046	5647140	0.50	0.30
12	Torres-Orozco et al	Palmernd1	12	1700164	5643623	1.00	0.50
13	Torres-Orozco et al	Mangawrd	10	1692722	5639506	0.60	0.30
14	Torres-Orozco et al	4	10	1700761	5640679	0.40	0.30
15	Torres-Orozco et al	5	12	1700885	5642305	0.60	0.40
16	Torres-Orozco et al	Kp1	10	1692692	5638691	0.50	0.30
17	Torres-Orozco et al	Kp2	6	1698913	5640250	0.50	0.30
18	Torres-Orozco et al	Kp3	11	1700677	5642642	0.60	0.50
19	Torres-Orozco et al	Kp4	20	1702369	5644613	0.50	0.30
20	Torres-Orozco et al	Kp5	12	1701566	5645353	0.60	0.40
21	Torres-Orozco et al	Kp6	17	1701154	5646062	0.70	0.50
22	Torres-Orozco et al	Kp7	10	1703563	5644516	0.50	0.30
23	Torres-Orozco et al	Kp8	5	1702315	5646703	0.60	0.40
24	Torres-Orozco et al	Kp9	6	1703016	5646676	0.50	0.40
25	Torres-Orozco et al	Kp10	12	1703610	5646190	0.30	0.10
26	Torres-Orozco et al	Kp11	2	1702719	5648589	0.20	0.20
27	Torres-Orozco et al	Kp12	7	1701910	5648589	0.20	0.20
28	Torres-Orozco et al	Kp13	16	1695160	5640626	0.70	0.50
29	Torres-Orozco et al	Kp14	17	1695700	5640617	0.60	0.40
30	Torres-Orozco et al	Kp15	14	1694663	5640601	0.70	0.50
31	Torres-Orozco et al	Kp16	17	1696402	5641114	0.70	0.50
32	Torres-Orozco et al	Kp17	11	1696367	5643166	1.10	1.00
33	Torres-Orozco et al	Kp18	19	1696751	5643065	1.00	0.90
34	Torres-Orozco et al	Kp19	14	1698562	5642642	1.10	0.90
35	Torres-Orozco et al	Kp20	16	1698292	5642491	1.10	0.90
36	Torres-Orozco et al	Kp21	15	1698373	5642194	0.60	0.40
37	Torres-Orozco et al	Kp22	13	1698022	5642302	0.90	0.70
38	Torres-Orozco et al	Kp23	22	1697633	5642032	0.90	0.60
39	Torres-Orozco et al	Kp24	18	1697536	5641708	0.90	0.60
40	Torres-Orozco et al	Kp25	16	1697966	5646379	1.60	1.00
41	Torres-Orozco et al	Kp26	25	1696355	5648896	2.00	1.10
42	Torres-Orozco et al	Kp27	15	1696999	5649057	1.00	0.40
43	Torres-Orozco et al	Kp28	10	1696069	5648735	2.40	1.40
44	Torres-Orozco et al	Kp29	12	1695637	5648646	2.60	1.60
45	Torres-Orozco et al	Kp30	10	1695533	5648607	2.60	1.60
46	Torres-Orozco et al	Kp31	10	1695193	5648717	2.70	1.90
47	Torres-Orozco et al	Kp32	15	1694635	5648574	3.60	2.60
48	Torres-Orozco et al	Kp33	15	1694600	5648324	4.00	3.10
49	Torres-Orozco et al	Kp34	15	1694366	5648216	4.50	3.30
50	Torres-Orozco et al	Kp35	20	1693691	5648717	4.50	3.50

51	Torres-Orozco et al	Kp36	16	1693333	5648842	4.60	3.50
52	Torres-Orozco et al	Kp37	22	1694996	5646766	3.40	3.00
53	Torres-Orozco et al	Kp38	25	1696766	5644569	2.50	2.00
54	Torres-Orozco et al	Kp39	16	1694442	5643353	1.50	0.90
55	Torres-Orozco et al	Kp40	20	1693673	5642602	1.20	0.70
56	Torres-Orozco et al	Kp41	23	1695157	5645713	3.30	2.50
57	Torres-Orozco et al	Kp42	35	1694102	5645302	2.60	1.80
58	Torres-Orozco et al	Kp43	35	1693602	5645389	2.50	1.60
59	Torres-Orozco et al	Kp44	30	1693226	5645460	1.90	1.20
60	Torres-Orozco et al	Kp45	23	1692666	5645566	1.40	1.00
61	Torres-Orozco et al	Kp46	13	1692028	5645499	1.00	0.70
62	Torres-Orozco et al	Kp47	17	1691992	5646963	1.30	0.80
63	Torres-Orozco et al	Kp48	15	1692153	5647162	1.50	1.00
64	Torres-Orozco et al	Kp49	10	1691137	5645215	0.80	0.50
65	Torres-Orozco et al	Kp50	14	1691116	5644622	0.80	0.50
66	Torres-Orozco et al	Kp51	27	1692994	5647659	4.60	3.70
67	Torres-Orozco et al	Kp52	30	1693405	5647734	4.50	3.20
68	Torres-Orozco et al	Kp53	31	1693602	5647644	4.10	3.00
69	Torres-Orozco et al	Kp54	29	1693796	5647394	3.80	3.00
70	Torres-Orozco et al	Kp55	34	1694263	5647267	3.90	3.10
71	Torres-Orozco et al	Kp56	25	1694496	5647017	3.60	2.50
72	Torres-Orozco et al	Kp57	15	1694764	5646622	3.50	2.30
73	Torres-Orozco et al	A	32	1693677	5646093	2.60	1.60
74	Torres-Orozco et al	U	5	1693375	5651640	0.50	0.30
75	Torres-Orozco et al	W	4	1692493	5653010	0.50	0.30
76	Torres-Orozco et al	X2	3	1691773	5652670	0.50	0.30
77	Torres-Orozco et al	X1	4	1692029	5652917	0.50	0.30

Manganui-D bed-set (MD1-MD3)

Id	Section's author	Section	Th cm	UTM coordinates		MD1 (vj) cm	MD2 (vj) cm	MD3 (vj) cm
				x	y			
1	Alloway et al. 1995	4	23.2	1700781	5640579	0.60	0.63	0.94
2	Alloway et al. 1995	17	9.3	1711555	5664166	0.50	0.60	0.80
3	Alloway et al. 1995	23-25	2.0	1717839	5663007	0.00	0.00	0.00
4	Damaschke et al. 2017	LRI	3.0	1707184	5668927	0.30	0.30	0.30
5	Damaschke et al. 2017	TS1	7.0	1712191	5658610	0.30	0.30	0.30
6	Damaschke et al. 2017	TS2	7.0	1713206	5658974	0.30	0.30	0.30
7	Damaschke et al. 2017	NS1	6.0	1715630	5637964	0.40	0.40	0.40
8	Damaschke et al. 2017	NS2	6.0	1716103	5638697	0.40	0.40	0.40
9	Damaschke et al. 2017	ES1	6.0	1714635	5634444	0.30	0.30	0.30
10	Damaschke et al. 2017	ES2	6.0	1713471	5632211	0.30	0.30	0.30
11	Franks 1964	2	19.6	1704256	5660976	0.91	0.95	1.10
12	May 2003	5	13.5	1700631	5642062	0.60	0.60	1.10
13	McGlone et al. 1966	Borehole	25.0	1690924	5654961	-	-	-
14	McGlone et al. 1966	Borehole	25.0	1698839	5647500	-	-	-
15	Torres-Orozco et al	R	41.1	1693692	5651940	3.10	3.30	4.50
16	Torres-Orozco et al	S	42.6	1694358	5652419	3.30	4.20	4.10
17	Torres-Orozco et al	T	25.3	1694514	5653261	2.09	2.00	2.00
18	Torres-Orozco et al	X1	25.0	1691766	5652672	1.60	1.35	1.35
19	Torres-Orozco et al	X2	25.0	1691367	5652937	1.20	1.38	1.30
20	Torres-Orozco et al	Y	20.0	1690952	5652652	1.20	1.35	1.30
21	Torres-Orozco et al	B	41.1	1692564	5645603	2.60	4.60	2.10
22	Torres-Orozco et al	A	26.4	1693646	5646069	3.10	4.10	1.95
23	Torres-Orozco et al	C	129.5	1693657	5647246	6.20	6.60	4.00
24	Torres-Orozco et al	D	56.6	1694163	5647731	6.05	6.21	4.00
25	Torres-Orozco et al	G	72.6	1694576	5646147	5.95	5.40	3.90
26	Torres-Orozco et al	H	65.2	1695054	5646216	3.50	3.12	4.00
27	Torres-Orozco et al	L_UPBrd	34.7	1695464	5646699	2.60	3.50	5.10
28	Torres-Orozco et al	F	101.5	1694126	5646670	4.90	4.95	6.10
29	Torres-Orozco et al	J	61.6	1695117	5650296	3.10	3.50	5.67

30	Torres-Orozco et al	N	41.0	1694630	5651331	2.90	3.10	3.95
31	Torres-Orozco et al	W	24.9	1692442	5653002	1.62	1.35	1.50
32	Torres-Orozco et al	M	44.2	1695136	5651214	2.95	3.00	4.20
33	Torres-Orozco et al	DFrd1	33.7	1696311	5642852	0.99	0.91	1.50
34	Torres-Orozco et al	DFrd2	62.0	1695390	5646375	3.00	2.61	2.00
35	Torres-Orozco et al	MThouse	35.2	1696426	5648665	2.20	3.46	3.10
36	Torres-Orozco et al	MTrd2	20.1	1695304	5654649	1.85	2.10	2.00
37	Torres-Orozco et al	Korlford1	7.3	1695017	5664075	0.97	0.94	0.98
38	Torres-Orozco et al	WP1	40.0	1694472	5647235	3.10	3.20	4.10
39	Torres-Orozco et al	DFvc2	54.0	1694559	5645376	2.95	2.16	2.30
40	Torres-Orozco et al	LowKaupp	24.6	1695676	5644152	1.85	1.20	1.50
41	Torres-Orozco et al	Pouakal1	24.3	1686696	5655036	1.30	1.21	1.30
42	Torres-Orozco et al	Pouakal2	22.7	1692455	5657593	1.19	1.21	1.21
43	Torres-Orozco et al	Pouakal3	23.9	1689455	5656100	1.19	1.15	1.20
44	Torres-Orozco et al	S2	41.5	1693930	5652357	3.00	4.30	4.10
45	Torres-Orozco et al	V	39.6	1693006	5651792	4.00	4.10	3.90
46	Torres-Orozco et al	J2	31.5	1697107	5649655	3.00	2.75	5.10
47	Torres-Orozco et al	F2	60.1	1695073	5649016	2.80	3.50	5.10
48	Torres-Orozco et al	W2	25.2	1692074	5652926	1.60	1.35	1.51
49	Torres-Orozco et al	W3	25.3	1692665	5653417	1.60	1.36	1.40
50	Torres-Orozco et al	W4	25.5	1692296	5653343	1.59	1.36	1.50
51	Torres-Orozco et al	V2	40.6	1693136	5652153	3.00	4.21	4.20
52	Torres-Orozco et al	Mauderd	11.1	1695342	5662276	0.90	0.92	1.20
53	Torres-Orozco et al	Korlford2	9.6	1693373	5662010	0.98	0.95	1.10
54	Torres-Orozco et al	Maude-Kent	14.2	1694597	5661035	0.97	0.95	1.10
55	Torres-Orozco et al	N2	36.7	1695604	5651639	3.00	3.00	3.70
56	Torres-Orozco et al	M2	27.7	1696607	5651467	3.00	2.64	3.90
57	Torres-Orozco et al	M3	26.4	1696242	5652127	2.19	2.60	3.50
58	Turner 2006	LU	0.2	1698317	5673076	0.20	0.20	0.20
59	Turner 2006	LRotok	1.5	1721299	5632014	0.00	0.00	0.00
60	Whitehead 1976	Hill rd	7.1	1696432	5661645	0.94	0.98	1.20
61	Whitehead 1976	Egmitrd1	26.0	1697091	5656727	1.50	2.30	1.50
62	Whitehead 1976	Egmitrd2	33.0	1696242	5659473	1.50	2.00	1.50
63	Whitehead 1976	Egmitrd3	19.4	1696466	5660026	1.30	2.00	1.50
64	Whitehead 1976	Bedfordrd	19.6	1700572	5662709	0.69	1.35	1.20
65	Whitehead 1976	Egmitrd4	20.1	1696986	5664259	0.91	1.10	0.98
66	Whitehead 1976	Egmitrd5	16.6	1696909	5664654	0.67	1.10	1.00
67	Whitehead 1976	Egmitrd6	12.7	1696932	5665266	0.90	1.15	0.97
68	Whitehead 1976	Egmitrd7	13.1	1699011	5665969	0.60	0.95	0.97
69	Whitehead 1976	Uplandrd1	20.2	1699690	5664903	0.67	1.00	1.00
70	Whitehead 1976	Uplandrd2	9.9	1700176	5666216	0.69	0.95	0.98
71	Whitehead 1976	Lepperrd	6.9	1702303	5665899	0.79	0.95	0.96
72	Whitehead 1976	Manga_st	6.1	1701659	5666350	0.61	0.96	0.96
73	Whitehead 1976	SH3_1	6.5	1705563	5661996	0.90	0.95	0.98
74	Whitehead 1976	SH3_2	6.1	1705966	5660311	0.91	0.96	0.94
75	Whitehead 1976	Norfolk1	7.6	1705036	5660141	0.90	0.95	0.94
76	Whitehead 1976	Maket_st	6.9	1705233	5660277	0.90	0.95	0.94
77	Whitehead 1976	Norfkrd1	6.4	1706070	5659960	0.67	0.97	0.97
78	Whitehead 1976	Norfkrd2	7.1	1705655	5659700	0.65	0.94	0.97
79	Whitehead 1976	Rugbyrd	5.4	1706096	5656546	0.60	0.92	0.96
80	Whitehead 1976	Johnsrd	6.0	1706265	5656164	0.64	0.97	0.94
81	Whitehead 1976	Norfkrd3	9.3	1704101	5657709	0.95	1.30	1.30
82	Whitehead 1976	Norfkrd4	12.1	1703502	5657462	0.92	1.30	1.30
83	Whitehead 1976	Durhamrd1	12.6	1703253	5656659	0.94	1.35	1.35
84	Whitehead 1976	Bedfdrd1	15.2	1703909	5655661	0.60	1.20	1.36
85	Whitehead 1976	Bedfdrd2	11.9	1704215	5655606	0.64	1.26	1.35
86	Whitehead 1976	Bedfdrd3	13.6	1704396	5655469	0.62	1.25	1.30
87	Whitehead 1976	Bedfdrd4	21.1	1704271	5654926	0.61	1.20	1.35
88	Whitehead 1976	Bedfdrd5	15.7	1704676	5653617	0.60	1.15	1.30
89	Whitehead 1976	Durhamrd2	19.6	1700934	5656626	0.95	1.60	1.35
90	Whitehead 1976	Norfkrd5	19.2	1702359	5654656	0.90	1.26	1.40

40	Torres-Orozco et al	MThouse	25.0	1696426	5646665	2.20	2.00
41	Torres-Orozco et al	MTrd2	22.0	1695304	5654649	1.85	1.70
42	Torres-Orozco et al	Korlford1	21.0	1695017	5664075	1.30	1.00
43	Torres-Orozco et al	WP1	32.0	1694472	5647235	3.10	2.90
44	Torres-Orozco et al	DFvc2	10.0	1694559	5645376	1.61	1.50
45	Torres-Orozco et al	LowKaupo	6.1	1695676	5644152	1.65	1.20
46	Torres-Orozco et al	Pouakal1	6.5	1666696	5655636	1.10	0.80
47	Torres-Orozco et al	Pouakal2	12.0	1692455	5657593	1.20	1.00
48	Torres-Orozco et al	Pouakal3	6.9	1669455	5656100	1.10	0.90
49	Torres-Orozco et al	S2	40.0	1693930	5652357	3.00	2.50
50	Torres-Orozco et al	V	35.0	1693006	5651792	4.00	3.10
51	Torres-Orozco et al	J2	49.0	1697107	5649655	3.00	2.40
52	Torres-Orozco et al	F2	35.0	1695073	5649016	2.60	2.60
53	Torres-Orozco et al	W2	24.0	1692074	5652926	2.60	2.20
54	Torres-Orozco et al	W3	23.1	1692665	5653417	2.70	2.00
55	Torres-Orozco et al	W4	23.4	1692296	5653343	2.60	2.00
56	Torres-Orozco et al	V2	34.7	1693136	5652153	3.00	2.60
57	Torres-Orozco et al	Mauderd	24.1	1695342	5662276	1.20	0.90
58	Torres-Orozco et al	Korlford2	21.0	1693373	5662010	1.20	0.90
59	Torres-Orozco et al	N2	32.0	1695604	5651639	3.00	2.60
60	Torres-Orozco et al	M2	29.1	1696607	5651467	3.00	2.40
61	Torres-Orozco et al	M3	27.5	1696242	5652127	2.19	2.10
62	Torres-Orozco et al	Hill rd	23.2	1696432	5661645	1.30	1.00
63	Torres-Orozco et al	Egmtrd1	21.0	1697691	5656727	1.50	1.20
64	Torres-Orozco et al	Egmtrd2	20.6	1696242	5659473	1.50	1.20
65	Torres-Orozco et al	Bedfdrd	19.6	1700572	5662709	1.20	0.90
66	Torres-Orozco et al	Egmtrd4	17.0	1696966	5664259	1.15	0.90
67	Torres-Orozco et al	Egmtrd7	10.1	1699011	5655969	1.00	0.80
68	Torres-Orozco et al	Uplandr1	16.6	1699690	5664903	1.20	0.90
69	Torres-Orozco et al	Manga_st	7.6	1701659	5666350	1.00	0.90
70	Torres-Orozco et al	SH3_1	10.5	1705663	5661996	1.20	0.90
71	Torres-Orozco et al	SH3_2	16.5	1705966	5660311	1.10	1.00
72	Torres-Orozco et al	Maket_st	10.5	1705233	5660277	1.10	1.00
73	Torres-Orozco et al	Johnsr1	16.6	1706295	5656164	1.10	1.00
74	Torres-Orozco et al	Norfkrd4	23.5	1703502	5657462	1.61	1.30
75	Torres-Orozco et al	Bedfdrd3	17.0	1704396	5655469	1.75	1.30
76	Torres-Orozco et al	Bedfdrd4	19.7	1704271	5654926	1.73	1.40
77	Torres-Orozco et al	Bedfdrd5	17.6	1704676	5653817	1.77	1.30
78	Torres-Orozco et al	Durhamrd2	21.0	1700934	5656626	1.49	1.30
79	Torres-Orozco et al	Norfkrd5	24.0	1702359	5654656	1.60	1.50
80	Torres-Orozco et al	Derbyrd	16.0	1703219	5653625	1.65	1.30
81	Torres-Orozco et al	Tariki2	19.0	1706129	5655456	1.26	1.20
82	Torres-Orozco et al	SH3_3	15.0	1706165	5653942	1.30	1.20
83	Torres-Orozco et al	Radnord1	9.5	1702667	5646059	1.67	1.20
84	Torres-Orozco et al	Pembroke2	6.7	1704691	5646710	1.12	1.20
85	Torres-Orozco et al	Pembroke4	16.0	1696999	5647954	1.65	1.70
86	Torres-Orozco et al	Pembroke3	21.2	1701046	5647140	1.60	1.20
87	Torres-Orozco et al	Polard	9.3	1703617	5643215	1.24	0.90
88	Torres-Orozco et al	Hastingsrd	10.1	1702656	5642763	1.20	0.90
89	Torres-Orozco et al	Palmerd1	10.1	1700164	5643623	1.34	1.10
90	Torres-Orozco et al	S	9.0	1700631	5642062	1.10	0.80
91	Torres-Orozco et al	Q	26.0	1693957	5651445	3.00	3.00
92	Turner 2006	LU	0.3	1696317	5673076	0.10	0.05

Kokowai bed-set (Kw7)

Id	Section's author	Section	Th cm	UTM coordinates		P cm	L cm
				x	y		
1	Damaschke et al. 2017	LRI	3.0	1707164	5666927	0.25	0.25
2	Torres-Orozco et al	X1	36.5	1691766	5652672	5.10	4.10
3	Torres-Orozco et al	X2	37.0	1691367	5652937	5.10	4.20

40	Torres-Orozco et al	MThouse	25.0	1696426	5646665	2.20	2.00
41	Torres-Orozco et al	MTrd2	22.0	1695304	5654649	1.85	1.70
42	Torres-Orozco et al	Korlford1	21.0	1695017	5664075	1.30	1.00
43	Torres-Orozco et al	WP1	32.0	1694472	5647235	3.10	2.90
44	Torres-Orozco et al	DFvc2	10.0	1694559	5645376	1.81	1.50
45	Torres-Orozco et al	LowKaupo	6.1	1695678	5644152	1.85	1.20
46	Torres-Orozco et al	Pouakai1	6.5	1665696	5655636	1.10	0.80
47	Torres-Orozco et al	Pouakai2	12.0	1692455	5657593	1.20	1.00
48	Torres-Orozco et al	Pouakai3	6.9	1669455	5656100	1.10	0.90
49	Torres-Orozco et al	S2	40.0	1693930	5652357	3.00	2.50
50	Torres-Orozco et al	V	35.0	1693006	5651792	4.00	3.10
51	Torres-Orozco et al	J2	49.0	1697107	5649655	3.00	2.40
52	Torres-Orozco et al	F2	35.0	1695073	5649016	2.60	2.60
53	Torres-Orozco et al	W2	24.0	1692074	5652926	2.60	2.20
54	Torres-Orozco et al	W3	23.1	1692665	5653417	2.70	2.00
55	Torres-Orozco et al	W4	23.4	1692296	5653343	2.60	2.00
56	Torres-Orozco et al	V2	34.7	1693136	5652153	3.00	2.60
57	Torres-Orozco et al	Mauderd	24.1	1695342	5662276	1.20	0.90
58	Torres-Orozco et al	Korlford2	21.0	1693373	5662010	1.20	0.90
59	Torres-Orozco et al	N2	32.0	1695604	5651639	3.00	2.60
60	Torres-Orozco et al	M2	29.1	1696607	5651467	3.00	2.40
61	Torres-Orozco et al	M3	27.5	1696242	5652127	2.19	2.10
62	Torres-Orozco et al	Hill rd	23.2	1696432	5661645	1.30	1.00
63	Torres-Orozco et al	Egmtrd1	21.0	1697691	5656727	1.50	1.20
64	Torres-Orozco et al	Egmtrd2	20.6	1696242	5659473	1.50	1.20
65	Torres-Orozco et al	Bedfordrd	19.6	1700572	5662709	1.20	0.90
66	Torres-Orozco et al	Egmtrd4	17.0	1698966	5664259	1.15	0.90
67	Torres-Orozco et al	Egmtrd7	10.1	1699011	5665969	1.00	0.80
68	Torres-Orozco et al	Uplandrd1	16.6	1699690	5664903	1.20	0.90
69	Torres-Orozco et al	Manga_st	7.8	1701859	5666350	1.00	0.90
70	Torres-Orozco et al	SH3_1	10.5	1705563	5661996	1.20	0.90
71	Torres-Orozco et al	SH3_2	16.5	1705966	5660311	1.10	1.00
72	Torres-Orozco et al	Maket_st	10.5	1705233	5660277	1.10	1.00
73	Torres-Orozco et al	Johnsrđ	16.6	1706265	5656164	1.10	1.00
74	Torres-Orozco et al	Norflkrđ4	23.5	1703502	5657462	1.61	1.30
75	Torres-Orozco et al	Bedfđrd3	17.0	1704396	5655469	1.75	1.30
76	Torres-Orozco et al	Bedfđrd4	19.7	1704271	5654926	1.73	1.40
77	Torres-Orozco et al	Bedfđrd5	17.6	1704676	5653617	1.77	1.30
78	Torres-Orozco et al	Durhamrd2	21.0	1700934	5656626	1.49	1.30
79	Torres-Orozco et al	Norflkrđ5	24.0	1702359	5654656	1.60	1.50
80	Torres-Orozco et al	Derbyrd	18.0	1703219	5653625	1.85	1.30
81	Torres-Orozco et al	Tarłkđ2	19.0	1706129	5655456	1.26	1.20
82	Torres-Orozco et al	SH3_3	15.0	1706165	5653942	1.30	1.20
83	Torres-Orozco et al	Radnorrd1	9.5	1702667	5648059	1.67	1.20
84	Torres-Orozco et al	Pembroke2	6.7	1704691	5646710	1.12	1.20
85	Torres-Orozco et al	Pembroke4	16.0	1698999	5647954	1.85	1.70
86	Torres-Orozco et al	Pembroke3	21.2	1701046	5647140	1.60	1.20
87	Torres-Orozco et al	Potord	8.3	1703617	5643215	1.24	0.90
88	Torres-Orozco et al	Hastingsrd	10.1	1702656	5642763	1.20	0.90
89	Torres-Orozco et al	Palmerrd1	10.1	1700164	5643623	1.34	1.10
90	Torres-Orozco et al	S	9.0	1700631	5642062	1.10	0.80
91	Torres-Orozco et al	Q	26.0	1693957	5651445	3.00	3.00
92	Turner 2006	LU	0.3	1696317	5673076	0.10	0.05

Kokowai bed-set (Kw7)

Id	Section's author	Section	Th cm	UTM coordinates		P cm	L cm
				x	y		
1	Damaschke et al. 2017	LRI	3.0	1707164	5668927	0.25	0.25
2	Torres-Orozco et al	X1	36.5	1691766	5652672	5.10	4.10
3	Torres-Orozco et al	X2	37.0	1691367	5652937	5.10	4.20

4	Torres-Orozco et al	Y	35.0	1690952	5652652	4.90	4.00
5	Torres-Orozco et al	W	37.0	1692442	5653002	5.20	4.10
6	Torres-Orozco et al	WP1	9.0	1694472	5647235	3.20	2.50
7	Torres-Orozco et al	W2	38.0	1692074	5652925	5.20	4.00
8	Torres-Orozco et al	W3	37.0	1692665	5653417	5.20	4.20
9	Torres-Orozco et al	W4	37.5	1692296	5653343	5.30	4.20
10	Torres-Orozco et al	Q	16.0	1693957	5651445	4.20	3.00
11	Torres-Orozco et al	P	27.0	1693703	5651211	4.20	3.10
12	Torres-Orozco et al	Kw7_1	20.0	1699279	5653040	3.20	2.40
13	Torres-Orozco et al	Kw7_2	23.0	1694261	5661266	2.90	2.40
14	Torres-Orozco et al	Kw7_3	21.0	1692958	5662672	2.60	2.10
15	Torres-Orozco et al	Kw7_4	31.0	1690497	5652653	5.00	4.00
16	Turner 2006	LU	1.0	1698317	5673076	0.20	0.20

Kokowai bed-set (Kw4)

id	Section's author	Section	Th cm	UTM coordinates		P cm	L cm
				x	y		
1	Alloway et al. 1995	Onaero1	2.00	1718009	5662966	0.20	0.20
2	Alloway et al. 1995	Onaero2	2.00	1717400	5662966	0.20	0.20
3	Damaschke et al. 2017	LRI	4.50	1707184	5668927	2.30	1.40
4	Torres-Orozco et al	X1	23.00	1691766	5652672	5.70	5.00
5	Torres-Orozco et al	X2	22.00	1691367	5652937	5.60	4.90
6	Torres-Orozco et al	Y	19.50	1690952	5652652	5.10	4.50
7	Torres-Orozco et al	W	14.00	1692442	5653002	5.30	4.10
8	Torres-Orozco et al	WP1	63.00	1694472	5647235	5.60	5.00
9	Torres-Orozco et al	W2	15.10	1692074	5652925	5.30	4.30
10	Torres-Orozco et al	W3	16.00	1692665	5653417	5.30	4.10
11	Torres-Orozco et al	W4	14.20	1692296	5653343	5.10	4.10
12	Torres-Orozco et al	Q	170.00	1693957	5651445	6.30	5.20
13	Torres-Orozco et al	P	176.00	1693703	5651211	6.30	5.00
14	Torres-Orozco et al	Kw4_1	72.00	1699279	5653040	4.50	3.90
15	Torres-Orozco et al	Kw4_2	49.00	1694261	5661266	4.10	3.30
16	Torres-Orozco et al	Kw4_3	43.00	1692958	5662672	3.70	2.90
17	Torres-Orozco et al	Kw4_4	75.00	1694372	5646564	4.20	3.70
18	Torres-Orozco et al	Kw4_5	60.00	1693706	5646696	4.10	4.30
19	Torres-Orozco et al	Kw4_6	100.00	1690497	5652653	5.00	4.50
20	Turner 2006	LU	4.00	1698317	5673076	1.50	1.50

Th: deposit thickness, P: average pumice diameter, L: average lithic diameter, vj: average diameter of vesicular juvenile clasts ("dense pumice")

The average diameter corresponds to the mean estimate of three axes measured on five different clasts

UTM coordinates in NZGD 2000 New Zealand Transverse Mercator

Appendix 4.2 Density and volume analyses and porosity determinations of pyroclasts from different bed-sets produced by large eruptions at Mt. Taranaki

Burrell bed-set

	Wgt g	Envelope (Bulk) Density				Skeletal Density			Solid Density			Porosity			
		cm3	SD	g/cm3	SD	cm3	g/cm3	Vol SD	cm3	g/cm3	Vol SD	Bulk %	Conn %	Iso %	
Top Dense pumice (dark-grey / brown, banded)	3.23	3.40	0.0056	0.95	0.0015	1.34	2.42	0.0026	1.25	2.54	0.0012	62.65	60.76	1.88	
	3.73	3.40	0.0022	0.94	0.0013	1.33	2.43	0.0015	1.26	2.52	0.0014	62.71	60.96	1.75	
	3.20	3.39	0.0065	0.96	0.0043	1.34	2.42	0.0016	1.25	2.54	0.0016	62.14	60.61	1.53	
	1.51	1.64	0.0020	0.99	0.0013	1.14	2.45	0.0021	1.07	2.55	0.0025	61.28	30.27	31.00	
	2.60	2.26	0.0029	1.14	0.0029	1.34	2.42	0.0039	1.24	2.54	0.0014	54.96	40.90	14.06	
	2.59	2.26	0.0060	1.25	0.0017	1.72	2.19	0.0019	0.65	2.40	0.0032	48.02	23.61	24.41	
	2.62	2.25	0.0016	1.21	0.0014	1.14	2.44	0.0029	1.08	2.54	0.0066	52.22	49.29	2.93	
	1.62	1.64	0.0157	0.99	0.0096	0.73	2.21	0.0076	0.66	2.40	0.0036	58.60	55.23	3.57	
	3.23	3.40	0.0017	0.92	0.0077	1.33	2.43	0.0026	1.25	2.54	0.0046	63.67	60.60	3.07	
	3.24	3.41	0.0022	0.96	0.0053	1.73	2.21	0.0043	0.66	2.42	0.0041	60.31	49.24	11.07	
	1.62	1.65	0.0026	1.00	0.0022	0.74	2.20	0.0026	0.67	2.38	0.0014	58.21	55.37	2.85	
	1.66	1.61	0.0016	0.99	0.0035	1.14	2.45	0.0020	1.07	2.54	0.0065	61.16	28.99	32.19	
	2.75	2.25	0.0006	1.23	0.0017	1.90	2.20	0.0034	0.66	2.41	0.0023	48.63	15.46	33.35	
	2.60	2.26	0.0035	1.12	0.0015	1.12	2.43	0.0107	1.09	2.51	0.0020	55.25	50.17	5.07	
	2.60	2.25	0.0163	1.24	0.0100	1.14	2.45	0.0050	1.07	2.54	0.0026	51.16	49.26	1.88	
	3.19	3.36	0.0029	0.95	0.0076	1.33	2.43	0.0022	1.25	2.54	0.0016	62.71	60.54	2.17	
	3.30	3.42	0.0039	0.95	0.0023	1.32	2.21	0.0016	0.67	2.37	0.0013	59.64	61.52	-1.67	
	1.59	1.64	0.0040	1.01	0.0020	1.14	2.44	0.0012	1.07	2.54	0.0011	60.33	30.27	30.07	
	1.59	1.63	0.0097	1.01	0.0026	1.14	2.46	0.0016	1.07	2.55	0.0101	60.46	30.23	30.25	
	2.79	2.26	0.0032	1.24	0.0016	1.37	2.40	0.0017	1.23	2.53	0.0021	51.05	39.36	11.67	
	2.60	2.27	0.0029	1.11	0.0032	1.22	2.20	0.0029	0.64	2.41	0.0011	53.63	46.21	7.62	
	3.22	3.39	0.0050	0.93	0.0029	1.33	2.43	0.0013	1.26	2.52	0.0021	63.17	60.69	2.48	
	3.02	3.40	0.0017	0.96	0.0014	1.34	2.41	0.0012	1.25	2.54	0.0020	62.02	60.69	1.33	
	3.43	3.40	0.0043	0.96	0.0062	2.73	2.23	0.0012	0.66	2.40	0.0015	59.30	19.88	39.42	
	1.62	1.64	0.0013	1.01	0.0005	0.72	2.24	0.0016	0.66	2.41	0.0021	58.34	55.93	2.41	
	1.92	1.66	0.0021	0.99	0.0016	0.74	2.16	0.0032	0.66	2.39	0.0031	58.72	50.09	3.63	
	1.62	1.62	0.0034	0.99	0.0006	1.15	2.44	0.0022	1.07	2.55	0.0032	61.27	29.23	32.04	
	1.62	1.63	0.0060	1.00	0.0015	1.15	2.44	0.0037	1.08	2.53	0.0039	60.61	29.47	31.14	
	2.60	2.27	0.0016	1.24	0.0065	1.37	2.42	0.0043	1.25	2.50	0.0026	50.35	39.36	10.97	
	2.62	2.25	0.0014	1.24	0.0034	1.14	2.45	0.0019	1.09	2.54	0.0034	51.05	49.52	1.53	
	Grey pumice	1.73	2.19	0.0147	0.79	0.0053	0.77	2.24	0.0019	0.69	2.44	0.0020	67.62	64.79	2.64
		1.46	2.11	0.0036	0.70	0.0013	0.74	2.05	0.0017	0.63	2.34	0.0013	69.92	65.10	4.63
1.51		2.12	0.0015	0.67	0.0034	0.76	2.27	0.0034	0.69	2.44	0.0037	72.41	64.06	6.35	
1.62		2.23	0.0016	0.76	0.0006	1.19	0.55	0.0016	0.49	2.35	0.0034	67.76	46.70	21.06	
1.73		2.19	0.0020	0.79	0.0025	1.14	0.56	0.0052	0.49	2.36	0.0040	66.76	47.99	16.77	
1.17		1.61	0.0016	0.67	0.0023	0.77	2.26	0.0046	0.69	2.46	0.0036	72.77	57.35	15.41	
1.20		1.60	0.0016	0.61	0.0043	0.55	2.12	0.0039	0.47	2.34	0.0013	73.71	69.59	4.12	
1.51		2.11	0.0095	0.72	0.0035	0.74	2.05	0.0032	0.64	2.32	0.0019	69.19	60.13	4.06	
1.50		2.10	0.0050	0.69	0.0050	0.74	2.04	0.0011	0.63	2.35	0.0022	70.90	64.76	6.15	
1.51		2.10	0.0039	0.71	0.0046	0.74	2.04	0.0019	0.64	2.32	0.0043	69.25	64.60	4.45	

Top	Grey pumice	1.92	2.22	0.0039	0.79	0.0066	0.77	2.25	0.0016	0.69	2.43	0.0007	67.65	65.41	2.24
		1.73	2.16	0.0015	0.79	0.0015	1.16	0.56	0.0023	0.49	2.38	0.0097	66.76	46.44	20.34
		1.98	1.81	0.0019	0.66	0.0016	0.73	2.06	0.0021	0.63	2.34	0.0021	71.11	59.58	11.52
		1.20	1.81	0.0021	0.65	0.0014	0.56	2.13	0.0017	0.48	2.35	0.0026	72.11	69.21	2.90
		1.21	2.10	0.0022	0.72	0.0008	0.74	2.04	0.0013	0.64	2.31	0.0012	69.04	64.79	4.24
		1.52	2.13	0.0097	0.72	0.0018	0.76	2.26	0.0015	0.69	2.42	0.0017	70.47	64.09	6.38
		1.72	2.19	0.0029	0.77	0.0011	0.77	2.24	0.0014	0.69	2.45	0.0013	68.57	64.73	3.84
		1.70	2.19	0.0025	0.76	0.0016	1.16	0.55	0.0040	0.46	2.40	0.0020	67.61	46.81	20.80
		1.63	2.19	0.0058	0.79	0.0101	1.13	0.56	0.0022	0.49	2.37	0.0016	66.53	46.52	19.01
		1.18	1.80	0.0026	0.66	0.0015	0.74	2.06	0.0040	0.59	2.32	0.0026	71.70	59.22	12.48
		1.19	1.80	0.0018	0.65	0.0013	0.77	2.24	0.0013	0.70	2.44	0.0016	73.50	57.07	16.42
		1.51	2.11	0.0025	0.71	0.0029	0.74	2.05	0.0026	0.64	2.31	0.0013	69.50	65.06	4.42
		1.71	2.19	0.0043	0.76	0.0021	0.77	2.24	0.0020	0.69	2.43	0.0012	68.05	64.74	3.31
		1.21	1.76	0.0015	0.67	0.0013	0.74	2.05	0.0040	0.64	2.33	0.0012	71.38	56.69	12.69
		1.19	1.81	0.0043	0.66	0.0015	0.56	2.13	0.0013	0.49	2.37	0.0023	72.27	69.18	3.09
		1.50	2.11	0.0021	0.71	0.0029	0.73	2.06	0.0020	0.63	2.33	0.0015	69.37	65.32	4.05
		1.48	2.11	0.0020	0.72	0.0097	0.77	2.26	0.0020	0.68	2.45	0.0026	70.54	63.76	6.78
		1.74	2.16	0.0008	0.81	0.0032	1.63	0.56	0.0048	0.49	2.35	0.0015	65.60	16.19	49.41
		1.56	1.80	0.0022	0.64	0.0043	0.81	2.24	0.0008	0.72	2.45	0.0076	73.99	55.01	18.99
		1.20	1.80	0.0031	0.66	0.0103	0.55	2.12	0.0020	0.49	2.36	0.0014	72.16	69.52	2.64
Middle	Dense pumice	2.02	2.00	0.0031	1.01	0.0015	0.98	2.06	0.0042	0.64	2.35	0.0010	57.23	51.24	5.99
		2.71	2.64	0.0147	1.03	0.0057	1.19	2.28	0.0032	1.07	2.48	0.0036	56.64	54.66	3.76
		2.62	2.36	0.0136	1.19	0.0068	1.19	2.36	0.0046	1.11	2.50	0.0061	52.45	49.64	2.61
		1.99	1.96	0.0006	1.00	0.0051	0.97	2.06	0.0016	0.64	2.35	0.0026	57.35	51.03	6.32
		2.34	2.00	0.0026	1.00	0.0029	0.97	2.06	0.0034	0.63	2.36	0.0090	57.42	51.50	5.92
		2.14	1.99	0.0006	1.01	0.0012	0.97	2.06	0.0029	0.63	2.37	0.0026	57.52	51.42	6.10
		2.01	1.97	0.0026	0.96	0.0017	0.97	2.07	0.0011	0.64	2.36	0.0029	56.57	50.73	7.64
		2.93	1.99	0.0024	1.00	0.0015	0.98	2.06	0.0001	0.64	2.35	0.0031	57.47	50.93	6.54
		1.97	2.01	0.0016	1.00	0.0009	0.98	2.05	0.0007	0.64	2.35	0.0061	57.43	51.03	6.40
		2.02	2.01	0.0034	1.01	0.0025	1.17	2.31	0.0096	1.07	2.46	0.0026	59.42	41.72	17.70
		2.17	2.01	0.0001	1.01	0.0018	1.19	2.28	0.0006	1.07	2.49	0.0013	59.36	40.80	18.55
		2.02	2.02	0.0090	1.01	0.0020	1.16	2.30	0.0062	1.06	2.50	0.0016	59.77	41.66	18.09
		2.70	2.63	0.0026	1.12	0.0011	1.16	2.29	0.0016	1.06	2.47	0.0001	54.55	54.89	-0.34
		2.71	2.63	0.0007	1.13	0.0026	1.19	2.27	0.0017	1.07	2.49	0.0001	54.79	54.75	0.04
		2.71	2.63	0.0017	1.03	0.0011	1.19	2.28	0.0016	1.07	2.49	0.0011	56.60	54.62	3.99
		2.67	2.62	0.0030	1.00	0.0017	1.17	2.40	0.0073	1.11	2.49	0.0017	59.95	55.32	4.63
		2.70	2.62	0.0069	1.00	0.0019	1.16	2.36	0.0020	1.11	2.49	0.0043	59.95	54.94	5.01
		2.69	2.61	0.0031	1.02	0.0017	1.19	2.37	0.0041	1.11	2.51	0.0032	59.31	54.44	4.87
		2.70	2.62	0.0061	1.07	0.0012	1.19	2.37	0.0016	1.10	2.52	0.0049	57.35	54.66	2.67
		2.71	2.64	0.0020	1.06	0.0059	1.19	2.37	0.0097	1.10	2.51	0.0011	57.79	55.04	2.76
2.71	2.66	0.0097	1.03	0.0017	1.20	2.35	0.0017	1.11	2.49	0.0026	56.65	54.94	3.71		
2.61	2.36	0.0040	1.24	0.0027	0.97	2.06	0.0069	0.64	2.35	0.0026	47.13	56.95	-11.82		
2.61	2.36	0.0094	1.20	0.0034	0.93	2.05	0.0007	0.64	2.35	0.0030	46.63	60.35	-11.52		
2.61	2.36	0.0026	1.17	0.0015	0.96	2.07	0.0016	0.63	2.35	0.0011	50.11	56.36	-6.25		
2.60	2.36	0.0012	1.19	0.0075	1.16	2.26	0.0011	1.05	2.51	0.0097	52.57	51.23	1.35		
2.78	2.37	0.0022	1.22	0.0024	1.16	2.26	0.0032	1.06	2.49	0.0029	51.11	51.11	0.01		
2.61	2.36	0.0096	1.16	0.0016	1.19	2.30	0.0024	1.07	2.51	0.0040	53.02	49.46	3.57		
2.61	2.36	0.0029	1.19	0.0034	1.16	2.36	0.0017	1.12	2.49	0.0075	52.10	51.29	0.81		
2.61	2.36	0.0046	1.22	0.0019	1.16	2.36	0.0006	1.11	2.50	0.0025	51.19	49.90	1.30		

Middle	Grey pumice	2.50	2.37	0.0013	1.19	0.0021	1.19	2.35	0.0052	1.10	2.45	0.0015	51.53	49.55	1.75
		1.95	2.45	0.0001	0.70	0.0017	0.57	2.23	0.0034	0.79	2.40	0.0025	70.79	64.71	5.07
		2.10	2.44	0.0007	0.77	0.0011	0.55	2.20	0.0023	0.79	2.41	0.0021	65.11	63.95	4.13
		1.93	2.40	0.0023	0.69	0.0005	0.72	2.23	0.0045	0.55	2.43	0.0025	71.57	69.93	1.53
		1.71	2.35	0.0021	0.76	0.0095	0.91	2.21	0.0012	0.74	2.39	0.0025	65.17	61.46	5.71
		1.50	2.50	0.0097	0.73	0.0015	0.70	2.22	0.0075	0.55	2.40	0.0027	69.73	72.10	-2.37
		1.65	2.43	0.0005	0.67	0.0071	0.72	2.12	0.0015	0.55	2.42	0.0011	72.15	70.31	1.54
		1.60	2.43	0.0011	0.69	0.0059	0.74	2.22	0.0009	0.54	2.41	0.0052	71.22	69.43	1.50
		1.93	2.45	0.0105	0.75	0.0032	0.55	2.21	0.0027	0.79	2.42	0.0017	67.74	64.57	3.07
		1.95	2.55	0.0034	0.77	0.0031	0.55	2.20	0.0009	0.75	2.43	0.0020	65.43	65.91	2.51
		2.19	2.45	0.0004	0.73	0.0001	0.57	2.21	0.0025	0.75	2.42	0.0011	69.95	64.75	5.20
		1.52	2.44	0.0022	0.55	0.0073	0.72	2.24	0.0022	0.55	2.41	0.0001	71.75	70.51	1.27
		1.50	2.41	0.0015	0.55	0.0012	0.55	2.19	0.0097	0.72	2.42	0.0075	72.59	63.59	9.00
		1.54	2.39	0.0017	0.59	0.0019	0.71	2.23	0.0011	0.51	2.32	0.0001	70.32	70.14	0.15
		1.49	2.51	0.0097	0.77	0.0107	0.77	2.20	0.0007	0.71	2.35	0.0005	67.55	69.33	-1.67
		1.51	2.41	0.0145	0.57	0.0040	0.72	2.23	0.0031	0.55	2.42	0.0014	72.35	70.05	2.33
		2.24	2.45	0.0020	0.74	0.0020	0.72	2.23	0.0055	0.55	2.40	0.0001	69.31	70.57	-1.25
		1.93	2.52	0.0015	0.71	0.0010	0.73	2.22	0.0015	0.55	2.42	0.0011	70.53	71.15	-0.51
		1.51	2.39	0.0011	0.55	0.0051	0.90	2.19	0.0049	0.79	2.41	0.0017	72.73	62.41	10.32
		1.51	2.39	0.0020	0.57	0.0031	0.75	2.20	0.0015	0.59	2.40	0.0015	72.22	57.55	4.55
		1.45	2.43	0.0051	0.55	0.0029	0.70	2.17	0.0024	0.54	2.42	0.0025	71.92	71.44	0.45
		2.14	2.45	0.0009	0.75	0.0031	0.57	2.21	0.0007	0.75	2.43	0.0013	69.23	54.59	4.54
		1.93	2.39	0.0001	0.75	0.0020	0.55	2.20	0.0019	0.79	2.41	0.0051	67.74	63.30	4.43
		1.93	2.51	0.0011	0.74	0.0011	0.72	2.23	0.0013	0.55	2.35	0.0011	65.95	71.20	-2.22
		1.53	2.45	0.0017	0.55	0.0004	0.72	2.23	0.0025	0.55	2.42	0.0013	71.95	70.45	1.50
1.93	2.59	0.0095	0.70	0.0055	0.79	2.20	0.0059	0.59	2.42	0.0055	70.59	69.57	1.32		
1.71	2.45	0.0012	0.75	0.0051	0.55	2.21	0.0017	0.55	2.39	0.0010	57.45	55.45	1.95		
1.59	2.49	0.0019	0.77	0.0029	0.55	2.20	0.0005	0.75	2.41	0.0012	55.15	55.55	2.52		
1.59	2.40	0.0017	0.77	0.0013	0.75	2.15	0.0055	0.75	2.41	0.0030	55.17	55.44	-0.27		
1.55	2.41	0.0040	0.55	0.0022	0.79	2.20	0.0041	0.51	2.41	0.0007	72.70	57.27	5.43		
1.51	2.42	0.0011	0.59	0.0024	0.71	2.21	0.0097	0.55	2.40	0.0011	71.33	70.51	0.52		
Base	Grey pumice	1.75	2.15	0.0032	0.52	0.0011	0.55	2.10	0.0021	0.73	2.35	0.0010	55.79	51.10	4.59
		2.54	2.42	0.0011	1.12	0.0012	1.33	1.99	0.0037	1.13	2.31	0.0001	51.55	44.59	5.59
		1.90	2.25	0.0012	0.90	0.0051	0.55	2.25	0.0013	0.50	2.47	0.0024	53.57	51.12	2.45
		2.15	2.30	0.0007	1.05	0.0045	0.95	2.20	0.0010	0.59	2.39	0.0051	55.97	57.29	-1.32
		2.14	2.05	0.0012	0.93	0.0013	1.00	2.17	0.0033	0.55	2.41	0.0012	51.20	52.20	9.00
		1.93	1.53	0.0021	0.94	0.0021	0.53	2.19	0.0025	0.74	2.43	0.0010	51.22	54.35	5.54
		2.00	2.25	0.0125	0.59	0.0049	0.55	2.27	0.0017	0.50	2.45	0.0014	53.90	50.94	2.95
		2.52	2.39	0.0001	1.05	0.0020	1.33	1.99	0.0015	1.13	2.31	0.0001	54.27	44.22	10.05
		1.77	2.15	0.0015	0.55	0.0041	0.55	2.10	0.0020	0.73	2.35	0.0037	53.95	51.05	2.90
		2.14	2.31	0.0001	0.94	0.0004	0.99	2.15	0.0020	0.55	2.41	0.0009	50.75	57.02	3.74
		2.15	2.17	0.0055	0.90	0.0011	1.00	2.17	0.0022	0.55	2.41	0.0012	52.55	54.05	5.49
		1.50	1.59	0.0032	1.02	0.0025	0.54	2.15	0.0021	0.74	2.43	0.0035	55.05	55.52	2.53
		1.53	1.53	0.0050	0.95	0.0041	0.54	2.17	0.0021	0.74	2.42	0.0029	50.25	53.90	5.35
		2.24	2.40	0.0025	1.10	0.0021	1.33	2.00	0.0029	1.13	2.31	0.0029	52.52	44.52	7.90
		1.50	2.15	0.0012	0.55	0.0017	0.53	2.14	0.0023	0.73	2.39	0.0012	54.50	51.40	3.20
		2.31	2.27	0.0027	0.91	0.0021	0.55	2.29	0.0012	0.51	2.44	0.0025	52.55	51.43	1.14
		2.15	2.05	0.0079	0.92	0.0015	0.99	2.15	0.0035	0.55	2.41	0.0025	52.05	51.52	10.23
		1.55	2.00	0.0053	0.95	0.0053	0.54	2.15	0.0021	0.74	2.43	0.0013	50.33	55.04	2.29

Base	Grey pumice	2.65	2.42	0.0139	1.10	0.0063	1.33	1.99	0.0006	1.13	2.30	0.0012	52.41	44.66	7.52
		2.43	2.51	0.0029	1.08	0.0014	1.32	2.01	0.0021	1.13	2.31	0.0021	53.43	47.46	5.97
		1.77	2.16	0.0007	0.90	0.0012	0.84	2.12	0.0007	0.72	2.40	0.0001	62.76	61.46	1.30
		1.99	2.25	0.0062	0.89	0.0023	0.88	2.26	0.0019	0.80	2.47	0.0037	64.19	60.86	3.33
		2.11	2.26	0.0006	0.86	0.0001	0.88	2.27	0.0046	0.80	2.46	0.0022	64.37	61.01	3.36
		1.63	1.94	0.0009	0.97	0.0013	0.83	2.20	0.0015	0.74	2.41	0.0016	59.55	57.03	2.52
		1.89	1.80	0.0020	0.95	0.0022	0.84	2.17	0.0001	0.74	2.42	0.0014	60.66	53.06	7.60
		2.16	2.26	0.0055	0.95	0.0022	1.00	2.17	0.0010	0.88	2.41	0.0033	60.66	56.33	4.33
		2.57	2.43	0.0001	1.10	0.0010	1.32	2.00	0.0010	1.13	2.29	0.0010	51.86	45.59	6.27
		1.76	2.16	0.0001	0.81	0.0019	0.84	2.13	0.0020	0.72	2.40	0.0012	66.07	61.60	4.46
		1.76	2.15	0.0012	1.00	0.0020	0.85	2.10	0.0001	0.73	2.39	0.0016	58.10	60.62	-2.52
		1.88	2.22	0.0001	0.87	0.0007	0.88	2.26	0.0065	0.80	2.46	0.0051	64.71	60.13	4.58
		Average			0.90			2.16			2.42		62.76	55.91	6.41
		Top			0.88			2.09			2.43		63.88	52.38	11.51
Middle			0.90			2.22			2.43		62.96	59.86	3.10		
Base			0.95			2.15			2.40		60.13	55.50	4.63		
D.lith	4.32	3.27	0.0011	2.64	0.0047	3.21	2.90	0.0023	2.97	2.91	0.0005	2.56	1.77	0.60	

Kaupokonui bed-set

	Wgt	Envelope (Bulk) Density				Skeletal Density			Solid Density			Porosity			
		g	cm3	SD	g/cm3	SD	cm3	g/cm3	Vol SD	cm3	g/cm3	Vol SD	Bulk %	Conn %	Iso %
Top	Grey-brown pumice	2.91	2.61	0.0249	1.12	0.0105	1.16	2.51	0.0010	0.55	2.58	0.0016	56.78	55.49	1.30
		4.64	2.93	0.0022	1.22	0.0039	1.61	2.56	0.0031	1.76	2.60	0.0021	53.23	38.10	15.12
		2.91	2.61	0.0012	1.13	0.0012	1.16	2.50	0.0019	0.55	2.49	0.0007	54.71	55.48	-0.77
		3.42	2.99	0.0022	1.14	0.0036	1.33	2.57	0.0033	1.29	2.62	0.0025	56.31	55.40	0.91
		4.26	3.80	0.0441	1.12	0.0130	1.73	2.46	0.0001	1.65	2.55	0.0023	56.05	54.36	1.68
		4.63	2.92	0.0007	1.36	0.0019	1.62	2.54	0.0019	1.77	2.59	0.0016	47.73	37.56	10.17
		4.26	3.80	0.0062	1.12	0.0018	1.74	2.45	0.0006	1.66	2.54	0.0006	55.94	54.19	1.75
		4.25	3.79	0.0011	1.11	0.0021	1.74	2.45	0.0009	1.66	2.55	0.0022	56.39	54.17	2.22
		2.88	2.61	0.0016	1.11	0.0018	1.16	2.50	0.0011	0.57	2.41	0.0061	54.06	55.37	-1.31
		2.50	2.33	0.0007	1.08	0.0012	1.00	2.49	0.0016	0.96	2.58	0.0009	56.26	57.24	1.04
		2.47	2.32	0.0023	1.06	0.0016	1.00	2.46	0.0033	0.94	2.63	0.0021	59.63	56.63	3.00
		3.41	2.97	0.0011	1.14	0.0013	1.34	2.57	0.0006	1.30	2.59	0.0032	55.64	54.99	0.65
		4.64	2.92	0.0078	1.59	0.0042	1.62	2.55	0.0045	1.76	2.60	0.0025	39.02	37.80	1.22
		4.26	3.81	0.0042	1.13	0.0027	1.73	2.46	0.0026	1.65	2.56	0.0037	55.70	54.46	1.23
		2.91	2.60	0.0023	1.10	0.0024	1.16	2.51	0.0014	0.55	2.47	0.0011	55.31	55.25	0.06
		2.49	2.34	0.0030	1.10	0.0031	1.01	2.47	0.0036	0.96	2.59	0.0046	57.60	57.02	0.59
		3.43	2.98	0.0016	1.15	0.0011	1.33	2.58	0.0009	1.28	2.64	0.0062	56.53	55.64	0.89
		2.49	2.33	0.0035	1.07	0.0016	1.00	2.49	0.0015	0.95	2.62	0.0049	59.26	57.16	2.12
		3.43	2.99	0.0056	1.15	0.0021	1.33	2.55	0.0020	1.28	2.64	0.0026	56.55	55.89	0.66
		4.65	2.92	0.0030	1.32	0.0016	1.62	2.54	0.0021	1.77	2.60	0.0034	49.30	37.65	11.65
		4.26	3.79	0.0009	1.12	0.0022	1.74	2.45	0.0011	1.67	2.52	0.0006	55.57	54.12	1.45
		4.27	3.82	0.0044	1.14	0.0011	1.73	2.46	0.0015	1.66	2.55	0.0026	55.20	54.56	0.61
		4.64	2.91	0.0017	1.49	0.0034	1.62	2.55	0.0006	1.76	2.58	0.0013	42.39	37.56	4.83
		2.91	2.56	0.0004	1.09	0.0009	1.16	2.52	0.0010	0.56	2.46	0.0023	55.63	55.12	0.71
		2.94	2.61	0.0007	1.12	0.0024	1.16	2.51	0.0005	0.55	2.57	0.0016	56.56	55.52	1.06
		2.51	2.33	0.0007	1.07	0.0013	0.99	2.51	0.0006	0.97	2.55	0.0036	56.02	57.63	0.39

		2.48	2.33	0.0011	1.07	0.0018	1.00	2.49	0.0048	0.95	2.60	0.0027	59.02	57.19	1.83
		3.43	2.99	0.0007	1.15	0.0025	1.33	2.59	0.0010	1.29	2.62	0.0020	56.30	55.69	0.61
		3.44	3.00	0.0022	1.16	0.0021	1.33	2.58	0.0007	1.26	2.63	0.0037	55.97	55.86	0.11
		4.63	2.92	0.0016	1.56	0.0013	1.64	2.52	0.0010	1.79	2.56	0.0011	36.16	37.04	1.14
Base	Grey-brown pumice	3.27	2.56	0.0004	1.24	0.0063	1.23	2.58	0.0050	0.55	2.59	0.0024	52.13	52.05	0.08
		3.57	2.52	0.0026	1.26	0.0033	1.57	2.51	0.0015	1.76	2.53	0.0019	50.30	37.61	12.49
		3.22	2.69	0.0095	1.20	0.0032	1.26	2.52	0.0006	0.55	2.59	0.0011	53.71	53.31	0.41
		3.48	2.78	0.0024	1.20	0.0006	1.35	2.50	0.0035	1.29	2.52	0.0036	52.38	51.37	1.02
		3.29	2.60	0.0017	1.19	0.0029	1.50	2.52	0.0095	1.65	2.53	0.0021	53.10	42.40	10.70
		2.99	2.64	0.0090	1.21	0.0011	1.58	2.41	0.0012	1.77	2.56	0.0056	53.08	44.44	8.63
		3.21	3.01	0.0012	1.22	0.0008	1.55	2.40	0.0031	1.66	2.42	0.0028	49.49	46.69	0.79
		3.00	2.01	0.0018	1.31	0.0005	1.24	2.42	0.0019	1.66	2.43	0.0021	46.37	36.42	7.94
		2.65	3.00	0.0010	1.31	0.0014	1.71	2.51	0.0044	0.57	2.53	0.0020	46.33	42.90	5.42
		2.55	2.01	0.0061	1.22	0.0066	1.25	2.56	0.0047	0.96	2.56	0.0037	52.61	37.59	15.22
		3.15	3.25	0.0040	1.25	0.0009	1.78	2.46	0.0012	0.94	2.51	0.0094	50.19	45.32	4.67
		3.01	3.11	0.0028	1.16	0.0094	1.76	2.54	0.0076	1.30	2.56	0.0016	54.76	43.41	11.35
		3.01	3.60	0.0035	1.15	0.0063	1.61	2.57	0.0063	1.76	2.59	0.0049	55.71	56.62	-2.91
		3.01	2.96	0.0022	1.20	0.0007	1.68	2.57	0.0032	1.65	2.60	0.0061	53.79	43.77	10.02
		3.66	3.01	0.0026	1.21	0.0015	1.64	2.58	0.0024	0.55	2.60	0.0040	53.51	45.39	8.13
		3.15	3.08	0.0013	1.23	0.0020	1.56	2.44	0.0041	0.96	2.45	0.0052	50.00	49.28	0.72
		3.00	2.96	0.0033	1.25	0.0025	1.50	2.50	0.0046	1.26	2.52	0.0010	50.40	49.79	0.61
		2.95	2.55	0.0023	1.21	0.0029	1.29	2.50	0.0015	0.95	2.52	0.0013	51.79	49.35	2.45
		3.00	2.13	0.0022	1.18	0.0040	1.20	2.49	0.0037	1.26	2.51	0.0014	53.11	43.67	9.45
		3.11	2.15	0.0027	1.30	0.0010	1.20	2.51	0.0071	1.77	2.53	0.0023	46.52	44.24	4.26
		3.23	2.09	0.0037	1.25	0.0094	1.31	2.55	0.0026	1.67	2.57	0.0014	51.42	37.30	14.11
		2.59	2.03	0.0105	1.19	0.0035	1.30	2.59	0.0051	1.66	2.60	0.0020	54.33	36.03	16.29
		2.69	2.16	0.0029	1.13	0.0016	1.19	2.57	0.0032	1.76	2.59	0.0016	56.60	44.91	11.69
		2.94	2.42	0.0025	1.21	0.0018	1.16	2.55	0.0018	0.56	2.57	0.0020	52.97	52.27	0.70
		3.11	2.32	0.0027	1.20	0.0033	1.16	2.53	0.0045	0.55	2.55	0.0079	52.65	49.94	2.91
		3.20	2.67	0.0034	1.20	0.0043	1.42	2.58	0.0036	0.97	2.59	0.0021	53.68	46.71	6.96
		3.20	2.74	0.0020	1.25	0.0024	1.40	2.58	0.0026	0.95	2.60	0.0021	51.97	46.65	3.11
		2.93	3.12	0.0041	1.19	0.0027	1.41	2.59	0.0022	1.29	2.62	0.0014	54.47	54.66	-0.40
2.66	3.01	0.0032	1.21	0.0025	1.51	2.49	0.0094	1.26	2.51	0.0021	51.75	49.96	1.76		
2.74	2.13	0.0046	1.26	0.0001	1.23	2.44	0.0030	1.79	2.46	0.0049	46.11	42.12	5.99		
Average				1.20			2.52		2.56		53.41	49.29	4.12		
Top				1.16			2.51		2.57		54.25	52.01	2.24		
Base				1.22			2.52		2.55		52.05	46.16	5.69		
D.lith	3.90	2.33	0.0015	2.54	0.0006	2.21	2.57	0.0021	1.32	2.61	0.0006	2.60	5.25	-2.44	

Manganui-D bed-set

	Wgt g	Envelope (Bulk) Density				Skeletal Density			Solid Density			Porosity		
		cm3	SD	g/cm3	SD	cm3	g/cm3	Vol SD	cm3	g/cm3	Vol SD	Bulk %	Conn %	Iso %
MD3 Top Brown pumice	4.51	2.15	0.0028	2.11	0.0024	1.48	3.06	0.0011	1.46	3.09	0.0019	31.71	31.00	0.71
	4.53	2.16	0.0012	2.11	0.0012	1.49	3.05	0.0019	1.46	3.06	0.0014	31.47	30.62	0.65
	4.52	2.15	0.0032	2.11	0.0061	1.48	3.06	0.0035	1.46	3.09	0.0076	31.70	30.96	0.74
	4.53	2.15	0.0098	2.11	0.0064	1.46	3.06	0.0041	1.46	3.09	0.0041	31.69	31.85	-0.26
	4.53	2.15	0.0004	2.12	0.0067	1.48	3.06	0.0034	1.47	3.09	0.0015	31.36	31.06	0.30

MD3 Top	Vesicular brown purpice	4.53	2.15	0.0034	2.11	0.0033	1.48	3.06	0.0064	1.46	3.09	0.0004	31.70	31.03	0.68
		4.51	2.16	0.0033	2.12	0.0013	1.48	3.05	0.0022	1.46	3.09	0.0006	31.37	31.39	-0.01
		4.51	2.15	0.0040	2.11	0.0040	1.47	3.06	0.0049	1.46	3.06	0.0004	31.51	31.53	-0.01
		4.51	2.13	0.0045	2.11	0.0018	1.48	3.06	0.0012	1.46	3.09	0.0055	31.70	30.45	1.25
		4.51	2.15	0.0067	2.10	0.0042	1.49	3.06	0.0017	1.45	3.09	0.0019	32.03	30.61	1.42
		4.51	2.15	0.0112	2.11	0.0006	1.49	3.06	0.0039	1.46	3.10	0.0006	31.93	30.51	1.42
		4.53	2.15	0.0056	2.10	0.0112	1.48	3.06	0.0016	1.45	3.10	0.0003	32.25	31.01	1.24
		4.51	2.15	0.0053	2.11	0.0041	1.48	3.06	0.0062	1.46	3.09	0.0009	31.69	31.07	0.62
		4.51	2.14	0.0017	2.11	0.0020	1.48	3.06	0.0005	1.46	3.09	0.0042	31.72	31.07	0.66
		4.53	2.14	0.0035	2.11	0.0018	1.48	3.06	0.0032	1.45	3.09	0.0041	31.70	30.70	0.99
		4.53	2.14	0.0076	2.11	0.0032	1.48	3.06	0.0018	1.46	3.09	0.0004	31.73	31.00	0.73
		4.53	2.14	0.0014	2.11	0.0058	1.48	3.06	0.0032	1.46	3.10	0.0006	31.94	30.99	0.95
		4.51	2.15	0.0024	2.11	0.0017	1.48	3.06	0.0112	1.45	3.06	0.0032	31.49	31.01	0.48
		4.51	2.15	0.0011	2.11	0.0032	1.48	3.06	0.0029	1.46	3.09	0.0034	31.71	31.07	0.64
		4.52	2.15	0.0069	2.12	0.0016	1.48	3.05	0.0092	1.46	3.09	0.0011	31.36	31.03	0.33
		4.53	2.14	0.0006	2.10	0.0050	1.45	3.06	0.0056	1.47	3.09	0.0003	32.02	30.71	1.31
		4.53	2.15	0.0018	2.10	0.0053	1.48	3.06	0.0020	1.46	3.09	0.0015	32.02	31.01	1.01
		4.53	2.16	0.0042	2.11	0.0006	1.48	3.06	0.0032	1.46	3.09	0.0041	31.71	31.36	0.35
		4.53	2.14	0.0012	2.11	0.0035	1.48	3.06	0.0035	1.48	3.10	0.0017	31.92	30.93	1.00
		4.53	2.16	0.0031	2.12	0.0011	1.48	3.05	0.0011	1.46	3.09	0.0013	31.37	31.37	0.01
4.51	2.14	0.0018	2.11	0.0044	1.48	3.06	0.0042	1.46	3.09	0.0002	31.71	30.78	0.93		
4.51	2.15	0.0004	2.11	0.0069	1.48	3.06	0.0028	1.46	3.06	0.0015	31.46	31.07	0.39		
4.52	2.14	0.0044	2.11	0.0020	1.48	3.07	0.0061	1.46	3.09	0.0031	31.73	30.99	0.75		
4.53	2.15	0.0042	2.11	0.0011	1.48	3.06	0.0006	1.46	3.09	0.0009	31.71	30.99	0.72		
MD3 Middle	Vesicular brown purpice	6.06	3.92	0.0032	1.54	0.0034	2.16	2.64	0.0006	2.11	2.67	0.0012	46.25	44.86	1.39
		6.06	3.91	0.0056	1.55	0.0026	2.15	2.63	0.0020	2.10	2.66	0.0029	45.69	44.98	0.71
		6.09	3.94	0.0013	1.55	0.0029	2.15	2.64	0.0010	2.10	2.66	0.0013	45.66	45.39	0.29
		6.09	3.92	0.0034	1.55	0.0094	2.14	2.65	0.0019	2.11	2.66	0.0006	46.06	45.36	0.69
		6.10	3.92	0.0056	1.55	0.0068	2.15	2.63	0.0012	2.09	2.66	0.0027	45.62	45.22	0.40
		6.07	3.94	0.0018	1.56	0.0059	2.15	2.63	0.0020	2.09	2.67	0.0010	45.55	45.40	0.14
		6.08	3.92	0.0039	1.55	0.0026	2.15	2.64	0.0031	2.11	2.67	0.0035	45.90	45.11	0.79
		6.08	3.92	0.0029	1.55	0.0022	2.15	2.63	0.0007	2.09	2.66	0.0006	45.63	45.11	0.72
		6.08	3.92	0.0021	1.55	0.0050	2.16	2.63	0.0034	2.10	2.66	0.0006	45.69	44.86	0.83
		6.09	3.91	0.0020	1.55	0.0036	2.15	2.63	0.0015	2.10	2.67	0.0009	46.02	44.97	1.06
		6.09	3.91	0.0045	1.56	0.0076	2.15	2.61	0.0026	2.07	2.64	0.0005	44.92	45.04	-0.12
		6.09	3.91	0.0022	1.55	0.0021	2.15	2.63	0.0005	2.09	2.66	0.0024	46.04	45.03	1.01
		6.10	3.92	0.0018	1.56	0.0012	2.15	2.62	0.0009	2.08	2.65	0.0006	45.43	45.09	0.34
		6.10	3.92	0.0045	1.56	0.0022	2.15	2.62	0.0026	2.08	2.65	0.0020	45.34	45.09	0.25
		6.09	3.92	0.0094	1.55	0.0013	2.15	2.63	0.0010	2.10	2.65	0.0021	45.39	45.10	0.28
		6.09	3.92	0.0062	1.55	0.0026	2.14	2.62	0.0033	2.08	2.65	0.0026	45.45	45.35	0.09
		6.09	3.92	0.0011	1.55	0.0035	2.15	2.62	0.0026	2.09	2.65	0.0012	45.66	45.10	0.59
		6.11	3.92	0.0044	1.56	0.0015	2.15	2.61	0.0023	2.07	2.65	0.0031	45.27	45.16	0.10
		6.06	3.92	0.0042	1.55	0.0018	2.15	2.63	0.0015	2.10	2.66	0.0006	45.70	45.11	0.58
		6.06	3.92	0.0033	1.54	0.0012	2.16	2.65	0.0024	2.11	2.66	0.0006	46.37	44.86	1.52
6.09	3.92	0.0040	1.55	0.0056	2.16	2.63	0.0004	2.09	2.66	0.0034	45.65	44.67	0.78		
6.09	3.92	0.0047	1.55	0.0019	2.15	2.63	0.0016	2.09	2.66	0.0011	45.67	45.10	0.56		
6.09	3.92	0.0011	1.56	0.0029	2.15	2.62	0.0036	2.08	2.64	0.0011	44.67	45.15	-0.28		
6.11	3.92	0.0016	1.56	0.0015	2.15	2.62	0.0001	2.08	2.65	0.0016	45.34	45.09	0.25		
6.07	3.92	0.0004	1.56	0.0026	2.16	2.65	0.0036	2.11	2.66	0.0016	45.63	44.86	0.77		

		6.09	3.92	0.0020	1.55	0.0035	2.15	2.83	0.0024	2.10	2.87	0.0032	45.88	45.11	0.78
		6.09	3.92	0.0018	1.55	0.0034	2.15	2.85	0.0017	2.12	2.86	0.0028	45.67	45.10	0.57
		6.09	3.92	0.0018	1.55	0.0013	2.15	2.83	0.0009	2.09	2.86	0.0035	45.66	45.15	0.51
		6.09	3.92	0.0032	1.55	0.0031	2.15	2.83	0.0014	2.09	2.86	0.0029	45.64	45.10	0.54
		2.29	1.41	0.0041	1.66	0.0041	0.77	3.03	0.0076	0.77	3.06	0.0020	45.61	44.94	0.67
		2.30	1.39	0.0047	1.65	0.0021	0.76	3.02	0.0032	0.75	3.05	0.0011	45.97	45.28	0.69
		2.30	1.42	0.0015	1.67	0.0018	0.78	3.03	0.0012	0.77	3.07	0.0017	45.68	45.05	0.63
		2.30	1.39	0.0022	1.65	0.0020	0.76	3.01	0.0029	0.75	3.05	0.0021	46.00	45.19	0.81
		2.31	1.39	0.0045	1.65	0.0011	0.76	3.01	0.0019	0.75	3.05	0.0008	46.00	45.34	0.66
		2.28	1.40	0.0032	1.65	0.0014	0.76	3.01	0.0046	0.75	3.05	0.0039	45.98	45.38	0.60
		2.29	1.40	0.0033	1.65	0.0007	0.76	3.02	0.0013	0.76	3.05	0.0058	45.96	45.66	0.30
		2.29	1.39	0.0033	1.65	0.0014	0.76	3.01	0.0080	0.75	3.05	0.0064	45.98	45.30	0.68
		2.30	1.40	0.0006	1.65	0.0018	0.76	3.02	0.0035	0.76	3.05	0.0025	45.96	45.58	0.38
		2.30	1.39	0.0011	1.65	0.0031	0.76	3.01	0.0042	0.75	3.05	0.0031	45.99	45.33	0.66
		2.30	1.38	0.0029	1.64	0.0059	0.75	3.00	0.0024	0.74	3.04	0.0059	46.13	45.64	0.50
		2.30	1.39	0.0016	1.65	0.0021	0.76	3.01	0.0042	0.75	3.05	0.0062	45.98	45.30	0.67
		2.32	1.38	0.0040	1.64	0.0016	0.75	3.00	0.0033	0.74	3.04	0.0037	46.14	45.66	0.48
		2.28	1.40	0.0005	1.65	0.0035	0.76	3.01	0.0022	0.75	3.05	0.0043	45.97	45.33	0.64
		2.30	1.40	0.0039	1.65	0.0034	0.76	3.01	0.0022	0.75	3.05	0.0032	45.97	45.37	0.60
		2.30	1.41	0.0092	1.67	0.0020	0.78	3.03	0.0011	0.77	3.07	0.0034	45.69	44.68	1.01
		2.30	1.39	0.0029	1.65	0.0006	0.76	3.01	0.0032	0.75	3.05	0.0020	45.98	45.31	0.67
		2.32	1.34	0.0022	1.63	0.0019	0.75	3.00	0.0012	0.74	3.04	0.0036	46.21	44.28	1.93
		2.29	1.40	0.0095	1.66	0.0011	0.77	3.02	0.0015	0.76	3.06	0.0018	45.82	44.96	0.86
		2.29	1.40	0.0017	1.65	0.0046	0.76	3.01	0.0021	0.75	3.05	0.0016	45.97	45.33	0.64
		2.30	1.37	0.0039	1.63	0.0034	0.74	2.99	0.0006	0.73	3.03	0.0021	46.29	45.98	0.31
		2.30	1.38	0.0020	1.64	0.0064	0.75	3.00	0.0019	0.74	3.04	0.0056	46.14	45.65	0.49
		2.31	1.38	0.0021	1.64	0.0118	0.75	3.01	0.0015	0.74	3.04	0.0013	46.12	45.60	0.51
		2.32	1.37	0.0046	1.63	0.0055	0.74	2.99	0.0039	0.73	3.03	0.0028	46.33	46.06	0.27
		2.28	1.41	0.0039	1.67	0.0036	0.78	3.03	0.0034	0.77	3.07	0.0096	45.68	44.66	1.02
		2.30	1.41	0.0091	1.67	0.0017	0.78	3.03	0.0034	0.77	3.07	0.0017	45.71	44.72	0.99
		2.30	1.41	0.0091	1.66	0.0053	0.77	3.02	0.0011	0.76	3.06	0.0011	45.85	45.41	0.44
		2.31	1.39	0.0018	1.65	0.0006	0.76	3.01	0.0046	0.75	3.05	0.0029	45.99	45.32	0.67
		2.32	1.38	0.0016	1.64	0.0020	0.75	3.00	0.0015	0.74	3.04	0.0026	46.15	45.68	0.47
		1.41	0.58	0.0012	2.43	0.0089	0.44	3.19	0.0032	0.44	3.22	0.0036	24.59	23.86	0.73
		1.41	0.58	0.0038	2.43	0.0020	0.44	3.19	0.0019	0.44	3.22	0.0118	24.60	23.93	0.67
		1.40	0.59	0.0007	2.44	0.0096	0.45	3.20	0.0016	0.45	3.23	0.0031	24.51	23.45	1.06
		1.41	0.59	0.0051	2.43	0.0035	0.45	3.19	0.0032	0.44	3.22	0.0064	24.57	23.76	0.81
		1.41	0.58	0.0021	2.43	0.0044	0.44	3.19	0.0011	0.44	3.22	0.0010	24.59	23.85	0.73
		1.41	0.58	0.0080	2.42	0.0014	0.44	3.18	0.0028	0.43	3.21	0.0086	24.62	24.05	0.58
		1.41	0.57	0.0019	2.42	0.0040	0.43	3.18	0.0046	0.43	3.21	0.0007	24.66	24.26	0.40
		1.42	0.57	0.0037	2.42	0.0025	0.44	3.18	0.0015	0.43	3.21	0.0016	24.66	24.25	0.41
		1.40	0.58	0.0063	2.43	0.0017	0.44	3.19	0.0046	0.44	3.22	0.0084	24.59	23.88	0.71
		1.41	0.58	0.0004	2.43	0.0039	0.44	3.19	0.0016	0.44	3.22	0.0007	24.59	23.86	0.72
		1.41	0.60	0.0017	2.45	0.0023	0.46	3.21	0.0016	0.46	3.24	0.0014	24.44	23.11	1.33
		1.41	0.58	0.0011	2.40	0.0043	0.42	3.16	0.0013	0.41	3.19	0.0055	24.80	25.05	-0.25
		1.43	0.57	0.0047	2.41	0.0064	0.43	3.17	0.0013	0.42	3.20	0.0032	24.71	24.50	0.20
		1.40	0.59	0.0011	2.43	0.0076	0.45	3.19	0.0013	0.44	3.22	0.0017	24.57	23.78	0.79
		1.41	0.58	0.0008	2.43	0.0018	0.44	3.19	0.0026	0.44	3.22	0.0020	24.59	23.87	0.72
		1.41	0.58	0.0028	2.43	0.0026	0.44	3.19	0.0021	0.44	3.22	0.0088	24.60	23.92	0.68

MD2 Top	Vesicular brown pumice	1.43	0.56	0.0012	2.42	0.0050	0.44	3.16	0.0037	0.43	3.21	0.0015	24.64	24.14	0.50	
		1.39	0.56	0.0025	2.43	0.0013	0.44	3.19	0.0055	0.44	3.22	0.0017	24.60	23.90	0.70	
		1.39	0.60	0.0008	2.45	0.0016	0.46	3.21	0.0056	0.46	3.24	0.0096	24.43	23.06	1.38	
		1.41	0.56	0.0035	2.43	0.0034	0.44	3.19	0.0015	0.44	3.22	0.0067	24.60	23.90	0.70	
		1.41	0.61	0.0042	2.45	0.0024	0.47	3.21	0.0056	0.46	3.24	0.0046	24.43	23.01	1.41	
		1.42	0.56	0.0026	2.42	0.0043	0.44	3.16	0.0009	0.43	3.21	0.0090	24.66	24.23	0.43	
		1.41	0.56	0.0062	2.43	0.0076	0.44	3.19	0.0031	0.44	3.22	0.0026	24.60	23.91	0.69	
		1.40	0.59	0.0036	2.44	0.0057	0.45	3.20	0.0077	0.45	3.23	0.0066	24.52	23.47	1.04	
		1.41	0.60	0.0072	2.44	0.0031	0.46	3.20	0.0011	0.46	3.24	0.0059	24.46	23.21	1.25	
		1.41	0.56	0.0029	2.43	0.0032	0.44	3.19	0.0015	0.44	3.22	0.0014	24.60	23.91	0.68	
		1.42	0.56	0.0031	2.43	0.0006	0.44	3.19	0.0033	0.44	3.22	0.0056	24.60	23.92	0.68	
		1.42	0.56	0.0092	2.42	0.0011	0.44	3.16	0.0041	0.43	3.21	0.0007	24.62	24.05	0.58	
		1.44	0.57	0.0024	2.42	0.0062	0.43	3.16	0.0051	0.43	3.21	0.0030	24.65	24.34	0.33	
		Dense (less vesicular) dark pumice	3.24	1.79	0.0034	1.67	0.0016	1.10	3.04	0.0021	1.06	3.05	0.0011	36.54	36.27	0.27
			3.25	1.77	0.0064	1.65	0.0008	1.05	3.02	0.0091	1.06	3.03	0.0039	36.60	36.71	0.09
	3.25		1.76	0.0025	1.66	0.0067	1.09	3.03	0.0036	1.07	3.04	0.0092	36.67	36.49	0.18	
	3.27		1.79	0.0026	1.67	0.0069	1.10	3.04	0.0026	1.06	3.05	0.0006	36.54	36.27	0.27	
	3.27		1.76	0.0013	1.65	0.0014	1.05	3.02	0.0033	1.06	3.03	0.0044	36.61	36.73	0.08	
	3.27		1.76	0.0013	1.65	0.0056	1.07	3.02	0.0017	1.06	3.02	0.0084	36.69	36.67	0.02	
	3.24		1.76	0.0015	1.65	0.0051	1.06	3.02	0.0012	1.06	3.03	0.0046	36.60	36.72	0.06	
	3.26		1.76	0.0023	1.67	0.0072	1.10	3.04	0.0090	1.06	3.04	0.0052	36.61	36.39	0.22	
	3.26		1.77	0.0092	1.66	0.0047	1.09	3.03	0.0017	1.07	3.03	0.0046	36.74	36.61	0.13	
	3.27		1.79	0.0010	1.67	0.0091	1.10	3.04	0.0012	1.06	3.05	0.0012	36.53	36.25	0.28	
	3.27		1.76	0.0037	1.64	0.0034	1.07	3.01	0.0091	1.05	3.02	0.0041	36.91	36.91	0.00	
	3.27		1.76	0.0017	1.65	0.0092	1.06	3.02	0.0099	1.06	3.02	0.0006	36.62	36.75	0.07	
	3.27		1.76	0.0007	1.64	0.0055	1.07	3.01	0.0057	1.05	3.02	0.0041	36.91	36.91	0.01	
	3.26		1.75	0.0009	1.64	0.0012	1.07	3.01	0.0077	1.05	3.01	0.0061	36.01	36.06	-0.07	
	3.26		1.76	0.0010	1.65	0.0011	1.06	3.02	0.0021	1.06	3.03	0.0031	36.61	36.72	0.06	
	3.27		1.76	0.0015	1.65	0.0016	1.06	3.02	0.0091	1.06	3.02	0.0024	36.61	36.74	0.07	
	3.26		1.76	0.0076	1.65	0.0023	1.06	3.02	0.0011	1.06	3.03	0.0046	36.61	36.74	0.06	
	3.26		1.76	0.0060	1.65	0.0029	1.06	3.02	0.0094	1.06	3.02	0.0064	36.63	36.76	0.07	
	3.29		1.76	0.0030	1.64	0.0053	1.07	3.01	0.0039	1.05	3.02	0.0096	36.92	36.92	0.00	
	3.26		1.77	0.0031	1.65	0.0050	1.06	3.02	0.0035	1.06	3.03	0.0014	36.76	36.69	0.10	
3.26	1.77		0.0010	1.65	0.0022	1.06	3.02	0.0022	1.06	3.03	0.0094	36.76	36.69	0.10		
3.27	1.76		0.0025	1.65	0.0011	1.06	3.02	0.0053	1.06	3.03	0.0026	36.61	36.72	0.06		
3.27	1.76		0.0009	1.65	0.0041	1.06	3.02	0.0066	1.06	3.02	0.0006	36.62	36.74	0.07		
3.29	1.74		0.0012	1.62	0.0011	1.05	2.99	0.0025	1.03	3.00	0.0020	39.17	39.36	-0.16		
3.26	1.76	0.0035	1.66	0.0027	1.09	3.03	0.0011	1.07	3.04	0.0023	36.66	36.47	0.16			
3.27	1.77	0.0067	1.65	0.0099	1.06	3.02	0.0063	1.06	3.03	0.0027	36.60	36.71	0.09			
3.27	1.77	0.0020	1.65	0.0026	1.06	3.02	0.0010	1.06	3.03	0.0026	36.60	36.71	0.09			
3.27	1.74	0.0015	1.63	0.0014	1.06	3.00	0.0023	1.04	3.00	0.0029	39.13	39.26	-0.15			
3.29	1.75	0.0042	1.64	0.0041	1.07	3.01	0.0039	1.05	3.01	0.0046	36.96	36.99	-0.03			
MD2 Base-Middle	Vesic. brown pumice	7.00	4.16	0.0036	1.69	0.0097	2.43	2.69	0.0014	2.43	2.90	0.0076	41.79	41.60	0.19	
		7.01	4.16	0.0011	1.69	0.0034	2.43	2.69	0.0046	2.44	2.90	0.0009	41.79	41.66	0.14	
		7.01	4.17	0.0039	1.71	0.0025	2.45	2.91	0.0019	2.44	2.90	0.0012	41.23	41.26	-0.03	
		7.01	4.16	0.0035	1.69	0.0022	2.43	2.69	0.0021	2.44	2.90	0.0024	41.76	41.59	0.17	
		6.99	4.19	0.0042	1.71	0.0011	2.45	2.91	0.0009	2.43	2.91	0.0067	41.24	41.50	-0.26	
		7.02	4.15	0.0011	1.66	0.0012	2.42	2.66	0.0072	2.42	2.90	0.0011	42.15	41.66	0.49	
		7.02	4.15	0.0015	1.69	0.0023	2.43	2.69	0.0025	2.42	2.69	0.0046	41.72	41.60	0.12	

MD2 Base-Middle	Vesicular brown pumice	7.02	4.15	0.0039	1.65	0.0021	2.41	2.55	0.0012	2.42	2.90	0.0039	42.14	41.97	0.17
		7.00	4.16	0.0059	1.69	0.0020	2.43	2.59	0.0031	2.44	2.94	0.0031	42.53	41.60	0.93
		7.01	4.16	0.0013	1.69	0.0037	2.43	2.59	0.0031	2.43	2.90	0.0026	41.79	41.70	0.08
		7.01	4.17	0.0025	1.71	0.0021	2.44	2.91	0.0061	2.43	2.90	0.0037	41.16	41.45	-0.28
		7.01	4.15	0.0016	1.69	0.0018	2.42	2.59	0.0050	2.43	2.90	0.0011	41.53	41.59	0.24
		7.02	4.14	0.0019	1.65	0.0020	2.42	2.55	0.0029	2.43	2.90	0.0057	42.09	41.47	0.62
		7.02	4.14	0.0057	1.67	0.0015	2.42	2.57	0.0012	2.41	2.57	0.0029	41.70	41.64	0.07
		7.01	4.16	0.0075	1.69	0.0112	2.43	2.59	0.0017	2.43	2.90	0.0017	41.79	41.51	0.15
		7.01	4.16	0.0022	1.70	0.0045	2.43	2.90	0.0012	2.43	2.90	0.0031	41.54	41.45	0.06
		7.01	4.16	0.0005	1.69	0.0055	2.43	2.59	0.0059	2.42	2.90	0.0015	41.50	41.62	0.15
		7.01	4.15	0.0039	1.65	0.0054	2.42	2.55	0.0017	2.42	2.90	0.0031	42.14	41.79	0.34
		7.02	4.16	0.0005	1.69	0.0115	2.43	2.59	0.0035	2.41	2.90	0.0010	41.75	41.62	0.16
		7.03	4.12	0.0012	1.65	0.0053	2.40	2.57	0.0050	2.40	2.59	0.0005	42.45	41.55	0.64
		6.99	4.15	0.0039	1.71	0.0033	2.45	2.91	0.0051	2.43	2.90	0.0052	41.10	41.39	-0.29
		7.00	4.17	0.0022	1.70	0.0004	2.44	2.90	0.0015	2.43	2.90	0.0025	41.44	41.49	-0.05
		7.01	4.16	0.0022	1.69	0.0025	2.43	2.59	0.0011	2.42	2.57	0.0015	41.22	41.62	-0.40
		7.01	4.16	0.0027	1.67	0.0055	2.40	2.57	0.0075	2.43	2.59	0.0015	42.35	42.20	0.15
		7.03	4.14	0.0005	1.65	0.0024	2.41	2.55	0.0024	2.43	2.59	0.0052	42.05	41.71	0.35
		7.00	4.16	0.0035	1.69	0.0032	2.43	2.59	0.0015	2.43	2.93	0.0011	42.41	41.62	0.75
		7.00	4.16	0.0012	1.70	0.0050	2.44	2.90	0.0034	2.45	2.90	0.0077	41.43	41.40	0.03
7.01	4.16	0.0012	1.69	0.0055	2.43	2.59	0.0047	2.44	2.90	0.0034	41.75	41.53	0.13		
7.02	4.14	0.0007	1.69	0.0015	2.42	2.59	0.0053	2.43	2.90	0.0029	41.50	41.35	0.44		
MD1 Middle-Top	Vesicular brown pumice	4.45	2.24	0.0005	1.99	0.0010	1.54	2.90	0.0013	1.50	2.95	0.0032	32.55	31.45	1.10
		4.45	2.24	0.0039	2.00	0.0094	1.53	2.90	0.0044	1.50	2.95	0.0029	32.45	31.54	0.52
		4.45	2.24	0.0045	1.97	0.0035	1.53	2.90	0.0050	1.50	2.95	0.0040	33.49	31.51	1.55
		4.45	2.24	0.0022	1.95	0.0015	1.53	2.90	0.0047	1.50	2.95	0.0020	32.91	31.55	1.27
		4.45	2.24	0.0032	1.95	0.0059	1.51	2.90	0.0055	1.50	2.95	0.0043	32.57	32.47	0.20
		4.43	2.24	0.0015	1.95	0.0020	1.54	2.93	0.0052	1.50	2.95	0.0054	33.01	31.54	1.45
		4.44	2.25	0.0004	1.99	0.0075	1.54	2.94	0.0022	1.50	2.97	0.0031	32.75	31.55	1.21
		4.45	2.25	0.0035	1.99	0.0012	1.55	2.91	0.0043	1.52	2.97	0.0031	32.51	31.75	1.05
		4.45	2.27	0.0039	1.99	0.0021	1.55	2.91	0.0032	1.52	2.95	0.0015	32.52	30.95	1.55
		4.45	2.22	0.0013	1.95	0.0005	1.53	2.90	0.0049	1.45	2.94	0.0052	32.53	30.55	1.77
		4.45	2.24	0.0020	1.95	0.0029	1.52	2.90	0.0012	1.49	2.94	0.0014	32.50	31.53	0.95
		4.45	2.24	0.0011	1.95	0.0011	1.51	2.90	0.0029	1.49	2.95	0.0013	32.55	32.33	0.35
		4.45	2.24	0.0005	1.95	0.0032	1.52	2.57	0.0053	1.45	2.95	0.0015	33.53	31.93	1.50
		4.45	2.25	0.0025	1.95	0.0053	1.53	2.90	0.0041	1.51	2.97	0.0004	33.10	31.75	1.32
		4.45	2.24	0.0005	2.00	0.0041	1.54	2.90	0.0015	1.50	2.95	0.0075	32.54	31.52	1.01
		4.45	2.24	0.0052	1.95	0.0035	1.53	2.57	0.0057	1.50	2.93	0.0014	32.45	31.51	0.55
		4.45	2.23	0.0015	1.97	0.0029	1.53	2.90	0.0055	1.49	2.95	0.0035	33.15	31.21	1.95
		4.45	2.22	0.0050	1.95	0.0040	1.50	2.90	0.0021	1.47	2.91	0.0055	32.92	32.15	0.77
		4.42	2.25	0.0025	1.95	0.0034	1.55	2.90	0.0057	1.52	2.95	0.0053	32.90	31.35	1.55
		4.45	2.24	0.0029	1.99	0.0044	1.54	2.90	0.0039	1.50	2.95	0.0010	33.14	31.31	1.53
		4.45	2.25	0.0021	1.99	0.0044	1.55	2.90	0.0033	1.52	2.95	0.0041	33.03	31.43	1.59
		4.45	2.24	0.0019	1.95	0.0047	1.53	2.90	0.0005	1.50	2.95	0.0017	32.57	31.51	1.05
		4.45	2.24	0.0015	1.95	0.0017	1.53	2.90	0.0019	1.49	2.95	0.0032	32.94	31.40	1.54
		4.45	2.23	0.0075	1.95	0.0050	1.52	2.90	0.0042	1.49	2.95	0.0055	32.55	31.54	0.51
		4.41	2.24	0.0051	1.99	0.0012	1.54	2.90	0.0025	1.50	2.95	0.0055	32.55	31.53	1.33
		4.45	2.24	0.0057	1.95	0.0015	1.53	2.90	0.0032	1.50	2.95	0.0055	32.55	31.52	1.24
4.44	2.25	0.0015	2.01	0.0021	1.54	2.90	0.0040	1.51	2.95	0.0042	32.00	31.75	0.22		

		4.45	2.26	0.0013	1.96	0.0049	1.55	2.90	0.0034	1.51	2.96	0.0035	33.03	31.46	1.56
		4.45	2.25	0.0032	1.99	0.0061	1.54	2.90	0.0056	1.50	2.96	0.0020	32.63	31.55	1.26
		4.45	2.24	0.0026	1.97	0.0040	1.53	2.90	0.0033	1.50	2.95	0.0011	33.15	31.61	1.54
MD1 Base	Dense (less vesicular) dark pumice	3.79	2.02	0.0017	1.87	0.0022	1.26	2.92	0.0064	1.25	3.02	0.0093	35.11	37.50	0.61
		3.60	2.02	0.0030	1.86	0.0015	1.26	2.93	0.0061	1.25	2.99	0.0095	37.02	37.61	-0.59
		3.60	2.02	0.0069	1.86	0.0034	1.26	2.95	0.0031	1.26	2.99	0.0014	37.66	36.41	1.25
		3.61	2.01	0.0097	1.86	0.0039	1.25	2.92	0.0060	1.25	2.96	0.0092	37.03	37.76	-0.75
		3.61	2.00	0.0053	1.86	0.0046	1.26	2.92	0.0055	1.25	2.96	0.0056	37.42	36.91	0.52
		3.61	2.01	0.0021	1.86	0.0099	1.26	2.92	0.0014	1.25	2.99	0.0064	37.66	37.41	0.25
		3.75	2.01	0.0026	1.87	0.0053	1.26	2.92	0.0006	1.26	2.99	0.0027	37.44	37.43	0.02
		3.60	2.02	0.0013	1.86	0.0008	1.26	2.93	0.0012	1.26	2.99	0.0015	37.26	36.71	0.56
		3.61	2.01	0.0011	1.85	0.0068	1.25	2.91	0.0056	1.25	2.99	0.0011	37.97	37.69	0.28
		3.61	2.01	0.0094	1.86	0.0012	1.25	2.90	0.0041	1.25	2.99	0.0094	37.91	37.76	0.15
		3.62	2.01	0.0055	1.86	0.0022	1.24	2.92	0.0023	1.25	2.99	0.0011	37.67	37.96	-0.29
		3.60	2.02	0.0027	1.86	0.0015	1.26	2.93	0.0031	1.25	2.99	0.0013	37.04	36.96	0.08
		3.60	2.02	0.0034	1.86	0.0010	1.26	2.92	0.0076	1.25	2.99	0.0080	37.67	37.74	-0.07
		3.60	2.03	0.0015	1.87	0.0015	1.26	2.92	0.0020	1.25	3.00	0.0017	37.55	37.66	-0.33
		3.62	1.99	0.0022	1.86	0.0012	1.25	2.91	0.0092	1.22	2.96	0.0041	37.46	37.27	0.19
		3.72	2.02	0.0071	1.86	0.0046	1.26	2.92	0.0006	1.25	2.99	0.0041	37.61	37.46	0.15
		3.77	2.02	0.0024	1.87	0.0017	1.26	2.94	0.0041	1.25	3.00	0.0015	37.74	36.43	1.30
		3.60	2.03	0.0076	1.87	0.0004	1.26	2.92	0.0009	1.25	2.99	0.0006	37.62	37.62	-0.20
		3.60	2.01	0.0049	1.86	0.0045	1.26	2.92	0.0035	1.25	2.99	0.0039	37.66	37.46	0.20
		3.60	2.01	0.0026	1.84	0.0024	1.26	2.92	0.0031	1.22	2.99	0.0094	36.26	37.42	0.66
		3.60	2.01	0.0015	1.85	0.0007	1.24	2.92	0.0061	1.25	2.99	0.0041	37.98	36.66	-0.70
		3.62	1.96	0.0007	1.82	0.0017	1.23	2.89	0.0099	1.25	2.99	0.0046	39.07	37.93	1.14
		3.75	2.04	0.0012	1.87	0.0017	1.27	2.92	0.0009	1.25	2.99	0.0022	37.64	37.75	-0.12
		3.79	2.02	0.0022	1.87	0.0067	1.26	2.92	0.0037	1.29	3.00	0.0027	37.51	37.67	-0.16
		3.79	2.01	0.0015	1.87	0.0051	1.27	2.93	0.0027	1.25	3.02	0.0006	36.03	36.66	1.15
		3.60	2.01	0.0022	1.87	0.0011	1.27	2.92	0.0013	1.25	2.99	0.0066	37.29	37.19	0.10
		3.61	2.01	0.0014	1.86	0.0032	1.26	2.91	0.0023	1.25	2.99	0.0006	37.63	37.60	0.03
		3.61	2.00	0.0099	1.86	0.0031	1.26	2.92	0.0061	1.25	2.99	0.0023	37.72	37.17	0.55
		3.62	2.01	0.0060	1.86	0.0010	1.26	2.90	0.0039	1.25	2.99	0.0015	37.91	37.53	0.36
		3.63	2.01	0.0060	1.85	0.0014	1.25	2.91	0.0007	1.24	2.95	0.0020	37.10	36.02	-0.92
Average					1.89			2.96			3.01		37.36	36.62	0.54
MD3					1.77			2.97			3.00		41.11	40.47	0.64
MD2					1.99			3.03			3.05		35.06	34.74	0.33
MD1					1.92			2.91			2.97		35.25	34.54	0.71
D.lith	7.65	2.13	0.0053	2.69	0.0092	2.71	2.90	0.0021	2.57	2.90	0.0047	7.31	-27.31	34.62	
D.lith	9.72	3.80	0.0029	2.56	0.0019	3.36	2.89	0.0012	2.66	2.90	0.0032	11.63	11.34	0.46	
D.lith	3.75	1.79	0.0035	2.90	0.0041	1.30	2.66	0.0004	1.23	2.96	0.0022	1.90	27.14	-25.24	
D.lith	9.51	2.93	0.0090	2.65	0.0012	3.31	2.66	0.0040	3.16	2.89	0.0016	1.20	-13.10	14.30	
D.lith	9.52	3.35	0.0049	2.64	0.0042	3.21	2.96	0.0044	2.90	2.97	0.0011	4.39	4.06	0.33	
Avg D.lith					2.77		2.90			2.92		5.33	0.43	4.90	

Upper Inglewood bed-set

	Wgt g	Envelope (Bulk) Density				Skeletal Density			Solid Density			Porosity		
		cm3	SD	g/cm3	SD	cm3	g/cm3	Vol SD	cm3	g/cm3	Vol SD	Bulk %	Conn %	Iso %
Dense grey pumice 1 (often banded)	3.47	3.26	0.0029	1.07	0.0091	1.25	2.79	0.0097	1.23	2.63	0.0024	61.96	61.62	0.37
	3.49	3.27	0.0060	1.06	0.0030	1.25	2.61	0.0067	1.24	2.63	0.0025	61.95	61.66	0.29
	3.49	3.27	0.0007	1.06	0.0022	1.26	2.61	0.0064	1.24	2.63	0.0064	61.76	60.81	0.97
	3.50	3.26	0.0006	1.07	0.0010	1.25	2.60	0.0011	1.24	2.63	0.0057	62.03	61.58	0.45
	3.50	3.26	0.0033	1.06	0.0008	1.25	2.61	0.0041	1.24	2.63	0.0006	61.69	61.66	-0.17
	3.50	3.26	0.0097	1.07	0.0022	1.25	2.79	0.0007	1.23	2.62	0.0061	62.09	61.61	0.46
	3.50	3.25	0.0037	1.07	0.0020	1.22	2.76	0.0095	1.23	2.63	0.0031	62.05	62.45	-0.41
	3.51	3.26	0.0037	1.07	0.0064	1.25	2.79	0.0060	1.23	2.62	0.0075	62.01	61.65	0.36
	3.50	3.26	0.0061	1.07	0.0020	1.25	2.79	0.0021	1.23	2.63	0.0043	62.04	61.62	0.42
	3.51	3.26	0.0099	1.06	0.0014	1.25	2.79	0.0013	1.21	2.62	0.0089	62.31	61.64	0.67
	3.49	3.26	0.0055	1.06	0.0010	1.26	2.60	0.0025	1.23	2.66	0.0064	62.20	61.37	0.63
	3.50	3.26	0.0017	1.07	0.0069	1.25	2.79	0.0014	1.23	2.63	0.0036	62.04	61.63	0.40
	3.51	3.25	0.0013	1.07	0.0006	1.25	2.76	0.0015	1.23	2.62	0.0099	62.03	61.44	0.59
	3.51	3.25	0.0015	1.07	0.0017	1.24	2.76	0.0017	1.22	2.60	0.0026	61.62	61.62	-0.19
	3.49	3.26	0.0032	1.06	0.0041	1.26	2.79	0.0050	1.23	2.63	0.0051	61.65	60.71	1.14
	3.50	3.24	0.0046	1.06	0.0025	1.25	2.77	0.0016	1.23	2.62	0.0017	62.34	61.39	0.95
	3.50	3.26	0.0024	1.06	0.0058	1.25	2.79	0.0027	1.21	2.62	0.0067	62.31	61.56	0.74
	3.52	3.23	0.0011	1.03	0.0095	1.25	2.77	0.0116	1.20	2.62	0.0023	63.46	61.29	2.16
	3.48	3.26	0.0012	1.06	0.0021	1.26	2.61	0.0067	1.25	2.63	0.0026	61.95	61.62	0.33
	3.48	3.26	0.0076	1.06	0.0006	1.25	2.60	0.0026	1.23	2.66	0.0012	62.22	61.60	0.62
	3.50	3.26	0.0053	1.09	0.0072	1.25	2.61	0.0009	1.25	2.63	0.0020	61.33	61.72	-0.39
	3.50	3.26	0.0056	1.06	0.0039	1.26	2.60	0.0031	1.23	2.63	0.0026	61.77	61.40	0.36
	3.50	3.26	0.0011	1.07	0.0095	1.25	2.62	0.0059	1.26	2.63	0.0037	62.13	61.67	0.26
	3.50	3.25	0.0062	1.06	0.0018	1.25	2.76	0.0022	1.22	2.63	0.0023	62.40	61.56	0.62
	3.53	3.25	0.0014	1.06	0.0007	1.21	2.76	0.0071	1.22	2.62	0.0021	62.30	62.77	-0.47
	3.50	3.26	0.0015	1.09	0.0035	1.25	2.60	0.0027	1.24	2.63	0.0094	61.33	61.57	-0.24
	3.50	3.27	0.0041	1.06	0.0016	1.25	2.60	0.0015	1.23	2.63	0.0093	61.66	61.66	0.00
	3.48	3.26	0.0096	1.07	0.0004	1.25	2.60	0.0014	1.23	2.63	0.0012	61.97	61.59	0.38
3.50	3.26	0.0055	1.05	0.0033	1.25	2.79	0.0062	1.23	2.60	0.0007	62.39	61.71	0.66	
3.50	3.26	0.0094	1.07	0.0031	1.24	2.79	0.0027	1.23	2.62	0.0039	62.04	61.97	0.07	
Very Dense grey pumice 2	5.99	4.39	0.0003	1.37	0.0015	2.27	2.64	0.0020	2.25	2.66	0.0020	46.60	46.20	0.40
	6.00	4.42	0.0066	1.36	0.0096	2.27	2.65	0.0035	2.25	2.67	0.0001	46.43	46.63	-0.20
	6.00	4.39	0.0026	1.37	0.0041	2.29	2.66	0.0059	2.25	2.67	0.0016	46.60	47.62	0.97
	6.01	4.39	0.0010	1.37	0.0049	2.29	2.67	0.0012	2.27	2.66	0.0027	46.57	47.62	0.74
	6.02	4.36	0.0026	1.37	0.0010	2.26	2.64	0.0045	2.23	2.65	0.0023	46.44	46.44	0.00
	6.02	4.36	0.0015	1.33	0.0031	2.26	2.63	0.0037	2.23	2.65	0.0032	49.97	46.39	1.56
	5.99	4.39	0.0003	1.36	0.0030	2.29	2.66	0.0007	2.26	2.67	0.0023	46.32	47.75	0.56
	6.00	4.42	0.0033	1.37	0.0027	2.27	2.64	0.0007	2.25	2.67	0.0001	46.67	46.56	0.11
	6.01	4.39	0.0019	1.37	0.0051	2.28	2.65	0.0012	2.25	2.66	0.0001	46.52	47.96	0.56
	6.01	4.39	0.0003	1.40	0.0025	2.28	2.66	0.0059	2.25	2.67	0.0001	47.57	47.97	-0.40
	6.01	4.39	0.0003	1.40	0.0022	2.27	2.65	0.0035	2.25	2.67	0.0013	47.54	46.20	-0.66
	6.02	4.39	0.0023	1.37	0.0021	2.27	2.64	0.0056	2.25	2.66	0.0036	46.90	46.20	0.70
	5.96	4.39	0.0010	1.37	0.0037	2.29	2.66	0.0104	2.26	2.66	0.0009	46.66	47.79	1.06
	6.00	4.39	0.0026	1.37	0.0024	2.26	2.65	0.0031	2.24	2.67	0.0001	46.76	46.03	0.75
	6.00	4.39	0.0045	1.37	0.0029	2.27	2.64	0.0036	2.25	2.66	0.0012	46.54	46.20	0.34

Very Dense grey pumice 2	6.01	4.39	0.0010	1.37	0.0034	2.27	2.64	0.0036	2.24	2.66	0.0016	45.56	45.18	0.38
	6.01	4.39	0.0010	1.36	0.0023	2.27	2.64	0.0032	2.25	2.67	0.0106	45.45	45.18	0.27
	6.03	4.39	0.0098	1.37	0.0046	2.27	2.64	0.0022	2.24	2.66	0.0007	45.57	45.20	0.37
	5.96	4.36	0.0027	1.37	0.0011	2.27	2.64	0.0043	2.24	2.64	0.0031	45.29	47.87	0.43
	6.00	4.36	0.0018	1.37	0.0012	2.25	2.62	0.0032	2.24	2.65	0.0022	45.44	45.60	-0.16
	6.00	4.39	0.0047	1.37	0.0008	2.27	2.64	0.0080	2.24	2.66	0.0026	45.63	45.23	0.40
	5.97	4.36	0.0018	1.37	0.0041	2.27	2.64	0.0094	2.24	2.66	0.0093	45.54	45.21	0.33
	6.01	4.39	0.0014	1.34	0.0010	2.26	2.64	0.0026	2.24	2.66	0.0027	49.70	45.43	1.27
	6.03	4.36	0.0043	1.36	0.0010	2.27	2.64	0.0021	2.24	2.66	0.0011	49.01	45.20	0.81
	6.00	4.36	0.0037	1.37	0.0010	2.26	2.64	0.0043	2.22	2.65	0.0024	45.46	45.40	0.06
	6.00	4.36	0.0013	1.37	0.0010	2.27	2.64	0.0026	2.24	2.66	0.0029	45.60	45.16	0.44
	6.00	4.36	0.0013	1.37	0.0025	2.27	2.64	0.0030	2.22	2.65	0.0015	45.46	45.21	0.25
	6.01	4.36	0.0003	1.37	0.0040	2.26	2.63	0.0055	2.24	2.66	0.0034	45.57	45.43	0.14
	6.01	4.35	0.0003	1.36	0.0021	2.26	2.64	0.0024	2.23	2.66	0.0009	45.94	45.19	0.75
	6.01	4.36	0.0003	1.37	0.0035	2.25	2.62	0.0058	2.21	2.62	0.0038	47.75	45.67	-0.92
Vesicular Y-W pumice 1	1.97	2.95	0.0013	0.65	0.0017	0.69	2.86	0.0055	0.68	2.91	0.0089	76.51	76.64	0.13
	1.97	2.91	0.0007	0.67	0.0031	0.69	2.86	0.0012	0.67	2.88	0.0014	76.77	76.47	0.30
	1.95	2.94	0.0051	0.67	0.0027	0.69	2.86	0.0039	0.67	2.90	0.0037	76.92	76.67	0.25
	1.95	2.95	0.0020	0.65	0.0041	0.69	2.90	0.0041	0.69	2.91	0.0057	76.55	76.64	-0.09
	1.97	2.94	0.0061	0.67	0.0038	0.70	2.87	0.0008	0.68	2.90	0.0022	76.91	76.32	0.59
	1.95	2.95	0.0023	0.69	0.0091	0.69	2.86	0.0095	0.70	2.90	0.0027	76.15	76.64	-0.49
	1.97	2.94	0.0011	0.66	0.0015	0.69	2.83	0.0012	0.67	2.90	0.0006	77.20	76.72	0.48
	1.95	2.94	0.0025	0.65	0.0095	0.65	2.86	0.0013	0.66	2.90	0.0062	77.46	76.94	0.52
	1.93	2.94	0.0059	0.67	0.0016	0.69	2.86	0.0017	0.68	2.90	0.0016	76.91	76.60	0.31
	1.95	2.94	0.0014	0.69	0.0010	0.69	2.87	0.0097	0.70	2.90	0.0014	76.21	76.61	-0.40
	1.97	2.94	0.0024	0.67	0.0025	0.69	2.87	0.0064	0.68	2.92	0.0006	77.07	76.46	0.61
	1.97	2.94	0.0099	0.65	0.0021	0.70	2.87	0.0050	0.69	2.92	0.0075	76.55	76.35	0.20
	1.97	2.94	0.0028	0.67	0.0041	0.70	2.87	0.0011	0.68	2.91	0.0056	76.96	76.14	0.82
	1.97	2.94	0.0046	0.67	0.0028	0.69	2.86	0.0006	0.67	2.90	0.0017	77.02	76.64	0.38
	1.97	2.94	0.0015	0.67	0.0032	0.68	2.86	0.0029	0.67	2.90	0.0021	76.92	76.96	-0.05
	1.95	2.94	0.0006	0.67	0.0011	0.69	2.86	0.0080	0.67	2.89	0.0094	76.90	76.62	0.28
	1.99	2.94	0.0035	0.64	0.0027	0.66	2.86	0.0031	0.65	2.86	0.0007	77.56	77.62	-0.06
	1.95	2.94	0.0095	0.65	0.0009	0.71	2.87	0.0023	0.69	2.90	0.0020	76.56	75.72	0.85
	1.95	2.95	0.0012	0.67	0.0067	0.70	2.87	0.0006	0.68	2.91	0.0093	76.93	76.61	0.33
	1.97	2.95	0.0031	0.69	0.0008	0.70	2.86	0.0004	0.69	2.91	0.0015	76.29	76.36	-0.07
	1.97	2.94	0.0044	0.67	0.0010	0.69	2.86	0.0018	0.68	2.90	0.0014	76.92	76.63	0.29
	1.97	2.94	0.0020	0.64	0.0006	0.69	2.86	0.0097	0.65	2.89	0.0006	77.69	76.61	1.09
	1.95	2.94	0.0037	0.66	0.0099	0.69	2.86	0.0022	0.67	2.89	0.0096	77.07	76.63	0.43
	1.95	2.91	0.0094	0.66	0.0007	0.67	2.85	0.0014	0.66	2.90	0.0024	77.22	77.07	0.14
	1.99	2.94	0.0010	0.66	0.0009	0.69	2.82	0.0022	0.66	2.89	0.0084	77.25	76.60	0.64
	1.96	2.95	0.0007	0.67	0.0028	0.69	2.87	0.0009	0.68	2.91	0.0072	76.95	76.66	0.07
	1.95	2.94	0.0015	0.67	0.0033	0.69	2.89	0.0021	0.68	2.91	0.0067	76.89	76.49	0.41
	1.97	2.94	0.0039	0.67	0.0017	0.70	2.87	0.0025	0.68	2.90	0.0016	76.90	76.19	0.72
1.95	2.94	0.0071	0.67	0.0053	0.67	2.85	0.0076	0.68	2.90	0.0030	76.94	77.27	-0.33	
1.95	2.94	0.0026	0.66	0.0037	0.68	2.86	0.0043	0.66	2.89	0.0033	77.11	76.81	0.30	
3.20	4.15	0.0051	0.75	0.0023	1.22	2.72	0.0018	1.15	2.75	0.0012	71.51	70.72	0.79	
3.23	4.15	0.0032	0.79	0.0034	1.21	2.72	0.0036	1.15	2.75	0.0023	71.33	71.09	0.24	
3.23	4.15	0.0016	0.79	0.0011	1.20	2.71	0.0041	1.15	2.75	0.0018	71.41	71.30	0.11	
3.23	4.15	0.0045	0.75	0.0032	1.20	2.70	0.0019	1.16	2.75	0.0036	71.59	71.07	0.52	

Ug7		Intermediate Y-W pumice 2													
		3.23	4.14	0.0029	0.75	0.0014	1.19	2.70	0.0054	1.15	2.75	0.0048	71.60	71.30	0.30
		3.23	4.13	0.0033	0.75	0.0024	1.20	2.70	0.0015	1.13	2.74	0.0009	71.60	71.08	0.52
		3.24	4.14	0.0025	0.77	0.0011	1.18	2.70	0.0022	1.15	2.74	0.0015	71.68	71.63	0.25
		3.22	4.15	0.0027	0.75	0.0033	1.20	2.71	0.0073	1.18	2.75	0.0026	71.51	71.08	0.43
		3.23	4.15	0.0091	0.79	0.0024	1.21	2.72	0.0033	1.16	2.75	0.0089	71.22	70.89	0.34
		3.23	4.14	0.0033	0.77	0.0011	1.20	2.68	0.0058	1.15	2.74	0.0019	71.93	71.15	0.79
		3.24	4.14	0.0027	0.75	0.0021	1.18	2.70	0.0048	1.13	2.72	0.0021	71.26	71.40	-0.12
		3.19	4.15	0.0037	0.75	0.0048	1.20	2.70	0.0079	1.15	2.75	0.0006	71.54	71.10	0.45
		3.23	4.15	0.0105	0.79	0.0093	1.20	2.71	0.0104	1.16	2.75	0.0031	71.63	71.15	0.48
		3.23	4.15	0.0016	0.80	0.0018	1.21	2.72	0.0012	1.16	2.75	0.0021	70.87	70.82	0.05
		3.23	4.15	0.0035	0.75	0.0008	1.20	2.70	0.0029	1.16	2.75	0.0020	71.53	71.17	0.36
		3.19	4.14	0.0022	0.76	0.0053	1.20	2.70	0.0039	1.15	2.72	0.0030	72.06	71.14	0.92
		3.23	4.15	0.0028	0.75	0.0102	1.20	2.70	0.0040	1.14	2.74	0.0085	71.66	71.16	0.50
		3.26	4.15	0.0013	0.74	0.0008	1.16	2.68	0.0010	1.12	2.74	0.0050	73.08	71.91	1.18
		3.23	4.15	0.0022	0.79	0.0018	1.20	2.71	0.0019	1.15	2.75	0.0010	71.22	71.15	0.07
		3.15	4.15	0.0084	0.75	0.0021	1.23	2.73	0.0030	1.15	2.75	0.0014	71.07	70.43	1.23
		3.23	4.14	0.0030	0.77	0.0023	1.19	2.70	0.0014	1.14	2.75	0.0005	71.97	71.39	0.59
		3.24	4.14	0.0101	0.75	0.0014	1.20	2.70	0.0017	1.15	2.74	0.0019	71.58	71.17	0.41
		3.24	4.15	0.0022	0.75	0.0017	1.19	2.69	0.0034	1.14	2.74	0.0030	71.60	71.19	0.41
		3.26	4.10	0.0032	0.77	0.0009	1.18	2.69	0.0006	1.15	2.74	0.0016	71.69	71.18	0.71
		3.22	4.15	0.0012	0.79	0.0019	1.20	2.70	0.0033	1.15	2.75	0.0011	71.67	71.11	0.57
		3.23	4.15	0.0041	0.80	0.0011	1.20	2.70	0.0020	1.15	2.75	0.0006	70.87	71.00	-0.13
		3.23	4.15	0.0063	0.79	0.0020	1.20	2.70	0.0036	1.16	2.75	0.0021	71.32	71.14	0.18
		3.23	4.15	0.0057	0.75	0.0066	1.20	2.70	0.0011	1.15	2.75	0.0009	71.60	71.16	0.44
		3.23	4.12	0.0022	0.75	0.0023	1.20	2.70	0.0011	1.15	2.75	0.0008	71.61	70.98	0.64
		3.24	4.14	0.0054	0.77	0.0038	1.18	2.70	0.0030	1.15	2.74	0.0105	71.69	71.63	0.25
		3.20	3.72	0.0028	0.87	0.0069	1.17	2.81	0.0033	1.16	2.75	0.0027	68.31	68.58	-0.27
		3.22	3.70	0.0017	0.87	0.0042	1.15	2.81	0.0043	1.16	2.76	0.0069	68.38	68.97	-0.58
		3.22	3.70	0.0015	0.84	0.0027	1.15	2.79	0.0013	1.13	2.75	0.0086	69.33	68.95	0.37
		3.23	3.69	0.0100	0.87	0.0034	1.15	2.81	0.0069	1.16	2.75	0.0086	68.43	68.95	-0.52
		3.20	3.70	0.0035	0.90	0.0059	1.15	2.82	0.0032	1.19	2.75	0.0024	67.18	68.95	-1.80
		3.22	3.70	0.0077	0.87	0.0041	1.15	2.81	0.0006	1.16	2.75	0.0013	68.31	68.95	-0.64
		3.21	3.70	0.0036	0.87	0.0032	1.16	2.81	0.0010	1.16	2.75	0.0042	68.61	68.69	-0.08
		3.21	3.70	0.0028	0.91	0.0066	1.15	2.82	0.0008	1.20	2.76	0.0026	67.01	68.95	-1.93
		3.22	3.70	0.0032	0.87	0.0047	1.15	2.81	0.0008	1.16	2.77	0.0034	68.46	68.92	-0.47
		3.22	3.70	0.0007	0.87	0.0012	1.15	2.82	0.0012	1.16	2.77	0.0013	68.46	68.94	-0.48
		3.23	3.69	0.0101	0.87	0.0012	1.14	2.81	0.0016	1.16	2.75	0.0050	68.28	69.21	-0.93
		3.23	3.70	0.0039	0.87	0.0025	1.15	2.81	0.0016	1.16	2.73	0.0027	68.12	68.95	-0.83
		3.24	3.69	0.0039	0.87	0.0076	1.14	2.81	0.0110	1.16	2.74	0.0017	68.25	69.23	-0.98
		3.22	3.70	0.0035	0.87	0.0029	1.15	2.81	0.0032	1.16	2.75	0.0034	68.35	68.97	-0.62
		3.22	3.70	0.0014	0.87	0.0035	1.16	2.82	0.0064	1.16	2.75	0.0042	68.23	68.71	-0.49
		3.23	3.70	0.0010	0.87	0.0009	1.13	2.80	0.0009	1.16	2.75	0.0064	68.51	69.50	-0.99
		3.23	3.70	0.0004	0.87	0.0016	1.15	2.81	0.0010	1.16	2.74	0.0064	68.23	68.96	-0.74
		3.24	3.66	0.0050	0.84	0.0011	1.13	2.81	0.0085	1.13	2.73	0.0089	69.20	69.25	-0.06
		3.24	3.66	0.0048	0.87	0.0017	1.12	2.77	0.0086	1.16	2.72	0.0089	68.14	69.31	-1.17
		3.19	3.70	0.0027	0.87	0.0091	1.15	2.81	0.0052	1.16	2.75	0.0018	68.32	68.97	-0.65
		3.22	3.70	0.0011	0.87	0.0030	1.15	2.83	0.0045	1.16	2.75	0.0065	68.36	69.00	-0.64
		3.22	3.71	0.0016	0.87	0.0039	1.17	2.83	0.0045	1.16	2.76	0.0041	68.40	68.58	-0.18
		3.23	3.69	0.0008	0.87	0.0024	1.15	2.81	0.0013	1.16	2.75	0.0026	68.31	68.93	-0.62

Dense Y-W pumice 3

Ug7

Intermediate Y-W pumice 2

		3.24	3.66	0.0096	0.87	0.0013	1.15	2.80	0.0042	1.16	2.75	0.0006	66.37	66.51	-0.44
		3.25	3.66	0.0092	0.87	0.0096	1.14	2.80	0.0041	1.15	2.75	0.0053	66.53	69.15	-0.62
		3.21	3.71	0.0036	0.87	0.0052	1.16	2.82	0.0021	1.16	2.75	0.0016	66.24	66.74	-0.50
		3.20	3.71	0.0042	0.88	0.0015	1.17	2.82	0.0012	1.17	2.76	0.0025	66.21	66.51	-0.30
		3.22	3.73	0.0067	0.88	0.0042	1.17	2.81	0.0009	1.17	2.75	0.0043	66.07	66.66	-0.59
		3.23	3.69	0.0051	0.87	0.0016	1.14	2.80	0.0091	1.16	2.75	0.0096	66.26	69.15	-0.69
		3.23	3.66	0.0014	0.87	0.0054	1.14	2.80	0.0061	1.16	2.75	0.0076	66.33	69.03	-0.69
Crystalline Y-W pumice 4		4.16	4.10	0.0035	1.03	0.0022	1.55	2.66	0.0027	1.52	2.71	0.0021	62.11	62.06	0.05
		4.16	4.10	0.0074	1.03	0.0035	1.55	2.69	0.0026	1.53	2.72	0.0079	62.09	62.06	0.03
		4.13	4.10	0.0022	1.02	0.0053	1.57	2.66	0.0035	1.52	2.74	0.0021	62.96	61.66	1.30
		4.16	4.10	0.0013	1.02	0.0013	1.55	2.66	0.0040	1.52	2.71	0.0030	62.52	62.12	0.40
		4.16	4.10	0.0041	1.01	0.0038	1.54	2.65	0.0045	1.49	2.71	0.0006	62.66	62.33	0.35
		4.17	4.09	0.0064	1.02	0.0011	1.55	2.66	0.0043	1.52	2.69	0.0023	62.32	62.10	0.22
		4.15	4.10	0.0018	1.02	0.0104	1.56	2.71	0.0019	1.55	2.73	0.0016	62.75	61.83	0.92
		4.15	4.10	0.0049	1.02	0.0061	1.55	2.71	0.0019	1.55	2.72	0.0039	62.47	62.09	0.36
		4.16	4.07	0.0016	1.01	0.0043	1.55	2.66	0.0025	1.52	2.71	0.0031	62.67	61.83	0.84
		4.17	4.10	0.0024	1.00	0.0066	1.55	2.67	0.0016	1.51	2.71	0.0010	63.29	62.08	1.20
		4.17	4.09	0.0015	1.01	0.0043	1.54	2.66	0.0050	1.52	2.71	0.0024	62.92	62.34	0.58
		4.17	4.07	0.0010	1.00	0.0015	1.54	2.67	0.0006	1.51	2.70	0.0016	63.16	62.18	0.98
		4.12	4.10	0.0013	1.02	0.0044	1.55	2.66	0.0019	1.52	2.72	0.0036	62.60	62.08	0.51
		4.14	4.10	0.0024	1.02	0.0053	1.57	2.69	0.0013	1.53	2.74	0.0042	62.65	61.60	1.26
		4.16	4.10	0.0031	1.02	0.0099	1.55	2.66	0.0060	1.52	2.72	0.0042	62.50	62.08	0.42
		4.16	4.10	0.0044	1.01	0.0032	1.55	2.66	0.0017	1.52	2.71	0.0037	62.96	62.09	0.87
		4.17	4.10	0.0019	1.02	0.0004	1.54	2.66	0.0052	1.52	2.69	0.0067	62.32	62.30	0.02
		4.16	4.09	0.0041	0.99	0.0045	1.53	2.66	0.0026	1.52	2.66	0.0025	63.26	62.60	0.66
		4.15	4.10	0.0030	1.04	0.0059	1.56	2.66	0.0006	1.53	2.72	0.0054	61.66	61.83	-0.17
		4.16	4.10	0.0097	1.02	0.0026	1.55	2.66	0.0011	1.52	2.71	0.0042	62.59	62.09	0.51
		4.15	4.14	0.0046	1.03	0.0073	1.55	2.69	0.0027	1.53	2.72	0.0049	62.27	62.42	-0.15
		4.16	4.10	0.0097	1.02	0.0046	1.57	2.66	0.0017	1.52	2.73	0.0050	62.49	61.64	0.85
		4.16	4.10	0.0015	1.02	0.0053	1.56	2.66	0.0015	1.52	2.72	0.0030	62.56	61.90	0.66
		4.16	4.10	0.0029	1.02	0.0044	1.55	2.66	0.0115	1.52	2.72	0.0026	62.31	62.08	0.22
		4.17	4.09	0.0096	1.01	0.0042	1.55	2.66	0.0041	1.52	2.71	0.0097	62.66	62.06	0.60
		4.16	4.09	0.0026	1.01	0.0016	1.54	2.64	0.0042	1.46	2.70	0.0034	62.44	62.31	0.13
	4.15	4.13	0.0064	1.02	0.0091	1.55	2.66	0.0034	1.52	2.72	0.0024	62.62	62.37	0.26	
	4.16	4.10	0.0047	1.02	0.0040	1.57	2.66	0.0045	1.52	2.73	0.0029	62.41	61.66	0.75	
	4.16	4.09	0.0032	1.01	0.0014	1.53	2.66	0.0041	1.52	2.71	0.0023	62.61	62.53	0.08	
	4.17	4.10	0.0066	1.01	0.0013	1.54	2.66	0.0014	1.52	2.70	0.0012	62.66	62.34	0.31	
Crystalline violet pumice		4.27	2.05	0.0002	2.12	0.0011	1.56	2.79	0.0010	1.51	2.65	0.0011	25.37	23.66	1.71
		4.30	2.04	0.0010	2.14	0.0002	1.56	2.80	0.0003	1.51	2.64	0.0002	24.61	23.72	0.90
		4.30	2.03	0.0010	2.11	0.0003	1.52	2.79	0.0003	1.50	2.60	0.0011	24.63	25.14	-0.52
		4.31	2.01	0.0011	2.11	0.0003	1.54	2.79	0.0011	1.51	2.62	0.0002	25.16	23.24	1.93
		4.29	2.03	0.0011	2.13	0.0011	1.54	2.79	0.0003	1.54	2.62	0.0011	24.66	23.97	0.71
		4.30	2.03	0.0002	2.14	0.0002	1.54	2.79	0.0003	1.51	2.62	0.0002	24.20	24.16	0.03
		4.30	2.03	0.0003	2.13	0.0002	1.55	2.79	0.0003	1.51	2.63	0.0002	24.67	23.65	1.01
		4.30	2.03	0.0003	2.12	0.0010	1.54	2.80	0.0003	1.51	2.62	0.0002	24.90	24.06	0.84
		4.30	2.04	0.0010	2.13	0.0003	1.56	2.80	0.0010	1.51	2.65	0.0002	25.05	23.31	1.74
		4.30	2.03	0.0010	2.12	0.0003	1.54	2.76	0.0002	1.51	2.62	0.0011	24.96	23.94	1.02
		4.30	2.02	0.0002	2.11	0.0002	1.53	2.76	0.0002	1.51	2.62	0.0010	25.07	23.94	1.13
		4.30	2.03	0.0010	2.12	0.0010	1.54	2.79	0.0011	1.50	2.62	0.0002	24.93	23.91	1.02

Ulg6	Crystalline violet pumice	4.31	2.03	0.0011	2.12	0.0003	1.53	2.78	0.0011	1.51	2.81	0.0010	24.50	24.84	-0.14		
		4.26	2.03	0.0002	2.12	0.0011	1.54	2.79	0.0002	1.51	2.82	0.0011	24.87	23.99	0.88		
		4.30	2.03	0.0002	2.12	0.0003	1.54	2.80	0.0011	1.51	2.82	0.0003	24.86	23.88	0.98		
		4.30	2.03	0.0010	2.13	0.0010	1.54	2.80	0.0011	1.51	2.82	0.0003	24.85	23.99	0.67		
		4.30	2.03	0.0002	2.12	0.0003	1.54	2.77	0.0002	1.51	2.82	0.0003	24.90	23.95	0.95		
		4.31	2.01	0.0011	2.12	0.0010	1.53	2.77	0.0011	1.48	2.82	0.0003	24.88	23.87	0.81		
		4.29	2.03	0.0011	2.13	0.0003	1.54	2.80	0.0002	1.55	2.83	0.0003	24.80	23.94	0.67		
		4.30	2.04	0.0011	2.13	0.0002	1.55	2.79	0.0002	1.51	2.84	0.0003	24.94	23.79	1.16		
		4.30	2.02	0.0003	2.12	0.0003	1.54	2.79	0.0010	1.51	2.82	0.0011	24.83	23.83	1.00		
		4.33	2.00	0.0011	2.08	0.0002	1.51	2.76	0.0011	1.50	2.80	0.0003	25.66	24.15	1.52		
		4.33	2.01	0.0011	2.11	0.0011	1.53	2.79	0.0011	1.50	2.81	0.0011	24.95	24.01	0.93		
		4.29	2.03	0.0011	2.12	0.0003	1.55	2.81	0.0010	1.51	2.84	0.0010	25.11	23.53	1.58		
		4.30	2.03	0.0010	2.13	0.0002	1.54	2.79	0.0002	1.51	2.83	0.0010	24.77	23.93	0.84		
		4.26	2.06	0.0010	2.12	0.0011	1.56	2.79	0.0011	1.52	2.85	0.0003	25.49	23.96	1.52		
		4.30	2.03	0.0096	2.12	0.0012	1.54	2.79	0.0017	1.51	2.82	0.0024	24.91	23.92	0.98		
		4.30	2.03	0.0003	2.10	0.0003	1.54	2.79	0.0003	1.48	2.82	0.0011	25.83	23.95	1.88		
		4.30	2.03	0.0002	2.12	0.0010	1.53	2.78	0.0002	1.51	2.82	0.0010	24.70	24.30	0.40		
		4.30	2.01	0.0010	2.11	0.0002	1.54	2.79	0.0010	1.51	2.82	0.0002	25.03	23.47	1.56		
		Ulg6	Dense grey pumice 1 (often banded)	0.47	0.42	0.0030	1.26	0.0035	0.18	2.84	0.0025	0.18	3.20	0.0039	60.42	57.06	3.36
				0.49	0.40	0.0042	1.27	0.0029	0.19	2.82	0.0023	0.18	3.20	0.0011	60.50	53.28	7.22
0.50	0.40			0.0102	1.26	0.0061	0.18	2.82	0.0021	0.16	3.21	0.0041	60.78	55.01	5.77		
0.50	0.39			0.0018	1.23	0.0033	0.18	2.81	0.0018	0.15	3.19	0.0018	61.57	55.47	6.10		
0.50	0.38			0.0108	1.26	0.0034	0.17	2.82	0.0050	0.15	3.19	0.0051	60.70	55.32	5.38		
0.45	0.40			0.0009	1.26	0.0048	0.18	2.82	0.0060	0.15	3.20	0.0066	60.66	55.38	5.28		
0.50	0.40			0.0087	1.26	0.0042	0.18	2.82	0.0034	0.15	3.20	0.0045	60.74	55.79	4.95		
0.50	0.40			0.0030	1.25	0.0016	0.16	2.82	0.0034	0.15	3.19	0.0025	60.73	60.70	0.03		
0.50	0.40			0.0083	1.25	0.0047	0.17	2.80	0.0082	0.13	3.19	0.0022	60.72	58.20	2.52		
0.51	0.38			0.0020	1.25	0.0031	0.18	2.81	0.0021	0.15	3.17	0.0018	60.72	54.01	6.71		
0.49	0.40			0.0020	1.26	0.0033	0.18	2.82	0.0024	0.16	3.20	0.0018	60.83	53.99	6.84		
0.49	0.40			0.0014	1.26	0.0025	0.18	2.83	0.0011	0.17	3.22	0.0031	60.90	55.32	5.58		
0.50	0.41			0.0025	1.26	0.0036	0.20	2.84	0.0040	0.17	3.20	0.0029	60.88	52.21	8.68		
0.50	0.41			0.0044	1.26	0.0010	0.19	2.84	0.0026	0.18	3.20	0.0053	60.77	53.79	6.98		
0.50	0.40			0.0037	1.26	0.0012	0.18	2.82	0.0029	0.15	3.19	0.0015	60.66	55.48	5.18		
0.50	0.40			0.0034	1.26	0.0063	0.17	2.82	0.0061	0.15	3.18	0.0041	60.54	55.95	4.59		
0.50	0.38			0.0036	1.26	0.0036	0.17	2.81	0.0041	0.15	3.19	0.0058	60.69	55.26	5.43		
0.53	0.36			0.0040	1.26	0.0029	0.13	2.80	0.0017	0.13	3.18	0.0039	60.29	63.24	-2.96		
0.50	0.40			0.0034	1.29	0.0035	0.18	2.82	0.0045	0.16	3.20	0.0019	59.77	54.47	5.30		
0.50	0.40			0.0057	1.26	0.0087	0.18	2.82	0.0056	0.16	3.21	0.0020	60.61	53.82	6.79		
0.50	0.40			0.0062	1.25	0.0057	0.18	2.82	0.0031	0.15	3.18	0.0043	60.80	55.56	5.24		
0.50	0.39			0.0031	1.26	0.0030	0.18	2.81	0.0018	0.14	3.19	0.0049	60.55	55.41	5.14		
0.53	0.38			0.0030	1.21	0.0040	0.17	2.81	0.0014	0.14	3.19	0.0019	61.97	56.55	5.41		
0.49	0.41			0.0022	1.29	0.0105	0.18	2.84	0.0017	0.17	3.20	0.0041	59.89	54.83	4.87		
0.50	0.40			0.0049	1.26	0.0030	0.20	2.82	0.0037	0.15	3.20	0.0019	60.67	51.27	9.40		
0.50	0.40			0.0020	1.26	0.0022	0.19	2.83	0.0034	0.16	3.20	0.0033	60.66	52.70	7.95		
0.49	0.43			0.0025	1.26	0.0121	0.18	2.84	0.0023	0.18	3.20	0.0039	60.67	58.60	2.06		
0.50	0.39			0.0022	1.26	0.0048	0.17	2.81	0.0019	0.15	3.19	0.0027	60.65	57.02	3.63		
0.50	0.39			0.0031	1.26	0.0084	0.18	2.82	0.0031	0.15	3.19	0.0031	60.67	55.58	5.09		
0.34	0.33			0.0003	1.07	0.0010	0.11	3.12	0.0003	0.10	3.37	0.0010	68.10	66.07	2.03		
0.34	0.34			0.0007	1.09	0.0007	0.11	3.14	0.0007	0.12	3.37	0.0007	67.59	66.93	0.66		

Crystalline Y-W pumice 4	0.34	0.32	0.0010	1.09	0.0003	0.11	3.14	0.0010	0.12	3.37	0.0003	67.51	65.56	1.95
	0.34	0.31	0.0016	1.07	0.0002	0.11	3.12	0.0007	0.10	3.36	0.0003	68.13	65.11	3.02
	0.34	0.32	0.0003	1.06	0.0010	0.11	3.13	0.0003	0.11	3.37	0.0002	67.62	65.03	2.60
	0.34	0.33	0.0003	1.07	0.0002	0.12	3.12	0.0002	0.10	3.37	0.0007	68.17	63.96	4.21
	0.34	0.32	0.0064	1.07	0.0022	0.11	3.12	0.0012	0.10	3.37	0.0011	68.11	65.61	2.50
	0.34	0.32	0.0010	1.07	0.0010	0.11	3.12	0.0002	0.10	3.36	0.0010	68.13	66.13	2.00
	0.34	0.32	0.0019	1.07	0.0007	0.11	3.12	0.0007	0.10	3.36	0.0003	68.11	65.91	2.20
	0.35	0.32	0.0002	1.06	0.0010	0.11	3.10	0.0016	0.09	3.37	0.0003	68.43	65.66	2.77
	0.34	0.33	0.0002	1.06	0.0007	0.14	3.13	0.0002	0.11	3.40	0.0007	68.07	57.01	11.06
	0.34	0.34	0.0007	1.07	0.0007	0.11	3.12	0.0007	0.10	3.37	0.0007	68.12	67.18	0.94
	0.34	0.30	0.0010	1.07	0.0010	0.11	3.12	0.0003	0.10	3.36	0.0010	68.08	64.33	3.76
	0.34	0.31	0.0010	1.05	0.0010	0.11	3.09	0.0003	0.08	3.36	0.0063	68.70	65.12	3.58
	0.37	0.28	0.0003	1.05	0.0002	0.11	3.09	0.0002	0.07	3.37	0.0002	68.79	60.41	8.38
	0.31	0.32	0.0003	1.07	0.0003	0.11	3.12	0.0003	0.10	3.37	0.0003	68.11	65.74	2.37
	0.34	0.32	0.0007	1.07	0.0007	0.14	3.12	0.0007	0.10	3.40	0.0007	68.39	56.85	11.54
	0.34	0.33	0.0010	1.09	0.0003	0.11	3.14	0.0002	0.12	3.37	0.0010	67.53	66.62	0.71
	0.34	0.32	0.0010	1.07	0.0003	0.11	3.12	0.0019	0.10	3.37	0.0010	68.10	65.41	2.69
	0.34	0.33	0.0010	1.07	0.0003	0.12	3.12	0.0025	0.10	3.37	0.0010	68.14	64.23	3.92
	0.34	0.32	0.0015	1.06	0.0007	0.08	3.11	0.0007	0.09	3.34	0.0007	68.12	75.09	-6.97
	0.34	0.32	0.0003	1.07	0.0007	0.10	3.12	0.0007	0.10	3.35	0.0007	68.00	69.31	-1.30
0.34	0.31	0.0003	1.06	0.0007	0.11	3.11	0.0007	0.09	3.36	0.0010	68.41	65.03	3.37	
0.35	0.32	0.0003	1.06	0.0010	0.10	3.11	0.0010	0.09	3.36	0.0003	68.47	66.71	-0.23	
0.38	0.31	0.0003	1.06	0.0010	0.07	3.11	0.0003	0.08	3.32	0.0003	68.05	76.14	-10.09	
0.31	0.32	0.0003	1.09	0.0002	0.12	3.14	0.0003	0.12	3.37	0.0002	67.59	63.43	4.16	
0.34	0.32	0.0010	1.07	0.0002	0.11	3.12	0.0007	0.10	3.37	0.0002	68.11	65.32	2.79	
0.34	0.32	0.0009	1.07	0.0002	0.11	3.12	0.0002	0.10	3.37	0.0002	68.13	65.44	2.70	
0.34	0.31	0.0003	1.06	0.0007	0.11	3.11	0.0007	0.09	3.36	0.0010	68.37	65.07	3.30	
Dense grey pumice 1 (often banded)	0.26	0.27	0.0042	1.21	0.0031	0.10	3.19	0.0006	0.07	4.12	0.0102	70.65	63.85	6.81
	0.26	0.23	0.0015	1.21	0.0076	0.08	3.18	0.0021	0.07	4.11	0.0036	70.65	62.77	7.88
	0.26	0.22	0.0007	1.21	0.0101	0.08	3.18	0.0024	0.05	4.11	0.0023	70.66	65.51	5.16
	0.26	0.26	0.0013	1.21	0.0103	0.09	3.19	0.0025	0.07	4.11	0.0049	70.63	64.06	6.57
	0.26	0.23	0.0012	1.22	0.0010	0.09	3.20	0.0066	0.07	4.12	0.0033	70.39	61.03	9.36
	0.27	0.23	0.0013	1.23	0.0022	0.10	3.21	0.0094	0.08	4.11	0.0066	70.13	57.66	12.25
	0.27	0.23	0.0010	1.23	0.0094	0.09	3.21	0.0061	0.10	4.11	0.0023	70.10	63.19	6.91
	0.27	0.23	0.0101	1.20	0.0032	0.09	3.18	0.0019	0.06	4.11	0.0109	70.70	62.09	8.61
	0.26	0.23	0.0054	1.20	0.0032	0.08	3.18	0.0026	0.05	4.11	0.0025	70.78	65.56	5.22
	0.26	0.20	0.0006	1.20	0.0014	0.09	3.17	0.0021	0.05	4.10	0.0065	70.76	56.19	14.59
	0.23	0.23	0.0013	1.21	0.0028	0.09	3.19	0.0037	0.07	4.11	0.0071	70.63	61.43	9.19
	0.26	0.23	0.0027	1.22	0.0071	0.09	3.20	0.0019	0.08	4.14	0.0102	70.57	56.93	11.64
	0.26	0.23	0.0101	1.21	0.0053	0.09	3.19	0.0016	0.07	4.14	0.0029	70.61	59.61	11.00
	0.27	0.23	0.0025	1.22	0.0041	0.11	3.20	0.0022	0.08	4.12	0.0096	70.26	53.27	17.01
	0.27	0.23	0.0019	1.21	0.0054	0.09	3.19	0.0021	0.07	4.11	0.0014	70.64	62.01	8.63
	0.27	0.23	0.0011	1.21	0.0052	0.09	3.19	0.0093	0.07	4.12	0.0032	70.63	61.26	9.37
	0.26	0.23	0.0018	1.21	0.0076	0.09	3.19	0.0093	0.07	4.10	0.0020	70.57	62.12	8.45
	0.26	0.22	0.0028	1.19	0.0049	0.09	3.17	0.0097	0.07	4.11	0.0090	71.02	62.04	8.98
	0.29	0.22	0.0017	1.16	0.0035	0.04	3.16	0.0056	0.04	4.11	0.0066	71.32	60.29	-6.97
	0.25	0.23	0.0009	1.23	0.0041	0.09	3.21	0.0014	0.09	4.12	0.0041	70.16	60.96	9.20
0.27	0.23	0.0007	1.21	0.0104	0.09	3.19	0.0071	0.07	4.12	0.0015	70.67	56.74	11.93	
0.27	0.23	0.0027	1.21	0.0015	0.09	3.19	0.0029	0.07	4.11	0.0026	70.64	62.06	8.58	

Ulg5 Top	Crystalline Y-W pumice 4	0.29	0.22	0.0010	1.20	0.0018	0.05	3.17	0.0095	0.05	4.07	0.0021	70.52	65.45	5.14
		0.27	0.23	0.0091	1.21	0.0095	0.11	3.19	0.0012	0.07	4.12	0.0011	70.64	53.25	17.40
		0.27	0.23	0.0028	1.21	0.0065	0.10	3.19	0.0029	0.07	4.11	0.0025	70.50	57.62	12.88
		0.27	0.20	0.0033	1.21	0.0017	0.07	3.19	0.0099	0.07	4.11	0.0032	70.63	67.06	3.57
		0.25	0.23	0.0047	1.20	0.0056	0.09	3.15	0.0075	0.07	4.05	0.0011	70.62	62.20	8.42
		0.25	0.23	0.0019	1.20	0.0022	0.05	3.17	0.0035	0.06	4.11	0.0017	70.62	66.62	4.20
		0.25	0.22	0.0042	1.21	0.0032	0.09	3.19	0.0061	0.07	4.11	0.0044	70.64	61.69	8.94
		0.23	0.25	0.0023	1.11	0.0045	0.05	3.01	0.0032	0.07	4.22	0.0044	73.63	65.39	5.24
	0.24	0.22	0.0096	1.10	0.0056	0.10	3.01	0.0023	0.07	4.19	0.0025	73.63	55.35	18.25	
	0.24	0.22	0.0021	1.10	0.0030	0.10	3.00	0.0023	0.06	4.19	0.0014	73.64	55.36	18.25	
	0.24	0.22	0.0067	1.10	0.0034	0.05	3.00	0.0025	0.06	4.15	0.0012	73.60	63.19	10.41	
	0.25	0.22	0.0019	1.10	0.0016	0.07	3.00	0.0011	0.06	4.15	0.0060	73.62	67.27	6.35	
	0.23	0.25	0.0034	1.10	0.0053	0.05	3.00	0.0057	0.06	4.21	0.0025	73.75	67.70	6.05	
	0.23	0.22	0.0034	1.13	0.0097	0.09	3.00	0.0023	0.06	4.15	0.0017	72.55	55.35	14.52	
	0.24	0.22	0.0090	1.11	0.0027	0.05	3.00	0.0044	0.06	4.15	0.0020	73.55	63.10	10.45	
	0.24	0.21	0.0103	1.10	0.0024	0.05	3.00	0.0034	0.06	4.17	0.0042	73.62	71.57	1.74	
	0.25	0.19	0.0021	1.09	0.0037	0.05	2.95	0.0022	0.04	4.15	0.0102	73.64	65.35	8.30	
	0.23	0.22	0.0012	1.11	0.0030	0.09	3.02	0.0007	0.05	4.15	0.0045	73.54	55.34	15.20	
	0.24	0.22	0.0054	1.11	0.0040	0.10	3.01	0.0027	0.07	4.15	0.0053	73.54	54.52	15.72	
	0.24	0.22	0.0097	1.10	0.0102	0.09	3.00	0.0093	0.06	4.15	0.0030	73.61	59.64	13.95	
	0.24	0.22	0.0034	1.11	0.0009	0.05	3.01	0.0079	0.07	4.15	0.0015	73.43	62.74	10.59	
	0.24	0.22	0.0034	1.07	0.0025	0.07	2.99	0.0027	0.05	4.15	0.0032	74.32	67.52	6.51	
	0.25	0.22	0.0025	1.10	0.0095	0.07	2.99	0.0015	0.05	4.15	0.0070	73.64	65.00	5.54	
	0.25	0.22	0.0010	1.10	0.0074	0.07	2.99	0.0067	0.05	4.15	0.0032	73.60	67.97	5.53	
	0.25	0.21	0.0015	1.10	0.0025	0.05	2.97	0.0105	0.03	4.15	0.0102	73.57	73.12	0.45	
	0.20	0.22	0.0024	1.10	0.0025	0.05	3.00	0.0053	0.05	4.15	0.0033	73.60	63.15	10.44	
	0.24	0.22	0.0023	1.10	0.0004	0.05	3.01	0.0092	0.07	4.15	0.0070	73.55	63.15	10.42	
	0.24	0.22	0.0110	1.10	0.0057	0.05	3.00	0.0020	0.05	4.15	0.0050	73.64	63.75	9.55	
	0.25	0.22	0.0067	1.10	0.0020	0.05	3.00	0.0065	0.05	4.15	0.0097	73.62	63.43	10.19	
	0.25	0.21	0.0014	1.05	0.0022	0.07	3.00	0.0095	0.05	4.17	0.0050	74.57	67.52	7.05	
	0.22	0.22	0.0035	1.11	0.0030	0.10	3.00	0.0077	0.05	4.15	0.0025	73.41	54.02	19.40	
	0.23	0.22	0.0100	1.13	0.0055	0.05	3.00	0.0019	0.05	4.15	0.0049	72.55	63.21	9.57	
	0.24	0.22	0.0023	1.11	0.0044	0.05	3.01	0.0041	0.07	4.15	0.0010	73.57	62.79	10.75	
0.24	0.19	0.0034	1.10	0.0015	0.05	3.00	0.0092	0.05	4.15	0.0072	73.50	57.75	15.74		
0.24	0.22	0.0039	1.10	0.0091	0.05	2.99	0.0015	0.05	4.15	0.0024	73.60	63.35	10.24		
0.25	0.21	0.0040	1.10	0.0015	0.05	3.00	0.0035	0.05	4.15	0.0101	73.60	62.57	10.93		
Very Dense grey pumice 4 (-banded)	0.39	0.30	0.0035	1.47	0.0021	0.15	2.75	0.0100	0.15	3.15	0.0055	53.52	49.00	4.52	
	0.41	0.25	0.0029	1.45	0.0055	0.15	2.75	0.0077	0.13	3.19	0.0024	54.45	43.71	10.75	
	0.41	0.29	0.0039	1.45	0.0099	0.15	2.75	0.0009	0.14	3.19	0.0042	54.17	45.53	8.54	
	0.41	0.25	0.0037	1.45	0.0095	0.15	2.75	0.0030	0.13	3.19	0.0025	54.41	44.55	9.85	
	0.41	0.25	0.0027	1.45	0.0020	0.15	2.77	0.0024	0.13	3.15	0.0071	54.45	45.55	8.90	
	0.41	0.27	0.0014	1.44	0.0025	0.14	2.75	0.0027	0.12	3.17	0.0105	54.60	45.33	9.25	
	0.41	0.27	0.0015	1.43	0.0005	0.14	2.75	0.0020	0.12	3.17	0.0115	54.94	47.53	7.41	
	0.41	0.25	0.0050	1.45	0.0055	0.15	2.77	0.0044	0.13	3.19	0.0024	54.45	42.54	11.54	
	0.41	0.25	0.0055	1.45	0.0021	0.15	2.77	0.0062	0.13	3.15	0.0095	54.31	45.94	8.37	
	0.41	0.30	0.0014	1.45	0.0017	0.15	2.77	0.0054	0.15	3.19	0.0095	54.25	45.59	8.35	
	0.41	0.25	0.0025	1.45	0.0013	0.15	2.75	0.0015	0.13	3.15	0.0005	54.43	45.05	9.37	
	0.42	0.25	0.0015	1.45	0.0095	0.15	2.75	0.0090	0.13	3.15	0.0044	54.44	45.25	9.17	
0.42	0.25	0.0072	1.43	0.0035	0.14	2.75	0.0055	0.13	3.17	0.0025	54.94	45.79	9.15		

Very Dense grey pumice 4 (-banded)	0.41	0.29	0.0031	1.45	0.0052	0.15	2.79	0.0091	0.14	3.16	0.0035	54.34	47.26	7.05
	0.41	0.26	0.0107	1.46	0.0027	0.17	2.77	0.0025	0.13	3.20	0.0033	54.49	36.90	15.59
	0.41	0.26	0.0017	1.45	0.0029	0.13	2.76	0.0026	0.13	3.16	0.0012	54.13	53.42	0.71
	0.42	0.26	0.0066	1.45	0.0065	0.15	2.75	0.0011	0.11	3.16	0.0045	54.47	42.99	11.48
	0.45	0.25	0.0063	1.42	0.0055	0.11	2.73	0.0014	0.10	3.14	0.0027	54.61	56.66	-2.05
	0.36	0.26	0.0042	1.45	0.0034	0.15	2.76	0.0110	0.13	3.16	0.0107	54.37	45.64	8.73
	0.41	0.26	0.0026	1.45	0.0023	0.16	2.76	0.0062	0.13	3.19	0.0100	54.56	43.23	11.34
	0.41	0.26	0.0020	1.44	0.0039	0.15	2.76	0.0031	0.13	3.16	0.0021	54.62	45.53	9.09
	0.41	0.27	0.0025	1.45	0.0047	0.15	2.76	0.0094	0.12	3.16	0.0063	54.45	44.56	9.89
	0.42	0.27	0.0030	1.44	0.0047	0.15	2.74	0.0015	0.12	3.16	0.0026	54.63	44.36	10.45
	0.45	0.27	0.0023	1.44	0.0039	0.14	2.76	0.0044	0.12	3.17	0.0021	54.70	47.41	7.29
	0.41	0.29	0.0051	1.46	0.0067	0.17	2.77	0.0096	0.14	3.20	0.0036	54.25	42.10	12.15
	0.41	0.26	0.0029	1.45	0.0090	0.16	2.76	0.0035	0.13	3.19	0.0072	54.46	43.42	11.04
	0.41	0.30	0.0015	1.46	0.0032	0.15	2.76	0.0034	0.15	3.16	0.0027	53.46	50.00	3.46
	0.41	0.26	0.0056	1.45	0.0031	0.15	2.75	0.0021	0.13	3.16	0.0016	54.41	46.67	7.74
	0.41	0.26	0.0007	1.45	0.0095	0.15	2.74	0.0030	0.13	3.16	0.0025	54.43	46.07	8.36
Crystalline violet pumice	0.39	0.20	0.0032	2.01	0.0052	0.14	2.64	0.0069	0.11	3.26	0.0047	38.77	30.05	8.72
	0.39	0.19	0.0032	2.00	0.0021	0.14	2.65	0.0096	0.11	3.26	0.0040	38.96	26.74	12.22
	0.39	0.20	0.0031	1.99	0.0032	0.14	2.64	0.0051	0.11	3.29	0.0027	39.45	29.67	9.57
	0.37	0.19	0.0040	1.99	0.0030	0.16	2.66	0.0035	0.12	3.26	0.0052	39.31	16.35	20.97
	0.39	0.16	0.0017	1.99	0.0011	0.14	2.64	0.0035	0.11	3.26	0.0019	38.95	25.42	13.53
	0.40	0.19	0.0025	1.96	0.0029	0.13	2.63	0.0011	0.11	3.26	0.0026	39.53	32.36	7.15
	0.40	0.19	0.0013	1.96	0.0022	0.14	2.64	0.0036	0.11	3.26	0.0011	39.54	29.66	9.66
	0.37	0.20	0.0067	1.99	0.0065	0.16	2.66	0.0092	0.11	3.26	0.0093	39.22	21.95	17.27
	0.36	0.20	0.0047	2.00	0.0062	0.14	2.64	0.0091	0.14	3.26	0.0026	39.06	29.54	9.53
	0.39	0.20	0.0026	2.01	0.0009	0.15	2.65	0.0053	0.11	3.29	0.0100	36.64	22.61	16.22
	0.39	0.20	0.0064	1.99	0.0039	0.14	2.64	0.0027	0.11	3.29	0.0017	39.47	29.64	9.64
	0.39	0.19	0.0022	1.99	0.0033	0.13	2.64	0.0069	0.11	3.26	0.0037	39.29	30.51	8.77
	0.39	0.16	0.0097	1.99	0.0044	0.13	2.63	0.0039	0.11	3.26	0.0061	39.25	21.57	17.66
	0.40	0.19	0.0023	1.99	0.0092	0.12	2.63	0.0031	0.11	3.27	0.0014	39.13	37.61	1.52
	0.40	0.16	0.0016	1.99	0.0100	0.13	2.62	0.0020	0.06	3.26	0.0077	38.92	30.51	8.41
	0.36	0.20	0.0069	2.00	0.0040	0.14	2.64	0.0015	0.15	3.29	0.0101	39.17	31.73	7.44
	0.39	0.20	0.0092	2.00	0.0022	0.14	2.64	0.0036	0.11	3.29	0.0041	39.32	31.75	7.56
	0.39	0.19	0.0024	1.97	0.0073	0.14	2.64	0.0057	0.06	3.26	0.0034	39.66	26.66	11.21
	0.39	0.19	0.0016	1.96	0.0091	0.11	2.62	0.0012	0.11	3.26	0.0066	39.61	41.73	-2.12
	0.41	0.19	0.0016	1.95	0.0096	0.11	2.61	0.0016	0.11	3.25	0.0061	40.02	44.00	-3.96
	0.36	0.23	0.0027	2.00	0.0039	0.15	2.65	0.0013	0.11	3.26	0.0047	39.05	34.01	5.04
	0.36	0.22	0.0046	2.00	0.0066	0.14	2.64	0.0017	0.11	3.26	0.0042	39.21	36.20	1.01
	0.39	0.19	0.0096	2.00	0.0021	0.16	2.66	0.0029	0.12	3.29	0.0024	39.10	16.62	20.26
	0.40	0.19	0.0099	1.99	0.0024	0.14	2.64	0.0051	0.11	3.26	0.0044	39.27	29.30	9.96
	0.39	0.19	0.0007	1.99	0.0076	0.14	2.64	0.0010	0.11	3.26	0.0012	39.29	29.63	9.66
	0.35	0.19	0.0043	1.99	0.0095	0.14	2.64	0.0061	0.11	3.26	0.0024	39.26	29.36	9.90
0.36	0.20	0.0029	1.99	0.0032	0.15	2.65	0.0069	0.11	3.31	0.0039	39.71	25.01	14.70	
0.39	0.19	0.0095	1.99	0.0031	0.14	2.64	0.0059	0.11	3.27	0.0073	39.16	29.60	9.36	
0.40	0.19	0.0042	1.96	0.0100	0.13	2.63	0.0026	0.11	3.27	0.0036	39.51	33.07	6.43	
	1.73	1.10	0.0017	1.59	0.0093	0.66	2.67	0.0016	0.63	2.79	0.0034	42.96	36.06	4.89
	1.74	1.10	0.0024	1.60	0.0016	0.65	2.66	0.0019	0.63	2.76	0.0027	42.29	40.63	1.67
	1.74	1.10	0.0010	1.59	0.0053	0.66	2.66	0.0022	0.63	2.76	0.0067	42.75	40.13	2.62
	1.74	1.09	0.0009	1.57	0.0040	0.65	2.67	0.0069	0.62	2.76	0.0101	42.96	40.65	2.33

Very Dense grey pumice 4 (-banded)	1.74	1.10	0.0097	1.58	0.0054	0.65	2.67	0.0014	0.63	2.78	0.0046	43.01	40.75	2.25
	1.75	1.10	0.0096	1.57	0.0019	0.65	2.67	0.0016	0.62	2.77	0.0047	43.28	40.79	2.50
	1.73	1.10	0.0009	1.58	0.0095	0.65	2.70	0.0013	0.63	2.79	0.0010	43.14	40.51	2.62
	1.74	1.10	0.0013	1.58	0.0027	0.65	2.68	0.0023	0.63	2.78	0.0018	43.00	40.70	2.30
	1.74	1.11	0.0097	1.58	0.0030	0.65	2.67	0.0031	0.63	2.80	0.0047	43.42	41.12	2.30
	1.74	1.10	0.0102	1.58	0.0028	0.65	2.66	0.0023	0.62	2.78	0.0040	43.06	40.71	2.35
	1.75	1.10	0.0097	1.57	0.0021	0.65	2.67	0.0014	0.62	2.77	0.0042	43.11	40.82	2.30
	1.76	1.07	0.0016	1.58	0.0062	0.64	2.65	0.0074	0.59	2.76	0.0054	42.70	39.99	2.71
	1.71	1.10	0.0012	1.58	0.0056	0.65	2.67	0.0026	0.63	2.78	0.0022	42.96	40.75	2.21
	1.73	1.14	0.0034	1.59	0.0065	0.66	2.68	0.0024	0.66	2.78	0.0008	42.66	42.00	0.66
	1.74	1.10	0.0028	1.58	0.0009	0.65	2.68	0.0014	0.63	2.78	0.0043	42.96	40.64	2.32
	1.74	1.10	0.0012	1.58	0.0007	0.65	2.67	0.0013	0.63	2.77	0.0097	42.98	40.90	2.09
	1.75	1.10	0.0023	1.58	0.0032	0.65	2.67	0.0077	0.62	2.78	0.0015	43.02	40.64	2.38
	1.76	1.10	0.0092	1.54	0.0032	0.65	2.64	0.0092	0.62	2.75	0.0042	44.06	40.50	3.56
	1.72	1.10	0.0010	1.58	0.0057	0.66	2.67	0.0020	0.63	2.80	0.0033	43.32	40.65	3.27
	1.72	1.13	0.0006	1.59	0.0012	0.65	2.67	0.0036	0.66	2.78	0.0032	42.77	42.34	0.42
	1.74	1.10	0.0092	1.59	0.0025	0.65	2.67	0.0039	0.63	2.78	0.0027	42.79	40.87	1.91
	1.74	1.10	0.0090	1.58	0.0028	0.64	2.65	0.0016	0.62	2.78	0.0093	43.02	41.79	1.23
	1.75	1.10	0.0098	1.58	0.0013	0.65	2.66	0.0020	0.62	2.77	0.0016	42.80	40.71	2.09
	1.77	1.09	0.0070	1.57	0.0040	0.61	2.67	0.0024	0.62	2.76	0.0013	43.13	44.28	-1.13
1.73	1.10	0.0029	1.59	0.0019	0.68	2.67	0.0010	0.63	2.78	0.0065	42.62	38.03	4.79	
1.74	1.10	0.0022	1.60	0.0012	0.65	2.68	0.0031	0.63	2.79	0.0040	42.67	40.55	2.12	
1.74	1.11	0.0070	1.59	0.0013	0.65	2.68	0.0031	0.63	2.80	0.0013	42.98	41.05	1.93	
1.74	1.07	0.0016	1.56	0.0092	0.65	2.67	0.0081	0.60	2.78	0.0060	43.75	39.48	4.27	
1.74	1.10	0.0100	1.58	0.0023	0.62	2.67	0.0016	0.63	2.77	0.0067	42.81	43.50	-0.69	
Dense grey pumice 1	2.39	2.14	0.0017	1.12	0.0032	0.92	2.61	0.0044	0.89	2.73	0.0010	58.91	57.06	1.85
	2.39	2.14	0.0063	1.13	0.0015	0.92	2.63	0.0044	0.89	2.69	0.0041	58.25	57.01	1.24
	2.39	2.16	0.0104	1.13	0.0032	0.92	2.62	0.0014	0.91	2.70	0.0034	58.18	57.50	0.68
	2.39	2.11	0.0011	1.12	0.0031	0.92	2.59	0.0076	0.87	2.69	0.0094	58.43	56.68	1.74
	2.39	2.14	0.0014	1.12	0.0023	0.92	2.60	0.0036	0.89	2.69	0.0093	58.50	57.08	1.42
	2.39	2.13	0.0078	1.11	0.0103	0.92	2.59	0.0023	0.88	2.69	0.0089	58.68	57.01	1.67
	2.36	2.14	0.0035	1.12	0.0015	0.92	2.61	0.0012	0.89	2.69	0.0025	58.42	57.09	1.33
	2.39	2.14	0.0015	1.12	0.0025	0.93	2.62	0.0048	0.89	2.73	0.0004	58.99	56.71	2.29
	2.39	2.16	0.0033	1.13	0.0014	0.92	2.62	0.0009	0.90	2.69	0.0006	57.96	57.28	0.68
	2.39	2.14	0.0012	1.12	0.0015	0.92	2.58	0.0022	0.89	2.67	0.0025	58.07	57.23	0.84
	2.39	2.14	0.0015	1.12	0.0062	0.91	2.60	0.0025	0.89	2.69	0.0071	58.51	57.63	0.88
	2.39	2.14	0.0057	1.12	0.0042	0.92	2.60	0.0028	0.89	2.69	0.0021	58.47	57.13	1.34
	2.36	2.16	0.0018	1.14	0.0011	0.93	2.61	0.0008	0.91	2.69	0.0016	57.75	57.14	0.61
	2.39	2.14	0.0024	1.12	0.0094	0.95	2.61	0.0056	0.89	2.69	0.0053	58.41	55.71	2.70
	2.39	2.15	0.0041	1.12	0.0044	0.92	2.62	0.0030	0.90	2.70	0.0027	58.54	57.19	1.34
	2.39	2.14	0.0102	1.12	0.0072	0.92	2.61	0.0024	0.89	2.69	0.0012	58.51	57.04	1.47
	2.39	2.14	0.0092	1.12	0.0030	0.93	2.61	0.0017	0.89	2.70	0.0010	58.42	56.76	1.66
	2.39	2.14	0.0041	1.11	0.0039	0.92	2.60	0.0094	0.89	2.69	0.0020	58.74	57.10	1.63
	2.39	2.13	0.0062	1.10	0.0099	0.92	2.60	0.0032	0.88	2.69	0.0031	59.24	57.01	2.23
	2.39	2.14	0.0020	1.10	0.0007	0.92	2.60	0.0019	0.89	2.69	0.0091	59.23	57.12	2.11
2.40	2.12	0.0093	1.12	0.0067	0.92	2.60	0.0013	0.88	2.69	0.0091	58.55	56.78	1.77	
2.40	2.13	0.0093	1.11	0.0029	0.91	2.60	0.0011	0.87	2.66	0.0014	58.51	57.37	1.14	
2.42	2.11	0.0041	1.09	0.0042	0.92	2.56	0.0021	0.86	2.69	0.0027	59.59	56.52	3.07	
2.39	2.15	0.0011	1.12	0.0067	0.92	2.61	0.0066	0.90	2.69	0.0008	58.36	57.18	1.19	

Ulg5 Base														
Vesicular Y-W pumice 1	2.39	2.14	0.0025	1.12	0.0017	0.92	2.61	0.0014	0.89	2.70	0.0035	56.38	57.04	1.34
	2.39	2.14	0.0057	1.12	0.0061	0.92	2.60	0.0008	0.89	2.69	0.0017	55.51	57.08	1.43
	2.39	2.15	0.0011	1.13	0.0007	0.95	2.61	0.0070	0.90	2.70	0.0018	55.10	55.89	2.22
	2.39	2.16	0.0056	1.15	0.0012	0.92	2.61	0.0017	0.91	2.70	0.0021	57.51	57.51	-0.01
	2.39	2.13	0.0010	1.12	0.0092	0.89	2.60	0.0014	0.88	2.69	0.0095	56.53	56.34	0.19
	0.80	1.18	0.0014	0.74	0.0108	0.30	3.01	0.0076	0.29	3.06	0.0076	75.89	74.79	1.10
	0.83	1.17	0.0049	0.72	0.0015	0.28	3.02	0.0056	0.27	3.07	0.0023	76.57	76.05	0.52
	0.83	1.19	0.0041	0.74	0.0011	0.30	3.01	0.0027	0.29	3.06	0.0033	75.87	74.91	0.96
	0.84	1.16	0.0027	0.72	0.0008	0.27	3.01	0.0064	0.27	3.06	0.0026	76.57	76.28	0.29
	0.84	1.14	0.0027	0.71	0.0026	0.27	3.00	0.0063	0.26	3.05	0.0012	76.76	76.27	0.49
	0.79	1.17	0.0015	0.72	0.0019	0.28	3.01	0.0013	0.27	3.06	0.0054	76.54	76.16	0.38
	0.83	1.17	0.0012	0.72	0.0062	0.28	3.03	0.0031	0.27	3.08	0.0102	76.67	76.28	0.39
	0.83	1.16	0.0008	0.72	0.0008	0.28	3.01	0.0018	0.27	3.06	0.0029	76.51	76.08	0.43
	0.84	1.16	0.0022	0.70	0.0041	0.25	3.00	0.0021	0.25	3.05	0.0044	77.12	76.29	-1.17
	0.84	1.16	0.0105	0.71	0.0019	0.27	3.01	0.0030	0.26	3.06	0.0018	76.86	76.84	0.02
	0.84	1.14	0.0025	0.72	0.0019	0.28	3.00	0.0037	0.27	3.05	0.0039	76.50	75.86	0.64
	0.82	1.17	0.0044	0.72	0.0074	0.28	3.02	0.0080	0.27	3.06	0.0020	76.56	76.14	0.43
	0.83	1.17	0.0029	0.72	0.0076	0.28	3.02	0.0010	0.27	3.06	0.0019	76.56	76.05	0.52
	0.83	1.17	0.0016	0.72	0.0099	0.28	3.01	0.0092	0.27	3.06	0.0036	76.52	76.21	0.31
	0.84	1.16	0.0032	0.72	0.0029	0.28	3.01	0.0068	0.27	3.06	0.0025	76.54	76.19	0.35
0.84	1.16	0.0029	0.72	0.0025	0.28	3.01	0.0023	0.27	3.06	0.0022	76.54	76.16	0.37	
0.87	1.13	0.0027	0.69	0.0029	0.25	2.97	0.0018	0.24	3.02	0.0100	76.96	77.98	-1.02	
0.83	1.17	0.0017	0.73	0.0038	0.29	3.01	0.0055	0.28	3.06	0.0030	76.20	75.30	0.90	
0.84	1.16	0.0051	0.72	0.0031	0.28	3.01	0.0017	0.27	3.06	0.0053	76.53	76.16	0.37	
0.83	1.16	0.0040	0.73	0.0079	0.28	3.02	0.0023	0.28	3.07	0.0069	76.33	75.67	0.65	
0.83	1.17	0.0010	0.74	0.0063	0.30	3.02	0.0021	0.29	3.07	0.0031	75.98	74.59	1.39	
0.83	1.17	0.0004	0.72	0.0012	0.28	3.02	0.0014	0.27	3.07	0.0022	76.55	76.14	0.40	
0.84	1.16	0.0107	0.72	0.0015	0.28	3.01	0.0025	0.27	3.06	0.0020	76.53	76.21	0.32	
0.84	1.16	0.0014	0.71	0.0040	0.26	3.01	0.0046	0.26	3.06	0.0047	76.88	77.48	-0.60	
0.84	1.15	0.0036	0.70	0.0017	0.27	3.01	0.0068	0.26	3.06	0.0031	77.03	76.64	0.39	
0.87	1.15	0.0031	0.71	0.0009	0.27	3.00	0.0020	0.26	3.05	0.0107	76.83	76.91	-0.08	
0.83	1.16	0.0020	0.74	0.0039	0.29	3.03	0.0039	0.29	3.08	0.0092	76.09	75.14	0.94	
0.84	1.16	0.0027	0.72	0.0053	0.28	2.99	0.0042	0.27	3.04	0.0056	76.38	76.20	0.18	
0.84	1.15	0.0025	0.71	0.0043	0.27	3.00	0.0030	0.26	3.05	0.0021	76.80	76.64	0.16	
Intermediate Y-W pumice 2	1.32	1.79	0.0067	0.76	0.0022	0.46	2.64	0.0064	0.47	2.89	0.0024	73.63	73.36	0.47
	1.33	1.79	0.0023	0.76	0.0033	0.49	2.65	0.0039	0.47	2.90	0.0037	73.73	72.66	1.07
	1.33	1.79	0.0094	0.75	0.0039	0.47	2.64	0.0014	0.46	2.88	0.0041	74.13	73.77	0.36
	1.34	1.79	0.0030	0.74	0.0095	0.46	2.64	0.0018	0.45	2.88	0.0019	74.16	74.21	-0.05
	1.30	1.79	0.0020	0.75	0.0049	0.47	2.64	0.0036	0.46	2.88	0.0016	74.13	73.89	0.44
	1.32	1.79	0.0063	0.76	0.0025	0.47	2.67	0.0029	0.47	2.89	0.0018	73.78	73.64	0.15
	1.33	1.79	0.0040	0.77	0.0094	0.48	2.65	0.0021	0.48	2.89	0.0076	73.50	73.19	0.31
	1.33	1.76	0.0031	0.75	0.0008	0.45	2.64	0.0024	0.46	2.88	0.0034	74.15	74.52	-0.37
	1.33	1.79	0.0031	0.75	0.0019	0.47	2.63	0.0067	0.46	2.88	0.0011	74.14	73.86	0.28
	1.34	1.76	0.0013	0.75	0.0102	0.47	2.64	0.0015	0.46	2.88	0.0018	74.13	73.75	0.38
	1.31	1.82	0.0079	0.75	0.0015	0.48	2.64	0.0111	0.46	2.88	0.0009	74.12	73.85	0.28
	1.33	1.79	0.0051	0.75	0.0018	0.47	2.65	0.0061	0.46	2.88	0.0018	74.09	73.48	0.61
	1.33	1.79	0.0110	0.75	0.0028	0.48	2.64	0.0025	0.46	2.88	0.0056	73.93	73.19	0.75
	1.33	1.79	0.0020	0.74	0.0022	0.47	2.64	0.0094	0.46	2.88	0.0022	74.17	73.77	0.40
	1.34	1.79	0.0012	0.74	0.0028	0.46	2.64	0.0007	0.45	2.87	0.0015	74.31	74.35	-0.03

		1.34	1.79	0.0005	0.73	0.0039	0.47	2.83	0.0009	0.44	2.88	0.0041	74.66	73.78	0.89
		1.31	1.79	0.0029	0.77	0.0071	0.47	2.84	0.0109	0.48	2.90	0.0015	73.59	73.63	-0.04
		1.32	1.79	0.0063	0.77	0.0008	0.47	2.84	0.0060	0.48	2.91	0.0026	73.64	73.67	-0.23
		1.33	1.78	0.0009	0.72	0.0027	0.46	2.84	0.0094	0.43	2.88	0.0011	74.99	74.29	0.70
		1.35	1.76	0.0008	0.74	0.0038	0.47	2.82	0.0114	0.45	2.87	0.0014	74.31	73.32	0.99
		1.32	1.83	0.0058	0.75	0.0012	0.48	2.85	0.0019	0.46	2.88	0.0062	74.09	73.78	0.31
		1.33	1.79	0.0094	0.75	0.0031	0.49	2.85	0.0031	0.46	2.89	0.0018	74.16	72.65	1.53
		1.33	1.79	0.0078	0.75	0.0098	0.47	2.85	0.0046	0.46	2.89	0.0011	74.15	73.76	0.40
		1.33	1.79	0.0066	0.75	0.0037	0.47	2.86	0.0053	0.46	2.88	0.0080	74.10	73.67	0.43
		1.33	1.79	0.0012	0.74	0.0035	0.47	2.84	0.0025	0.45	2.88	0.0021	74.40	73.79	0.62
		1.34	1.79	0.0023	0.74	0.0042	0.47	2.82	0.0007	0.46	2.88	0.0030	74.15	73.78	0.37
		1.34	1.79	0.0008	0.74	0.0012	0.46	2.84	0.0011	0.46	2.88	0.0011	74.00	74.21	-0.21
		1.35	1.78	0.0021	0.72	0.0016	0.43	2.81	0.0110	0.43	2.88	0.0046	74.83	76.06	-1.23
		1.36	1.78	0.0032	0.73	0.0014	0.46	2.84	0.0053	0.45	2.87	0.0017	74.42	74.23	0.19
		0.48	0.57	0.0029	0.88	0.0022	0.15	3.30	0.0017	0.13	3.72	0.0029	76.20	73.16	3.03
		0.49	0.57	0.0100	0.86	0.0065	0.15	3.30	0.0018	0.13	3.72	0.0063	77.01	74.02	2.99
		0.48	0.59	0.0021	0.85	0.0040	0.15	3.33	0.0018	0.14	3.71	0.0010	76.88	74.85	2.04
		0.49	0.56	0.0022	0.82	0.0108	0.15	3.30	0.0096	0.13	3.71	0.0012	77.78	73.67	4.11
		0.51	0.56	0.0091	0.85	0.0031	0.15	3.30	0.0021	0.13	3.70	0.0039	76.93	73.86	3.27
		0.47	0.57	0.0016	0.86	0.0023	0.16	3.30	0.0011	0.16	3.71	0.0056	76.96	72.89	4.07
		0.49	0.57	0.0107	0.86	0.0034	0.15	3.30	0.0027	0.13	3.73	0.0025	77.03	73.79	3.23
		0.49	0.57	0.0041	0.85	0.0034	0.15	3.29	0.0025	0.13	3.71	0.0050	77.03	74.04	2.98
		0.50	0.56	0.0020	0.85	0.0030	0.14	3.28	0.0020	0.13	3.71	0.0012	77.01	75.10	1.91
		0.51	0.56	0.0091	0.84	0.0008	0.15	3.29	0.0019	0.10	3.69	0.0073	77.13	73.39	3.73
		0.46	0.57	0.0037	0.85	0.0031	0.15	3.30	0.0011	0.13	3.71	0.0080	76.99	73.83	3.16
		0.48	0.57	0.0089	0.86	0.0029	0.16	3.30	0.0014	0.17	3.72	0.0036	76.80	72.37	4.43
		0.49	0.59	0.0064	0.85	0.0060	0.16	3.31	0.0014	0.14	3.72	0.0029	77.04	72.93	4.10
		0.49	0.57	0.0033	0.85	0.0019	0.15	3.30	0.0026	0.13	3.70	0.0008	76.92	74.38	2.54
		0.50	0.57	0.0021	0.85	0.0071	0.14	3.28	0.0044	0.13	3.71	0.0020	77.02	75.48	1.53
		0.51	0.55	0.0039	0.85	0.0004	0.11	3.27	0.0028	0.12	3.68	0.0017	76.80	80.65	-3.86
		0.47	0.59	0.0009	0.86	0.0039	0.15	3.32	0.0022	0.13	3.71	0.0055	76.77	74.52	2.25
		0.49	0.57	0.0015	0.85	0.0023	0.15	3.30	0.0010	0.13	3.71	0.0080	76.98	74.08	2.90
		0.49	0.59	0.0020	0.86	0.0038	0.17	3.31	0.0026	0.13	3.72	0.0011	76.97	71.51	5.46
		0.49	0.56	0.0031	0.85	0.0020	0.16	3.30	0.0018	0.13	3.71	0.0077	76.98	72.56	4.42
		0.49	0.57	0.0033	0.86	0.0031	0.16	3.30	0.0007	0.13	3.73	0.0016	76.88	72.78	4.10
		0.49	0.55	0.0053	0.85	0.0023	0.14	3.30	0.0026	0.12	3.71	0.0107	77.04	75.08	1.96
		0.49	0.56	0.0023	0.85	0.0028	0.14	3.29	0.0028	0.13	3.71	0.0026	77.00	75.44	1.55
		0.51	0.56	0.0032	0.81	0.0007	0.14	3.29	0.0025	0.12	3.71	0.0027	78.11	75.32	2.80
		0.48	0.58	0.0015	0.89	0.0045	0.16	3.31	0.0044	0.13	3.71	0.0044	76.15	73.23	2.92
		0.48	0.57	0.0012	0.86	0.0080	0.17	3.31	0.0049	0.13	3.72	0.0015	76.97	70.59	6.38
		0.49	0.57	0.0015	0.85	0.0083	0.13	3.30	0.0043	0.10	3.71	0.0111	77.06	77.68	-0.62
		0.49	0.57	0.0040	0.84	0.0028	0.15	3.30	0.0096	0.13	3.69	0.0011	77.19	74.15	3.04
		0.50	0.57	0.0093	0.85	0.0017	0.15	3.30	0.0056	0.13	3.71	0.0020	77.00	74.19	2.81
		1.36	1.08	0.0087	1.29	0.0032	0.52	2.85	0.0042	0.50	2.81	0.0022	54.07	51.42	2.65
		1.37	1.08	0.0008	1.28	0.0019	0.49	2.84	0.0072	0.50	2.80	0.0018	54.26	54.97	-0.72
		1.38	1.08	0.0017	1.28	0.0021	0.48	2.84	0.0022	0.49	2.80	0.0020	54.26	54.96	-0.69
		1.39	1.07	0.0034	1.28	0.0015	0.48	2.84	0.0010	0.48	2.80	0.0015	54.27	55.05	-0.78
		1.36	1.08	0.0034	1.28	0.0031	0.52	2.84	0.0014	0.50	2.80	0.0031	54.26	52.03	2.24
		1.37	1.08	0.0026	1.28	0.0032	0.48	2.84	0.0105	0.51	2.80	0.0009	54.17	54.94	-0.78

Ulg4		Dense grey pumice 1											Crystalline violet pumice 4										
1.37	1.10	0.0012	1.29	0.0025	0.49	2.54	0.0007	0.50	2.50	0.0023	54.05	55.30	-1.22										
1.30	1.07	0.0034	1.25	0.0014	0.45	2.54	0.0077	0.49	2.50	0.0055	54.27	54.55	-0.55										
1.30	1.07	0.0033	1.25	0.0059	0.45	2.54	0.0045	0.45	2.50	0.0055	54.27	54.75	-0.50										
1.39	1.05	0.0103	1.27	0.0039	0.45	2.54	0.0035	0.49	2.79	0.0019	54.45	54.41	0.04										
1.39	1.07	0.0110	1.25	0.0040	0.45	2.53	0.0053	0.49	2.75	0.0015	54.55	57.45	-2.51										
1.30	1.10	0.0015	1.25	0.0032	0.45	2.55	0.0015	0.49	2.50	0.0015	54.25	55.50	-1.54										
1.37	1.05	0.0027	1.25	0.0023	0.45	2.57	0.0022	0.50	2.50	0.0015	54.15	55.00	-0.52										
1.37	1.05	0.0041	1.29	0.0010	0.49	2.55	0.0052	0.50	2.51	0.0033	53.95	54.93	-0.95										
1.35	1.05	0.0013	1.25	0.0037	0.45	2.54	0.0034	0.45	2.79	0.0045	54.25	54.44	-0.16										
1.35	1.07	0.0011	1.27	0.0090	0.45	2.54	0.0025	0.45	2.79	0.0091	54.37	54.55	-0.29										
1.40	1.05	0.0039	1.25	0.0113	0.45	2.54	0.0024	0.45	2.77	0.0045	54.55	54.21	0.54										
1.34	1.05	0.0025	1.25	0.0021	0.45	2.54	0.0012	0.49	2.50	0.0022	54.25	54.97	-0.73										
1.37	1.09	0.0045	1.25	0.0015	0.49	2.57	0.0057	0.50	2.50	0.0015	54.25	55.27	-1.01										
1.37	1.10	0.0014	1.25	0.0005	0.49	2.54	0.0024	0.49	2.50	0.0019	54.24	55.22	-0.95										
1.35	1.07	0.0045	1.25	0.0024	0.45	2.54	0.0029	0.47	2.79	0.0055	54.30	57.51	-3.30										
1.35	1.07	0.0117	1.25	0.0015	0.45	2.51	0.0013	0.49	2.79	0.0027	54.32	54.52	-0.31										
1.41	1.05	0.0034	1.25	0.0115	0.45	2.50	0.0050	0.45	2.79	0.0021	54.25	55.05	-0.75										
1.35	1.09	0.0035	1.31	0.0021	0.45	2.54	0.0025	0.49	2.52	0.0012	53.75	55.40	-1.55										
1.37	1.09	0.0012	1.29	0.0025	0.45	2.54	0.0055	0.51	2.50	0.0007	54.10	55.55	-1.45										
1.37	1.05	0.0029	1.29	0.0014	0.49	2.54	0.0025	0.49	2.50	0.0079	54.05	54.59	-0.50										
1.35	1.05	0.0119	1.27	0.0025	0.45	2.54	0.0115	0.49	2.79	0.0057	54.45	55.02	-0.55										
1.35	1.07	0.0107	1.25	0.0017	0.45	2.53	0.0011	0.49	2.75	0.0057	54.53	55.00	-0.37										
1.35	1.05	0.0050	1.25	0.0057	0.45	2.54	0.0024	0.49	2.79	0.0007	54.30	55.33	-1.02										
3.21	1.50	0.0052	2.03	0.0054	1.14	2.55	0.0029	1.15	2.51	0.0041	27.55	25.75	-1.07										
3.22	1.52	0.0037	2.03	0.0092	1.14	2.55	0.0027	1.15	2.54	0.0011	25.37	29.52	-1.25										
3.25	1.50	0.0039	2.01	0.0012	1.13	2.55	0.0097	1.15	2.51	0.0039	25.31	29.45	-1.17										
3.25	1.59	0.0024	2.02	0.0014	1.14	2.55	0.0042	1.15	2.50	0.0039	27.94	25.25	-0.35										
3.24	1.50	0.0013	2.03	0.0031	1.14	2.55	0.0022	1.15	2.51	0.0057	27.70	25.71	-1.01										
3.25	1.50	0.0100	2.04	0.0057	1.14	2.55	0.0015	1.17	2.51	0.0055	27.55	25.55	-1.02										
3.25	1.50	0.0052	2.04	0.0012	1.14	2.55	0.0041	1.15	2.51	0.0024	27.15	25.71	-1.53										
3.25	1.50	0.0020	2.02	0.0055	1.14	2.55	0.0022	1.15	2.51	0.0025	25.00	25.72	-0.73										
3.25	1.59	0.0025	2.03	0.0055	1.14	2.55	0.0029	1.14	2.79	0.0052	27.13	25.41	-1.25										
3.25	1.59	0.0023	2.01	0.0025	1.13	2.52	0.0015	1.15	2.79	0.0101	25.03	25.59	-0.55										
3.25	1.50	0.0059	2.03	0.0029	1.17	2.55	0.0015	1.15	2.51	0.0012	27.55	25.57	0.59										
3.25	1.51	0.0039	2.03	0.0059	1.14	2.55	0.0032	1.15	2.51	0.0052	27.54	29.13	-1.49										
3.25	1.50	0.0024	2.05	0.0022	1.15	2.55	0.0005	1.15	2.51	0.0053	27.19	25.35	-1.15										
3.25	1.50	0.0015	2.03	0.0011	1.14	2.55	0.0025	1.15	2.51	0.0054	27.70	25.51	-1.10										
3.25	1.55	0.0029	2.00	0.0015	1.14	2.55	0.0017	1.11	2.75	0.0027	27.92	27.72	0.20										
3.25	1.50	0.0010	2.04	0.0013	1.15	2.59	0.0020	1.15	2.51	0.0035	27.37	25.24	-0.57										
3.25	1.50	0.0022	2.04	0.0045	1.14	2.55	0.0031	1.15	2.51	0.0032	27.41	25.70	-1.25										
3.25	1.55	0.0051	2.03	0.0077	1.14	2.54	0.0021	1.14	2.51	0.0017	27.55	27.95	-0.30										
3.25	1.59	0.0035	2.03	0.0055	1.14	2.55	0.0011	1.14	2.50	0.0023	27.55	25.39	-0.51										
3.25	1.59	0.0024	2.03	0.0034	1.10	2.54	0.0027	1.14	2.79	0.0012	27.33	30.55	-3.55										
3.22	1.52	0.0051	2.03	0.0051	1.15	2.55	0.0059	1.15	2.53	0.0057	25.15	29.14	-0.99										
3.24	1.51	0.0015	2.05	0.0034	1.14	2.55	0.0054	1.15	2.51	0.0051	25.79	29.05	-2.25										
3.25	1.51	0.0005	2.03	0.0075	1.17	2.55	0.0053	1.15	2.52	0.0035	27.94	27.34	0.50										
3.25	1.52	0.0055	2.04	0.0047	1.14	2.55	0.0035	1.17	2.52	0.0012	27.73	29.41	-1.55										
3.25	1.50	0.0031	2.03	0.0039	1.14	2.55	0.0025	1.15	2.51	0.0014	27.54	25.75	-1.10										
3.25	1.50	0.0040	2.03	0.0020	1.14	2.52	0.0032	1.13	2.51	0.0007	27.72	25.94	-1.22										

Ulg3	Crystalline violet purpice 4	3.25	1.60	0.0038	2.03	0.0061	1.14	2.65	0.0039	1.15	2.60	0.0042	27.50	26.60	-1.30
		3.26	1.59	0.0030	2.03	0.0057	1.11	2.65	0.0065	1.15	2.61	0.0024	27.72	30.20	-2.46
		3.26	1.60	0.0011	2.03	0.0016	1.14	2.65	0.0047	1.14	2.79	0.0026	27.13	26.76	-1.65
	2.53	1.13	0.0011	2.24	0.0029	0.90	2.62	0.0031	0.69	2.63	0.0016	20.79	20.20	0.60	
	2.53	1.13	0.0039	2.24	0.0056	0.91	2.62	0.0053	0.69	2.63	0.0024	20.79	19.62	0.97	
	2.53	1.13	0.0026	2.24	0.0052	0.91	2.63	0.0027	0.69	2.63	0.0039	20.79	19.36	1.41	
	2.53	1.13	0.0101	2.21	0.0011	0.69	2.62	0.0026	0.69	2.60	0.0067	21.01	20.76	0.23	
	2.53	1.13	0.0053	2.24	0.0029	0.69	2.62	0.0097	0.69	2.63	0.0020	20.60	21.49	-0.66	
	2.54	1.13	0.0022	2.24	0.0024	0.68	2.62	0.0017	0.69	2.63	0.0064	20.60	22.25	-1.45	
	2.53	1.13	0.0039	2.24	0.0077	0.90	2.62	0.0021	0.69	2.63	0.0063	20.60	20.63	0.17	
	2.52	1.13	0.0100	2.27	0.0055	0.90	2.62	0.0036	0.69	2.66	0.0062	20.56	20.67	-0.11	
	2.53	1.13	0.0032	2.24	0.0024	0.91	2.63	0.0066	0.69	2.63	0.0031	20.60	19.53	1.26	
	2.51	1.15	0.0016	2.25	0.0051	0.90	2.64	0.0022	0.91	2.64	0.0023	20.74	22.04	-1.29	
	2.54	1.12	0.0014	2.24	0.0067	0.69	2.61	0.0019	0.66	2.63	0.0026	20.60	20.55	0.25	
	2.54	1.13	0.0010	2.24	0.0013	0.90	2.62	0.0091	0.69	2.63	0.0026	20.61	20.54	0.27	
	2.51	1.15	0.0047	2.24	0.0060	0.90	2.64	0.0027	0.91	2.63	0.0065	20.79	22.03	-1.24	
	2.52	1.14	0.0040	2.24	0.0056	0.92	2.63	0.0035	0.90	2.63	0.0016	20.60	19.02	1.77	
	2.52	1.13	0.0066	2.24	0.0020	0.90	2.62	0.0032	0.69	2.63	0.0029	20.79	20.36	0.41	
	2.53	1.13	0.0030	2.24	0.0061	0.90	2.63	0.0034	0.90	2.63	0.0029	20.76	20.99	-0.21	
	2.53	1.12	0.0096	2.24	0.0012	0.69	2.61	0.0015	0.66	2.63	0.0096	20.60	20.29	0.50	
	2.54	1.13	0.0017	2.24	0.0069	0.69	2.62	0.0091	0.69	2.63	0.0066	20.63	20.60	0.03	
	2.54	1.11	0.0066	2.24	0.0021	0.69	2.61	0.0039	0.66	2.63	0.0020	20.61	20.34	0.46	
	2.54	1.12	0.0037	2.21	0.0032	0.66	2.61	0.0016	0.67	2.60	0.0016	21.02	21.60	-0.76	
	2.55	1.10	0.0073	2.24	0.0021	0.67	2.60	0.0024	0.67	2.63	0.0014	20.63	21.34	-0.51	
	2.52	1.14	0.0046	2.24	0.0094	0.90	2.64	0.0026	0.90	2.63	0.0052	20.76	21.43	-0.65	
	2.53	1.15	0.0035	2.25	0.0016	0.91	2.64	0.0041	0.91	2.64	0.0061	20.75	21.26	-0.52	
	2.53	1.13	0.0089	2.24	0.0011	0.90	2.62	0.0031	0.69	2.63	0.0094	20.60	20.45	0.35	
	2.54	1.12	0.0066	2.24	0.0047	0.90	2.62	0.0021	0.66	2.63	0.0039	20.60	20.21	0.59	
	2.55	1.12	0.0061	2.24	0.0039	0.90	2.61	0.0016	0.66	2.62	0.0017	20.64	19.66	0.96	
	2.52	1.13	0.0066	2.26	0.0011	0.91	2.63	0.0031	0.69	2.67	0.0066	20.51	19.69	0.62	
2.53	1.14	0.0022	2.24	0.0077	0.90	2.64	0.0061	0.91	2.63	0.0014	20.79	20.97	-0.17		
2.53	1.10	0.0099	2.24	0.0022	0.90	2.60	0.0047	0.67	2.62	0.0051	20.64	16.90	1.94		
1.56	0.79	0.0093	2.06	0.0010	0.56	2.91	0.0030	0.56	2.66	0.0055	26.47	26.99	1.46		
1.61	0.61	0.0066	2.06	0.0019	0.56	2.69	0.0104	0.56	2.66	0.0019	27.67	31.16	-3.26		
1.61	0.79	0.0101	2.06	0.0066	0.56	2.69	0.0096	0.56	2.66	0.0036	26.05	26.46	-0.43		
1.61	0.76	0.0016	2.04	0.0099	0.55	2.66	0.0061	0.55	2.65	0.0065	26.15	29.99	-1.64		
1.60	0.79	0.0029	2.06	0.0097	0.56	2.90	0.0023	0.57	2.67	0.0023	26.24	26.61	-0.36		
1.61	0.62	0.0096	2.06	0.0017	0.57	2.90	0.0097	0.57	2.67	0.0021	26.06	30.12	-2.05		
1.61	0.79	0.0026	2.06	0.0021	0.57	2.69	0.0033	0.56	2.66	0.0030	27.36	26.12	-0.76		
1.61	0.76	0.0073	2.03	0.0014	0.56	2.69	0.0011	0.56	2.66	0.0037	26.77	26.59	0.16		
1.61	0.76	0.0027	2.06	0.0065	0.55	2.69	0.0011	0.56	2.66	0.0022	26.03	29.51	-1.49		
1.62	0.76	0.0026	2.05	0.0016	0.56	2.66	0.0066	0.55	2.65	0.0020	27.60	29.04	-1.24		
1.60	0.79	0.0071	2.06	0.0066	0.56	2.69	0.0046	0.56	2.66	0.0096	27.62	26.65	-0.63		
1.61	0.79	0.0041	2.06	0.0075	0.57	2.91	0.0026	0.56	2.66	0.0027	27.62	27.21	0.60		
1.61	0.76	0.0013	2.07	0.0012	0.57	2.91	0.0096	0.56	2.66	0.0036	26.13	27.45	0.69		
1.61	0.79	0.0060	2.06	0.0041	0.56	2.69	0.0054	0.56	2.66	0.0032	27.61	29.16	-1.37		
1.61	0.76	0.0020	2.05	0.0060	0.56	2.69	0.0011	0.56	2.66	0.0032	26.10	26.66	-0.76		
1.62	0.76	0.0019	2.05	0.0069	0.54	2.66	0.0102	0.56	2.65	0.0053	26.11	31.33	-3.22		
1.62	0.76	0.0044	2.05	0.0026	0.56	2.69	0.0096	0.56	2.66	0.0016	26.07	26.66	-0.79		

Ulg1-2	Crystalline fully altered pumice	1.61	0.76	0.0012	2.06	0.0031	0.56	2.69	0.0045	0.56	2.66	0.0036	26.06	26.66	-0.62
		1.64	0.76	0.0006	2.01	0.0032	0.53	2.67	0.0020	0.53	2.63	0.0023	26.96	32.62	-3.66
		1.57	0.76	0.0094	2.06	0.0016	0.56	2.69	0.0036	0.56	2.66	0.0091	26.01	26.57	-0.56
		1.61	0.76	0.0103	2.07	0.0012	0.56	2.90	0.0026	0.57	2.67	0.0023	27.69	26.65	-0.96
		1.61	0.79	0.0076	2.06	0.0011	0.56	2.69	0.0011	0.56	2.66	0.0024	26.01	26.96	-0.97
		1.61	0.76	0.0055	2.06	0.0015	0.59	2.91	0.0031	0.56	2.66	0.0041	26.56	25.06	3.50
		1.61	0.75	0.0015	2.06	0.0061	0.56	2.66	0.0026	0.55	2.65	0.0056	27.61	26.11	1.70
		1.62	0.76	0.0027	2.05	0.0017	0.54	2.69	0.0041	0.56	2.66	0.0039	26.32	31.31	-2.99
		1.64	0.74	0.0027	2.05	0.0043	0.55	2.66	0.0024	0.55	2.65	0.0053	26.11	26.60	1.52
		1.61	0.79	0.0011	2.07	0.0099	0.56	2.69	0.0034	0.56	2.66	0.0043	27.73	29.30	-1.57
1.61	0.76	0.0017	2.04	0.0061	0.56	2.67	0.0022	0.54	2.64	0.0026	27.92	26.69	-0.77		
1.61	0.77	0.0020	2.05	0.0016	0.56	2.69	0.0071	0.56	2.66	0.0029	26.06	27.61	0.26		
Ulg1-2	Crystalline grey-violet pumices 4	6.09	3.12	0.0012	1.96	0.0022	2.23	2.75	0.0035	2.22	2.74	0.0016	26.29	26.65	-0.36
		6.13	3.13	0.0031	1.97	0.0037	2.23	2.76	0.0025	2.22	2.75	0.0019	26.23	26.64	-0.61
		6.13	3.13	0.0025	1.96	0.0094	2.23	2.75	0.0035	2.24	2.74	0.0031	26.42	26.65	-0.23
		6.13	3.10	0.0040	1.94	0.0069	2.23	2.73	0.0015	2.22	2.73	0.0016	26.72	26.15	0.57
		6.13	3.12	0.0007	1.96	0.0030	2.23	2.75	0.0015	2.20	2.74	0.0033	26.25	26.71	-0.45
		6.14	3.12	0.0022	1.96	0.0094	2.21	2.75	0.0021	2.22	2.73	0.0012	26.06	29.33	-1.25
		6.13	3.14	0.0042	1.97	0.0015	2.24	2.77	0.0102	2.22	2.74	0.0103	26.05	26.61	-0.56
		6.13	3.12	0.0095	1.96	0.0016	2.23	2.75	0.0056	2.23	2.76	0.0019	26.77	26.50	0.27
		6.13	3.12	0.0026	1.96	0.0015	2.23	2.75	0.0096	2.23	2.74	0.0037	26.26	26.60	-0.34
		6.13	3.13	0.0041	1.96	0.0094	2.23	2.75	0.0042	2.23	2.74	0.0026	26.27	26.73	-0.46
		6.08	3.15	0.0036	1.96	0.0042	2.26	2.76	0.0022	2.22	2.74	0.0026	27.52	26.26	-0.74
		6.13	3.12	0.0095	1.96	0.0072	2.23	2.75	0.0024	2.22	2.74	0.0026	26.26	26.72	-0.46
		6.14	3.12	0.0025	1.96	0.0076	2.23	2.75	0.0050	2.22	2.74	0.0016	26.25	26.73	-0.48
		6.14	3.11	0.0015	1.95	0.0099	2.23	2.74	0.0057	2.21	2.74	0.0006	26.64	26.41	0.24
		6.10	3.15	0.0045	1.96	0.0030	2.25	2.77	0.0013	2.22	2.74	0.0079	27.59	26.54	-0.95
		6.13	3.13	0.0026	1.96	0.0025	2.23	2.76	0.0092	2.23	2.74	0.0042	26.39	26.67	-0.28
		6.13	3.15	0.0072	1.96	0.0024	2.24	2.77	0.0099	2.23	2.75	0.0020	27.65	26.64	-0.96
		6.13	3.12	0.0022	1.96	0.0032	2.23	2.75	0.0067	2.21	2.73	0.0022	26.23	26.71	-0.48
		6.13	3.12	0.0010	1.95	0.0012	2.22	2.75	0.0045	2.22	2.73	0.0024	26.37	26.66	-0.49
		6.16	3.10	0.0045	1.94	0.0097	2.20	2.73	0.0034	2.19	2.69	0.0064	27.99	29.07	-1.09
		6.12	3.13	0.0010	1.96	0.0016	2.23	2.75	0.0011	2.22	2.74	0.0063	26.42	26.66	-0.24
		6.13	3.14	0.0102	1.96	0.0016	2.24	2.77	0.0099	2.23	2.76	0.0030	26.11	26.60	-0.48
		6.13	3.12	0.0023	1.96	0.0055	2.22	2.75	0.0026	2.22	2.74	0.0020	26.30	26.65	-0.35
6.14	3.12	0.0094	1.95	0.0014	2.21	2.75	0.0029	2.20	2.74	0.0031	26.61	26.93	-0.12		
6.16	3.11	0.0069	1.95	0.0067	2.21	2.74	0.0026	2.22	2.73	0.0024	26.42	26.67	-0.45		
6.12	3.14	0.0064	1.97	0.0049	2.23	2.76	0.0042	2.25	2.74	0.0056	27.93	26.64	-0.91		
6.13	3.13	0.0034	1.96	0.0071	2.23	2.76	0.0104	2.23	2.75	0.0062	26.46	26.67	-0.16		
6.13	3.12	0.0015	1.96	0.0036	2.23	2.75	0.0019	2.22	2.72	0.0100	27.72	26.71	-0.99		
6.13	3.12	0.0004	1.95	0.0072	2.23	2.75	0.0016	2.22	2.74	0.0037	26.62	26.55	0.06		
Average				1.33			2.65			3.04		55.25	53.05	2.21	
Ulg7				0.96			2.75			2.77		65.01	64.78	0.23	
Ulg4-6				1.13			2.92			3.27		64.62	60.67	3.76	
Ulg3				2.15			2.66			2.64		24.43	24.71	-0.27	
Ulg1-2				1.96			2.75			2.74		26.25	26.70	-0.45	
Ulg7 i2	9.16	3.49	0.0046	2.63	0.0036	3.23	2.64	0.0016	3.06	2.66	0.0033	7.95	7.40	0.56	
Ulg7 i2	7.71	3.20	0.0046	2.41	0.0035	2.95	2.61	0.0025	2.67	2.64	0.0012	6.62	7.66	0.96	
Ulg7 i2	5.76	2.22	0.0090	2.61	0.0011	2.06	2.60	0.0026	1.76	2.65	0.0021	6.66	7.00	1.66	

Ulg7 i3	9.94	3.97	0.0067	2.50	0.0042	3.00	3.31	0.0034	3.25	2.76	0.0031	9.42	24.40	-14.95
Ulg7 i2	10.77	4.05	0.0094	2.66	0.0060	3.00	2.83	0.0011	3.43	2.81	0.0010	5.39	6.20	-0.81
Ulg4-6 i6	2.55	0.94	0.0050	2.72	0.0015	0.90	2.82	0.0020	0.84	2.89	0.0024	5.91	3.43	2.45
Ulg4-6 i1	0.59	0.29	0.0094	2.04	0.0080	0.21	2.83	0.0006	0.16	3.10	0.0009	34.27	28.03	6.24
Ulg4-6 i2	0.76	0.29	0.0062	2.59	0.0055	0.27	2.77	0.0004	0.25	2.97	0.0015	12.77	6.52	6.25
Ulg4-6 i2	0.29	0.11	0.0024	2.57	0.0056	0.11	2.64	0.0007	0.09	3.15	0.0011	16.50	2.89	15.61
Ulg4-6 i3	0.67	0.26	0.0037	2.35	0.0011	0.23	2.91	0.0032	0.20	3.15	0.0041	25.44	19.41	6.02
Ulg4-6 i4	0.52	0.21	0.0099	2.43	0.0084	0.17	3.05	0.0015	0.15	3.37	0.0014	27.91	20.43	7.45
Ulg4-6 i4	0.64	0.24	0.0020	2.62	0.0023	0.25	2.61	0.0007	0.22	2.91	0.0006	9.74	-0.45	10.19
Ulg4-6 i2	3.53	1.37	0.0093	2.57	0.0092	1.28	2.75	0.0007	1.24	2.80	0.0027	8.22	6.56	1.65
Ulg4-6 i3	7.06	3.26	0.0095	2.17	0.0099	2.61	2.70	0.0017	2.49	2.71	0.0022	20.22	19.86	0.36
Ulg4-6 i5	3.24	1.24	0.0013	2.62	0.0026	1.16	2.79	0.0030	1.10	2.85	0.0027	6.14	6.24	1.69
Ulg4-6 i6	2.35	0.67	0.0071	2.71	0.0091	0.85	2.76	0.0041	0.82	2.76	0.0031	1.71	1.52	0.19
Ulg4-6 i5	6.21	2.56	0.0089	2.40	0.0091	2.26	2.75	0.0033	2.21	2.73	0.0018	12.06	12.53	-0.47
Ulg4-6 i2	3.62	1.47	0.0061	2.46	0.0092	1.26	2.67	0.0026	1.19	2.85	0.0011	13.55	14.22	-0.67
Ulg4-6 i3	2.61	1.12	0.0022	2.32	0.0047	0.94	2.79	0.0032	0.89	2.73	0.0057	14.84	16.70	-1.86
Ulg3 i2	1.99	0.80	0.0011	2.49	0.0035	0.71	2.79	0.0034	0.70	2.76	0.0013	10.13	10.54	-0.41
Ulg1-2 i2	3.67	1.71	0.0039	2.26	0.0051	1.44	2.69	0.0010	1.37	2.73	0.0026	17.40	16.11	1.29
Average				2.46			2.61			2.66		13.38	11.31	2.06
Ulg7 lith				2.56			2.66			2.76		6.05	10.57	-2.52
Ulg4-6 lith				2.47			2.79			2.93		15.23	11.26	3.96
Ulg3 lith				2.49			2.79			2.76		10.13	10.54	-0.41
Ulg1-2 lith				2.26			2.69			2.73		17.40	16.11	1.29

Kokowai bed-set

	Wgt g	Envelope (Bulk) Density				Skeletal Density			Solid Density			Porosity		
		cm3	SD	g/cm3	SD	cm3	g/cm3	Vol SD	cm3	g/cm3	Vol SD	Bulk %	Conn %	Iso %
	2.56	3.29	0.0013	0.79	0.0032	0.93	2.61	0.0021	0.89	2.66	0.0011	72.43	71.62	0.62
	2.60	3.29	0.0039	0.79	0.0076	0.96	2.61	0.0046	0.89	2.66	0.0023	72.45	70.90	1.55
	2.60	3.29	0.0014	0.79	0.0049	0.93	2.61	0.0012	0.89	2.69	0.0040	72.60	71.63	0.77
	2.61	3.29	0.0008	0.79	0.0037	0.90	2.60	0.0037	0.86	2.66	0.0010	72.53	72.74	-0.21
	2.61	3.29	0.0063	0.78	0.0024	0.93	2.60	0.0047	0.86	2.67	0.0014	72.75	71.67	0.89
	2.61	3.29	0.0011	0.79	0.0026	0.93	2.79	0.0065	0.86	2.66	0.0015	72.55	71.62	0.74
	2.60	3.29	0.0026	0.80	0.0022	0.96	2.62	0.0076	0.89	2.89	0.0021	72.17	70.90	1.27
	2.60	3.29	0.0089	0.79	0.0021	0.93	2.61	0.0024	0.89	2.66	0.0037	72.50	71.62	0.69
	2.60	3.26	0.0062	0.79	0.0015	0.92	2.61	0.0105	0.86	2.66	0.0012	72.31	71.67	0.64
	2.61	3.26	0.0007	0.78	0.0026	0.92	2.60	0.0051	0.87	2.66	0.0023	72.95	71.66	1.09
	2.59	3.29	0.0053	0.80	0.0023	0.93	2.62	0.0016	0.91	2.66	0.0046	72.39	71.74	0.65
	2.60	3.29	0.0025	0.80	0.0047	0.93	2.61	0.0029	0.90	2.66	0.0050	72.37	71.79	0.58
	2.55	3.30	0.0021	0.82	0.0094	0.93	2.63	0.0033	0.89	2.66	0.0031	71.46	71.67	-0.41
	2.60	3.29	0.0011	0.79	0.0026	0.93	2.61	0.0052	0.86	2.66	0.0015	72.49	71.61	0.66
	2.61	3.29	0.0016	0.77	0.0021	0.93	2.60	0.0046	0.89	2.67	0.0025	73.12	71.64	1.26
	2.63	3.26	0.0004	0.76	0.0045	0.93	2.78	0.0026	0.86	2.64	0.0032	73.19	71.76	1.41
	2.59	3.32	0.0023	0.79	0.0043	0.93	2.61	0.0006	0.89	2.89	0.0040	72.49	72.06	0.43
	2.60	3.29	0.0016	0.81	0.0097	0.93	2.62	0.0050	0.90	2.90	0.0032	72.16	71.75	0.44
	2.60	3.30	0.0022	0.80	0.0063	0.93	2.63	0.0035	0.90	2.89	0.0021	72.23	71.66	0.36
	2.60	3.26	0.0009	0.79	0.0011	0.92	2.78	0.0031	0.89	2.67	0.0022	72.40	71.64	0.57

		2.61	3.29	0.0022	0.79	0.0009	0.93	2.61	0.0009	0.66	2.66	0.0014	72.52	71.62	0.70
		2.63	3.26	0.0007	0.76	0.0024	0.89	2.60	0.0066	0.69	2.67	0.0012	72.66	73.04	-0.16
		2.57	3.29	0.0022	0.81	0.0035	0.94	2.63	0.0016	0.69	2.66	0.0023	71.61	71.56	0.24
		2.60	3.33	0.0019	0.79	0.0046	0.94	2.61	0.0023	0.90	2.69	0.0094	72.50	71.66	0.62
		2.60	3.29	0.0036	0.80	0.0096	0.93	2.61	0.0020	0.69	2.90	0.0029	72.45	71.77	0.66
		2.60	3.29	0.0031	0.79	0.0012	0.93	2.61	0.0024	0.90	2.69	0.0049	72.49	71.60	0.66
		2.60	3.29	0.0012	0.79	0.0006	0.93	2.61	0.0021	0.69	2.66	0.0015	72.72	71.67	0.65
		2.61	3.29	0.0095	0.79	0.0023	0.92	2.61	0.0023	0.67	2.66	0.0037	72.51	72.17	0.34
		2.61	3.29	0.0016	0.77	0.0014	0.93	2.61	0.0007	0.69	2.67	0.0032	73.12	71.64	1.26
		2.60	3.29	0.0009	0.79	0.0043	0.94	2.61	0.0006	0.66	2.66	0.0010	72.55	71.57	0.99
		1.20	1.63	0.0024	0.67	0.0026	0.44	3.03	0.0033	0.37	3.12	0.0092	76.44	75.96	2.46
		1.21	1.63	0.0012	0.67	0.0037	0.40	3.03	0.0064	0.36	3.12	0.0059	76.57	76.06	0.49
		1.21	1.63	0.0017	0.67	0.0013	0.40	3.03	0.0096	0.36	3.12	0.0039	76.46	76.04	0.42
		1.21	1.62	0.0007	0.66	0.0013	0.40	3.03	0.0100	0.35	3.11	0.0019	76.76	76.00	0.76
		1.22	1.62	0.0030	0.66	0.0012	0.40	3.01	0.0070	0.36	3.11	0.0016	76.70	76.06	0.64
		1.22	1.61	0.0011	0.65	0.0011	0.40	3.02	0.0046	0.35	3.10	0.0016	76.93	77.97	0.96
		1.19	1.65	0.0038	0.66	0.0030	0.40	3.05	0.0013	0.36	3.11	0.0007	76.66	76.32	0.35
		1.20	1.63	0.0034	0.67	0.0031	0.40	3.03	0.0060	0.36	3.12	0.0069	76.56	76.09	0.49
		1.21	1.63	0.0023	0.66	0.0067	0.40	3.03	0.0045	0.37	3.12	0.0023	76.36	76.10	0.27
		1.21	1.63	0.0034	0.65	0.0066	0.40	3.03	0.0069	0.36	3.10	0.0014	76.95	76.13	0.61
		1.22	1.63	0.0036	0.66	0.0006	0.40	3.03	0.0090	0.36	3.11	0.0046	76.75	76.31	0.44
		1.22	1.62	0.0013	0.64	0.0066	0.37	3.01	0.0079	0.35	3.09	0.0045	79.20	79.67	-0.47
		1.20	1.63	0.0036	0.66	0.0039	0.43	3.03	0.0042	0.37	3.11	0.0050	76.69	76.35	2.34
		1.21	1.64	0.0010	0.67	0.0036	0.40	3.04	0.0060	0.36	3.12	0.0100	76.46	76.26	0.22
		1.21	1.65	0.0016	0.66	0.0069	0.41	3.06	0.0050	0.36	3.11	0.0027	76.66	77.97	0.69
		1.21	1.62	0.0016	0.66	0.0096	0.40	3.02	0.0056	0.36	3.11	0.0013	76.70	76.07	0.64
		1.23	1.60	0.0095	0.63	0.0052	0.40	2.99	0.0099	0.34	3.06	0.0034	79.46	76.02	1.45
		1.17	1.63	0.0025	0.66	0.0046	0.40	3.03	0.0014	0.36	3.11	0.0004	76.67	76.09	0.56
		1.21	1.63	0.0021	0.66	0.0012	0.40	3.03	0.0015	0.37	3.11	0.0096	76.66	76.03	0.66
		1.21	1.63	0.0011	0.66	0.0047	0.40	3.03	0.0016	0.37	3.13	0.0039	76.32	76.07	0.26
		1.21	1.60	0.0027	0.66	0.0023	0.39	3.03	0.0017	0.34	3.11	0.0014	76.71	76.11	0.60
		1.22	1.63	0.0051	0.64	0.0019	0.40	3.03	0.0057	0.36	3.09	0.0072	79.16	76.13	1.05
		1.23	1.61	0.0021	0.66	0.0029	0.39	3.01	0.0030	0.35	3.11	0.0011	76.71	76.30	0.41
		1.20	1.64	0.0015	0.69	0.0025	0.40	3.03	0.0024	0.36	3.14	0.0046	76.02	76.22	-0.20
		1.20	1.64	0.0035	0.66	0.0024	0.40	3.04	0.0012	0.36	3.11	0.0091	76.69	76.13	0.56
		1.21	1.63	0.0022	0.66	0.0006	0.40	3.03	0.0019	0.36	3.11	0.0031	76.69	76.09	0.60
		1.21	1.63	0.0016	0.66	0.0022	0.37	3.03	0.0011	0.36	3.11	0.0015	76.75	79.66	-0.91
		1.22	1.62	0.0013	0.66	0.0015	0.40	3.02	0.0096	0.35	3.11	0.0044	76.63	76.02	0.61
		1.22	1.63	0.0064	0.66	0.0015	0.40	3.01	0.0063	0.36	3.11	0.0017	76.70	76.16	0.54
		1.21	1.63	0.0011	0.66	0.0011	0.40	3.03	0.0013	0.36	3.11	0.0007	76.70	76.09	0.61
		3.60	3.26	0.0023	1.16	0.0060	1.41	2.77	0.0016	1.35	2.61	0.0074	66.10	66.76	1.32
		3.61	3.26	0.0036	1.17	0.0033	1.36	2.76	0.0049	1.35	2.61	0.0030	66.34	67.66	0.66
		3.61	3.26	0.0035	1.16	0.0046	1.39	2.76	0.0065	1.35	2.62	0.0030	66.16	67.46	0.66
		3.61	3.25	0.0029	1.17	0.0030	1.36	2.76	0.0019	1.35	2.60	0.0013	66.22	67.64	0.56
		3.62	3.24	0.0022	1.16	0.0012	1.36	2.76	0.0097	1.35	2.60	0.0047	66.51	67.44	1.07
		3.60	3.26	0.0037	1.16	0.0071	1.36	2.76	0.0066	1.35	2.60	0.0040	67.97	67.67	0.30
		3.61	3.27	0.0016	1.19	0.0099	1.36	2.76	0.0044	1.37	2.61	0.0012	67.63	67.76	-0.15
		3.61	3.26	0.0016	1.15	0.0051	1.36	2.76	0.0026	1.35	2.60	0.0042	66.93	67.77	1.16
		3.62	3.25	0.0026	1.16	0.0013	1.36	2.76	0.0070	1.34	2.60	0.0013	66.51	67.59	0.92

Dense grey pumice	3.62	3.25	0.0019	1.17	0.0017	1.35	2.75	0.0040	1.34	2.79	0.0029	55.09	57.66	0.44
	3.77	3.26	0.0017	1.17	0.0050	1.35	2.76	0.0005	1.35	2.80	0.0026	55.16	57.70	0.45
	3.60	3.26	0.0014	1.16	0.0064	1.39	2.77	0.0013	1.35	2.81	0.0016	55.01	57.43	0.55
	3.61	3.26	0.0012	1.16	0.0030	1.35	2.77	0.0017	1.36	2.80	0.0012	57.53	57.67	0.16
	3.76	3.29	0.0014	1.17	0.0090	1.35	2.79	0.0012	1.37	2.80	0.0026	56.24	56.05	0.19
	3.61	3.26	0.0047	1.16	0.0013	1.35	2.74	0.0027	1.33	2.80	0.0027	56.60	57.73	0.66
	3.62	3.26	0.0021	1.17	0.0021	1.35	2.76	0.0101	1.35	2.80	0.0067	56.21	57.69	0.52
	3.62	3.24	0.0007	1.17	0.0010	1.37	2.76	0.0067	1.33	2.75	0.0031	57.92	57.60	0.12
	3.79	3.26	0.0026	1.17	0.0096	1.39	2.79	0.0064	1.37	2.80	0.0033	56.14	57.69	0.44
	3.61	3.26	0.0020	1.19	0.0100	1.35	2.76	0.0067	1.35	2.81	0.0046	57.56	57.71	-0.13
	3.61	3.26	0.0016	1.17	0.0045	1.35	2.76	0.0097	1.35	2.81	0.0021	56.35	57.63	0.72
	3.61	3.26	0.0021	1.17	0.0064	1.35	2.76	0.0093	1.34	2.80	0.0036	56.19	56.59	-0.40
	3.61	3.26	0.0097	1.17	0.0052	1.35	2.76	0.0015	1.35	2.80	0.0059	56.22	57.67	0.55
	3.63	3.23	0.0012	1.13	0.0041	1.35	2.74	0.0053	1.33	2.77	0.0017	59.29	57.26	2.02
	3.60	3.26	0.0036	1.17	0.0091	1.35	2.75	0.0069	1.36	2.83	0.0011	55.53	57.63	0.90
	3.60	3.27	0.0012	1.16	0.0047	1.41	2.76	0.0023	1.36	2.80	0.0021	57.94	56.66	1.06
	3.61	3.27	0.0035	1.16	0.0096	1.35	2.79	0.0010	1.37	2.81	0.0013	57.93	57.61	0.13
	3.61	3.26	0.0041	1.17	0.0036	1.35	2.76	0.0049	1.35	2.79	0.0037	56.14	57.67	0.47
	3.62	3.24	0.0035	1.16	0.0095	1.35	2.76	0.0060	1.34	2.80	0.0043	56.51	57.44	1.07
	3.63	3.24	0.0016	1.16	0.0026	1.34	2.75	0.0030	1.34	2.80	0.0013	56.56	56.79	-0.23
3.61	3.26	0.0014	1.17	0.0064	1.35	2.76	0.0019	1.35	2.80	0.0029	56.16	57.70	0.46	
Kw7 Middle Yellow pumice	1.67	2.64	0.0047	0.67	0.0015	0.61	2.91	0.0003	0.59	2.96	0.0010	77.63	77.05	0.58
	1.70	2.64	0.0023	0.65	0.0004	0.59	2.92	0.0090	0.57	2.97	0.0021	76.06	77.76	0.30
	1.70	2.63	0.0046	0.66	0.0025	0.61	2.92	0.0001	0.56	2.96	0.0040	77.94	77.00	0.94
	1.69	2.63	0.0006	0.66	0.0031	0.61	2.91	0.0026	0.60	2.99	0.0023	77.32	76.97	0.34
	1.70	2.63	0.0019	0.65	0.0016	0.56	2.91	0.0011	0.57	2.94	0.0014	77.96	76.50	-0.52
	1.71	2.63	0.0007	0.65	0.0057	0.57	2.90	0.0001	0.57	2.95	0.0046	76.10	76.15	-0.05
	1.70	2.63	0.0046	0.65	0.0011	0.59	2.91	0.0003	0.57	2.96	0.0020	76.09	77.73	0.36
	1.70	2.63	0.0025	0.66	0.0042	0.60	2.92	0.0095	0.56	2.96	0.0040	77.76	77.07	0.72
	1.70	2.63	0.0063	0.63	0.0024	0.56	2.91	0.0001	0.55	2.96	0.0025	76.63	77.77	1.06
	1.71	2.62	0.0022	0.63	0.0096	0.57	2.89	0.0001	0.56	2.95	0.0046	76.53	76.24	0.29
	1.70	2.63	0.0022	0.65	0.0006	0.60	2.93	0.0003	0.57	2.97	0.0050	76.11	77.36	0.75
	1.70	2.66	0.0017	0.65	0.0014	0.59	2.91	0.0056	0.57	2.97	0.0049	76.06	77.99	0.09
	1.70	2.63	0.0011	0.65	0.0024	0.59	2.91	0.0036	0.57	2.97	0.0019	76.20	77.41	0.79
	1.70	2.63	0.0021	0.65	0.0022	0.59	2.92	0.0033	0.57	2.96	0.0035	76.17	77.72	0.45
	1.70	2.63	0.0019	0.65	0.0056	0.56	2.90	0.0011	0.57	2.96	0.0021	76.16	77.77	0.40
	1.70	2.63	0.0034	0.65	0.0006	0.59	2.91	0.0019	0.57	2.96	0.0064	76.16	77.74	0.42
	1.70	2.63	0.0015	0.64	0.0069	0.57	2.90	0.0011	0.56	2.96	0.0021	76.44	76.13	0.32
	1.70	2.63	0.0023	0.63	0.0001	0.56	2.91	0.0011	0.55	2.96	0.0037	76.60	76.06	0.72
	1.73	2.63	0.0016	0.62	0.0094	0.56	2.86	0.0001	0.54	2.94	0.0090	79.01	76.61	0.40
	1.70	2.66	0.0053	0.66	0.0007	0.60	2.91	0.0001	0.56	2.96	0.0020	77.65	77.57	0.26
	1.70	2.63	0.0095	0.65	0.0033	0.59	2.92	0.0001	0.57	2.96	0.0026	76.03	77.73	0.30
	1.70	2.63	0.0015	0.64	0.0015	0.56	2.91	0.0011	0.56	2.96	0.0020	76.35	77.76	0.56
	1.70	2.60	0.0014	0.65	0.0094	0.56	2.90	0.0037	0.57	2.96	0.0026	76.13	77.67	0.26
	1.74	2.59	0.0011	0.63	0.0037	0.57	2.91	0.0001	0.56	2.95	0.0069	76.52	77.62	0.70
	1.67	2.63	0.0023	0.65	0.0011	0.59	2.91	0.0003	0.57	2.96	0.0007	76.06	77.74	0.35
	1.70	2.63	0.0016	0.65	0.0013	0.59	2.91	0.0069	0.56	2.96	0.0031	77.93	77.74	0.16
	1.70	2.64	0.0007	0.65	0.0016	0.59	2.92	0.0026	0.57	2.96	0.0043	76.06	77.76	0.32
1.70	2.63	0.0033	0.65	0.0007	0.59	2.91	0.0011	0.57	2.96	0.0007	76.16	77.72	0.44	

Kw7 Base	Yellow pumice (and banded)	1.70	2.63	0.0009	0.65	0.0001	0.59	2.91	0.0006	0.57	2.96	0.0014	76.19	77.75	0.44	
		1.70	2.63	0.0021	0.65	0.0018	0.55	2.91	0.0003	0.57	2.96	0.0025	76.16	77.76	0.35	
		2.32	3.52	0.0007	0.67	0.0016	0.62	2.88	0.0045	0.60	2.93	0.0001	77.02	76.63	0.38	
		2.35	3.52	0.0011	0.70	0.0026	0.62	2.89	0.0028	0.61	2.96	0.0047	76.34	76.64	-0.30	
		2.36	3.53	0.0064	0.66	0.0077	0.62	2.89	0.0036	0.61	2.94	0.0023	76.62	76.75	0.07	
		2.33	3.51	0.0025	0.67	0.0042	0.63	2.90	0.0023	0.62	2.93	0.0066	77.01	76.43	0.58	
		2.36	3.51	0.0022	0.67	0.0007	0.62	2.87	0.0019	0.60	2.93	0.0008	77.05	76.63	0.42	
		2.37	3.51	0.0027	0.66	0.0019	0.62	2.86	0.0011	0.79	2.92	0.0043	77.29	76.66	0.63	
		2.36	3.51	0.0075	0.67	0.0033	0.62	2.86	0.0029	0.60	2.93	0.0036	77.04	76.63	0.41	
		2.36	3.53	0.0031	0.66	0.0035	0.63	2.90	0.0066	0.62	2.94	0.0055	76.60	76.54	0.25	
		2.36	3.49	0.0016	0.67	0.0013	0.79	2.88	0.0003	0.60	2.93	0.0026	77.10	77.31	-0.21	
		2.37	3.51	0.0021	0.65	0.0012	0.62	2.86	0.0029	0.60	2.91	0.0011	77.54	76.65	0.89	
		2.37	3.51	0.0067	0.65	0.0007	0.79	2.87	0.0011	0.78	2.91	0.0026	77.57	77.50	0.07	
		2.35	3.52	0.0011	0.67	0.0041	0.65	2.86	0.0025	0.60	2.93	0.0049	77.04	75.77	1.27	
		2.36	3.52	0.0011	0.66	0.0034	0.62	2.86	0.0011	0.60	2.93	0.0006	76.93	76.65	0.27	
		2.36	3.53	0.0041	0.67	0.0057	0.62	2.86	0.0016	0.61	2.93	0.0076	77.03	76.63	0.40	
		2.36	3.52	0.0014	0.66	0.0079	0.62	2.86	0.0013	0.60	2.94	0.0046	76.60	76.61	0.19	
		2.36	3.52	0.0014	0.69	0.0012	0.62	2.86	0.0066	0.60	2.94	0.0066	76.66	76.66	-0.01	
		2.37	3.51	0.0024	0.67	0.0026	0.62	2.87	0.0012	0.79	2.93	0.0010	77.11	76.63	0.46	
		2.37	3.51	0.0016	0.67	0.0012	0.62	2.87	0.0040	0.79	2.93	0.0011	77.05	76.59	0.45	
		2.37	3.51	0.0011	0.67	0.0021	0.62	2.86	0.0020	0.60	2.93	0.0020	77.10	76.74	0.36	
		2.39	3.47	0.0025	0.64	0.0094	0.62	2.85	0.0011	0.77	2.90	0.0032	77.64	76.46	1.36	
		2.33	3.52	0.0011	0.67	0.0069	0.62	2.90	0.0024	0.62	2.93	0.0001	77.02	76.64	0.39	
		2.36	3.52	0.0004	0.67	0.0034	0.62	2.89	0.0026	0.61	2.93	0.0016	77.04	76.63	0.41	
		2.36	3.52	0.0016	0.69	0.0011	0.62	2.86	0.0046	0.60	2.94	0.0093	76.70	76.64	0.06	
		2.36	3.51	0.0015	0.66	0.0007	0.62	2.86	0.0013	0.60	2.92	0.0012	77.30	76.64	0.66	
		2.37	3.50	0.0009	0.67	0.0036	0.62	2.87	0.0032	0.79	2.92	0.0022	77.16	76.57	0.61	
		2.39	3.50	0.0006	0.67	0.0062	0.62	2.87	0.0013	0.79	2.93	0.0031	77.06	76.74	0.32	
		2.36	3.52	0.0015	0.66	0.0016	0.66	2.86	0.0066	0.60	2.94	0.0021	76.76	75.59	1.19	
		2.33	3.50	0.0012	0.67	0.0007	0.62	2.85	0.0026	0.78	2.93	0.0012	77.06	76.72	0.34	
		2.37	3.51	0.0095	0.67	0.0040	0.62	2.86	0.0029	0.60	2.93	0.0013	77.04	76.62	0.43	
		2.36	3.52	0.0011	0.67	0.0069	0.62	2.86	0.0040	0.60	2.93	0.0032	77.00	76.65	0.35	
		Dense grey pumice	3.16	2.69	0.0011	1.20	0.0011	1.16	2.70	0.0007	1.13	2.77	0.0007	56.76	56.07	0.70
			3.19	2.69	0.0032	1.19	0.0011	1.16	2.71	0.0001	1.13	2.76	0.0001	56.67	56.12	0.75
			3.19	2.70	0.0023	1.19	0.0001	1.19	2.70	0.0007	1.14	2.76	0.0001	56.97	56.06	0.91
			3.19	2.69	0.0019	1.20	0.0001	1.16	2.70	0.0007	1.13	2.77	0.0001	56.71	56.11	0.60
			3.19	2.66	0.0020	1.16	0.0007	1.17	2.69	0.0011	1.12	2.75	0.0001	57.09	56.25	0.64
			3.20	2.66	0.0011	1.16	0.0017	1.16	2.70	0.0003	1.12	2.75	0.0012	57.17	56.54	0.63
			3.16	2.70	0.0011	1.21	0.0011	1.19	2.71	0.0022	1.14	2.76	0.0012	56.43	55.89	0.53
			3.19	2.71	0.0015	1.19	0.0011	1.20	2.72	0.0007	1.15	2.76	0.0001	56.61	55.85	0.95
			3.19	2.69	0.0003	1.20	0.0001	1.16	2.70	0.0007	1.13	2.77	0.0011	56.66	56.12	0.56
			3.19	2.69	0.0007	1.16	0.0007	1.16	2.70	0.0019	1.13	2.75	0.0007	57.19	56.13	1.05
			3.19	2.66	0.0021	1.19	0.0016	1.17	2.66	0.0011	1.12	2.76	0.0001	56.96	56.21	0.77
			3.20	2.67	0.0011	1.17	0.0016	1.17	2.69	0.0003	1.11	2.74	0.0020	57.40	56.20	1.20
			3.17	2.71	0.0011	1.19	0.0006	1.20	2.72	0.0034	1.15	2.76	0.0012	56.97	55.66	1.29
			3.16	2.69	0.0014	1.19	0.0011	1.16	2.70	0.0001	1.13	2.76	0.0001	56.69	56.06	0.63
			3.19	2.71	0.0026	1.19	0.0001	1.20	2.71	0.0016	1.15	2.76	0.0001	56.79	55.67	1.12
		3.19	2.67	0.0003	1.16	0.0007	1.15	2.70	0.0003	1.11	2.75	0.0007	56.99	56.72	0.27	
		3.19	2.69	0.0014	1.17	0.0009	1.16	2.70	0.0019	1.13	2.74	0.0001	57.37	56.15	1.22	

Kw4 Top	Dense grey pumice	3.21	2.67	0.0011	1.16	0.0025	1.15	2.67	0.0003	1.10	2.73	0.0029	57.61	56.80	0.81		
		3.14	2.69	0.0011	1.19	0.0018	1.18	2.70	0.0010	1.13	2.76	0.0020	56.96	56.11	0.85		
		3.19	2.69	0.0032	1.19	0.0001	1.18	2.71	0.0007	1.13	2.76	0.0001	56.79	56.12	0.66		
		3.19	2.71	0.0033	1.19	0.0001	1.20	2.73	0.0007	1.15	2.76	0.0011	56.95	55.64	1.31		
		3.19	2.69	0.0095	1.19	0.0096	1.18	2.70	0.0019	1.13	2.76	0.0016	56.96	56.13	0.83		
		3.20	2.69	0.0029	1.19	0.0011	1.18	2.68	0.0011	1.13	2.76	0.0029	56.96	56.16	0.82		
		3.21	2.68	0.0011	1.18	0.0028	1.17	2.69	0.0003	1.12	2.75	0.0025	56.99	56.38	0.62		
		3.18	2.69	0.0011	1.19	0.0011	1.18	2.70	0.0011	1.13	2.76	0.0008	56.96	56.11	0.87		
		3.18	2.70	0.0021	1.19	0.0011	1.19	2.71	0.0001	1.14	2.76	0.0001	56.97	55.88	1.10		
		3.19	2.69	0.0003	1.18	0.0012	1.18	2.70	0.0003	1.13	2.75	0.0007	57.02	56.14	0.88		
		3.19	2.68	0.0009	1.18	0.0007	1.17	2.70	0.0015	1.12	2.75	0.0001	57.03	56.27	0.77		
		3.19	2.69	0.0026	1.18	0.0011	1.18	2.70	0.0011	1.13	2.75	0.0001	57.02	56.13	0.89		
		3.19	2.69	0.0003	1.19	0.0025	1.18	2.70	0.0018	1.13	2.76	0.0020	57.00	56.16	0.84		
		Kw4 Top	Dense grey pumice	3.77	3.26	0.0038	1.17	0.0012	1.38	2.77	0.0024	1.35	2.80	0.0021	58.25	57.64	0.61
				3.81	3.30	0.0072	1.18	0.0012	1.39	2.77	0.0014	1.39	2.80	0.0012	57.95	57.87	0.08
				3.81	3.26	0.0019	1.17	0.0021	1.39	2.76	0.0059	1.35	2.80	0.0082	58.24	57.39	0.85
				3.81	3.25	0.0030	1.17	0.0048	1.38	2.75	0.0020	1.34	2.80	0.0014	58.30	57.61	0.69
				3.81	3.26	0.0105	1.16	0.0011	1.38	2.76	0.0022	1.35	2.80	0.0035	58.64	58.24	0.41
				3.82	3.25	0.0027	1.17	0.0023	1.38	2.76	0.0019	1.35	2.78	0.0111	57.97	57.65	0.32
				3.81	3.26	0.0097	1.17	0.0052	1.38	2.76	0.0015	1.35	2.80	0.0059	58.22	57.67	0.55
3.81	3.26			0.0037	1.17	0.0014	1.38	2.76	0.0097	1.35	2.81	0.0026	58.27	57.51	0.76		
3.81	3.23			0.0012	1.17	0.0016	1.38	2.74	0.0042	1.32	2.80	0.0025	58.34	57.35	0.98		
3.81	3.25			0.0071	1.17	0.0020	1.38	2.76	0.0023	1.35	2.80	0.0067	58.25	57.68	0.58		
3.82	3.23			0.0052	1.16	0.0028	1.38	2.76	0.0035	1.32	2.79	0.0088	58.38	57.88	0.50		
3.80	3.29			0.0014	1.17	0.0092	1.38	2.77	0.0009	1.38	2.80	0.0019	58.22	58.07	0.15		
3.81	3.26			0.0031	1.20	0.0028	1.38	2.77	0.0107	1.35	2.80	0.0019	57.19	57.54	-0.35		
3.81	3.26			0.0044	1.17	0.0038	1.39	2.76	0.0054	1.35	2.82	0.0074	58.35	57.41	0.94		
3.81	3.26			0.0103	1.17	0.0038	1.39	2.77	0.0107	1.35	2.80	0.0088	58.17	57.26	0.91		
3.81	3.26			0.0021	1.17	0.0096	1.37	2.76	0.0029	1.35	2.80	0.0015	58.22	57.98	0.26		
3.81	3.26			0.0044	1.17	0.0017	1.38	2.76	0.0037	1.35	2.78	0.0069	57.96	57.68	0.30		
3.84	3.25			0.0024	1.17	0.0019	1.35	2.72	0.0021	1.35	2.77	0.0078	57.76	58.53	-0.77		
3.78	3.26			0.0009	1.18	0.0088	1.38	2.77	0.0021	1.35	2.82	0.0022	58.24	57.65	0.59		
3.81	3.26			0.0082	1.17	0.0037	1.38	2.76	0.0027	1.35	2.80	0.0088	58.22	57.68	0.54		
3.78	3.26	0.0019	1.17	0.0024	1.38	2.76	0.0035	1.36	2.83	0.0117	58.66	57.72	0.94				
3.81	3.26	0.0013	1.17	0.0009	1.38	2.76	0.0018	1.35	2.79	0.0032	58.19	57.67	0.52				
3.81	3.26	0.0101	1.17	0.0017	1.37	2.75	0.0035	1.35	2.79	0.0012	58.13	57.83	0.31				
3.84	3.25	0.0054	1.13	0.0013	1.38	2.75	0.0045	1.34	2.79	0.0119	58.54	57.60	1.93				
3.81	3.26	0.0014	1.20	0.0043	1.38	2.77	0.0096	1.35	2.81	0.0018	57.30	57.68	-0.38				
3.81	3.26	0.0021	1.17	0.0027	1.39	2.76	0.0020	1.36	2.81	0.0065	58.38	57.45	0.93				
3.81	3.26	0.0029	1.18	0.0015	1.39	2.77	0.0028	1.35	2.80	0.0118	58.08	57.22	0.78				
3.81	3.26	0.0030	1.14	0.0064	1.38	2.76	0.0028	1.35	2.80	0.0032	58.29	57.75	1.54				
3.82	3.25	0.0088	1.17	0.0032	1.37	2.76	0.0050	1.35	2.80	0.0110	58.21	57.94	0.27				
3.81	3.26	0.0014	1.17	0.0048	1.38	2.76	0.0020	1.35	2.80	0.0019	58.18	57.68	0.52				
1.94	2.36	0.0085	0.84	0.0043	0.68	2.93	0.0029	0.68	2.90	0.0030	70.99	71.30	-0.31				
1.98	2.36	0.0014	0.84	0.0023	0.68	2.93	0.0096	0.68	2.90	0.0016	71.03	71.34	-0.31				
1.98	2.36	0.0028	0.86	0.0011	0.68	2.93	0.0023	0.69	2.93	0.0006	70.58	71.01	-0.43				
1.99	2.35	0.0017	0.83	0.0023	0.68	2.93	0.0103	0.68	2.89	0.0015	71.24	71.24	-0.01				
1.99	2.36	0.0011	0.84	0.0031	0.67	2.93	0.0075	0.68	2.88	0.0013	70.81	71.36	-0.55				
1.97	2.36	0.0048	0.84	0.0024	0.71	2.93	0.0037	0.72	2.90	0.0041	70.98	69.94	1.04				

Vesicular yellow pumice	1.97	2.36	0.0035	0.85	0.0026	0.65	2.96	0.0050	0.69	2.91	0.0089	70.70	71.21	-0.52
	1.98	2.36	0.0021	0.86	0.0060	0.65	2.93	0.0060	0.65	2.91	0.0031	70.49	71.39	-0.90
	1.98	2.37	0.0021	0.84	0.0017	0.65	2.94	0.0012	0.65	2.90	0.0010	70.96	71.44	-0.48
	1.98	2.36	0.0014	0.84	0.0068	0.65	2.93	0.0021	0.65	2.89	0.0027	70.95	71.30	-0.34
	1.99	2.35	0.0024	0.84	0.0024	0.67	2.93	0.0017	0.65	2.89	0.0114	70.96	71.44	-0.48
	1.99	2.34	0.0011	0.83	0.0074	0.65	2.92	0.0020	0.65	2.86	0.0044	71.37	72.36	-0.98
	1.97	2.37	0.0053	0.84	0.0022	0.72	2.94	0.0020	0.72	2.90	0.0044	70.97	69.76	1.20
	1.98	2.37	0.0055	0.86	0.0046	0.65	2.93	0.0019	0.69	2.91	0.0038	70.41	71.16	-0.76
	1.98	2.36	0.0070	0.82	0.0095	0.67	2.93	0.0010	0.65	2.90	0.0034	71.68	71.53	0.15
	1.99	2.34	0.0046	0.84	0.0044	0.65	2.92	0.0104	0.65	2.90	0.0011	70.97	71.09	-0.12
	1.98	2.36	0.0057	0.84	0.0020	0.65	2.93	0.0018	0.65	2.90	0.0038	70.97	71.29	-0.32
	1.96	2.36	0.0071	0.86	0.0024	0.65	2.94	0.0021	0.65	2.92	0.0033	70.49	71.29	-0.80
	1.97	2.36	0.0018	0.84	0.0037	0.65	2.96	0.0013	0.65	2.90	0.0109	71.00	71.33	-0.33
	1.98	2.36	0.0051	0.85	0.0069	0.65	2.93	0.0023	0.69	2.90	0.0059	70.67	71.20	-0.52
	1.98	2.37	0.0020	0.84	0.0026	0.65	2.93	0.0030	0.65	2.90	0.0013	70.94	71.45	-0.51
	1.98	2.35	0.0024	0.84	0.0045	0.65	2.93	0.0051	0.65	2.90	0.0029	70.99	71.21	-0.22
	1.99	2.36	0.0016	0.83	0.0032	0.65	2.93	0.0055	0.65	2.86	0.0076	71.06	71.32	-0.24
	1.99	2.35	0.0007	0.83	0.0096	0.65	2.93	0.0022	0.65	2.89	0.0014	71.33	71.23	0.10
	2.00	2.36	0.0015	0.83	0.0009	0.67	2.89	0.0021	0.65	2.88	0.0025	71.24	71.56	-0.32
	1.97	2.36	0.0024	0.85	0.0043	0.65	2.93	0.0044	0.65	2.90	0.0044	70.64	71.61	-0.97
1.98	2.37	0.0075	0.84	0.0024	0.65	2.93	0.0027	0.65	2.90	0.0021	70.99	71.37	-0.37	
1.98	2.35	0.0046	0.84	0.0075	0.65	2.92	0.0012	0.65	2.90	0.0035	70.96	72.49	-1.51	
1.98	2.35	0.0017	0.83	0.0014	0.65	2.90	0.0064	0.65	2.89	0.0015	71.31	71.26	0.05	
1.98	2.35	0.0016	0.84	0.0022	0.65	2.93	0.0023	0.65	2.90	0.0025	70.99	71.28	-0.29	
Dense grey pumice	2.36	2.51	0.0036	0.95	0.0108	0.64	2.86	0.0034	0.64	2.84	0.0003	66.50	66.71	-0.21
	2.36	2.51	0.0014	0.96	0.0054	0.64	2.86	0.0037	0.64	2.84	0.0047	66.38	66.57	-0.19
	2.39	2.53	0.0029	0.96	0.0056	0.64	2.86	0.0025	0.65	2.86	0.0015	66.37	66.63	-0.26
	2.39	2.51	0.0034	0.96	0.0096	0.65	2.86	0.0016	0.64	2.84	0.0036	66.28	66.17	0.10
	2.39	2.51	0.0076	0.95	0.0058	0.63	2.86	0.0020	0.63	2.84	0.0086	66.51	66.74	-0.23
	2.39	2.50	0.0030	0.95	0.0033	0.63	2.85	0.0026	0.64	2.83	0.0011	66.46	66.72	-0.26
	2.40	2.51	0.0024	0.95	0.0020	0.63	2.86	0.0011	0.64	2.84	0.0007	66.56	66.82	-0.26
	2.41	2.50	0.0077	0.95	0.0031	0.63	2.84	0.0011	0.64	2.83	0.0031	66.37	66.97	-0.60
	2.38	2.52	0.0019	0.95	0.0078	0.66	2.87	0.0043	0.64	2.85	0.0048	66.59	66.81	0.77
	2.38	2.51	0.0012	0.97	0.0062	0.64	2.86	0.0043	0.65	2.84	0.0029	66.64	66.54	-0.71
	2.39	2.51	0.0016	0.95	0.0078	0.64	2.86	0.0048	0.64	2.84	0.0026	66.53	66.38	0.15
	2.39	2.51	0.0020	0.95	0.0026	0.62	2.86	0.0102	0.64	2.84	0.0064	66.60	67.13	-0.53
	2.40	2.50	0.0030	0.94	0.0032	0.63	2.85	0.0015	0.62	2.84	0.0009	66.76	66.63	0.13
	2.41	2.50	0.0089	0.95	0.0032	0.61	2.85	0.0016	0.63	2.83	0.0017	66.44	67.34	-0.90
	2.39	2.51	0.0065	0.95	0.0024	0.63	2.86	0.0023	0.64	2.84	0.0020	66.54	66.74	-0.20
	2.39	2.53	0.0023	0.97	0.0057	0.64	2.87	0.0002	0.65	2.86	0.0038	66.02	66.65	-0.63
	2.39	2.51	0.0074	0.93	0.0046	0.63	2.86	0.0091	0.64	2.84	0.0004	67.27	66.82	0.44
	2.41	2.49	0.0077	0.91	0.0039	0.60	2.83	0.0021	0.61	2.81	0.0013	67.71	67.65	0.06
	2.37	2.51	0.0003	0.96	0.0103	0.64	2.86	0.0044	0.64	2.84	0.0018	66.31	66.75	-0.44
	2.39	2.52	0.0020	0.96	0.0007	0.64	2.86	0.0032	0.64	2.85	0.0017	66.22	66.64	-0.62
2.38	2.53	0.0035	0.95	0.0066	0.64	2.86	0.0048	0.67	2.86	0.0002	66.60	66.96	-0.16	
2.39	2.51	0.0023	0.95	0.0040	0.62	2.86	0.0018	0.64	2.84	0.0017	66.55	67.49	-0.95	
2.41	2.50	0.0067	0.94	0.0077	0.63	2.85	0.0074	0.63	2.83	0.0017	66.75	66.62	0.14	
2.37	2.53	0.0021	0.95	0.0065	0.64	2.86	0.0020	0.66	2.86	0.0046	66.70	66.96	-0.29	
2.38	2.52	0.0050	0.96	0.0071	0.64	2.87	0.0020	0.65	2.85	0.0016	66.40	66.66	-0.46	

Kwet Middle		2.39	2.51	0.0048	0.95	0.0013	0.85	2.86	0.0043	0.84	2.84	0.0037	66.49	66.23	0.25
		2.39	2.49	0.0054	0.94	0.0030	0.83	2.83	0.0018	0.84	2.82	0.0009	66.63	66.49	0.14
		2.39	2.50	0.0039	0.94	0.0021	0.83	2.85	0.0049	0.83	2.83	0.0006	66.62	66.62	0.00
		2.40	2.51	0.0037	0.94	0.0025	0.83	2.86	0.0006	0.82	2.84	0.0009	66.62	66.73	0.08
		2.39	2.51	0.0014	0.95	0.0020	0.83	2.86	0.0046	0.84	2.84	0.0006	66.46	66.70	-0.29
	Vesicular yellow pumice	1.96	2.36	0.0028	0.86	0.0065	0.70	2.93	0.0011	0.69	2.90	0.0032	70.26	70.44	-0.18
		1.96	2.36	0.0025	0.86	0.0100	0.69	2.94	0.0029	0.69	2.90	0.0043	70.46	70.52	-0.06
		1.96	2.36	0.0063	0.84	0.0032	0.66	2.94	0.0021	0.66	2.90	0.0032	70.97	71.26	-0.29
		1.96	2.36	0.0095	0.84	0.0108	0.66	2.92	0.0046	0.66	2.89	0.0010	70.96	71.31	-0.35
		1.99	2.36	0.0026	0.84	0.0033	0.67	2.92	0.0018	0.66	2.89	0.0049	71.01	71.74	-0.73
		1.97	2.39	0.0039	0.84	0.0051	0.66	2.93	0.0007	0.66	2.93	0.0040	71.20	71.65	-0.45
		1.98	2.36	0.0014	0.85	0.0056	0.68	2.93	0.0021	0.69	2.90	0.0025	70.73	71.28	-0.56
		1.98	2.36	0.0095	0.85	0.0023	0.70	2.94	0.0020	0.68	2.90	0.0043	70.64	70.53	0.11
		1.96	2.36	0.0091	0.83	0.0009	0.66	2.93	0.0043	0.66	2.90	0.0013	71.16	71.34	-0.18
		1.99	2.36	0.0079	0.82	0.0091	0.67	2.93	0.0039	0.66	2.89	0.0078	71.65	71.67	-0.02
		1.99	2.33	0.0026	0.83	0.0019	0.66	2.91	0.0023	0.67	2.87	0.0047	71.11	71.57	-0.47
		1.94	2.36	0.0019	0.84	0.0038	0.66	2.93	0.0016	0.66	2.90	0.0014	70.66	71.29	-0.40
		1.97	2.40	0.0046	0.84	0.0107	0.66	2.94	0.0023	0.69	2.93	0.0025	71.25	71.72	-0.46
		1.96	2.36	0.0022	0.87	0.0019	0.70	2.93	0.0014	0.66	2.90	0.0043	70.00	70.52	-0.52
1.96		2.35	0.0006	0.84	0.0021	0.66	2.93	0.0026	0.66	2.89	0.0035	70.92	72.09	-1.16	
1.99		2.36	0.0057	0.83	0.0057	0.67	2.92	0.0057	0.66	2.90	0.0053	71.31	71.74	-0.43	
2.00		2.35	0.0045	0.81	0.0015	0.65	2.90	0.0076	0.66	2.89	0.0091	71.99	72.21	-0.21	
1.98		2.36	0.0057	0.84	0.0020	0.66	2.93	0.0016	0.66	2.90	0.0036	70.97	71.29	-0.32	
1.96		2.36	0.0035	0.84	0.0028	0.69	2.93	0.0021	0.66	2.90	0.0026	70.96	70.95	0.03	
1.96		2.36	0.0016	0.84	0.0028	0.66	2.94	0.0026	0.69	2.90	0.0035	70.66	71.25	-0.37	
1.96	2.36	0.0063	0.84	0.0104	0.67	2.93	0.0054	0.65	2.90	0.0046	70.99	71.72	-0.73		
1.99	2.35	0.0033	0.82	0.0031	0.66	2.93	0.0013	0.66	2.89	0.0097	71.64	71.32	0.33		
2.00	2.35	0.0024	0.83	0.0019	0.67	2.93	0.0046	0.64	2.89	0.0090	71.36	71.70	-0.35		
1.97	2.36	0.0023	0.84	0.0067	0.69	2.96	0.0010	0.69	2.90	0.0014	70.63	70.84	-0.01		
1.97	2.36	0.0060	0.84	0.0058	0.66	2.93	0.0042	0.71	2.90	0.0016	70.67	71.29	-0.42		
1.96	2.36	0.0006	0.84	0.0037	0.66	2.94	0.0037	0.66	2.90	0.0034	70.64	71.29	-0.44		
1.96	2.33	0.0013	0.84	0.0024	0.66	2.93	0.0066	0.66	2.87	0.0026	70.66	70.95	-0.27		
1.99	2.36	0.0015	0.84	0.0047	0.66	2.91	0.0034	0.67	2.89	0.0021	70.97	71.29	-0.32		
1.99	2.35	0.0023	0.84	0.0066	0.66	2.93	0.0026	0.66	2.89	0.0098	70.95	71.26	-0.31		
1.96	2.36	0.0006	0.84	0.0015	0.66	2.93	0.0014	0.66	2.90	0.0016	70.97	71.26	-0.31		
Dense grey pumice	2.36	2.51	0.0013	0.95	0.0066	0.64	2.67	0.0079	0.84	2.67	0.0066	66.77	66.64	0.14	
	2.36	2.51	0.0067	0.96	0.0027	0.64	2.66	0.0015	0.84	2.65	0.0044	66.41	66.67	-0.26	
	2.39	2.52	0.0089	0.96	0.0049	0.65	2.66	0.0077	0.84	2.65	0.0020	66.23	66.44	-0.21	
	2.39	2.51	0.0037	0.93	0.0039	0.63	2.66	0.0035	0.61	2.64	0.0023	67.25	66.75	0.50	
	2.39	2.51	0.0056	0.95	0.0058	0.63	2.66	0.0050	0.63	2.64	0.0022	66.54	66.76	-0.22	
	2.37	2.53	0.0016	0.95	0.0023	0.66	2.66	0.0066	0.64	2.64	0.0019	66.46	66.20	0.26	
	2.39	2.53	0.0067	0.97	0.0006	0.65	2.67	0.0050	0.64	2.65	0.0021	65.94	66.35	-0.41	
	2.39	2.50	0.0047	0.95	0.0016	0.63	2.66	0.0064	0.64	2.64	0.0033	66.54	66.91	-0.37	
	2.39	2.50	0.0100	0.94	0.0106	0.62	2.65	0.0045	0.64	2.64	0.0076	66.65	67.01	-0.17	
	2.39	2.51	0.0065	0.95	0.0024	0.63	2.66	0.0023	0.64	2.64	0.0020	66.54	66.74	-0.20	
	2.36	2.51	0.0016	0.96	0.0022	0.64	2.66	0.0065	0.67	2.64	0.0054	66.30	66.66	-0.36	
	2.36	2.52	0.0012	0.96	0.0099	0.65	2.67	0.0067	0.64	2.64	0.0056	66.27	66.43	-0.16	
	2.39	2.51	0.0069	0.95	0.0016	0.64	2.66	0.0020	0.64	2.65	0.0014	66.63	66.64	-0.01	
2.39	2.51	0.0046	0.95	0.0046	0.63	2.66	0.0039	0.64	2.63	0.0061	66.49	66.75	-0.26		

Kw4 Base	Dense grey putrifice	2.39	2.49	0.0073	0.94	0.0060	0.61	2.65	0.0033	0.64	2.64	0.0014	66.63	67.26	-0.45	
		2.40	2.49	0.0032	0.94	0.0031	0.61	2.66	0.0063	0.64	2.64	0.0023	66.63	67.26	-0.45	
		2.40	2.50	0.0019	0.95	0.0052	0.62	2.65	0.0040	0.61	2.62	0.0035	66.31	67.09	-0.78	
		2.41	2.46	0.0051	0.91	0.0095	0.60	2.63	0.0046	0.63	2.61	0.0021	67.66	67.56	0.10	
		2.34	2.51	0.0036	0.95	0.0021	0.64	2.66	0.0062	0.64	2.64	0.0043	66.50	66.66	-0.16	
		2.36	2.51	0.0009	0.96	0.0056	0.64	2.66	0.0110	0.66	2.65	0.0099	66.30	66.66	-0.36	
		2.39	2.51	0.0046	0.96	0.0040	0.64	2.66	0.0052	0.64	2.66	0.0012	66.44	66.67	-0.23	
		2.39	2.51	0.0012	0.95	0.0069	0.63	2.65	0.0047	0.64	2.64	0.0106	66.52	66.76	-0.24	
		2.41	2.50	0.0012	0.94	0.0032	0.62	2.65	0.0094	0.63	2.64	0.0017	66.66	67.09	-0.21	
		2.39	2.52	0.0022	0.97	0.0026	0.64	2.66	0.0020	0.64	2.65	0.0024	65.90	66.56	-0.66	
		2.39	2.51	0.0014	0.96	0.0019	0.64	2.66	0.0021	0.64	2.64	0.0009	66.16	66.74	-0.58	
		2.39	2.51	0.0062	0.95	0.0031	0.64	2.66	0.0022	0.64	2.65	0.0042	66.63	66.74	-0.11	
		2.36	2.54	0.0026	0.95	0.0013	0.67	2.66	0.0023	0.65	2.64	0.0016	66.55	66.95	0.60	
		2.39	2.51	0.0023	0.94	0.0015	0.63	2.63	0.0043	0.63	2.64	0.0051	66.92	66.75	0.17	
		2.39	2.51	0.0060	0.95	0.0109	0.63	2.66	0.0016	0.64	2.62	0.0049	66.33	66.75	-0.42	
		2.39	2.51	0.0009	0.95	0.0006	0.63	2.66	0.0020	0.64	2.64	0.0023	66.50	66.77	-0.27	
		Vesicular yellow putrifice	2.66	3.29	0.0070	0.79	0.0027	0.93	2.61	0.0014	0.69	2.66	0.0045	72.50	71.79	0.71
			2.60	3.29	0.0027	0.79	0.0044	0.94	2.63	0.0026	0.90	2.90	0.0016	72.60	71.56	1.03
	2.55		3.26	0.0037	0.79	0.0013	0.93	2.61	0.0015	0.69	2.66	0.0016	72.62	71.63	0.98	
	2.61		3.29	0.0013	0.79	0.0054	0.93	2.60	0.0043	0.66	2.67	0.0016	72.46	71.62	0.64	
	2.59		3.32	0.0072	0.79	0.0032	0.93	2.61	0.0014	0.69	2.66	0.0054	72.46	72.06	0.39	
	2.60		3.29	0.0016	0.79	0.0049	0.94	2.61	0.0049	0.69	2.66	0.0069	72.47	71.54	0.93	
	2.55		3.30	0.0042	0.79	0.0020	0.93	2.63	0.0033	0.91	2.90	0.0013	72.69	71.64	0.85	
	2.61		3.29	0.0027	0.79	0.0026	0.92	2.60	0.0014	0.66	2.67	0.0036	72.47	71.96	0.49	
	2.61		3.29	0.0013	0.79	0.0065	0.93	2.61	0.0034	0.69	2.66	0.0026	72.54	71.61	0.73	
	2.57		3.29	0.0050	0.80	0.0036	0.93	2.63	0.0025	0.91	2.90	0.0030	72.42	71.60	0.62	
	2.59		3.29	0.0021	0.79	0.0019	0.95	2.62	0.0032	0.90	2.69	0.0040	72.51	71.00	1.52	
	2.60		3.29	0.0069	0.79	0.0021	0.93	2.61	0.0024	0.69	2.66	0.0037	72.50	71.62	0.69	
	2.60		3.26	0.0032	0.79	0.0007	0.93	2.79	0.0023	0.66	2.66	0.0026	72.36	71.79	0.60	
	2.60		3.29	0.0017	0.79	0.0017	0.92	2.61	0.0026	0.69	2.66	0.0019	72.50	72.11	0.39	
	2.61		3.29	0.0019	0.79	0.0062	0.92	2.60	0.0033	0.67	2.67	0.0029	72.41	72.09	0.32	
	2.63		3.26	0.0020	0.79	0.0079	0.90	2.79	0.0041	0.66	2.66	0.0037	72.29	72.69	-0.40	
	2.60	3.29	0.0096	0.82	0.0016	0.93	2.62	0.0030	0.90	2.69	0.0060	71.55	71.63	-0.26		
	2.60	3.29	0.0024	0.79	0.0017	0.93	2.62	0.0016	0.69	2.69	0.0099	72.56	71.63	0.76		
2.60	3.30	0.0033	0.79	0.0099	0.94	2.63	0.0069	0.91	2.90	0.0021	72.69	71.56	1.10			
2.60	3.29	0.0070	0.80	0.0014	0.94	2.61	0.0046	0.69	2.66	0.0017	72.27	71.36	0.89			
2.61	3.29	0.0025	0.76	0.0044	0.91	2.61	0.0021	0.69	2.66	0.0029	72.92	72.39	0.53			
2.61	3.29	0.0009	0.79	0.0061	0.93	2.61	0.0025	0.69	2.66	0.0021	72.54	71.65	0.70			
2.61	3.26	0.0011	0.76	0.0039	0.91	2.79	0.0025	0.66	2.66	0.0021	72.70	72.17	0.54			
2.63	3.26	0.0030	0.75	0.0037	0.93	2.60	0.0016	0.66	2.67	0.0013	73.66	71.76	2.06			
2.60	3.33	0.0016	0.80	0.0029	0.94	2.61	0.0021	0.69	2.66	0.0020	72.21	71.65	0.36			
2.60	3.29	0.0024	0.82	0.0036	0.93	2.61	0.0023	0.69	2.66	0.0061	71.46	71.69	-0.23			
2.60	3.29	0.0039	0.79	0.0067	0.94	2.61	0.0110	0.69	2.66	0.0036	72.47	71.42	1.05			
2.60	3.29	0.0034	0.79	0.0012	0.93	2.61	0.0032	0.66	2.66	0.0019	72.55	71.62	0.73			
2.61	3.29	0.0023	0.76	0.0006	0.92	2.60	0.0019	0.66	2.67	0.0022	73.46	71.90	1.57			
2.61	3.29	0.0016	0.79	0.0032	0.93	2.61	0.0014	0.69	2.66	0.0019	72.51	71.62	0.69			
Avg Kw7			0.65						2.91			70.27	69.66	0.59		
Avg Kw4			0.92						2.66			67.63	67.60	0.03		
D.lith	7.00	2.56	0.0037	2.71	0.0039	2.43	2.69	0.0046	2.29	2.91	0.0056	6.63	6.96	0.67		

Appendix 4.3 Summary of key lithostratigraphic characteristics of deposits produced by large eruptions at Mt. Taranaki (modified from Torres-Orozco et al. 2017)

Layer	Lithofacies description	Interpretation
<i>AD 1655 Burrell bed-set (units modified from Platz et al. 2007)</i>		
unit 3	Matrix-supported, massive deposit of pale-grey pumice blocks and lapilli, similar to unit 1.	C-PDC
unit 2	Matrix-supported, normal to reversely-graded, partially welded deposit of brown to dark-brown pumice blocks and lapilli, grey and dark-grey lithic blocks and lapilli concentrated towards the base, black glassy clasts and altered lithic lapilli and blocks.	C-PDC
unit 1	Matrix-supported, massive deposit of pale-grey pumice blocks and lapilli in a medium-coarse ash.	C-PDC
Bu	Clast-supported, reverse to massive to normally-graded deposit of grey pumice lapilli and grey, dark-grey and bluish lithic lapilli.	Fall
unit baf	Matrix-supported, massive deposit of brownish-grey medium ash and grey lithic blocks and lapilli, bearing rare grey pumice, charcoal twigs and imbricated charcoal logs.	BAF
<i>-1.2 cal ka B.P. Kaupokonui bed-set</i>		
Kp	Clast-supported, reversely-graded deposit of brownish pumice lapilli and grey lithic lapilli	Fall
<i>-2.6 cal ka B.P. Manganui-O bed-set</i>		
U-DF	Firm, matrix-supported, reversely-graded to massive deposits of clay-rich, coarse sands and gravels, bearing abundant pyroclasts from the underlying layers.	Debris flow
MD2b	Coherent, massive deposits of dense, poorly vesicular or non-vesicular porphyritic andesitic rocks; resting on chaotic breccias and passing upwards into highly vesicular, rough lithofacies.	aa lava flow
MD3	Clast-supported deposit of four reversely-graded beds comprising vesicular/microvesicular juvenile lapilli and diverse hetero-lithic lapilli: grey and dark-grey clasts, orange, red and white bleached altered lithics and gabbroic accidentals.	Fall
MD2	Very friable, clast-supported, reverse to massive to normally-graded deposit of vesicular/microvesicular juvenile lapilli	Fall
MD1	Very friable, clast-supported, reverse to normally-graded deposit of vesicular/microvesicular juvenile lapilli and common violet and orange altered lithics	Fall
L-DF	Firm, matrix-supported, massive weathered deposits of coarse sand, rich in dark juvenile clasts from older pyroclastic deposits	Debris flow
<i>3.3 cal ka B.P. Upper Inglewood bed-set</i>		
Ulg7	Clast-supported, massive deposit of yellowish pumice lapilli and grey, dark-grey and orange-altered lithic lapilli	Fall
Ulg6	Matrix-supported, parallel and cross-stratified, pinching-swelling deposit of pumice and lithic ash and lapilli, bearing charcoal	Lateral-PDC
Ulg5	Firm, matrix-supported, massive, pinching-swelling deposit of faintly imbricated pumice and lithic lapilli and ash	Lateral-PDC
Ulg4	Matrix-supported, parallel-stratified, pinching deposit of pumice and lithic ash	Lateral-PDC
Ulg3	Matrix-supported, parallel and cross-stratified, pinching-swelling deposit of grey lithic ash and lapilli and scarce pumice lapilli	BAF
Ulg2	Firm, matrix-supported, reverse to faintly parallel and cross-stratified deposit of imbricated grey lithic lapilli and ash	BAF
Ulg1	Friable, matrix-supported, reverse to massive to normally-graded deposit of grey lithic blocks, ash and less lapilli	BAF
<i>4.7-4.6 cal ka B.P. Kokowai bed-set</i>		
Kw6	Matrix-supported, massive, pinching deposit of yellowish pumice ash and lapilli and grey, black and orange-altered lithic lapilli	C-PDC
Kw7	Clast-supported, reverse to massive to normally-graded deposit of yellow pumice and grey and orange-altered lithic lapilli	Fall
Kw6	Matrix-supported, massive, pinching deposit of yellow pumice ash and lapilli, free crystals and grey and orange lithic lapilli	C-PDC
Kw5	Matrix-supported, reverse, parallel and faintly cross-stratified, pinching deposit of grey lithic ash, free crystals and scarce pumice ash, bearing charcoal.	BAF
Kw4	Clast-supported, reverse to massive and faintly normally-graded deposit of pumice lapilli and blocks, and grey, dark-grey and orange-altered lithic lapilli and few blocks. The latter concentrate and occasionally form a reversely-graded top deposit level	Fall
Kw3	Matrix-supported, massive, pinching deposit of yellow pumice ash and lapilli, free crystals, few grey lithic lapilli and charcoal	C-PDC
Kw2	Friable, matrix-supported, reverse to normally-graded deposit of grey lithic ash and lapilli	BAF
Kw1	Friable, matrix-supported, reverse to massive to normally-graded deposit of grey lithic blocks and ash, bearing charcoal	BAF

BAF: block-and-ash flow, PDC: pyroclastic density current, C-PDC: column collapse PDC

Appendix 4.4 Whole-rock analyses of juvenile pyroclasts from different bed-sets deposited by eruptions from Mt. Taranaki

Sample	Kw4_p	Kw4_j	Kw7t	Kw7m	Kw7b	Ulg1	Ulg2	Ulg3	Ulg4	Ulg5t	Ulg5b	Ulg6t	Ulg6b	Ulg7_p	Ulg7_j	
Section	A	A	A	A	A	D	C	C	C	C	C	C	C	C	C	
Type	Pumice	Grey Lt	Pumice	Pumice	Pumice	Grey Lt	Bulk	Bulk	Pumice	Bulk	Pumice	Bulk	Pumice	Pumice	Grey Lt	
Major elements (wt. %)																
SiO ₂	50.72	56.37	52.35	51.13	51.67	57.94	57.56	56.93	57.39	57.96	57.45	54.92	56.59	56.46	59.92	
Al ₂ O ₃	19.21	17.82	19.69	20.01	19.66	16.23	16.82	19.37	16.71	16.94	16.72	19.44	16.40	16.69	16.57	
Fe ₂ O ₃ (t)	7.47	7.07	7.29	7.29	7.31	5.91	6.16	5.70	6.02	5.69	5.95	6.76	6.25	5.84	5.69	
MgO	2.71	2.57	2.44	2.39	2.41	1.65	2.01	2.15	1.75	1.66	1.76	2.15	1.73	1.70	1.71	
CaO	7.97	7.40	7.67	7.62	7.66	6.83	7.22	7.56	6.43	5.95	6.54	7.04	6.36	6.52	6.46	
Na ₂ O	3.50	3.96	3.57	3.44	3.46	4.15	4.12	4.15	4.07	3.82	4.06	3.80	4.01	3.99	4.30	
K ₂ O	1.83	2.46	1.85	1.70	1.75	2.34	2.20	1.95	2.26	2.26	2.27	1.75	2.26	2.19	2.43	
TiO ₂	0.83	0.78	0.80	0.81	0.81	0.61	0.64	0.59	0.61	0.65	0.61	0.71	0.61	0.61	0.60	
P ₂ O ₅	0.35	0.26	0.34	0.32	0.32	0.29	0.30	0.19	0.26	0.29	0.26	0.26	0.26	0.27	0.26	
MnO	0.16	0.17	0.17	0.16	0.16	0.17	0.17	0.16	0.16	0.14	0.17	0.16	0.16	0.16	0.17	
LOI	4.26	-0.01	3.60	4.72	4.32	0.44	0.72	0.89	2.25	2.05	2.16	2.05	2.43	2.62	0.15	
Total	99.03	98.96	99.97	99.76	99.84	96.76	99.94	99.64	99.92	99.66	99.99	99.66	99.06	99.33	100.26	

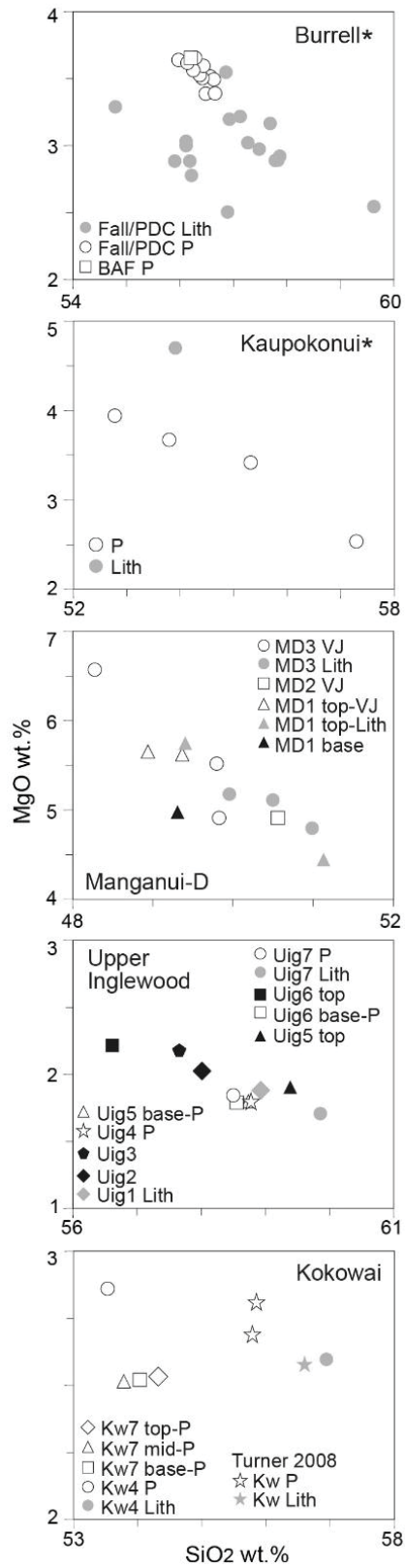
All samples were analysed at the University of Auckland, New Zealand, using a PANalytical Axios 1 KW wavelength dispersive X-ray fluorescence spectrometer.

Sample codes stand for bed-sets Kokowai (layers Kw4 and Kw7), Upper Inglewood (layers Ulg1-7), Manganui-D (layers MD1-3), Manganui-A (MA) and Manganui-C (MC); base (b), middle (m) and top (t) stratigraphic levels; and pumice (p), lithic (l) or vesicular juvenile (v) clasts analysed. Bulk: Bulk-deposit, Lt: Lithic, VJ: Vesicular Juvenile.

(continue)

Sample	MD1	MD1U	MD1L	MD1LV	MD1LJ	MD2	MD3b_v	MD3b_L	MD3m	MD3L_v	MD3LJ	MD3LJ	MA	MC
Section	F	F	F	F	F	F	F	F	F	F	F	F	F	F
Type	Bulk	Black Lt	VJ	VJ	Grey Lt	VJ	VJ	Black Lt	VJ	Black Lt	Black Lt	Grey Lt	Bulk	Bulk
Major elements (wt. %)														
SiO ₂	48.54	48.06	48.92	48.22	51.19	50.13	49.36	50.30	48.59	47.69	49.12	51.02	49.68	47.59
Al ₂ O ₃	17.54	16.89	17.13	17.65	18.18	17.75	17.24	17.31	17.75	16.35	17.07	17.71	16.89	14.86
Fe ₂ O ₃ (t)	10.79	10.63	10.56	10.66	9.91	10.10	10.73	10.32	10.24	11.36	10.32	10.15	10.07	11.07
MgO	4.90	5.71	5.56	5.56	4.45	4.07	5.47	5.09	4.79	6.49	5.09	4.80	3.89	7.39
CaO	10.20	10.86	10.78	10.60	9.93	10.02	10.18	10.18	9.88	11.24	10.31	9.94	9.48	12.53
Na ₂ O	3.26	3.06	3.06	2.90	3.28	3.17	3.06	3.21	3.15	2.73	3.23	3.22	3.26	2.37
K ₂ O	1.70	1.59	1.57	1.42	1.72	1.64	1.57	1.70	1.60	1.33	1.69	1.75	1.67	1.20
TiO ₂	1.07	1.10	1.09	1.11	1.03	1.04	1.09	1.06	1.06	1.16	1.06	1.05	1.08	1.19
P ₂ O ₅	0.27	0.25	0.25	0.25	0.26	0.26	0.25	0.25	0.27	0.23	0.25	0.25	0.28	0.19
MnO	0.17	0.17	0.17	0.16	0.17	0.17	0.17	0.17	0.17	0.17	0.17	0.17	0.17	0.17
LOI	0.61	0.06	0.07	1.24	0.24	0.89	0.60	0.30	1.46	1.02	0.53	0.17	1.66	0.27
Total	99.05	99.40	99.16	99.77	100.36	100.04	99.92	99.91	98.95	99.50	98.86	100.23	100.13	99.55

Appendix 4.5



Appendix 4.6 Isopach data of individual or combined fall deposit layers and resulting geometrical values

Isopach cm	Area km ²	A ^{1/2} km	P km	Shp Fcl	Axis1 km	Axis2 km	Asp Ratio	Dc km	Da km	Ecc
<i>Burrell (modified from Platz et al. 2007)</i>										
40	7.4	2.7	13.7	0.49	5.0	1.2	4.0	2.9	3.0	0.97
30	21.1	4.6	19.2	0.72	5.0	3.3	2.4	4.0	4.1	0.96
20	42.4	6.5	26.0	0.79	10.0	5.0	2.0	5.0	5.2	0.96
10	149.9	12.2	45.9	0.90	15.0	11.0	1.4	7.9	10.0	0.79
5 (f-int)	725.0	26.9	96.0	0.99	37.3	19.9	1.9	16.7	20.4	0.91
1 (p-ext)	1165.5	34.4	136.1	0.80	54.5	25.6	2.1	27.3	26.6	0.96
<i>Kaupokonui (modified from Whitehead 1976)</i>										
30	7.9	2.8	15.2	0.43	7.0	1.3	5.4	3.5	3.6	0.96
25	13.6	3.7	16.4	0.50	6.3	2.1	4.0	4.2	4.5	0.92
20	20.6	4.5	21.3	0.57	9.5	2.9	3.3	4.6	4.9	0.96
15	46.0	6.8	27.4	0.77	11.3	5.3	2.1	5.7	5.8	0.97
10	109.3	10.5	39.2	0.90	14.6	10.5	1.4	7.3	6.7	0.84
5 (p-ext)	417.4	20.4	74.4	0.95	27.3	21.2	1.3	13.7	16.4	0.83
<i>Manganui-D, layers MD1-3</i>										
130	7.4	2.7	9.6	1.00	3.0	3.0	1.0	1.5	2.2	0.66
100	10.9	3.3	11.7	1.00	3.7	3.6	1.0	1.9	2.6	0.66
80	15.6	4.0	14.1	1.00	4.5	4.4	1.0	2.2	3.3	0.67
70	22.1	4.7	16.7	0.99	5.3	5.2	1.0	2.7	3.9	0.66
60	29.0	5.4	19.1	1.00	6.0	5.9	1.0	3.0	4.6	0.65
50	36.9	6.2	22.2	1.00	7.0	6.6	1.0	3.5	5.3	0.66
40	56.9	7.7	27.3	1.00	6.7	6.3	1.0	4.4	6.7	0.65
30	92.4	9.6	34.2	1.00	11.0	10.4	1.1	5.5	6.4	0.65
20	622.1	24.9	69.3	0.96	31.3	25.7	1.2	15.7	21.3	0.73
10 (p-ext)	945.2	30.7	110.0	0.96	36.7	31.6	1.2	19.4	25.6	0.75
5 (p-ext)	1492.1	38.6	136.4	0.96	46.7	39.5	1.2	24.4	33.1	0.74
1 (p-ext)	2469.0	49.9	176.2	0.96	61.3	51.0	1.2	30.7	40.0	0.77
0.1 (ext)	6753.2	82.2	307.5	0.90	100.5	70.5	1.4	50.3	57.1	0.66
<i>Upper Inglewood, layer Ulg7</i>										
110	4.1	2.0	6.6	0.69	3.7	1.3	3.0	1.9	2.0	0.94
50	7.7	2.8	11.5	0.73	4.6	1.9	2.5	2.4	2.4	0.96
40	19.1	4.4	16.0	0.94	5.9	4.0	1.5	3.0	3.6	0.82
30	32.7	5.7	20.7	0.96	7.3	5.6	1.3	3.7	4.7	0.76
20	366.4	19.1	69.1	0.96	24.1	16.7	1.3	12.1	15.6	0.77
10	663.6	25.6	93.0	0.96	32.7	24.9	1.3	16.4	21.2	0.77
5 (p-ext)	1043.7	32.3	115.6	0.96	39.7	32.5	1.2	19.9	25.0	0.79
1 (p-ext)	1463.6	38.3	137.1	0.96	47.6	36.7	1.2	23.9	31.4	0.76
0.3 (ext)	2211.4	47.0	169.0	0.97	59.2	46.1	1.3	29.6	36.2	0.77
<i>Kokowai, layer Kw7</i>										
30	16.6	4.3	17.4	0.76	6.9	3.1	2.2	3.4	3.5	0.96
20	91.1	9.5	36.5	0.77	15.2	7.1	2.1	7.6	6.5	0.89
10	221.6	14.9	56.7	0.81	23.0	11.1	2.1	11.5	12.6	0.90

(continue)

Isopach	Area	A ^{1/2}	P	Shp	Axis1	Axis2	Asp	Dc	Da	Ecc
cm	km ²	km	km	Fct	km	km	Ratio	km	km	
<i>Kokowai, layer Kw7</i>										
5	313.8	17.7	69.0	0.83	26.7	13.6	2.0	13.4	15.3	0.67
1 (ext)	510.9	22.6	85.8	0.81	34.7	18.0	1.9	17.4	20.2	0.66
<i>Kokowai, layer Kw4</i>										
170	7.7	2.8	9.9	0.98	3.5	2.8	1.3	1.8	2.3	0.77
150	8.9	3.0	10.7	0.98	3.8	3.0	1.3	1.9	2.4	0.79
140	10.4	3.2	11.5	0.99	4.1	3.2	1.3	2.1	2.9	0.72
130	12.1	3.5	12.5	0.97	4.4	3.5	1.3	2.2	2.7	0.81
120	13.4	3.7	13.1	0.98	4.6	3.7	1.2	2.3	2.8	0.82
110	15.1	3.9	13.9	0.98	4.9	3.9	1.3	2.5	3.0	0.82
100	21.0	4.6	16.4	0.98	5.8	4.6	1.3	2.9	3.6	0.81
90	47.6	6.9	24.7	0.98	8.7	6.9	1.3	4.4	5.5	0.79
80	70.5	8.4	30.1	0.98	10.6	8.4	1.3	5.3	6.7	0.79
70	93.8	9.7	34.7	0.98	12.3	9.7	1.3	6.2	7.7	0.80
60 (f-int)	136.0	11.7	41.8	0.98	14.8	11.7	1.3	7.4	9.1	0.81
50	174.3	13.2	47.3	0.98	16.7	13.1	1.3	8.4	10.3	0.81
40	255.6	16.0	57.3	0.98	20.2	15.9	1.3	10.1	12.3	0.82
30 (f-int)	326.7	18.1	64.8	0.98	22.8	18.0	1.3	11.4	14.1	0.81
20 (f-int)	421.0	20.5	73.5	0.98	25.9	20.6	1.3	13.0	15.6	0.83
10	522.7	22.9	81.9	0.98	28.9	22.9	1.3	14.5	18.0	0.80
5 (f-int)	830.0	28.8	102.7	0.99	36.2	28.7	1.3	18.1	21.8	0.83
4 (ext)	889.4	29.8	106.9	0.98	37.7	29.8	1.3	18.9	22.5	0.84
2 (ext)	1548.5	39.4	141.0	0.98	49.5	39.3	1.3	24.8	29.8	0.83

A^{1/2}: area^{1/2}, P: perimeter, Shp Fct: shape factor = $4\pi A/P^2$, Axis1: long axis, Axis2: short axis, Asp Ratio: aspect ratio = Axis1/Axis2, Dc: distance from the centre of the ellipse to a focus = $1/2(\text{Axis1})$, Da: distance from the focus to a vertex = $(\text{Db}^2 + \text{Dc}^2)^{1/2}$ where "Db" (distance from the centre to the vertex) is perpendicular to Dc. Ecc: eccentricity = Dc/Da.

Isopachs are fully extrapolated (ext), partially extrapolated (p-ext), fully interpolated (f-int), and in most cases partially (or solely) interpolated from field data.

Shp Fct < 1 = ellipse and circle = 1. Asp Ratio > 1 = ellipse and circle = 1. Ecc = 0.1 to -1.05 = ellipse, circle = 0 and line = ->1.05

Appendix 4.7 Isoleth data of individual fall deposit layers and resulting geometrical values

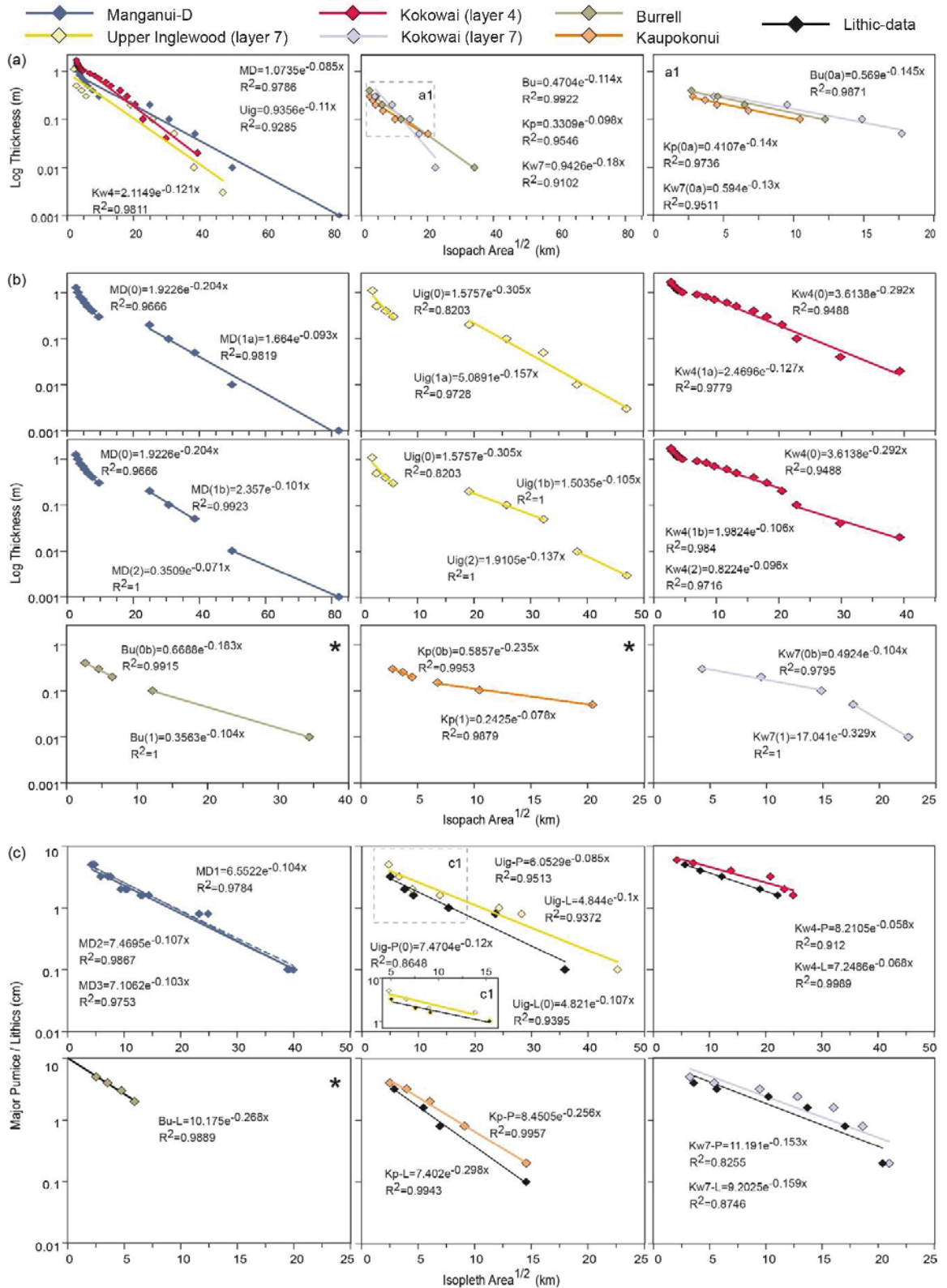
Isoleth cm	Area km ²	A ^{1/2} km	P km	Shp Fct	Axis1 km	Axis2 km	Asp Ratio	Dc km	Da km	Ecc	Dw km	Cw km
<i>Burrell lithics (modified from Platz et al. 2007)</i>												
5	6.5	2.5	10.7	0.71	4.5	1.7	2.6	2.3	2.3	0.96	4.0	0.9
4	12.4	3.5	14.1	0.76	5.9	2.6	2.3	3.0	3.0	0.96	5.0	1.3
3	22.6	4.8	16.7	0.81	6.5	5.0	1.3	3.3	4.0	0.81	5.7	2.5
2	35.0	5.9	21.7	0.94	7.7	5.9	1.3	3.9	5.1	0.75	6.7	3.0
1.6 (ext)	40.0	6.3	22.9	0.96	8.2	6.3	1.3	4.1	5.5	0.75	7.1	3.2
<i>Kaupokonui pumice</i>												
4	6.3	2.5	9.3	0.92	3.5	2.1	1.7	1.8	1.9	0.92	3.5	1.1
3.2	15.9	4.0	16.9	0.70	7.5	2.8	2.7	3.8	4.0	0.94	7.3	1.4
2	36.6	6.0	23.4	0.84	9.6	4.5	2.1	4.8	5.3	0.91	9.4	2.5
1.6 (f-int)	52.1	7.2	26.6	0.93	10.4	5.9	1.8	5.2	5.9	0.89	10.1	3.1
0.8	83.1	9.1	32.96	0.96	12.0	8.9	1.4	6.0	7.0	0.86	11.5	4.5
0.2 (p-ext)	212.0	14.6	51.05	0.99	17.7	15.3	1.2	8.9	11.5	0.77	15.3	7.8
<i>Kaupokonui lithics</i>												
3.2	6.4	2.9	10.7	0.93	4.1	2.5	1.6	2.1	2.4	0.85	3.3	1.3
1.6	30.1	5.5	21.7	0.80	9.1	4.1	2.2	4.6	4.9	0.93	8.2	2.1
0.8	46.0	6.9	26.6	0.84	11.2	5.5	2.0	5.6	6.2	0.90	10.0	2.6
0.1 (p-ext)	212.0	14.6	51.9	0.99	17.6	15.4	1.1	6.8	11.8	0.75	15.2	7.8
<i>Manganui-D, layer MD1, dense vesicular juveniles</i>												
5	17.9	4.2	15.1	0.99	5.2	4.3	1.2	2.6	3.2	0.81	3.4	2.2
3.2	34.8	5.9	21.0	0.99	6.1	5.9	1.0	3.1	4.0	0.76	4.7	3.2
2	66.7	8.4	33.7	0.96	11.9	9.5	1.3	6.0	7.6	0.78	9.2	4.9
1.6	166.0	13.0	46.4	0.96	16.0	13.0	1.2	6.0	10.4	0.77	13.2	6.6
0.8	543.9	23.3	83.5	0.96	29.2	23.7	1.2	14.6	17.5	0.83	24.5	12.1
0.1 (p-ext)	1514.9	38.9	136.2	1.00	44.6	42.0	1.1	22.4	29.0	0.77	36.0	21.7
<i>Manganui-D, layer MD2, dense vesicular juveniles</i>												
5	22.4	4.7	18.0	0.87	6.9	3.8	1.8	3.5	3.8	0.91	5.1	1.9
3.2	51.4	7.2	27.4	0.86	10.7	5.8	1.8	5.4	5.9	0.91	6.6	2.9
2	111.9	10.6	41.5	0.82	16.7	8.1	2.1	6.4	9.1	0.82	14.3	4.1
1.6	207.3	14.4	53.4	0.91	20.2	12.7	1.6	10.1	11.7	0.86	17.0	6.4
0.8	540.4	23.2	83.4	0.96	29.3	23.4	1.3	14.7	16.2	0.80	24.1	11.7
0.1 (p-ext)	1543.9	39.3	139.7	0.99	45.2	42.5	1.1	22.6	30.6	0.73	36.6	21.8
<i>Manganui-D, layer MD3, dense vesicular juveniles</i>												
5	20.8	4.6	18.5	0.77	7.8	3.2	2.4	3.9	4.0	0.96	6.3	1.6
3.2	56.2	7.6	31.0	0.76	13.1	5.4	2.4	6.6	6.9	0.95	11.0	2.7
2	105.4	10.3	36.7	0.88	15.1	8.5	1.8	7.6	8.3	0.91	12.6	4.3
1.6	177.1	13.3	49.3	0.92	18.6	11.4	1.6	9.3	10.7	0.87	15.2	5.8
0.8	619.1	24.9	86.6	0.99	29.9	26.6	1.1	15.0	16.2	0.82	24.7	13.5
0.1 (p-ext)	1594.6	39.9	141.8	1.00	47.1	43.6	1.1	23.6	31.4	0.75	37.4	21.8
<i>Upper Inglewood, layer Ulg7, pumice</i>												
5	22.8	4.8	17.3	0.96	6.2	4.4	1.4	3.1	3.4	0.91	4.5	2.3
3.2	43.8	6.6	24.0	0.96	8.5	6.2	1.4	4.3	4.9	0.87	6.6	3.2
2	80.8	9.0	32.6	0.96	11.7	8.6	1.4	5.9	7.3	0.80	9.4	4.3

(continue)

Isopleth cm	Area km ²	A ^{1/2} km	P km	Shp Fct	Axis1 km	Axis2 km	Asp Ratio	Dc km	Da km	Ecc	Dw km	Cw km
Upper Inglewood, layer Uig7, pumice												
1.6	192.1	13.9	50.2	0.96	16.1	13.3	1.4	9.1	11.1	0.82	15.7	6.7
1	590.9	24.3	66.4	0.99	26.6	25.6	1.1	14.4	16.4	0.76	26.0	12.6
0.6	799.6	28.3	100.6	0.99	33.7	29.6	1.1	16.9	21.6	0.76	30.3	14.6
0.1	2049.4	45.3	161.0	0.99	52.6	47.5	1.1	26.3	34.6	0.76	50.3	23.3
Upper Inglewood, layer Uig7, lithics												
3.2	25.5	5.0	16.0	0.99	5.6	5.4	1.1	2.9	4.0	0.73	4.7	2.6
2	57.4	7.6	27.2	0.96	9.6	7.5	1.3	4.6	5.6	0.63	6.1	3.6
1.6	63.3	9.1	32.6	0.97	11.7	9.1	1.3	5.9	7.0	0.64	9.7	4.5
1	235.6	15.3	55.0	0.96	19.6	15.4	1.3	9.6	11.9	0.62	17.6	7.7
0.6	556.6	23.6	84.2	0.99	26.6	24.7	1.2	14.3	16.4	0.76	25.6	12.6
0.1	1290.0	35.9	127.9	0.99	43.3	37.4	1.2	21.7	29.3	0.74	36.6	16.6
Kokowai, layer Kw7, pumice												
5	10.5	3.2	12.5	0.65	5.0	2.6	1.9	2.5	2.7	0.93	4.3	1.3
4	29.2	5.4	20.6	0.65	6.5	4.3	2.0	4.3	4.9	0.66	7.4	2.2
3.2	69.5	8.5	36.1	0.66	14.3	7.6	1.9	7.2	6.3	0.66	10.9	3.6
2.4	164.5	12.6	46.6	0.67	19.1	10.5	1.6	9.6	11.0	0.67	14.6	5.3
1.6 (f-int)	257.3	16.0	60.1	0.90	23.3	14.0	1.7	11.7	13.4	0.67	16.4	7.0
0.6 (f-int)	347.3	18.6	69.7	0.90	26.6	16.4	1.6	13.3	15.7	0.65	21.9	6.2
0.2	440.4	21.0	75.3	0.90	29.9	16.4	1.6	15.0	17.7	0.65	25.0	9.4
Kokowai, layer Kw7, lithics												
4	12.6	3.6	14.5	0.77	5.6	2.7	2.1	2.9	3.2	0.91	4.5	1.4
3.2	31.6	5.6	23.0	0.75	9.3	4.4	2.1	4.7	5.0	0.93	7.5	2.3
2.4	104.7	10.2	36.3	0.90	14.6	6.9	1.6	7.3	6.1	0.90	12.0	4.4
1.6 (f-int)	166.1	13.7	51.4	0.89	16.9	11.9	1.6	9.5	11.0	0.66	16.4	6.0
0.6 (f-int)	290.9	17.1	63.7	0.90	24.6	15.0	1.6	12.3	14.1	0.67	20.6	7.5
0.2	416.1	20.4	76.1	0.90	29.0	16.0	1.6	14.5	17.0	0.65	25.0	9.1
Kokowai, layer Kw4, pumice												
6	17.7	4.2	15.0	0.99	5.1	4.3	1.2	2.6	3.2	0.60	4.5	2.1
5.3	50.6	7.1	25.5	0.96	6.6	7.2	1.2	4.3	5.4	0.60	7.5	3.5
4	190.7	13.6	49.5	0.96	17.4	13.6	1.3	6.7	10.7	0.62	15.6	6.6
3.2	434.3	20.6	74.9	0.97	26.5	20.7	1.3	13.3	16.0	0.63	24.2	10.3
2 (f-int)	544.6	23.3	83.6	0.96	29.5	23.4	1.3	14.6	16.3	0.61	26.1	11.7
1.6	620.7	24.9	89.3	0.96	31.5	25.0	1.3	15.6	19.6	0.60	27.6	12.5
Kokowai, layer Kw4, lithics												
5	31.9	5.6	20.3	0.97	7.0	5.6	1.3	3.5	4.4	0.60	6.1	2.6
4	70.0	8.4	30.1	0.97	10.6	6.2	1.3	5.3	6.5	0.62	6.5	4.1
3.2	146.9	12.2	43.6	0.96	15.4	12.1	1.3	7.7	10.2	0.75	13.1	6.5
2 (f-int)	360.0	19.0	66.2	0.97	24.2	16.6	1.3	12.1	14.5	0.63	21.2	9.4
1.6	490.5	22.1	79.6	0.97	26.2	21.9	1.3	14.1	16.3	0.77	24.5	11.0

For most abbreviations, definitions and formulas see Online Resource 6. Dw: downwind and Cw: crosswind distances measured on the isopleth maps according to Carey and Sparks (1966).

Appendix 4.8



Appendix 4.9

9a Column height (HT) in kilometres, calculated by applying different methods using isopleth and isopach data

Bu	Kp	MD1	MD2	MD3	Ulg7	Kw7	Kw4
<i>Carey and Sparks (1986; from isopleth data _a)</i>							
6.0	9.0	17.0	16.5	16.0	15.1	14.5	24.0
10.0	10.0	22.5	22.0	21.0	16.5	15.0	24.5
7.5	11.0	26.0	27.5	29.0	17.0	16.9	26.3
12.0	11.0				17.6	19.6	29.7
12.5	12.0				16.0	20.5	27.2
14.0	15.0				16.6	21.2	26.3
15.5					22.4	21.4	29.0
					24.2	22.4	29.0
					27.6	23.0	
					26.5		
<i>Sparks (1986) and Pyle (1989; from isopleth data _b)</i>							
16.7	17.4	33.0	32.6	33.0	30.5	26.6	42.8
	19.3				32.3	26.0	40.1
<i>Sulpizio (2005; from isopach and isopleth data _c)</i>							
14.1	13.4	22.0	21.7	22.0	13.3	17.0	20.5
16.6	14.4	23.2	24.2	26.4	16.1	16.0	20.1
16.6	15.0				19.3	16.4	21.6
21.1	19.2				20.6	19.6	22.9
22.0	22.6				21.5	22.0	26.9
					21.7		29.0
					21.9		
					22.4		
					24.2		
<i>Bonadonna and Costa (2013; from isopleth data _d)</i>							
13.1	14.4	26.2	25.7	26.3	26.1	19.5	30.7

Bed-sets: Burrell (Bu), Kaupokonui (Kp), Manganui-D layers 1-3 (MD1-MD3), Upper Inglewood layer 7 (Ulg7), and Kokowai layers 7 and 4 (Kw7 and Kw4).

_a Available pumice and lithic isopleths within 0.6-5.3 cm clast-diameters were employed.

_b Calculated from grain-size exponential decreasing rates of pumice and lithic isopleths.

_c Calculated from total (klot) and proximal (k0) bulk-deposit thinning and grain-size decreasing exponential rates.

_d Calculated from grain-size decreasing rates using a Weibull function

9b Eruption classification parameters calculated from isopleth and isopach data

	Bu	Kp	MD1	MD2	MD3	Ulg7	Kw7	Kw4
<i>Walker (1973)</i>								
<i>D (km²)</i>	1576	2206	3672 (MD1-3)			3396	655	2121
<i>Pyle (1989)</i>								
<i>bt (km)</i>	3.4	4.0	5.2 (MD1-3)			5.0	2.6	3.9
<i>bc (km)</i>		1.4	3.8 (MD1-3)			3.5	2.5	6.3
<i>bc(p)</i>		1.5	3.6	3.7	3.6	3.7	2.6	6.7
<i>bc(l)</i>	1.5	1.3				3.3	2.5	5.6
<i>bc/bt</i>		0.36	0.73			0.70	0.97	1.60
<i>bc/bt(p)</i>		0.36	0.73	0.71	0.74	0.74	0.96	1.72
<i>bc/bt(l)</i>	0.43	0.33				0.66	0.95	1.47
<i>Bonadonna and Costa (2013)</i>								
<i>Ath(1)</i>	19.4	45.2	25.4	25.4	25.4	20.4	12.0	15.7
<i>Ath(2)</i>			52.2	52.2	52.2	26.3	12.9	51.9
<i>AML</i>	5.7	6.9	20.3	19.5	20.3	20.1	11.6	27.0
<i>AML/Ath1</i>	0.3	0.2	0.6	0.6	0.6	1.0	1.0	1.7
<i>AML/Ath2</i>			0.4	0.4	0.4	0.7	0.9	0.5

Bed-sets: Burrell (Bu), Kaupokonui (Kp), Manganui-D layers 1-3 (MD1-MD3), Upper Inglewood layer 7 (Ulg7), Kokowai layers 7 and 4 (Kw7 and Kw4).

D: Area of dispersal.

bt: half distance of the maximum thickness extrapolated.

bc: total half distance of the maximum clasts extrapolated. Letters (p) or (l) stand for calculations made with either pumice and vesicular juvenile clasts or lithics, respectively.

Ath: Decay length scale of deposit thickness, using interpolated-extrapolated isopachs (1) or field-interpolated isopachs alone (2).

AML: Decay length scale of clast diameter, using lithic isopleth data.

Appendix 5.1

Geographic location of the studied sections

Section	NZTM2000*		WGS84†	
	Northing	Easting	Latitude	Longitude
A	5646089.0 m	1693647.9 m	39° 19' 46.3" S	174° 05' 11.5" E
B	5645802.5 m	1692564.1 m	39° 19' 56.1" S	174° 04' 26.4" E
C	5647245.5 m	1693657.3 m	39° 19' 08.8" S	174° 05' 11.3" E
D	5647730.6 m	1694183.4 m	39° 18' 52.9" S	174° 05' 33.1" E
E	5647992.4 m	1693868.5 m	39° 18' 44.5" S	174° 05' 19.8" E
F	5648669.8 m	1694125.8 m	39° 18' 22.5" S	174° 05' 30.2" E
G	5648147.3 m	1694575.6 m	39° 18' 39.2" S	174° 05' 49.2" E
H	5648217.9 m	1695053.5 m	39° 18' 36.8" S	174° 06' 09.1" E
I	5648699.3 m	1695464.5 m	39° 18' 21.0" S	174° 06' 26.0" E
J	5650296.4 m	1695116.9 m	39° 17' 29.3" S	174° 06' 10.7" E
K	5650170.5 m	1693243.8 m	39° 17' 34.1" S	174° 04' 52.6" E
L	5650609.5 m	1694645.3 m	39° 17' 19.4" S	174° 05' 50.9" E
M	5651214.4 m	1695135.5 m	39° 16' 59.5" S	174° 06' 11.0" E
N	5651331.0 m	1694630.4 m	39° 16' 56.0" S	174° 05' 49.9" E
O	5651200.5 m	1693598.4 m	39° 17' 00.6" S	174° 05' 06.9" E
P	5651436.9 m	1693936.1 m	39° 16' 52.8" S	174° 05' 20.9" E
Q	5651588.9 m	1694088.1 m	39° 16' 47.8" S	174° 05' 27.1" E
R	5651939.7 m	1693892.2 m	39° 16' 36.5" S	174° 05' 18.8" E
S	5652418.9 m	1694358.4 m	39° 16' 20.8" S	174° 05' 38.0" E
T	5653260.8 m	1694513.8 m	39° 15' 53.4" S	174° 05' 44.1" E
U	5651453.8 m	1693243.8 m	39° 16' 52.5" S	174° 04' 52.0" E
V	5651792.2 m	1693007.9 m	39° 16' 41.6" S	174° 04' 41.9" E
W	5653001.8 m	1692441.6 m	39° 16' 02.6" S	174° 04' 17.7" E
X1	5652872.2 m	1691768.1 m	39° 16' 07.1" S	174° 03' 49.7" E
X2	5652937.0 m	1691366.6 m	39° 16' 05.1" S	174° 03' 32.9" E
Y	5652652.1 m	1690952.1 m	39° 16' 14.5" S	174° 03' 15.7" E

*New Zealand Transverse Mercator 2000

†World Geodetic System 1984

B. Statements of contribution



MASSEY UNIVERSITY
GRADUATE RESEARCH SCHOOL

**STATEMENT OF CONTRIBUTION
TO DOCTORAL THESIS CONTAINING PUBLICATIONS**

(To appear at the end of each thesis chapter/section/appendix submitted as an article/paper or collected as an appendix at the end of the thesis)

We, the candidate and the candidate's Principal Supervisor, certify that all co-authors have consented to their work being included in the thesis and they have accepted the candidate's contribution as indicated below in the *Statement of Originality*.

Name of Candidate: Rafael Torres-Orozco

Name/Title of Principal Supervisor: Shane J Cronin

Name of Published Research Output and full reference:

Torres-Orozco R, Cronin SJ, Pardo N, Palmer AS (2017) New insights into Holocene eruption episodes from proximal deposit sequences at Mt. Taranaki (Egmont), New Zealand. *Bulletin of Volcanology* 79:3, doi: 10.1007/s00445-016-1085-5

In which Chapter is the Published Work: Chapter 3

Please indicate either:

- The percentage of the Published Work that was contributed by the candidate:
and / or
- Describe the contribution that the candidate has made to the Published Work:
Field descriptions, mapping and sampling, laboratory preparation of samples, manuscript and figures preparation, writing and submission.

Rafael
Torres-Orozco
Digital Signature of Rafael Torres-Orozco
Date: 2017.02.26 09:29:03
Signed by Rafael Torres-Orozco
Date: 2017.02.26 09:29:03

Candidate's Signature

26/02/2017

Date

Shane Cronin
Digital Signature of Shane Cronin
Date: 2017.02.26 09:29:03
Signed by Shane Cronin
Date: 2017.02.26 09:29:03

Principal Supervisor's signature

28/02/2017

Date



MASSEY UNIVERSITY
GRADUATE RESEARCH SCHOOL

**STATEMENT OF CONTRIBUTION
TO DOCTORAL THESIS CONTAINING PUBLICATIONS**

(To appear at the end of each thesis chapter/section/appendix submitted as an article/paper or collected as an appendix at the end of the thesis)

We, the candidate and the candidate's Principal Supervisor, certify that all co-authors have consented to their work being included in the thesis and they have accepted the candidate's contribution as indicated below in the *Statement of Originality*.

Name of Candidate: Rafael Torres-Orozco

Name/Title of Principal Supervisor: Shane J Cronin

Name of Published Research Output and full reference:

Torres-Orozco R, Cronin SJ, Damaschke M, Pardo N (2017) Diverse dynamics of Holocene mafic-intermediate Plinian eruptions at Mt. Taranaki (Egmont), New Zealand. In review by editor at Bulletin of Volcanology.

In which Chapter is the Published Work: Chapter 4

Please indicate either:

- The percentage of the Published Work that was contributed by the candidate:
and / or
- Describe the contribution that the candidate has made to the Published Work:
Field descriptions, mapping and sampling, laboratory preparation of samples, analyses of granulometry, componentry and picnometry, calculation of eruptive parameters, manuscript and figures preparation, writing and submission.

Rafael
Torres-Orozco

Candidate's Signature

Digitally signed by Rafael Torres-Orozco
DN: cn=Rafael Torres-Orozco, o=Massey University,
ou=Graduate Research School, email=Rafael.Torres-Orozco@massey.ac.nz,
serial=1000000000

26/02/2017

Date

Shane Cronin

Principal Supervisor's signature

Digitally signed by Shane Cronin
DN: cn=Shane Cronin, o=University of
Auckland, ou=School of Environment,
email=s.cronin@auckland.ac.nz, c=NZ,
date=2017.02.28 09:30:08 +1200

28/02/2017

Date



MASSEY UNIVERSITY
GRADUATE RESEARCH SCHOOL

**STATEMENT OF CONTRIBUTION
TO DOCTORAL THESIS CONTAINING PUBLICATIONS**

(To appear at the end of each thesis chapter/section/appendix submitted as an article/paper or collected as an appendix at the end of the thesis)

We, the candidate and the candidate's Principal Supervisor, certify that all co-authors have consented to their work being included in the thesis and they have accepted the candidate's contribution as indicated below in the *Statement of Originality*.

Name of Candidate: Rafael Torres-Orozco

Name/Title of Principal Supervisor: Shane J Cronin

Name of Published Research Output and full reference:

Torres-Orozco R, Cronin SJ, Pardo N, Palmer AS (submitted) Volcanic hazard scenarios for multi-phase andesitic Plinian eruptions from lithostratigraphy: Mt. Taranaki (Egmont), New Zealand. Submitted to Geological Society of America Bulletin.

In which Chapter is the Published Work: Chapter 5

Please indicate either:

- The percentage of the Published Work that was contributed by the candidate:
and / or
- Describe the contribution that the candidate has made to the Published Work:
Field descriptions, mapping and sampling, laboratory preparation of samples, analyses of componentry, manuscript and figures preparation, writing and submission.

Rafael
Torres-Orozco
Digital signature of Rafael Torres-Orozco
Date: 2017.02.26 09:30:00
Signed by Rafael Torres-Orozco
Date: 2017.02.26 09:30:00

Candidate's Signature

26/02/2017
Date

Date

Shane Cronin
Digital signature of Shane Cronin
Date: 2017.02.28 09:30:00
Signed by Shane Cronin
Date: 2017.02.28 09:30:00

Principal Supervisor's signature

28/02/17
Date

Date